eCAM
Evidence-Based Complementary and Alternative Medicine

Biological Values of Acupuncture and Chinese Herbal Medicine: Impact on the Life Science

Guest Editors: Yong Qing Yang, Chen Yan, Chris J. Branford-White, and Xiang-Yu Hou

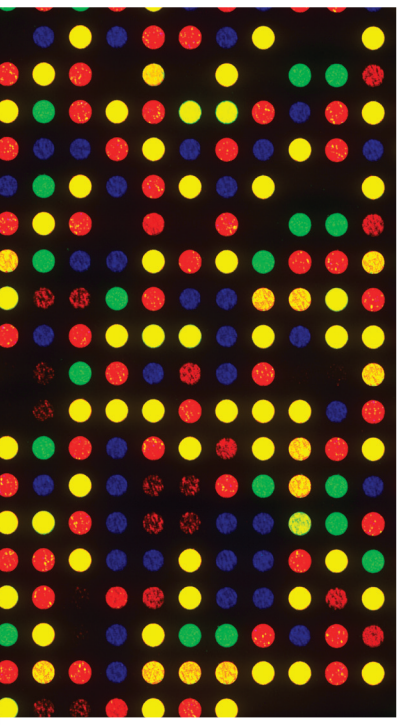

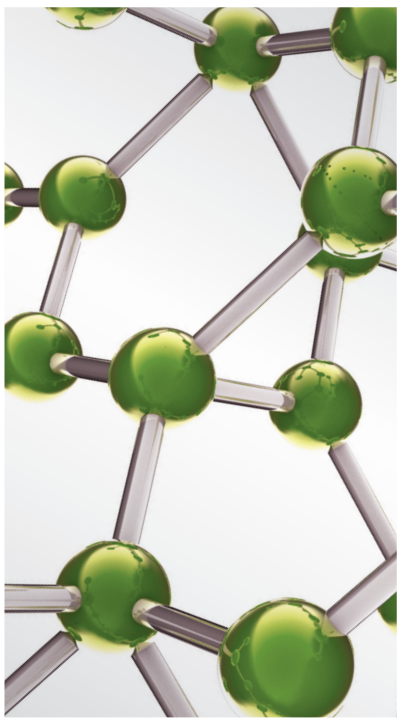


Biological Values of Acupuncture and Chinese Herbal Medicine: Impact on the Life Science

Evidence-Based Complementary and Alternative Medicine

Biological Values of Acupuncture and Chinese Herbal Medicine: Impact on the Life Science

Guest Editors: Yong Qing Yang, Chen Yan,
Chris J. Branford-White, and Xiang-Yu Hou

Editorial Board

Contents

Editorial

Biological Values of Acupuncture and Chinese Herbal Medicine: Impact on the Life Science

Yong-Qing Yang,[1] Chen Yan,[2] Chris J. Branford-White,[3] and Xiang-Yu Hou[4]

[1] *Shanghai Research Institute of Acupuncture and Meridian, Yueyang Hospital, Shanghai University of Traditional Chinese Medicine, Shanghai 201203, China*
[2] *Cardiovascular Research Institute, University of Rochester School of Medicine and Dentistry, Rochester, NY 14642, USA*
[3] *Institute for Health Research and Policy, London Metropolitan University, UK*
[4] *School of Public Health, Queensland University of Technology, Victoria Park Road, Kelvin Grove, QLD 4059, Australia*

Correspondence should be addressed to Yong-Qing Yang; yyq@shutcm.edu.cn

Received 19 November 2013; Accepted 19 November 2013; Published 12 January 2014

As treasures of the traditional Chinese medicine (TCM), acupuncture and Chinese herbal medicine have a history of more than 2,500 years and have achieved sound effects in the clinical practice [1]. The effects of acupuncture and Chinese herbs have usually been demonstrated by biological regulations of physiological and pathological processes [2, 3], which are inherent responses of human beings and of great importance in the life science research.

In recent years, the researches of acupuncture and Chinese herbal medicine have improved significantly due to the prosperity and development of modern life science technology [4–7]. At the same time, the studies of acupuncture and Chinese herbal medicine have in turn enhanced the development of biomedical science as well as the understanding of life [8–10] and offered new perspectives that can benefit modern medicine [11, 12]. However, the major challenge of the integration of TCM with modern medicine is the inadequate understanding of the biological foundation of TCM experience and concepts. In order to deepen our knowledge of TCM, it is important to clarify the biological value and mechanistic action of acupuncture and Chinese herbal medicine, which may turn hypothesis to solid data-based research and creative discovery of life science.

We are excited to present our readers with this special issue that summarizes recent discoveries and knowledge of acupuncture and Chinese herbal medicine. This specialized issue collects 24 original research articles and 4 reviews that provide the clinical or animal-based evidence elucidating the impacts of acupuncture and Chinese herbal medicine on the life science. Among these original research articles, the biological functions and potential mechanisms of acupuncture and Chinese herbal drugs in disease treatment were demonstrated in animal models of diseases such as focal cerebral ischemia, pain, atopic dermatitis, insomnia, fatty liver, and Crohn's disease. Two papers are on cancer cells: Han-Peng Kuo et al. reported that Ganoderma tsugae extract inhibited the growth of HER2-overexpressing cancer cells and enhanced the growth inhibitory effect of antitumor drugs via the modulation of HER2/PI3K/Akt signaling pathway; Xiu-Feng Wang et al. showed that PC-SPESII herbal extract could impair human breast cancer metastasis by regulating proteolytic enzymes and matrix dynamics through the p38MAPK and SAPK/JNK pathway. Additionally, You Ning et al. reported the molecular mechanisms underlying the antiproliferative and prodifferentiative effects of psoralen on adult neural stem cells using DNA microarray. Interestingly, two research articles (Lei-Miao Yin et al. and Xiang-Gen Zhong et al.) simultaneously focused on the same issue, specific link between the lung and the large intestine, which provide new lines of evidence for the modern biological theory of "exterior-interior correlation between *Zang* and *Fu*

organs." The review by Yu Wang et al. presented a comprehensive overview of the researches on acupuncture effective biomolecules, covered diverse carriers such as cerebrospinal fluid, serum, organs, and tissues, and discussed how to promote the development of biological medicine based on the discovery of acupuncture effective biomolecules. The other 3 review articles also provided us with current understanding of biological values of acupuncture and Chinese herbal medicine on inflammatory bowel diseases, amblyopia, and glucose and lipids metabolism, respectively.

In summary, this special issue provides up-to-date and valuable information about the role of acupuncture and Chinese herbs in the life science. Accordingly, future researches with modern technologies would further advance our understanding of the biological effects and cellular/molecular bases for acupuncture and Chinese herbal medicine in diverse diseases.

Acknowledgments

We, the editorial team, would like to thank all of the authors for their contributions to this special issue and we are also grateful to the reviewers for their timely responses and constructive feedback to authors. We also thank Dr. Lei-Miao Yin and Dr. Yu-Dong Xu for their excellent secretary assistance for the special issue.

Yong-Qing Yang
Chen Yan
Chris J. Branford-White
Xiang-Yu Hou

References

[1] F. Cheung, "TCM: made in China," *Nature*, vol. 480, no. 7378, pp. S82–S83, 2011.

[2] Z.-Q. Zhao, "Neural mechanism underlying acupuncture analgesia," *Progress in Neurobiology*, vol. 85, no. 4, pp. 355–375, 2008.

[3] W. Lam, S. Bussom, F. Guan et al., "The four-herb Chinese medicine PHY906 reduces chemotherapy-induced gastrointestinal toxicity," *Science Translational Medicine*, vol. 2, no. 45, article 45ra59, 2010.

[4] X.-W. Zhang, X.-J. Yan, Z.-R. Zhou et al., "Arsenic trioxide controls the fate of the PML-RARα oncoprotein by directly binding PML," *Science*, vol. 328, no. 5975, pp. 240–243, 2010.

[5] Y. D. Xu, J. M. Cui, Y. Wang et al., "Proteomic analysis reveals the deregulation of inflammation-related proteins in acupuncture-treated rats with asthma onset," *Evidence-Based Complementary and Alternative Medicine*, vol. 2012, Article ID 850512, 14 pages, 2012.

[6] L.-M. Yin, G.-H. Jiang, Y. Wang et al., "Use of serial analysis of gene expression to reveal the specific regulation of gene expression profile in asthmatic rats treated by acupuncture," *Journal of Biomedical Science*, vol. 16, no. 1, article 46, 2009.

[7] R. Stone, "Biochemistry: lifting the veil on traditional Chinese medicine," *Science*, vol. 319, no. 5864, pp. 709–710, 2008.

[8] N. Goldman, M. Chen, T. Fujita et al., "Adenosine A1 receptors mediate local anti-nociceptive effects of acupuncture," *Nature Neuroscience*, vol. 13, no. 7, pp. 883–888, 2010.

[9] C.-X. Liu, Q.-Q. Yin, H.-C. Zhou et al., "Adenanthin targets peroxiredoxin I and II to induce differentiation of leukemic cells," *Nature Chemical Biology*, vol. 8, no. 5, pp. 486–493, 2012.

[10] S. R. Meshnick, T. E. Taylor, and S. Kamchonwongpaisan, "Artemisinin and the antimalarial endoperoxides: from herbal remedy to targeted chemotherapy," *Microbiological Reviews*, vol. 60, no. 2, pp. 301–315, 1996.

[11] P. Tian, "Convergence: where West meets East," *Nature*, vol. 480, no. 7378, pp. S84–S86, 2011.

[12] F. Qi, A. Li, Y. Inagaki et al., "Chinese herbal medicines as adjuvant treatment during chemo- or radio-therapy for cancer," *Bioscience Trends*, vol. 4, no. 6, pp. 297–307, 2010.

Hindawi Publishing Corporation
Evidence-Based Complementary and Alternative Medicine
Volume 2013, Article ID 360302, 12 pages
http://dx.doi.org/10.1155/2013/360302

Research Article

Microarray Analysis of mRNA and MicroRNA Expression Profile Reveals the Role of β-Sitosterol-D-glucoside in the Proliferation of Neural Stem Cell

Li-hua Jiang,[1] Nian-yun Yang,[2] Xiao-lin Yuan,[3] Yi-jie Zou,[4] Ze-qun Jiang,[3] Feng-ming Zhao,[3] Jian-ping Chen,[3] Ming-yan Wang,[3] and Da-xiang Lu[1]

[1] *Medical College of Jinan University, 601 Huangpu Road West, Guangzhou 510632, China*
[2] *Department of Pharmacognosy, Nanjing University of Chinese Medicine, Nanjing 210038, China*
[3] *Basic Medical College of Nanjing University of Chinese Medicine, Nanjing 210038, China*
[4] *Jiangsu Province Hospital of Traditional Chinese Medicine, Nanjing 210029, China*

Correspondence should be addressed to Ming-yan Wang; dmwmy@163.com and Da-xiang Lu; ldx@jnu.edu.cn

Received 11 June 2013; Accepted 27 September 2013

Academic Editor: Xiang-Yu Hou

Neural stem cells (NSCs) are self-regenerating cells, but their regenerative capacity is limited. The present study was conducted to investigate the effect of β-sitosterol-D-glucoside (BSSG) on the proliferation of hippocampal NSCs and to determine the corresponding molecular mechanism. Results of CCK-8 assay showed that BSSG significantly increased NSC proliferation and the effectiveness of BSSG was similar to that of basic fibroblast growth factor and epidermal growth factor. mRNA expression profiling showed that 960 genes were differentially expressed after NSCs were treated with BSSG. Among the 960 genes, IGF1 is considered as a key regulatory gene that functionally promotes NSC proliferation. MicroRNA (miRNA) expression profiling indicated that 30 and 84 miRNAs were upregulated and downregulated, respectively. miRNA-mRNA relevance analysis revealed that numerous mRNAs including IGF1 mRNA were negatively regulated by miRNAs with decreased expression, thereby increasing the corresponding mRNA expression. The increased expression of IGF1 protein was validated by ELISA. Picropodophyllin (PPP, an inhibitor of IGF-1R) inhibition test confirmed that the proliferation-enhancing effect depended on IGF1. This study provided information about BSSG as an efficient and inexpensive growth factor alternative, of which the effect is closely involved in IGF1.

1. Introduction

Neural stem cells (NSCs) are defined as undifferentiated cells that have the ability of self-renewal and the potential to generate neurons, astrocytes, or oligodendrocytes in the central nervous system [1, 2]. NSCs are located in the subventricular zone (SVZ) and the subgranular zone (SGZ) of hippocampus. NSCs and neural regeneration have been extensively studied to provide proper treatment for encephalic diseases [3, 4] by cell transplantation. However, a majority of NSCs are arrested at the G0 phase of the mitotic cell cycle; such a limited regenerative capacity of endogenous and grafted NSCs is attributed to the inhibition of NSC proliferation and neurogenesis [5]. Studies have also suggested that several active components of herbs such as Tenuigenin [6] and mitogens such as epidermal growth factor (EGF) [7] and basic fibroblast growth factor (bFGF) [8] accelerate NSC proliferation. However, these active components are costly or chemically unstable, limiting their application. Therefore, reliable alternative chemical components should be identified.

In this study, the first confirmation that β-sitosterol-D-glucoside (BSSG, a sterolin) increases the proliferation of hippocampal NSCs was presented. Studies have showed multiple biological activity of BSSG, including anti-inflammatory effects [9, 10], anthelmintic activity [11], and immunomodulating activity [12, 13]. In the study, BSSG promoted NSC proliferation as a result of regulation of numerous genes, especially increasing IGF1 expression.

Recent advances in bioinformatics and high-throughput technologies such as microarray analysis are bringing about

a revolution in our understanding of the molecular mechanisms underlying biological processes. In this study, mRNA and microRNA (miRNA) expression microarray analyses were performed to understand the molecular mechanism of the effect on NSCs. miRNAs are small endogenous, noncoding RNAs that are highly conserved and that have been recognized as a powerful tool for regulating gene expression through the RNA interference pathway [14, 15]. With the ability of one miRNA to bind and regulate numerous mRNAs and the potential for a single mRNA to be targeted by multiple miRNAs, it is possible to fine-tune the expression of proteins within the cell in a very precise manner [16].

Some analytical methods are applied in the microarray analysis, including Gene Ontology (GO) analysis. GO analysis (http://www.geneontology.org/) provides a controlled vocabulary to describe the gene and the gene product attributes in any organism. GO covers three domains: biological process, cellular component, and molecular function [17]. Biological process refers to a biological objective to which the gene or gene product contributes. A process is accomplished via one or more ordered assemblies of molecular functions. Molecular function is defined as the biochemical activity of a gene product. Cellular component refers to the place in the cell where a gene product is active. These terms reflect our understanding of eukaryotic cell structure. Among these domains, biological process helps understand the biological functions specifying where or when the event actually occurs. Thus, biological process was used to describe the specific biological functions of differentially expressed genes. In addition, genic network analysis helps understand the interacting genes.

2. Materials and Methods

2.1. Preparation of BSSG. BSSG (purity: 98%, provided by Department of Pharmacognosy, Nanjing University of Chinese Medicine) stock solution was prepared in Dimethyl Sulfoxide (DMSO). Before each experiment was performed, the solution was diluted in a fresh medium to obtain a final DMSO concentration of ≤0.1%.

2.2. Primary NSC Culture and Identification. Primary NSC culture was established according to a previously published protocol [18]. In brief, the hippocampus of a Sprague-Dawley rat embryo at 16 d of embryonic stage was dissected in cold CMF-HBSS and then dissociated mechanically. The cells were collected by centrifugation and resuspended in a neurobasal medium (Gibco, CA, USA) supplemented with epidermal growth factor (EGF, 20 ng/mL; PeproTech Inc., Rocky Hill, NJ, USA), basic fibroblast growth factor (bFGF, 20 ng/mL; PeproTech Inc. USA), B27 supplement (2%; Gibco, USA), penicillin (50 U/mL), and streptomycin (50 μg/mL). The cells were adjusted to a density of 1×10^5 cells/mL and planted in culture flasks. The medium was replaced with 1/2 of the same medium at an interval of 3 d. The cells were stained by immunocytochemistry with primary antibody against nestin (Boshide, Wuhan, China) to make the identification of NSCs.

2.3. CCK-8 Assay

2.3.1. Dose-Dependent Cell Proliferation Detection. Dose-dependent cell viability was monitored using a cell counting kit-8 (CCK-8) assay. CCK-8 is a sensitive nonradioactive colorimetric assay used to determine the number of viable cells in cell proliferation and cytotoxicity assays. In the study, NSCs were cultured in 96-well plates containing the growth culture medium at a cell density of 5×10^3 cells per well. The cells were divided into nine groups: control group and BSSG treatment groups (1.25, 2.5, 5, 10, 20, 40, 80, and 100 μM BSSG). Each group was designed to establish six double-pore treatments. Each BSSG treatment group was treated with the corresponding amount of BSSG. The cells were treated for 72 h as described, whereafter CCK-8 solution (Beyotime Biotech, Haimen, China) was added to the cell culture medium to a final concentration of 10 μL/100 μL and incubated for another 4 h at 37°C. Absorbance was measured at 450 nm to determine cell viability as a percentage, using a microplate reader (ELx800, BioTek Instruments, Inc., Winooski, VT, USA).

2.3.2. Comparison of NSC Proliferation Promoted by BSSG, bFGF, and EGF. To understand the effectiveness of BSSG on enhancing NSCs proliferation, we compared BSSG with bFGF and EGF by performing CCK-8 assay. The cells were cultured in 96-well plates at a cell density of 1×10^4 cells per well and then divided into six treatment groups: bFGF and EGF vacancy group ($bFGF^-EGF^-$: with neurobasal medium and B27 supplement); bFGF group (with neurobasal medium, B27 supplement, and bFGF 20 ng/mL); EGF group (with neurobasal medium, B27 supplement, and EGF 20 ng/mL); and $bFGF^-EGF^-$ + BSSG groups (10, 20, and 40 μM). The cells were treated for 72 h as described above, and CCK-8 assay was performed.

2.4. mRNA Expression Microarray Analysis

2.4.1. mRNA Expression Profiling. mRNA expression microarray analysis was performed by use of Roche-NimbleGen Rattus norvegicus 12 × 135 K Array (Roche, supplied by KangChen Corp), in order to understand the effect of BSSG on regulation of mRNA, disclosing the mechanism of BSSG promoting NSCs proliferation.

Total RNA was obtained from each sample (five samples from the control group and five samples from the BSSG-treated group (40 μM), the cells were treated for 72 h as described above) and quantified by NanoDrop ND-1000. The total RNA was used for labeling and array hybridization based on the following steps: (1) reverse transcription using superscript ds-cDNA synthesis kit (Invitrogen, USA); (2) ds-cDNA labeling using one-color DNA labeling kit (Roche NimbleGen, USA); (3) array hybridization using NimbleGen hybridization system and washed using NimbleGen wash buffer kit; and (4) array scanning using the Axon GenePix 4000B microarray scanner (Molecular Devices Corporation, Sunnyvale, CA, USA).

The scanned images were imported into the NimbleScan software (version 2.6) for grid alignment and expression data

Table 1: Primer sequences of the reference gene and the genes selected.

Gene	Primer sequence	Annealing temperature (°C)	Product length (bp)
GAPDH	F: 5′-GGAAAGCTGTGGCGTGAT-3′ R: 5′-AAGGTGGAAGAATGGGAGTT-3′	60	308
IGF1	F: 5′-CTGGCACTCTGCTTGCTCAC-3′ R: 5′-CTCATCCACAATGCCCGTCT-3′	60	180
cdkn1c	F: 5′-CCTCCCGTTCCCTTCTTTCT-3′ R: 5′-CGTTCCATCGCTGTTCTGC-3′	60	96
Espl1	F: 5′-TGACTACCTGGGCGTGACTG-3′ R: 5′-CTGGCTCTGAGATGGCACAA-3′	60	98
Pttg1	F: 5′-TGGAGACAGTTGTTTGGGTGC-3′ R: 5′-GCTGCCTGGCTCTTCGTTAT-3′	60	270
Ptpru	F: 5′-ACCCTGAGCGAGAACGACA-3′ R: 5′-GGGATGGCTGAATAGCAAGAT-3′	60	285

To validate the mRNA expression profiling, five genes (Igf1, cdkn1c, Espl1, Pttg1, and Ptpru) were selected to performed real time-PCR. Primer sequences of the GAPDH gene and the genes selected were listed in Table 1. Igf1: Insulin-like growth factor-1; cdkn1c: cyclin-dependent kinase inhibitor 1C; Espl1: extra spindle pole bodies homolog 1, Pttg1: pituitary tumor-transforming 1; Ptpru: protein tyrosine phosphatase, receptor type, U.

analysis. The expression data were normalized by quartile normalization and robust multichip average (RMA) algorithm included in the NimbleScan software. The probe level files and the gene level files were generated after normalization. The ten gene level files were imported into Agilent GeneSpring GX software (version 11.5.1) for further analysis. Differentially expressed genes were identified by volcano plot filtering (P value < 0.05; fold change ≥2.0 or ≤0.5).

The genic network was plotted by use of the search tool STRING (http://string-db.org/) and drawing tool cytoscape. Then the connectivity analysis of the network was performed to obtain the "hubs" of the gene nodes, using one-side Fisher's exact test [19]. Network "nodes" (or "components") represent genes. Nodes with large degree values are commonly referred to as "hubs." The hub genes were considered as the important genes, which play significant roles in the functions and structure of cells.

2.4.2. Real-Time PCR Validation for mRNA Expression Profiling. Real-time PCR was performed to validate the mRNA expression profiling obtained. Total RNA (obtained from the same samples as mentioned in mRNA microarray analysis) was reverse transcribed with SuperScript II reverse transcriptase (Invitrogen). Real-time PCR was performed using the ABI PRISM7900 system (Applied Biosystems, Foster City, CA, USA), in the presence of forward and reverse primers for the target genes, or forward and reverse primers for the GAPDH gene used as reference. Relative quantification of the target gene is determined by calculating the ratio between the concentration of the target gene and that of the reference.

The primer sequences of the GAPDH gene and the target genes are listed in Table 1.

2.5. miRNA Microarray Analysis

2.5.1. miRNA Expression Profiling. Evidence showed the important functions of miRNAs in stem cell regulation [20, 21]. Specific miRNAs modulate the functions of many types of stem cells, including neural stem/progenitor cells [22, 23]. In the present study, the miRNA expression profiling was analyzed to understand the effect of BSSG on regulation of miRNA, describing the correlation of miRNA and mRNA. In brief, total RNA (obtained from the same samples as mentioned in mRNA microarray analysis) was harvested using TRIZOL (Invitrogen) and miRNeasy mini kit (QIAGEN) according to the manufacturer's instructions. After the total RNA was measured using NanoDrop 1000, the samples were labeled using the miRCURY Hy3/Hy5 power labeling kit and hybridized in miRCURY LNA Array (v.18.0). Following the washing steps, the slides were scanned by the Agilent Scanner G2505C.

The scanned images were imported into GenePix Pro 6.0 software (Axon) for grid alignment and data extraction. The replicated miRNAs were averaged and the miRNAs with intensities ≥30 in all of the samples were chosen to calculate the normalization factor. The expressed data were normalized by median normalization. After normalization, significantly and differentially expressed miRNAs were identified by volcano plot filtering.

2.5.2. Real-Time PCR Validation for miRNA Expression Profiling. Real-time PCR was performed to validate the differential miRNA expression profiling obtained. Total RNA was reverse-transcribed to cDNA using AMV reverse transcriptase (Epicentre), RNase (Epicentre), dNTP (HyTest Ltd), RT buffer, and RT primers (Invitrogen). The mixture was incubated at 16°C for 30 min, 42°C for 40 min, and 85°C for 5 min to generate a library of miRNA cDNAs. U6 is used as an internal control for normalization. Real-time PCR was subsequently performed using an ABI PRISM7900 system (Applied Biosystems, Foster City, CA, USA) according to a standardized protocol. The reactions were incubated at 95°C for 10 min, followed by 40 cycles at an interval of 10 s at 95°C and an interval of 1 min at 60°C. Data were analyzed by $2^{-\Delta\Delta CT}$. The primer sequences of the internal control gene and the target genes are listed in Tables 2 and 3.

Table 2: RT Primer sequence of the internal control gene and the target genes for cDNA synthesis.

Genes	RT primer sequence
U6	5′-CGCTTCACGAATTTGCGTGTCAT-3′
rno-miR-129-5p	5′-GTCGTATCCAGTGCGTGTCGTGGAGTCGGCAATTGCACTGGATACGACGCAAGCC-3′
rno-miR-322-5p	5′-GTCGTATCCAGTGCGTGTCGTGGAGTCGGCAATTGCACTGGATACGACTCCAAAA-3′
rno-miR-301a-3p	5′-GTCGTATCCAGTGCGTGTCGTGGAGTCGGCAATTGCACTGGATACGACGCTTTG-3′

To validate the miRNA expression profiling, three genes were selected to performed real time-PCR. RT primer sequences of the U6 gene used as reference and the genes selected were listed in Table 2.

Table 3: Primer sequences of the internal control gene and the target genes for PCR.

Genes	Primer sequence	Annealing temperature (°C)	Product length (bp)
U6	F: 5′GCTTCGGCAGCACATATACTAAAAT3′ R: 5′CGCTTCACGAATTTGCGTGTCAT3′	60	89
rno-miR-129-5p	GSP: 5′GGAACTTTTTGCGGTCTGG3′ R: 5′GTGCGTGTCGTGGAGTCG3′	60	63
rno-miR-322-5p	GSP: 5′GGGCAGCAGCAATTCAT3′ R: 5′CAGTGCGTGTCGTGGAG3′	60	65
rno-miR-301a-3p	GSP: 5′CCCCGTGCAATAGTATTGT3′ R: 5′CAGTGCGTGTCGTGGAGT3′	60	65

Primer sequences of the internal control gene and the target genes for PCR were listed in Table 3. GSP is the specific primer for the corresponding miRNA and R is the matching primer for the corresponding RT Primer.

2.6. IGF1 Protein Determination. IGF1 protein determination were performed to investigate the key regulator by which BSSG promotes NSC proliferation. The cells were cultured in 24-well plates at a cell density of 5×10^4 cells per well and divided into four groups: a control group and BSSG-treated groups (10, 20, and 40 μM). Each group was designed to establish six double-pore treatments. The cells were treated for 72 h as described above. The supernatant was collected and processed using the Quantikine rat IGF1 ELISA kit (R&D Systems, Inc., Minneapolis, MN, USA), following the instructions provided by the manufacturer. The absorbance of each well was determined using a microplate reader (EL×800, BioTek instruments, Inc., Winooski, VT, USA) set at 450 nm; the readings at 570 nm were subtracted from the readings at 450 nm. The quantity of cells in each well was counted using a cell counting plate. IGF1 levels were reported in pg/10,000 cells.

2.7. PPP Inhibition Test. IGF1 is mediated by type 1 IGF receptor (IGF1R). PPP is an inhibitor of IGF1R [24]. The inhibitory effect of PPP on IGF1R did not coinhibit the insulin receptor (IR) or compete with ATP in vitro kinase assays, suggesting that PPP may inhibit IGF1R autophosphorylation at the substrate level [25]. If PPP prevents BSSG-induced NSC proliferation, then the function of BSSG depends on IGF1.

In the study, PPP (Tocris Bioscience, Bristol, UK) stock solutions were prepared in DMSO and stored at 4°C. Before each experiment was performed, these solutions were diluted in a fresh medium to obtain a final DMSO concentration of <0.1%. The cells were cultured in 96-well plates at a cell density of 1×10^4 cells per well and divided among the PPP-BSSG treated groups (pair-wise; with PPP doses of 0, 0.01, 0.1, 1, and 2 μM and BSSG doses of 0, 10, 20, and 40 μM). Each group was designed to establish four double-pore experiments. The cells were treated for 72 h, and CCK-8 assay was performed. Absorbance was measured at 450 nm to determine cell viability as a percentage.

2.8. Statistical Analyses. Statistical analyses were performed by use of SPSS version 16.0 software program for windows (SPSS, Inc., Chicago, IL). Multiple comparisons were made using one-way ANOVA, followed by the Bonferroni posttest. All data are presented as Mean ± SD, and statistical significance was accepted at the 5% level.

3. Results

3.1. Identification of NSCs. NSCs were positive for nestin (Figure 1).

3.2. Dose-Dependent Cell Proliferation Detection. BSSG significantly increased NSC proliferation at concentration of 40 μM ($P < 0.01$). The same result was observed at 5, 10, and 20 μM BSSG ($P < 0.05$, Figure 2).

3.3. Comparison of NSC Proliferation Promoted by BSSG, BFGF, and EGF. NSCs proliferation was induced by adding bFGF (20 ng/mL; $P < 0.001$), EGF (20 ng/mL; $P < 0.001$), and BSSG at different concentrations (10 and 20 μM, $P < 0.01$; 40 μM, $P < 0.001$). The effect of BSSG on NSC proliferation at 40 μM was similar to those of bFGF and EGF (Figure 3).

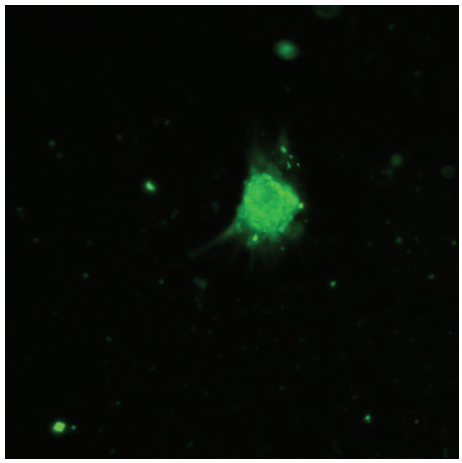

Figure 1: Identification of NSCs. Cultured NSCs were stained by immunocytochemistry with primary antibody against nestin (original magnification: 100x).

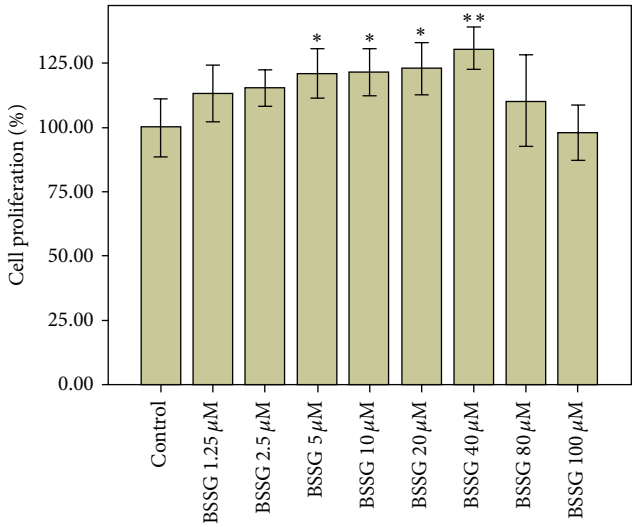

Figure 2: Dose-dependent effects of BSSG on cell proliferation. Dose-dependent effects of BSSG on cell proliferation were determined by CCK-8 assay and the data are plotted as percentages of control cell proliferation. Data are presented as Mean ± SD ($n = 6$); $^{*}P < 0.05$ and $^{**}P < 0.01$ compared with the control. BSSG significantly increased cell proliferation percentage at a concentration of 40 μM ($P < 0.01$) and at concentrations of 5, 10, and 20 μM ($P < 0.05$).

3.4. mRNA Expression Profiling. The result of mRNA expression microarray analysis showed that 960 genes were differentially expressed after NSCs were treated with BSSG, including 333 upregulation genes (fold change ≥2) and 627 downregulation genes (fold change ≤0.5). The differential expression genes were described using GO term analysis (biological process). The main differentially expressed genes are listed in Tables 4 and 5.

Tables 4 and 5 revealed that the majority of upregulation genes were involved in mitotic cell cycle particularly in the M phase, enhancing cell proliferation. By contrast, the majority

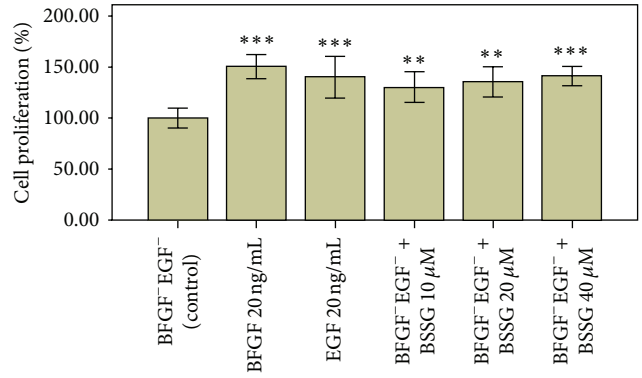

Figure 3: Comparison of NSC Proliferation Promoted by BSSG, BFGF, and EGF. Comparison of NSC proliferation promoted by BSSG, bFGF and EGF was determined by CCK-8 assay and the data are plotted as percentages of control cell proliferation. Data are presented as Mean ± SD ($n = 6$); $^{**}P < 0.01$, $^{***}P < 0.001$ compared with the control. NSCs proliferation was induced by adding bFGF (20 ng/mL, $P < 0.001$), EGF (20 ng/mL; $P < 0.001$), and BSSG at different concentrations (10 and 20 μM, $P < 0.01$; 40 μM, $P < 0.001$). The effect of BSSG on NSC proliferation at 40 μM was similar to those of bFGF and EGF.

of the downregulation genes were involved in cell differentiation, indicating that cell differentiation was inhibited, and accordingly, more possibility of cell proliferation was afforded.

3.5. Genic Network Analysis. The genic network consists of the majority of the upregulation and downregulation genes (Figure 4(a)). The "hubs" of the gene nodes in the genic network include Bub1b (budding uninhibited by benzimidazoles 1 homolog, beta), Cdc20 (cell division cycle 20 homolog), Plk1 (polo-like kinase 1), Spp1 (Sialoprotein/osteopontin), IGF1 (insulin-like growth factor I), Aurkb (aurora kinase B), and Ndc80 (kinetochore associated 2) based on the results of connectivity analysis (Figure 4(b)). BSSG increased the expression of the hub genes, which are mostly involved in cell cycle (the functions of these genes see Genecards, http://www.genecards.org/), thereby enhancing NSC proliferation.

3.6. Real-Time PCR Validation for mRNA Expression Profiling. The mRNA expression profiling was validated by real-time PCR. The comparison of quantified mRNA expressions obtained using real-time PCR and microarray analysis was performed to determine the reliability of microarray analysis (Table 6). Table 6 showed that the fold changes (test versus control) of microarray analysis were almost similar to those of PCR; an increase or a decrease in gene expression quantified by microarray analysis was consistent with the result of PCR. This result indicated that the result of the microarray analysis was reliable.

3.7. miRNA Expression Profiling. A total of 30 upregulated miRNAs (test versus control, fold change ≥2) and 84 downregulated miRNAs (test versus control, fold change ≤0.5)

Table 4: Upregulation genes.

GO ID	Term	*P* value	Genes
GO:0000087	M phase of the cell cycle	$9.58E-09$	AURKB; CCNF; KIF2C; BUB1B; CDCA3; IGF1; CENPF; DLGAP5; CDC20; SPAG5; MAD2L1; TRAF4AF1; NUSAP1; ESPL1; CCNB1; PLK1; PTTG1
GO:0000278	Mitotic cell cycle	$8.23E-08$	SPAG5; MAD2L1; TRAF4AF1; NUSAP1; ESPL1; CDKN1B; CENPF; DLGAP5; CENPA; NDC80; CCNB1; PTTG1; CDC20; AURKB; CCNF;
GO:0000280	Nuclear division	$1.82E-07$	SPAG5; MAD2L1; TRAF4AF1; NUSAP1; ESPL1; CCNB1; PLK1; PTTG1; CDC20; AURKB; CCNF; KIF2C; BUB1B; CDCA3; IGF1
GO:0007059	Chromosome segregation	$4.12E-07$	SPAG5; MAD2L1; TRAF4AF1; NUSAP1; ESPL1; CCNB1; NDC80; PTTG1; CENPF; KIF2C; TOP2A
GO:0048285	Organelle fission	$4.86E-07$	SPAG5; MAD2L1; TRAF4AF1; NUSAP1; ESPL1; CCNB1; CDCA3; PLK1; PTTG1; CDC20; AURKB; CCNF; KIF2C; BUB1B; IGF1
GO:0000226	Microtubule cytoskeleton organization	$1.87E-06$	CENPA; NDC80; ESPL1; PLK1; KIF20A; KIF2C; SPAG5; TEKT1; TRAF4AF1; CCNF; TACC3; CDKN1B; NUSAP1; CCNB1; AURKB
GO:0048545	Response to steroid hormone stimulus	$2.36E-06$	CAR9; GBA; A2M; HP; IGF1; ADM; and so forth, a total of 22 genes
GO:0051301	Cell division	$3.80E-06$	NUSAP1; PLK1; AURKB; KIF20A; NUMBL; TOP2A; TXNIP; CCNB2; CCNB1; PTTG1; CDC20; CCNF; KIF2C; BUB1B; CDCA3; TRAF4AF1
GO:0008283	Cell proliferation	$6.93E-06$	CDC20; AURKB; CCNB1; PTTG1; IGF1; and so forth, a total of 39 genes
GO:0019932	Second messenger-mediated signaling	$1.12E-05$	CALCA; ADORA2A; GRM3; EDNRB; GRM5; CXCR4; TOX3; RASD1; ADM; PDE7B; CDH13; IGF1; LMCD1; MT1A
GO:0009605	Response to external stimulus	$1.25E-05$	A2M; LBP; CCNB1; ENPP2; CKLF; IGF1; and so forth, a total of 35 genes
GO:0009719	Response to endogenous stimulus	$1.94E-05$	ADORA2A; IGF1; SPP1; A2M; and so forth, a total of 32 genes
GO:0008608	Attachment of spindle microtubules to kinetochores	$2.25E-05$	CCNB1; SPAG5; TRAF4AF1; NDC80
GO:0009056	Catabolism	$2.78E-05$	TOP2A; FBXO32; MANBA; IGF1; CDC20; and so forth, totle 41 genes
GO:0007051	Spindle organization	$3.11E-05$	ESPL1; NDC80; TACC3; CCNB1; AURKB; SPAG5; TRAF4AF1
GO:0051313	Attachment of spindle microtubules to chromosomes	$4.44E-05$	NDC80; CCNB1; SPAG5; TRAF4AF1
GO:0009725	Response to hormone stimulus	$5.00E-05$	IGF1; LOX; SPP1; A2M; HP; ALPL; and so forth, a total of 27 genes
GO:0010941	Regulation of cell death	$2.39E-04$	AURKB; IGF1; ADORA2A; and so forth, a total of 32 genes
GO:0043470	Regulation of carbohydrate catabolism	$8.83E-04$	PFKFB3; DDIT4; IER3; IGF1
GO:0048016	Inositol phosphate-mediated signaling	$1.28E-03$	EDNRB; GRM5; CALCA; IGF1; LMCD1

Upregulation genes obtained from the mRNA expression profiling were listed in Table 4. The upregulation genes were mostly involved in the mitotic cell cycle, enhancing cell proliferation. *P* value, the significance testing value of the GO ID, results from the top GO of a bioconductor.

Table 5: Downregulation genes.

GO ID	Term	*P* value	Genes
GO:0030154	Cell differentiation	$3.02E-06$	FOXC2; IGF2; JAG1; SEMA3C; HMGA2; and so forth, a total of 38 genes
GO:0006950	Response to stress	$2.05E-04$	PENK; BDNF; CRYAB; TRH; PLAU; MMP3; and so forth, a total of 32 genes
GO:2000736	Regulation of stem cell differentiation	$4.89E-04$	HMGA2; JAG1; HES1
GO:0032103	Positive regulation of response to external stimulus	$6.01E-04$	NPY; IL1RL1; SCG2; TNFSF11; CD74; THBS4
GO:0048710	Regulation of astrocyte differentiation	$8.72E-04$	HES1; CLCF1; HMGA2
GO:0045597	Positive regulation of cell differentiation	$1.16E-03$	TGFB1I1; CD74; FRZB; JAG1; BDNF; MAP1B; IFI204; TNFSF11; TNFRSF12A; HES1; CLCF1
GO:0048584	Positive regulation of response to stimulus	$2.06E-03$	CD74; TNFSF11; TGFB1I1; CDKN1C; GPC3; HES1; NPY; CLCF1; IGF2; JAG1; PRRX2; IL1RL1; SCG2; THBS4; HMGA2; TNFRSF12A
GO:0000904	Cell morphogenesis involved in differentiation	$5.26E-03$	HMGA2; MAP1B; BDNF; TGFB1I1; CHST3; FOXC2; TNFRSF12A; HES1; XYLT1; NPTX1
GO:0050920	Regulation of chemotaxis	$6.38E-03$	SCG2; CD74; THBS4; EFNB2
GO:0030182	Neuron differentiation	$7.29E-03$	MAP1B; BDNF; CHST3; NPY; MFRP; JAG1; HES1; CDKN1C; TNFRSF12A; HCN1; XYLT1; THBS4; NPTX1; BYSL
GO:0060326	Cell chemotaxis	$1.53E-02$	TNFSF11; SCG2; CD74; THBS4
GO:0090398	Cellular senescence	$1.67E-02$	HMGA2; RGD1305645
GO:0016477	Cell migration	$2.55E-02$	SEMA3C; EFNB2; TNFSF11; TNFRSF12A; PLAU; MMP3; UNC5C; SCG2; THBS4; CD74; HES1
GO:0016126	Sterol biosynthesis	$4.53E-02$	HMGCS2; HSD17B7
GO:0033554	Cellular response to stress	$4.91E-02$	HMGA2; TNFSF11; MAP1B; CHST3; XYLT1; DHX9

Downregulation genes obtained from the mRNA expression profiling were listed in Table 5. The downregulation genes were mostly involved in differentiation and the regulation of differentiation, indicating that cell differentiation was inhibited, and accordingly, more possibility of cell proliferation was afforded. *P* value, the significance testing value of the GO ID, results from the top GO of a bioconductor.

were obtained after the NSCs were treated with BSSG (Figure 5).

3.8. Real-Time PCR Validation for miRNA Microarray Analysis. The miRNA expression profiling was validated by real-time PCR. The comparison of quantified miRNA expressions obtained using real-time PCR and microarray analysis was performed to determine the reliability of microarray analysis (Table 7). Table 7 showed that the fold changes (test versus control) obtained by microarray analysis were almost similar to those obtained by PCR. An increase or a decrease in gene expression quantified by microarray analysis was consistent with the result of PCR. This result indicated that the result of microarray analysis was reliable.

3.9. miRNA-mRNA Correlation Analysis. miRNAs are recognized as a powerful tool used to regulate gene expression via the RNA interference pathway [14, 15]. Thus, miRNA-mRNA correlation analysis was carried out to further understand the effect of BSSG on regulating NSCs genes. Five downregulated miRNAs, miR-322-5p, miR-301a-3p, miR-129-5p, miR-322-3p, and miR-129-2-3p, of which the target mRNAs are involved in regulation of cell proliferation (based on miRWalk database http://www.ma.uni-heidelberg.de/apps/zmf/mirwalk/ and DAVID Bioinformatics Resources 6.7 http://david.abcc.ncifcrf.gov/tools.jsp), were selected to perform correlation analysis. The interactions between the five miRNAs and predicted target mRNAs (included in the differential expression genes obtained by the mRNA microarray analysis) were visualized as a network (Figure 6). The network was generated by use of cytoscape (with a fold change ≥ 2 or ≤ 0.5, $P < 0.05$), miRanda target prediction, and negative-correlation filtering, revealing that numerous mRNAs including IGF1 mRNA were negatively regulated by the five miRNAs, which were downregulated, thereby increasing the expression of the corresponding mRNA.

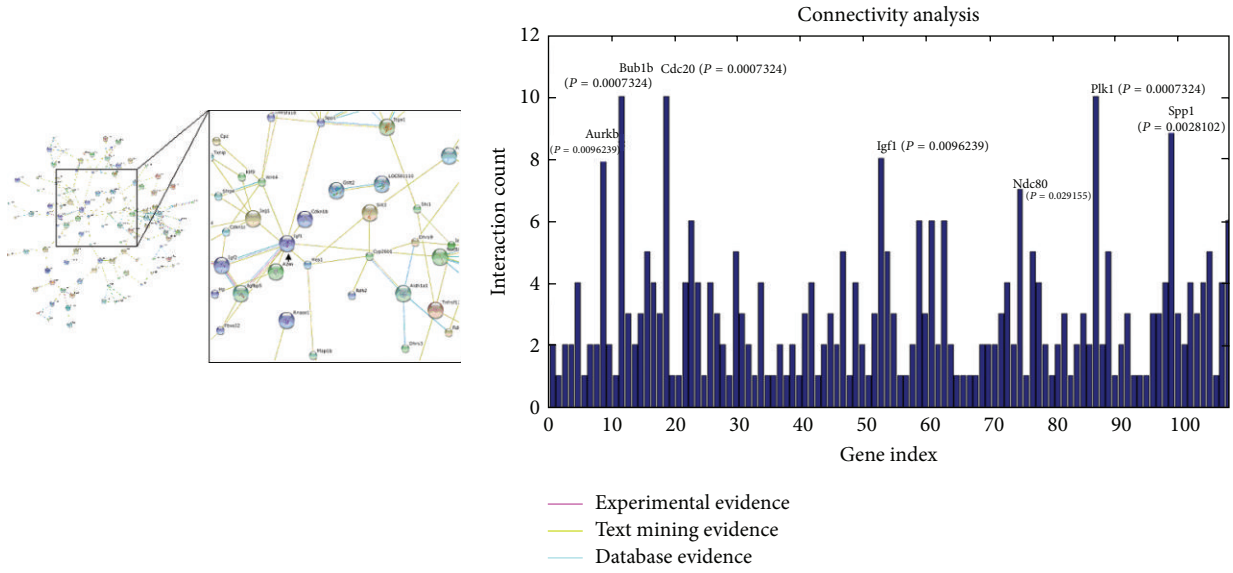

Figure 4: Genic network analysis. (a) Genic network. The genic network was plotted by use of the search tool STRING and drawing tool cytoscape to understand the interacting genes. The genic network consists of the majority of the upregulated and downregulated genes. The integral network and its magnified image are shown on the left and right parts, respectively. IGF1 is indicated by an arrow. (b) Connectivity analysis on the network. The "hubs" of the gene nodes were determined by interaction count and P value; thus, Bub1b, Cdc20, 1Plk1, Spp1, IGF1, Aurkb, and Ndc80 are the hub genes.

Table 6: Comparison of quantified mRNA expressions obtained using real-time PCR and microarray analysis.

Genes	PCR		Microarray analysis		Fold change (test versus control)	
	Control	Test	Control	Test	PCR	Microarray analysis
IGF1	0.061 ± 0.0043	0.196 ± 0.0098	230.514 ± 49.286	1079.355 ± 144.074	3.20 ↑	4.75 ↑
Pttg1	0.025 ± 0.0007	0.051 ± 0.007	319.160 ± 31.644	931.231 ± 116.161	2.09 ↑	2.91 ↑
Adora2a	0.053 ± 0.0028	0.125 ± 0.025	590.370 ± 64.092	1544.692 ± 112.533	2.34 ↑	2.62 ↑
Espl1	0.008 ± 0.002	0.028 ± 0.008	349.823 ± 33.064	730.605 ± 135.345	3.41 ↑	2.07 ↑
Ptpru	0.028 ± 0.010	0.078 ± 0.011	537.963 ± 83.725	1321.925 ± 187.830	2.74 ↑	2.46 ↑
cdkn1c	0.058 ± 0.028	0.018 ± 0.017	2536.464 ± 115.441	1196.195 ± 188.255	0.30 ↓	0.47 ↓

3.10. IGF1 Protein Quantitation. IGF1 protein in the cell culture supernatant was quantified. IGF1 protein levels were remarkably increased after the NSCs were treated with BSSG at 20 and 40 μM ($P < 0.05$, Figure 7).

3.11. PPP Inhibition Test. PPP inhibited the BSSG-induced cell proliferation at suitable concentrations (Figure 8). The inhibition of PPP on NSC proliferation was weak at 0.01 μM; however, the inhibition was remarkable at 0.1 μM ($P < 0.05$) as well as 1 ($P < 0.001$) and 2 μM ($P < 0.001$). Analogously, the inhibition of PPP on BSSG-induced cell proliferation was weak at 0.01 μM. By contrast, BSSG-induced cell proliferation was inhibited when the cells were exposed to PPP ≥ 0.1 μM. This result showed that if the function of IGF1 was blocked up, then the cell proliferation induced by BSSG ceased to exist.

4. Discussion

NSC proliferation is necessary to facilitate neurogenesis [26, 27]. Neurogenesis is enhanced when NSC proliferation is promoted appropriately. The present study provided an efficient alternative substance BSSG, which is inexpensive and chemically stable (BSSG powder remains stable at room temperature for a maximum of two years).

BSSG is present in many higher plants [28]. The procedure of isolation of BSSG is simple [29]. Moreover, it had been synthetically prepared since 1913 [30]; therefore, BSSG can be easily obtained. In the study, the minimal effective concentration was 5 μM, and the effectiveness of BSSG was similar to that of bFGF (20 ng/mL) and EGF (20 ng/mL) at concentrations of 40 μM, revealing the excellent proliferation-promoting activity.

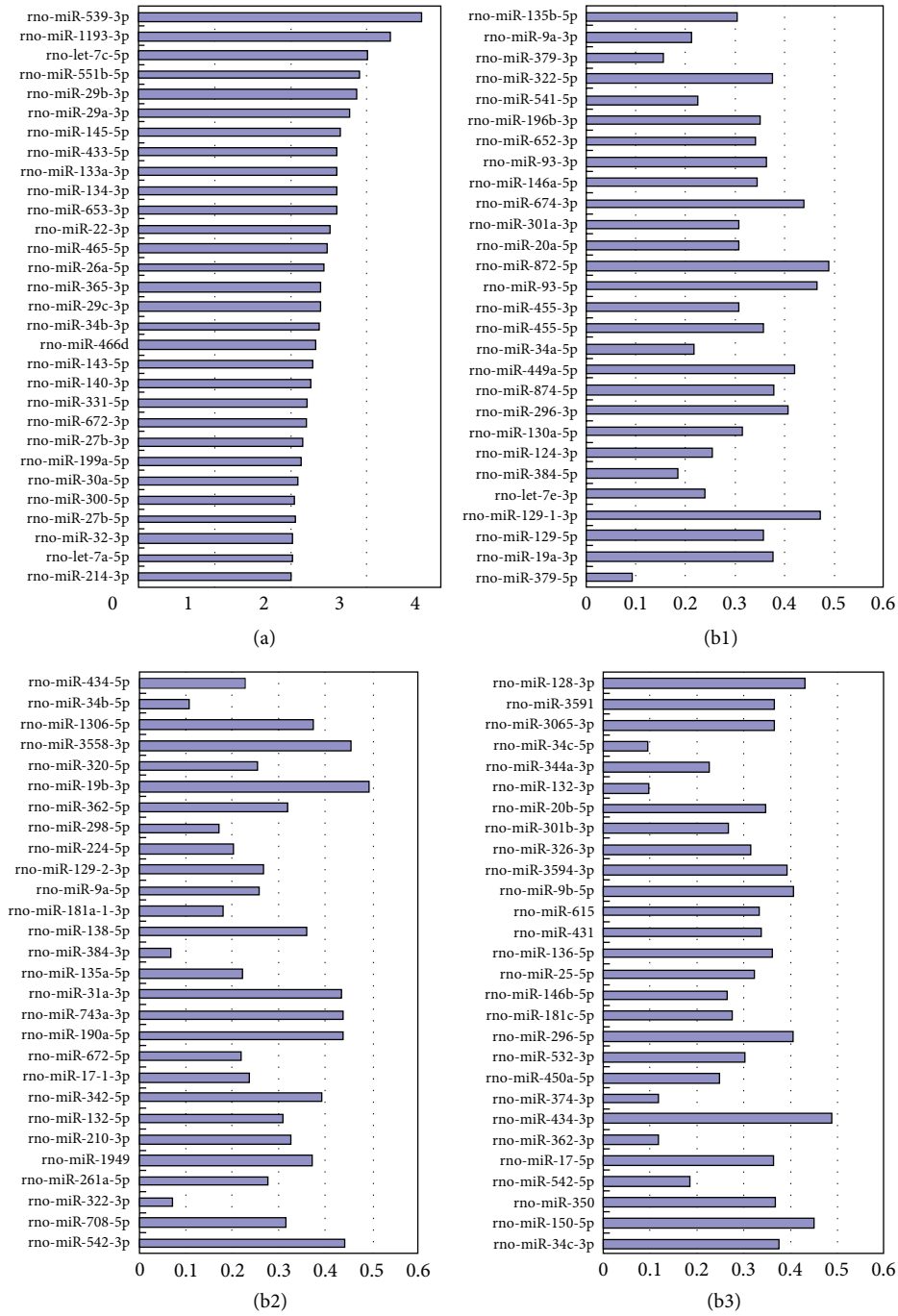

Figure 5: Differentially expressed miRNA. *Y*-axis shows the differentially expressed mRNAs; *X*-axis represents the fold change (test versus control), or the ratio of miRNA expression in the BSSG-treated group (test group) to the miRNA expression in the control group. (a) Upregulation miRNA; (b1), (b2), and (b3): downregulation miRNA.

Table 7: Comparison of the quantified miRNA expressions obtained by real-time PCR and microarray analysis.

miRNA	PCR		Microarray analysis		Fold change (test versus control)	
	Control	Test	Control	Test	PCR	Microarray analysis
rno-miR-129-5p	1.00 ± 0.055	0.29 ± 0.090	0.88 ± 0.17	0.32 ± 0.08	0.29 ↓	0.36 ↓
rno-miR-301a-3p	0.89 ± 0.11	0.29 ± 0.12	3.47 ± 1.15	1.08 ± 0.27	0.33 ↓	0.31 ↓
rno-miR-322-5p	1.34 ± 0.33	0.46 ± 0.15	1.95 ± 0.55	0.73 ± 0.11	0.34 ↓	0.37 ↓

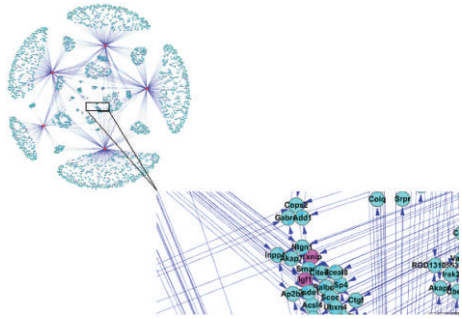

Figure 6: miRNA-mRNA Interactome Network. The integral chart and its magnified image were shown on the upper left and lower right corners, respectively. Red square nodes represented the five miRNAs: miR-322-5p; miR-301a-3p; miR-129-5p; miR-322-3p, and miR-129-2-3p. Turquoise round nodes represented the target genes of these miRNAs. Pink round nodes represented the upregulated mRNAs correlated with these miRNAs; green round nodes represented the downregulated mRNAs. The network revealed that numerous mRNAs were regulated by the miRNAs and the expressions of many mRNAs including IGF1 were increased.

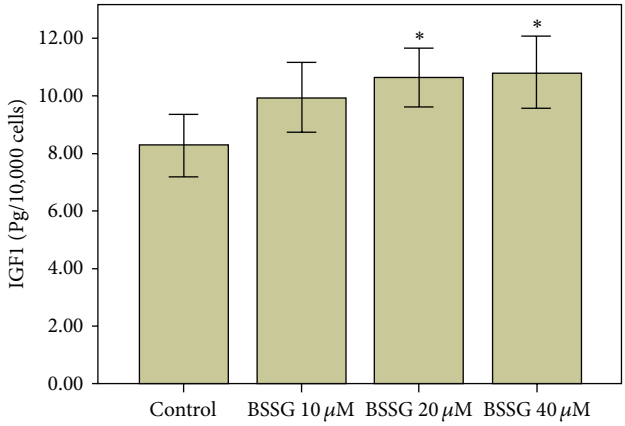

Figure 7: IGF1 protein quantitation. IGF1 protein levels were reported in pg/10,000 cells. IGF1 protein levels were significantly increased after the NSCs were treated with BSSG at 20 and 40 μM. Data are presented as Mean ± SD ($n = 6$); $^{*}P < 0.05$ compared with the control.

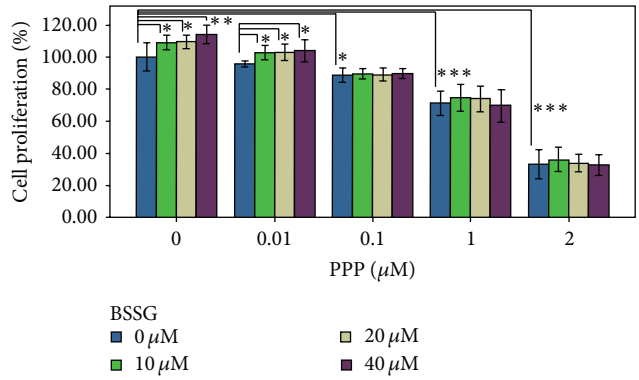

Figure 8: PPP inhibited the BSSG-induced cell proliferation. The inhibition of PPP on NSC proliferation was weak at 0.01 μM; however, the inhibition was remarkable at 0.1 μM ($P < 0.05$) as well as 1 ($P < 0.001$) and 2 μM ($P < 0.001$). Analogously, the inhibition of PPP on BSSG-induced cell proliferation was weak at 0.01 μM. By contrast, BSSG-induced cell proliferation was inhibited when the cells were exposed to PPP ≥ 0.1 μM. This result showed that if the function of IGF1 was blocked up; then the cell proliferation induced by BSSG ceased to exist. Data are presented as Mean ± SD ($n = 4$). $^{*}P < 0.05$, $^{**}P < 0.01$, and $^{***}P < 0.001$.

The proliferation-promoting activity of BSSG is the result of regulation of numerous genes. mRNA expression profiling revealed that the majority of upregulation genes were involved in mitotic cell cycle particularly in the M phase, enhancing cell proliferation. By contrast, the majority of the downregulated expression genes were involved in cell differentiation, indicating that cell differentiation was inhibited and accordingly, more possibility of cell proliferation was afforded. Among the differential expression genes, the "hubs" of the gene nodes were Bub1b, Cdc20, Plk1, Spp1, Aurkb, IGF1, and Ndc80, all of which were upregulated. Most of these "hub" genes are necessary to complete a cell cycle according to Genecards (http://www.genecards.org/), of which the importance is self-evident. However, the primary regulatory gene that induces the cells to enter the cell cycle or accelerate the course of the cell cycle is more substantial to cell proliferation. IGF1 is the key regulatory gene in these "hub" genes, since it exhibits a notable growth-promoting activity.

IGF1 gene encodes a protein with functions and structure similar to insulin, but IGF1 exhibits a higher growth-promoting activity. Experimental evidence demonstrates that IGF1 functions in CNS development by promoting neural cell proliferation, survival, and differentiation, in which IGF1 likely functions in a paracrine or autocrine fashion [31]. In vivo activities of IGF1, including the stimulation of NSC and progenitor cell proliferation during embryonic and early postnatal development, have been examined [32]. Moreover, endogenous IGF1 serves an important role in dentate granule cell survival during the course of postnatal brain development [33]. Also, IGF1 is an endogenous mediator of focal ischemia-induced neural progenitor proliferation [34]. BSSG increases the expression of endogenous IGF1 with even more biological activities, since IGF1 plays important role in growth and development of NSCs.

BSSG increased the expression of endogenous IGF1 as showed in mRNA expression microarray analysis, miRNA-mRNA correlation analysis and IGF1 Protein Quantitation. In particular, IGF1 mRNA was negatively regulated by miRNAs (miR-129-5p, miR-301a-3p, and miR-322-5p), which were downregulated after NSCs were treated with BSSG. In other words, the expression of IGF1 mRNA was increased. And as a result, the IGF1 protein level was increased. Emerging evidence supported the close relationship between the abilities of BSSG and IGF1 to promote cell proliferation. PPP inhibition test confirmed that the function of BSSG depended on IGF1, in which the function was inhibited when the cells were exposed to suitable doses of PPP.

The present study provided information about BSSG, an inexpensive and stable compound, which could promote

NSC proliferation. BSSG could be potentially developed as a growth factor alternative that could be used in clinical medicine and research applications.

Acknowledgments

This work was supported by the National Program on Key Basic Research Project (973 Program 2011CB707501), the Key Project of Science and Technology of Guangzhou (11BppZXaa2070006), and the Sixth Batch of projects of Jiangsu Province Six Talent Peak of China and a project funded by the Priority Academic Program Development of Jiangsu Higher Education Institutions, PAPD (TCM combined with western medicine).

References

[1] B. A. Reynolds, W. Tetzlaff, and S. Weiss, "A multipotent EGF-responsive striatal embryonic progenitor cell produces neurons and astrocytes," *Journal of Neuroscience*, vol. 12, no. 11, pp. 4565–4574, 1992.

[2] B. A. Reynolds and S. Weiss, "Generation of neurons and astrocytes from isolated cells of the adult mammalian central nervous system," *Science*, vol. 255, no. 5052, pp. 1707–1710, 1992.

[3] P. Miltiadous, G. Kouroupi, A. Stamatakis et al., "Subventricular zone-derived neural stem cell grafts protect against hippocampal degeneration and restore cognitive function in the mouse following intrahippocampal kainic Acid administration," *Stem Cells Translational Medicine*, vol. 2, no. 3, pp. 185–198, 2013.

[4] H. Ma, B. Yu, L. Kong, Y. Zhang, and Y. Shi, "Neural stem cells over-expressing brain-derived neurotrophic factor (BDNF) stimulate synaptic protein expression and promote functional recovery following transplantation in rat model of traumatic brain injury," *Neurochemical Research*, vol. 37, no. 1, pp. 69–83, 2012.

[5] X. Li, H. Su, Q. L. Fu et al., "Soluble NgR fusion protein modulates the proliferation of neural progenitor cells via the notch pathway," *Neurochemical Research*, vol. 36, no. 12, pp. 2363–2372, 2011.

[6] Y. Chen, X. Huang, W. Chen, N. Wang, and L. Li, "Tenuigenin promotes proliferation and differentiation of hippocampal neural stem cells," *Neurochemical Research*, vol. 37, no. 4, pp. 771–777, 2012.

[7] R. W. C. Wong and L. Guillaud, "The role of epidermal growth factor and its receptors in mammalian CNS," *Cytokine and Growth Factor Reviews*, vol. 15, no. 2-3, pp. 147–156, 2004.

[8] I. Mason, "Initiation to end point: the multiple roles of fibroblast growth factors in neural development," *Nature Reviews Neuroscience*, vol. 8, no. 8, pp. 583–596, 2007.

[9] P. J. D. Bouic, S. Etsebeth, R. W. Liebenberg, C. F. Albrecht, K. Pegel, and P. P. Van Jaarsveld, "Beta-sitosterol and beta-sitosterol glucoside stimulate human peripheral blood lymphocyte proliferation: implications for their use as an immunomodulatory vitamin combination," *International Journal of Immunopharmacology*, vol. 18, no. 12, pp. 693–700, 1996.

[10] J. N. Choi, Y. H. Choi, J. M. Lee et al., "Anti-inflammatory effects of β-sitosterol-β-D-glucoside from Trachelospermum jasminoides (Apocynaceae) in lipopolysaccharide-stimulated RAW 264.7 murine macrophages," *Natural Product Research*, vol. 26, no. 24, pp. 2340–2343, 2012.

[11] M. Deepak, G. Dipankar, D. Prashanth, M. K. Asha, A. Amit, and B. V. Venkataraman, "Tribulosin and β-sitosterol-D-glucoside, the anthelmintic principles of Tribulus terrestris," *Phytomedicine*, vol. 9, no. 8, pp. 753–756, 2002.

[12] P. J. D. Bouic and J. H. Lamprecht, "Plant sterols and sterolins: a review of their immune-modulating properties," *Alternative Medicine Review*, vol. 4, no. 3, pp. 170–177, 1999.

[13] J.H. Lee, J. Y. Lee, J. H. Park et al., "Immunoregulatory activity by daucosterol, a β-sitosterol glycoside, induces protective Th1 immune response against disseminated Candidiasis in mice," *Vaccine*, vol. 25, no. 19, pp. 3834–3840, 2007.

[14] V. Ambros, "The functions of animal microRNAs," *Nature*, vol. 431, no. 7006, pp. 350–355, 2004.

[15] D. P. Bartel, "MicroRNAs: genomics, biogenesis, mechanism, and function," *Cell*, vol. 116, no. 2, pp. 281–297, 2004.

[16] L. P. Lim, N. C. Lau, P. Garrett-Engele et al., "Microarray analysis shows that some microRNAs downregulate large numbers of-target mRNAs," *Nature*, vol. 433, no. 7027, pp. 769–773, 2005.

[17] M. Ashburner, C. A. Ball, J. A. Blake et al., "Gene ontology: tool for the unification of biology. The Gene Ontology Consortium," *Nature Genetics*, vol. 25, no. 1, pp. 25–29, 2000.

[18] J. Guo, Y. Zeng, Y. Liang, L. Wang, H. Su, and W. Wu, "Cyclosporine affects the proliferation and differentiation of neural stem cells in culture," *NeuroReport*, vol. 18, no. 9, pp. 863–868, 2007.

[19] F. Azuaje, Y. Devaux, and D. R. Wagner, "Coordinated modular functionality and prognostic potential of a heart failure biomarker-driven interaction network," *BMC Systems Biology*, vol. 4, pp. 60–78, 2010.

[20] C. Liu and X. Zhao, "MicroRNAs in adult and embryonic neurogenesis," *Neuromolecular Medicine*, vol. 11, no. 3, pp. 141–152, 2009.

[21] Q. Shen and S. Temple, "Fine control: microRNA regulation of adult neurogenesis," *Nature Neuroscience*, vol. 12, no. 4, pp. 369–370, 2009.

[22] L. C. Cheng, E. Pastrana, M. Tavazoie, and F. Doetsch, "MiR-124 regulates adult neurogenesis in the subventricular zone stem cell niche," *Nature Neuroscience*, vol. 12, no. 4, pp. 399–408, 2009.

[23] C. Zhao, G. Sun, S. Li, and Y. Shi, "A feedback regulatory loop involving microRNA-9 and nuclear receptor TLX in neural stem cell fate determination," *Nature Structural and Molecular Biology*, vol. 16, no. 4, pp. 365–371, 2009.

[24] A. Girnita, L. Girnita, F. del Prete, A. Bartolazzi, O. Larsson, and M. Axelson, "Cyclolignans as inhibitors of the isulin-like growth factor-1 receptor and malignant cell growth," *Cancer Research*, vol. 64, no. 1, pp. 236–242, 2004.

[25] D. Vasilcanu, A. Girnita, L. Girnita, R. Vasilcanu, M. Axelson, and O. Larsson, "The cyclolignan PPP induces activation loop-specific inhibition of tyrosine phosphorylation of the insulin-like growth factor-1 receptor link to the phosphatidyl inositol-3 kinase/Akt apoptotic pathway," *Oncogene*, vol. 23, no. 47, pp. 7854–7862, 2004.

[26] M. Iwai, K. Sato, N. Omori et al., "Three steps of neural stem cells development in gerbil dentate gyrus after transient ischemia," *Journal of Cerebral Blood Flow and Metabolism*, vol. 22, no. 4, pp. 411–419, 2002.

[27] M. Iwai, K. Sato, H. Kamada et al., "Temporal profile of stem cell division, migration, and differentiation from subventricular zone to olfactory bulb after transient forebrain ischemia in gerbils," *Journal of Cerebral Blood Flow and Metabolism*, vol. 23, no. 3, pp. 331–341, 2003.

[28] "Monograph. Plant sterols and sterolins," *Alternative Medicine Review*, vol. 6, no. 2, pp. 203–206, 2001.

[29] F. Aylward and B. W. Nichols, "Isolation of β-sitosterol-D-glucoside from groundnut phospholipids," *Nature*, vol. 181, no. 4615, article 1064, 1958.

[30] A. H. Salway, "The synthetical preparation of the d-glucosides of sitosterol, cholesterol, and some fatty alcohols," *Journal of the Chemical Society*, vol. 103, pp. 1022–1029, 1913.

[31] A. J. D'Ercole, P. Ye, and A. S. Calikoglu, "The role of the insulin-like growth factors in the central nervous system," *Molecular Neurobiology*, vol. 13, no. 3, pp. 227–255, 1996.

[32] G. J. Popken, R. D. Hodge, P. Ye et al., "*In vivo* effects of insulin-like growth factor-I (IGF-I) on prenatal and early postnatal development of the central nervous system," *The European Journal of Neuroscience*, vol. 19, no. 8, pp. 2056–2068, 2004.

[33] C. M. Cheng, M. Cohen, V. Tseng, and C. A. Bondy, "Endogenous IGF1 enhances cell survival in the postnatal dentate gyrus," *Journal of Neuroscience Research*, vol. 64, no. 4, pp. 341–347, 2001.

[34] Y. P. Yan, K. A. Sailor, R. Vemuganti, and R. J. Dempsey, "Insulin-like growth factor-1 is an endogenous mediator of focal ischemia-induced neural progenitor proliferation," *The European Journal of Neuroscience*, vol. 24, no. 1, pp. 45–54, 2006.

Hindawi Publishing Corporation
Evidence-Based Complementary and Alternative Medicine
Volume 2013, Article ID 763213, 9 pages
http://dx.doi.org/10.1155/2013/763213

Research Article

Exploring Potential Chemical Transformation by Chemical Profiling Approach for Rapidly Evaluating Chemical Consistency between Sun-Dried and Sulfur-Fumigated Radix Paeoniae Alba Using Ultraperformance Liquid Chromatography Coupled with Time-of-Flight Mass Spectrometry

Jida Zhang,[1] Hao Cai,[2] Gang Cao,[2,3] Xiao Liu,[2] Chengping Wen,[1] and Yongsheng Fan[1]

[1] *College of Basic Medical Science, Zhejiang Chinese Medical University, Hangzhou 310053, China*
[2] *College of Pharmacy, Nanjing University of Chinese Medicine, Nanjing 210023, China*
[3] *Research Center of TCM Processing Technology, Zhejiang Chinese Medical University, Hangzhou 310053, China*

Correspondence should be addressed to Hao Cai; haocai_98@126.com and Gang Cao; caogang33@163.com

Received 18 April 2013; Accepted 22 August 2013

Academic Editor: Chris J. Branford-White

Ultraperformance liquid chromatography coupled with time-of-flight mass spectrometry (UPLC-QTOF/MS) based on a chemical profiling method was applied to rapidly evaluate the chemical consistency between sun-dried and sulfur-fumigated Radix Paeoniae Alba. By virtue of the high resolution, high speed of UPLC, and the accurate mass measurement of TOFMS coupled with reliable MarkerLynx software, five newly assigned monoterpene glycoside sulfonates were found and identified in sulfur-fumigated Radix Paeoniae Alba samples. This method could be applied for rapid quality evaluation of different kinds of sulfur-fumigated Radix Paeoniae Alba among commercial samples.

1. Introduction

Sulfur-fumigation processing is one of the traditional preservative approaches for most food, agricultural product, and herbal medicine. Moreover, some herbal farmers even sprinkle sulfur powder onto the herbs to infiltrate sulfur into the herbs. The sulfur-fumigation process uses sulfur dioxide, obtained from the heating of sulfur, for the fumigation of herbal medicines as well as processed drugs, for the purposes of torrefaction, sterilization, mildew proofing, insect prevention, and bleaching [1, 2]. However, the medicinal properties and chemical profiles are likely to be changed after the sulfur-fumigation process. Besides, residual sulfur dioxide in herbal medicine is harmful to human health. According to some reports, a sulfur dioxide concentration of greater than 0.05% in the medicine can cause an unpleasant taste sensation [3]. Long-term administration of such sulfur-fumigated medicine may cause heavy metal intoxication in the body. Furthermore, excess sulfur dioxide in herbal medicine may cause a sore throat and stomachache, and more seriously it can even lead to a toxic reaction in the liver and kidneys [4, 5].

Radix Paeoniae Alba, derived from the dried root of *Paeonia lactiflora* Pall., is one of the oldest and most frequently used herbal medicines [6]. Radix Paeoniae Alba has been applied clinically in traditional Chinese Medicine to calm liver wind, relieve pain, nourish blood, regulate menstrual functions, and suppress sweating [7, 8]. Furthermore, Radix Paeoniae Alba contains significant amounts of monoterpenoid glucosides, tannins, phenolic acids, triterpenes, saponins, and other substances that are considered to be the biologically active components critical in many TCM formulas [9, 10]. Traditionally, the Radix Paeoniae Alba was dried naturally under sun or in the shade, but in recent decades, this practice has been replaced by sulfur-fumigation, a faster and cheaper method. Accumulated studies showed

that sulfur-fumigation can induce chemical transformation of paeoniflorin, the main bioactive component of Radix Paeoniae Alba, into its artifact paeoniflorin sulfonates and consequently alter the bioactivities and pharmacokinetics of Radix Paeoniae Alba [11]. Whether the constituents of sulfur-fumigated Radix Paeoniae Alba changed or not is a very important issue referring to both efficacy and safety when applied in clinic. Development of a rapid and specific approach to determine the potential chemical changes is the key to the quality evaluation of sulfur-fumigated Radix Paeoniae Alba.

Ultraperformance liquid chromatography (UPLC) coupled with time-of-flight mass spectrometry (QTOF/MS) is a powerful hyphenated technique and has been used as a major tool for the quality assurance of herbal medicine and its preparations [12, 13]. Compared to conventional liquid chromatography, UPLC using short columns packed with 1.7-1.8 μm porous particles holds enhanced retention time reproducibility, high chromatographic resolution, improved sensitivity, and increased operation speed.

In the present study, UPLC-QTOF/MS coupled with a chemical profiling approach was developed to investigate the influence of sulfur-fumigation on the quality of Radix Paeoniae Alba. Under the chromatographic and MS conditions, the significantly changed components, in particular those newly generated components in sulfur-fumigated Radix Paeoniae Alba, were identified or tentatively assigned by comparing their mass spectra with the LC-MS/MS library and/or tentatively assigned by matching empirical molecular formula with that of published compounds and/or elucidating quasimolecular ions and fragment ions referring to the available literature information. This method could be applied for rapid quality evaluation of different kinds of sulfur-fumigated Radix Paeoniae Alba among commercial samples.

2. Experimental

2.1. Chemicals, Solvents, and Herbal Materials. The reference sun-dried Radix Paeoniae Alba samples were acquired from the suppliers of Bozhou (Anhui, China). The identities of the collected reference sun-dried Radix Paeoniae Alba samples were authenticated to be the dried root of *Paeonia lactiflora* Pall. using morphological and histological methods according to Chinese Pharmacopoeia (version 2010) by an expert in the field. HPLC-grade acetonitrile, was obtained from Merck (Darmstadt, Germany). Deionized water was purified using the Milli-Q system (Millipore, Bedford, MA, USA); formic acid was of HPLC grade and was obtained from Honeywell Company (Morristown, New Jersey, USA). All other chemicals were of analytical grade and commercially available.

2.2. Liquid Chromatography. UPLC was performed with a Waters ACQUITY UPLC system (Waters Corp., MA, USA), equipped with a binary solvent delivery system, autosampler, and a PDA detector. The column was a Waters ACQUITY BEH C_{18} (100 mm × 2.1 mm, 1.7 μm). The mobile phase consisted of (A) 0.1% (v/v) aqueous formic acid and (B) acetonitrile. The UPLC elution condition was optimized as follows: 2–15% B (0–8 min), 15–30% B (8–11 min), 30–50% B (11–13 min), 50–2% B (13–13.05 min), and 2% B (13.05–15 min). The detection wavelength was set at 270 nm, and the flow rate was at 0.5 mL·min^{-1}. The temperatures of column and autosampler were maintained at 35 and 10°C, respectively, and the injection volume of sample was 2.0 μL.

2.3. Mass Spectrometry. Mass spectrometry was performed on a Waters Xevo QTOF/MS system (Waters Corp., MA, USA), equipped with an electrospray ionization (ESI) source. The nebulization gas was set at 650 L·h^{-1}. At temperature of 350°C, the cone gas was set at 50 L·h^{-1}, and the source temperature was set at 120°C. Detection was performed in negative ion modes in the m/z range of 100–1000 Da, with an acquisition time of 0.3 s in centroid mode. The ESI conditions were as follows: capillary voltage 2500 V, cone voltage 30 V, source temperature 120°C, desolvation temperature 400°C, cone gas flow 50 L·h^{-1}, and desolvation gas flow 800 L·h^{-1}.

2.4. Accurate Mass Measurement. All MS data were acquired using the LockSpray to ensure mass accuracy and reproducibility. Mass axis was calibrated during the experiment by continuous infusion of a solution of 2 g·mL^{-1} leucine enkephalin in acetonitrile/water (50 : 50). The data were collected using MassLynx v4.1 software and analyzed using MassFragment (Waters Corp., Milford, MA, USA).

2.5. Sample Preparation

2.5.1. Sulfur-Fumigated Radix Paeoniae Alba Samples. The sulfur-fumigated samples were prepared from the reference sun-dried Radix Paeoniae Alba samples, following procedures similar to that employed by farmers and wholesalers: 150 g of the reference sun-dried Radix Paeoniae Alba sample was wetted with 15 mL of water and then put to stand for 1.5 h; 15 g of sulfur powder was heated until burning; the burning sulfur and the wetted reference sun-dried Radix Paeoniae Alba sample were carefully put into the lower and upper layers of a desiccator, respectively. The desiccator was then kept closed for 5 h. After fumigation, the sulfur-fumigated Radix Paeoniae Alba sample was dried in a ventilated drying oven at 40°C for 5 h.

2.5.2. Radix Paeoniae Alba Sample Solutions. The powder of sun-dried or sulfur-fumigated Radix Paeoniae Alba sample was precisely weighed (0.5 g) and extracted with 5 mL of 50% methanol in an ultrasonic bath (power 200 W, frequency 40 kHz) for 25 min and cooled at room temperature; then 50% methanol was added to compensate for the lost weight. The sample solution was centrifuged for 10 min and the supernatant was further diluted to a proper concentration and filtered through a 0.45 μm filter membrane before being injected into the UPLC system for analysis.

Table 1: Details of the five identified monoterpene glycoside sulfonate derivatives.

No.	t_R (min)	$[M\text{-}H]^-/(m/z)$	Molecular formula	Assigned identity	Source sample
1	1.709	559.1106	$C_{23}H_{28}O_{14}S$	Oxypaeoniflorin sulfonate	Sulfur-fumigated sample
2	2.338	589.1216	$C_{24}H_{30}O_{15}S$	Mudanpioside E sulfonate	Sulfur-fumigated sample
3	3.002	543.1139	$C_{23}H_{28}O_{13}S$	Paeoniflorin sulfonate	Sulfur-fumigated sample
4	6.016	695.1207	$C_{30}H_{32}O_{17}S$	Galloylpaeoniflorin sulfonate	Sulfur-fumigated sample
5	9.863	647.1406	$C_{30}H_{32}O_{14}S$	Benzoylpaeoniflorin sulfonate	Sulfur-fumigated sample

2.6. Multivariate Statistical Analysis. All data were processed using the MarkerLynx application manager for MassLynx 4.1 software (Waters Corp., Milford, USA). The unsupervised segregation was checked by principal component analysis (PCA) using Pareto-scaled data. The first objective in the data analysis process is to reduce the dimensionality of the complex data set to enable easy visualization of any component clustering of the different groups of samples. Thus, the loading plot gives an indication of the components that most strongly influence the patterns in the score plot. From the loading plot of orthogonal to partial least squares discriminant analysis (OPLS-DA), various components could be identified as being responsible for the differentiation between sun-dried and sulfur-fumigated samples and were therefore viewed as potential chemical transformations.

3. Results and Discussion

3.1. Chromatographic and MS Conditions Development. In the present study, different kinds of UPLC columns and mobile phases were used to optimize the chromatographic and MS conditions. The BEH C_{18} column was chosen as stationary phase, which provided a relatively even distribution of the target analytes throughout the whole polarity range. This enabled us to substantially shorten the duration of chromatography to 15 min including equilibration. Different mobile phase compositions were tested: water-methanol, water-acetonitrile, 0.1% (v/v) aqueous formic acid–methanol, and 0.1% (v/v) aqueous formic acid–acetonitrile. As a result, the combination of 0.1% (v/v) aqueous formic acid–acetonitrile for the mobile phase gave the best separation. The gradient elution profile and MS conditions were optimized with respect to the separation of major peaks and the sensitivity of MS detector. Under the optimized chromatographic and MS conditions, the major components in sun-dried and sulfur-fumigated Radix Paeoniae Alba samples were well separated and detected within 15 min. The representative chromatograms monitored by UPLC-QTOF/MS are shown in Figure 1.

3.2. Multivariate Statistical Analysis and Chemical Consistency Evaluation. Unsupervised principal component analysis (PCA) and supervised orthogonal partial squared discriminant analysis (OPLS-DA) were performed to compare the difference between sun-dried and sulfur-fumigated Radix Paeoniae Alba samples. After Pareto scaling with mean centering, the data from both negative ion modes were displayed as score plot (Figure 2). The score plot showed that the determined samples clearly clustered into three groups, that is, the blank, the sun-dried, and the sulfur-fumigated Radix Paeoniae Alba, indicating that the sulfur-fumigation caused changes in the composition and/or content of components in Radix Paeoniae Alba.

To find out potential chemical markers contributing to the significant difference between sun-dried and sulfur-fumigated Radix Paeoniae Alba samples, the extensive statistical analysis was performed to generate S-plot (Figure 3). In the S-plot, each point represents an ion t_R-m/z pair; the x-axis represents variable contribution: when the distance of the ion t_R-m/z pair points is farther from zero, the ion has more contribution to the difference between the two groups; the y-axis represents variable confidence: when the distance of the ion t_R-m/z pair points is farther from zero, the ion has higher confidence level for the difference between two groups. Thus, the t_R-m/z pair points at the two ends of "S" represent characteristic markers with the most confidence to each group. According to the S-plot, five ions at the bottom left corner of "S" were the ions contributing most to the difference between sun-dried and sulfur-fumigated Radix Paeoniae Alba. It was found that ions A (t_R 1.709 min, m/z 559.1106), B (t_R 2.338 min, m/z 589.1216), C (t_R 3.002 min, m/z 543.1139), D (t_R 6.016 min, m/z 695.1207), and E (t_R 9.863 min, m/z 647.1406) were detected in sulfur-fumigated Radix Paeoniae Alba but not found in the sun-dried sample, which suggested that during the storage and marketing process, in order to preserve its white appearance, Radix Paeoniae Alba was often nonofficially fumigated with toxic sulfur dioxide gas, which is generated by burning sulfur. This nonofficial postharvest handling method was recently revealed leading to the conversion of the main component paeoniflorin into its sulfonate derivative paeoniflorin sulfonate.

3.3. Identity Assignment and Confirmation of the Significantly Transformed Components. In the present study, significant differences in their chemical profiles were found between sun-dried and sulfur-fumigated Radix Paeoniae Alba samples. Five monoterpene glycoside sulfonate derivatives were detected in sulfur-fumigated Radix Paeoniae Alba samples according to the present chromatographic and MS conditions. The details of the five identified components are summarized in Table 1. Five monoterpene glycoside sulfonate derivatives were newly detected and identified along with oxypaeoniflorin sulfonate, paeoniflorin sulfonate, mudanpioside E sulfonate, benzoylpaeoniflorin sulfonate, and galloylpaeoniflorin sulfonate by MassFragment system and MarkerLynx system. MarkerLynx is a peak detection algorithm,

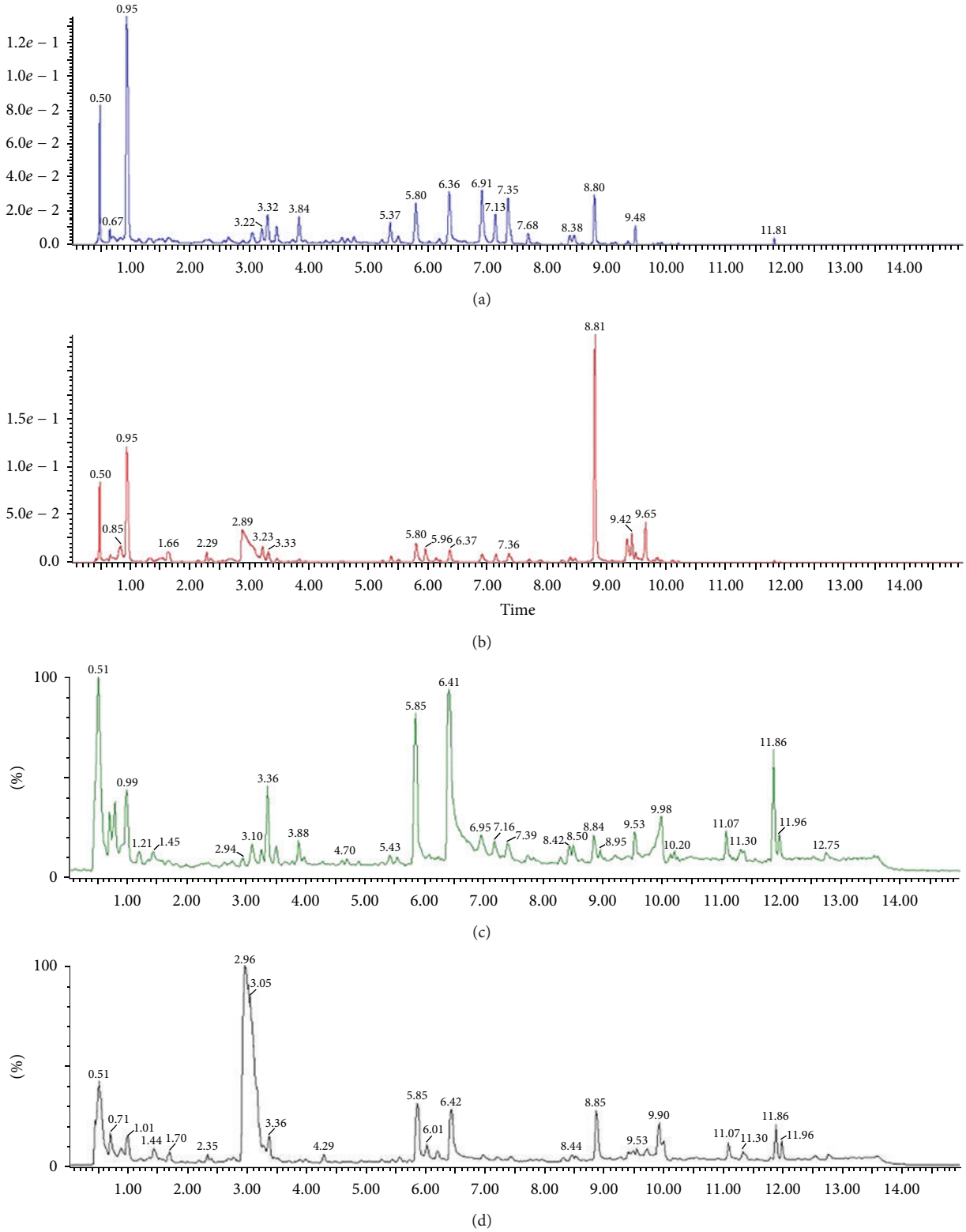

Figure 1: Representative chromatograms of sun-dried and sulfur-fumigated Radix Paeoniae Alba samples in negative ion mode. (a) UPLC chromatogram of sun-dried Radix Paeoniae Alba; (b) UPLC chromatogram of sulfur-fumigated Radix Paeoniae Alba; (c) total ion chromatogram of sun-dried Radix Paeoniae Alba; (d) total ion chromatogram of sulfur-fumigated Radix Paeoniae Alba.

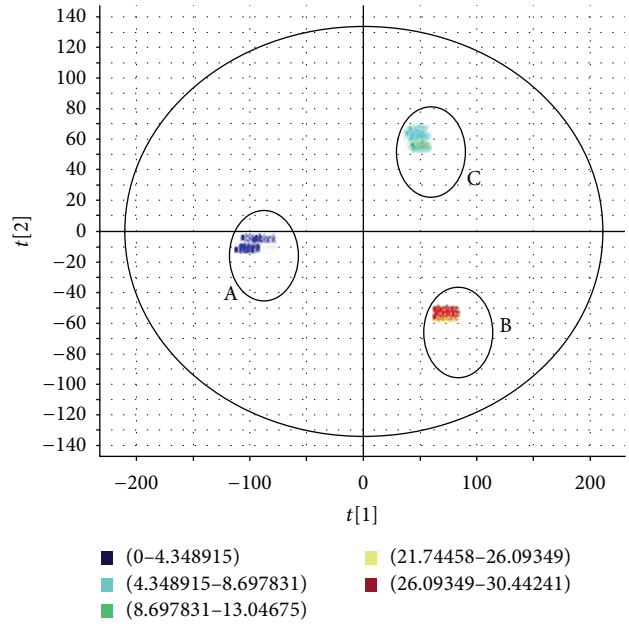

Figure 2: PCA score plot of sun-dried and sulfur-fumigated Radix Paeoniae Alba samples. A: blank; B: sun-dried Radix Paeoniae Alba samples; C: sulfur-fumigated Radix Paeoniae Alba samples.

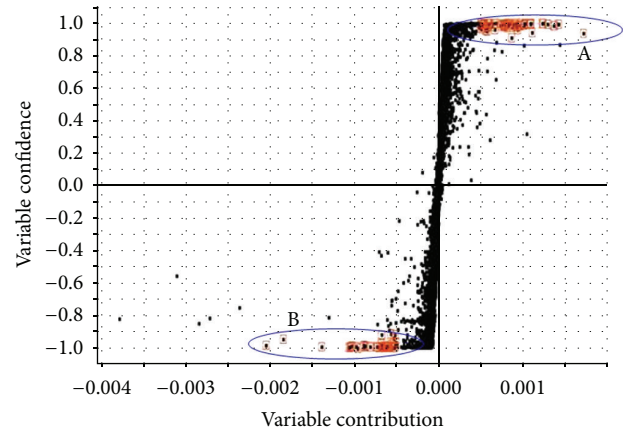

Figure 3: OPLS-DA/S-plot of sun-dried and sulfur-fumigated Radix Paeoniae Alba samples obtained using Pareto scaling with mean centering. A: sun-dried Radix Paeoniae Alba samples; B: sulfur-fumigated Radix Paeoniae Alba samples.

where each mass number is analyzed separately in search of peaks. The software MarkerLynx has been used to process the complex data quickly and reliably. In this paper, we firstly applied the MarkerLynx to the analysis of the structure of paeoniflorin in Radix Paeoniae Alba samples. This software is a repeatable and reliable analytical method when we should compare the MS data generated by using paeoniflorin assay standard. The chromatograms and fragmentations and mode assignments of paeoniflorin assay standard are shown in Figure 4, and the fragmentations and mode assignments of those five monoterpene glycoside sulfonate derivatives are shown in Figure 5. As sulfur-fumigation can cause chemical transformation of Radix Paeoniae Alba, the bioactivities and toxicities of sulfur-fumigated Radix Paeoniae Alba and five monoterpene glycoside sulfonate derivatives need further investigation.

4. Conclusion

In this paper, chemical consistency between sun-dried and sulfur-fumigated Radix Paeoniae Alba samples was rapidly evaluated by UPLC-QTOF/MS based on chemical profiling approach to guarantee clinical safety. This method was also developed to reveal chemical transformation of main compounds in Radix Paeoniae Alba during sulfur-fumigation process. The results showed that there were obvious differences in chemical components between sun-dried and sulfur-fumigated Radix Paeoniae Alba samples following the same

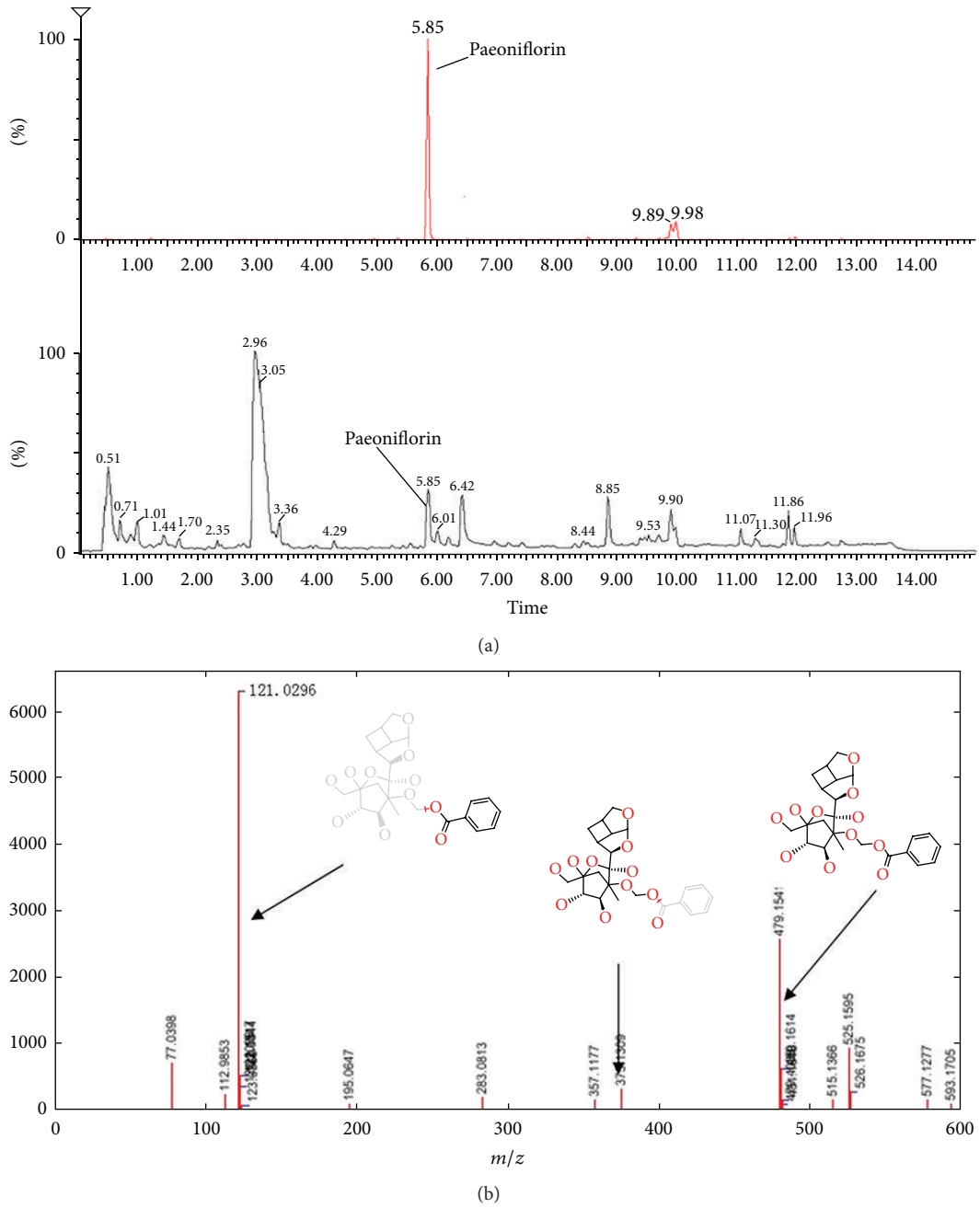

FIGURE 4: Chromatograms and fragmentations and mode assignments of paeoniflorin. (a) Radix Paeoniae Alba sample; (b) paeoniflorin assay standard.

dosage ratio. The established method should be useful for assessing the quality of herbal medicines.

Authors' Contribution

Jida Zhang, Hao Cai, Gang Cao, and Xiao Liu contributed equally to this work.

Acknowledgments

The authors are grateful to the financial support of the National Natural Science Foundation of China (nos. 81173546, 30940093, and 81202918); the Natural Science Foundation of Jiangsu Province, China (no. BK2009495); the International Science and Technology Cooperation Project of Jiangsu Province, China (no. BZ2011053); the Project of Science Technology Department of Zhejiang Province, China (nos. 2012D60SA1C0065, 2013C33SA1C0002 and 2012D60SA1C0066); the Open Project of National First-Class Key Discipline for Science of Chinese Materia Medica, Nanjing University of Chinese Medicine (nos. 2011ZYX2-006 and 2011ZYX2-001); the Chinese Medicine Research Program of Zhejiang Province, China (no. 2008ZA002); the Science Foundation of Zhejiang Chinese Medical University

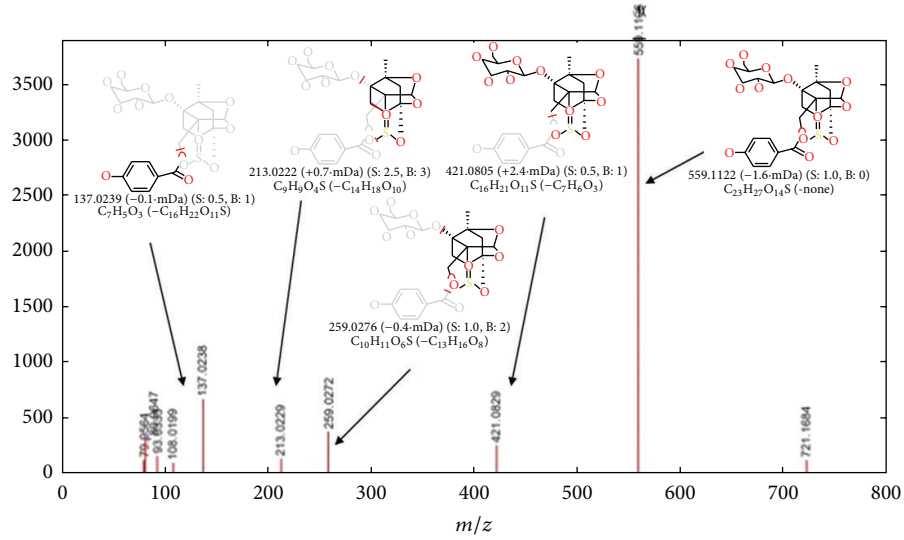

(a)

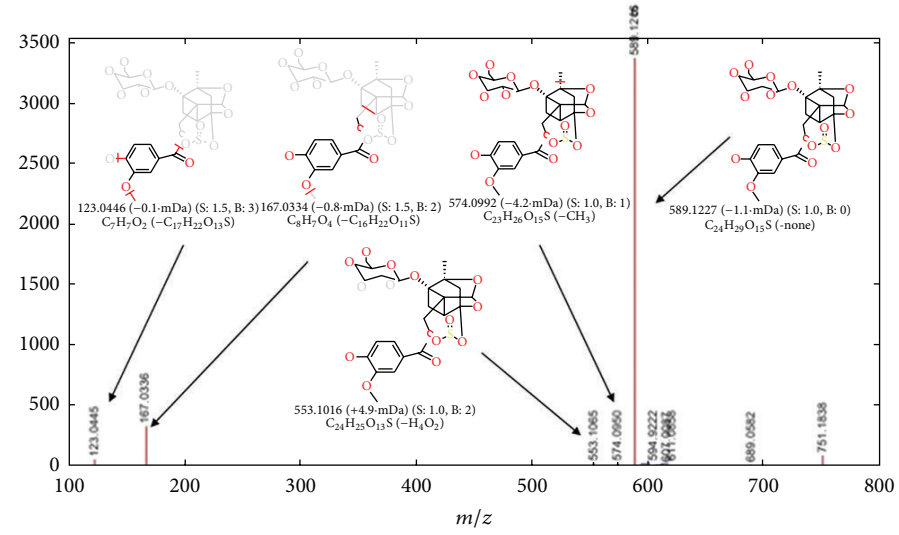

(b)

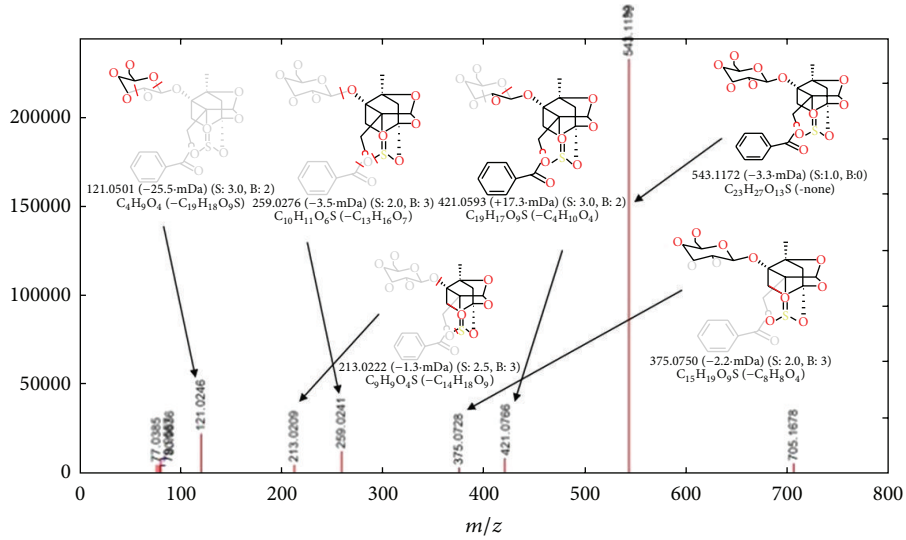

(c)

Figure 5: Continued.

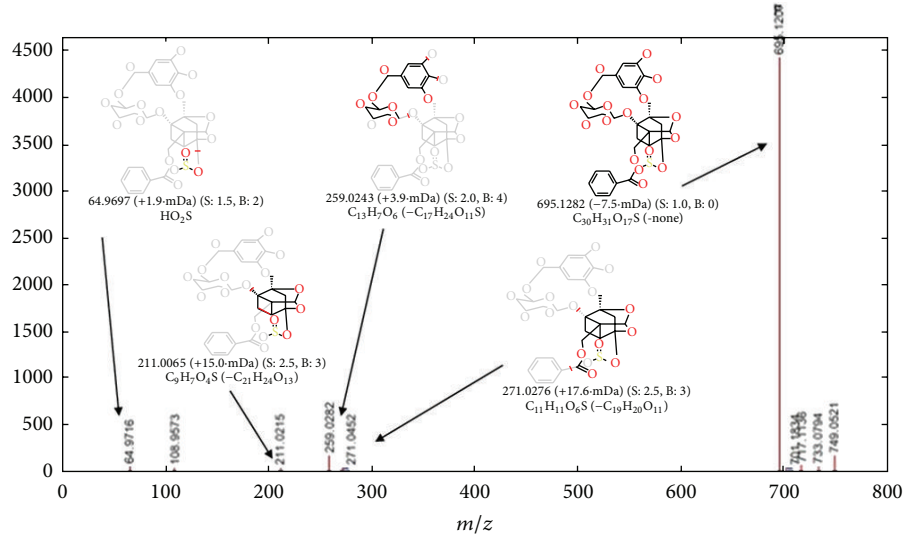

(d)

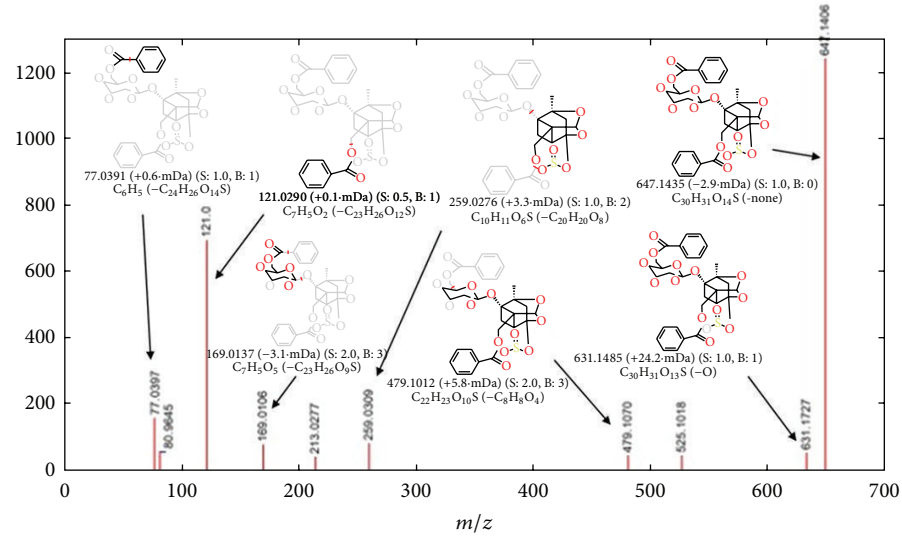

(e)

Figure 5: Fragmentations and mode assignments of five monoterpene glycoside sulfonate derivatives. (a) Oxypaeoniflorin sulfonate; (b) mudanpioside E sulfonate; (c) paeoniflorin sulfonate; (d) galloylpaeoniflorin sulfonate; (e) benzoylpaeoniflorin sulfonate.

(nos. 2011ZY25 and 2011ZR01); the Project of Science and Technology for Chinese Medicine of Zhejiang Province, China (no. 2013KYB183); the Project of Science Technology Department of Hangzhou, China (no. 20130533B68); and the Fund of Zhejiang Modernization of Traditional Chinese Medicine Item (nos. [2008]436 and [2012]680).

References

[1] G. Cao, H. Cai, X. D. Cong et al., "Global detection and analysis of volatile components from sun-dried and sulfur-fumigated herbal medicine by comprehensive two-dimensional gas chromatography/time-of-flight mass spectrometry," *Analyst*, vol. 137, pp. 3828–3835, 2012.

[2] Y. Qiu, X. Lu, T. Pang, C. Ma, X. Li, and G. Xu, "Determination of radix ginseng volatile oils at different ages by comprehensive two-dimensional gas chromatography/time-of-flight mass spectrometry," *Journal of Separation Science*, vol. 31, no. 19, pp. 3451–3457, 2008.

[3] X. Jiang, L. F. Huang, S. H. Zheng, and S. L. Chen, "Sulfur fumigation, a better or worse choice in preservation of traditional Chinese medicine?" *Phytomedicine*, vol. 20, pp. 97–105, 2013.

[4] L. Z. Chou, H. X. Zhao, and B. G. Li, "Screening of sulfur fumigation technology for achyranthes bidentata," *Chinese Journal of Experimental Traditional Medical Formulae*, vol. 18, pp. 35–37, 2012.

[5] B. Duan, L. Huang, and S. Chen, "Study on the destructive effect to inherent quality of *Fritillaria thunbergii* Miq. (Zhebeimu) by sulfur-fumigated process using chromatographic fingerprinting analysis," *Phytomedicine*, vol. 19, no. 6, pp. 562–568, 2012.

[6] Y. Li, M. Wang, X. Wang et al., "Pharmacokinetic properties of albiflorin and paeoniflorin after oral administration of pure compound, Radix Paeoniae alba extract and Danggui-Shaoyao-San extract to rats," *Journal of Asian Natural Products Research*, vol. 13, no. 2, pp. 117–127, 2011.

[7] L. Tong, M. Wan, D. Zhou, J. Gao, Y. Zhu, and K. Bi, "LC-MS/MS determination and pharmacokinetic study of albiflorin and paeoniflorin in rat plasma after oral administration of Radix Paeoniae Alba extract and Tang-Min-Ling-Wan," *Biomedical Chromatography*, vol. 24, no. 12, pp. 1324–1331, 2010.

[8] K. Wang, R. Zhang, Z. Fang, and M. Shen, "Analysis of benzoic acid content in Radix Paeoniae Alba treated by different process," *Journal of Chinese Medicinal Materials*, vol. 31, no. 10, pp. 1476–1478, 2008.

[9] K. S. Huang, J. G. Lin, H. C. Lee et al., "Paeoniae alba Radix promotes peripheral nerve regeneration," *Evidence-Based Complementary and Alternative Medicine*, vol. 2011, Article ID 109809, 8 pages, 2011.

[10] J. Li, C. Peng, and J. Ji, "Mechanism study of action on compatible using of total alkaloids of Radix Aconiti Praeparata and total glycosides or polysaccharides of Radix Paeoniae Alba therapy on rheumatoid arthritis in rats," *China Journal of Chinese Materia Medica*, vol. 34, no. 22, pp. 2937–2942, 2009.

[11] K. B. Kwon, E. K. Kim, M. J. Han et al., "Induction of apoptosis by Radix Paeoniae Alba extract through cytochrome c release and the activations of caspase-9 and caspase-3 in HL-60 cells," *Biological and Pharmaceutical Bulletin*, vol. 29, no. 6, pp. 1082–1086, 2006.

[12] E. X. Shang, Z. H. Zhu, L. Liu, Y. P. Tang, and J. A. Duan, "UPLC-QTOF-MS with chemical profiling approach for rapidly evaluating chemical consistency between traditional and dispensing granule decoctions of Tao-Hong-Si-Wu decoction," *Chemistry Central Journal*, vol. 6, p. 143, 2012.

[13] W. Zhou, S. Su, J. Duan et al., "Characterization of the active constituents in Shixiao San using bioactivity evaluation followed by UPLC-QTOF and Markerlynx analysis," *Molecules*, vol. 15, no. 9, pp. 6217–6230, 2010.

Hindawi Publishing Corporation
Evidence-Based Complementary and Alternative Medicine
Volume 2013, Article ID 410793, 11 pages
http://dx.doi.org/10.1155/2013/410793

Review Article

Extracts of *Tripterygium wilfordii* Hook F in the Treatment of Rheumatoid Arthritis: A Systemic Review and Meta-Analysis of Randomised Controlled Trials

Yafei Liu, Shenghao Tu, Weina Gao, Yu Wang, Peilin Liu, Yonghong Hu, and Hui Dong

Institute of Integrated Traditional Chinese and Western Medicine, Tongji Hospital, Tongji Medical College, Huazhong University of Science and Technology, 1095 Jiefang Avenue, Wuhan, Hubei 430030, China

Correspondence should be addressed to Shenghao Tu; shtu@tjh.tjmu.edu.cn and Hui Dong; tjhdonghui@163.com

Received 6 June 2013; Accepted 25 September 2013

Academic Editor: Xiang-Yu Hou

Clinical trials have reported the effects of *Tripterygium wilfordii* Hook F (TwHF) extracts (TEs) in the treatment of rheumatoid arthritis (RA); however, the results have been inconsistent. This meta-analysis is aimed to assess the safety of TEs and their effects on the treatment of RA. Randomised controlled trials (RCTs) comparing the effects of TEs and placebo (PBO) or disease-modifying antirheumatic drugs (DMARDs) in patients with RA were included. Weighted mean differences (MDs) were calculated for net changes by employing fixed-effect or random-effects models. After filtering, ten RCTs (involving 733 participants) were included in this study. The methodological quality of these studies was generally low. Compared with DMARDs, TEs alone produced a mild increase in grip strength (GS) ($P = 0.02$; standard mean difference (SMD) = 0.81; 95% confidence interval (CI): 0.14 to 1.48). The most common adverse effects (AEs) of TEs were gastrointestinal discomfort, menstruation disorders, and amenorrhea. In conclusion, TEs, as a sort of "herbal DMARD," could be as effective as synthetic DMARDs in the treatment of RA. However, the efficacy of TEs in treating RA should be further estimated with better designed, fully powered, confirmatory RCTs that apply the American College of Rheumatology (ACR) improvement criteria to evaluate their outcomes.

1. Introduction

Rheumatoid arthritis (RA) is an autoimmune disease of unknown aetiology that is characterised by pain, stiffness, and swelling of peripheral joints [1]. RA affects approximately 1% of the population worldwide [2]. Uncontrolled disease can result in progressive joint destruction, deformity, disability, and increased mortality. According to the guidelines proposed by the American College of Rheumatology (ACR) for the management of RA [3], nonsteroidal antiinflammatory drugs (NSAIDs) and disease-modifying antirheumatic drugs (DMARDs) are recommended to relieve joint damage. Recently, based on an evolving understanding of the pathogenic mechanisms of RA [4], specific targeted therapies (including inhibitors of tumour necrosis factor and other novel biological compounds) [5] have been introduced to interfere with the disease process in RA.

However, many patients discontinue the above treatments because of adverse events (AEs) [6] or poor clinical response to biological agents. Furthermore, biologics are unlikely to be of general benefit in the developing world because of the financial constraints [7], and the relatively high medical care costs for RA [8] restrict the application of these drugs in the developing world.

Tripterygium wilfordii Hook F (TwHF), commonly known as thunder god vine, is a member of the Celastraceae family. It is a perennial vine-like plant that is abundant in south China [9]. Anti-inflammatory and immunosuppressive compounds extracted from TwHF have been used for the treatment of a wide spectrum of autoimmune and

inflammatory diseases, including RA [10, 11], ankylosing spondylitis [12, 13], and systemic lupus erythematosus [14]. Additionally, TwHF extracts (TEs) have been demonstrating beneficial effects on nephrotic syndrome [15], Crohn's disease [16], and solid tumours [17].

Among the approximately 380 secondary metabolites isolated from *Tripterygium* species, 95% are terpenoids [18]. Triptolide and tripdiolide, the ethyl acetate extract and chloroform-methanol extract [19], respectively, are the major components that account for the immunosuppressive effects of TwHF. It has been reported that these extracts exert better therapeutic effects and cause fewer AEs than other crude preparations. Therefore, these two preparations have been used most widely in China [10].

Meanwhile, many studies have been dedicated to elucidating the potential molecular mechanisms underlying the anti-inflammatory and immunosuppressive effects of TEs [18], including the inhibition of platelet activation [20], the induction of nitric oxide [21], and prostaglandin E_2 [22] production. Based on studies both *in vitro* and *in vivo*, it is easy to speculate that TEs are likely to be types of herbal DMARDs, which differ from synthetic DMARDs.

While the extracts of TwHF have been most frequently used for a long time in treating RA, there exist a number of issues. In this regard, most of this clinical information comes from uncontrolled clinical trials or from retrospective reports, and few multicentre clinical trials have been performed to confirm the effects of TEs in the treatment of RA. In addition, the scientific evidence verifying that TEs are as effective as other conventional treatments in treating RA remains to be further validated. In terms of security, the safety of a long-term TE intake for chronic RA is uncertain. Given these uncertainties, it is necessary to assess the pertinent trials to systematically review the potential effects and safety of the long-term application of TEs in the treatment of RA.

2. Materials and Methods

To ensure the accuracy of our systemic review and meta-analysis, we designed and reported our results by employing a checklist of items that was as consistent as possible with the Preferred Reporting Items for Systemic Review and Meta-Analyses (PRISMA) statement.

2.1. Search Strategy. We searched the following digital databases to identify trials: PubMed, Embase, the Cochrane Library, and Clinical Trials.gov. In addition, we searched the Chinese databases, such as the CNKI Database, VIP Database, CBM Database, WanFang Database, and Chinese Clinical Trial Register. All of the databases were searched from their available dates of inception to the latest issue (January 2013).

Different search strategies were combined as follows. For the English databases, we used free text terms, such as "*Tripterygium wilfordii* Hook F," "lei gong teng," "thunder god vine," or "yellow vine" (which are all alternative names in Chinese for *Tripterygium wilfordii* Hook F) and "rheumatoid arthritis," or "RA." For the Chinese databases, free text terms were used, such as "lei gong teng" or "huang teng" (which means *Tripterygium wilfordii* Hook F in Chinese) and "lei feng shi guan jie yan" (which means rheumatoid arthritis in Chinese). A filter for clinical trials was applied. To collect an adequate number of trials, the reference lists of relevant publications were also searched to identify additional studies.

2.2. Selection Criteria. Randomised controlled trials (RCTs) were included regardless of blinding, publication status, or language. Studies were selected for analysis if they satisfied the following criteria: (1) the subjects took extracts of TwHF alone or with other DMARDs for at least 4 weeks; (2) the study was an RCT with a parallel or crossover design; (3) TEs were used as an active treatment intervention; and (4) people enrolled were diagnosed with RA, according to the 1987 guidelines of the American Rheumatology Association [23].

"TEs," in this review, mainly refer to the two root extracts of TwHF that have shown therapeutic promise, tripterygium glycosides tablets and tripterygium tablets. Therefore, studies using any TwHF-containing herbs or other herbal extracts were excluded. We also excluded case reports, reviews, retrospective studies, or studies without control groups. For obviously repeated studies, the authors of the reports were contacted to clarify any ambiguities. If the author could not be reached, the first published study was considered to be original. Studies were also excluded if the dose of TEs was not available. RCTs that lacked sufficient data to allow for the calculation of the net changes in outcomes and their variances from the baseline to the endpoint were also eliminated from our analysis. Two reviewers selected the articles independently. Based on the PRISMA requirements, a flow diagram of the study selection has been generated.

2.3. Data Extraction and Management. The relevant data was extracted by two independent reviewers, and divergences were resolved by consensus or were arbitrated by a third reviewer. The validated Jadad instrument was adopted to assess each study's quality independently [24]. The Jadad score included the following items: randomisation (0–2 points); double-blinding (0–2 points); and description of withdrawals and dropouts (0-1 point). Allocation concealment was estimated by the criteria adopted from Schulz et al. [25]. Studies with Jadad scores of no less than 3 were regarded as being of high quality.

The primary outcomes were tender joint count (TJC), swollen joint count (SJC), duration of morning stiffness (DMS), and grip strength (GS). The secondary outcomes consisted of rheumatoid factor (RF), erythrocyte sedimentation rate (ESR), and C-reactive protein (CRP). AEs were also collected from the studies. For the trials that applied a three-armed group design, the outcomes of the groups were extracted if they met the inclusion criteria and were excluded otherwise. In case of vagueness or absence in the articles of the outcomes, the authors were contacted and related data has been extracted by consensus if the authors were unavailable.

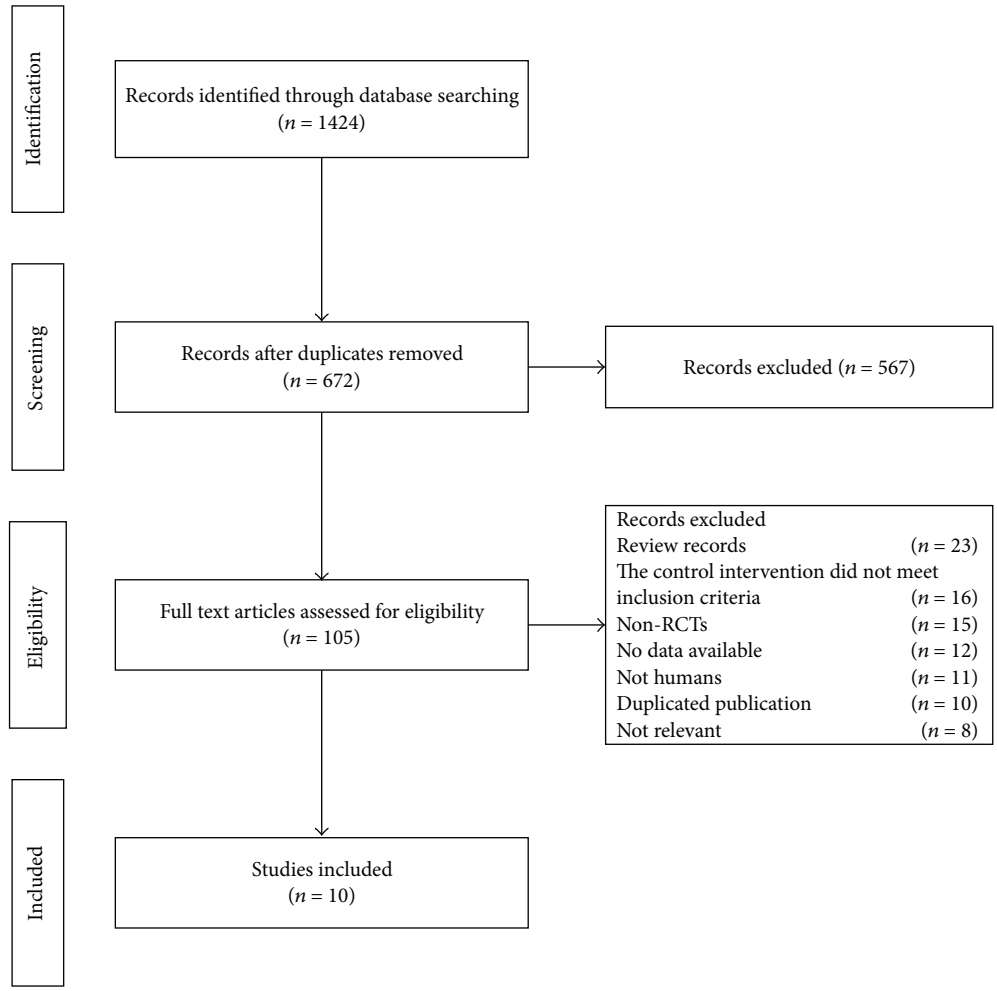

Figure 1: Process of searching for and screening studies.

2.4. Data Synthesis and Analysis. The effects of TE intake on patients with RA were calculated as differences between the treatment groups and the no TE control group, by employing Review Manager meta-analysis software, version 5.2. To ensure the credibility of the results, the net changes in all of the outcomes were calculated as the mean differences (TEs minus control) in changes (endpoint minus baseline) for parallel trials. We calculated weighted mean differences (MDs) or standard mean differences (SMDs) and 95% confidence intervals (CIs) for continuous data. MDs were used if the outcomes were evaluated in the same manner among trials, while SMDs were used if the same outcomes were evaluated by adopting different approaches. Heterogeneity was evaluated via the chi-square test, the tau^2 test, and Higgins I^2 test. A fixed-effect model was employed when the studies in the group were sufficiently alike ($P > 0.10$); otherwise, a random-effects model was used. A Z score was calculated to test the overall effect, with significance set at $P < 0.05$. Publication bias was detected by funnel plots, Egger's regression asymmetry test, and Begg's test when the number of included trials ≥5 (Stata software, version 12.0). We performed subgroup analyses to verify whether the use of TEs alone or with DMARDs had different effects on the outcomes.

To minimise the clinical heterogeneity, we performed three subgroup analyses: TEs compared with a placebo (PBO); TEs compared with DMARDs; and TEs with DMARDs compared with DMARDs alone.

3. Results

3.1. Study Selection. The process of study selection is shown in Figure 1. According to the prespecified selection criteria defined in the Methods section, ten RCTs were included in the meta-analysis. In the PBO group, three studies were searched [26–28]. Two RCTs were crossover studies with two courses [26, 27]. One study was excluded for all of the outcomes were graphic representations [28]. Two studies [29, 30] that compared TEs with nonsteroidal anti-inflammatory drugs (NSAIDs) were also excluded from our review. The trial of Fu et al. [29] compared TEs with NSAIDs and physiotherapy, and in the other trial [30], the doses of NSAIDs changed during the treatment; thus, it was difficult to determine the effects of the intervention and the control

Table 1: The characteristics of the included trials.

Author	Number of patients		Intervention and TwHF dose (g)		Duration (wks)	Outcomes
	Experimental	Control	Experimental	Control		
Tao et al. 1989 [26]	27	31	TEs (0.06)	PBO	12	SJC, DMS, GS, RF, ESR, AE
Huang et al. 1989 [27]	18	16	TEs (0.03)	PBO	16	SJC, DMS, GS, RF, ESR, AE
Tan et al. 2000 [31]	40	35	TEs (0.06)	MTX + PA	12	TJC, SJC, DMS, RF, ESR, CRP, AE
Wang et al. 2006 [32]	45	45	TEs (0.06)	MTX	20	TJC, SJC, RF, ESR, CRP, AE
Yang and Zhang 2007 [33]	60	60	TEs (0.06)	MTX	4	TJC, SJC, DMS, GS, RF, ESR, CRP, AE
Yang 2011 [34]	74	72	TEs (1.8)	MTX	12	TJC, SJC, DMS, GS, AE
Liu et al. 2006 [35]	10	10	TEs (0.09)	MTX	12	TJC, SJC, DMS, RF, ESR, CRP
Goldbach-Mansky et al. 2009 [36]	37	25	TEs (0.18)	SSZ	4	RF, AE
Chen et al. 2011 [37]	34	34	TEs (0.06), MTX	MTX + LEF	12	ESR, CRP, AE
Li and Ji 2008 [38]	30	30	TEs (0.01–0.02), SSZ	MTX + SSZ	4	ESR, CRP

Note: TEs: TwHF extracts; MTX: methotrexate; LEF: leflunomide; SSZ: sulfasalazine; PA: penicillamine; TJC: tender joint count; SJC: swollen joint count; DMS: duration of morning stiffness; GS: grip strength; RF: rheumatoid factor; ESR: erythrocyte sedimentation rate; CRP: C-reactive protein; AE: adverse effect.

groups. The characteristics of the studies are summarised in Table 1. Together, these studies included a total of 733 participants.

3.2. Study Descriptions. The included studies were published as full texts between 1988 and 2011. All of the RCTs originated in China, except for one [36]. Eight studies were published in Chinese, while two studies were in English [26, 36]. Nine studies were conducted as single-centre trials, and one study [36] was a multicentre trial.

3.3. Interventions and Controls. Two studies compared TEs with a PBO. Six studies randomised the participants to receive TEs alone versus a control of DMARDs. Two trials compared a cointervention of TEs and DMARDs (methotrexate, or sulfasalazine) with a control of DMARDs alone. There were three types of TE preparations applied in the included trials, consisting of tripterygium glycosides tablets, tripterygium tablets, and an unknown TE capsule. Different doses of TEs were used in these trials. The TE intake ranged from 0.01 g to 1.8 g per day. Except for two trials in which the TEs doses were not less than 0.18 g, the doses of TEs in most of the included trials were moderate (≤0.09 g). The total daily TE intake was divided into one to three doses. One trial [37] reduced the dose of TEs during the period of study when liver function abnormalities occurred. In the event of gastrointestinal intolerance, the protocol of one trial [36] allowed for a temporary dose reduction of 50%.

The duration of the interventions in the included studies also differed, ranging from four to twenty weeks. In the trial by Wang et al., the outcomes were detected at three time points: 20 weeks, 40 weeks, and 80 weeks [32]. Another trial had two time points: 4 weeks and 24 weeks [36]. To ensure homogeneity among the studies, we chose only 20 weeks and 4 weeks from the above two trials. The interventions lasted for four weeks in three trials [33, 36, 38], twelve weeks in five trials [26, 31, 34, 35, 37], and sixteen weeks in one trial [27]. Only one trial [32] reported that the patients had received TEs for twenty weeks.

3.4. Objectives and Outcomes. The majority of the outcomes of the study [36], such as TJC, SJC, ESR, CRP, were graphic representations, rather than outcomes reported in a table that allowed for the extraction of data for re-analysis. AEs were reported in eight trials. Eight trials performed treated-per-protocol analysis, and two [27, 36] performed intention-to-treat analysis which was generally interpreted as including all participants, regardless of the entry criteria, the treatment actually received, and ensuing withdrawal or deviation from the protocol.

3.5. Quality of the Included Studies. Compared with the four trials [26, 27, 36, 37] that were of high quality, most of the included trials were of low quality (Jadad score < 3) because of unclear randomisation, deficient allocation concealment, inadequate blinding, and undescribed withdrawals and dropouts. An adequate double blind was also performed in two of the four trials [26, 36]. Meanwhile, withdrawals and dropouts were described in four trials [26, 27, 36, 37].

3.6. Publication Bias. Egger's publication bias plots and Begg's test showed that there were no significant publication biases for three outcomes in which the numbers of the included trials were not less than 5. As shown in Figure 2, the calculated P values exceeded 0.05 in three outcomes among the studies (TJC, $P = 0.335$; SJC, $P = 0.467$; RF, $P = 0.785$), and the

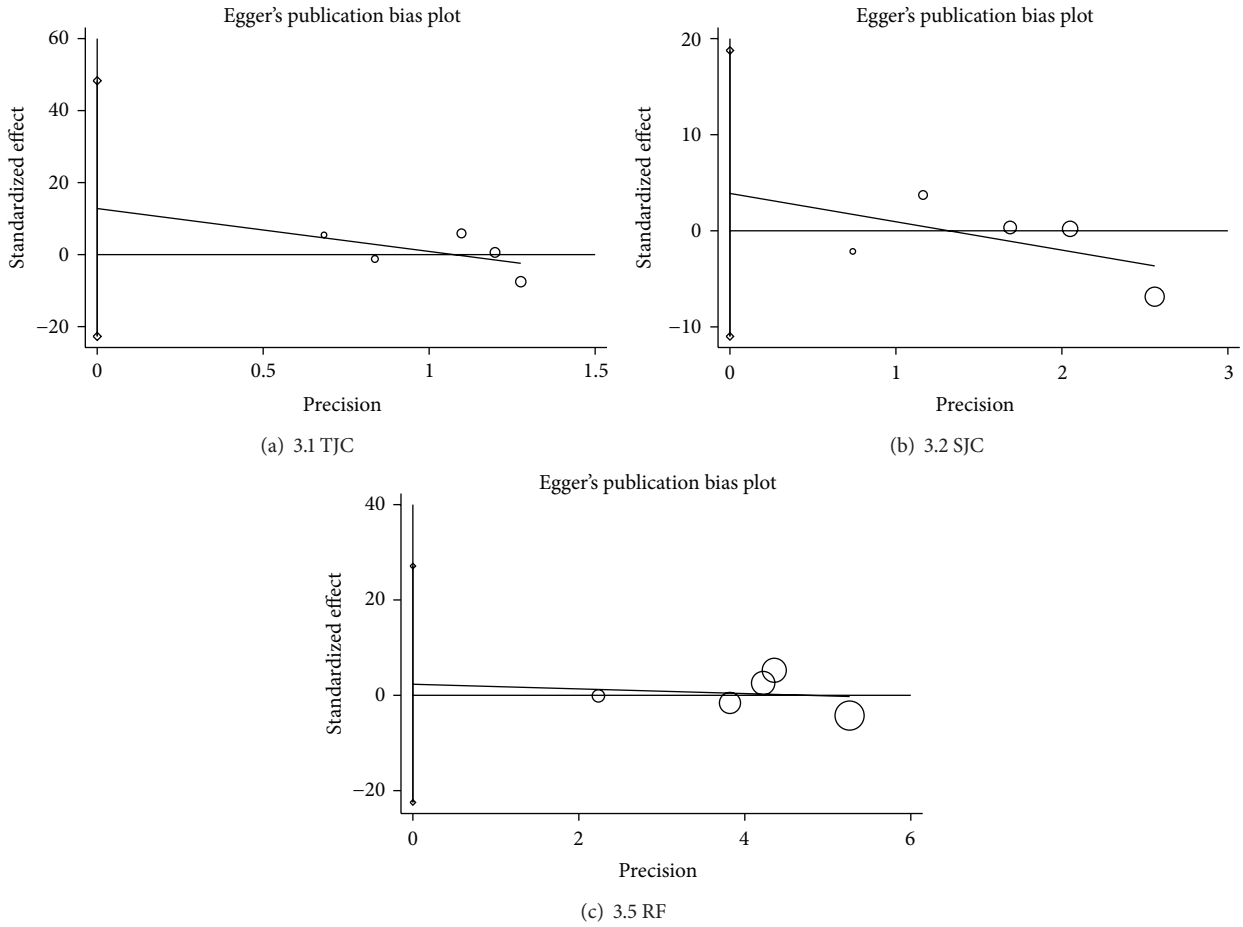

(a) 3.1 TJC

(b) 3.2 SJC

(c) 3.5 RF

Figure 2: Publication bias in the included trials. Egger's linear regression test for detecting publication bias. TJC: tender joint count; SJC: swollen joint count; RF: rheumatoid factor. "◯" is a size graph symbol for the weight of each included study. The distance between two diamonds on the second vertical bar on the left represents the 95% CI for the intercept.

95% CI for the intercept included zero. However, these results cannot be considered convincing because there were fewer than ten trials.

3.7. Effects of Interventions

3.7.1. TEs Compared with a PBO. Two trials (involving 92 patients) compared the therapeutic effects of TEs and a PBO [26, 27]. The number of trial participants ranged from 16 to 31 with trial durations in the range of twelve to sixteen weeks. As shown in Figure 3, the statistical heterogeneity among the studies was found to be significant regarding the results for GS ($P = 0.01$). The pooled results indicated a significant difference between TE-treated group and the PBO group, aside from RF ($P = 0.27$; MD = −32.40; 95% CI: −89.76 to 24.96). The significant difference was identified between TEs and PBO in terms of the SJC ($P < 0.00001$; MD = −4.13; 95% CI: −5.69 to −2.58), DMS ($P < 0.0001$; MD = −88.41 min; 95% CI: −129.64 to −47.18), and ESR ($P < 0.0001$; MD = −28.63 mm/H; 95% CI: −42.12 to −15.14). A small but significant increase in GS ($P = 0.003$; MD = 53.82; 95% CI: 18.63 to 89.01) was also found.

3.7.2. TEs Compared with DMARDs. Six trials (involving 513 patients) compared the therapeutic effects of TEs with those of DMARDs [31–36]. The number of trial participants ranged from 10 to 74, with the trial duration varying from four to twenty weeks. As illustrated in Figure 4, there was significant heterogeneity among the studies (all $P < 0.10$). Consequently, a random-effects model was employed to pool the results. The pooled results displayed no significant differences between TE-treated group and the DMARDs group, aside from GS ($P = 0.02$; SMD = 0.81; 95% CI: 0.14 to 1.48). However, no effects were found for TJC ($P = 0.60$; MD = 1.26; 95% CI: −3.52 to 6.05), SJC ($P = 0.72$; MD = −0.37; 95% CI: −2.35 to 1.61), DMS ($P = 0.94$; MD = −2.50 min; 95% CI: −67.08 to 62.08), RF ($P = 0.79$; SMD = 0.11; 95% CI: −0.70 to 0.92), ESR ($P = 0.54$; MD = 5.28 mm/H; 95% CI: −11.62 to 22.17), or CRP ($P = 0.73$; SMD = −0.22; 95% CI: −1.47 to 1.03). Only one trial [36] described the results, which were a 20% improvement in RA as defined by ACR (ACR 20) [39], ACR 50, and ACR 70, so we did not pool these results.

3.7.3. TEs with DMARDs Compared with DMARDs Alone. Two trials (involving 128 patients) compared a combined

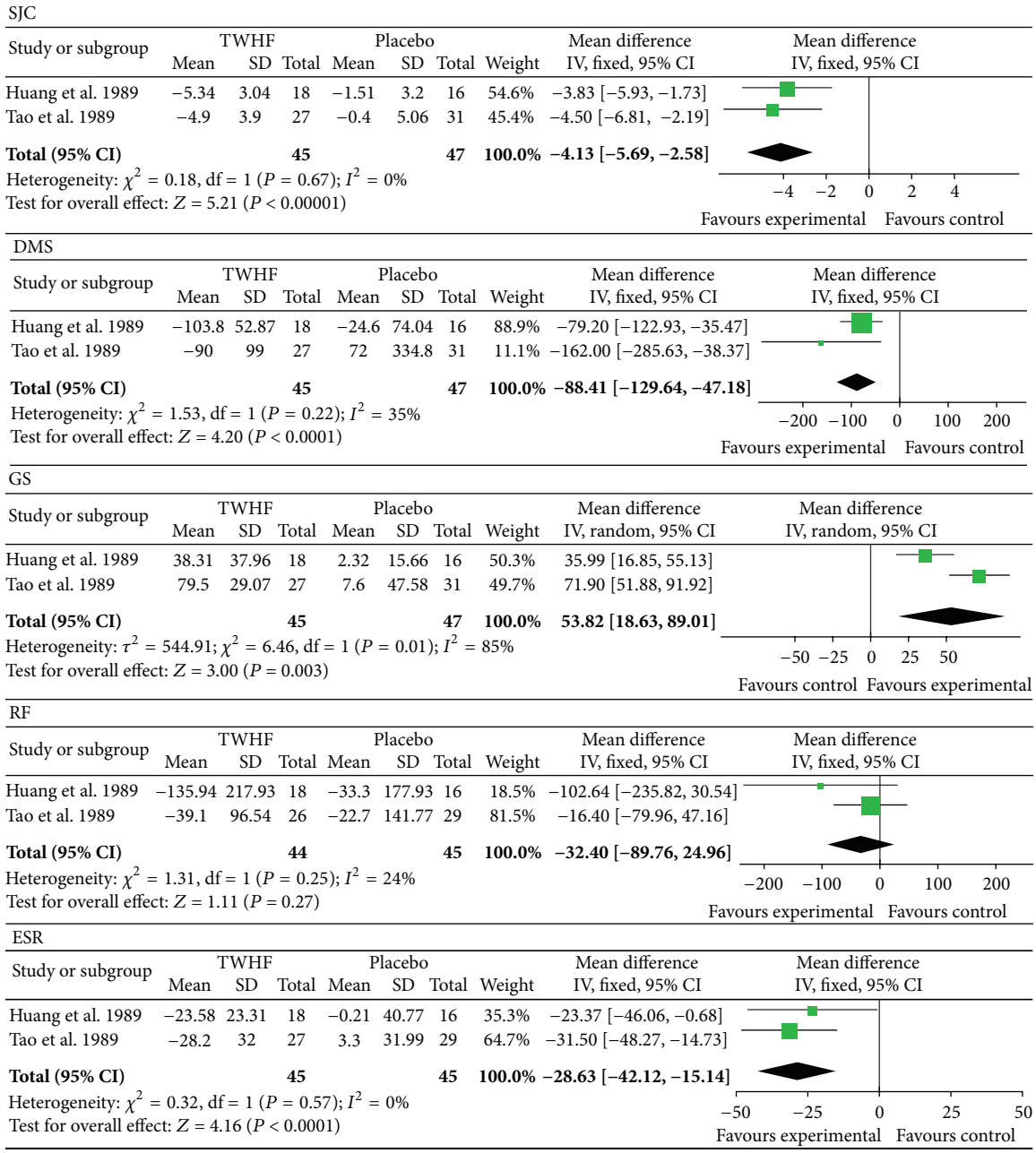

Figure 3: The first subgroup analyses comparing the effects of TEs and a PBO. Forest plots of TE treatment compared with a PBO. TEs: TwHF extracts; PBO: placebo; SJC: swollen joint count; DMS: duration of morning stiffness; GS: grip strength; RF: rheumatoid factor; ESR: erythrocyte sedimentation rate.

therapy of TEs and DMARDs with DMARDs alone [37, 38]. The number of trial participants ranged from 30 to 34 with trial durations varying from four to twelve weeks. As shown in Figure 5, the statistical heterogeneity among the studies was found to be significant regarding the results for ESR ($P = 0.05$). The pooled results showed no significant differences between the two groups in terms of ESR ($P = 0.39$; MD = −7.27 mm/H; 95% CI: −24.02 to 9.48) or CRP ($P = 0.62$; SMD = −0.09; 95% CI: −0.43 to 0.26). Unfortunately, none of the included trials reported its results: ACR 20, ACR 50, or ACR 70.

3.8. AEs. Eight trials reported outcomes for AEs. Seven trials [26, 27, 31, 33, 34, 36, 37] reported mild to moderate gastrointestinal events in a few of the participants who received TEs. Menstruation disorders or amenorrhea was reported in six trials [26, 27, 31, 33, 36, 37] in the TE group. Three trials [27, 33, 37] reported mild liver function abnormalities in a few patients caused by the intake of TEs. In the trial by Chen et al. [37], study discontinuation occurred in one patient in each group, and another trial [36] reported that seventeen patients who received sulfasalazine and eight patients who received TEs discontinued the study because of AEs

3.1 TJC

Study or subgroup	Experimental Mean	SD	Total	Control Mean	SD	Total	Weight	Mean difference IV, random, 95% CI
Liu et al. 2006	−3.3	2.06	10	−3.82	1.65	10	20.3%	0.52 [−1.12, 2.16]
Tan et al. 2000	−3.2	3.78	35	−8.6	4.11	40	20.2%	5.40 [3.61, 7.19]
Wang et al. 2006	1	6.95	45	−7	6.93	45	19.3%	8.00 [5.13, 10.87]
Yang and Zhang 2007	−10.35	3.95	60	−4.44	4.61	60	20.4%	−5.91 [−7.45, −4.37]
Yang et al. 2011	−6.7	6.8	74	−5.3	7.61	72	19.8%	−1.40 [−3.74, 0.94]
Total (95% CI)			**224**			**227**	**100.0%**	**1.26 [−3.52, 6.05]**

Heterogeneity: $\tau^2 = 28.68$; $\chi^2 = 123.60$, df = 4 ($P < 0.00001$); $I^2 = 97\%$
Test for overall effect: $Z = 0.52$ ($P = 0.60$)

Mean difference IV, random, 95% CI
−10 −5 0 5 10
Favours experimental Favours control

3.2 SJC

Study or subgroup	Experimental Mean	SD	Total	Control Mean	SD	Total	Weight	Mean difference IV, random, 95% CI
Liu et al. 2006	−3.1	0.97	10	−3.2	1.2	10	21.5%	0.10 [−0.86, 1.06]
Tan et al. 2000	−2.2	3.98	35	−5.4	3.38	40	19.5%	3.20 [1.52, 4.88]
Wang et al. 2006	−1.8	2.64	45	−2	2.97	45	21.0%	0.20 [−0.96, 1.36]
Yang and Zhang 2007	−3.7	2.15	60	−1.02	2.13	60	21.9%	−2.68 [−3.45, −1.91]
Yang et al. 2011	−6.8	7.35	74	−3.9	8.88	72	16.4%	−2.90 [−5.55, −0.25]
Total (95% CI)			**224**			**227**	**100.0%**	**−0.37 [−2.35, 1.61]**

Heterogeneity: $\tau^2 = 4.51$; $\chi^2 = 53.37$, df = 4 ($P < 0.00001$); $I^2 = 93\%$
Test for overall effect: $Z = 0.36$ ($P = 0.72$)

Mean difference IV, random, 95% CI
−4 −2 0 2 4
Favours experimental Favours control

3.3 DMS

Study or subgroup	Experimental Mean	SD	Total	Control Mean	SD	Total	Weight	Mean difference IV, random, 95% CI
Liu et al. 2006	−104.4	79.57	10	−85.8	72.2	10	21.5%	−18.60 [−85.19, 47.99]
Tan et al. 2000	−40.8	60.75	35	−132	65.86	40	25.8%	91.20 [62.54, 119.86]
Yang and Zhang 2007	−94.8	26.94	60	−46.2	34.38	60	27.0%	−48.60 [−59.65, −37.55]
Yang et al. 2011	−82.9	71.41	74	−48.5	78.58	72	26.2%	−34.40 [−58.78, −10.02]
Total (95% CI)			**179**			**182**	**100.0%**	**−2.50 [−67.08, 62.08]**

Heterogeneity: $\tau^2 = 3995.28$; $\chi^2 = 79.77$, df = 3 ($P < 0.00001$); $I^2 = 96\%$
Test for overall effect: $Z = 0.08$ ($P = 0.94$)

Mean difference IV, random, 95% CI
−100 −50 0 50 100
Favours experimental Favours control

3.4 GS

Study or subgroup	Experimental Mean	SD	Total	Control Mean	SD	Total	Weight	Mean difference IV, random, 95% CI
Yang and Zhang 2007	7.53	4.68	60	2.54	3.81	60	48.8%	1.16 [0.77, 1.55]
Yang et al. 2011	19.4	24.38	74	8.4	21.28	72	51.2%	0.48 [0.15, 0.81]
Total (95% CI)			**134**			**132**	**100.0%**	**0.81 [0.14, 1.48]**

Heterogeneity: $\tau^2 = 0.20$; $\chi^2 = 6.95$, df = 1 ($P = 0.008$); $I^2 = 86\%$
Test for overall effect: $Z = 2.37$ ($P = 0.02$)

Mean difference IV, random, 95% CI
−1 −0.5 0 0.5 1
Favours control Favours experimental

3.5 RF

Study or subgroup	Experimental Mean	SD	Total	Control Mean	SD	Total	Weight	Mean difference IV, random, 95% CI
Goldbach-Mansky et al. 2009	−336.38	943.46	37	−27.59	91.61	25	20.2%	−0.42 [−0.93, 0.10]
Liu et al. 2006	−66.11	79.42	10	−60.33	133.68	10	17.5%	−0.05 [−0.93, 0.83]
Tan et al. 2000	−18.6	21.5	35	−33.5	26.62	40	20.5%	0.61 [0.14, 1.07]
Wang et al. 2006	−13.4	9.1	45	−26	11.6	45	20.6%	1.20 [0.75, 1.65]
Yang and Zhang 2007	−102.17	88.62	60	−27.97	94.87	60	21.1%	−0.80 [−1.18, −0.43]
Total (95% CI)			**187**			**180**	**100.0%**	**0.11 [−0.70, 0.92]**

Heterogeneity: $\tau^2 = 0.78$; $\chi^2 = 53.84$, df = 1 ($P < 0.00001$); $I^2 = 93\%$
Test for overall effect: $Z = 0.26$ ($P = 0.79$)

Mean difference IV, random, 95% CI
−1 −0.5 0 0.5 1
Favours experimental Favours control

Figure 4: Continued.

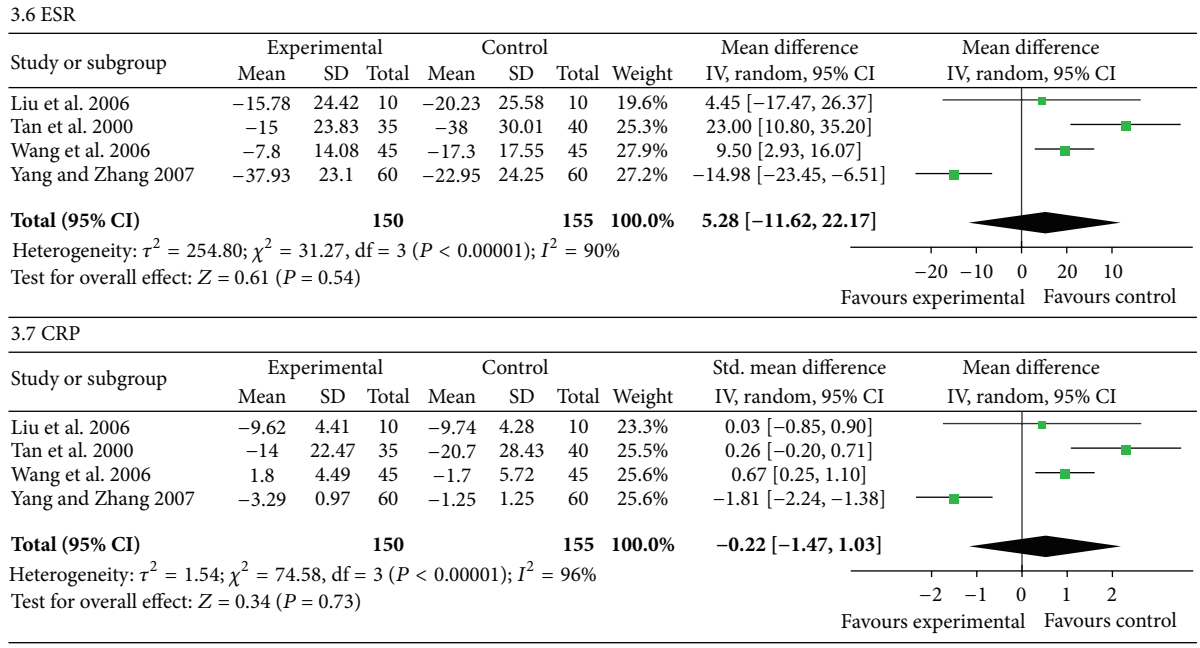

Figure 4: The second subgroup analyses comparing the effects of TEs with those of DMARDs. Forest plots comparing the effects of TE treatment with DMARDs. Note: TEs: TwHF extracts; DMARDs: disease-modifying antirheumatic drugs; TJC: tender joint count; SJC: swollen joint count; DMS: duration of morning stiffness; GS: grip strength; RF: rheumatoid factor; ESR: erythrocyte sedimentation rate; CRP: C-reactive protein.

($P = 0.071$). In addition, the same trial [36] reported that two patients became pregnant while receiving TEs or sulfasalazine, and mild prolongation of the corrected QT interval was seen on electrocardiography in patients receiving TEs.

4. Discussion

Although several systematic reviews and meta-analyses regarding the efficacy of TEs in the treatment of RA have been conducted, these systematic reviews achieved contradictory conclusions [40–43], which resulted from the differences of the search strategies, selection criteria, and data extraction and analysis, although all of these aspects have been recognised to some extent in these reviews. The meta-analysis published by Jiang et al. [43] (7 trials with 393 participants) performed two subgroup analyses: TEs versus PBO and TEs versus DMARDs. The systematic review published by Canter et al. [41] reported that TEs are associated with serious AEs, which render the risk-benefit analysis for TEs negative, and consequently, their application is not recommended. The most recent review, published by Cameron et al. [40] in the Cochrane Collaboration in 2011, could not pool its data due to differing interventions, comparisons, and outcomes. The Cochrane review concluded that TEs can reduce some RA symptoms; however, AEs can arise from oral use. We included ten trials and set three subgroups to minimize the heterogeneity, along with more new studies which made our systematic review differ from the previous ones.

Compared with a PBO, our results were consistent with those of Jiang et al. [43] in terms of SJC, RF, and ESR. In addition, TEs were found to be able to improve the DMS and GS. Although only two studies were included in this subgroup, the results showed that TEs were superior to PBO in improving joint function and reducing disease activity in RA.

Many of our results were consistent with the findings of Jiang et al. [43] between the TE-treated group and the DMARDs group, in terms of TJC, RF, and CRP. Unlike the previous review by Jiang et al. [43], there were no beneficial effects on SJC, DMS, or ESR in our review when comparing TEs with DMARDs. Furthermore, our review showed that the TE group had increased GS (SMD = 0.81) compared with the DMARDs group.

As shown in Figure 5, no beneficial effects on ESR and CRP were observed when the coadministration of TEs and DMARDs was compared with the administration of DMARDs alone. Although only two studies were included in this subgroup and two results were pooled, the analysis showed that TEs plus DMARDs had the same effects as those of two synthetic DMARDs alone in terms of lowering disease activity in RA. Additionally, the control groups, containing different efficient DMARDs, might have been responsible for the lack of intergroup differences in most of the endpoints.

The most common AEs with TEs were gastrointestinal discomfort, menstruation disorders, and amenorrhea, and they could be relieved with or without dose reductions. Due to different interventions, limited data, and the low quality of the included studies, the AEs were not ultimately combined. Identical to the synthetic DMARDs, the toxicity of TEs

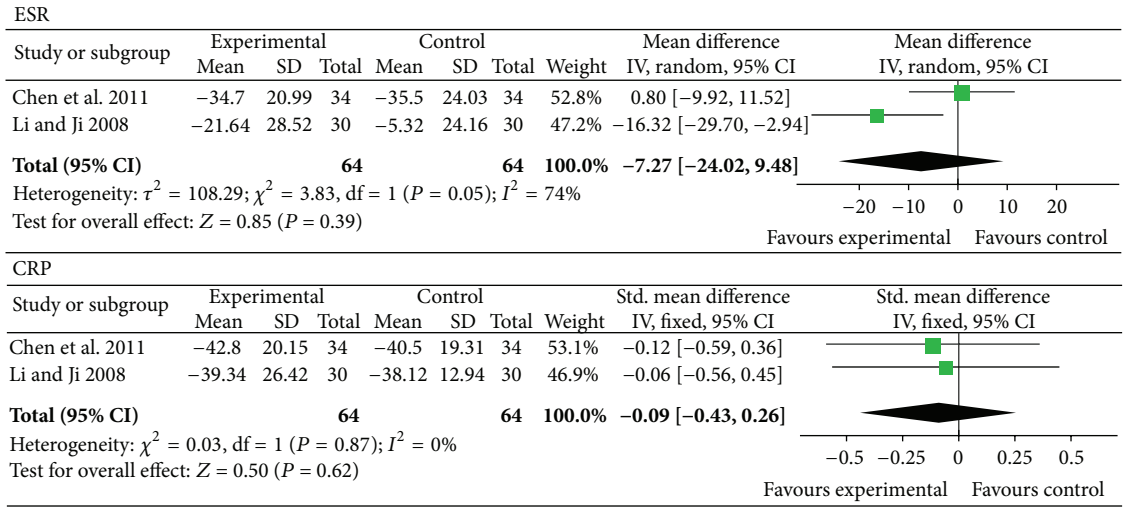

Figure 5: The third subgroup analyses comparing the effects of the coadministration of TEs and DMARDs with the effects of DMARDs alone. Forest plots comparing the effects of the coadministration of TEs and DMARDs with those of DMARDs alone. TEs: TwHF extracts; DMARDs: disease-modifying antirheumatic drugs; ESR: erythrocyte sedimentation rate; CRP: C-reactive protein.

requires monitoring regularly to prevent AEs. Additionally, the doses of TEs should be controlled to avoid AEs.

However, some limitations of this meta-analysis should be noted. First, nine of the included trials were conducted in Chinese populations, which implies a high risk of selection bias. This fact could have influenced the applicability of TEs to populations of other ethnic origins. Second, most of the studies published in Chinese were of poor quality regarding their designs, reporting, and methodologies. Only one multicentre RCT was identified [36], which applied adequate randomisation, double-blinding, and allocation concealment in the included trials. As we know, if investigators, participants, and outcome assessors are not blinded, knowledge of group assignment can influence responses to an intervention [44]. Furthermore, inadequate allocation concealment resulted in exaggerated estimates of treatment effect [45]. Third, the limited number (from two to five) of the trials included in each subgroup obscured the positive evidence of TEs for RA. Fourth, the heterogeneity between the trials included in each subgroup was also significant, especially in the subgroup of TEs versus DMARDs. We believe that differences in the quality of the reports, intervention methods, doses, and durations of treatment were responsible for the heterogeneity. Different efficacy, applicability, and toxicity presented in different synthetic DMARDs also gave rise to heterogeneity. Finally, the most important criteria (ACR 20, ACR 50, ACR 70) were not reported in nearly any of the trials except for one study [36]. In view of this, we should carefully explain all of the conclusions due to the considerable methodological and clinical variety of the studies.

5. Conclusion

In summary, TEs alone or combined with DMARDs might not be inferior to DMARDs in the treatment of RA. Based on their bioactivity, TEs, which function as a type of "herbal DMARD," appear to have the same effects as those of synthetic DMARDs. Meanwhile, the AEs of TEs should be assessed periodically, as with synthetic DMARDs. Considering the low methodological quality of the randomised trials, more RCTs are needed before we can recommend TEs to replace synthetic DMARDs or to be combined with them.

Conflict of Interests

The authors declare that they have no conflict of interests.

Acknowledgment

The authors acknowledge the authors of the original studies that they included in their meta-analysis.

References

[1] D. M. Lee and M. E. Weinblatt, "Rheumatoid arthritis," *The Lancet*, vol. 358, no. 9285, pp. 903–911, 2001.

[2] E. D. Harris Jr., "Rheumatoid arthritis: pathophysiology and implications for therapy," *New England Journal of Medicine*, vol. 322, no. 18, pp. 1277–1289, 1990.

[3] C. K. Kwoh, L. G. Anderson, J. M. Greene et al., "Guidelines for the management of rheumatoid arthritis: 2002 update—American College of Rheumatology Subcommittee on Rheumatoid Arthritis Guidelines," *Arthritis and Rheumatism*, vol. 46, no. 2, pp. 328–346, 2002.

[4] G. S. Firestein, "Evolving concepts of rheumatoid arthritis," *Nature*, vol. 423, no. 6937, pp. 356–361, 2003.

[5] J. S. Smolen, D. Aletaha, M. Koeller, M. H. Weisman, and P. Emery, "New therapies for treatment of rheumatoid arthritis," *The Lancet*, vol. 370, no. 9602, pp. 1861–1874, 2007.

[6] T. Bongartz, A. J. Sutton, M. J. Sweeting, I. Buchan, E. L. Matteson, and V. Montori, "Anti-TNF antibody therapy in rheumatoid arthritis and the risk of serious infections and malignancies: systematic review and meta-analysis of rare

harmful effects in randomized controlled trials," *Journal of the American Medical Association*, vol. 295, no. 19, pp. 2275–2285, 2006.

[7] A. A. Kalla and M. Tikly, "Rheumatoid arthritis in the developing world," *Best Practice and Research: Clinical Rheumatology*, vol. 17, no. 5, pp. 863–875, 2003.

[8] E. Yelin and L. A. Wanke, "An assessment of the annual and long-term direct costs of rheumatoid arthritis: the impact of poor function and functional decline," *Arthritis and Rheumatism*, vol. 42, no. 6, pp. 1209–1218, 1999.

[9] X. Tao and P. E. Lipsky, "The Chinese anti-inflammatory and immunosuppressive herbal remedy *Tripterygium wilfordii* Hook F," *Rheumatic Disease Clinics of North America*, vol. 26, no. 1, pp. 29–50, 2000.

[10] X. Tao, J. J. Cush, M. Garret, and P. E. Lipsky, "A phase I study of ethyl acetate extract of the Chinese antirheumatic herb *Tripterygium wilfordii* Hook F in rheumatoid arthritis," *Journal of Rheumatology*, vol. 28, no. 10, pp. 2160–2167, 2001.

[11] W. Zhang, Q. Shi, L.D. Zhao et al., "The safety and effectiveness of a chloroform/methanol extract of *Tripterygium wilfordii* Hook F (T2) plus methotrexate in treating rheumatoid arthritis," *Journal of Clinical Rheumatology*, vol. 16, no. 8, pp. 375–378, 2010.

[12] W. Ji, J. Li, Y. Lin et al., "Report of 12 cases of ankylosing spondylitis patients treated with *Tripterygium wilfordii*," *Clinical Rheumatology*, vol. 29, no. 9, pp. 1067–1072, 2010.

[13] J. L. Guo, Z. G. Gao, A. C. Zang, and R. X. Bai, "Radix *Tripterygium wilfordii* Hook F in rheumatoid arthritis, ankylosing spondylitis and juvenile rheumatoid arthritis," *Chinese Medical Journal*, vol. 99, no. 4, pp. 317–320, 1986.

[14] T. Patavino and D. M. Brady, "Natural medicine and nutritional therapy as an alternative treatment in systemic lupus erythematosus," *Alternative Medicine Review*, vol. 6, no. 5, pp. 460–471, 2001.

[15] X. Jiang, "Clinical observations on the use of the Chinese herb *Tripterygium wilfordii* Hook for the treatment of nephrotic syndrome," *Pediatric Nephrology*, vol. 8, no. 3, pp. 343–344, 1994.

[16] J. Ren, Q. Tao, X. Wang, Z. Wang, and J. Li, "Efficacy of T2 in active Crohn's disease: a prospective study report," *Digestive Diseases and Sciences*, vol. 52, no. 8, pp. 1790–1797, 2007.

[17] S. Yang, J. Chen, Z. Guo et al., "Triptolide inhibits the growth and metastasis of solid tumors," *Molecular Cancer Therapeutics*, vol. 2, no. 1, pp. 65–72, 2003.

[18] A. M. Brinker, J. Ma, P. E. Lipsky, and I. Raskin, "Medicinal chemistry and pharmacology of genus *Tripterygium* (Celastraceae)," *Phytochemistry*, vol. 68, no. 6, pp. 732–766, 2007.

[19] X. Tao, J. J. Cai, and P. E. Lipsky, "The identity of immunosuppressive components of the ethyl acetate extract and chloroform methanol extract (T2) of *Tripterygium wilfordii* Hook.F," *Journal of Pharmacology and Experimental Therapeutics*, vol. 272, no. 3, pp. 1305–1312, 1995.

[20] H. Hu, A. Straub, Z. Tian, N. Bassler, J. Cheng, and K. Peter, "Celastrol, a triterpene extracted from *Tripterygium wilfordii* Hook F, inhibits platelet activation," *Journal of Cardiovascular Pharmacology*, vol. 54, no. 3, pp. 240–245, 2009.

[21] B. Wang, L. Ma, X. Tao, and P. E. Lipsky, "Triptolide, an active component of the Chinese herbal remedy *Tripterygium wilfordii* Hook F, inhibits production of nitric oxide by decreasing inducible nitric oxide synthase gene transcription," *Arthritis and Rheumatism*, vol. 50, no. 9, pp. 2995–3003, 2004.

[22] X. Tao, H. Schulze-Koops, L. Ma, J. Cai, Y. Mao, and P. E. Lipsky, "Effects of *Tripterygium wilfordii* Hook F extracts on induction of cyclooxygenase 2 activity and prostaglandin E2 production," *Arthritis and Rheumatism*, vol. 41, no. 1, pp. 130–138, 1998.

[23] F. C. Arnett, S. M. Edworthy, D. A. Bloch et al., "The American Rheumatism Association 1987 revised criteria for the classification of rheumatoid arthritis," *Arthritis and Rheumatism*, vol. 31, no. 3, pp. 315–324, 1988.

[24] A. R. Jadad, R. A. Moore, D. Carroll et al., "Assessing the quality of reports of randomized clinical trials: is blinding necessary?" *Controlled Clinical Trials*, vol. 17, no. 1, pp. 1–12, 1996.

[25] K. F. Schulz, L. Chalmers, R. J. Hayes, and D. G. Altman, "Empirical evidence of bias: dimensions of methodological quality associated with estimates of treatment effects in controlled trials," *Journal of the American Medical Association*, vol. 273, no. 5, pp. 408–412, 1995.

[26] X. L. Tao, Y. Sun, Y. Dong et al., "A prospective, controlled, double-blind, cross-over study of *Tripterygium wilfodii* hook F in treatment of rheumatoid arthritis," *Chinese Medical Journal*, vol. 102, no. 5, pp. 327–332, 1989.

[27] C. Huang, C. Wu, Z. Shen, M. Lin et al., "Study on the treatment of rheumatoid arthritis with polyglycosides of *Tripterygium wilfordii* Hook F: randomized, controlled, crossover clinical trial," in *Proceedings of the 3rd National Meeting of Rheumatology of China. Shijiazhuang, China, 1989*, pp. 31–35, Chinese Association of Medicine, Beijing, China, 1989.

[28] X. Tao, J. Younger, F. Z. Fan, B. Wang, and P. E. Lipsky, "Benefit of an extract of *Tripterygium wilfordii* Hook F in patients with rheumatoid arthritis: a double-blind, placebo-controlled study," *Arthritis and Rheumatism*, vol. 46, no. 7, pp. 1735–1743, 2002.

[29] J. Fu, S. Liang, L. Ren, W. Li, and S. Guo, "The effect of tripterygium glycosides on plasma TNFα in patients with rheumatoid arthritis," *The Journal of Traditional Chinese Orthopedics and Traumatology*, vol. 13, no. 9, pp. 13–14, 2001.

[30] N. Li, "The effect of tripterygium glycosides on plasma TNFα and IL-6 in patients with rheumatoid arthritis," *Journal of Guangxi Medical University*, vol. 22, no. 5, pp. 681–683, 2005.

[31] Y. Tan, C. Wu, and Y. You, "Clinical analysis of methotrexate combined with penicillamine in the treatment of rheumatoid arthritis," *China Journal of Modern Medicine*, vol. 10, no. 12, pp. 71–72, 2000.

[32] Y. Wang, Q. Wu, J. Wei, H. Shen, L. Wang, and Q. Zhu, "Total glucosides of paeony, methotrexate and *Tripterygium wilfordii* in the treatment of 150 cases of rheumatoid arthritis," *Journal of Zhengzhou University(Medical Sciences)*, vol. 41, no. 5, pp. 1002–1003, 2006.

[33] X. Yang and L. Zhang, "Clinical observation of tripterygium for treatment of 60 cases of rheumatoid arthritis," *Chinese Journal of Traditional Medical Science and Technology*, vol. 14, no. 2, pp. 130–131, 2007.

[34] Z. Yang, "The clinic effect of *Tripterygium wilfordii* Hook F on rheumatoid arthritis," *China Pharmaceuticals*, vol. 20, no. 14, pp. 76–77, 2011.

[35] J. Liu, H. Li, and X. Chen, "Effects of traditional Chinese medicine for invigorating spleen to resolve dampness and dredging collaterals on patients with rheumatoid arthritis and anemia," *Journal of Chinese Integrative Medicine*, vol. 4, no. 4, pp. 348–354, 2006.

[36] R. Goldbach-Mansky, M. Wilson, R. Fleischmann et al., "Comparison of *Tripterygium wilfordii* Hook F versus sulfasalazine in the treatment of rheumatoid arthritis: a randomized trial," *Annals of Internal Medicine*, vol. 151, no. 4, pp. 229–240, 2009.

[37] P. Chen, L. Zhu, X. Zou, H. Du, Y. Zhou, and X. Gu, "Tripterygium glucosides combined with methotrexate in treatment of rheumatoid arthritis: a randomised controlled trial," *Journal of Anhui Traditional Chinese Medical College*, vol. 30, no. 6, pp. 28–32, 2011.

[38] N. Li and H. Ji, "*Tripterygium wilfordii* combines with sulfasalazine on the related indexes of active rheumatoid arthritis," *Journal of Liaoning University of Traditional Chinese Medicine*, vol. 10, no. 12, pp. 89–90, 2008.

[39] D. T. Felson, J. J. Anderson, M. Boers et al., "American College of Rheumatology preliminary definition of improvement in rheumatoid arthritis," *Arthritis and Rheumatism*, vol. 38, no. 6, pp. 727–735, 1995.

[40] M. Cameron, J. J. Gagnier, and S. Chrubasik, "Herbal therapy for treating rheumatoid arthritis," *Cochrane Database of Systematic Reviews*, no. 2, Article ID CD002948, 2011.

[41] P. H. Canter, H. S. Lee, and E. Ernst, "A systematic review of randomised clinical trials of *Tripterygium wilfordii* for rheumatoid arthritis," *Phytomedicine*, vol. 13, no. 5, pp. 371–377, 2006.

[42] C. Little and T. Parsons, "Herbal therapy for treating rheumatoid arthritis," *Cochrane Database of Systematic Reviews*, no. 4, Article ID CD002948, 2000.

[43] Q. Jiang, W. Cao, X. Tang, and J. Juan, "*Tripterygium wilfordii* extract for treating rheumatoid arthritis: systematic review," *China Journal of Chinese Materia Medica*, vol. 34, no. 20, pp. 2637–2643, 2009.

[44] K. F. Schulz and D. A. Grimes, "Blinding in randomised trials: hiding who got what," *The Lancet*, vol. 359, no. 9307, pp. 696–700, 2002.

[45] K. F. Schulz and D. A. Grimes, "Allocation concealment in randomised trials: defending against deciphering," *The Lancet*, vol. 359, no. 9306, pp. 614–618, 2002.

Hindawi Publishing Corporation
Evidence-Based Complementary and Alternative Medicine
Volume 2013, Article ID 137631, 10 pages
http://dx.doi.org/10.1155/2013/137631

Research Article

Electroacupuncture-Induced Neuroprotection against Cerebral Ischemia in Rats: Role of the Dopamine D2 Receptor

Ming-Shu Xu,[1] Shu-Jing Zhang,[1] Dan Zhao,[2] Cheng-Yong Liu,[3] Chang-Zhi Li,[4] Chun-Yan Chen,[2] Li-Hui Li,[1] Ming-Zhe Li,[1] Jia Xu,[4] and Lin-Bao Ge[2,5]

[1] *Neurobiology Laboratory of Brain, Shanghai Research Institute of Acupuncture and Meridians, Shanghai 200030, China*
[2] *Shanghai Research Institute of Qigong, Shanghai 200030, China*
[3] *Jiangsu Provincial Hospital of Traditional Chinese Medicine, Nanjing 210029, China*
[4] *Yueyang Hospital of Integrative Chinese & Western Medicine Affiliated to Shanghai University of TCM, Shanghai 200437, China*
[5] *Shanghai Research Center of Acupuncture and Meridians, Shanghai 201203, China*

Correspondence should be addressed to Lin-Bao Ge; gelinbao@vip.163.com

Received 3 June 2013; Revised 24 July 2013; Accepted 30 July 2013

Academic Editor: Yong-Qing Yang

Background. Cerebral ischemia is known to produce brain damage and related behavioural deficits, including memory deficits and motor disorders. Evidence shows that EA significantly promotes recovery of neurological function and thus improves quality of life. *Objective*. Evidence exists for the involvement of catecholamines in human neuroplasticity. A better understanding of dopaminergic (DAergic) modulation in this process will be important. *Methods*. A total of 72 adult male Sprague-Dawley (SD) rats were divided into 6 groups: normal, model, EA, spiperone group, EA + spiperone group, and pergolide. The middle cerebral artery occlusion (MCAO) model was used in all 6 groups except the normal group. A behavioural assessment was conducted at 1, 3, 5, and 7 days after MCAO. The percent of brain infarct area was also determined 7 days after MCAO. Tyrosine hydroxylase (TH) and growth-associated protein 43 (GAP-43) fluorescence double labeling was performed in the striatum. *Results*. In this study, we found that EA at Fengchi (GB20) acupoints resulted in marked improvements based on a behavioural assessment. Both TTC staining and GAP-43 immunofluorescence labeling results showed that EA treatment reduced ischemia injury and promoted neuroplasticity compared with the model group. The D2R-selective agonist, pergolide, showed similar results, but these results were reversed by the D2R-selective antagonist, spiperone. We also found that there were more colocalization and expression of GAP-43 and TH in the EA and pergolide groups than those in the other groups. *Conclusion*. These results suggest that the neuroplasticity induced by EA was mediated by D2 autoreceptors in DAergic neurons.

1. Introduction

Cerebrovascular injury is one of the most prevalent diseases in the world, especially in developed countries and developing countries with continuously increasing standards of living, such as China. Stroke can be either ischemic or hemorrhagic, but more than 80% of stroke cases are caused by cerebral ischemia [1].

Cerebral ischemia is known to produce brain damage and related behavioural deficits, including memory deficits and motor disorders. Middle cerebral artery occlusion reportedly occurred in 10–15% of stroke patients [2]. The main areas affected by middle artery occlusion are the cerebral cortex, the hippocampus, and the striatum [3]. Memory and motor deficits are associated with interruption of blood flow to these areas [4–8].

Survivors of stroke are often affected by serious, long-term disabilities, including paralysis and disruption of higher cognitive functions, such as speech and memory. Some patients may even have mental disorders, such as depressive symptoms. Individuals with such disabilities often require extensive long-term care by health care professionals and family.

Due to the high and wide-ranging social impact of cerebrovascular disease, there is great interest in researching methods to increase the cure rate of cerebrovascular diseases,

reduce the financial burden of both government agencies and affected families, and improve the quality of life of ischemic patients.

Although many neuroprotective agents have been proven to reduce infarction volume and improve neurological recovery in basic research with animal stroke models, few have shown positive effects in clinical trials [9, 10]. There is a wide gap between current treatments and our expectations. Currently, no clinical modality has demonstrated promising efficacy in terms of stroke treatment. Therefore, new strategies should be developed to establish better preventative measures and treatments for this serious disease.

Traditional Chinese medicines (TCMs) have been used successfully for centuries to treat a wide variety of ailments and have attracted increasing attention from industry and academia in China [11–13].

EA is a therapy based on traditional acupuncture, combined with modern electrotherapy. Acupuncture to different brain areas is known to have beneficial effects, and EA has been seen as an improvement on traditional acupuncture. Evidence shows that EA significantly promotes recovery of neurological function and thus improves quality of life [14].

Numerous studies have confirmed that acupuncture can be beneficial to patients during convalescence from ischemic apoplexy [15]. Animal experiments [16] have also demonstrated that acupuncture can accelerate the restoration of function and help heal the cerebral tissue lesion during cerebral ischemia-reperfusion. Dopamine plays an important role in this process.

Some key concepts for developing effective rehabilitation interventions are the heterogeneity of mechanisms underlying stroke as well as the plastic processes leading to recovery of function after neuronal injury.

DAergic neurons are subject to modulation by a variety of factors. Some of the factors involved in intrinsic regulation of central DA neurotransmission during physical activity include TH, D1, and D2 receptors.

Evidence exists for the participation of catecholamines in human neuroplasticity. Regional discrepancies observed in the action of dopamine on synaptic plasticity [17] could be explained by differences in dopamine content and dopamine receptor subtype distribution, resulting in differences in the level of dopamine receptor activation during LTP or LTD induction.

Dopamine neurons are important for neuroplasticity after ischemia. Electroacupuncture (EA) significantly promotes recovery of neurological function. Previous studies have shown that dopamine D2 receptor plays a importance role in the induction of neuroplasticity. The recovery of neurological function is interrelated and inextricably linked with neuroplasticity. Given the recovery of EA and the importance of the dopamine system in neuroplasticity after ischemia, we hypothesized that Dopamine D2 receptor may play an important role in the neuroprotection induced by EA. To reflect the progression of the disease and recovery, the behavioural observations should be combined with histopathology. A better understanding of DAergic modulation will be important for understanding neuroplastic processes after ischemia.

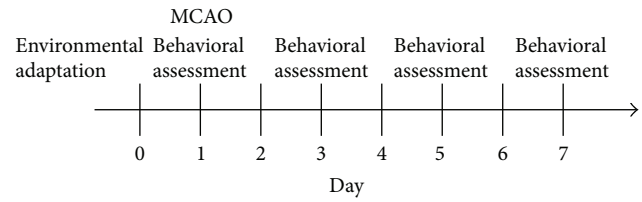

Figure 1: Experimental procedure. Normal group: behavioural assessment, but no MCAO. The other group: behavioural assessment and MCAO. EA, pergolide, or spiperone treatment was given each day after MCAO.

2. Materials and Methods

2.1. Animals. A total of 72 adult male Sprague-Dawley (SD) rats (8-9 wks of age, 300 ± 20 g, Shanghai Laboratory Animal Center, Chinese Academy of Sciences, Shanghai, China) were raised in groups of 4–6 per cage under controlled conditions (23 ± 1°C, 50% ± 10% relative humidity, 12/12 hr alternate light/dark cycles, and food and water ad libitum) for at least 1 week before the experiments. All animals were handled with care to prevent infection and minimize stress.

The experimental protocols were approved by the Institutional Animal Care and Use Committee. The minimum number of animals and duration of observations required to obtain reliable data were used.

2.2. Environmental Adaptation and Grouping. Based on a random number table, the rats were divided into 6 groups: normal, model, EA, spiperone group, EA + spiperone group, and pergolide group, with 12 rats in each group. The middle cerebral artery occlusion (MCAO) model was established in all 6 groups except the normal group. The D2R antagonist, spiperone, was delivered by peritoneal injection in the D2R antagonist group and the EA + spiperone group once a day for 7 days. The D2R agonist, pergolide, was delivered by peritoneal injection in the pergolide group once a day for 7 days. EA was applied once a day for 7 days in the EA group and the EA + spiperone group. In this study, the doses of spiperone and pergolide were selected based on our pilot study and earlier reports. Behavioural assessments were conducted 1, 3, 5, and 7 days after MCAO. The brain infarct area was also determined 7 days after MCAO. The schedule for drug treatment, surgery, and behavioural testing is shown in Figure 1.

2.3. Reagents. 10% chloral hydrate; gentamycin sulfate injection; 1% heparin sodium solution; D2R agonist pergolide (P8828, Sigma, America); D2R antagonist spiperone (108587, Sigma, America); GAP-43 antibody (G9264, Sigma, America); TH antibody (ab6211, Abcam, America).

2.4. Instruments. SD-78 bipolar coagulator; G6805-2 electroacupuncture instrument (Shanghai Huayi Medical Instrument Factory); YP1201N electronic balance (Shanghai Precision Scientific and Balance Instrument Factory); 40-90-8C rat temperature control pad (Frederick Haer, America); acupuncture needles (0.25 mm in diameter and 13 mm in length, Suzhou Acupuncture Supplies Factory).

2.5. Induction of the MCAO Rat Model. Plug lines were prepared with 3.0 cm nylon monofilament (4-0) suture (DG, America). The tips were rounded by heating near a flame and then washed with normal saline and placed in tubes filled with heparin sodium 1% solution.

The rat model of middle cerebral artery ischemia-reperfusion was established according to the literature [1]. Briefly, rats were anesthetized with chloral hydrate (400 mg/kg, i.p.). The right common carotid artery (CCA) and internal carotid artery (ICA) were exposed via a midline incision in the neck. The pterygopalatine artery was ligated close to its origin. The nylon filament suture was advanced from the right external carotid artery, through the CCA and up to the ICA for a distance of 18 ± 0.5 mm to block the origin of the middle cerebral artery (MCA), until a mild resistance was felt. The right MCA was occluded for 90 min. After that, cerebral blood flow (CBF) was restored by withdrawal of the nylon thread. The rectal temperature was maintained at 37°C–37.5°C during and after surgery. The sham group underwent the same surgical procedure without insertion of the nylon thread [18, 19].

2.6. Behavioural Assessment. Researchers and an assistant who was not involved in this experiment scored the neurological deficits.

2.6.1. Index of Neurological Deficits Test. Neural function defect score (NFDS) standard [3]: rats show no asymmetric activity, 0 points; rats are unable to stretch the left forelimb when the tail is lifted, 1 point; the left forelimb could not straightly downwards accompanied by the abduction of the left shoulder, 2 points; left forelimb is close to the chest wall, 3 points; rats turn left in free activities, 4 points; accompanied by obvious left-front paw pushing back, 5 points; rats can only rotate around the origin to the left, 6 points; limbs cannot support the body weight on the left side, and the rats can only lie on the left side, 7 points.

2.6.2. Balance Beam Test (BBT). Rats were placed on a wooden bar of 300 mm × 25 mm. Rats can maintain balance with four feet and walk across the wooden bar, 0 point; rats can't walk across the wooden bar, but can maintain balance with four feet, 1 point; rat's claws grip the side of the wooden bar or rat's body shakes on the bar, 2 points; one limb slips from the bar, 3 points; two limbs slip from the bar, 4 points; rats try to keep their balance but slip, 5 points; rats fail to keep their balance, hang on the bar and fall down, 6 points; rats fall down directly without trying to keep their balance, 7 points [20].

2.6.3. Limb Placement Test. In this study, sensorimotor integration was evaluated over a 7-day period by an investigator blind to the rats' treatment regimen. In the forelimb placement test (FPT), animals were held gently by the torso and moved slowly toward a table top until the dorsal forepaw surface barely touched the edge. Normal animals rapidly place their forelimb on the table top. Performance was scored between 0 (normal) and 10 (maximal impairment). Similarly, the hindlimb placing test (HPT) evaluated the animal's ability to place the hindpaw on a table in response to light stimulation and was scored on a 0–6 scale [20, 21].

2.7. EA Intervention Scheme. The location of the rat Fengchi (GB 20) is similar to that in the human body under the occipital bone in the hollow between the trapezius and sternocleidomastoid muscles. Two stainless steel needles were perpendicularly inserted 8 mm into the Fengchi (GB 20) and connected to the EA instrument. The parameters were as follows: frequency of 2 Hz, continuous wave, and current intensity of 3.0 mA (oscilloscope detection), with mild jittering of the rat auricle. The EA lasted for 20 min, was stopped for 10 min, and then resumed for another 20 min.

2.8. Infarct Area Assessment. Following neurological function evaluation, 6 rats in each group were deeply anesthetized by an intraperitoneal dose of 400 mg/kg chloral hydrate and then decapitated. Each brain was removed and sliced in 2 mm sections using a rodent brain matrix slicer (RBM-4000C; ASI Instruments, Warren, MI, USA). Sections were stained with 2,3,5-triphenyltetrazolium chloride (TTC) (Nanjing Green Synthesis Biochemical Co., Ltd., Nanjing, Jiangsu, China). The percent of infarct area of the entire brain represented the degree of cerebral infarction. Serial coronal sections were prepared and soaked in 2% TTC phosphate buffer at 37°C for 10 minutes in the dark. Normal brain tissues were stained red, while infarct tissues were not stained (white). The sections were soaked in 4% paraformaldehyde phosphate buffer for 30 minutes, arranged in order, and scanned. Areas of red and white staining were measured using a computer colour multimedia image analysis system (Image J 1.46R, NIH, USA). The percent of infarction is given by the equation: %infarct area = infarct area/total area of slice × 100 [22].

2.9. Double Immunofluorescent Labeling. Following anaesthesia with chloral hydrate (60 mg/kg body weight), 6 rats in each group were transcardially perfused with fixative containing 4% paraformaldehyde in 0.1 M phosphate buffer (pH 7.3). The brains were removed and stored overnight in the same fixative. They were infiltrated with 30% sucrose solution and kept at 4°C. The specimens were rapidly frozen and sectioned with a vibratome (30 μm sections) on a cryostat. In order to examine the relation between TH and GAP-43 in the striatum, fluorescence double labeling was performed. After washing in PBS (pH 7.3), striatal sections were incubated for 30 min at room temperature in 10% goat serum diluted in PBS. They were then incubated for 48 h at 4°C with a mixture of antisera against TH and GAP-43 diluted 1 : 1000 and 1 : 100 in PBS, respectively. After washing in PBS, they were incubated for 1 h at room temperature with a mixture of pig antisera against IgG of mouse antisera conjugated to Cy3 diluted 1 : 100 and goat antisera against IgG of rabbit antisera conjugated to fluorescein isothiocyanate (FITC) diluted 1 : 100 in PBS. DAPI was used as an additional nuclear counterstain. The sections were mounted on glass slides. Image analysis of the double immunofluorescent labeling was performed by a SP5-AOBS confocal laser-scanning microscope (Leica Microsystems, Mannheim, Germany) through a 20 × 0.5 NA air

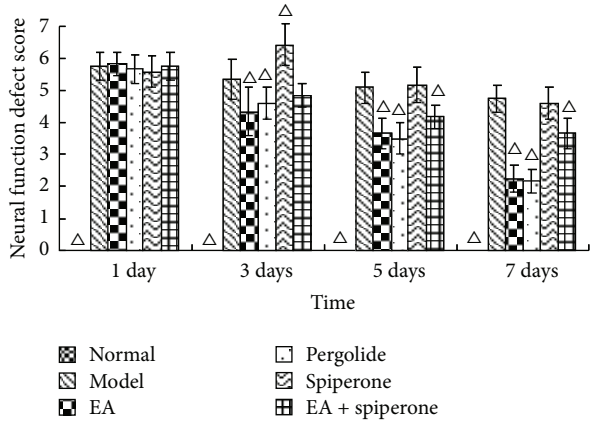

Figure 2: NFDS changes in all groups except the normal group 1, 3, 5, and 7 days after MCAO. The columns represent the normal, model, EA, pergolide, spiperone, and EA + spiperone groups, respectively. The score for the normal group on each day was 0 (data not shown), $\Delta P < 0.05$ versus model group at the same time point.

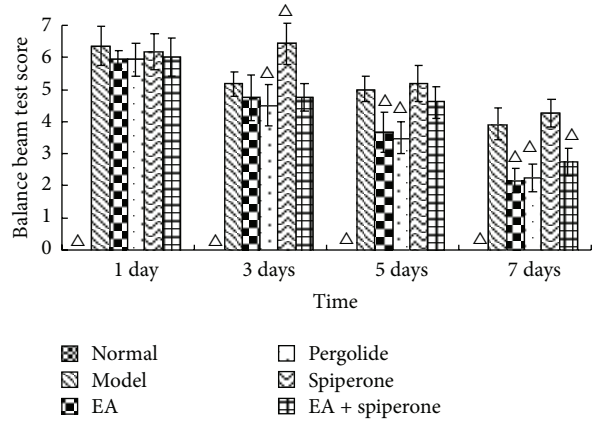

Figure 3: BBT score changes for all groups except the normal group 1, 3, 5, and 7 days after MCAO. The score for the normal group on each day was 0 (data not shown). $\Delta P < 0.05$ versus model group at the same time-point.

objective and a 40 × 1.2 NA oil-immersion objective, using laser excitation at 488 and 561 nm. Images were assembled into montages with Image J software (NIH; http://rsb.info.nih.gov/ij/) and Adobe Photoshop 7.0 (Adobe Systems, Mountain View, CA, USA). The size distribution of positive cell profiles was determined using NIH Image software. The somas of neurons of interest were outlined manually, and their sizes were determined. Only neurons with a distinguishable nucleus in the section were counted [23, 24].

2.10. Statistical Analysis. Data are expressed as mean ± SD. Data from all groups were compared using a one-way ANOVA followed by post hoc analysis for significance with the Student-Newman-Keuls multiple comparison test. A probability value of less than 0.05 was considered statistically significant.

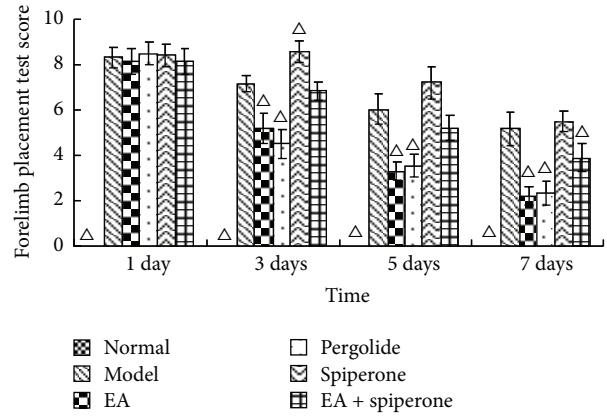

Figure 4: FPT score changes in all groups except the normal group 1, 3, 5, and 7 days after MCAO. The score for the normal group on each day was 0 (data not shown). $\Delta P < 0.05$ versus model group at the same time-point.

3. Results

3.1. Behavioural Assessment. All 72 rats were included in the results analysis, without any animals being lost in the course of the experiment. NFDS and BBT scores may reflect the neurological deficit and the impaired balancing ability in rat brain function. Before MCAO, the NFDS and BBT scores for all groups were 0. In the experiment, we observed that the neurological deficit was aggravated after MCAO. The situation was stable until 24 h after reperfusion. NFDS and BBT scores taken 1, 3, 5, and 7 days after reperfusion are shown in Figures 2 and 3. There were significant differences in NFDS and balance beam test scores before and after MCAO ($P < 0.05$). After the EA and pergolide interventions, the NFDS and BBT scores in the EA group and the pergolide group had improved more significantly than those in the model group ($P < 0.05$). The NFDS and BBT scores in the spiperone group had worsened 3 days after reperfusion and were significantly different from the model group. The NFDS and BBT scores in the EA + spiperone group had noticeably improved compared with those in the spiperone only group. (Figures 2 and 3).

FPT and HPT score changes appear similar to the changes in NFDS and BBT at 1, 3, 5, and 7 days after modeling. The FPT and HPT scores were both 0 in the normal group on each day. The neurological deficit was aggravated after MCAO. EA and pergolide improved the score compared with the model group ($P < 0.05$). The spiperone group showed decreased FPT and HPT scores 3 days after reperfusion; however, these scores noticeably improved in the EA + spiperone group. (Figures 4 and 5).

3.2. TTC Staining. TTC staining may reflect the neurological deficit in the rat brain. There were significant differences in lesion area between rats in the normal and model groups ($P < 0.05$). After interventions with EA and pergolide, the lesion

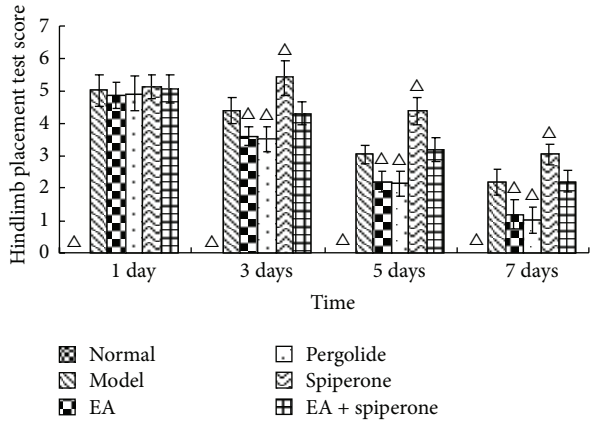

FIGURE 5: HPT score changes in all groups except the normal group 1, 3, 5, and 7 days after MCAO. The score for the normal group on each day was 0 (data not shown). $\Delta P < 0.05$ versus model group at the same time-point.

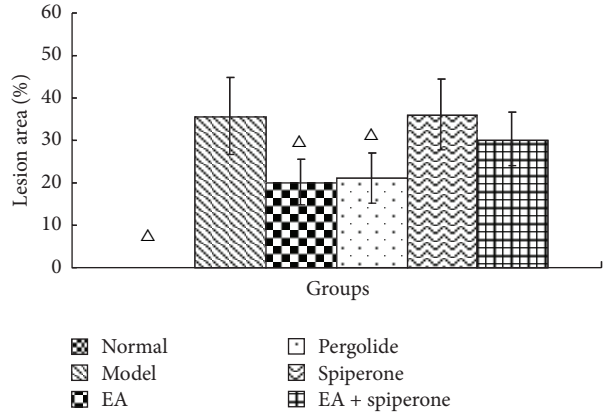

FIGURE 6: Percent lesion area in the contralateral hemisphere ($\overline{X} \pm$ SD) ($n = 6$). The percent lesion area in the normal group was 0 (data not shown). $\Delta P < 0.05$ versus model group at the same time-point.

TABLE 1: Percent lesion area in the contralateral hemisphere ($\overline{X} \pm$SD) ($n = 6$).

Group	Lesion area, %
Normal	0
Model	35.7 ± 9.1
EA	20.1 ± 5.2
Pergolide	21.1 ± 6.1
Spiperone	35.9 ± 8.4
EA + spiperone	30.2 ± 6.3

area in the EA and the pergolide groups was reduced noticeably compared with the model group ($P < 0.05$). The area of the lesion in the spiperone group had worsened and showed no significant difference from the model group. In the spiperone and EA group, the area of the lesion was reduced, but no significant difference was found when compared with the spiperone group (Table 1 and Figures 6 and 7).

3.3. Double Immunofluorescent Labeling (GAP-43 and TH Immunocolocalization). As shown in Figure 8, colocalization experiments indicated that TH-positive cells (green) and GAP-43-positive cells (red) were colocalized in some neurons of the striatum. The double immunostaining revealed that only a third of TH-positive cells produced GAP-43, meaning that the colocalization was only partial. EA and pergolide led to increased GAP-43 expression in DAergic neurons 7 days after the onset of ischemia compared with the model group ($P < 0.05$) (data not shown) (Figure 8, resp.). There was no variation between the two groups of animals (data not shown). The colocalization of both GAP-43 and TH decreased in the spiperone group compared to the EA and pergolide groups ($P < 0.05$). Indeed, no GAP-43/TH double-labeled cells were observable in the spiperone group. Such an effect could be partly reversed by EA. No significant differences in co-localization were found between the model group and the EA + spiperone group ($P > 0.05$).

Photomicrographs show neurons in the rat striatum after double labeling with TH antiserum (shown in green) and GAP-43 antiserum (shown in red) of normal Figures 8(a)–8(c), model Figures 8(d)–8(f), EA Figures 8(g)–8(i), pergolide Figures 8(j)–8(l), spiperone Figures 8(m)–8(o), and EA + spiperone groups Figures 8(p)–8(r). The immunoreactivity of TH and GAP-43 decreased after spiperone treatment while EA or pergolide treatment increased the immunoreactivity of these neurons. There was colocalization of TH and GAP-43 (yellow) in some neurons in the model Figure 8(f), EA Figure 8(i), pergolide Figure 8(l), and EA + spiperone Figure 8(r) groups. Scale bar is 30 μm.

4. Discussion

Although two systematic reviews have indicated that there is no enough evidence to support the claim that acupuncture has a positive effect on functional recovery after stroke [15, 25], certain clinical studies have revealed that acupuncture may be an effective therapy for ischemic stroke [26]. Many recent clinical trials have verified that acupuncture can improve balance function [27] and spastic states [28] in stroke patients reduce muscle spasticity, and improve motor function in chronic stroke survivors with moderate or severe muscle spasticity [29]. Lewith et al. [30] systematically researched and reviewed the literature, looking at how acupuncture affects brain activation as measured by functional magnetic resonance imaging and positron emission tomography, and found that specific and largely predictable areas of brain activation and deactivation occur when traditional Chinese acupuncture is applied to certain specific acupuncture points. In addition, 46% of stroke survivors in the United States use some form of complementary and alternative medicine (CAM) therapy. Acupuncture was the most frequently used CAM therapy in stroke survivors [31]. However, the beneficial effects of acupuncture in stroke patients required more high-quality evidence [32]. Integrated with electrotherapy, EA is conducted by inserting acupuncture needles into acupoints and then changing

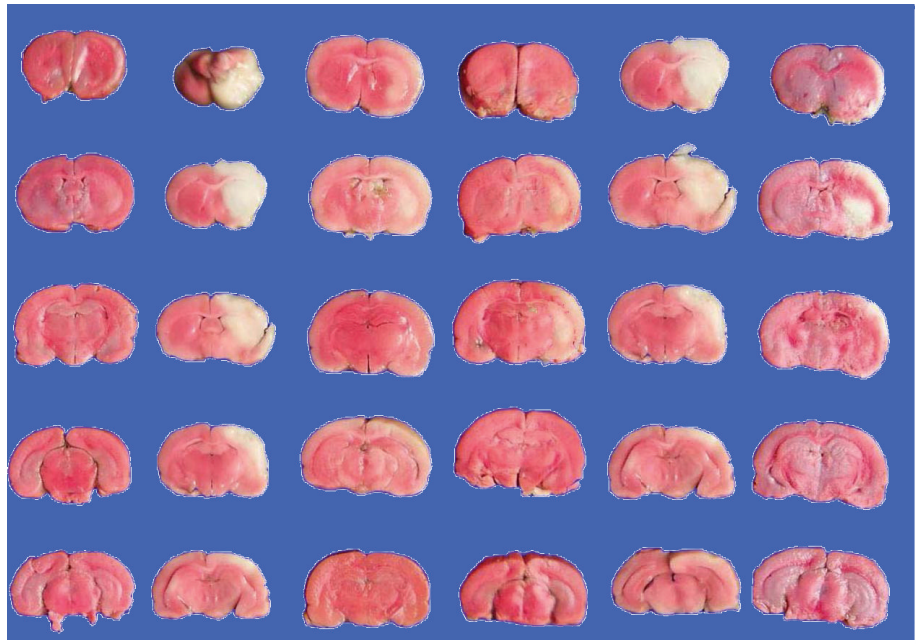

Figure 7: Effect of EA, pergolide, and spiperone on brain infarct area. Brain infarct area was determined using TTC staining. (a) Normal, (b) model, (c) EA, (d) pergolide, (e) spiperone, (f) EA + spiperone. Sections are arranged from rostral (top) to caudal (bottom).

electrical stimulation parameters, including the stimulation frequency, current intensity, pulse width, and pulse interval. Thus, EA not only inherits the benefits of traditional acupuncture but also combines the physiological effects of electric stimulation [33].

A large number of animal studies have shown that EA can reduce neural apoptosis, promote cell proliferation, increase cerebral blood flow (CBF), and improve neurological function after stroke [34–36]. These results provide some evidence for further translational studies.

Recent evidence suggests that nitric oxide, serotonin, catecholamines, and amino acids such as glutamate and γ-aminobutyric acid (GABA) are mediators of the neurobiological effects of acupuncture, but at present their role is still poorly understood. Therefore, acquiring further information about the neurobiological mechanisms of acupuncture should be the aim of research in the future [19].

There have often been discrepancies between neuroprotective drug studies in animals and clinical studies in humans. Many drugs appear to work in animal experiments but fail in clinical studies. In preclinical studies, determination of neuroprotection has relied heavily on assessment of infarct volume (instead of functional outcomes), short-term (instead of long-term) end points, short (instead of extended) time windows for drug administration, and protection of cerebral gray matter (instead of both gray and white matter). Current methodologies have been reevaluated. New concepts in ischemic pathophysiology should encourage researchers to think beyond the hyperacute phase of ischemia and consider multiagent therapies that exploit the brain's capacity for neuroplasticity and repair [37]. The reorganization of functional areas after ischemia and methods for assessing the restoration of function should compensate for the above shortcomings.

Functional restoration after a stroke relies on neuroplasticity, and neuroscience research has increasingly focused on studying this neuroplasticity [38]. Neuroplasticity has been defined as the ability of neurons and circuits to modify (1) their functional activity (short- or long-term potentiation/depression) and/or (2) their synaptic organization in accordance with variations in activity [39, 40]. Neuroplasticity is present at all points in an individual's lifespan: development, adulthood, after injury, during memory formation and/or learning, and so forth.

Even though neuroplasticity is especially intense and a key process during development, it is still present and necessary in adulthood [41]. The maintenance of neuroplastic activities is also necessary for nerve recovery after damage, such as stroke [42].

Behavioural examinations are the main means to determine early neuronal death after cerebral ischemic injury and are also a way to evaluate the restoration of neurological function caused by neuroplasticity. Since Longa et al. [43] developed their criteria for the evaluation of neurological deficits caused by cerebral ischemia in animals, this neurological deficit score has improved greatly and is now broadly applied to estimate the curative effects of diverse treatments on many kinds of animals [44]. Our research showed a rapid decline in rat behavioural scores after MCAO. BBT and NFDS scores were significantly improved after interventions with EA and D2R agonists, which indicate that these compounds promote recovery of neurological function after cerebral ischemic injury. FPT and HPT score changes appeared similar to the NFDS and BBT score changes seen 1, 3, 5, and 7 days after

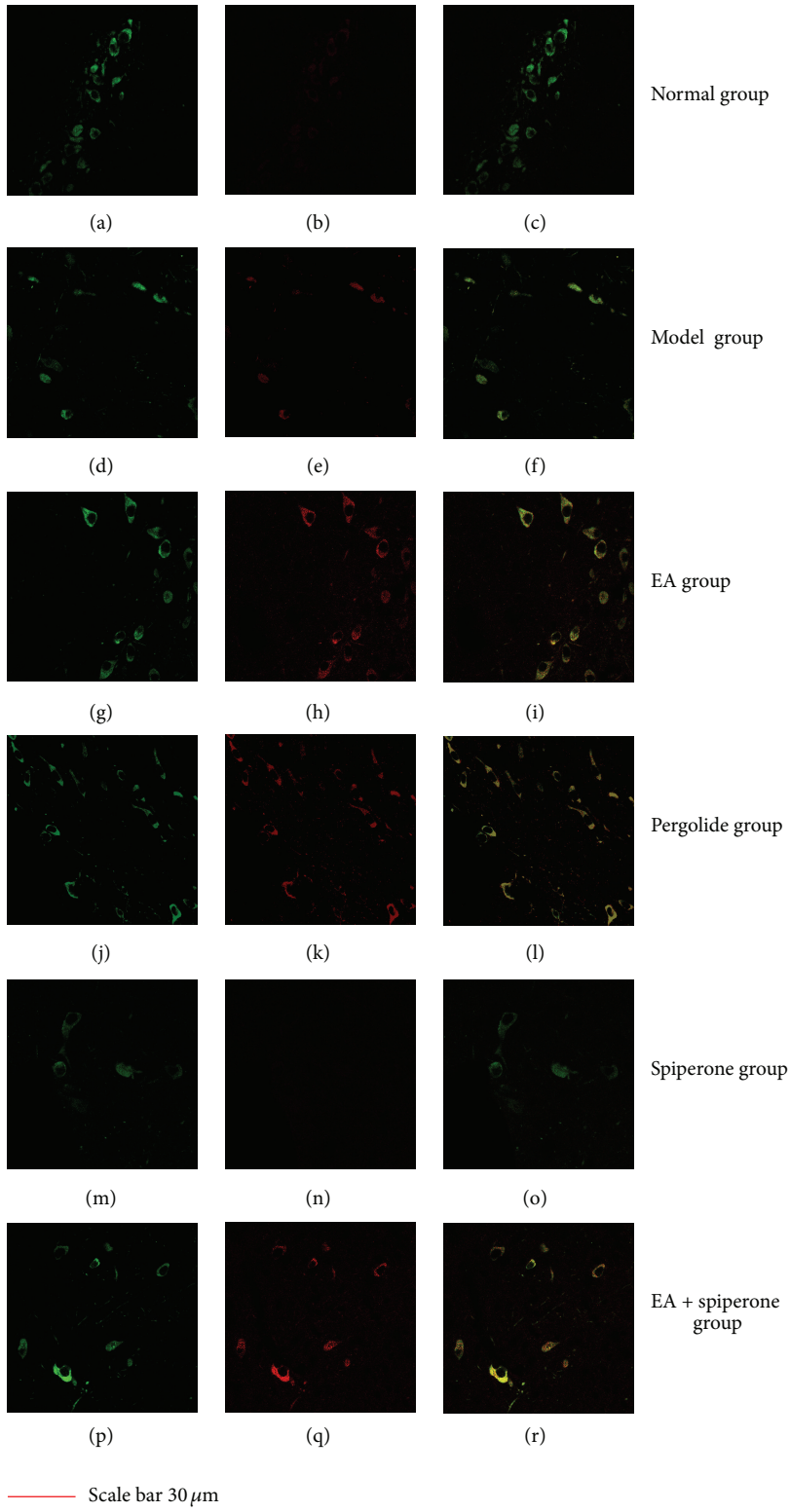

Figure 8: Fluorescence double staining of TH (tyrosine hydroxylase) and GAP-43 (growth-associated protein 43).

modeling. Spiperone decreased the FPT and HPT scores at 3 days after reperfusion. FPT and HPT scores were improved with spiperone and EA. EA has been shown to promote the expression of neurotrophic factors [15], effectively improve functional neural impairment, and promote brain plasticity. Studies have shown that D1R can enhance excitotoxicity and increase nerve damage [4].

It is necessary to combine behavioural observations with histopathology in order to reflect the progression of the disease and treatment more objectively. The results of TTC staining suggested that EA and D2R agonists could decrease the infarct area. Furthermore, D2R antagonists could increase the infarct area. The infarct area of each group with MCAO should be similar, but in fact, there was a significant difference between the EA group and the model group, similar to the difference seen between the pergolide group and the model group. These results suggest that EA and pergolide might save the ischemic penumbra and decrease the infarct volume through reducing or stopping the secondary injury after cerebral ischemia and reperfusion. On the contrary, spiperone aggravated the secondary injury. EA was able to partially reduce the injurious effects of spiperone. Our results indicate that D2R plays an important role in the injury-reducing effect of EA treatment for ischemia and reperfusion.

In addition to reducing injury after ischemia, DAergic neurons are important for neuroplasticity after ischemia. Research has shown that endogenous DA plays a physiological role through DR and TH. Dopamine receptors are classified into two categories: D1-like and D2-like. D1 receptors function primarily as postsynaptic heteroreceptors on non-DAergic neurons. In contrast, D2 receptors have dual roles in DA neurotransmission as autoreceptors and postsynaptic receptors [45].

A better understanding of DAergic neuroplasticity modulation will be important for understanding the rehabilitation processes, not only in animals but also in humans. Evidence exists for the participation of catecholamines in human plasticity. As previously shown, amphetamine (a catecholamine reuptake blocker) stabilizes use-dependent motor cortex plasticity, accelerates recovery of motor function in stroke patients, and improves learning and consolidation of verbal material [46–48]. Recent work has demonstrated that application of a single dose of levodopa significantly improves the formation of a motor memory in healthy subjects as well as in chronic stroke patients [49].

There is agreement that dopamine increases NMDA currents through D1 receptors [50]. Both D1 and NMDA receptors were suggested to contribute to the mechanisms of LTP by inducing the accumulation of cAMP and the activation of PKA [51].

The importance of D2 receptors for the induction of neuroplasticity has been described in animal experiments [52]. Moreover, it was demonstrated that D2 receptors determine the direction of neuroplastic changes in the striatum of mice [53]. In healthy humans, the D2 antagonist, SULP, and the predominant D2 antagonist, haloperidol, [54] impaired learning. This adds further behavioural evidence to the importance of D2 receptors for neuroplasticity in humans.

To further evaluate the role of DAergic neurons in neuroplasticity, cellular localization of GAP-43 formation was assessed in DAergic neurons by double immunostaining experiments (immunohistofluorescence for TH and GAP-43) performed after 7 days of ischemia. According to previous research, tyrosine hydroxylase was widely accepted as the marker of DAergic neurons [55]. GAP-43 is a calmodulin-binding phosphoprotein found in growing axons and growth cones of developing neurons and also in regenerating axons. The expression of GAP-43 might indicate the existence of a regeneration or neuroplasticity process, such as long-term potentiation. GAP-43 is considered a useful marker of developing neural connections and neuroplasticity or regenerating nerve fibres [56].

EA and pergolide led to an increase in GAP-43 expression in DAergic neurons. Spiperone decreased the co-localization of both. This effect of spiperone could be partly reversed by EA. The results of this study are additional evidence for a plasticity-enhancing effect of D2 receptor activity after ischemia and favour the hypothesis that for rehabilitation after stroke, DAergic treatment could enhance plastic reorganization of cortical areas. Indeed, some studies report a beneficial effect of DAergic medication, when combined with motor learning paradigms or physiotherapeutic rehabilitation after stroke [57].

Previous research has shown that transcranial direct current stimulation (tDCS) leads to modulation of cortical network plasticity by application of weak direct currents through the surface of the scalp. DA is necessary to induce this kind of neuroplasticity and it also strengthens and consolidates it [51, 57]. The EA treatment used in our research applied weak direct currents to acupoints near the scalp and produced a similar result. Moreover, our results indicate that the neuroplasticity induced by EA is mediated by a D2 autoreceptor in DAergic neurons.

In conclusion, the present findings imply that DAergic neurons play an important role in the induction of neuroplastic changes after ischemia, through a D2-like receptor, and that this receptor plays an important role in EA treatment for ischemia. Although important progress has been made in the comprehension of DAergic neuron function, the identification of the neuroplastic mechanisms of DAergic neurons in the CNS is a prerequisite in determining future research and rehabilitation strategies. A targeted protection of DAergic neurons could represent a novel and exciting approach to potentiate poststroke neuroregenerative responses [37].

Conflict of Interests

The authors declare that there is no conflict of interests.

Acknowledgments

This work was supported by the National Basic Research Program of China (973 Program, 2009CB522900), the National Natural Science Foundation of China (81001547), and Shanghai Leading Academic Discipline Project (S30304).

References

[1] G. A. Donnan, M. Fisher, M. Macleod, and S. M. Davis, "Stroke," *The Lancet*, vol. 371, no. 9624, pp. 1612–1623, 2008.

[2] W. Hacke, S. Schwab, M. Horn, M. Spranger, M. De Georgia, and R. Von Kummer, "'Malignant' middle cerebral artery territory infarction: clinical course and prognostic signs," *Archives of Neurology*, vol. 53, no. 4, pp. 309–315, 1996.

[3] Y.-G. Zhang, T.-P. Liu, Z.-Y. Qian, and D. Liu, "Influence of total saponins of Panax ginseng on infarct size and polyamine contents in rat brain after middle cerebral artery occlusion," *Chinese Journal of Pharmacology and Toxicology*, vol. 8, no. 4, pp. 250–255, 1994.

[4] S. Ishibashi, T. Kuroiwa, N. Katsumata, S. L. Yuan, S. Endo, and H. Mizusawa, "Extrapyramidal motor symptoms versus striatal infarction volume after focal ischemia in mongolian gerbils," *Neuroscience*, vol. 127, no. 2, pp. 269–275, 2004.

[5] H. Hodges, A. Nelson, D. Virley, T. R. Kershaw, and J. D. Sinden, "Cognitive deficits induced by global cerebral ischaemia: prospects for transplant therapy," *Pharmacology Biochemistry and Behavior*, vol. 56, no. 4, pp. 763–780, 1997.

[6] A. Nelson, A. Lebessi, P. Sowinski, and H. Hodges, "Comparison of effects of global cerebral ischaemia on spatial learning in the standard and radial water maze: relationship of hippocampal damage to performance," *Behavioural Brain Research*, vol. 85, no. 1, pp. 93–115, 1997.

[7] J. Nunn and H. Hodges, "Cognitive deficits induced by global cerebral ischaemia: relationship to brain damage and reversal by transplants," *Behavioural Brain Research*, vol. 65, no. 1, pp. 1–31, 1994.

[8] C. A. Netto, H. Hodges, J. D. Sinden et al., "Effects of fetal hippocampal field grafts on ischaemic-induced deficits in spatial navigation in the water maze," *Neuroscience*, vol. 54, no. 1, pp. 69–92, 1993.

[9] L. Zhihong, X. Lize, and Z. Zhenghua, "Acupoint specificity of electroacupuncture preconditioning effect on cerebral ischemia injury in rats," *Chinese Acuponcture & Moxibustion*, vol. 10, no. 013, 2002.

[10] K. R. Lees, J. A. Zivin, T. Ashwood et al., "NXY-059 for acute ischemic stroke," *The New England Journal of Medicine*, vol. 354, no. 6, pp. 588–600, 2006.

[11] B. Liu, Y. Liu, Y. Ling et al., "The herb medicine formula "chong Lou Fu Fang" increases the cytotoxicity of chemotherapeutic agents and down-regulates the expression of chemotherapeutic agent resistance-related genes in human gastric cancer cells in vitro," *Evidence-Based Complementary and Alternative Medicine*, vol. 2011, Article ID 834231, 10 pages, 2011.

[12] C.-S. Shia, Y.-C. Hou, S.-H. Juang et al., "Metabolism and Pharmacokinetics of San-Huang-Xie-Xin-Tang, a polyphenol-Rich chinese medicine formula, in rats and *Ex-Vivo* antioxidant activity," *Evidence-Based Complementary and Alternative Medicine*, vol. 2011, Article ID 721293, 9 pages, 2011.

[13] C.-J. Wu, J.-T. Chen, T.-L. Yen et al., "Neuroprotection by the traditional Chinese medicine, Tao-Hong-Si-Wu-Tang, against middle cerebral artery occlusion-induced cerebral ischemia in rats," *Evidence-Based Complementary and Alternative Medicine*, vol. 2011, Article ID 803015, 9 pages, 2011.

[14] P. Chou, H. Chu, and J.-G. Lin, "Effects of electroacupuncture treatment on impaired cognition and quality of life in Taiwanese stroke patients," *Journal of Alternative and Complementary Medicine*, vol. 15, no. 10, pp. 1067–1073, 2009.

[15] P. Wu, E. Mills, D. Moher, and D. Seely, "Acupuncture in poststroke rehabilitation: a systematic review and meta-analysis of randomized trials," *Stroke*, vol. 41, no. 4, pp. e171–e179, 2010.

[16] H. Liu, X. Shen, H. Tang, J. Li, T. Xiang, and W. Yu, "Using microPET imaging in quantitative verification of the acupuncture effect in ischemia stroke treatment," *Scientific Reports*, vol. 3, Article ID 1070, 2013.

[17] T. M. Jay, "Dopamine: a potential substrate for synaptic plasticity and memory mechanisms," *Progress in Neurobiology*, vol. 69, no. 6, pp. 375–390, 2003.

[18] S.-Y. Su, C.-Y. Cheng, T.-H. Tsai, and C.-L. Hsieh, "Paeonol protects memory after ischemic stroke via inhibiting β-secretase and apoptosis," *Evidence-Based Complementary and Alternative Medicine*, vol. 2012, Article ID 932823, 11 pages, 2012.

[19] S. Zhong, Z. Li, L. Huan, and B.-Y. Chen, "Neurochemical mechanism of electroacupuncture: anti-injury effect on cerebral function after focal cerebral ischemia in rats," *Evidence-Based Complementary and Alternative Medicine*, vol. 6, no. 1, pp. 51–56, 2009.

[20] T. Freret, P. Schumann-Bard Boulouard M, and V. Bouet, "On the importance of long-term functional assessment after stroke to improve translation from bench to bedside," *Experimental & Translational Stroke Medicine*, vol. 3, no. 6, pp. 1–5, 2011.

[21] Y. Zhou, N. Fathali, T. Lekic et al., "Remote limb ischemic postconditioning protects against neonatal hypoxic-ischemic brain injury in rat pups by the opioid receptor/akt pathway," *Stroke*, vol. 42, no. 2, pp. 439–444, 2011.

[22] F. Cheng, X. Zhong, Y. Lu et al., "Refined Qingkailing protects MCAO mice from endoplasmic reticulum stress-induced apoptosis with a broad time window," *Evidence-Based Complementary and Alternative Medicine*, vol. 2012, Article ID 567872, 12 pages, 2012.

[23] S. Kaewsuk, K. Sae-ung, P. Phansuwan-Pujito, and P. Govitrapong, "Melatonin attenuates methamphetamine-induced reduction of tyrosine hydroxylase, synaptophysin and growth-associated protein-43 levels in the neonatal rat brain," *Neurochemistry International*, vol. 55, no. 6, pp. 397–405, 2009.

[24] G. Maraula, C. Traini, T. Mello et al., "Effects of oxygen and glucose deprivation on synaptic transmission in rat dentate gyrus: role of A(2A) adenosine receptors," *Neuropharmacology*, vol. 67, pp. 511–520, 2013.

[25] J. C. Kong, M. S. Lee, B.-C. Shin, Y.-S. Song, and E. Ernst, "Acupuncture for functional recovery after stroke: a systematic review of sham-controlled randomized clinical trials," *Canadian Medical Association Journal*, vol. 182, no. 16, pp. 1723–1729, 2010.

[26] Y.-S. Kim, H. Jun, Y. Chae et al., "The practice of Korean medicine: an overview of clinical trials in acupuncture," *Evidence-Based Complementary and Alternative Medicine*, vol. 2, no. 3, pp. 325–352, 2005.

[27] S.-Y. Liu, C.-L. Hsieh, T.-S. Wei, P.-T. Liu, Y.-J. Chang, and T.-C. Li, "Acupuncture stimulation improves balance function in stroke patients: a single-blinded cotrolled, randomized study," *American Journal of Chinese Medicine*, vol. 37, no. 3, pp. 483–494, 2009.

[28] J.-G. Zhao, C.-H. Cao, C.-Z. Liu et al., "Effect of acupuncture treatment on spastic states of stroke patients," *Journal of the Neurological Sciences*, vol. 276, no. 1-2, pp. 143–147, 2009.

[29] W. Liu, M. Mukherjee, C. Sun, H. Liu, and L. K. McPeak, "Electroacupuncture may help motor recovery in chronic stroke survivors: a pilot study," *Journal of Rehabilitation Research and Development*, vol. 45, no. 4, pp. 587–595, 2008.

[30] G. T. Lewith, P. J. White, and J. Pariente, "Investigating acupuncture using brain imaging techniques: the current state of play," *Evidence-Based Complementary and Alternative Medicine*, vol. 2, no. 3, pp. 315–319, 2005.

[31] S. H. Shah, R. Engelhardt, and B. Ovbiagele, "Patterns of complementary and alternative medicine use among United States stroke survivors," *Journal of the Neurological Sciences*, vol. 271, no. 1-2, pp. 180–185, 2008.

[32] Z. Junhua, F. Menniti-Ippolito, G. Xiumei et al., "Complex traditional chinese medicine for poststroke motor dysfunction: a systematic review," *Stroke*, vol. 40, no. 8, pp. 2797–2804, 2009.

[33] X. Li, P. Luo, Q. Wang, and L. Xiong, "Electroacupuncture pretreatment as a novel avenue to protect brain against ischemia and reperfusion injury," *Evidence-Based Complementary and Alternative Medicine*, vol. 2012, Article ID 195397, 12 pages, 2012.

[34] J. Tao, X.-H. Xue, L.-D. Chen et al., "Electroacupuncture improves neurological deficits and enhances proliferation and differentiation of endogenous nerve stem cells in rats with focal cerebral ischemia," *Neurological Research*, vol. 32, no. 2, pp. 198–204, 2010.

[35] Y. Du, L. Shi, J. Li, J. Xiong, B. Li, and X. Fan, "Angiogenesis and improved cerebral blood flow in the ischemic boundary area were detected after electroacupuncture treatment to rats with ischemic stroke," *Neurological Research*, vol. 33, no. 1, pp. 101–107, 2011.

[36] Y. Liu, L.-P. Zou, J.-B. Du, and V. Wong, "Electro-acupuncture protects against hypoxic-ischemic brain-damaged immature rat via hydrogen sulfide as a possible mediator," *Neuroscience Letters*, vol. 485, no. 1, pp. 74–78, 2010.

[37] D. J. Gladstone, S. E. Black, and A. M. Hakim, "Toward wisdom from failure: lessons from neuroprotective stroke trials and new therapeutic directions," *Stroke*, vol. 33, no. 8, pp. 2123–2136, 2002.

[38] A. Nishiyama, M. Komitova, R. Suzuki, and X. Zhu, "Polydendrocytes (NG2 cells): multifunctional cells with lineage plasticity," *Nature Reviews Neuroscience*, vol. 10, no. 1, pp. 9–22, 2009.

[39] M. A. Nitsche, D. Liebetanz, W. Paulus, and F. Tergau, "Pharmacological characterisation and modulation of neuroplasticity in humans," *Current Neuropharmacology*, vol. 3, no. 3, pp. 217–229, 2005.

[40] J. Syka, "Plastic changes in the central auditory system after hearing loss, restoration of function, and during learning," *Physiological Reviews*, vol. 82, no. 3, pp. 601–636, 2002.

[41] P. Gil-Loyzaga, "Biological bases of neuroplasticity-In vivo and in vitro studies: interest for the auditory system," *Audiological Medicine*, vol. 7, no. 1, pp. 3–10, 2009.

[42] A. Sterr and A. B. Conforto, "Plasticity of adult sensorimotor system in severe brain infarcts: challenges and opportunities," *Neural Plasticity*, vol. 2012, Article ID 970136, 10 pages, 2012.

[43] E. Z. Longa, P. R. Weinstein, S. Carlson, and R. Cummins, "Reversible middle cerebral artery occlusion without craniectomy in rats," *Stroke*, vol. 20, no. 1, pp. 84–91, 1989.

[44] R. Ahmed, B. F. Zuberi, and S. Afsar, "Stroke scale score and early prediction of outcome after stroke," *Journal of the College of Physicians and Surgeons Pakistan*, vol. 14, no. 5, pp. 267–269, 2004.

[45] T. E. Foley and M. Fleshner, "Neuroplasticity of dopamine circuits after exercise: implications for central fatigue," *NeuroMolecular Medicine*, vol. 10, no. 2, pp. 67–80, 2008.

[46] H. R. Dinse, P. Ragert, B. Pleger, P. Schwenkreis, and M. Tegenthoff, "Pharmacological modulation of perceptual learning and associated cortical reorganization," *Science*, vol. 301, no. 5629, pp. 91–94, 2003.

[47] D. J. Gladstone, C. J. Danells, A. Armesto et al., "Physiotherapy coupled with dextroamphetamine for rehabilitation after hemiparetic stroke: a randomized, double-blind, placebo-controlled trial," *Stroke*, vol. 37, no. 1, pp. 179–185, 2006.

[48] D. Walker-Batson, P. Smith, S. Curtis, H. Unwin, and R. Greenlee, "Amphetamine paired with physical therapy accelerates motor recovery after stroke: further evidence," *Stroke*, vol. 26, no. 12, pp. 2254–2259, 1995.

[49] A. Flöel, C. Breitenstein, F. Hummel et al., "Dopaminergic influences on formation of a motor memory," *Annals of Neurology*, vol. 58, no. 1, pp. 121–130, 2005.

[50] J. K. Seamans and C. R. Yang, "The principal features and mechanisms of dopamine modulation in the prefrontal cortex," *Progress in Neurobiology*, vol. 74, no. 1, pp. 1–57, 2004.

[51] M.-F. Kuo, W. Paulus, and M. A. Nitsche, "Boosting focally-induced brain plasticity by dopamine," *Cerebral Cortex*, vol. 18, no. 3, pp. 648–651, 2008.

[52] D. Manahan-Vaughan and A. Kulla, "Regulation of depotentiation and long-term potentiation in the dentate gyrus of freely moving rats by dopamine D2-like receptors," *Cerebral Cortex*, vol. 13, no. 2, pp. 123–135, 2003.

[53] P. Calabresi, A. Saiardi, A. Pisani et al., "Abnormal synaptic plasticity in the striatum of mice lacking dopamine D2 receptors," *Journal of Neuroscience*, vol. 17, no. 12, pp. 4536–4544, 1997.

[54] K. Monte-Silva, D. Ruge, J. T. Teo, W. Paulus, J. C. Rothwell, and M. A. Nitsche, "D2 receptor block abolishes theta burst stimulation-induced neuroplasticity in the human motor cortex," *Neuropsychopharmacology*, vol. 36, no. 10, pp. 2097–2102, 2011.

[55] M. A. Raghanti, C. D. Stimpson, J. L. Marcinkiewicz, J. M. Erwin, P. R. Hof, and C. C. Sherwood, "Cortical dopaminergic innervation among humans, chimpanzees, and macaque monkeys: a comparative study," *Neuroscience*, vol. 155, no. 1, pp. 203–220, 2008.

[56] P. Gil-Loyzaga, F. Carricondo, M. V. Bartolomé, M. C. Iglesias, F. Rodríguez, and J. Poch-Broto, "Cellular and molecular bases of neuroplasticity: brainstem effects after cochlear damage," *Acta Oto-Laryngologica*, vol. 130, no. 3, pp. 318–325, 2010.

[57] M. A. Nitsche, C. Lampe, A. Antal et al., "Dopaminergic modulation of long-lasting direct current-induced cortical excitability changes in the human motor cortex," *European Journal of Neuroscience*, vol. 23, no. 6, pp. 1651–1657, 2006.

Hindawi Publishing Corporation
Evidence-Based Complementary and Alternative Medicine
Volume 2013, Article ID 608026, 6 pages
http://dx.doi.org/10.1155/2013/608026

Review Article

The Research of Acupuncture Effective Biomolecules: Retrospect and Prospect

Yu Wang, Lei-Miao Yin, Yu-Dong Xu, Yan-Yan Lui, Jun Ran, and Yong-Qing Yang

Molecular Biology Laboratory, Shanghai Research Institute of Acupuncture and Meridian, Yue Yang Hospital, Shanghai University of Traditional Chinese Medicine, Shanghai 200030, China

Correspondence should be addressed to Yong-Qing Yang; yyq@shutcm.edu.cn

Received 6 June 2013; Accepted 27 September 2013

Academic Editor: Xiang-Yu Hou

Acupuncture is an effective, safe and convenient therapy that has been applied for 2,500 years. The acupuncture researches have obtained significant improvement with the technical support of the life sciences and the studies of acupuncture have in turn accelerated the development of biomedical science. The effects of acupuncture influence important physiopathologic and biological activities, including gene expression, protein-protein interactions, and other biological processes. Cerebrospinal fluid, serum, organs, and tissues are reported to be carriers of the biomolecules of the effects of acupuncture. The paper summarized the progress of acupuncture effective biomolecules researches and found that biomolecules play important roles in the mechanism of acupuncture. With the development of omics technologies and translational medicine, the acupuncture research will meet both opportunities and challenges.

1. Introduction

Acupuncture is one of the key components of traditional Chinese medicine involving the insertion of solid filiform needles into the skin at specific points on the body to achieve therapeutic effects, acupuncture is considered to be the ancient Chinese art of healing [1, 2]. Using ancient scientific principles, acupuncture treats illnesses by bringing a person's body into harmony and regulating the balance of yin and yang. Since the Warring States period (475 BC–221 BC), acupuncture has been utilized for more than 2,500 years in China [3]. This technique spread throughout the Far East and Europe, then to America during the 19th century [4].

There have been two waves of development of acupuncture research since 1950s [5], when acupuncture was used as a technique to induce analgesic effect in the place of anesthetics during surgical procedures. The first wave was started in the late 1950s [6]. The Chinese government began to invest in research on acupuncture, and this nonconventional practice raised the interest of not only medical professionals over the world, but also basic researchers who would like to explore the possible mechanisms. What really launched acupuncture in the West, however, was a report in the New York Times in 1971 [7]. The report inspired a rush of American medical doctors to China to investigate acupuncture analgesia. There was a marked increase in acupuncture research in the 1990s. In terms of the increase in the number of SCI-Expanded journal papers, acupuncture literature can be divided into two phases. The first phase dated from 1973 to 1997, and during these years, the number of articles fluctuated to plateau at an average of 85 papers per year. The number of articles showed a dramatic 40% increase in 1998 and continued to increase [5]. This growth might be encouraged by two events. The first one was the "NIH Consensus Development Conference on Acupuncture" held in 1997 in Bethesda, MD. The second event was that the National Center for Complementary and Alternative Medicine (NCCAM) was inaugurated under the USA NIH in 1998 [5].

In recent years, the researches of Chinese medicine, specifically acupuncture, have shown significant improvement with technical supports of the life sciences. Simultaneously studies in acupuncture have in turn accelerated the development of medicine as well as understanding of biomedical science. For example, the achievements of fifty years of acupuncture anesthesia research and application have enriched the gate control theory of pain and clarified the underlying

mechanism of endorphin release. In the last half of century scientific research on acupuncture, coupled with advances in knowledge about pain control mechanisms, has yielded facts sufficient to develop acupuncture analgesia [8]. The principle research has been developing for nearly half century, during which acupuncture anesthesia has played an important role and made remarkable contribution to research hypotheses and methods. The research of acupuncture is not only a method but also the source of the development of concept, cognition, and methodology. A systematic review outlining 50 years of principal research of acupuncture in China and summarizing the basic regulation and characteristics of acupuncture may play a guiding role in the future development of this discipline.

Biological systems are composed of two factors of information: genes and networks of regulatory interactions. This information is hierarchical in nature: DNA → mRNA → protein → protein interactions → informational pathways → informational networks → cells → tissues or networks of cells → an organism → populations → ecologies [9]. Other macromolecules and small molecules also participate in these information hierarchies [9]. The effects of acupuncture are through the influences on physiological and pathological processes after the stimulation on acupoints. The research on biomolecules of acupuncture goes a long way towards explaining the biological processes from gene expression and protein functional expression as well as the information reaction sequence and rule of protein interaction.

The acupuncture effective biomolecules are biological molecules which have similar acupuncture effect and were produced by a living organism response to acupuncture, including macromolecules and small molecules, such as proteins, polysaccharides, lipids, nucleic acids, and primary and secondary metabolites. It is reported that the cerebrospinal fluid, serum, organs, and tissues of the acupoint are the carriers of biomolecules of acupuncture effects, which contain various acupuncture effective biomolecules and have acupuncture-like effect added into experimental system *in vivo* or *in vitro*. This review aims to summarize the progress of acupuncture effective biomolecules researches, which provides clues and guides for the acupuncture development.

2. Acupuncture Effective Biomolecules in the Cerebrospinal Fluid

The effect of acupuncture analgesia for surgery is based on chemical mediations. The transfer of the cerebrospinal fluid (CSF) of rabbit under acupuncture analgesia to the third ventricle of a naive recipient animal produced an analgesic effect in the second rabbit. The results showed that transmitters in the CSF were responsible for the analgesic effect [10]. Li et al. showed that the classical neurotransmitter serotonin was an important mediator of acupuncture analgesia [11]. Han et al. [12, 13] used the antibody injection technique to show that enkephalins and beta-endorphin are mediators for acupuncture analgesia in the brain. Dynorphins were effective in the spinal cord but not in the brain [14]. Important correlations of the endorphins in acupuncture analgesia hypothesis were found in the report of Sjolund et al. [15], which showed that endorphins were increased in the CSF after electroacupuncture stimulation.

Different frequencies of stimulation can affect the release of different neuropeptides. Han et al. [16] showed with serial samples of CSF from human volunteers that different types of neuropeptides can be released in the CNS by simply changing the frequency of electrical stimulation without moving the position of the needle. Low frequency (2 Hz) electroacupuncture increases the content of beta-endorphin and met-enkephalin in the CSF, whereas high frequency (100 Hz) accelerated the release of dynorphin. This scientific evidence of frequency-specific effects that are wide spread throughout the CNS was different from the symptom-specific metaphysical theories of specific acupoint needle stimulation. However, stimulation of different points representing different neurotomes can also produce action on those body structures innervated by the neurotomes.

The above-mentioned work was the milestone of acupuncture research. The National Institute of Health consensus conference in 1997 recognized acupuncture (and by extension Traditional Chinese Medicine) as a legitimate branch of scientific medicine. Acupuncture has received an enormous boost in the last few years and seems destined to be accepted and incorporated into Western medicine. Research on acupuncture analgesia has shown a substantial basis for acupuncture and promoted the development of neurophysiology.

3. Acupuncture Effective Biomolecules in Serum

Serum includes all of the proteins not used in blood clotting (coagulation) and all the electrolytes, antibodies, antigens, hormones, and any exogenous substances (e.g., drugs and microorganisms). The serum of an animal is used to provide immunity to a pathogen or toxin by inoculation or as a diagnostic agent [17]. With biological activity, as carrier of acupuncture effective components, serum has received a great deal of attention during the past twenty years in China.

In the regular experiment, serum was considered to be an ordinary sample. However, serum was now recognized as carrier of acupuncture effective biomolecules. Regardless of the source of human or animal, sera that prior to or after acupuncture treatment were added into an *in vitro* reaction system as an effect substance. Through contacting with target objectives biomolecules of acupuncture effects, serum effects can be observed to evaluate the function of acupuncture and moxibustion [18]. The acupuncture effect is closely associated with the induced specific proteins by acupuncture and moxibustion. This will become an epoch-making discovery when "the needling or moxibustion can induce specific proteins" and can be proved as a universal phenomenon [18].

Serum after acupuncture (SA) shows biological activity similar to acupuncture *in vivo* and *in vitro*. In the *in vivo* experimental system, the SA was injected into an experimental animal. After the intravenous injection of SA, SA can decreased the eosinophil counts in the peripheral blood [19]. To observe the SA effects on a cell *in vitro*, a cell was cultured

within a culture media containing SA. A different research work showed that SA can reduce the number of osteoclasts *in vitro* [20], decrease the Ca^{2+} level in cultured myocardial cells [21], decrease the Ca^{2+} level in cultured cells of the cerebral cortex [22, 23], and promote the growth of a tumor-infiltration lymphocyte both in the aspects of proliferation and phenotypes [24].

The research on SA *in vivo* and *in vitro* provides direct evidence of biomolecules in SA. The acupuncture serum samples were separated by gel filtration into three segments according to molecular weight [25], and each segments could decreased the eosinophil counts in the peripheral blood. The effective components of acupuncture serum from asthmatic rats treated by acupuncture for eosinophils were not single component, and acupuncture stimulation may produce many types of components of antiasthma [19]. In further research, two-dimensional protein electrophoresis was employed to analyze the differential proteins in the serum with antiasthma activity of acupuncture, and differential proteins such as cyclophilin A and zinc finger protein 91 were identified with mass spectrometry. There were multitarget effects regulating the whole body in acupuncture treating asthma relating to immunoregulation, gene expression, and proteins synthesization. The effects of acupuncture on the response of proteins warrant further research [26, 27].

4. Acupuncture Effective Biomolecules in Organs

Clinical observation and principal research on acupuncture focus on the adjustment of the zang-fu organ and have shown that the adjustment by acupuncture relied largely on the neuroendocrine-immune network, which also provide new evidences for the acupuncture effective components in different organs.

Four SAGE libraries of the lungs of the control rats (CK), asthmatic rats (AS), asthmatic rats treated by acupuncture (ASAC), and control rats treated by acupuncture (CKAC) were established and bioinformatics analyses were conducted. The study found that the gene expression profile of the AS and ASAC was more similar than that of the other groups by the hierarchical dendrogram; 21 specific genes regulated by acupuncture in the asthmatic model, such as the S100 calcium binding protein A9 (S100A9), metallothionein-2 (MT-2), and the dual specificity protein phosphatase 1 (Dusp1) were found by Venn graph; three key gene categories, such as "immune response," "response to steroid hormone stimulus," and "homeostatic process," were closely associated with acupuncture treatment for asthma via DAVID functional analysis; DAG analysis suggested that acupuncture was a biological process which regulated the genesis of endocorticosteroids and inhibited immune response in asthma treatment; the KEGG pathways indicated that the genesis and regulation of the hormone and immune response were involved in acupuncture treatment for asthma [28]. Using two-dimensional gel electrophoresis (2DE) and mass spectrometry, pulmonary proteins such as S100A8, S100A11, and the Clara cell 10-kDa protein (CC10) were found, which could be used to identify new drug candidates for the prophylaxis and treatment of asthma [29].

Several key effective molecules of acupuncture were selected for validation of their function. As a member of the S100 family, the S100A9 protein, which originate from lung, elicits dose-dependent antiasthmatic effects and may provide further insight into the treatment of asthma [30]. The CC10 protein that is secreted by the nonciliated, nonmucous, secretary epithelial Clara cells of the pulmonary airways showed that it could inhibit the proliferation of airway smooth muscle cells and migration induced by platelet-derived growth factor (PDGF), and this suppressive effect might be associated with the inhibition of cyclin D1 expression [31].

Pulmonary functions changes were closely related to the rectal resting pressure in the rat model of asthma and constipation, and the lung homogenate could significantly contract the large intestine muscle strip [32]. This relationship could be effectively regulated by acupuncture, and the phenomenon suggested that there were effective biomolecules in the lung homogenate.

5. Acupuncture Effective Biomolecules in Acupoints Tissues

Researchers have investigated the specific structure of the acupoint tissues, but there has been limited progress without convincing results. In the last 20 years, research on the local molecular mechanism of acupuncture has progressed gradually. Preliminary research suggested that histamine and adenosine were effective biomolecules of acupuncture information generated locally at acupoint.

During the needling manipulation process, the needle is being grasped by connective tissue as a result of collagen and elastic fibers winding and tightening around the needle, delivering a cellular signal conducted along the pathway of channels (meridians) and leading to downstream effects that activate certain cellular pathways and facilitate healing [33]. Collagen fibers play an important role in acupuncture-induced analgesia, and they participate in signal transmission and transform processes [34]. The analgesic effect was more pronounced after stimulation of the Zusanli (ST36) point than after stimulation of a sham point near the true acupuncture point. The density of mast cells from the Zusanli (ST36) point of rats was higher than that from a nearby sham point. In addition, acupuncture resulted in a remarkable increase in degranulation of mast cells. Disodium cromoglycate (DSCG) is in the mast cell stabilizers, caused a concentration-dependent inhibition of histamine release [35, 36]. Pretreatment of the acupuncture point with disodium cromoglycate (DSCG) not only counteracted the phenomenon of degranulation but also reduced the analgesic effect of acupuncture. Experiments on inhibition of the degranulation of mast cells in tissue from acupuncture points demonstrate the possible role of mast cells in the effects of acupuncture [37].

The mast cell densities were higher in the acupoints than in the nonacupoints. Effective nerve conduction signaling in manual acupuncture (MA) analgesia was generated after

the degranulation of mast cells in the process of acupoints activation or needle sense, which was the direct cause of generation of the nerve signals [38]. There was a positive correlation between the mast cell degranulation rate and the analgesic effects [39]. After activation, mast cells express histamine, leukotrienes, and prostanoids, as well as proteases, and many cytokines and chemokines [40, 41]. These mediators were pivotal to the genesis of an inflammatory response [42]. Transmitters released by mast calls can increase vascular permeability and induce local edema and mild authigenic inflammatory response [43]. On one hand, this possibly promotes aggregation of mast cells in focal and other places towards acupoints via induced adhesion molecules and chemotactic factors; on the other hand, it can activate immune system, and expand local acupuncture effect to the entire body [44]. Acupuncture has a significant analgesia and enhances the degranulation of mast apparently cells, which was weakened by injection of disodium cromoglycate (DSC) in the acupoint area, suggesting an important role of mast cells in acupuncture-induced analgesia [45].

Adenosine is a neuromodulator with antinociceptive properties [46]. ATP is released in response to mechanical and electrical stimulation or heat. Once released, ATP acts as a transmitter that binds to the purinergic receptors [47, 48], and it cannot be transported back into a cell but was rapidly degraded to adenosine by several ectonucleotidases before reuptake [48]. Thus, adenosine acted as an analgesic agent that suppresses pain through Gi-coupled A1-adenosine receptors [49, 50]. A researcher collected samples of interstitial fluid by a microdialysis probe implanted in the tibialis anterior muscle/subcutis of adult mice at a distance of 0.4–0.6 mm from the Zusanli (ST36) point, and the adenine nucleotides and adenosine were quantified using high-performance liquid chromatography (HPLC) before, during, and after acupuncture. Adenosine was released during acupuncture and its antinociceptive actions required the adenosine A1 receptor expression. Direct injection of an adenosine A1 receptor agonist replicated the analgesic effect of acupuncture. Inhibition of the enzymes involved in adenosine degradation potentiated the acupuncture-elicited increase in adenosine, as well as its antinociceptive effect. The observations indicate that adenosine mediates the effects of acupuncture and interfering with adenosine metabolism may prolong the clinical benefit of acupuncture [51].

Further research was conducted with human subjects. The interstitial adenosine concentration increased significantly during acupuncture and remained elevated for 30 minutes after acupuncture. Acupuncture-mediated adenosine release was not observed if acupuncture was not administered in the Zusanli (ST36) point or if the acupuncture needle was inserted, but not rotated. The study strengthened the role of adenosine in acupuncture-mediated antinociception by directly providing such evidence in humans [52]. The research presents further evidence of the role of adenosine in acupuncture-mediated antinociception by demonstrating that local adenosine concentrations increase in the acupoint in human subjects receiving traditional acupuncture.

6. Perspective

Acupuncture is the pilot subject to increase global acceptance of Chinese medicine. This technique is accepted by the scientific community because it is an effective therapy, the biological effect of acupuncture is unique, and it has biological significance for the research of the human biology. Previous research on acupuncture anesthesia principle research played an important role by establishing the basis and methodology of acupuncture research, which has made an important scientific contribution. The research investigating acupuncture anesthesia and acupuncture analgesia promoted the knowledge of pain physiology.

Since 1998, global acupuncture research has developed rapidly [5]. In the beginning of the 21st century, the acupuncture research has also passed on to the postgenome era [53]. The effects of acupuncture comprise a complicated biological process, and many biological molecules are involved. Systems biology techniques, such as functional genomics and proteomics, are involved in an increasing number of applications in the field of acupuncture research. With the development of biological technology such as high-throughput omics technology (genomics, transcriptomics, proteomics, metabolomics, and beyond) [54], the fundamental biological processes of acupuncture can be studied by applying the full range of omics technologies to reveal the mechanism of the effect of acupuncture.

The effects of acupuncture include non-specific effects and specific effects and acupuncture effective biomolecules can be either nonspecific effective biomolecules or specific effective biomolecules. Endogenous opioid peptides (enkephalin, dynorphin, endorphins, and orphanin) and purine (adenosine) were significant but non-specific effective biomolecules of acupuncture anesthesia and acupuncture analgesia. These non-specific effective biomolecules are produced by the acupuncture and are not based on a specific body state. Biomolecules originate from specific organs of the disease model, such as S100A9 and CC10, and represented the specific effect of acupuncture. Additional specific effective biomolecules could be discovered by more research into the different types of diseases.

Translational medicine is a relatively young area of biomedicine, and it has developed rapidly and become more interdisciplinary in the past 10 years [55], which is becoming ever-more interdisciplinary. The combination of translational medicine and acupuncture effectiveness and target drug discovery based on acupuncture effect biomolecules will promote the application of acupuncture. These combined processes will also promote the development of biological medicine.

Conflict of Interests

The authors have declared that no competing interests exist.

Authors' Contribution

Yu Wang and Lei-Miao Yin contributed equally to this work.

Acknowledgments

This work was supported by the National Natural Science Foundation of China (nos. 81001548, 81173341, 81173332, and 81202753) and the Project Supported by Open Research Fund of Zhejiang First-foremost Key Subject-Acupuncture & Moxibustion (no. ZTK2010A02).

References

[1] F. Mann, *Acupuncture: The Ancient Chinese Art of Healing and How It Works Scientifically*, Vintage Books, New York, NY, USA, 1973.

[2] G. Li, J.-M. Liang, P.-W. Li et al., "Physiology and cell biology of acupuncture observed in calcium signaling activated by acoustic shear wave," *Pflugers Archiv European Journal of Physiology*, vol. 462, no. 4, pp. 587–597, 2011.

[3] J.-N. Wu, "A short history of acupuncture," *Journal of Alternative and Complementary Medicine*, vol. 2, no. 1, pp. 19–21, 1996.

[4] E. Lee, "Chinese American families," *Working with Asian Americans: A Guide for Clinicians*, pp. 46–78, 1997.

[5] J.-S. Han and Y.-S. Ho, "Global trends and performances of acupuncture research," *Neuroscience and Biobehavioral Reviews*, vol. 35, no. 3, pp. 680–687, 2011.

[6] G.-C. Wu, "Acupuncture anesthesia in China: retrospect and prospect," *Chinese Journal of Integrative Medicine*, vol. 13, no. 3, pp. 163–165, 2007.

[7] Reston, *Now, About my Operation in Peking; Now, Let Me Tell You about my Appendectomy in Peking*, The New York Times, 1971.

[8] G. A. Ulett, S. Han, and J.-S. Han, "Electroacupuncture: mechanisms and clinical application," *Biological Psychiatry*, vol. 44, no. 2, pp. 129–138, 1998.

[9] T. Ideker, T. Galitski, and L. Hood, "A new approach to decoding life: systems biology," *Annual Review of Genomics and Human Genetics*, vol. 2, pp. 343–372, 2001.

[10] Research Group of Acupuncture Anesthesia PMC, "The role of some neurotransmitters of the brain in finger-acupuncture analgesia," *Scientia Sinica*, vol. 17, no. 1, pp. 112–130, 1974.

[11] S. J. Li, J. Tang, and J. S. Han, "The implication of central serotonin in electro-acupuncture tolerance in the rat," *Scientia Sinica B*, vol. 25, no. 6, pp. 620–629, 1982.

[12] J. S. Han, G. X. Xie, Z. F. Zhou, R. Folkesson, and L. Terenius, "Enkephalin and beta-endorphin as mediators of electroacupuncture analgesia in rabbits: an antiserum microinjection study," *Advances in Biochemical Psychopharmacology*, vol. 33, pp. 369–377, 1982.

[13] G. X. Xie, J. S. Han, and V. Hollt, "Electroacupuncture analgesia blocked by microinjection of anti-beta-endorphin antiserum into periaqueductal gray of the rabbit," *International Journal of Neuroscience*, vol. 18, no. 3-4, pp. 287–291, 1983.

[14] Q. S. Chen, C. W. Xie, J. Tang, and J. S. Han, "Effect of electi oacupuncture on the content of immunoreactive beta endorphin in the rat's brain regions," *Kexue Tong Bao*, vol. 28, no. 5, pp. 312–312, 1983.

[15] B. Sjolund, L. Terenius, and M. Eriksson, "Increased cerebrospinal fluid levels of endorphins after electro-acupuncture," *Acta Physiologica Scandinavica*, vol. 100, no. 3, pp. 382–384, 1977.

[16] J. S. Han, X. H. Chen, S. L. Sun et al., "Effect of low- and high-frequency TENS on Met-enkephalin-Arg-Phe and dynorphin A immunoreactivity in human lumbar CSF," *Pain*, vol. 47, no. 3, pp. 295–298, 1991.

[17] The Oxford English Dictionary and Oxford Dictionaries, http://oxforddictionaries.com/.

[18] Y.-Q. Yang, Y. Wang, and L.-M. Yin, "Prof. CHEN Han-ping: a thinker in principles and practice of acupuncture-moxibustion," *Journal of Acupuncture and Tuina Science*, vol. 8, no. 4, pp. 199–203, 2010.

[19] H. M. Xu, S. L. Ma, Y. Q. Yang, and Y. Y. Zhang, "Effects of different segments of acupuncture serum on eosinophil counts in the rat with eosinophilia," *Zhongguo Zhen Jiu*, vol. 25, no. 4, pp. 272–274, 2005.

[20] Y.-X. Zhao, J. Wang, Y.-R. Qin et al., "Effect of acupuncture serum on the number of osteclast cultured in vitro," *Zhongguo Zhen Jiu*, vol. 27, no. 7, pp. 521–524, 2007.

[21] M.-F. Luo, C.-H. Li, J.-L. Zhang et al., "Acupuncture-serum decreases $Ca2^{+}$ content in cultured rat myocardial cells," *Zhongguo Zhen Jiu*, vol. 26, no. 5, pp. 367–370, 2006.

[22] R. W. Li, J. L. Zhang, Y. Guo, and C. H. Li, "Preliminary study on effect of acupuncture serum on $Ca2^{+}$ content in cultured neurons of cerebral cortex," *Zhongguo Zhen Jiu*, vol. 25, no. 5, pp. 351–354, 2005.

[23] J.-L. Zhang, Y. Guo, R.-W. Li, C.-H. Li, and M.-F. Luo, "Protecting action of acupuncture serum on calcium over-loaded neurons of the hippocampus in rats of ischemia-reperfusion," *Zhongguo Zhen Jiu*, vol. 29, no. 1, pp. 45–47, 2009.

[24] Y. Chen, C. Zhao, H. Chen, H. Qin, and F. Fang, "Effects of "moxibustion serum" on proliferation and phenotypes of tumor infiltrating lymphocytes," *Journal of Traditional Chinese Medicine*, vol. 23, no. 3, pp. 225–229, 2003.

[25] H. M. Xu, S. L. Ma, Y. Q. Yang, L. P. Cui, and Y. Wang, "Study on serum segments separated from the acupuncture serum by gel filtration "Abstract"," *Journal of Acupuncture and Tuina Science*, vol. 3, no. 3, 2005.

[26] Y. Wang, J. M. Cui, S. L. Ma, Y. Y. Liu, L. M. Yin, and Y. Q. Yang, "Proteomics analysis of component in serum with anti-asthma activity derived from rats treated by acupuncture," *Journal of Acupuncture and Tuina Science*, vol. 7, no. 1, 2009.

[27] Y. Wang, Y.-Q. Yang, S.-L. Ma, J.-M. Cui, and Y.-Y. Liu, "SDS-PAGE analysis of components in serum with anti-asthma activity derived from rats treated by acupuncture," *Journal of Acupuncture and Tuina Science*, vol. 7, no. 1, pp. 8–12, 2009.

[28] L.-M. Yin, G.-H. Jiang, Y. Wang et al., "Use of serial analysis of gene expression to reveal the specific regulation of gene expression profile in asthmatic rats treated by acupuncture," *Journal of Biomedical Science*, vol. 16, no. 1, article 46, 2009.

[29] Y. D. Xu, J. M. Cui, Y. Wang et al., "Proteomic analysis reveals the deregulation of inflammation-related proteins in acupuncture-treated rats with asthma onset," *Evidence-Based Complementary and Alternative Medicine*, vol. 2012, Article ID 850512, 14 pages, 2012.

[30] L.-M. Yin, H.-Y. Li, Q.-H. Zhang et al., "Effects of S100A9 in a rat model of asthma and in isolated tracheal spirals," *Biochemical and Biophysical Research Communications*, vol. 398, no. 3, pp. 547–552, 2010.

[31] Y. Wei, Y. D. Xu, L. M. Yin et al., "Recombinant rat CC10 protein inhibit PDGF-induced airway smoothmuscle cells proliferation 5 andmigration," *BioMed Research International*, vol. 2013, Article ID 690937, 8 pages, 2013.

[32] L. M. Yin, G. Q. Zhang, X. K. Yan, Y. Wang, Y. D. Xu, and Y. Q. Yang, "An In Vivo and In Vitro Evaluation of the Mutual

Interactions between the Lung and the Large Intestine," *Evidence-Based Complementary and Alternative Medicine*, vol. 2013, Article ID 695641, 9 pages, 2013.

[33] H. M. Langevin, D. L. Churchill, and M. J. Cipolla, "Mechanical signaling through connective tissue: a mechanism for the therapeutic effect of acupuncture," *The FASEB Journal*, vol. 15, no. 12, pp. 2275–2282, 2001.

[34] X. Yu, G. Ding, H. Huang, J. Lin, W. Yao, and R. Zhan, "Role of collagen fibers in acupuncture analgesia therapy on rats," *Connective Tissue Research*, vol. 50, no. 2, pp. 110–120, 2009.

[35] E. J. Kusner, B. Dubnick, and D. J. Herzig, "The inhibition by disodium cromoglycate in vitro of anaphylactically induced histamine release from rat peritoneal mast cells," *Journal of Pharmacology and Experimental Therapeutics*, vol. 184, no. 1, pp. 41–46, 1973.

[36] A. B. Kay, G. M. Walsh, and R. Moqbel, "Disodium cromoglycate inhibits activation of human inflammatory cells in vitro," *Journal of Allergy and Clinical Immunology*, vol. 80, no. 1, pp. 1–8, 1987.

[37] D. Zhang, G. Ding, X. Shen et al., "Role of mast cells in acupuncture effect: a pilot study," *Explore*, vol. 4, no. 3, pp. 170–177, 2008.

[38] H. Huang, R. Zhan, X.-J. Yu, D. Zhang, W.-M. Li, and G.-H. Ding, "Different effects and peripheral mechanism between manual-acupuncture and electroacupuncture on mast cell function and acupuncture analgesia by nerve block in acupionts," *Journal of Acupuncture and Tuina Science*, vol. 6, no. 5, pp. 273–275, 2008.

[39] K. Cheng, G. H. Ding, X. Y. Shen, and F. Wu, "Relationship between and laser acupuncture analgesia and the function of mast cells in adjuvant arthritis rats," *Journal of Acupuncture and Tuina Science*, vol. 7, no. 1, 7 pages, 2009.

[40] E. Crivellato, D. Ribatti, F. Mallardi, and C. A. Beltrami, "The mast cell: a multifunctional effector cell," *Advances in Clinical Pathology*, vol. 7, no. 1, pp. 13–26, 2003.

[41] D. D. Metcalfe, D. Baram, and Y. A. Mekori, "Mast cells," *Physiological Reviews*, vol. 77, no. 4, pp. 1033–1079, 1997.

[42] G. Krishnaswamy, O. Ajitawi, and D. S. Chi, "The human mast cell: an overview," *Methods in Molecular Biology*, vol. 315, pp. 13–34, 2006.

[43] D. Zhou, P. Pan, Y. Guo, Y.-M. Guo, and L.-P. Wu, "Inflammatory reaction caused by acupuncture is one of the initial factors of acupuncture effect," *Zhongguo Zhen Jiu*, vol. 29, no. 1, pp. 32–34, 2009.

[44] M.-F. Luo, J.-N. He, Y. Guo, C.-H. Li, and J.-L. Zhang, "Effect of electroacupuncture and moxibustion of "Dazhui" (GV14) on the number and distribution of degranulated mast cells in GV14 region," *Zhen Ci Yan Jiu*, vol. 32, no. 5, pp. 327–329, 2007.

[45] D. Zhang, G.-H. Ding, X.-Y. Shen et al., "Influence of mast cell function on the analgesic effect of acupuncture of "Zusanli" (ST 36) in rats," *Zhen Ci Yan Jiu*, vol. 32, no. 3, pp. 147–152, 2007.

[46] J. Giordano, "The neurobiology of nociceptive and anti-nociceptive systems," *Pain Physician*, vol. 8, no. 3, pp. 277–290, 2005.

[47] B. D. Gulbransen and K. A. Sharkey, "Purinergic neuron-to-glia signaling in the enteric nervous system," *Gastroenterology*, vol. 136, no. 4, pp. 1349–1358, 2009.

[48] G. Burnstock, "Physiology and pathophysiology of purinergic neurotransmission," *Physiological Reviews*, vol. 87, no. 2, pp. 659–797, 2007.

[49] K.-F. Sjölund, M. Segerdahl, and A. Sollevi, "Adenosine reduces secondary hyperalgesia in two human models of cutaneous inflammatory pain," *Anesthesia and Analgesia*, vol. 88, no. 3, pp. 605–610, 1999.

[50] S. Maione, V. de Novellis, L. Cappellacci et al., "The antinociceptive effect of 2-chloro-2′-C-methyl-N6-cyclopentyladenosine (2′-Me-CCPA), a highly selective adenosine A1 receptor agonist, in the rat," *Pain*, vol. 131, no. 3, pp. 281–292, 2007.

[51] N. Goldman, M. Chen, T. Fujita et al., "Adenosine A1 receptors mediate local anti-nociceptive effects of acupuncture," *Nature Neuroscience*, vol. 13, no. 7, pp. 883–888, 2010.

[52] T. Takano, X. Chen, F. Luo et al., "Traditional acupuncture triggers a local increase in adenosine in human subjects," *Journal of Pain*, vol. 13, no. 12, pp. 1215–1223, 2012.

[53] G. L. Kenyon, D. M. DeMarini, E. Fuchs et al., "Defining the mandate of proteomics in the post-genomics era: workshop report," *Molecular & Cellular Proteomics*, vol. 1, no. 10, pp. 763–780, 2002.

[54] N. Morrison, G. Cochrane, N. Faruque et al., "Concept of sample in OMICS technology," *OMICS A Journal of Integrative Biology*, vol. 10, no. 2, pp. 127–137, 2006.

[55] X. Wu, F. M. Marincola, M. N. Liebman, and X. Wang, "A global resource to translational medicine: the International Park of Translational Medicine and BioMedicine (IPTBM)," *Journal of Translational Medicine*, vol. 11, article 8, 2013.

Hindawi Publishing Corporation
Evidence-Based Complementary and Alternative Medicine
Volume 2013, Article ID 795365, 12 pages
http://dx.doi.org/10.1155/2013/795365

Research Article

Postischemic Long-Term Treatment with Qiangli Tianma Duzhong Capsule Improves Brain Functional Recovery via the Improvement of Hemorrheology and the Inhibition of Platelet Aggregation in a Rat Model of Focal Cerebral Ischemia

Li-Zhi Hong,[1] Wei-wei Gu,[1] Yong Ni,[1] Min Xu,[1] Lei Yang,[1] Yan-Li Liu,[1] Shi-Ling Yang,[1] Qiang Zhou,[2] Xiu-Mei Gao,[3] and Hui-Ling Zhang[1]

[1] *Department of Pharmacology and Laboratory of Cerebrovascular Pharmacology, College of Pharmaceutical Science, Soochow University, Suzhou 215123, China*
[2] *ChunKe Guiyang Pharmaceutical R & D Co., Ltd., Guiyang 550018, China*
[3] *Xiyuan Hospital, China Academy of Chinese Medical Sciences, Beijing 100091, China*

Correspondence should be addressed to Hui-Ling Zhang; huilingzhang07@hotmail.com

Received 13 June 2013; Accepted 19 August 2013

Academic Editor: Chris J. Branford-White

Qiangli Tianma Duzhong capsule (TMDZ), a Chinese herbal drug, is clinically used to improve functional outcome in patients with ischemic stroke in China. This study was conducted to establish whether postischemic long-term treatment with TMDZ could reduce the loss of injured hemisphere and confer the improvements of neurological outcome in chronic survival of rats with 2 h middle cerebral artery occlusion (MCAO)/reperfusion brain injury and its primary mechanisms. We found that TMDZ (44.5, 89, or 178 mg/kg), administered per os 6 h after the onset of ischemia and for 28 consecutive days, significantly improved the behavior deficits, beginning on day 7, and further improved later. TMDZ treatment also markedly reduced the tissue loss of the injured hemisphere and improved histopathology. In the meantime, TMDZ treatment could improve hemorrheology and inhibit platelet aggregation. These results provide the first evidence that post-ischemic long-term treatment with TMDZ confers the improvements of neurological outcome and the loss of injured hemisphere in an animal ischemic stroke model, and its mechanisms might be associated with the improvements of hemorrheology and the inhibition of platelet aggregation.

1. Introduction

Cerebral ischemia or stroke, one of the leading causes of death and long-term disability in aged populations, often results in irreversible brain damage and subsequent loss of neuronal function. The medications commonly used for stroke can be divided into four groups: thrombolytic agents, antiplatelet agents, anticoagulants, and neuroprotective agents [1]. The only approved stroke medication, tissue plasminogen activator, is a thrombolytic that targets the thrombus in the blood vessel. Neuroprotective agents, which may make the brain more resistant to damage from stroke, have generated much interest as another approach to stroke treatment. To date, however, neuroprotective agents have not reached routine clinical use and remain less than ideal [2].

In recent years, much attention has been paid to traditional herbal medicines [3–7]. Qiangli Tianma Duzhong capsule (TMDZ) mainly comprises traditional herbal medicines, Tianma and Duzhong. From the view of traditional medicine, the function of TMDZ is promoting blood circulation, removing blood stasis, and relaxing the muscles pain and has been used in the treatment of ischemic stroke in China. So far, clinical studies have demonstrated a beneficial effect of TMDZ in functional recovery in patients with stroke. However, the details of functional recovery including characterization of how anatomical and histological recovery changes following brain ischemia are influenced by treatment with TMDZ, and its mechanisms are largely absent in the literature. Here, we demonstrated that after ischemia

administrated for 4 weeks, TMDZ can reduce the loss of damaged hemisphere and improve brain histopathology and neurological outcome, and its mechanisms might be associated with the improvements of hemorrheology and the inhibition of platelet aggregation in a rat model of 2 h MCAO and reperfusion.

2. Materials and Methods

2.1. Animals and Treatments. Sprague Dawley (SD) male rats (280–310 g) were purchased from the Center for Experimental Animals, Soochow University (certificate no. 20020008, Grade II). They were housed four per cage in a standard animal room with a 12 h light/dark cycle and given free access to food and water. NIH guidelines for the care and use of laboratory animals were followed in all animal procedures.

Qiangli Tianma Duzhong capsule (TMDZ) was provided by ChunKe Guiyang Pharmaceutical R & D Co., Ltd. TMDZ 44.5, 89, or 178 mg/kg (dissolved indistilled water) or vehicle (distilled water) was administrated per os 6 h after the onset of ischemia and consecutive 28 days after ischemia. Sham-operated or ischemic-reperfusion (IR) control animals received vehicle (distilled water) per os.

2.2. Rat Models of 2 h Middle Cerebral Artery Occlusion (MCAO) and Reperfusion. Rats (n = 10/group) were anesthetized with intraperitoneal injection of 4% choral hydrate (350 mg/kg). Through a ventral midline incision, the right common carotid artery (CCA), external carotid artery (ECA), and internal carotid artery (ICA) were isolated, and ECA and CCA were ligated. A 30 mm length of monofilament nylon suture (Φ0.22–0.24 mm), with its tip rounded by heating near a flame, was inserted from the right CCA to ICA through a small incision in the common carotid artery and then advanced to the Circle of Willis to occlude the origin of the right middle cerebral artery for 2 hours, and then the suture was withdrawn. Body temperature was closely monitored with a rectal probe and maintained in the range of 37.0 ± 0.5°C with a heating pad (Institute of Biomedical Engineering, CAMS, BME-412A ANIMAL REGULATOR, 308005669) during and after surgery until recovery from anesthesia. Sham-operated rats underwent the same procedures except for cutting a small incision and inserting a monofilament nylon suture to the artery. Behavioral tests were evaluated before stroke and at 2 h ischemia and 4 h, 1, 3, 7, 14, 21, and 28 days of reperfusion. Body weight was measured every week. For the observation of the brain damage, animals were killed, and the brains were dissected and sliced in a plastic module (Harvard Apparatus, 3 mm thickness) 28 days after ischemia. For morphology analysis, animals were sacrificed 28 days after ischemia (n = 3/group) by transcardial perfusion of 0.9% normal saline, followed by 4% paraformaldehyde in 100 mM phosphate buffer. The brains were then fixed, embedded with paraffin. Brain coronal sections at the level of the caudate putamen which showed typical infarction were selected and sectioned to 10 μm, and then brain coronal sections were stained with hematoxylin-eosin (HE). The pyramidal cortical cells were examined with a microscopy. For quantification of cells, 10 microscopic fields (magnification 20x) in each section across ischemic cortical regions in the ipsilateral hemisphere were analyzed. Three sections were used for each animal. The number of cells in each field was counted by an examiner who was blinded to the experimental conditions [8].

2.3. Behavioral Testing. Neurological deficits were examined at 2 h ischemia and 4 h reperfusion using a 5-point scale adapted and modified from Zhang et al. [9]. Specifically, no neurological deficit equals 0; right Horner's syndrome counts 1 point; failure to extend left forelimb and hindlimb counts 1 point each; turning to left counts 1 point; and circling to left counts 1 point.

2.4. Asymmetry in the Use of Forelimbs for Postural Support (Cylinder Test). Cylinder Tests were performed 1, 3, 7, 14, 21, and 28 days after ischemia reperfusion. Briefly, animals were placed into a plexiglass cylinder, and their behavior was observed for forelimb use asymmetry during vertical movements along the wall of the cylinder. The final score was calculated as (nonimpaired forelimb movement − impaired forelimb movement)/(nonimpaired forelimb movement + impaired forelimb movement + both movements), as previously described in the rat [10]. A total of 20 movements were recorded during the 10 min test.

2.5. Asymmetry-Corner Test. Corner tests were performed 1, 3, 7, 14, 21, and 28 days after ischemia reperfusion. Briefly, in the home cage, an animal was placed between the two angled boards. When entering deep into the corner, both sides of the vibrissae are stimulated together. The animal then rears forward and upward then turns back to face the open end. Twenty trials were performed for each rat, and the percentage of right turns versus left turns was calculated. Only turns involving full rearing along either boards were recorded [11, 12].

2.6. Magnetic Resonance Image (MRI) Analysis for Lesion Size. Rats were anesthetized with isoflurane, were placed in an animal holder/MRI probe apparatus, and were positioned inside the magnet. The animal's head was held in place inside the imaging coil. All MRI measurements were performed using a 7 Teslar, 18 cm bore superconducting magnet (Oxford Magnet Technologies) interfaced to a UNITYINOVA console (Oxford Instruments, UK, and Varian Inc., Palo Alto, CA, USA). T_2-weighted images (T_2WI) were obtained from a 1.0 mm thick coronal section with a 0.5 mm gap using a 30 mm × 30 mm field of view, TR = 3000 ms, TE = 37 ms, and b value = 0 and reconstructed using a 256 × 256 image matrix. Accurate positioning of the brain was performed to center the image slice 5 mm posterior to the rhinal fissure with the head of the rat held in a flat skull position. For each slice, the higher intensity lesions in T_2WI were marked as the ischemic lesion area [13]. MRI measurements were obtained 28 days after MCAO (n = 3 for each group).

2.7. Determination of Hemorrheology. Blood samples were taken from the abdominal aorta of rats and were mixed with

Heparin Li for blood viscosity and plasma viscosity, 3.2% citric acid for FBG, EDTA·K_2 for HCT, and 3.2% sodium citrate for ESR. Blood viscosity was measured with a cone-plate viscometer (Brookfield Engineering Laboratories, Inc., Stoughton, MA, USA). Plasma viscosity (PV) was centrifuged at 3000 rpm for 15 min in a centrifuge to obtain the plasma. The plasma viscosity was measured by an Automatic Blood Rheometer LBY-N6B (Beijing Precil Instrument CO., LTD, Beijing, China). Fibrinogen (Fb), heamatocrit (HCT), and erythrocyte sedimentation rate (ESR) were detected with a laser-assisted automatic hemorheological analyzer (modified MDK-B100, MDK, Inc., Chongqing, China). All measurements were conducted at 4°C.

2.8. Platelet Aggregation. Rat platelet suspensions were prepared as previously described [14]. In brief, blood was collected from rats with or without stroke which had taken TMDZ for 4 weeks and was mixed with 3.2% citrate for ADP or EDTA K_2 for thrombin. Platelet-rich plasma (PRP) was prepared by centrifugation at 500 rpm for 3 min at room temperature, and platelet aggregation induced by ADP (4 μmol/mL, Solarbio) was measured using an Aggregometer (TYXN-96, Shanghai General Machine Electricity Technological Research Institute, Shanghai, China). For thrombin, The PRP was then centrifuged at 1500 rpm for 5 min, and the resulting platelet pellet was resuspended in the washing buffer (NaCl 140 mM, KCl 2.7 mM, $NaH_2PO_4{\cdot}2H_2O$ 0.4 mM, $NaHCO_3$ 12 mM, $MgCl_2{\cdot}6H_2O$ 1 mM, glucose 5 mM, HEPES 10 mM, PGE1 100 nM, and BSA 3.5 mg/mL, pH 6.6) and then centrifuged at 1000 rpm for 5 min. The platelet was resuspended in the suspension buffer (NaCl 140 mM, KCl 2.7 mM, $NaH_2PO_4{\cdot}2H_2O$ 0.4 mM, $NaHCO_3$ 12 mM, $MgCl_2{\cdot}6H_2O$ 1 mM, glucose 5 mM, HEPES 10 mM, and BSA 3.5 mg/mL, pH 7.4), and the platelet aggregation induced by thrombin (3 U/mL, Sigma) was measured.

2.9. Statistical Analysis. Statistical analysis was carried out by one-way analysis of variance (ANOVA) followed by a post hoc Tukey test. Differences were considered significant when $P < 0.05$.

3. Results

3.1. Qiangli Tianma Duzhong Capsule (TMDZ) Increases Body Weight. Compared to the rats in ischemia-reperfusion control (IR control), TMDZ treatment significantly increased body weight from day 7 (the second week), which persisted throughout the 4-week survival period (Figure 1).

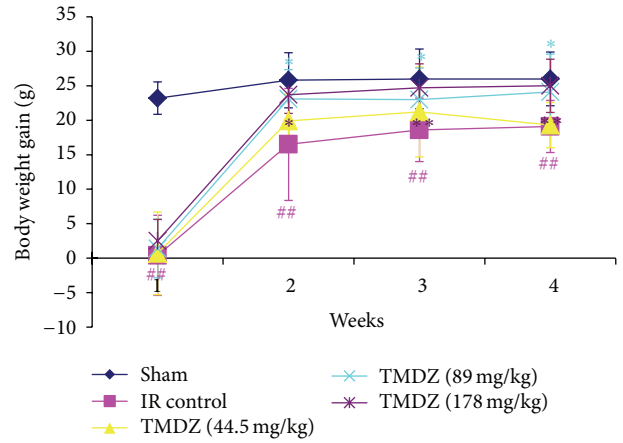

Figure 1: Post-ischemic long-term treatment with TMDZ increases the body weight after ischemic stroke. Animals underwent 2 h MCAO and reperfusion and received either an oral administration of TMDZ or vehicle (distilled water) at 2 h MCAO, 4 h reperfusion, and every day later for 28 days, and the body weight was measured every week. Compared to rats in ischemia-reperfusion control (IR Control), TMDZ treatment significantly increased body weight from day 7 (the second week), which persisted throughout the additional 3-week survival period. Values shown are mean ± S.D., $n = 10$. Statistical analysis was carried out with one-way ANOVA followed by a post hoc Tukey test. $^{\#\#}P < 0.01$ versus sham-operated group (Sham); $^{*}P < 0.05$ and $^{**}P < 0.01$ versus ischemia-reperfusion control group.

3.2. TMDZ Reduces Brain Loss and Lesion Size. To reduce errors associated with processing tissue for histological analysis, the residual brain volume is presented as the percentage of ipsilateral (right) hemisphere volume of the contralateral (left) hemisphere volume (indirect volume calculation). The residual brain volumes (the integrated right hemisphere volume) after a 4-week stroke were reduced compared with the sham-operated hemisphere or the contralateral hemisphere in both ischemia-reperfusion control and TMDZ-treated groups. However, compared with the residual brain volume in ischemia-reperfusion control rats, TMDZ treatment significantly increased the residual brain volumes after consecutive administration for 4 weeks (Figure 2). Being consistent with these results, HE staining analysis also found that ischemia-reperfusion control rats showed ipsilateral-hemisphere tissue loss and extensive zones of cystic necrosis. In contrast, rats treated with TMDZ showed less extensive cortical and subcortical damage (Figure 3). Treatment with TMDZ significantly increased the cortical cells compared to the vehicle-treated rats (Figure 3).

In addition, the ischemic lesion size was estimated using an in vivo MRI. T_2WIs were obtained 28 days after TMDZ or vehicle consecutive treatment. Coronal forebrain sections were obtained at the level of caudate-putamen complex (Figure 4). Lesion size (high intensity areas) was less in TMDZ-treated rats as compared to ischemia-reperfusion control rats (Figure 4).

These results suggest that post-ischemic long-term treatment with TMDZ reduces brain damage and brain tissue loss after stroke.

3.3. TMDZ Improves Neurological Outcome. Neurological score was normal in all animals before MCAO (score, 0). High-grade contralateral deficits (score, 2–5, Table 1) were presented at 2 h MCAO and 4 h reperfusion in all rats, and there was no significant difference among the groups

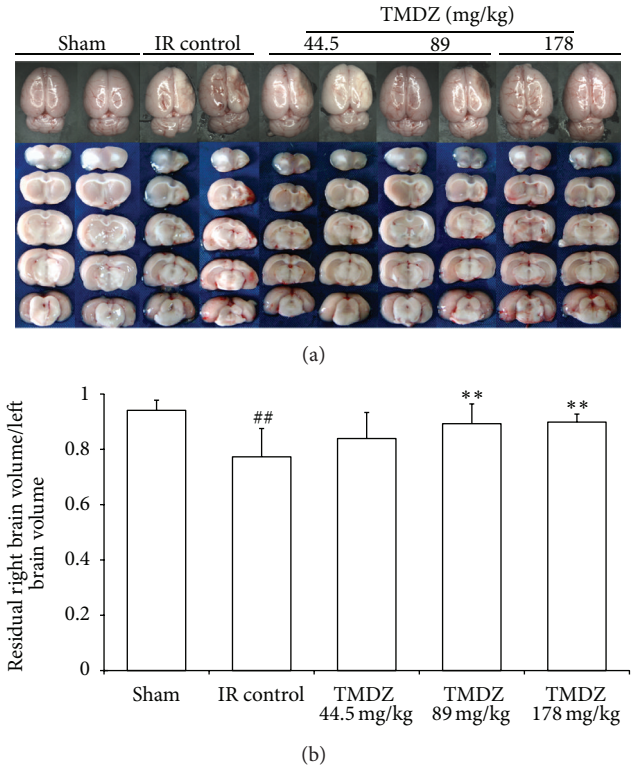

Figure 2: Post-ischemic long-term treatment with TMDZ reduces brain tissue loss after ischemic stroke. Animals underwent 2 h MCAO and reperfusion and received either an oral administration of TMDZ or vehicle (distilled water) at 2 h MCAO, 4 h reperfusion, and every day later for 28 days. The representative images of the whole brain and the sliced brain (a). The volume of right hemisphere (injured hemisphere) was indicated as the percentage of ipsilateral hemisphere volume of the contralateral hemisphere volume (indirect volume calculation) (b). Values shown are mean ± S.D., $n = 10$. Statistical analysis was carried out with one-way ANOVA followed by a post hoc Tukey test. $^{\#}P < 0.05$ and $^{\#\#}P < 0.01$ versus sham-operated group (Sham); $^{**}P < 0.01$ versus ischemic-reperfusion control group (IR Control).

(Table 1). After TMDZ consecutive treatment for 7 days, rats in TMDZ group showed a greater functional recovery than rats in ischemia-reperfusion control group and conferred a further improvement with time during the additional 3-week survival period in the corner test (Figure 5(a)) and cylinder test (Figure 5(b)). There were no adverse behavioral side effects observed with TMDZ administration. These results suggest that post-ischemic long-term treatment with TMDZ improves neurological outcome after stroke.

3.4. TMDZ Improves Hemorrheology. TMDZ did not change any of the hemorrheology parameters after normal rats were administrated with TMDZ for 4 weeks (Table 2). In rats, 4 weeks after stroke, the whole blood viscosity (WBV) of low shear rate, moderate shear rate, and high shear rate, the whole blood reduced viscosity (WBRV) of low shear rate, moderate shear rate, and high shear rate, and fibrinogen (Fb) were much higher as compared to sham-operated

Table 1: Neurological scores after stroke. Neurological function was measured by 5-point test after 2 h MCAO and 4 h reperfusion. High-grade contralateral deficits were presented at 2 h MCAO and 4 h reperfusion in all rats, and there was no significant difference among the groups.

Group	Ischemia/reperfusion	Tianma Duzhong capsule		
	Control	44.5 mg/kg	89 mg/kg	178 mg/kg
Score	2.5 ± 0.71	2.4 ± 0.52	2.4 ± 0.52	2.4 ± 0.70

rats (Table 3). In contrast, TMDZ treatment for 4 weeks significantly decreased the WBV, WBRV, and Fb (Table 3). In addition, stroke induced an increase in plasma viscosity (PV), heamatocrit (HCT), erythrocyte sedimentation rate (ESR), erythrocyte sedimentation rate equation K value (ESRK), red blood cell aggregation index (RBCAI), and red blood cell rigidity index (RBCRI), but these parameters did not reach a statistically significant level. However, TMDZ obviously reduced the stroke induced increases in PV, HCT, RBCAI, and RBCRI (Table 3). There were no significant differences in the red blood cell deformation index (RBCDI) and the red blood cell electrophoresis index (RBCEI) among all groups (Table 3).

3.5. TMDZ Inhibits Platelet Aggregation. TMDZ significantly decreased the in vitro ADP- or thrombin-induced platelet aggregation after normal rats were administrated with TMDZ for 4 weeks (Figure 6). Furthermore, the in vitro ADP- or thrombin-induced platelet aggregation in ischemia-reperfusion control rats was dramatically increased, and TMDZ treatment for 4 weeks significantly decreased the ischemia-reperfusion-induced increase in platelet aggregation (Figure 7). These results suggest that TMDZ has a strong inhibitory effect on the platelet aggregation.

4. Discussion

Ischemic hypoxic brain injury often causes irreversible brain damage and permanent behavioral performance deficits. A well-controlled animal model of MCAO in rats, which produces consistent cortical and subcortical infarcts, closely resembles the large hemispheric infarcts resulting from proximal MCAO in patients [15]. Most of the studies published so far have focused on the fact that histopathology changes in the damaged brain occur in acute period of ischemic stroke, and more recently, much attention has also been paid to the histopathology changes in the damaged that brain occur in subacute and remote period of ischemic stroke. It has been demonstrated that hemispheric edema will happen to in the acute ischemic stroke, whereas brain tissue loss and atrophy will occur in the ischemic hemisphere in the subacute and remote ischemic stroke and the volume of injured hemisphere is largely reduced as compared to the contralateral hemisphere [16, 17], which was also confirmed in our current study 4 weeks after stroke in a rat model of 2 h MCAO and reperfusion. As assessed by both neurobehavioral and histological methods, this study demonstrates that consecutive oral administration of Qiangli Tianma Duzhong

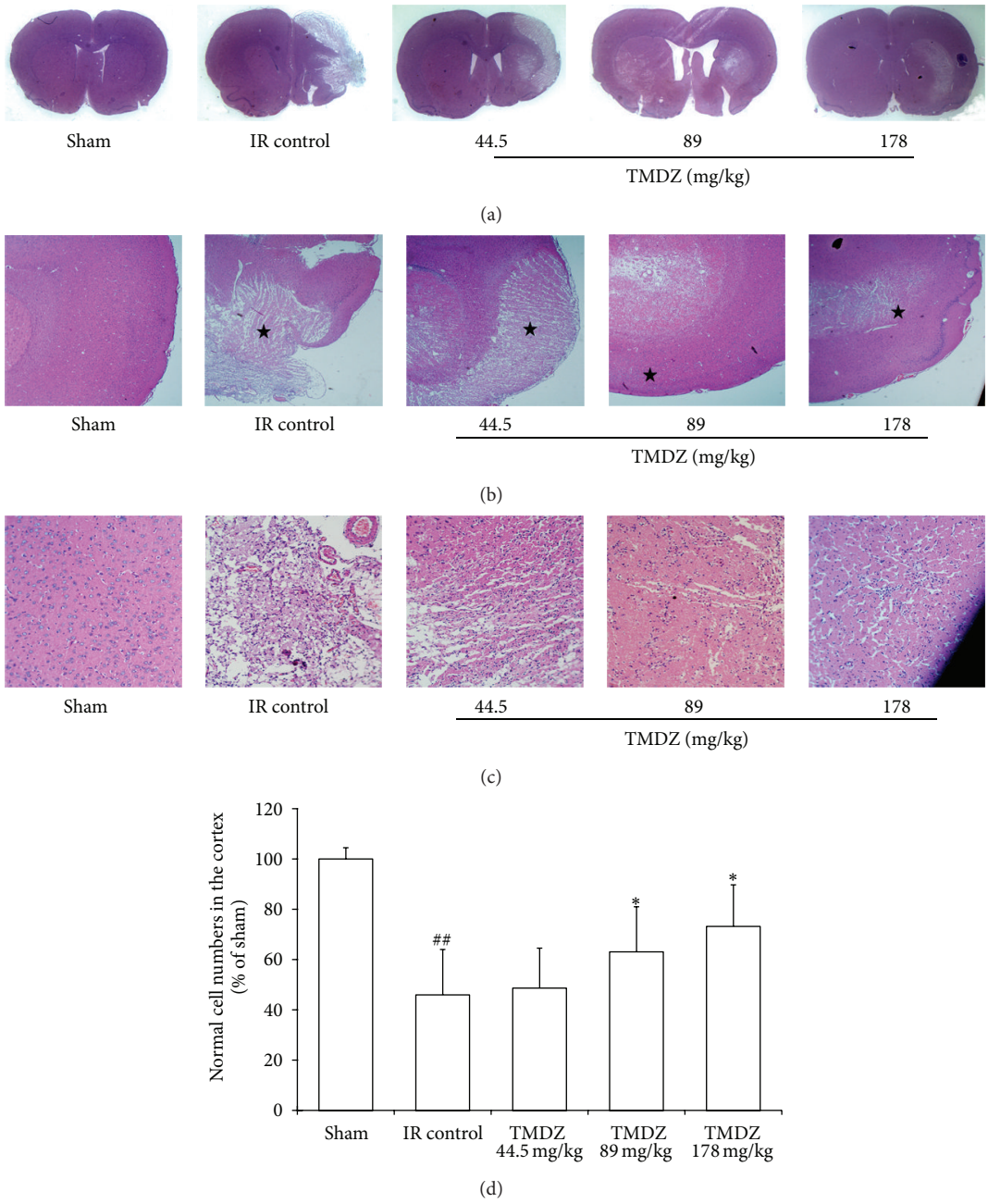

FIGURE 3: Post-ischemic long-term treatment with TMDZ improves the histopathological changes after ischemic stroke. Animals underwent 2 h MCAO and reperfusion and received either an oral administration of TMDZ or vehicle (distilled water) at 2 h MCAO, 4 h reperfusion, and every day later for 28 days, and the HE staining was measured 28 days after stroke. Computer generated MosaiX processed images (Carl Zeiss MicroImaging, Inc, Thornwood, NY, USA) of HE paraffin-embedded brain sections at coronal level (bregma +1.2 mm) from rats treated with vehicle or treated with TMDZ. The representative images of the entire slice (a), 4x (b), and 20x (c). The vehicle-treated rat (ischemia-reperfusion control group, IR Control) showed typical appearance of cystic necrosis, and pannecrosis involved the entire neocortical thickness, extending to subjacent regions. In contrast, rats treated with TMDZ showed less extensive damage. Values shown are mean ± S.D., $n = 6$. Statistical analysis was carried out with one-way ANOVA followed by a post hoc Tukey test. $^{\#\#}P < 0.01$ versus sham-operated group (Sham); $^{**}P < 0.01$ versus ischemia-reperfusion control group (IR Control).

capsule (TMDZ) for 4 weeks after cerebral infarction results in a reduction in brain tissue loss and ischemic lesion size estimated from brain slices measurements and MRI analysis, an increase in body weight, and an improvement in behavioral performance and histopathology from HE analysis.

At present, the remarkable effect of TMDZ is not largely understood. An elevated blood viscosity value has been demonstrated in patient after both acute cerebral ischemia (24 h after the onset of stroke) and remote cerebral ischemic episode (3–6 months after the onset of stroke) although

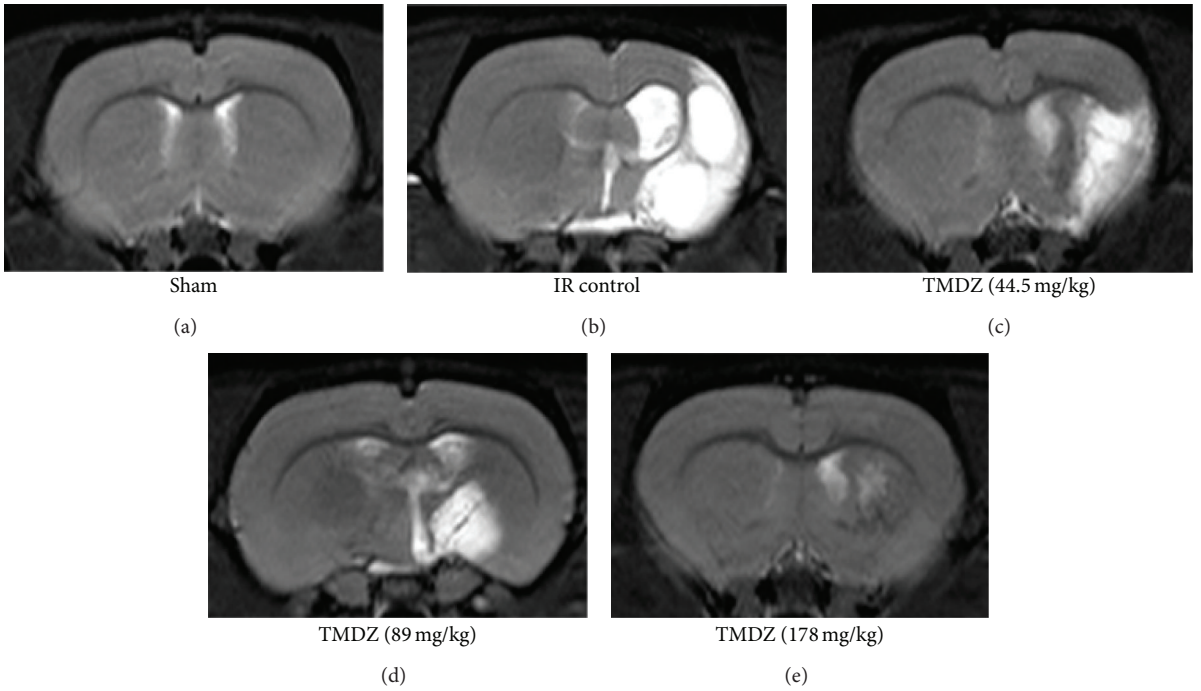

FIGURE 4: Post-ischemic long-term treatment with TMDZ reduces ischemic lesion with MRI. Animals underwent 2 h MCAO and reperfusion and received either an oral administration of TMDZ or vehicle (distilled water) at 2 h MCAO, 4 h reperfusion, and every day later for 28 days. T_2-weighted images were obtained from experimental animals 28 days after MCAO and TMDZ were administrated.

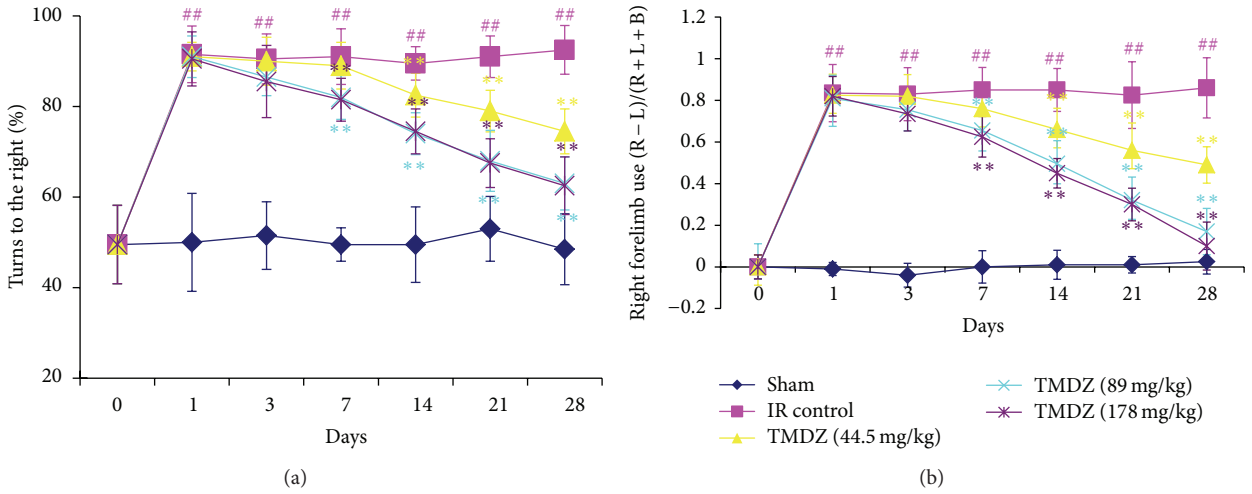

FIGURE 5: Post-ischemic long-term treatment with TMDZ improves neurological outcome after ischemic stroke. Animals underwent 2 h MCAO and reperfusion and received either an oral administration of TMDZ or vehicle (distilled water) at 2 h MCAO, 4 h reperfusion, and every day later for 28 days followed by neurological testing at 1, 3, 7, 14, 21, and 28 days. (a) The corner test demonstrated preferential turning to the right in animals that had undergone right MCAO/reperfusion and vehicle administration after stroke. Deficits persisted up to 28 days after stroke. Animals that received TMDZ, however, showed reduction of deficits over time. (b) The cylinder test demonstrated preferential right forearm placement in animals that had undergone right MCAO/reperfusion and vehicle administration after stroke. Deficits persisted up to 28 days after stroke. Animals that received TMDZ, however, showed reduction of deficits over time. Values shown are mean ± S.D., $n = 10$. Statistical analysis was carried out with one-way ANOVA followed by a post hoc Tukey test. $^{\#\#}P < 0.01$ versus sham-operated group (Sham); $^{**}P < 0.01$ versus ischemic-reperfusion control group (IR Control).

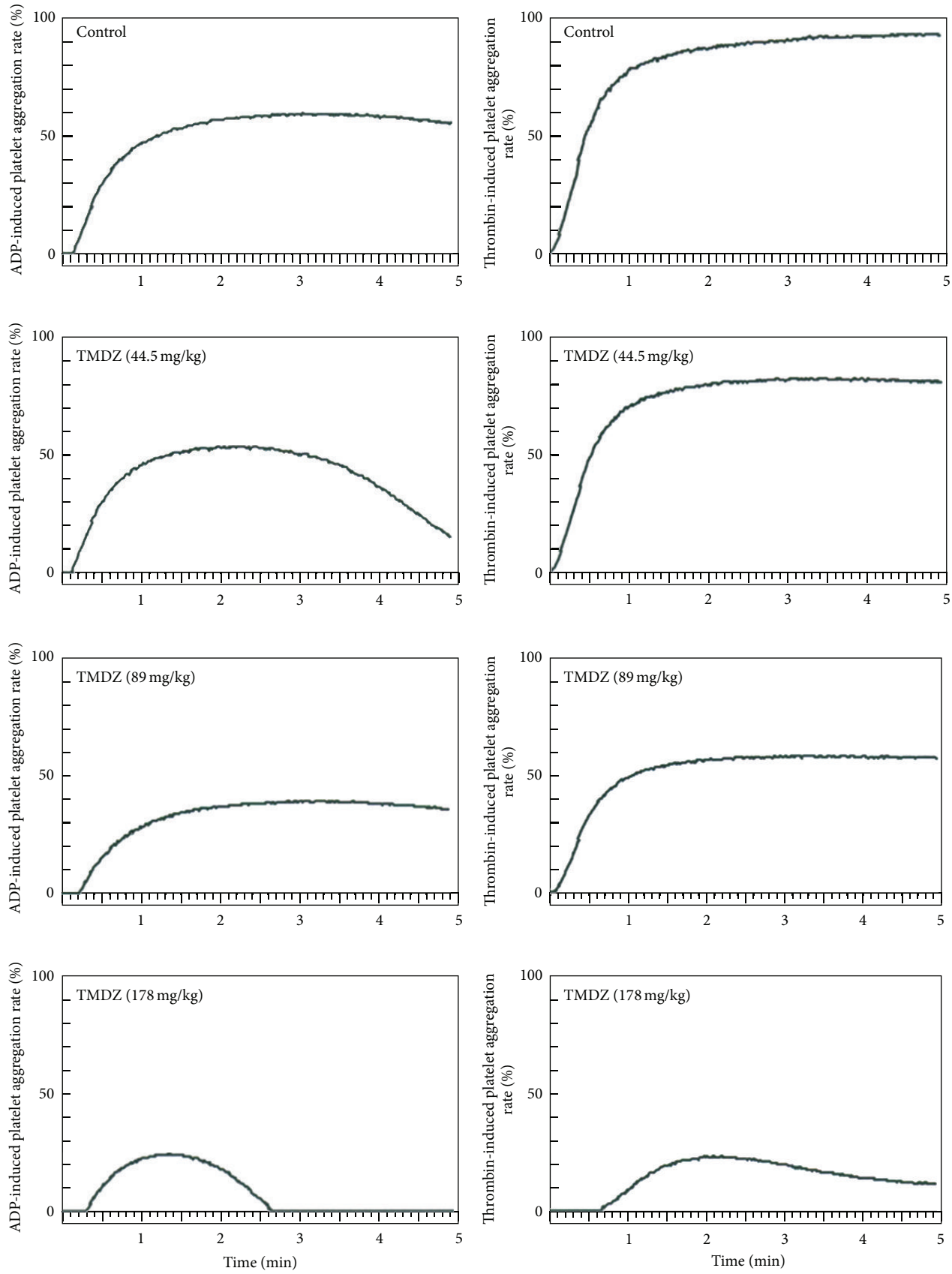

Figure 6: Continued.

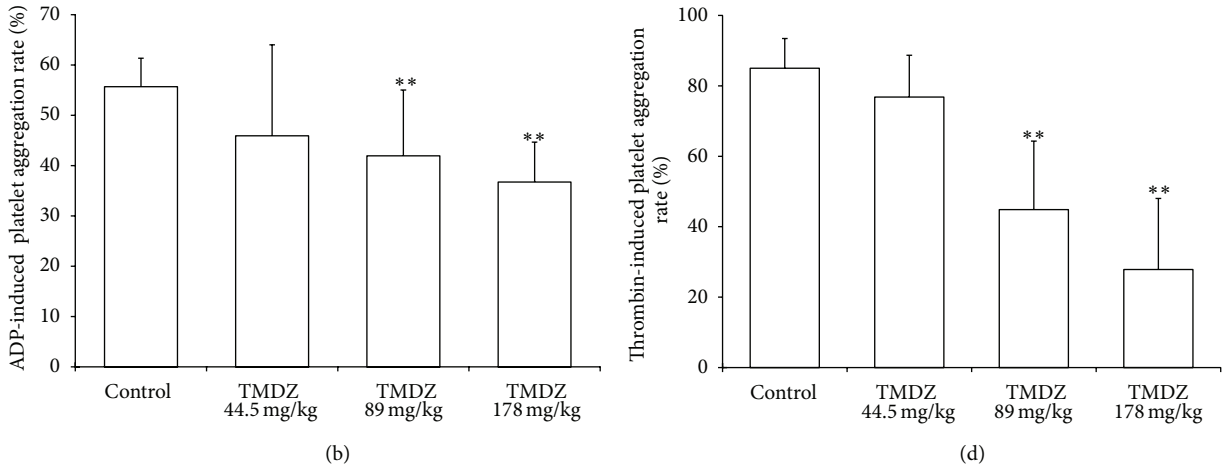

Figure 6: Long-term treatment with TMDZ inhibits ADP- or thrombin-induced platelet aggregation in normal rats. Animals received an oral administration of TMDZ or vehicle (distilled water) for 28 days, and then the blood was obtained, and the platelet aggregation induced by ADP or thrombin was detected. (a) and (c): representative curve of platelet aggregation induced by ADP (a) or thrombin (c). (b) and (d): quantitative analysis of changes in the platelet aggregation from 10 independent experiments of (a) and (c), respectively. Values shown are mean ± S.D., $n = 10$. Statistical analysis was carried out with one-way ANOVA followed by a post hoc Tukey test. $^{\#\#}P < 0.01$ versus vehicle-treated group (Control group).

Table 2: Hemorrheology parameters in normal rats. Animals received an oral administration of TMDZ or vehicle (distilled water) for 28 days, and then the blood was obtained, and hemorrheology parameters were detected. Values shown are mean ± SD, $n = 10$. TMDZ did not change any of the hemorrheology parameters after normal rats were administrated with TMDZ for 28 days.

Parameters	Control	Tianma Duzhong capsule		
		44.5 mg/kg	89 mg/kg	178 mg/kg
WBV: low shear (mPas) | 10 s^{-1}	9.86 ± 1.95	9.71 ± 1.56	10.16 ± 1.63	9.40 ± 1.58
WBV: moderate shear (mPas) | 60 s^{-1}	5.80 ± 0.97	5.61 ± 0.70	5.57 ± 0.41	9.03 ± 0.84
WBV: high shear (mPas) | 150 s^{-1}	4.54 ± 0.59	4.54 ± 0.48	4.63 ± 0.45	4.55 ± 0.67
PV	1.08 ± 0.03	1.06 ± 0.02	1.11 ± 0.04	1.09 ± 0.05
WBRV: low shear	21.36 ± 5.34	20.04 ± 3.77	17.62 ± 1.93	18.21 ± 2.79
WBRV: moderate shear	11.46 ± 2.17	10.54 ± 1.73	10.10 ± 0.92	10.24 ± 1.55
WBRV: high shear	8.39 ± 1.58	8.05 ± 1.18	7.93 ± 0.67	7.93 ± 1.19
Fb	2.10 ± 0.24	2.09 ± 0.17	2.19 ± 0.10	2.28 ± 0.43
HCT (%)	41.54 ± 2.11	43.34 ± 2.04	44.22 ± 3.22	43.30 ± 3.12
ESR(MM/H)	1.10 ± 0.18	1.10 ± 0.18	1.30 ± 0.67	2.30 ± 2.75
ESRK	3.77 ± 1.16	4.11 ± 1.23	4.29 ± 1.98	7.70 ± 8.23
RBCAI	2.15 ± 0.23	2.13 ± 0.17	2.40 ± 0.58	2.04 ± 0.25
RBCRI	7.79 ± 1.91	7.58 ± 1.41	7.70 ± 2.01	7.63 ± 1.32
RBCDI	1.05 ± 0.12	1.02 ± 0.09	1.06 ± 0.14	1.03 ± 0.09
RBCEI	5.21 ± 0.81	4.93 ± 0.54	5.93 ± 1.87	4.80 ± 0.69

WBV: whole blood viscosity; WBRV: whole blood reduced viscosity; PV: Plasma viscosity; Fb: fibrinogen; HCT: hematocrit; ESR: erythrocyte sedimentation rate; ESRK: erythrocyte sedimentation rate equation K value; RBCAI: red blood cell aggregation index; RBCRI: red blood cell rigidity index; RBCDI: red blood cell deformation index; RBCEI: red blood cell electrophoresis index.

there are some differences in hemorheological parameters between patient with acute cerebral ischemia and patient with remote cerebral ischemic episode [18, 19]. Therefore, clinically, one of the drug therapies in patient with ischemic stroke is modifying the hemorrheological properties and leading to a decrease in blood viscosity, and thus resulting in better perfusion of brain and promotion of the recovery of functional deficits after stroke. Consistent with the pieces of literature [18, 19], in the present study, we also confirmed a significant increase in the whole blood viscosity (WBV) of low shear rate, moderate shear rate, and high shear rate and the whole blood reduced viscosity (WBRV) of low shear rate, moderate shear rate, and high shear rate 4 weeks after stroke in a rat model of 2 h MCAO and reperfusion. Blood viscosity depends on many factors. The most important are hematocrit value, plasma viscosity, and elasticity of the red cells and their aggregability [18]. The increased blood viscosity in the current study may result from a stroke that induced

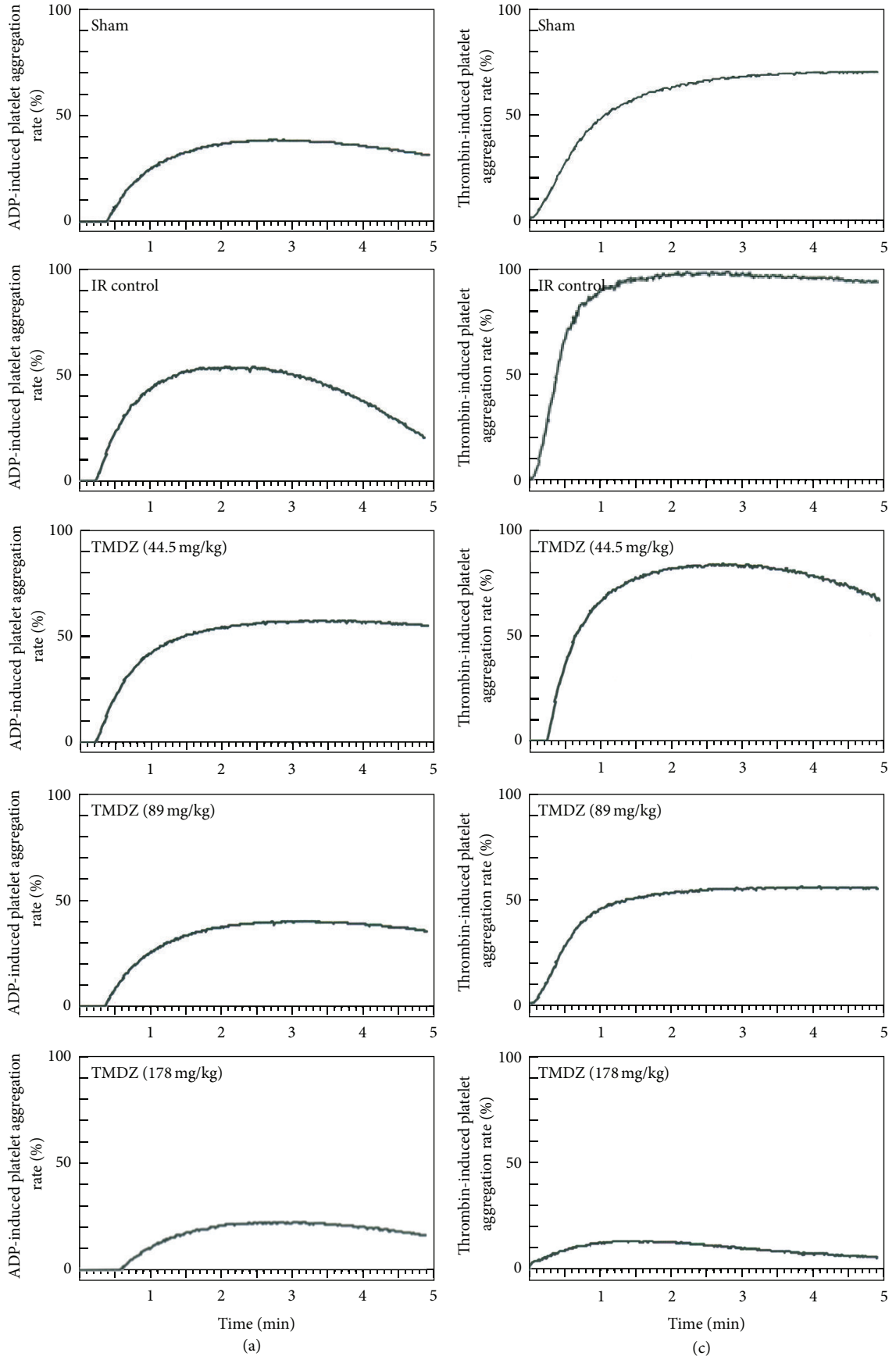

Figure 7: Continued.

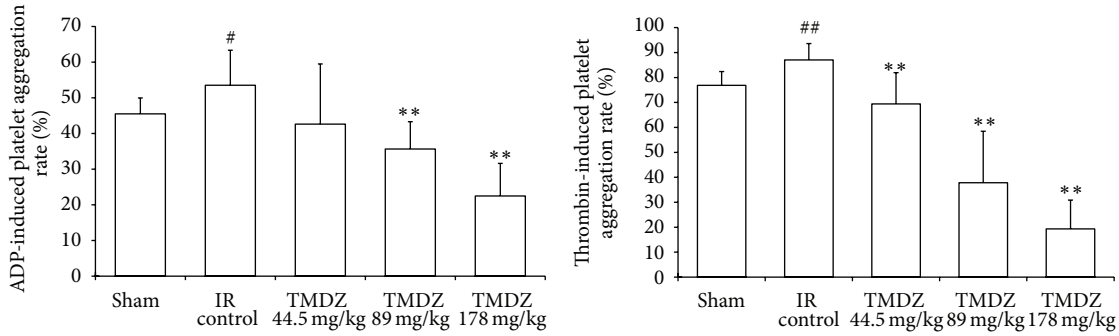

Figure 7: Long-term treatment with TMDZ inhibits ADP- or thrombin-induced platelet aggregation in ischemic stroke rats. Animals underwent 2 h MCAO and reperfusion and received either an oral administration of TMDZ or vehicle (distilled water) at 2 h MCAO, 4 h reperfusion and every day later for 28 days, and then the blood was obtained and the platelet aggregation induced by ADP or thrombin was detected. (a) and (c): representative curve of platelet aggregation induced by ADP (a) or thrombin (c). (b) and (d): quantitative analysis of changes in the platelet aggregation from 10 independent experiments of (a) and (c), respectively. Values shown are mean ± S.D., $n = 10$. Statistical analysis was carried out with one-way ANOVA followed by a post hoc Tukey test. $^{\#}P < 0.05$ and $^{\#\#}P < 0.01$ versus sham-operated group (Sham); $^{**}P < 0.01$ versus ischemia-reperfusion control group (IR Control).

Table 3: Hemorrheology parameters in stroke rats. Animals underwent 2 h MCAO and reperfusion and received either an oral administration of TMDZ or vehicle (distilled water) at 2 h MCAO, 4 h reperfusion, and every day later for 28 days, and then the blood was obtained, and hemorrheology parameters were detected. Values shown are mean ± S.D., $n = 10$. Statistical analysis was carried out with one-way ANOVA followed by a post hoc Tukey test.

Parameters	Sham	Ischemia/reperfusion control	Tianma Duzhong capsule		
			44.5 mg/kg	89 mg/kg	178 mg/kg
WBV: low shear (mPas) | 10 s^{-1}	9.08 ± 0.88	13.60 ± 3.10$^{\#\#}$	11.21 ± 2.10	8.75 ± 2.01**	9.14 ± 1.75**
WBV: moderate shear (mPas) | 60 s^{-1}	5.31 ± 0.37	6.74 ± 0.61$^{\#\#}$	5.95 ± 0.99*	5.08 ± 0.95**	5.22 ± 0.74**
WBV: high shear (mPas) | 150 s^{-1}	4.14 ± 0.41	5.26 ± 0.52$^{\#\#}$	4.67 ± 0.79	4.11 ± 0.77**	4.16 ± 0.47**
PV	1.04 ± 0.04	1.12 ± 0.06	1.12 ± 0.86	1.10 ± 0.06	1.07 ± 0.02*
WBRV: low shear	19.8 ± 2.98	28.18 ± 7.25$^{\#\#}$	25.02 ± 6.54	18.93 ± 3.04**	20.30 ± 4.27**
WBRV: moderate shear	10.53 ± 1.6	12.66 ± 1.59$^{\#\#}$	12.69 ± 4.75	9.99 ± 2.22**	10.40 ± 1.76**
WBRV: high shear	7.69 ± 1.74	9.30 ± 1.07$^{\#\#}$	8.66 ± 1.58	7.49 ± 1.56*	7.75 ± 1.08**
Fb	2.04 ± 0.26	2.90 ± 1.02$^{\#}$	2.64 ± 1.10	2.27 ± 0.32	2.10 ± 0.42*
HCT (%)	41.0 ± 4.41	44.61 ± 3.74	42.97 ± 6.71	40.14 ± 5.39	39.8 ± 3.30**
ESR(MM/H)	1.11 ± 0.33	2.90 ± 2.88	3.20 ± 4.96	1.38 ± 0.52	1.40 ± 0.52
ESRK	3.79 ± 1.46	10.54 ± 9.93	9.45 ± 9.20	4.26 ± 1.08	4.35 ± 1.44
RBCAI	2.22 ± 0.32	2.59 ± 0.51	2.41 ± 0.37	2.13 ± 0.21*	2.19 ± 0.27*
RBCRI	7.42 ± 1.89	8.29 ± 0.92	7.39 ± 1.21	6.83 ± 1.33*	7.22 ± 1.06*
RBCDI	1.05 ± 0.18	1.04 ± 0.08	1.02 ± 0.12	1.02 ± 0.13	1.05 ± 0.09
RBCEI	5.43 ± 0.70	5.86 ± 1.34	5.69 ± 0.92	5.35 ± 0.57	5.53 ± 0.86

$^{\#}P < 0.05$ and $^{\#\#}P < 0.01$ versus sham-operated group (Sham); $^{*}P < 0.05$ and $^{**}P < 0.01$ versus ischemic-reperfusion control group (IR Control). WBV: whole blood viscosity; WBRV: whole blood reduced viscosity; PV: Plasma viscosity; Fb: fibrinogen; HCT: heamatocrit; ESR: erythrocyte sedimentation rate; ESRK: erythrocyte sedimentation rate equation K value; RBCAI: red blood cell aggregation index; RBCRI: red blood cell rigidity index; RBCDI: red blood cell deformation index; RBCEI: red blood cell electrophoresis index.

some tendency towards higher value in hematocrit value, plasma viscosity and the aggregability of the red blood cells (statistically not significant), and lower value in the elasticity of the red blood cells (statistically not significant). TMDZ treatment for 4 weeks after stroke significantly decreased the WBV and WBRV and also simultaneously decreased plasma viscosity (PV), heamatocrit (HCT), red blood cell aggregation index (RBCAI), and red blood cell rigidity index (RBCRI), which may contribute to the fact that TMDZ induced a decrease in blood viscosity. In addition, we found that stroke induced a high fibrinogen level, which is in agreement with the observation in a patient by Velcheva and Nikolova [19], and TMDZ decreased it.

The cascade of events leading to neuronal injury and death in ischemia includes the release of cytokines, free radicals, and platelet activation [20, 21]. The participation of activated platelets has been observed in brain microvessels of the ischemic microvascular bed after experimental middle cerebral artery occlusion (MCAO) [21]. Microvascular thrombi continue to accumulate even after recanalization of

the MCAO, contributing to postischemic hypoperfusion and ongoing neuronal damage [22]. Thus, platelet aggregation may play a crucial role in MCAO-induced cerebral damage. In the present study, we showed that the platelet aggregation was significantly increased in ischemic rats 4 weeks after stroke by using an in vitro ADP- or thrombin-induced platelet aggregation and TMDZ treatment for 4 weeks significantly decreased the ischemia-induced increase in platelet aggregation. In addition, TMDZ also markedly decreased the platelet aggregation after normal rats were administrated with TMDZ for 4 weeks.

In summary, the present results firstly established that post-ischemic long-term treatment with TMDZ confers the improvements of neurological outcome and the loss of injured hemisphere in animal ischemic stroke models, and its mechanisms might be associated with the improvements of hemorrheology and the inhibition of platelet aggregation. These results are very encouraging for the wide application of TMDZ in patients with ischemic stroke. Whether post-ischemic long-term treatment with TMDZ produces neuroregeneration in the treatment of ischemic stroke remains to be further investigated in the near future.

Authors' Contribution

Li-Zhi Hong and Wei-wei Gu contributed equally to this work.

Acknowledgments

This work was supported by Grants from The National Natural Science Foundation of China (30973510 and 81171104), the Scientific Research Foundation for the Returned Overseas Chinese Scholars, State Education Ministry, and a project Funded by the Priority Academic Program Development of Jiangsu Higher Education Institutions (PAPD).

References

[1] Y. M. Mohammad, A. A. Divani, J. F. Kirmani, P. Harris-Lane, and A. I. Qureshi, "Acute treatment for ischemic stroke in 2004," *Emergency Radiology*, vol. 11, no. 2, pp. 83–86, 2004.

[2] Y. D. Cheng, L. Al-Khoury, and J. A. Zivin, "Neuroprotection for Ischemic Stroke: two decades of success and failure," *NeuroRx*, vol. 1, no. 1, pp. 36–45, 2004.

[3] M.-S. Lee, D.-Y. Yang, C.-L. Cheng, Y.-J. Liang, L.-L. Yang, and F.-C. Cheng, "Ginkgo biloba extract preserves pyruvate and enhances ascorbate in the cortex of gerbils during focal cerebral ischemia: a microdialysis-liquid chromatography study," *Journal of Chromatography A*, vol. 985, no. 1-2, pp. 387–394, 2003.

[4] X.-Q. Cao, X.-M. Zhang, X.-B. Wei, L.-X. Wang, and H.-Q. Liu, "Protective effects of gypenosides on focal brain ischemia-reperfusion injury in rats," *Chinese Pharmaceutical Journal*, vol. 37, no. 7, pp. 499–502, 2002.

[5] J. T. Hong, S. R. Ryu, H. J. Kim et al., "Protective effect of green tea extract on ischemia/reperfusion-induced brain injury in Mongolian gerbils," *Brain Research*, vol. 888, no. 1, pp. 11–18, 2001.

[6] B. Yan, D.-Y. Wang, D.-M. Xing et al., "The antidepressant effect of ethanol extract of radix puerariae in mice exposed to cerebral ischemia reperfusion," *Pharmacology Biochemistry and Behavior*, vol. 78, no. 2, pp. 319–325, 2004.

[7] Y. Numagami, S. Sato, and S. T. Ohnishi, "Attenuation of rat ischemic brain damage by aged garlic extracts: a possible protecting mechanism as antioxidants," *Neurochemistry International*, vol. 29, no. 2, pp. 135–143, 1996.

[8] H.-L. Zhang, Z.-L. Gu, S. I. Savitz, F. Han, K. Fukunaga, and Z.-H. Qin, "Neuroprotective effects of prostaglandin A1 in rat models of permanent focal cerebral ischemia are associated with nuclear factor-κB inhibition and peroxisome proliferator-activated receptor-γ up-regulation," *Journal of Neuroscience Research*, vol. 86, no. 5, pp. 1132–1141, 2008.

[9] R. L. Zhang, M. Chopp, Z. G. Zhang, Q. Jiang, and J. R. Ewing, "A rat model of focal embolic cerebral ischemia," *Brain Research*, vol. 766, no. 1-2, pp. 83–92, 1997.

[10] T. Schallert, S. M. Fleming, J. L. Leasure, J. L. Tillerson, and S. T. Bland, "CNS plasticity and assessment of forelimb sensorimotor outcome in unilateral rat models of stroke, cortical ablation, parkinsonism and spinal cord injury," *Neuropharmacology*, vol. 39, no. 5, pp. 777–787, 2000.

[11] B. Haelewyn, T. Freret, E. Pacary et al., "Long-term evaluation of sensorimotor and mnesic behaviour following striatal NMDA-induced unilateral excitotoxic lesion in the mouse," *Behavioural Brain Research*, vol. 178, no. 2, pp. 235–243, 2007.

[12] M. Brenneman, S. Sharma, M. Harting et al., "Autologous bone marrow mononuclear cells enhance recovery after acute ischemic stroke in young and middle-aged rats," *Journal of Cerebral Blood Flow and Metabolism*, vol. 30, no. 1, pp. 140–149, 2010.

[13] T. Neumann-Haefelin, A. Kastrup, A. de Crespigny et al., "Serial MRI after transient focal cerebral ischemia in rats: dynamics of tissue injury, blood-brain barrier damage, and edema formation," *Stroke*, vol. 31, no. 8, pp. 1965–1973, 2000.

[14] K. Yoneda, R. Iwamura, H. Kishi, Y. Mizukami, K. Mogami, and S. Kobayashi, "Identification of the active metabolite of ticlopidine from rat in vitro metabolites," *British Journal of Pharmacology*, vol. 142, no. 3, pp. 551–557, 2004.

[15] L. Belayev, O. F. Alonso, R. Busto, W. Zhao, and M. D. Ginsberg, "Middle cerebral artery occlusion in the rat by intraluminal suture: neurological and pathological evaluation of an improved model," *Stroke*, vol. 27, no. 9, pp. 1616–1623, 1996.

[16] L. Belayev, L. Khoutorova, K. Atkins, A. Cherqui, J. Alvarez-Builla, and N. G. Bazan, "LAU-0901, a novel platelet-activating factor receptor antagonist, confers enduring neuroprotection in experimental focal cerebral ischemia in the rat," *Brain Research*, vol. 1253, pp. 184–190, 2009.

[17] Y. Wang, Z. G. Zhang, K. Rhodes et al., "Post-ischemic treatment with erythropoietin or carbamylated erythropoietin reduces infarction and improves neurological outcome in a rat model of focal cerebral ischemia," *British Journal of Pharmacology*, vol. 151, no. 8, pp. 1377–1384, 2007.

[18] P. Kowal and A. Marcinkowska-Gapińska, "Hemorheological changes dependent on the time from the onset of ischemic stroke," *Journal of the Neurological Sciences*, vol. 258, no. 1-2, pp. 132–136, 2007.

[19] I. Velcheva and G. Nikolova, "Hemorheological disturbances and cognitive function in patients with cerebrovascular disease," *Clinical Hemorheology and Microcirculation*, vol. 39, no. 1–4, pp. 397–402, 2008.

[20] S. Kuroda and B. K. Siesjö, "Reperfusion damage following focal ischemia: pathophysiology and therapeutic windows," *Clinical Neuroscience*, vol. 4, no. 4, pp. 199–212, 1997.

[21] T. Abumiya, R. Fitridge, C. Mazur et al., "Integrin α(IIb)β3 inhibitor preserves microvascular patency in experimental acute focal cerebral ischemia," *Stroke*, vol. 31, no. 6, pp. 1402–1410, 2000.

[22] T. F. Choudhri, B. L. Hoh, H.-G. Zerwes et al., "Reduced microvascular thrombosis and improved outcome in acute murine stroke by inhibiting GP IIb/IIa receptor-mediated platelet aggregation," *Journal of Clinical Investigation*, vol. 102, no. 7, pp. 1301–1310, 1998.

Hindawi Publishing Corporation
Evidence-Based Complementary and Alternative Medicine
Volume 2013, Article ID 261217, 10 pages
http://dx.doi.org/10.1155/2013/261217

Research Article

The Effects of Acupuncture on Bladder Interstitial Cells of Cajal Excitability in Rats with Overactive Bladder

Qi-fan Feng, Yuen-hao Hou, Wen-guang Hou, Zhi-xian Lin, Kang-min Tang, and Yue-lai Chen

Shanghai University of Traditional Chinese Medicine, Shanghai 201203, China

Correspondence should be addressed to Yue-lai Chen; chenyuelai@163.com

Received 7 June 2013; Revised 9 August 2013; Accepted 12 August 2013

Academic Editor: Yong-Qing Yang

It is well known that acupuncture treatment has an effect on patients with an overactive bladder, but the mechanism of its action remains to be clarified. This study was aimed to investigate the effects of acupuncture on bladder overactivity, and the excitability of interstitial cells of Cajal of the bladder in a rat model of partial bladder outlet obstruction. Electroacupuncture (continuous wave, 30 Hz, 1 mA) was applied to stimulate the Ciliao point (BL32) and the Huiyang point (BL35) of rats for 20 min, 3 days. Results showed that acupuncture suppressed detrusor unstable contraction frequency and decreased detrusor maximum pressure in the bladder filling period. Compared with the normal control rats, HCN2 mRNA and protein expression within the bladder were upregulated and were reversed by electroacupuncture in overactive bladder rats as determined by RT-PCR, western blotting and immunohistochemistry. Moreover, in-vitro cell-cultured OAB rats bladder interstitial cells of Cajal intracellular Ca^{2+} concentration were higher than normal control rats, which were lowered after acupuncture treatment. These findings suggest that acupuncture stimulation can suppress bladder overactivity, and regulate the excitability of bladder interstitial cells of Cajal in treatment of overactive bladder myogenic mechanism.

1. Introduction

Overactive bladder (OAB) syndrome is characterized by urinary frequency and urgency with or without urge incontinence, and is often accompanied by nocturia. Acupuncture, as one of the traditional Chinese therapeutics, provides a nondrug therapy for OAB. It has been reported that the acupuncture stimulation to the sacral vertebrae has a suppressive effect on bladder activity, improves the symptom of nocturnal enuresis, decreases mean urge frequency, and diminishes voiding symptoms [1–5]. Our previous clinical studies have showed that acupuncture could improve urine dynamics condition, inhibit detrusor instability contraction, increase the bladder capacity, and improve quality of life significantly in OAB patients [6–8]. Although the effect of acupuncture on bladder activity has been confirmed, the mechanism of its action remains to be clarified. We previously found that the nitrergic neurotransmitter in bladder neck and detrusor was obviously decreased in rats with unstable bladder, the electroacupuncture treatment could significantly increase the contains of NOS in bladder tissue, regulate the bladder function, and inhibit bladder overactivity [9].

Many studies have found that interstitial cells of Cajal (ICCs) in bladder, like in gastrointestinal tract, act as primary pace maker cells that generate depolarizing currents into neighboring smooth muscles and coordinate muscle contractions, playing a fundamental role in signal transmission from bladder nerves to smooth muscle cells [10]. Bladder generates intrinsic autonomic contractions, and these intrinsic contractions are coordinated by the specialized system of ICCs [11]. c-Kit is used as an identification marker of ICCs, and Glivec (imatinib mesylate) is a c-kit receptor inhibitor, which reduces bladder overactivity. ICCs are linked to each other and to smooth muscle cells by gap junctions forming a continuous network, producing a syncytium of neurons enabling fast signal transduction [12]. c-Kit-positive ICCs are more numerous in human OAB detrusor than normal detrusor, suggesting that bladder ICCs one associated with the pathophysiology of OAB [13]. Hyperpolarization-activated cyclic nucleotide-gated (HCN) channels are unique among

vertebrate voltagegated ion channel, which lead to activation on hyperpolarization. The HCN cation channel protein is regarded as the structural basis of the hyperpolarization-activated inward (Ih) current, which plays a very important role in pacemaking [14]. HCN protein is identified in ICCs of rat bladder, the expression of HCN protein is enhanced obviously in OAB rats, which may be responsible for the increased bladder excitability [15]. The change of structure and cell communication function of pace maker ICCs in bladder result in bladder overactivity. Whether the effect of acupuncture stimulation merely acts on the detrusor smooth muscle cells or to achieve through regulating the pace marker ICCs excitability? Therefore, the present study was performed in rats to examine: (1) the effects of acupuncture stimulation on bladder overactivity; (2) whether the change of bladder ICCs excitability mediates detrusor unstable contraction; (3) how acupuncture regulates the bladder ICCs excitability in treatment of unstable bladder myogenic mechanism.

2. Materials and Methods

2.1. Animals and Study Design. All experiments were performed on female Wistar rats, obtained from the Experimental Animal Center, Shanghai University of Tranditional Chinese Medicine, weighing 180–200 g at the beginning of the experiment. Animals were housed in a 12 h light/dark cycle with food and water available ad libitum. The room temperature was maintained at 22 ± 1°C and relative humidity at 45–50%. Five animals were housed in each cage. All experiments were performed complying with international ethical standards in the care and use of animals, and passed the examination of animal ethics committee of Shanghai University of TCM.

Female Wistar rats ($n = 100$) firstly were randomly divided into two groups: normal control ($n = 15$), model ($n = 85$). Rats were anesthetized by intraperitoneal injection of 1% pentobarbital sodium (50 mg/kg). The normal control group underwent a sham operation. Partial bladder outlet obstruction (PBOO), the classical method to induce OAB [16], was performed in model group. After 6 weeks, the models were assessed by cystometrogram under urethane anesthesia. When the detrusor contraction caused by pressure fluctuation shows phase contraction wave, the model was set up [17]. The success models ($n = 46$) were randomly divided into 3 groups: model group ($n = 15$), acupuncture group ($n = 15$), Glivec group ($n = 16$). Model group were no treatment, acupuncture group were treated by electroacupuncture. Glivec group were irrigated in the bladder with ICCs blocker Glivec (10^{-5} mol/L, 1 mL/day, Santa Cruz Biotechnology), other groups were treated by bladder irrigation physiological saline, and every group was continuous treatment for 3 days.

2.2. Acupuncture Treatment. Conscious rats were treated by acupuncture. One acupuncture needle (diameter, 0.22 mm) was positioned almost vertically underneath the periosteum about 5 mm lateral to the midline of the S_2 (BL32, Ciliao) and the other acupuncture needle (diameter, 0.22 mm) was positioned almost vertically underneath the periosteum about 5 mm lateral to the midline of the coccyx (BL35, Huiyang), bilateral symmetry. Stimulated electrically at both right and left points with frequency of 30 Hz and intensity of 1 mA, the entire procedure lasting 20 min.

2.3. PBOO Operation and Cystometric Analysis. The operations of PBOO were performed under general anesthesia provided by intraperitoneal injection of 1% pentobarbital sodium (50 mg/kg). A 2-3 cm midline suprapubic skin incision was made, the fascia was reflected, the peritoneum was opened, and the bladder was identified. The urethra was inserted by a epidural catheter (diameter 1 mm), the proximal urethra was separated by a smooth forceps and tied with 2-0 sterile silk, the degree of tightness was that the catheter could be pulled easily, then the catheter was removed. The midline incision was closed in two layers with 5-0 polypropylene suture.

The models were assessed by cystometric analysis after 6 weeks. All Rats were anesthetized by intraperitoneal injection of 20% urethane (0.5 mL/100 g). One end of the transvesical catheter (polyethylene catheter-50) was inserted into the bladder through urethra and the other was connected to a pressure transducer and syringe pump via a 3-way stopcock to record intravesical pressure and infuse saline into the bladder. After the bladder was emptied, cystometry was performed with saline infused at 0.2 mL/min. The detrusor unstable contraction frequency and maximum pressure in the bladder filling period were recorded before and after treatment, the detrusor unstable contraction frequency was recorded by counting no-voiding contraction.

2.4. RNA Extraction and Quantitative RT-PCR. All rats were killed by cervical dislocation, the abdomen was opened, trigone of urinary bladder was aseptically isolated and immediately frozen in liquid nitrogen, and placed immediately to be stored at −80°C until it is used. Each Sample was collected in 1 mL ice-cold Trizol (Invitrogen, Carlsbad, CA, USA). After its homogenization and sonification, RNA was extracted with chloroform, precipitated with isopropyl alcohol, and dissolved in 30 μL RNAse-free DEPC. The RNA concentration and purity were analyzed by a Nanodrop spectrophotometer (Nanodrop Technologies, Wilmington, DE), with the spectral absorption at 260 and 280 nm. For cDNA synthesis, oligo(dT) primers, 1 μg of each total RNA sample, and the RevertAid First Strand cDNA Synthesis Kit (Fermentas, Ontario, Canada) were used, following the guidelines of the manufacturer. cDNA samples were placed on ice and stored at −20°C until further use. Prior to the analysis, 10 μL of each cDNA sample was diluted with 90 μL of MilliQ water.

Quantitative RT-PCR was carried out in 20 μL buffer solution containing 1 μL of diluted cDNA sample, 10 μL 2×SYBR green II qRT-PCR kit (Toyobo, Osaka, Japan), 1 μL of each primer (5 μM), and 8 μL of MilliQ water. Primers to detect the mRNAs of the housekeeping gene β-actin of Hcn were designed using Primer 3 (http://frodo.wi.mit.edu/). Primer pairs were for β-actin: 5′-TCTGTGTGGATTGGTGGCTCT-3′ and 5′-AGAAGCATTTGCGGTGCAC-3′, for Hcn: 5′-ACCCCCAGCTCGTCTACTCT-3′ and 5′-ACCCCATCTTGTTTCTGCAC-3′. Cycling conditions were 10 min

95°C, followed by 40 cycles of 15 sec at 95°C and 1 min at 60°C. After cycling, a melting protocol was performed with 15 sec at 95°C, 1 min at 60°C, and 15 sec at 95°C, to control product specificity. The fold change (FC) in target gene cDNA relative to selected endogenous control gene was determined as follows: $FC = 2^{-\Delta\Delta Ct}$, where $\Delta\Delta Ct = (Ct_{Target} - Ct_{Control})$ test $- (Ct_{Target} - Ct_{Control})$ control. Ct values were defined as the number of the PCR cycles at which the fluorescence signals were detected.

2.5. Western Blotting. Frozen tissues were homogenized in cold lysis buffer (Beyotime Biotechnology Co., Haimen, Jiangsu, China) and centrifuged at 13, 000 rpm for 5 min at 4°C, the supernatant total protein was quantified by Lowry method [18]. Samples (30 μg total protein per loading) were separated on a 10% sodium dodecyl sulfate-polyacrylamide gel, electrophoresis gel, and electrotransfered onto polyvinylidene difluoride membranes (Millipore, Bedford, MA, USA). The membranes were blocked with 5% nonfat milk overnight at 4°C, and then incubated with the primary antibodies recognizing β-actin (mouse monoclonal, 1 : 5000, Abcam, Cambridge, UK) or HCN2 antibody (rabbit polyclonal, 1 : 1000, Cell Signaling Technology, Danvers, MA, USA) for 2 h at 22°C. Then, the membranes were incubated with a horseradish peroxidase-conjugated antimouse (1 : 5000, Abcam, Cambridge, UK) or goat antirabbit HRP (1 : 4000, Abcam, Cambridge, UK) secondary antibodies. The signal was visualized with ECL plus reagent (GE healthcare, Buckinghamshire, UK) and exposed onto X-ray film (Kodak, Rochester, NY, USA). Protein ratios were calculated based on densitometrical quantification of scanned films in Image J software. HCN protein levels were normalized to actin levels and to levels of a control animal sample.

2.6. Immunohistochemistry. The bladder was fixed in buffered 10% formalin for 24 h, dehydrated and embedded in paraffin, then cut section at 3 μm for IF assay. In summary, slides were immersed to a boil (99°C~100°C) in 0.01 M sodium citrate buffer (pH 6.0) for 10 minutes. After the nonspecific binding was blocked with normal 5% goat serum, slides were incubated overnight with the primary antibodies c-Kit (H-300) antibody (sc5535, Santa Cruz Biotechnology) and Anti-HCN2 antibody (ab84817, Abcam), followed by the mixture of two fluorescent conjugated secondary antibodies for 30 min, Alexa Fluor 488 goat antirabbit IgG (Cat:A11034, Invitrogen, USA) and Alexa Fluor 555 goat anti-mouse IgG (Cat:A21424, Invitrogen, USA). Finally, the slides were mounted with DAPI mounting solution (P36935, Invitrogen, USA) and evaluated by 50i Nikon microscope in dark. The nucleus were visualized blue using a filter 330–380 nm and positive labeled expression with green by the filter 465–495 nm, with red by the filter 530–600 nm.

2.7. Primary Bladder ICCs Cell Culture and Identification. Referring to the previous experiments [19, 20], the rat bladder was dissected and placed in D-hanks' solution and the mucosal layer was removed. The smooth muscle was cut into small pieces and placed into 1 mg/mL collagenase type II (Worthington), 0.5 mg/mL trypsin (PAA), 1 mg/mL BSA (Huamei biological engineering company, China) solution. The smooth muscle was incubated in shaking bath for 8 min at 37°C 300 RPM, repeated 5 times. After incubation cells were centrifuged at 1500 RPM for 5 min, then the superfusate containing collagenase was removed. Cells were resuspended in 5 mL RPMI solution containing 30% FBS and centrifuged again at 1500 RPM for 5 min (twice). After the last cleaning process, 3 mL RPMI solution containing 30% FBS was added for the 1 plates (diameter 3 cm) having 2.5 mL cell suspension each, for measurement of intracellular-free Ca^{2+} concentration use 96 well plates. In our experiment, we found that while the ICCs took 3-4 hours to become attached to the plate of the culture disk, the detrusor cells would take 6 hours to do the same. Therefore, we used this time difference to separate these two types of cells concerned. Experiments were carried out on 1-2 days-old cultures. The ICCs in the cultures were morphologically distinct from the smooth muscle cells and their identity was confirmed with immunocytochemistry using primary antibodies against c-Kit.

Immunohistochemistry to visualize cells expressing c-Kit immunoreactivity, cells were fixed in 3.7% formaldehyde (Thremo fish) 10 min, blocked in 1% bovine serum albumin (BSA) for 20 min, and preparations were loaded in the dark incubated for 12 h in PBS containing c-Kit protein (SC 5535, diluted 1 : 200, Santa Cruz Biotechnology). The cell plate was washed and then incubated for another 1 h 37°C in antirabbit IgG antibody labelled with a fluorescent marker (IgG-Alexa Fluor 488, diluted 1 : 900, Cell Signaling Technology). After washing with PBS, the preparations were observed using an inverted fluorescence microscopy (Axiovert 40 CFL, Zeiss, Germany).

2.8. Measurement of Bladder ICCs Intracellular Free Ca^{2+} Concentration, $[Ca^{2+}]i$. Preparations were loaded in DMSO containing 5 μmol/L fura-2 AM (Dojindo Laboratories, Japan) for 40 min at 37°C. They were washed three times in PBS and de-esterified for 40 minutes at 37°C before the experiment. Varioskan flash (Thermo Fisher Scientific) was used for measuring $[Ca^{2+}]i$ concentration. Intensity ratios at 340 and 380 nm excitation (F_{340}/F_{380}) were calibrated using an in vitro method and converted into Ca^{2+} concentration according to the equation, $[Ca^{2+}]i = K_d\ ((R - R_{min})/(R_{max} - R))$, where K_d represents the dissociation constant with a value of 224 nM, R represents F_{340}/F_{380}, and R_{min} and R_{max} represent intensity ratios in 0 Ca^{2+} (added 0.1 M EGTA) and saturating Ca^{2+} (0.1% Triton X-100 and 0.1 M $CaCl_2$).

2.9. Data Analysis. All data were expressed as mean ± SD. Statistical significance was tested using one-way analysis of variance (ANOVA) and post hoc tests, with values of $P < 0.05$ considered significant.

3. Results

3.1. Effects of Acupuncture Treatment on Urodynamics

3.1.1. Effects of Acupuncture Treatment on the Detrusor Unstable Contraction Frequency in Bladder Filling Period. No

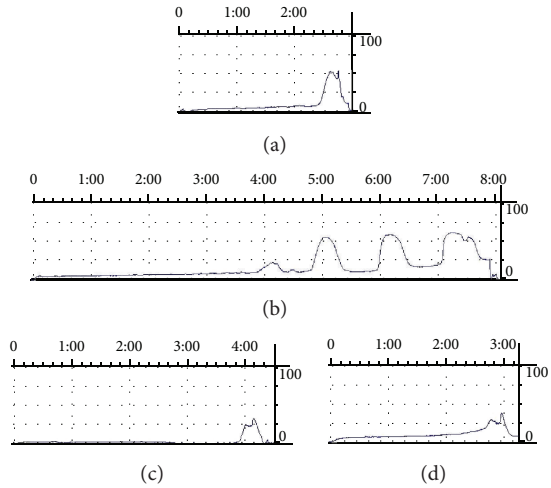

Figure 1: The original tracing of cystometrogram after treatment. (a) Normal control group (b) model group, and (c) acupuncture group; (d): Glivec group.

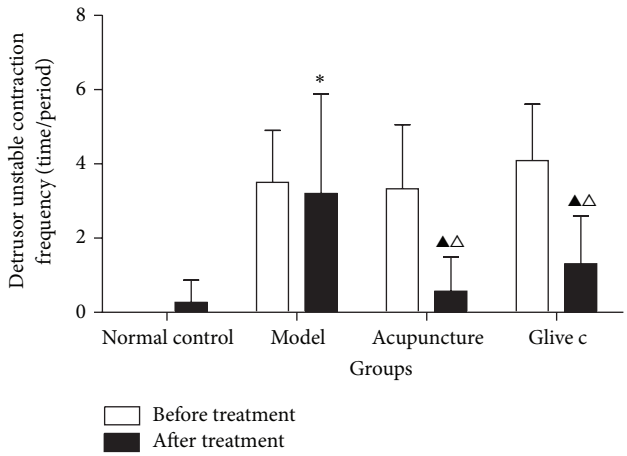

Figure 2: The detrusor unstable contraction frequency in bladder filling period before and after treatment for normal control, model, acupuncture, and Glivec groups. ▲ after treatment versus before treatment $P < 0.05$. ∗ versus normal control group $P < 0.05$. △ versus model group $P < 0.05$.

significant differences in body weight were observed among four groups before and after treatment. ($P = 0.227$ before treatment, $P = 0.77$ after treatment).

In cystometrograms performed six weeks after the operation, compared with normal control group (0.00 ± 0.00, $n = 13$), the detrusor unstable contraction frequency (time/period) in bladder filling period was significantly increased in the model group (3.50 ± 1.40, $n = 15$) ($P = 0.00$, $P > 0.05$), acupuncture group (3.33 ± 1.73, $n = 15$) ($P = 0.00$, $P > 0.05$), and Glivec group (4.09 ± 1.52, $n = 16$) ($P = 0.00$, $P > 0.05$), but no significant difference among model group, acupuncture group, and Glivec group ($P = 0.74$, $P = 0.24$, $P = 0.13$, $P > 0.05$). Comparison before and after treatment, there was no difference in the normal control group ($P = 0.13$, $P > 0.05$) and model group respectively, ($P = 0.64$, $P > 0.05$), and decreased in the acupuncture group ($P = 0.00$, $P < 0.05$), and Glivec group respectively, ($P = 0.00$, $P < 0.05$). Comparison among groups after treatment ($F = 9.805$, $P = 0.00$, $P < 0.05$), normal control group (0.27 ± 0.60) acupuncture group (0.57 ± 0.92), Glivec group (1.31 ± 1.29) were less than model group (3.20 ± 2.68) ($P = 0.00$, $P = 0.00$, and $P = 0.00$, $P < 0.05$), and there were no significant difference among the normal group, acupuncture group and Glivec group ($P = 0.63$, $P = 0.09$, and $P = 0.20$, $P > 0.05$) (Figures 1 and 2).

3.1.2. Effects of Acupuncture Treatment on the Detrusor Unstable Contraction Maximum Pressure in Bladder Filling Period. In cystometrograms performed six weeks after the operation, compared with the normal control group (4.32 ± 1.35, $n = 13$), the detrusor unstable contraction maximum pressure (cmH_2O) in bladder filling period was significantly raised in the model group (54.27 ± 22.39, $n = 15$) ($P = 0.00$, $P > 0.05$), acupuncture group (51.95 ± 20.33, $n = 15$) ($P = 0.00$, $P > 0.05$), and Glivec group (61.69 ± 16.28, $n = 16$) ($P = 0.00$, $P > 0.05$), but no significant difference among model group, acupuncture group, and Glivec group ($P = 0.72$, $P = 0.24$, and $P = 0.13$, $P > 0.05$). in a Comparison before and after treatment, there was no difference in the normal control group ($P = 0.06$, $P > 0.05$) and model group respectively ($P = 0.348$, $P > 0.05$), and decreased in the acupuncture group ($P = 0.00$, $P < 0.05$) and Glivec group respectively ($P = 0.00$, $P < 0.05$). Comparison among groups after treatment ($F = 15.305$, $P = 0.00$, $P < 0.05$), normal control group (7.68 ± 4.69) and acupuncture group (14.29 ± 10.94), Glivec group (18.24 ± 18.10) were lower than model group (45.69 ± 23.55) ($P = 0.00$, $P = 0.00$, and $P = 0.00$, $P < 0.05$), and there were no significant difference among normal group, acupuncture group, and Glivec group ($P = 0.29$, $P = 0.09$, and $P = 0.50$, $P > 0.05$) (Figures 1 and 3).

3.2. Effects of Acupuncture Treatment on Bladder HCN2 mRNA and Protein

3.2.1. Expression of HCN2 mRNA in Bladder Detected With RT-PCR. The expression of HCN2 mRNA in bladder was significantly different among groups ($F = 3.788$, $P = 0.024$, $P < 0.05$). Model group (2.21 ± 1.12, $n = 7$) is significantly higher than normal control group (1.21 ± 0.46, $n = 7$) ($P = 0.01$, $P < 0.05$), acupuncture group (1.36 ± 0.50, $n = 6$) ($P = 0.04$, $P < 0.05$), and Glivec Group (1.09 ± 0.41, $n = 7$), ($P = 0.00$, $P < 0.05$) (Figure 4).

3.2.2. Expression of HCN2 Protein in Bladder Detected by Western Blotting. Similar to the result from RT-PCR, the expression of HCN2 protein in bladder was different among groups ($F = 3.394$, $P = 0.05$). Model group (0.93 ± 0.17, $n = 4$) was increased compared with normal control group (0.62 ± 0.11, $n = 4$) ($P = 0.01$, $P < 0.05$), and significantly decreased in the acupuncture group (0.69 ± 0.14, $n = 4$) ($P = 0.04$, $P < 0.05$) and Glivec group (0.69 ± 0.16, $n = 4$) ($P = 0.04$, $P < 0.05$) (Figure 5).

3.3. Effects of Acupuncture Treatment on Bladder ICCs Distribution and Quantity. To detect the ICCs in rat bladder,

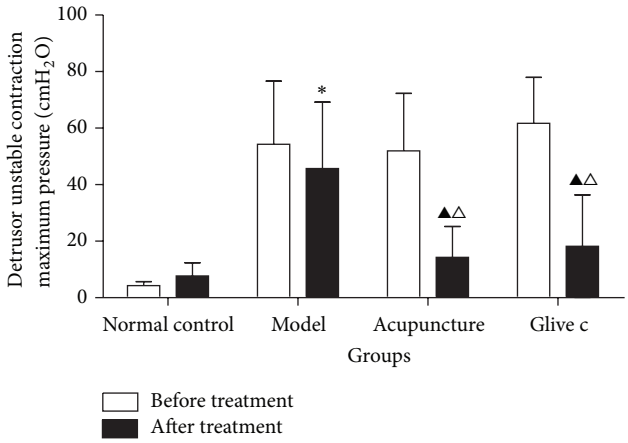

Figure 3: The detrusor unstable contraction maximum pressure in bladder filling period before and after treatment for normal control, model, acupuncture, and Glivec groups. ▲ after treatment versus before treatment $P < 0.05$. ∗ versus normal control group $P < 0.05$. △ versus model group $P < 0.05$.

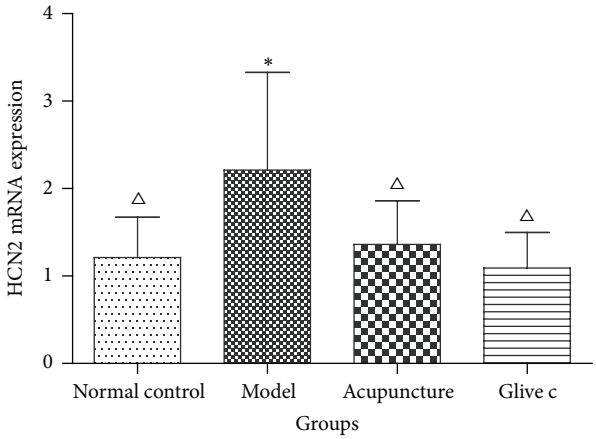

Figure 4: Relative expression level of the HCN2 mRNA in bladder determined by RT-PCR. ∗ versus normal control group $P < 0.05$. △ versus model group $P < 0.05$.

fluorescent staining method was applied, c-Kit-positive ICCs (red) were found in rat urothelium, suburothelium, and muscle layer by fluorescence microscope. Bladder ICCs were found in detrusor muscle layers that were mainly located along the boundary of smooth muscle bundles and between muscle bundles. The quantity of ICCs was counted in every visual field and 10 visual fields were observed by random in every group. The result showed a significant difference among groups ($F = 3.086$, $P = 0.039$, $P < 0.05$). Model group (2.70 ± 2.41) was more than normal control group (0.40 ± 0.84) ($P = 0.01$, $P < 0.05$), but there were no difference compared with acupuncture group (1.30 ± 0.95) ($P = 0.08$, $P > 0.05$) and Glivec group (1.60 ± 2.07) ($P = 0.16$, $P > 0.05$) (Figure 6).

3.4. Effects of Acupuncture Treatment on the Quantity of HCN2 Channel in Bladder ICCs. The relationship between

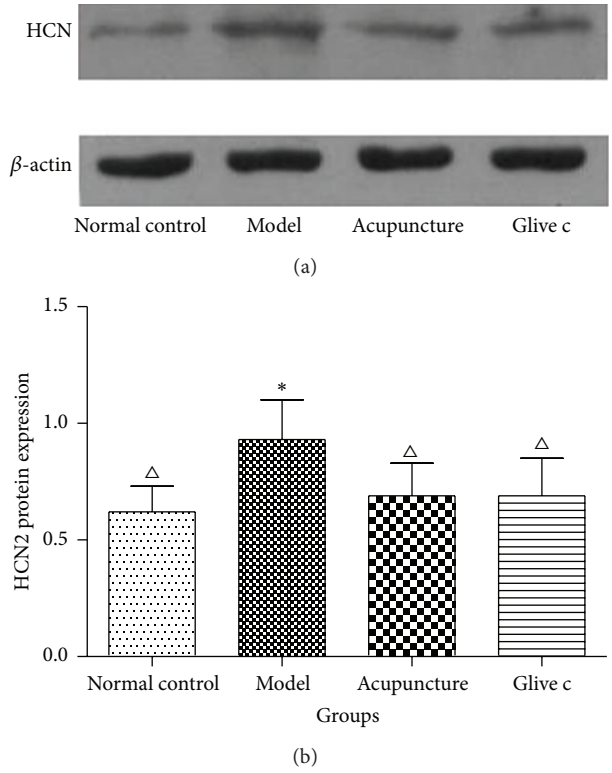

Figure 5: Relative expression level of the HCN2 protein in bladder determined by Western blotting. ∗ versus normal control group $P < 0.05$. △ versus model group $P < 0.05$.

bladder ICCs and HCN2 channel was investigated by double immunofluorescence experiments using c-Kit antibody followed by the antibody protein HCN2, known to be the important features of the pace maker. An relationship was noticed that the HCN2 staining was observed in c-Kit positive ICCs within the individual cell bodies, the HCN2 and c-Kit immunostaining were uniformly present throughout the cytoplasm. HCN2 immunostaining ICCs were also counted in every visual field and 10 visual fields were observed by random in every group. The results revealed a significant difference among these groups ($F = 6.756$, $P = 0.00$, $P < 0.05$), the quantity of HCN2 positive ICCs in model group (10.50 ± 8.53) was significantly increased compared with normal control group (0.40 ± 0.97) ($P = 0.00$, $P < 0.05$), and was less distributed in acupuncture treatment (4.20 ± 4.64) ($P = 0.01$, $P < 0.05$) and Glivec group (4.60 ± 2.80) ($P = 0.01$, $P < 0.05$) (Figure 7).

3.5. Effects of Acupuncture Treatment on Bladder ICCs Intracellular Free Ca^{2+} Concentration. Cultured cells were observed under inverted microscope. The morphology of ICCs was spindle-shaped, with several branches emanating from a central soma, and connected with neighboring cells, showing networks (Figure 8). The ICCs in the cultures were morphologically distinct from the smooth muscle cells and their identity was confirmed with immunocytochemistry using primary antibodies against c-Kit (Figures 9(a), 9(b), and 9(c)).

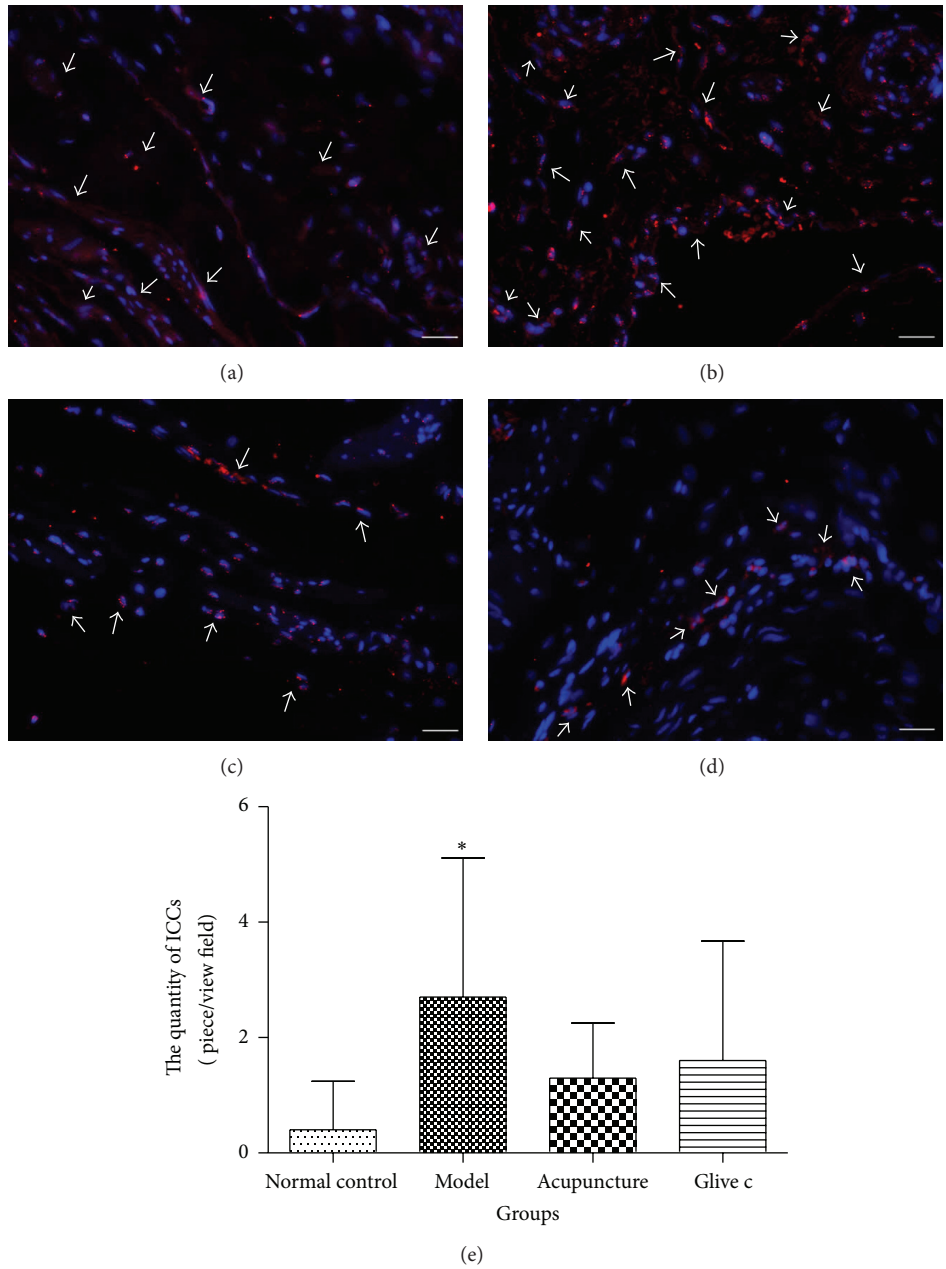

Figure 6: Changes of distribution and quantity in bladder ICCs. ((a), (b), (c), and (d)) Immunofluorescence of c-Kit in bladder. Nucleus stained by DAPI (blue), c-Kit (red) in urothelium, suburothelia, and muscle layer. c-Kit-positive ICCs (↑). (a) Normal control group, (b) model group, (c) acupuncture group, and (d) Glivec group. Scale bar is 50 μm. (e) Comparisons of relative quantity of ICCs in bladder after treatment. $*$ versus normal control group $P < 0.05$.

The ability of rat bladder ICCs to respond to the acupuncture stimulation and Glivec was investigated in primary cultured and fresh cells, loaded with Ca^{2+} indicator fura-2 AM. Varioskan flash (ThermoFisher Scientific) was used for measuring $[Ca^{2+}]i$ concentration, every well in 96-well plates was determined on 5 regions of interest, and 40 regions were selected in each group. According to the equation, $[Ca^{2+}]i = K_d((R-R_{min})/(R_{max}-R))$, to convert into Ca^{2+} concentration. The intracellular free Ca^{2+} concentration in bladder ICCs of model group (10.73 ± 3.05) was higher as compared to normal control group (5.24 ± 2.80), ($P = 0.00$, $P < 0.05$); acupuncture stimulation (5.57 ± 5.31) and Glivec bladder irrigation (6.21 ± 2.60) was significantly lower the OAB rats bladder ICCs intracellular Ca^{2+} concentration ($P = 0.00$, $P = 0.00$, $P < 0.05$) (Figure 10).

4. Discussion

This study demonstrated that acupuncture stimulation suppressed bladder overactivity, down-regulated the expression

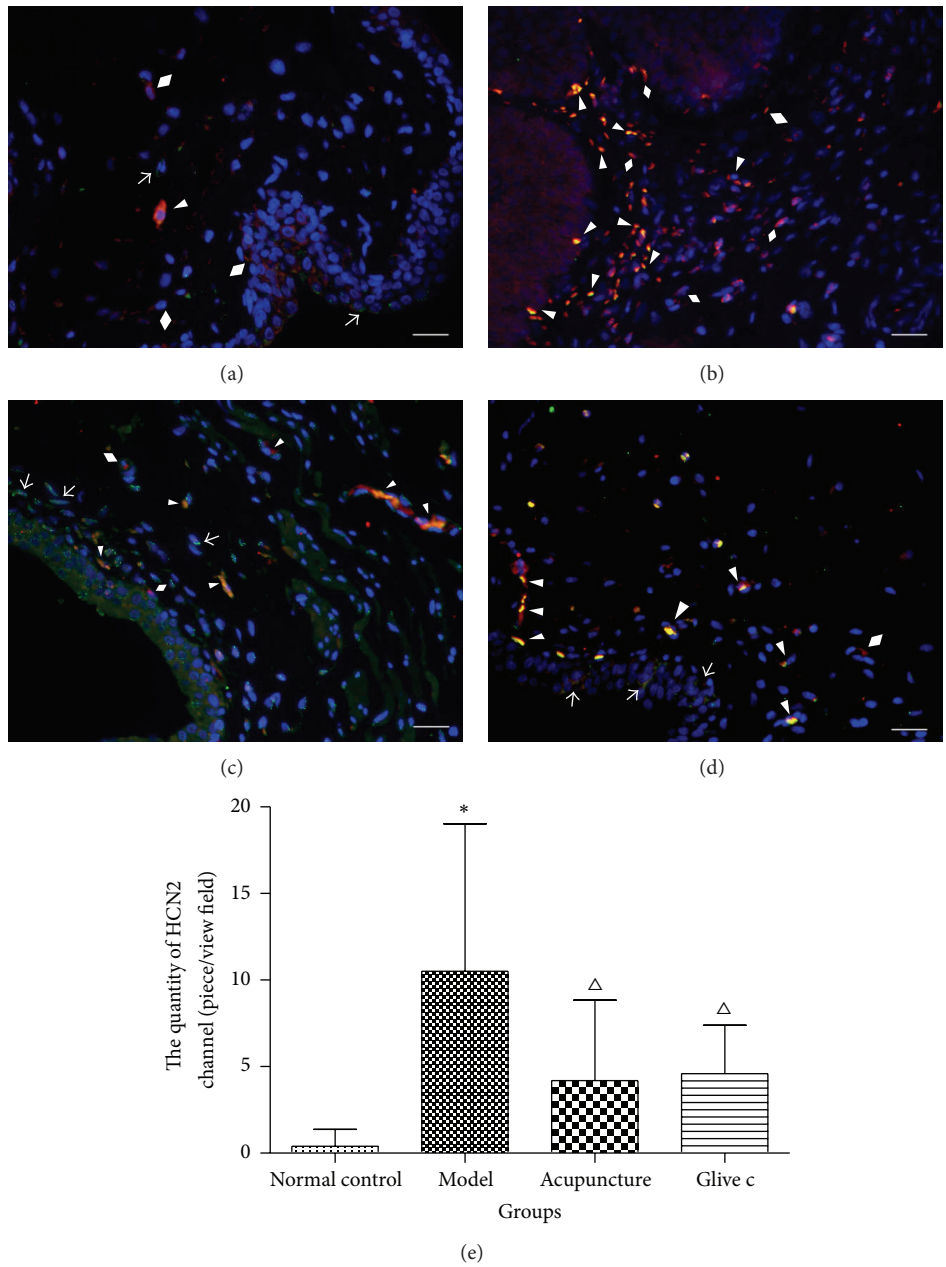

Figure 7: The quantity of HCN2 channel in bladder ICCs. ((a), (b), (c), and (d)) Double-labeled immunofluorescence of HCN2 and c-Kit in bladder. Nucleus stained by DAPI (blue), c-Kit (green), and HCN2 (red) staining in urothelium, suburothelium, and muscle layer. Some ICCs were c-kit positive (↑), some were HCN2 positive (◆), and some were double labeled (▲). (a) Normal control group, (b) model group, (c) acupuncture group, (d) Glivec group. Scale bar is 50 μm. (e) Comparisons of relative quantity of HCN2 channel in bladder ICCs after treatment. $*$ versus normal control group $P < 0.05$. $\triangle$ versus model group $P < 0.05$.

of HCN2 mRNA and protein in bladder, reduced the quantity of HCN2 channel in bladder ICCs, and also decreased bladder ICCs intracellular free Ca^{2+} concentration. This is the first evidence that acupuncture stimulation regulates the excitability of bladder ICCs in treatment of overactive bladder myogenic mechanism.

The points of stimulation in this study are the classical points BL32 and BL35 corresponding to sacral vertebrae S_2 level and coccyx, which belongs to the Bladder Meridian of Foot Taiyang in Traditional Chinese Medicine [21]. The clinical studies show that acupuncture stimulation to the sacral vertebrae increases bladder capacity and suppresses overactive bladder [22, 23]. In our previous clinical studies, we found that electroacupuncture with continuous wave, 30 Hz, 1 mA, 20 min, 3 days stimulation could suppress bladder unstable contraction frequency, and decrease detrusor maximum pressure in the bladder filling period thereby suppressing bladder overactivity. Therefore, we used the same therapy through the experiment.

ICCs have been widely recognized as playing key roles in the initiating contractile activity, mediating neurotransmission, conducting electrical impulses, and acting as a stretch

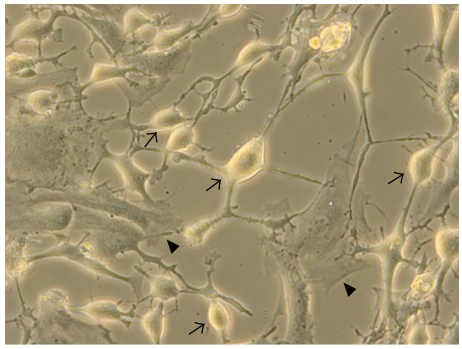

Figure 8: The morphology of ICCs (↑) and detrusor cell (▲) under inverted microscope (×400).

sensor [24]. The spontaneous action potentials identified in the ICCs indicate that changes in the excitability of this cell lead to a series of contractile abnormality. The number of ICCs was increased in overactive bladder, the changes in ICCs may account for pathologically increased signal transmission between cells [25]. The clinical significance of bladder ICC in bladder dysfunction has been investigated by studies of tissue from patients with unstable bladders which reportedly have larger numbers and density of distribution of ICC than control samples, Glivec (imatinib mesylate) 10^{-5} M, improved bladder capacity, compliance, voided volumes, urinary frequency, and reduced contraction thresholds and spontaneous activity [26]. Our results show that the quality of c-Kit-positive bladder ICCs in OAB rats was significantly increased compared with normal control rats, which was consistent with the results of above studies. However, the quatity was not significantly reduced by acupuncture stimulation and Glievc 10^{-5} mol/L bladder irrigation.

HCN channels are active at resting membrane potential and thus are believed to participate in autorhythmicity and excitability. Immunofluorescence and Western blotting revealed that HCN1, HCN2, HCN3, and HCN4 channels were all present in the ICCs of the human bladder [27]. HCN1, 2, 4 subtypes play important role in modulating bladder excitability by controlling the kit-positive ICC-like cells. HCN channel, and its Ih current may take part in the modulation of cell excitation and might control the excitability of bladder. HCN channel, as a potential peacemaker, was involved in the regulation of bladder excitation, presumably via bladder ICC-like cells [28]. In our study, immunohistochemistry was also used to detect HCN2 channel. The quality of HCN2 in ICCs in OAB rats was significantly increased compared with normal control rats, and significantly reduced by acupuncture stimulation and Glievc 10^{-5} M bladder irrigation. The results from RT-PCR and western blotting analysis revealed that HCN2 subtype was detected in bladder, and its mRNA and protein expression were increased in OAB rats, suggesting that there are some changes in the HCN2 channel in the pathologic conditions, with the excitability enhancement of HCN2 channel in bladder. HCN2 involved in the suppressing effect of acupuncture stimulation on bladder unstable contraction, acupuncture stimulation and Glivec 10^{-5} M bladder irrigation down-regulated the HCN2 mRNA and protein

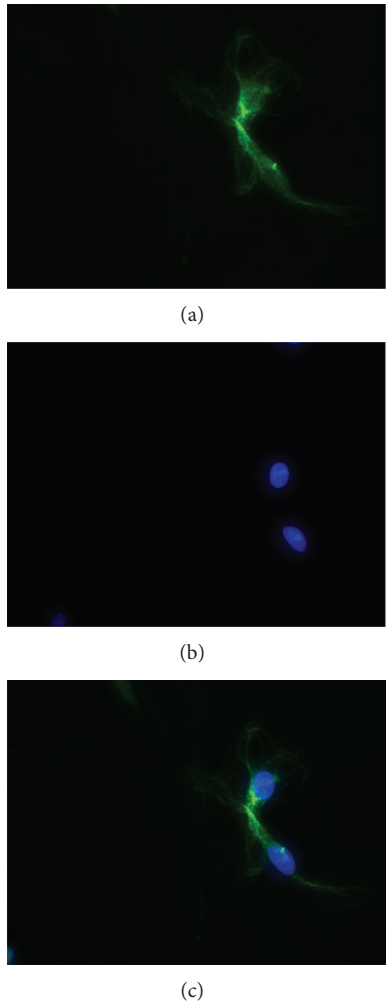

Figure 9: The c-Kit immunofluorescence of ICCs under Inverted Fluorescence Microscope (×400). (a) c-Kit-positive ICCs (green). (b) Nucleus stained by DAPI (blue). (c) Merge.

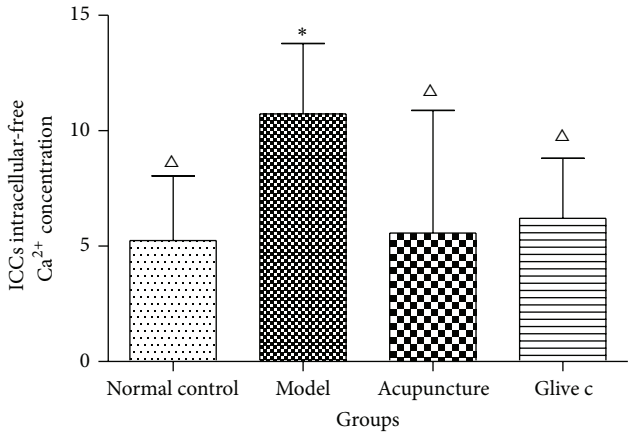

Figure 10: Comparisons of relative bladder ICCs intracellular-free Ca^{2+} concentration among four groups after treatment. ∗ versus normal control group $P < 0.005$, △ versus model group $P < 0.005$.

expression, suggesting that HCN channel in ICCs may be the new therapeutic target for OAB.

Modulation of cytoplasmic Ca^{2+} concentration is a mechanism common to signal transduction pathways regulating many cellular phenomena, the role of intracellular Ca^{2+} is of particular importance, as it is the main determinant of detrusor contractile activity. Spontaneous, autonomous cellular activity-Ca^{2+} and membrane potential oscillations, originate from detrusor smooth muscle in human bladders, mediated by extracellular Ca^{2+} influx and intracellular release [29]. Meanwhile, these pace maker cells ICCs generate the repetitive Ca^{2+} transients that activate inward currents that spread through the gap junctions to provide the depolarizing signal that triggers contraction through opening L-type voltage-operated channels (VOCs) allowing external Ca^{2+} to flood into the cell to trigger contraction [30]. In this study, we revealed that basal intracellular free Ca^{2+} concentration was elevated in Bladder ICCs from overactive bladders and was significantly decreased through acupuncture stimulation and Glivec, which suggest that acupuncture might have affected the membrane potential and made it difficult to induce Ca^{2+} influx, and the L-type calcium channel opened to trigger the action potential.

5. Conclusions

A systematic profile of the effects of acupuncture stimulation on bladder overactivity and the excitability of bladder ICCs were shown in the present study. The results show that acupuncture stimulation suppressed bladder overactivity, down-regulated the expression of HCN2 mRNA and protein in bladder, and reduced the quality of HCN2 chanel in bladder ICCs. Furthermore, acupuncture stimulation also decreased bladder ICCs intracellular-free Ca^{2+} concentration. The result may help to provide a scientific foundation to build the clinical acupuncture treatment in OAB.

Acknowledgments

The authors are grateful to The National Natural Science Foundation of China (no. 81072761), Science and Technology Commission of Shanghai Municipality (no. 11DZ1973502), and Shanghai Municipal Health and Family Planning Commission (no. ZYSNXD-CC-ZDYJ040) for financially supporting this work. They appreciate Dr. Rong Lu, (School of Basic Medicine of Shanghai university of Traditional Chinese Medicine), and Dr. Cheng-guang Li, (Institute of spinal decease research of Longhua Hospital affiliated to Shanghai University of Traditional Chinese Medicine) for their constructive discussion and suggestions for this work. They also thank Dr. Ke Wang, (Shuguang Hospital Affiliated to Shanghai University of Traditional Chinese Medicine) for his helps in data interpretation and revising of the paper.

References

[1] Y. Tanaka, Y. Koyama, E. Jodo et al., "Effects of acupuncture to the sacral segment on the bladder activity and electroencephalogram," *Psychiatry and Clinical Neurosciences*, vol. 56, no. 3, pp. 249–250, 2002.

[2] K. Hino, H. Honjo, M. Nakao, and H. Kitakoji, "The effects of sacral acupuncture on acetic acid-induced bladder irritation in conscious rats," *Urology*, vol. 75, no. 3, pp. 730–734, 2010.

[3] H. Wang, Y. Tanaka, A. Kawauchi, T. Miki, Y. Kayama, and Y. Koyama, "Acupuncture of the sacral vertebrae suppresses bladder activity and bladder activity-related neurons in the brainstem micturition center," *Neuroscience Research*, vol. 72, no. 1, pp. 43–49, 2012.

[4] S. H. Tjon Eng Soe, D. J. Kopsky, P. J. H. Jongen, H. C. W. de Vet, and C. L. Oei-Tan, "Multiple sclerosis patients with bladder dysfunction have decreased symptoms after electro-acupuncture," *Multiple Sclerosis*, vol. 15, no. 11, pp. 1376–1377, 2009.

[5] H. Kitakoji, T. Terasaki, H. Honjo et al., "Effect of acupuncture on the overactive bladder," *Japanese Journal of Urology*, vol. 86, no. 10, pp. 1514–1519, 1995.

[6] Y.-L. Chen, J. Cen, W.-G. Hou et al., "Clinical study on diferent needling methods for unstable bladder of kidney deficiency," *Shanghai Journal of Traditional Chinese Medicine*, vol. 39, no. 7, pp. 43–44, 2005.

[7] Q.-R. Huang and Y.-I. Chen, "Clinical observations on electroacupuncture treatment of unstable bladder," *Journal of Acpuncture and Tuina Science*, vol. 3, no. 5, pp. 56–58, 2005.

[8] Y.-L. Chen, J. Cen, W.-G. Hou, X.-M. Yu, and X.-M. Ma, "Study of the specificity of lumbosacral points in regulating unstable bladder," *Journal of Acupuncture and Tuina Science*, vol. 6, no. 2, pp. 99–103, 2008.

[9] Y.-L. Chen, J. Cen, W.-G. Hou, Z.-Q. Gao, X.-M. Yu, and X.-M. Ma, "Effects of electroacupuncture treatment on nitrergic neurotransmitter in bladder neck and detrusor of rats with unstable bladder," *Journal of Chinese Integrative Medicine*, vol. 4, no. 1, pp. 73–75, 2006.

[10] R. A. Davidson and K. D. McCloskey, "Morphology and localization of interstitial cells in the guinea pig bladder: structural relationships with smooth muscle and neurons," *Journal of Urology*, vol. 173, no. 4, pp. 1385–1390, 2005.

[11] J. I. Gillespie, M. Markerink-van Ittersum, and J. de Vente, "cGMP-generating cells in the bladder wall: identification of distinct networks of interstitial cells," *BJU International*, vol. 94, no. 7, pp. 1114–1124, 2004.

[12] L. Nemeth, S. Maddur, and P. Puri, "Immunolocalization of the Gap junction protein Connexin43 in the interstitial cells of Cajal in the normal and Hirschsprung's disease bowel," *Journal of Pediatric Surgery*, vol. 35, no. 6, pp. 823–828, 2000.

[13] S. M. Biers, J. M. Reynard, T. Doore, and A. F. Brading, "The functional effects of a c-kit tyrosine inhibitor on guinea-pig and human detrusor," *BJU International*, vol. 97, no. 3, pp. 612–616, 2006.

[14] C. Wahl-Schott and M. Biel, "HCN channels: structure, cellular regulation and physiological function," *Cellular and Molecular Life Sciences*, vol. 66, no. 3, pp. 470–494, 2009.

[15] L. L. Ding, Y. Q. Wang, Q. Fang et al., "Variation of HCN protein expression in interstitial cells of Cajal from rat with detrusor instability," *Journal of Third Military Medical University*, vol. 30, no. 7, pp. 578–581, 2008.

[16] C. Malmgren, B. Sjogren, and Uvrelius, "Cystometerical evaluation of bladder instability in rats with infravesical outflow obstruction," *Journal of Urology*, vol. 137, no. 6, pp. 1291–1376, 1987.

[17] C. R. Chapple and D. Smith, "The pathophysiological changes in the bladder obstructed by benign prostatic hyperplasia," *British Journal of Urology*, vol. 73, no. 2, pp. 117–123, 1994.

[18] O. H. Lowry, N. J. Rosebrough, A. L. Farr, and R. J. Randall, "Protein measurement with the Folin phenol reagent," *Journal of Biological Chemistry*, vol. 193, no. 1, pp. 265–275, 1951.

[19] D. Jianping, H. Peng, Z. Xiao et al., "Identification of T-type calcium channels in the interstitial cells of cajal in rat bladder," *Urology*, vol. 80, no. 6, pp. 1389.e1–1389.e7, 2012.

[20] Á. Jenes, F. Ruzsnavszky, A. Telek, G. P. Szigeti, and L. Csernoch, "A possible role of the cholinergic and purinergic receptor interaction in the regulation of the rat urinary bladder function," *Journal of Muscle Research and Cell Motility*, vol. 32, no. 6, pp. 421–431, 2012.

[21] M. L. Qiou and S. C. Zhang, *Acupointology*, Shanghai Science and Technology Publishing House, Shanghai, China, 1985.

[22] J. L. H. R. Bosch and J. Groen, "Sacral (S3) segmental nerve stimulation as a treatment for urge incontinence in patients with detrusor instability: results of chronic electrical stimulation using an implantable neural prosthesis," *Journal of Urology*, vol. 154, no. 2, part 1, pp. 504–507, 1995.

[23] H. Honjo, A. Kawauchi, O. Ukimura, J. Soh, Y. Mizutani, and T. Miki, "Treatment of monosymptomatic nocturnal enuresis by acupuncture: a preliminary study," *International Journal of Urology*, vol. 9, no. 12, pp. 672–676, 2003.

[24] M. Takaki, H. Suzuki, and S. Nakayama, "Recent advances in studies of spontaneous activity in smooth muscle: ubiquitous pacemaker cells," *Progress in Biophysics and Molecular Biology*, vol. 102, no. 2-3, pp. 129–135, 2010.

[25] Y. Kubota, H. Hashitani, N. Shirasawa et al., "Altered distribution of interstitial cells in the guinea pig bladder following bladder outlet obstruction," *Neurourology and Urodynamics*, vol. 27, no. 4, pp. 330–340, 2008.

[26] Y. Kubota, S. Kajioka, S. M. Biers, E. Yokota, K. Kohri, and A. F. Brading, "Investigation of the effect of the c-kit inhibitor Glivec on isolated guinea-pig detrusor preparations," *Autonomic Neuroscience: Basic and Clinical*, vol. 115, no. 1-2, pp. 64–73, 2004.

[27] L. Xue, Y. X. Li, X. J. Han et al., "Investigation of hyperpolarization-activated cyclic nucleotide-gated channels in interstitial cells of cajal of human bladder," *Urology*, vol. 80, no. 1, pp. 13–18, 2012.

[28] P. He, J. Deng, X. Zhong, Z. Zhou, B. Song, and L. Li, "Identification of a hyperpolarization-activated cyclic nucleotide-gated channel and its subtypes in the urinary bladder of the rat," *Urology*, vol. 79, no. 6, pp. 1411.e7–1411.e13, 2012.

[29] G. Sui, C. H. Fry, J. Malone-Lee, and C. Wu, "Aberrant Ca^{2+} oscillations in smooth muscle cells from overactive human bladders," *Cell Calcium*, vol. 45, no. 5, pp. 456–464, 2009.

[30] M. J. Berridge, "Smooth muscle cell calcium activation mechanisms," *Journal of Physiology*, vol. 586, no. 21, pp. 5047–5061, 2008.

Hindawi Publishing Corporation
Evidence-Based Complementary and Alternative Medicine
Volume 2013, Article ID 158352, 11 pages
http://dx.doi.org/10.1155/2013/158352

Review Article

Acupuncture and Moxibustion for Inflammatory Bowel Diseases: A Systematic Review and Meta-Analysis of Randomized Controlled Trials

Jun Ji, Yuan Lu, Huirong Liu, Hui Feng, Fuqing Zhang, Luyi Wu, Yunhua Cui, and Huangan Wu

Key Laboratory for Acupuncture-Moxibustion and Immunological Effects, Shanghai University of Traditional Chinese Medicine, 650 South WanPing Road, Shanghai 200030, China

Correspondence should be addressed to Huangan Wu; wuhuangan@126.com

Received 8 June 2013; Revised 9 August 2013; Accepted 12 August 2013

Academic Editor: Yong-Qing Yang

Background. Inflammatory bowel diseases (IBD) are recurrent and refractory which include ulcerative colitis (UC) and Crohn's disease (CD). Clinical researches about acupuncture and moxibustion treatments for IBD are increasing, while systematic reviews about their efficacy remains in a shortage. This study sought to evaluate the efficacy of acupuncture and moxibustion for IBD. *Methods*. Seven significant databases both in and abroad were searched for randomized controlled trials (RCTs) which compared acupuncture and moxibustion as the main intervention to pharmacotherapy in treating IBD. A meta-analysis was performed. *Results*. A total of 43 RCTs were included. Among the 43 included trials, 10 trials compared oral sulphasalazine (SASP) with acupuncture and/or moxibustion treatments. A meta-analysis of the 10 trials indicated that acupuncture and moxibustion therapy was superior to oral SASP. *Conclusion*. Acupuncture and moxibustion therapy demonstrates better efficacy than oral SASP in treating IBD. However, given the limitations of this systematic review and the included literature, definitive conclusions regarding the exact efficacy of acupuncture and moxibustion treatment for IBD cannot be drawn. Extant RCTs still cannot provide sufficient evidence and multicentre, double-blind RCTs with large sample sizes are needed to provide higher-quality evidence.

1. Introduction

Inflammatory bowel diseases (IBD) encompass a group of chronic nonspecific inflammatory diseases of the bowel with unknown aetiology. The main forms of IBD are ulcerative colitis (UC) and Crohn's disease (CD). UC and CD are similar with regard to their clinical manifestations, diagnosis, and treatment. Clinically, both UC and CD involve the primary symptoms of abdominal pain and diarrhoea. These conditions are refractory and recurrent, causing high levels of patient suffering.

The aetiology and pathogenesis of IBD are not fully understood and, moreover, there is currently no specific treatment. The primary therapeutic approaches in clinical practice are derived from western medicine including traditional treatment with sulphasalazine (SASP; also known as 5-aminosalicyclic acid (5-ASA)) or the administration of steroids, immunosuppressive agents, or new biological agents. However, long-term treatment with steroids and immunosuppressants can cause serious adverse reactions, whereas new types of biological agents not only are expensive and economically burdensome to patients but also have unsatisfactory long-term efficacy.

Since the 1990s, there have been an increasing number of clinical studies of acupuncture and moxibustion treatment for IBD, and the existing investigations have demonstrated that acupuncture and moxibustion can effectively control bowel inflammation by providing multitargeted regulation of the body's physiological balance [1, 2]. However, quality of these clinical studies is uneven, and types are varied. So far, systematic reviews or meta-analyses about acupuncture and moxibustion treatment for IBD are few. Therefore, it is necessary to conduct systematic evaluations and meta-analysis of randomized controlled trials (RCTs) of acupuncture and moxibustion in treating IBD. Also the studies could provide a reference for future clinical treatment and research.

2. Materials and Methods

2.1. Search and Retrieval Strategy. Foreign-language and Chinese databases were searched. The Medline, Embase, and Cochrane Library databases were searched for English-language reports regarding RCTs. The Medline database was searched from 1966 to December 31, 2012, and Embase from 1974 to December 31, 2012. The Chinese literature databases that were searched include the China National Knowledge Infrastructure Database (CNKI), the Chongqing VIP Chinese Science and Technology Periodical Database (VIP), and the Chinese Biomedical Literature Database (CBM). The CNKI and CBM were searched to retrieve relevant studies from January 1, 1949, to December 31, 2012, whereas the VIP was searched to retrieve relevant studies from January 1, 1989, to December 31, 2012. The keywords used to for the Chinese-language literature include "inflammatory bowel diseases," "ulcerative colitis", "Crohn's disease", "acupuncture", "moxibustion", "acupoint", and "acupuncture treatment"; the keywords used for English-language literature included "acupuncture", "moxibustion", "inflammatory bowel diseases," "ulcerative colitis", and "Crohn's disease" Based on the specific circumstances of the different databases, comprehensive searches for combinations of keywords and for wildcards were conducted to ensure the completeness of the search results.

2.2. Inclusion Criteria. (1) Research subjects: included studies were required to have enrolled patients with an unequivocal diagnosis of IBD (including UC and CD); no restrictions on race, age, or sex were imposed. (2) Study design: included studies were required to be RCTs in Chinese or English that evaluated the efficacy of acupuncture and/or moxibustion treatment for IBD. (3) Experimental group interventions: included studies were required to feature an experimental group that mainly received acupuncture and/or moxibustion treatment (including filiform needles, electroacupuncture, moxibustion, or cupping, among other techniques), either alone or in conjunction with other therapies (such as drug therapy), without differentiating among different acupuncture and moxibustion techniques, the selection of acupoints, or needle material. For studies in which the treatment group received acupuncture and/or moxibustion treatment combined with medication, the same drug had to be administered to both the treatment group and the control group. (4) Control group interventions: included studies were required to feature a control group that received medication, placebo, or sham acupuncture controlled treatment(s). (5) Outcome measurements: the outcome measurements of included studies had to include overall clinical efficacy, general conditions, changes in symptoms, serum inflammatory markers, and/or colonoscopic findings. (6) Availability: the full text or sufficiently informative abstracts of included studies had to be accessible.

2.3. Exclusion Criteria. The following types of studies were excluded from this analysis: (1) RCTs that lacked clear diagnostic criteria or basic information of the subjects or interventions; (2) serial observations, case reports, expert experiences, or descriptive analyses without control groups; (3) studies that compared different acupuncture and moxibustion techniques or selection of different acupoints to control groups; (4) studies that compared acupoint injections to drug therapy; (6) studies that were duplicate for retrieving or publishing.

Table 1: Modified Jadad quality scale.

Aspects	Details	Score
Randomization	Appropriate if random sequence is generated by computer or similar methods	2
	Unclear if a trial does not describe its method of randomization	1
	Inappropriate if a study uses an alternate assignment method, such as the allocation of odd and even numbers	0
Randomization concealment	Appropriate if either the distribution scheme is controlled by a center or pharmacy, containers with consistent serial numbers being used, on-site computer control, sealed opaque envelopes, or any other allocation method that clinicians and subjects are unable to predict	2
	Unclear if only a random number table or other random allocation scheme is employed	1
	Inappropriate if either of alternate allocation, case numbers, days of the week, an open-label random number table, serial coded envelopes, or any other method with predictable assignments is used	0
	Absent if randomization is not used	0
Blinding method	Appropriate if a completely identical placebo form or a similar method is used	2
	Unclear if the trial was described as blinded, but no methodological information regarding the blinding was provided	1
	Inappropriate if the double-blind method is not adopted or if the blinding method is improper, such as a comparison between tablets and injections	0
Withdrawal and exit	The number and reasons of patients who withdraw or exit are described	1
	The number and reasons of patients who withdraw or exit are not described	0

2.4. Quality Assessments of the Included RCTs. The methodological quality of the included trials was evaluated using a modified Jadad quality scale (Table 1). The total possible

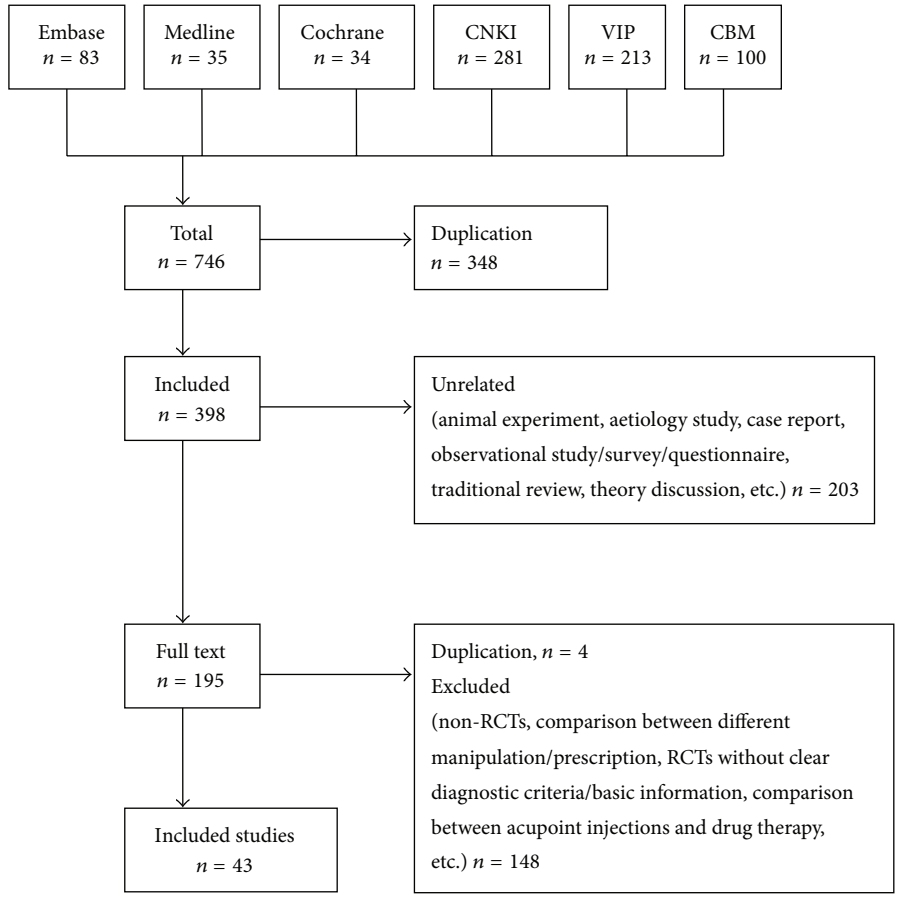

Figure 1: Flowchart of trial selection process. CNKI: China National Knowledge Infrastructure Database; VIP: Chongqing VIP Chinese Science and Technology Periodical Database; CBM: Chinese Biomedical Literature Database; RCT: randomized controlled trial.

score for study quality was 7 points. Studies with scores of 1–3 points were regarded as low-quality investigations, and studies with scores of 4–7 points were regarded as high-quality investigations.

2.5. Data Retrieval. In accordance with the predetermined inclusion criteria, two researchers independently performed a rigorous screening to identify qualified trials, and they extracted data from these trials using a predesigned data extraction form independently. The extracted data included methodological features of the studies, demographic characteristics, treatment and control measurements, and primary outcome indicators. A third evaluator verified the consistency of the data, and any inconsistencies were addressed through discussion.

2.6. Data Analysis. The RevMan software package from the Cochrane Collaboration (Oxford, UK), version 5.1, was used for meta-analysis of the data. In the analysis of clinical efficacy, count data were assessed in terms of risk ratios (RRs), and continuous variables were assessed in terms of mean difference (MD). Both count data and continuous variables are expressed as efficacy values with 95% confidence intervals (CIs). If the meta-analysis results exhibited heterogeneity (defined as results of tests of heterogeneity that indicated that $P < 0.1$ and $I^2 \geq 50\%$), then a random effects model will be used to assess combined efficacy values; otherwise, fixed effects models will be used for these assessments. Funnel plot analysis was used to evaluate the presence of publication bias.

3. Results

3.1. The Characteristics and Methodological Quality of the Included Trials. Using the search and retrieval strategy, a total of 746 studies were initially retrieved from the six aforementioned medical databases, including 152 English studies and 594 Chinese studies. The bibliographic information for these studies was imported into Microsoft Excel, and 348 duplicated titles were deleted. The titles and abstracts of the remaining studies were read to exclude irrelevant studies; after this process, 195 studies remained. These 195 studies were downloaded and full texts were read; using the predetermined exclusion criteria, 152 irrelevant studies were excluded. Finally, 43 studies were selected for inclusion [3–45], including 37 studies in Chinese and six studies in English. All of the included studies were published as journal articles. The flowchart for the literature search process is presented in Figure 1.

Among the 43 included studies, there was one CD study [43] and 42 UC studies. These studies included a total of 4,021 patients with IBD; 2,146 of these patients were male (55.9%), 1,691 were female (44.1%), and the gender of the remaining 184 patients (4.6%) was unknown because two studies did not report this information [5, 31]. The average sample size of each included RCT was 93.5 and ranged from 29 to 640.

Acupuncture and moxibustion therapy was the main intervention in the treatment groups of the examined RCTs. These treatments primarily involved acupuncture and/or moxibustion, although certain studies examined acupoint catgut embedding therapy, acupoint application, and auricular acupressure. In particular, among the 43 included studies, acupuncture and moxibustion therapy was used as the intervention method for the treatment group in 17 studies [5, 8, 9, 13–19, 21, 23–25, 28, 36, 45]; moxibustion treatment was used as the main intervention in 12 studies [5, 8, 9, 13–19, 28, 36]; acupuncture alone was used in one study [45]; acupoint catgut embedding therapy was used in two studies [24, 25]; balance cupping therapy was used in one study [21]; and acupoint application was used in one study [23]. Comprehensive treatment, using two forms of therapy as an intervention method, was used in 19 studies [3, 6, 7, 12, 20, 22, 26, 27, 29, 31, 33, 35, 37, 39–44]; in particular, combinations of two types of acupuncture and moxibustion treatments were used in 10 studies [3, 12, 22, 29, 35, 37, 41–44]; a combination of acupuncture and moxibustion with SASP treatments was used in three studies [6, 20, 39]; a combination of acupuncture and moxibustion with Chinese herbal treatments was used in one study [40]; and a combination of acupuncture and moxibustion with a retention enema, using traditional Chinese medicine, was used in five studies [7, 26, 27, 31, 33]. A combination of three treatments was used as an intervention method in a total of six studies [4, 10, 30, 32, 34, 38]; in particular, a combination of three types of acupuncture and moxibustion techniques was used in one study [38]; a combination of two types of acupuncture and moxibustion techniques and a retention enema using traditional Chinese medicine and/or western drugs was used in two studies [32, 34]; a combination of two types of acupuncture and moxibustion techniques with Chinese herbal medicine was used in one study [4]; and a combination therapy of two types of acupuncture and moxibustion techniques with oral western medicine was used in two studies [10, 30]. In addition, a combination of four interventions, including auricular acupressure, oral Chinese medicine, oral western medicine, and an enema with traditional Chinese medicine, was used in one study [11]. The interventions for the control groups consisted of drug therapy; in particular, most of these studies involved a control group that was administered SASP (27 studies). In addition, sham acupuncture was used as a control in two studies [41, 43].

The main outcome indicators reported in the included studies were overall efficacy, colonic activity indices, clinical symptom scores, fibre colonoscopy results, laboratory test findings (including evaluations of T lymphocyte subpopulations and immunoglobulin), and adverse reactions to treatments. The general data and methodological quality of the included studies are presented in Table 2, and the interventions and outcome measurements are presented in Table 3.

The assessments for bias risk revealed that among the 43 RCTs included in this systematic evaluation, nine RCTs reported their random allocation methods [10–12, 18, 25, 29, 40, 41, 43], three studies utilized appropriate allocation concealment [10, 41, 43], and the random allocation methods and allocation concealment of the remaining trials were either inappropriate or unclear. One study reported using a single-blind approach [41], one study addressed its implementation of a single-blind design and the reasons underlying the failure of final implementation [43], and unclear descriptions of blinding were provided in two trials [30, 37]. Two studies reported the numbers and the reasons of withdrawals from the trials [41, 43]. One study utilised preliminary screening to estimate its sample size before its main experiments [41]. In general, the methodological and report qualities of the included studies were low. Four trials reported follow-up data [10, 22, 41, 43]. In particular, Zhou and Jin [10] reported that at the 1-year followup, the recurrence rate was significantly lower in the treatment group than in the control group ($P < 0.05$). Li et al. [22] observed that by the 2-year followup, 11 patients in the treatment group and 12 patients in the control group had experienced recurrences. In a 2004 CD study, Joos et al. [43] found that the efficacy was fundamentally maintained for 12 weeks of followup after treatment ($P = 0.059$), and the same research group reported in their 2006 UC study [41] that after 16-week follow-up, the primary outcome measurements remained more significantly improved than receiving treatment before ($P < 0.001$). The remaining included RCTs did not mention follow-up.

3.2. Results of Studies with High Jadad Scores. Three of the 43 included trials were of high quality [10, 41, 43]. Zhou and Jin [10] utilised an RCT to observe the efficacy in UC patients of electroacupuncture combined with ginger-partitioned moxibustion and oral SASP treatment. 220 patients in this trial were randomly divided into the treatment group ($n = 110$) and the SASP control group ($n = 110$); the overall clinical efficacy of the treatment group was 84.5%, which was significantly better than the control treatment (68.2%, $P < 0.05$). In a 2004 study of CD [43] and a 2006 study of UC [41], Joos et al. examined the treatment efficacy of acupuncture combined with moxibustion, with sham acupuncture (i.e., shallow punctures at non-acupoints) as a control, in investigations that featured the rigorous design and implementation of a prospective, randomized, controlled, single-blind trial (although the researchers reported that the implementation of the single-blind design was unsuccessful in their 2004 CD study). In the 2004 study, Joos et al. randomly divided 51 CD patients into traditional Chinese medicine (TCM) group (acupuncture combined with moxibustion, $n = 27$) and control group (sham acupuncture, $n = 24$). After 4 weeks of treatment, the CD Activity Index (CDAI) of the patients in the TCM group had decreased significantly and was superior to the control group ($P = 0.003$). In their 2006 study, Joos et al. randomly divided 29 UC patients into TCM

Table 2: Characteristics and methodological quality of included studies.

Study	Sample size (n_1/n_2)	Sex (male/female)	Age (mean or range)	Type of IBD	Followup	Methodology quality score
Ma and Zhang, 1997 [3]	90 (60/30)	56/34	*T*: 23–68; *C*: 28–65	UC	No	1
Gao, 1997 [4]	66 (46/20)	27/39	*T*: 43.6; *C*: 39.5	UC	No	1
Wu et al., 1999 [5]	151 (65/56/30)	ND	*T*: 42.7; *C*: 38.4	UC	No	1
Li et al., 2008 [6]	67 (34/33)	42/25	35.5	UC	No	1
Mo et al., 2010 [7]	62 (31/31)	35/27	35.5	UC	No	1
X. Guo and F. Guo, 2010 [8]	55 (28/27)	38/17	38.77	UC	No	1
Yang et al., 2011 [9]	100 (50/50)	61/39	*T*: 54.6; *C*: 55.3	UC	No	1
Zhou and Jin, 2008 [10]	220 (110/110)	131/89	*T*: 48.60; *C*: 50.24	UC	Yes	4
Han et al., 2012 [11]	81 (41/40)	47/34	*T*: 36.5; *C*: 34.7	UC	No	1
Jiang, 2012 [12]	80 (40/40)	39/41	*T*: 38.65; *C*: 39.35	UC	No	3
Zhou, 2003 [13]	66 (34/32)	31/35	40.8	UC	No	1
Din et al., 2009 [14]	61 (30/31)	32/29	*T*: 44.9; *C*: 40.2	UC	No	1
Wu et al., 2000 [15]	46 (30/16)	25/21	*T*: 38.75; *C*: 37	UC	No	1
Wen, 2003 [16]	69 (39/30)	35/34	*T*: 41.2; *C*: 37.4	UC	No	1
Wang et al., 2006 [17]	60 (30/30)	28/32	38.5	UC	No	1
Xu et al., 2010 [18]	60 (28/32)	35/25	*T*: 35.0; *C*: 37.0	UC	No	2
Zhang, 2012 [19]	60 (30/30)	32/28	*T*: 28–52; *C*: 27–55	UC	No	1
Chi and Yu, 2011 [20]	84 (44/40)	36/48	*T*: 45; *C*: 43	UC	No	1
Luo, 2009 [21]	76 (40/36)	42/34	*T*: 53; *C*: 51.3	UC	No	1
Li et al., 2006 [22]	68 (40/28)	40/28	*T*: 36.4; *C*: 38.2	UC	Yes	1
Tian et al., 2012 [23]	106 (53/53)	46/60	*T*: 29–61; *C*: 32–63	UC	No	1
Chen, 2004 [24]	130 (100/30)	80/50	*T*: 42.5; *C*: 40.2	UC	No	1
Li et al., 2006 [25]	116 (56/60)	52/64	*T*: 37.1; *C*: 37.3	UC	No	2
Duan et al., 2012 [26]	640 (320/320)	406/234	*T*: 45.5; *C*: 46.5	UC	No	1
Sun and Wang, 1998 [27]	88 (45/43)	43/45	*T*: 34.6; *C*: 33.8	UC	No	1
Wang, 2008 [28]	108 (54/54)	78/30	*T*: 35; *C*: 33.5	UC	No	1
Ma and Xu, 2005 [29]	92 (47/45)	51/41	*T*: 52.5; *C*: 52.5	UC	No	2
Cui, 2010 [30]	48 (24/24)	27/21	*T*: 43; *C*: 44	UC	No	2
Guo et al., 2007 [31]	33 (22/11)	ND	ND	UC	No	1

Table 2: Continued.

Study	Sample size (n_1/n_2)	Sex (male/female)	Age (mean or range)	Type of IBD	Followup	Methodology quality score
Wang et al., 2009 [32]	78 (39/39)	44/34	*T*: 57.5; *C*: 55.0	UC	No	1
Long and Yang, 2010 [33]	46 (23/23)	20/26	*T*: 33.5; *C*: 33.4	UC	No	1
Chen, 2010 [34]	168 (84/84)	91/77	38.4	UC	No	1
Sun and Wang, 2001 [35]	55 (35/20)	32/23	*T*: 22–65; *C*: 25–70	UC	No	1
Wang et al., 2006 [36]	45 (27/18)	23/22	40.5	UC	No	1
Shi et al., 2006 [37]	60 (30/30)	34/26	*T*: 42.31; *C*: 43.64	UC	No	2
Qun et al., 2012 [38]	63 (33/30)	32/31	*T*: 46; *C*: 41	UC	No	1
Xu, 2006 [39]	110 (56/54)	59/51	*T*: 35.5; *C*: 33	UC	No	1
Zhang et al., 2011 [40]	60 (30/30)	38/22	*T*: 31.2; *C*: 30.6	UC	No	2
Joos et al., 2006 [41]	29 (15/14)	10/19	37.89 ± 12.0	UC	Yes	7
Yang and Yan, 1999 [42]	62 (32/30)	30/32	*T*: 45.5; *C*: 50.1	UC	No	1
Joos et al., 2004 [43]	51 (27/24)	15/36	ND	CD	Yes	5
Ma, 1999 [44]	90 (60/30)	56/34	*T*: 23–68; *C*: 28–65	UC	No	1
Ma, 2005 [45]	121 (76/45)	67/54	*T*: 42; *C*: 41.5	UC	No	1

n_1: sample size of test group; n_2: sample size of control group; *T*: test group; *C*: control group; ND: not described; IBD: inflammatory bowel disease; UC: ulcerative colitis; CD: Crohn's disease.

group (acupuncture combined with moxibustion, $n = 15$) and control group (sham acupuncture, $n = 14$); after 5 weeks of treatment, the Colitis Activity Index (CAI) of the patients in the traditional Chinese medicine group was significantly lower than the CAI of the control group ($P = 0.048$).

3.3. Meta-Analysis Results. The 43 included RCTs featured complex interventions and different reported outcomes, with no unified efficacy standard. To develop a general understanding of the therapeutic effect of acupuncture and moxibustion therapy for IBD, intervention measurements and therapies for control group were further refined. We limited the treatment group methods to acupuncture or moxibustion alone, or a combination of acupuncture and moxibustion; this limitation produced 10 studies that compared one of the these treatments with oral SASP for the treatment of UC [5, 14–16, 18, 19, 37, 42, 44, 45]. We then conducted a comprehensive efficacy evaluation of the interventions in the 10 RCTs, which featured simple interventions that could be readily compared with oral SASP. In addition, the efficacy criteria for these RCTs were similar, featuring the three outcomes of recently cured, effective, and ineffective; judgements of these outcomes were based on various indicators, such as clinical manifestations, routine stool test results, and colonoscopy findings. The definition of ineffective treatment was consistent among these 10 studies; therefore, a meta-analysis of the overall clinical efficacies determined in these studies could be performed.

3.3.1. Analysis of Overall Clinical Efficacy. The results of heterogeneity tests indicated that $I^2 < 50\%$ and $P > 0.1$ for the 10 examined studies and that the overall heterogeneity of subgroups was small ($P = 0.28$, $I^2 = 17\%$); therefore, a fixed effects model was used. The overall efficacy of acupuncture alone, moxibustion alone, or acupuncture combined with moxibustion was greater than the efficacy of western medicine (oral SASP) for the treatment of IBD ($P < 0.00001$, RR = 5.42, 95% CI [3.38, 8.68]) (Figure 2).

3.4. Funnel Plot. RevMan, version 5.1, was used to conduct a funnel plot analysis of the aforementioned 10 studies, and the resulting graph was symmetrical, suggesting that these studies demonstrated no obvious publication bias (Figure 3).

4. Discussion

4.1. Methodological Quality of the Included Trials. Based on the RCTs examined in this study, the methodological quality of the clinical trials regarding the examined topic was

Table 3: Interventions and outcomes of included studies.

Study	Intervention	Control	Outcome measurement
Ma and Zhang, 1997 [3]	Acupuncture + sparrow-pecking moxibustion	SASP + metronidazole	Efficacy
Gao, 1997 [4]	Acupoint application + moxibustion + decoction of traditional Chinese medicine	Traditional Chinese medicine	Efficacy
Wu et al., 1999 [5]	Drug-separated moxibustion	SASP	Efficacy, T lymphocyte subpopulations, HLA-DR antigen
Li et al., 2008 [6]	Moxa-box moxibustion + SASP	SASP	Efficacy, haemorheology, immunoglobulin, T lymphocyte subpopulations
Mo et al., 2010 [7]	Moxa-box moxibustion + traditional Chinese medicine enema	Traditional Chinese medicine enema	Efficacy
X. Guo and F. Guo, 2010 [8]	Warm moxibustion of acupoints	SASP + PAT	Efficacy, T lymphocyte subpopulations
Yang et al., 2011 [9]	Ginger moxibustion	Diphenoxylate	Efficacy
Zhou and Jin, 2008 [10]	Electroacupuncture + ginger moxibustion + SASP	SASP	Medical condition, efficacy, intestinal mucosa pathology, adverse reactions
Han et al., 2012 [11]	Auricular acupressure + salicylic acid preparations + traditional Chinese medicine + traditional Chinese medicine enema	Salicylic acid preparations + traditional Chinese medicine + traditional Chinese medicine enema	Enema retention time, efficacy
Jiang, 2012 [12]	Abdominal acupuncture + acupoint catgut embedding	Bupi Yichang pills	Symptom scores, efficacy, fibre colonoscopy
Zhou, 2003 [13]	Ginger moxibustion	SASP + prednisone tablets	Efficacy
Din et al., 2009 [14]	Ginger moxibustion	SASP	Efficacy
Wu et al., 2000 [15]	Moxibustion with herbal medicine underneath	SASP	Efficacy, colonic mucosal histopathology, mucin
Wen, 2003 [16]	Drug-separated moxibustion	SASP	Efficacy, immunoglobulin
Wang et al., 2006 [17]	Drug-separated moxibustion	SASP + metronidazole tablets	Efficacy, immunoglobulin, T lymphocyte subpopulations, NK content
Xu et al., 2010 [18]	Herb-partitioned moxibustion	SASP	Efficacy, adverse reactions
Zhang, 2012 [19]	Drug-separated moxibustion	SASP	Efficacy
Chi and Yu, 2011 [20]	Umbilical compression with traditional Chinese medicine + SASP	SASP	Efficacy
Luo, 2009 [21]	Balance cupping	Enteritidis tablet	Efficacy, symptom scores, immunoglobulin
Li et al., 2006 [22]	Application of musky warm umbilical cream + use of a specific electromagnetic spectrum therapeutic apparatus	SASP	Efficacy
Tian et al., 2012 [23]	Acupoint application	SASP	Efficacy, symptom scores
Chen, 2004 [24]	Acupoint catgut embedding	SASP	Efficacy
Li et al., 2006 [25]	Acupoint catgut embedding	SASP	Efficacy, stool characteristics, abdominal pain
Duan et al., 2012 [26]	Acupoint catgut embedding + traditional Chinese medicine enema	Traditional Chinese medicine enema	Efficacy, routine stool tests
Sun and Wang, 1998 [27]	Warm acupuncture + traditional Chinese medicine enema	Traditional Chinese medicine enema	Efficacy
Wang, 2008 [28]	Warm acupuncture	SASP + western medicine enema	Efficacy

Table 3: Continued.

Study	Intervention	Control	Outcome measurement
Ma and Xu, 2005 [29]	Acupuncture + TDP	SASP	Efficacy
Cui, 2010 [30]	Acupuncture + moxibustion + SASP	SASP	Efficacy, serum levels of TNF-α, IL-1, and IL-10
Guo et al., 2007 [31]	Acupuncture + traditional Chinese medicine enema	Traditional Chinese medicine enema	Efficacy, intestinal microscopy
Wang et al., 2009 [32]	Electroacupuncture + ginger moxibustion + traditional Chinese and western medicine enema	Traditional Chinese and western medicine enema	Efficacy
Long and Yang, 2010 [33]	Acupuncture + traditional Chinese medicine enema	Traditional Chinese medicine enema	Efficacy, colonoscopy
Chen, 2010 [34]	Acupuncture + ginger moxibustion + traditional Chinese medicine enema	Traditional Chinese medicine enema	Efficacy
Sun and Wang, 2001 [35]	Acupuncture + ginger moxibustion	Shuanghuanglian compound + norfloxacin + gentamicin	Efficacy
Wang et al., 2006 [36]	Warm acupuncture	SASP	Efficacy
Shi et al., 2006 [37]	Electroacupuncture + moxibustion	SASP	Efficacy, serum levels of TNF-α, IL-8, IL-l, and IL-10
Qun et al., 2012 [38]	Acupuncture + moxibustion + TDP	SASP	Efficacy, intestinal mucosa pathology, immunoglobulin
Xu, 2006 [39]	Ginger moxibustion + SASP	SASP	Efficacy
Zhang et al., 2011 [40]	Traditional acupuncture + Chinese medicine decoction	SASP	Efficacy, symptom scores, serum levels of IL-8 and IL-10
Joos et al., 2006 [41]	Traditional acupuncture + moxibustion	Sham acupuncture	CAI, QLO, general well-being, C-reactive protein, serum α_1-acid glycoprotein
Yang and Yan, 1999 [42]	Acupuncture + moxibustion	SASP	Efficacy, routine examination of faeces, electrogastrograms, sigmoidoscopy
Joos et al., 2004 [43]	Traditional acupuncture + moxibustion	Sham acupuncture	CDAI, QLO, general condition, C-reactive protein, serum α_1-acid glycoprotein
Ma, 1999 [44]	Acupuncture + sparrow-pecking moxibustion	SASP	Efficacy
Ma, 2005 [45]	Acupuncture	SASP	Efficacy

SASP: sulphasalazine; IBDQ: Inflammatory Bowel Disease Questionnaire; CAI: Colitis Activity Index; QOL: quality of life; CDAI: Crohn's Disease Activity Index; PAT: pipemidic acid tablet; sham acupuncture: superficial needling at nonacupoints.

generally low, and few studies provided robust evidence. Randomization and allocation concealment are among the ways in which bias can arise, and the vast majority of the examined trials only mentioned "randomization", without describing the specific methods used or whether allocation concealment was implemented. Thus, nonstandard "randomization" was widespread. The selective reporting of research results or the loss of trial data can also lead to reporting bias. Among the 43 included trials, only two studies reported the numbers of withdrawals from the study and the reasons; because none of the other trials reported exit data or cases lost to followup, the efficacy conclusions of these trials might be exaggerated. Most of the studies did not utilize blinding, producing a high probability of bias. The overall quality of the studies was low, affecting the strength of the evidence that was examined in this systematic evaluation.

4.2. Determinations of Sample Size. Adequate attention must be devoted to the important factor of sample size in RCTs that address the examined topic. At present, only two relevant RCTs have featured sample sizes of more than 200 individuals. Insufficient sample sizes can reduce the power of a test, resulting in limited reliability of the results and conclusions, that do not truly reflect the overall effects observed in a study. Low statistical power will reduce the magnitude of evidence that RCTs can provide.

4.3. Selection of Interventions. In this study, the specific interventions described in the included studies, which included acupuncture, herb-partitioned moxibustion, ginger-partitioned moxibustion, moxibustion, electroacupuncture, abdominal acupuncture, acupuncture catgut embedding, acupoint application, cupping, and auricular pressure, were

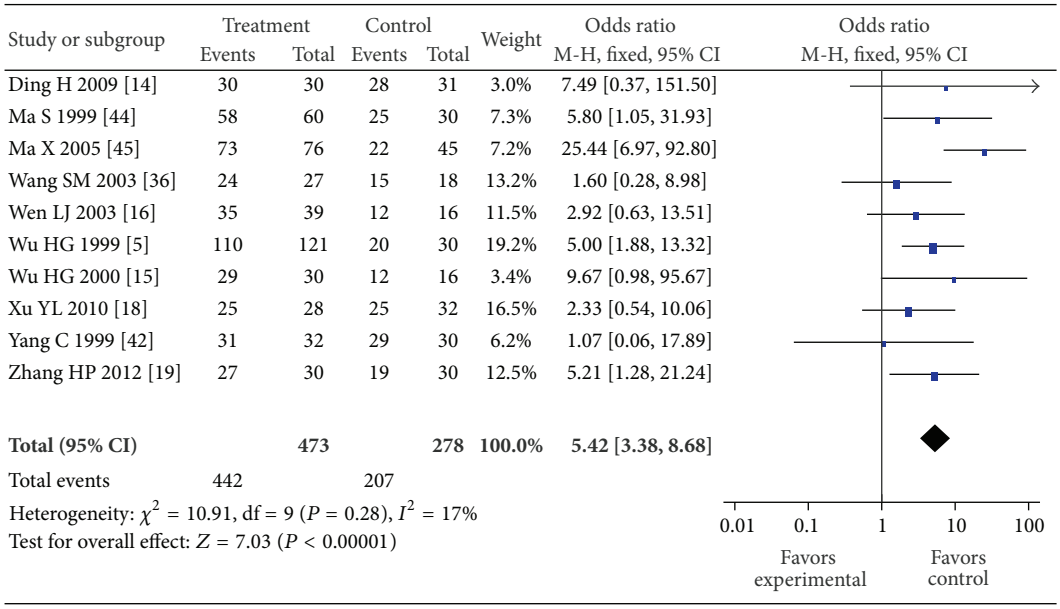

Figure 2: Forest plot of acupuncture and/or moxibustion for ulcerative colitis Compared to SASP.

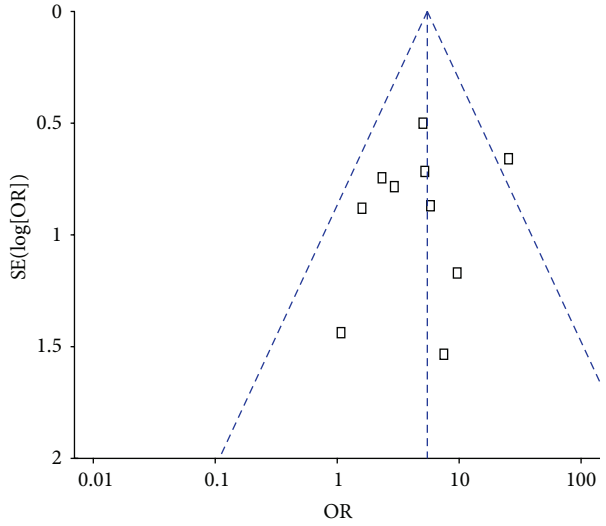

Figure 3: Funnel plot of randomized controlled trials using acupuncture and/or moxibustion for ulcerative colitis.

treated as one type of therapy, without considering the differences in acupoint selection or therapeutic techniques. Therefore, the results of this study might indicate overall efficacy trends, but they cannot be utilised to draw definitive conclusions, thus limiting the extent to which the conclusions of this investigation can be applied.

4.4. The Selection and Measurement of Outcome Indicators. The majority of the included studies selected clinical efficacy as the outcome measurement. Thus, there may exist subjectivity in the evaluations of the results. With little use of objective indicators, such as clinical symptom scores, endoscopic scores, or pathologic scores, the tendency towards subjective judgements weakened the credibility of conclusions regarding the effectiveness of acupuncture and moxibustion. With regard to long-term efficacy, most of the included studies did not conduct long-term followup, or if someone did, either the data for withdraw or the follow-up methods were not described. As a result, the long-term efficacy of acupuncture and moxibustion treatment for IBD cannot be determined.

4.5. Suggestions for Future Research. The objectivity and accuracy of systematic evaluations rely on high-quality RCTs. The findings of this systematic evaluation are somewhat limited due to the generally low quality of the existing studies. Thus, it is recommended that future research should be based on the Consolidated Standards of Reporting Trials (CONSORT) statement [46]. In particular, future studies should provide detailed reports regarding the generation of random allocation sequences and allocation concealment; moreover, to the greatest possible extent, these studies should be blinded and placebo controlled. In addition, a subject flowchart should be utilised to provide detailed accounts of patient withdrawals and loss during trials. Followup should be strengthened, and all of the trial data should be completely reported. In addition, intent-to-treat analysis should be conducted to evaluate therapeutic effects. These measurements will produce clinical RCTs that provide high levels of reliable evidence.

5. Conclusion

The results of this study suggest that acupuncture and moxibustion treatment demonstrated better overall efficacy than oral SASP in treating IBD. However, given the limitations of

this systematic evaluation and the included studies, definitive conclusions cannot be drawn with regard to the specific efficacy of acupuncture and moxibustion treatment for IBD. Currently published RCTs have not provided sufficient evidence for the effectiveness of acupuncture and moxibustion for IBD; thus, multicentre, double-blind RCTs with large sample sizes are still required to provide higher levels of evidence.

Conflict of Interests

The authors of this paper state that they have no conflict of interests associated with this investigation.

Authors' Contribution

Jun Ji, Yuan Lu, and Huirong Liu contributed equally to this work.

Acknowledgments

This study was financially supported by grants from the 973 Program of China (no. 2009CB522900), National Natural Science Foundation of China (no. 81173331), and Shanghai Municipal Health Bureau (no. 20124028; no. 2010QL025B).

References

[1] H. G. Wu, B. M. Zhang, and G. Q. An, "Herb-partitioned moxibustion modulates ulcerative colitis fibrosis TGF-β and its receptorsin rats," *Journal of Jiangxi College of Traditional Chinese Medicine*, vol. 15, no. 1, pp. 39–42, 2003.

[2] H. G. Wu, L. B. Zhou, C. Huang et al., "Discussion about cytokine gene expression modulated by acupuncture and moxibustion treatment of ulcerative colitis in rats," *The Chinese Journal of Gastroenterology*, vol. 6, no. 10, pp. 853–855, 1998.

[3] S. Ma and G. L. Zhang, "Efficacy of acupuncture and moxibustion treatment in 60 cases of ulcerative colitis," *Chinese Acupuncture and Moxibustion*, vol. 17, no. 5, pp. 275–276, 1997.

[4] Y. Gao, "Clinical observations of 46 cases of ulcerative colitis treated by medication combined with moxibustion," *Journal of Sichuan Continuing Education College of Medical Sciences*, vol. 16, no. 3, pp. 152–153, 1997.

[5] H. G. Wu, W. L. Tan, H. P. Chen et al., "The efficacy of moxibustion treatment of ulcerative colitis and the impact of the HLA-DR antigen on intestinal epithelial cells," *Acupuncture Research*, vol. 24, no. 1, pp. 12–16, 1999.

[6] H. Q. Li, Y. Zhou, D. Q. Zhang et al., "Effect of moxibustion in box in Shenque, Shangjuxu and Xiajuxu acupoints for chronic ulcerative colitis," *Clinical Acupuncture and Moxibustion*, vol. 24, no. 9, pp. 33–35, 2008.

[7] Y. X. Mo, X. F. Wang, W. R. Qu et al., "Observation on curative effect of moxa box moxibustion plus Chinese herbal medicine enema to treat patients with chronic ulcerative colitis," *Chinese Nursing Research*, vol. 24, no. 1, pp. 216–217, 2010.

[8] X. Guo and F. Guo, "The moxibustion of heat-sensitive acupoints as a therapy for ulcerative colitis," *China's Naturopathy*, vol. 18, no. 2, p. 12, 2010.

[9] H. J. Yang, Q. L. Zhao, and S. G. Zhao, "Efficacy of moxibustion at the Shenque acupoint for the treatment of 50 cases of chronic colitis," *Journal of Qilu Nursing*, vol. 17, no. 34, p. 125, 2011.

[10] G. Y. Zhou and J. H. Jin, "Effect of electroacupuncture plus moxibustion combined with medicine on ulcerative colitis," *Chinese Archives of Traditional Chinese Medicine*, vol. 26, no. 9, pp. 2069–2071, 2008.

[11] S. H. Han, Z. H. Xu, X. F. Chen et al., "Efficacy observation of seeds buried at ear acupuncture point in combined with traditional Chinese medicine enema for the treatment of ulcerative colitis," *Nursing and Rehabilitation Journal*, vol. 11, no. 6, pp. 570–571, 2012.

[12] X. P. Jiang, "Efficacy of treating ulcerative colitis by abdominal acupuncture plus catgut embedding," *Clinical Journal of Chinese Medicine*, vol. 4, no. 17, pp. 37–39, 2012.

[13] J. H. Zhou, "Clinical observations of ginger-partitioned moxibustion in 34 cases of ulcerative colitis," *Jiangsu Journal of Traditional Chinese Medicine*, vol. 24, no. 10, pp. 44–45, 2003.

[14] H. Din, H. Wang, T. Zhang et al., "Effects of ginger-partitioned moxibustion on 30 patients with asdthenic splenonephro-yang of ulcerative colitis," *Acta Academiae Medicinae CPAPF*, vol. 18, no. 6, pp. 509–511, 2009.

[15] H. G. Wu, L. B. Zhou, D. R. Shi et al., "Morphological study on colonic pathology ulcerative colitis treated by moxibustion," *World Journal of Gastroenterology*, vol. 6, no. 6, pp. 861–865, 2000.

[16] L. J. Wen, "Clinical Observation of herb-partitioned in treating chronic ulcerative colitis," *Journal of Jiangxi College of Traditional Chinese Medicine*, vol. 15, no. 2, pp. 35–36, 2003.

[17] S. M. Wang, L. Q. Zhang, J. Sun et al., "The clinical efficacy of acupuncture and moxibustion for the treatment of ulcerative colitis," *Practical Journal of Medicine and Pharmacy*, vol. 20, no. 2, p. 135, 2003.

[18] Y. L. Xu, Y. H. Du, and X. M. Xu, "Effect of herb-partitioned spread moxibustion for the treatment of chronic ulcerative colitis," *Chinese Acupuncture and Moxibustion*, vol. 30, no. 4, pp. 289–291, 2010.

[19] H. P. Zhang, "Efficacy of herb cake-partitioned moxibustion in treating 60 cases of chronic ulcerative colitis," *Nei Mongol Journal of Traditional Chinese Medicine*, vol. 31, no. 7, p. 79, 2012.

[20] L. L. Chi and M. M. Yu, "Shenque acupoint application of a spleen-strengthening ulcer-healing preparation combined with sulfasalazine for the treatment of 44 cases of chronic ulcerative colitis," *Journal of Practical Traditional Chinese Internal Medicine*, vol. 25, no. 8, pp. 55–57, 2011.

[21] Y. H. Luo, "Balanced cupping treatment for 40 cases of ulcerative colitis," *Jiangxi Journal of Traditional Chinese Medicine*, vol. 40, no. 2, pp. 63–64, 2009.

[22] D. P. Li, Q. Chen, L. Yi et al., "The use of umbilical application of musky warm cream combined with electromagnetic wave irradiation for the treatment of 40 cases of ulcerative colitis," *Shaanxi Journal of Traditional Chinese Medicine*, vol. 27, no. 1, pp. 49–50, 2006.

[23] J. R. Tian, X. J. Li, H. W. Han et al., "Clinical observation of Shenque acupoint in treating chronic ulcerative colitis," *Hebei Journal of Traditional Chinese Medicine*, vol. 34, no. 6, pp. 884–885, 2012.

[24] J. Chen, "Clinical observations of specific acupoint catgut-embedding treatment for chronic ulcerative colitis," *Journal of Sichuan of Traditional Chinese Medicine*, vol. 22, no. 5, pp. 89–90, 2004.

[25] H.-J. Li, G.-P. Li, and H.-Y. Li, "Clinical observation on acupoint catgut embedding therapy for treatment of ulcerative colitis," *Chinese Acupuncture and Moxibustion*, vol. 26, no. 4, pp. 261–263, 2006.

[26] D. J. Duan, L. N. Zhang, J. T. Yin et al., "Clinical observation of catgut embedding combined with Pulsatilla decoction enema for the treatment of chronic ulcerative colitis," *Hebei Journal of Traditional Chinese Medicine*, vol. 34, no. 5, pp. 721–722, 2012.

[27] Y. T. Sun and S. L. Wang, "Warm needle acupuncture combined with retention enema for the treatment of 45 cases of ulcerative colitis," *Journal of Chinese Acupuncture and Moxibustion*, vol. 9, p. 562, 1998.

[28] S. L. Wang, "Efficacy of warm needle acupuncture for the treatment of ulcerative colitis," *Journal of Chinese Community Doctors*, vol. 10, no. 22, pp. 132–133, 2008.

[29] T. A. Ma and Z. K. Xu, "Efficacy of acupuncture plus TDP for the treatment of chronic ulcerative colitis," *Central Plains Medical Journal*, vol. 32, no. 17, pp. 31–32, 2005.

[30] J. Cui, "The impact of acupuncture treatment on the cytokines of patients with ulcerative colitis," *Hebei Medical Journal*, vol. 32, no. 11, pp. 1409–1410, 2010.

[31] X. Y. Guo, Z. J. Long, X. Wu et al., "Observations of the efficacy of acupuncture and moxibustion combined with Chinese medicine enema treatment for 22 cases of ulcerative colitis," *Liaoning Journal of Traditional Chinese Medicine*, vol. 34, no. 5, pp. 654–655, 2007.

[32] D. M. Wang, X. G. Zhang, K. Chen et al., "Acupuncture and moxibustion combined with Chinese and Western medicine retention enema to treat ulcerative colitis," *Practical Pharmacy and Clinical Reme*, vol. 12, no. 3, pp. 224–225, 2009.

[33] Z. J. Long and X. L. Yang, "Acupuncture and moxibustion combined with traditional Chinese medicine enema for the treatment of 23 cases of ulcerative colitis," *Chinese Journal of Coloproctology*, vol. 30, no. 2, pp. 58–59, 2010.

[34] H. Y. Chen, "Efficacy and care-related observations of acupuncture and moxibustion combined with traditional Chinese medicine enema for ulcerative colitis," *Chinese and Foreign Medical Research*, vol. 8, no. 12, pp. 101–102, 2010.

[35] G. H. Sun and X. L. Wang, "Acupuncture and moxibustion treatment of 35 cases of chronic ulcerative colitis," *Journal of Practical Traditional Chinese Medicine*, vol. 17, no. 6, p. 32, 2001.

[36] S. H. Wang, X. G. Li, L. Q. Zhang et al., "Clinical study on herb-partitioned moxibustion at Shenque (CV 8) acupiont for treatment of ulcerative colitis," *Chinese Acupuncture and Moxibustion*, vol. 26, no. 2, pp. 97–99, 2006.

[37] Y. Q. Shi, S. P. Liu, and J. G. Liu, "The impact of acupuncture and moxibustion treatment on cytokine levels in patients with ulcerative colitis," *Hubei Journal of Traditional Chinese Medicine*, vol. 28, no. 2, pp. 11–12, 2006.

[38] S. Qun, J. Lu, and S. M. Guo, "Efficacy of acupuncture and moxibustion at crossed points as main treatment for ulcerative colitis," *Shanghai Journal of Acupuncture and Moxibustion*, vol. 31, no. 5, pp. 319–320, 2012.

[39] Q. J. Xu, "Clinical observation of an integrated traditional and western treatment for 56 cases of chronic ulcerative colitis," *Journal of Chinese Physician*, vol. 34, no. 1, pp. 48–49, 2006.

[40] Z. J. Zhang, S. Xie, G. F. Ma et al., "The impact of traditional Chinese medicine on serum IL-8 and IL-10 levels of ulcerative colitis patients," *Shaanxi Journal of Traditional Chinese Medicine*, vol. 32, no. 5, pp. 566–568, 2011.

[41] S. Joos, N. Wildau, R. Kohnen et al., "Acupuncture and moxibustion in the treatment of ulcerative colitis: a randomized controlled study," *Scandinavian Journal of Gastroenterology*, vol. 41, no. 9, pp. 1056–1063, 2006.

[42] C. Yang and H. Yan, "Efficacy of acupuncture and moxibustion in 62 cases of chronic colitis," *Journal of Traditional Chinese Medicine*, vol. 19, no. 2, pp. 111–114, 1999.

[43] S. Joos, B. Brinkhaus, C. Maluche et al., "Acupuncture and moxibustion in the treatment of active Crohn's disease: a randomized controlled study," *Digestion*, vol. 69, no. 3, pp. 131–139, 2004.

[44] S. Ma, "Observation on the therapeutic effect of combined treatment of 60 cases of ulcerative colitis with acupuncture and moxibustion," *World Journal of Acupuncture-Moxibustion*, vol. 9, no. 1, p. 24, 1999.

[45] X. Ma, "Acupuncture treatment for 76 cases of ulcerative colitis," *Journal of Traditional Chinese Medicine*, vol. 25, no. 4, pp. 264–265, 2005.

[46] K. F. Schulz, D. G. Altman, and D. Moher, "CONSORT 2010 statement: updated guidelines for reporting parallel group randomized trials," *Annals of Internal Medicine*, vol. 152, no. 11, pp. 726–732, 2010.

Hindawi Publishing Corporation
Evidence-Based Complementary and Alternative Medicine
Volume 2013, Article ID 890579, 7 pages
http://dx.doi.org/10.1155/2013/890579

Research Article

Gene Expression Profiles at Moxibustioned Site (ST36): A Microarray Analysis

Hai-Yan Yin,[1,2,3] Yong Tang,[1,2,3] Sheng-Feng Lu,[4] Ling Luo,[1] Jia-Ping Wang,[1] Xu-Guang Liu,[1] and Shu-Guang Yu[1,5]

[1] *Acupuncture & Tuina School, Chengdu University of Traditional Chinese Medicine, Chengdu 610075, China*
[2] *Joint Laboratory of Biochip between Chengdu University of Traditional Chinese Medicine and CapitalBio Co. Ltd., 37 Shi-er Qiao Road, Chengdu 610075, China*
[3] *Key Laboratory for Acupuncture & Chronobiology of Sichuan Province, Chengdu 610075, China*
[4] *Acupuncture & Tuina School, Nanjing University of Traditional Chinese Medicine, Nanjing 210029, China*
[5] *Laboratory for Acupuncture & Systematic Biology, Chengdu University of Traditional Chinese Medicine, Chengdu 610075, China*

Correspondence should be addressed to Shu-Guang Yu; ysg28588@126.com

Received 6 June 2013; Accepted 2 July 2013

Academic Editor: Yong-Qing Yang

As a major alternative therapy in Traditional Chinese Medicine, it has been demonstrated that moxibustion could generate a series of molecular events in blood, spleen, and brain, and so forth. However, what would happen at the moxibustioned site remained unclear. To answer this question, we performed a microarray analysis with skin tissue taken from the moxibustioned site also Zusanli acupoint (ST36) where 15-minute moxibustion stimulation was administrated. The results exhibited 145 upregulated and 72 downregulated genes which responded immediately under physiological conditions, and 255 upregulated and 243 downregulated genes under pathological conditions. Interestingly, most of the pathways and biological processes of the differentially expressed genes (DEGs) under pathological conditions get involved in immunity, while those under physiological conditions are involved in metabolism.

1. Introduction

In acupuncture research, microarray analysis has been widely employed to uncover gene expression profiles at different tissues or organs [1–19]. Based on these gene expression profiles, researchers would be able to have the possibility to find out more potentially interesting targeted genes to conduct further experiment to explain the molecular events induced by acupuncture. Moxibustion, as one of the main therapies in acupuncture clinical practice, has been demonstrated to it could be useful for pain relief [20, 21] and generated a series of molecular events in blood [22, 23], spleen [24, 25], colonic mucosa [26], brain [27], and so forth, by utilizing moxa cone or stick to stimulate acupoint or some areas (also named moxibustioned site). However, none of gene expression profiles at moxibustioned site to date has been reported. Therefore, we proposed that moxibustion could, to a considerable extent, yield a great deal of differentially expressed genes (DEGs) at moxibustioned site, and we also anticipate to find out potential molecular targets to explain how moxibustion works at the stimulated site.

2. Material and Methods

2.1. Animals. Adult male Sprague-Dawley rats weighing 200–220 g obtained from Chengdu University of Traditional Chinese Medicine, Experimental Animal Centre, were utilized in this study. Maintained in animal room of automatically controlled day cycles (12 : 12 = light : dark cycle) at 24 ± 2°C, all rats were allowed to freely take food and water *ad libitum* and randomly assigned to the various experimental groups ($n = 3$, for each group). The experimental procedures were conducted in accordance with the National Institutes of Health (NIH) Guide for the Care and Use of Laboratory Animals, and all experimental protocols were approved by

the Animal Ethics Committee of Chengdu University of Traditional Chinese Medicine.

2.2. Experimental Design. In this study, we aimed to explore what would take place at the moxibustioned site in the view of potential molecular target under physiological and pathological conditions. Thus, we designed two different parts of microarray experiment. One is designed for uncovering the gene expression profile at physiological condition in which it consisted of 2 group: healthy control group (C) and healthy control with moxibustion stimulation group (CM). The other one is designed for revealing the gene expression profile at pathological condition in which it composed of model control group (M) and model control with moxibustion stimulation group (MM).

2.3. Intervention

2.3.1. Physiological Condition. Under physiological condition, the rats in CM group received moxibustion at the left acupoint Zusanli (ST36), at the depression below the knee from the anterior crest of the tibia [28] for 15 min. The moxibustion stimulation was manipulated with lighting moxa stick (length: 12 cm, diameter: 0.6 cm, Nanyang Hanyi Moxibustion Technology Development Co., Ltd., China) for 15 min (Figure 1). In case of skin burnt, the tip of moxa stick was kept about 2-3 cm from the skin.

2.3.2. Pathological Condition. Firstly, the pathological condition was established by injecting subcutaneously with 0.1 mL Freund's Complete Adjuvant (FCA, Sigma, USA) into the plantar surface of the left hind paw of the rat [29]. The CFA injection immediately led to local inflammation, paw swelling and pain, which became apparent within 12 hours and persisted for at least 2 weeks after injection. In this experiment, the rats in MM group received moxibustion with the same procedure as mentioned above 1 week after injection.

2.4. RNA Extraction. Two hours after one time of moxibustion stimulation was completed, rats was euthanized by CO_2 inhalation. The cutaneous tissue (0.5 cm × 0.5 cm × 0.2 cm) located at moxibustioned site were immediately removed and preserved in RNAlater (Ambion, USA) to prevent RNA degradation. Total RNA was extracted using TRIzol Reagent (Invitrogen, USA) and purified with RNA clean-up Kit (MN, Germany) following the instructions of manufacturers, respectively. Total RNA was quantitated by spectrophotometry, and the integrity was assessed by formaldehyde denatured agarose gel electrophoresis.

2.5. Microarray Analysis. The microarray analysis service provided by CapitalBio Corporation (Beijing, China) was performed as described [30, 31]. Briefly, total RNA extracted from the samples was used to produce complementary RNA using in vitro transcription technique. Then cDNA was generated by reverse transcription and used as the template to synthesize the fluorescein-labeled cDNA by Klenow fragment polymerase. Universal rat reference RNA purchased from Stratagene was also labeled as common reference control. RNA from sample and common reference were fluorescently labeled by Cy5 or Cy3, respectively, and then were hybridized paired to 27K Rat Genome Array (CapitalBio, China). The array was comprised of 26,962 oligonucleotide probes covering 27,044 transcripts which represent about 22,012 genes. All arrays were scanned by LuxScan 10KA dual channel confocal laser scanner (CapitalBio, China). The obtained images were analyzed with LuxScan3.0 Image Analysis Software (CapitalBio, China), which employed the LOWESS normalization algorithm.

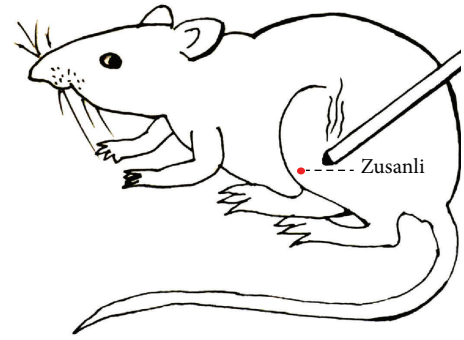

Figure 1: Rat received moxibustion at ST36 (Zusanli).

2.6. Data Analysis

2.6.1. Differentially Expressed Genes Selection. The detected signal intensities of all probes on the chip ≥400 were included for comparison analysis. We applied two-class unpaired algorithm in the Significant Analysis of Microarray software (SAM, Stanford) to identify significantly differentially expressed genes between CM and C groups, and MM and M groups. DEGs were determined with the threshold of false discovery rate, FDR ≤5% and fold change ≥2.0 or ≤0.5.

2.6.2. Pathway and Biological Processes Analysis of DEGs. We employed the online Molecule Annotation System (MAS) established by CapitalBio Corporation (http://bioinfo.capitalbio.com/mas3/) which integrated with KEGG and Gene Ontology (GO) database to perform pathway and GO Biological Process term enrichment analysis and calculate the statistical significance as described [32]. P value <0.001 was considered statistically significant.

2.7. Real Time PCR Confirmation. To validate the expression patterns obtained from microarray data, we used quantitative real time polymerase chain reaction (qPCR) to detect the expression of four DEGs, Hspa1a, Mcpt8, Slpi, and Clqa, which were randomly selected from the 27K Rat Genome Array. Table 1 showed the primers designed for these genes and the housekeeping gene Gapdh. cDNA was prepared from DNase-treated total RNA using the First Strand SuperScript II Kit (Invitrogen, USA). qPCR was performed with DNA Master SYBR Green I Kit (Roche, Germany) and LightCycler machine (Roche, Germany) following the manufacturer's protocols.

Table 1: The primer designed for validation.

Gene	Primer (5′-3′)	Temperature (°C)	Product size (bp)
Gapdh	FW: CCTTGTAAGGGCAAAACCAA RV: ATGGCCTTCCGTGTTCCTAC	59	156
Hspa1a	FW: GGTGAACTACAAGGGCGAGA RV: GCTGCGAGTCGTTGAAGTAG	58	152
Mcpt8	FW: CCAGGTCATCGCTGTTGTAAA RV: CCCAGGTTTCACCCAGTCC	62	382
Slpi	FW: ACAGACAGGGGCTCTCTTGA RV: CCTCCCAATAAGTGCCAGAA	60	216
Clqa	FW: AAGTGGGACCTTTGTCTGTCTATC RV: CCCTGCTAACACCTGGAAGAG	59	108

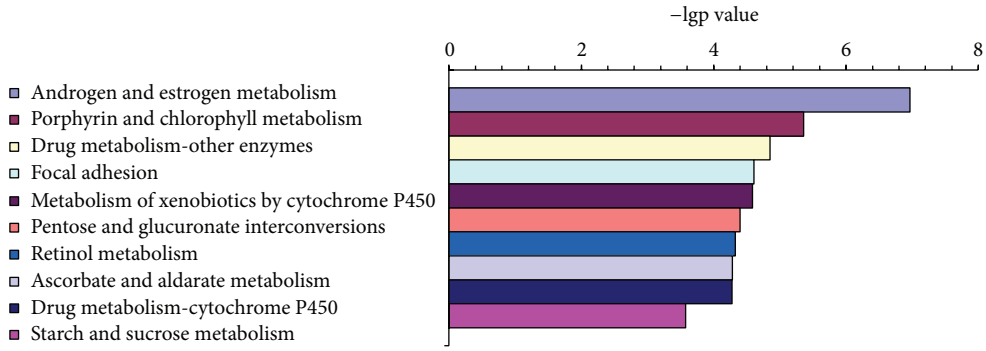

(a) Physiological condition

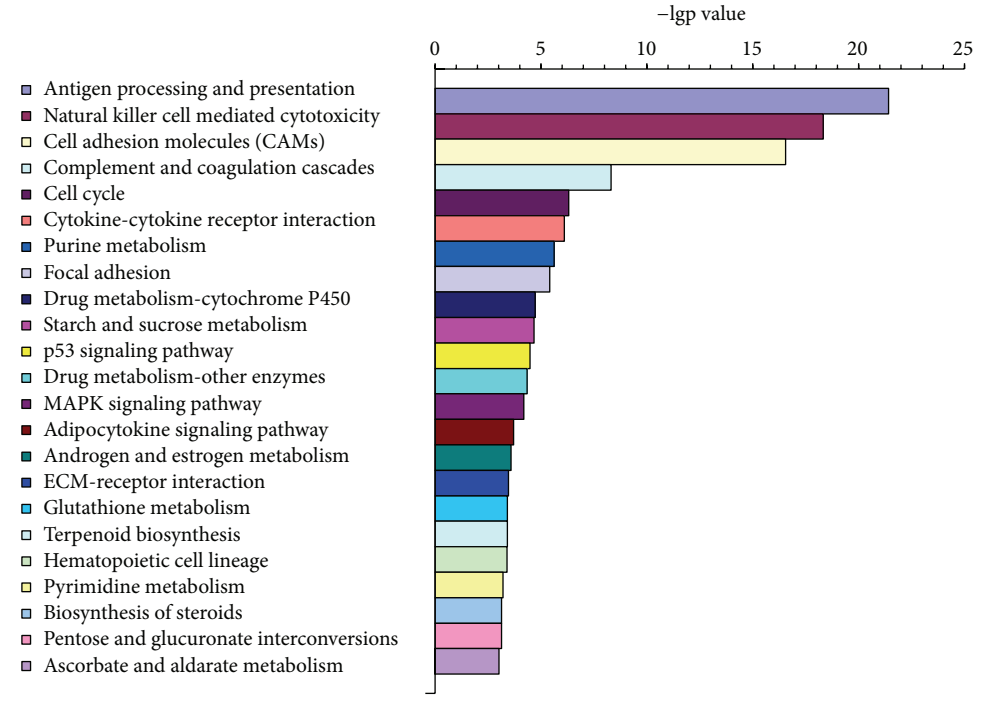

(b) Pathological condition

Figure 2: The statistically significant pathways (P value <0.001) involved in DEGs at moxibustioned site.

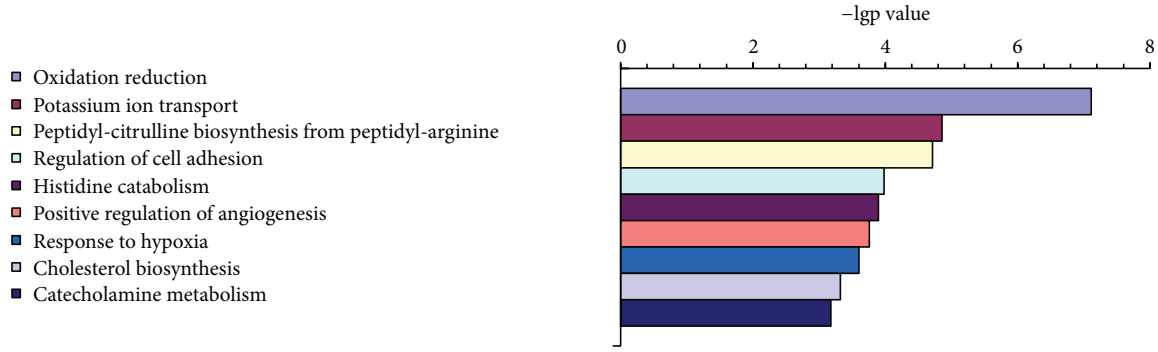

(a) Physiological condition

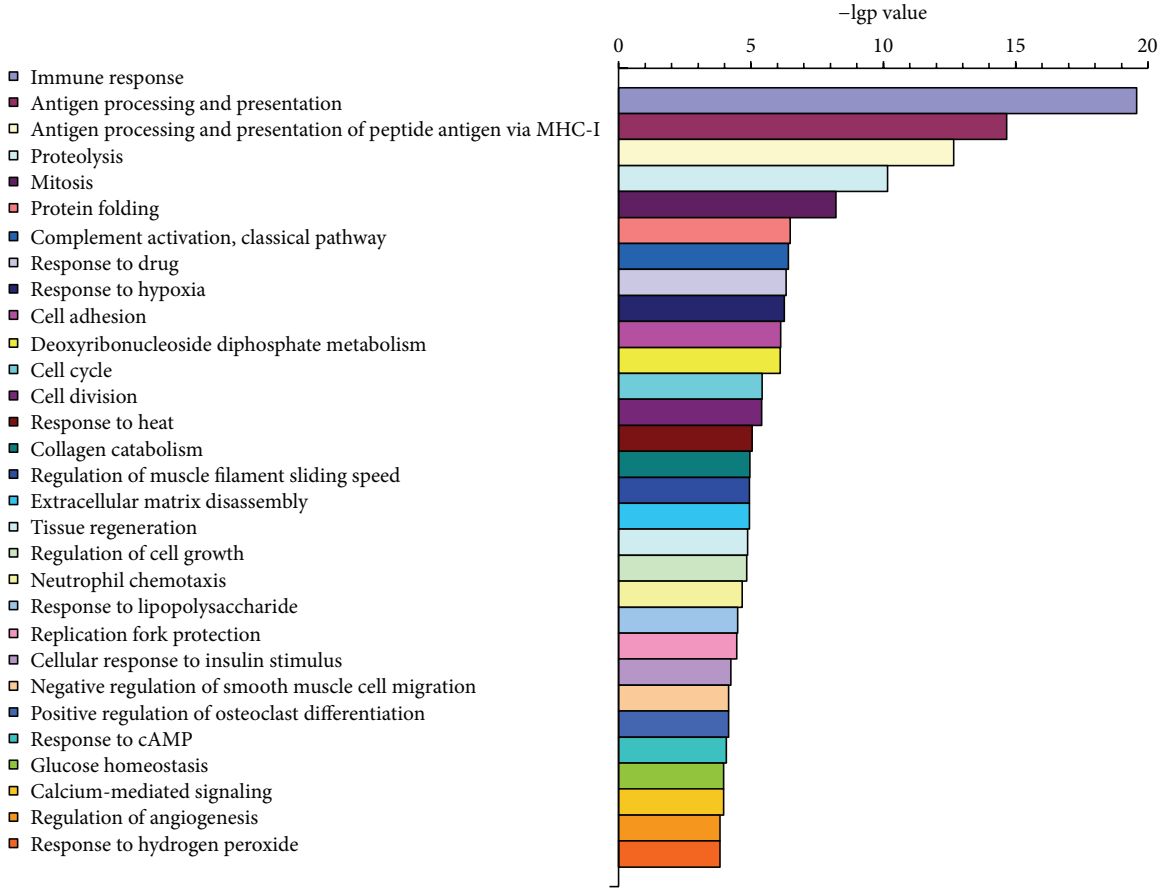

(b) Pathological condition

Figure 3: The statistically significant biological processes (P value <0.001) involved in DEGs at moxibustioned site.

3. Results

3.1. DEGs at Moxibustioned Site. Different numbers of DEGs at moxibustioned site were obtained from different condition. Under physiological condition, we obtained 145 upregulated and 72 downregulated DEGs (see Supplementary Table 1 in Supplementary Material available online at http://dx.doi.org/10.1155/2013/890579). While under pathological condition, the results displayed 255 upregulated and 243 downregulated DEGs (Supplementary Table 2).

3.2. Enriched Pathways at Moxibustioned Site. Figure 2 showed us statistically significant pathways (P value <0.001) at moxibustioned site. Under physiological condition (Figure 2(a)), it was found that 10 pathways were enriched based on all DEGs at moxibustioned Site. On the other hand, 21 enriched pathways were statistically significant under pathological condition (Figure 2(b)).

3.3. Enriched Biological Processes at Moxibustioned Site. From Figure 3, we would find out the biological processes with significantly statistical differences (P value <0.001) at moxibustioned site. Under physiological condition (Figure 3(a)), it was found out that 9 biological processes were involved. Under pathological condition (Figure 3(b)), 29 biological processes were enriched.

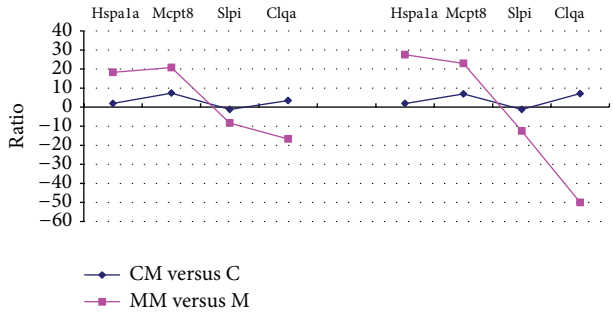

Figure 4: qPCR validation for 4 DEGs from microarray data.

3.4. Validation of the 4 Selected Genes. To validate the results of the microarray, we selected 4 genes, Hspa1a, Mcpt8, Slpi, and Clqa, by qPCR. The results indicated that the expression levels of confirmed genes in microarray were similar with that in qPCR (Figure 4).

4. Discussion

Here, we firstly reported the gene expression profiles at the moxibustioned site. The results imply that the moxibustioned site would also generate a setting of DEGs apart from those in other any tissue [16]. In other words, either under physiological condition or under pathological condition, we could find out a great number of DEGs responding to moxibustion stimulation at moxibustioned site. Based on these DEGs under different condition, we further seek out 22 coexpressed genes with similar expression tendency (Supplementary Table 3). To some extent, these genes (16 upnegulated and 6 downregulated genes) should be most likely to be considered as potential targets for continuing studies to determine which genes would be essential or critical in the role of moxibustion at moxibustioned site.

In this study, most (8/10) of the involved pathways at moxibustioned site were related to metabolism under physiological condition (Figure 2(a)). However, the significant pathways under pathological condition induced by FCA were most associated with immunity (Figure 2(b)), such as the pathway of antigen processing and presentation and natural killer cell-mediated cytotoxicity. It is suggested that different pathway at the moxibustioned site would get involved of the in different condition even with same moxibustion stimulation.

According to the biological processes analysis, we also could find out the difference from different state. Without FCA as the pathological stimulation, the biological progresses following moxibustion administration at moxibustioned site were most composed of oxidation reduction, potassium ion transport, and so forth. However, a variety of biological processes related to immunity, such as immune response, antigen processing and presentation, and antigen processing and presentation of peptide antigen via MHC class I, and were exhibited in this study.

Taken together, it seemed to be concluded that a series of molecular events would happen at moxibustioned site. Moreover, different pathways and biological progresses at moxibustioned site would be involved in different condition. However, this conclusion should be seriously taken for granted given the following limitations. Firstly, only one stimulation time point was used in this study. How about the time course or different time points, such as 5, 10, 15, 20, and 30 minutes, which were frequently practiced in moxibustion clinic, which needs to be answered in future study? Secondly, the pathological condition was induced by FCA injection in this study. To our knowledge, FCA injection will generate adjuvant arthritis through a series of immune actions [33, 34]. Moreover, previous studies also demonstrated that moxibustion would be useful to get better improved adjuvant arthritis [32, 35, 36]. Therefore, we cannot determine whether the DEGs at moxibustioned site under pathological condition would play important role in the moxibustion treatment of adjuvant arthritis. In this point of view, current data can only be used to explain what had happened at moxibustioned site under this condition. How about other pathological conditions? It is necessary to perform more researches to figure out the difference or similarity under different pathological conditions.

Additionally, in this study the tissue used for RNA extraction and microarray detection was taken from the skin of the moxibustioned site. So far, the skin has been also regarded as an important immune organ [37, 38] as well as a component of neuro-immuno-cutaneous system (NICS) [39–42]. In view of this aspect, we would be able to assure that the molecular event at moxibustioned site in this experiment will have the possibility to be applied to explain the initial mechanism of moxibustion activating the neuroimmune modulation which has been demonstrated in previous studies [43, 44]. This would be another potential mechanism of moxibustion apart from that it is currently considered as temperature-related and non-temperature-related work mechanisms [45].

5. Conclusions

The results suggested that a set of molecular events would have happened at moxibustioned site. Among those molecular events, different genes and different pathways and biological progresses at moxibustioned site would have got involved under different conditions.

Conflict of Interests

All authors manifest that there is no conflict of interests.

Authors' Contribution

Hai-Yan Yin and Yong Tang contributed equally to this work.

Acknowledgments

This work was funded by the National Basic Research Program of China (973 Program, no. 2009CB522903), the National Natural Science Foundation of China (nos. 81173320, 81102667), Sichuan province Education Bureau (no.

12ZA037), and the Scientific Research Foundation of Sichuan Province of China for Returned Chinese Scholars.

References

[1] S. K. Kim, J. Kim, E. Ko et al., "Gene expression profile of the hypothalamus in DNP-KLH immunized mice following electroacupuncture stimulation," *Evidence-Based Complementary and Alternative Medicine*, vol. 2011, Article ID 508689, 8 pages, 2011.

[2] Y.-G. Choi, S. Yeo, Y.-M. Hong, and S. Lim, "Neuroprotective changes of striatal degeneration-related gene expression by acupuncture in an MPTP mouse model of Parkinsonism: microarray analysis," *Cellular and Molecular Neurobiology*, vol. 31, no. 3, pp. 377–391, 2011.

[3] Y.-G. Choi, S. Yeo, Y.-M. Hong, S.-H. Kim, and S. Lim, "Changes of gene expression profiles in the cervical spinal cord by acupuncture in an MPTP-intoxicated mouse model: microarray analysis," *Gene*, vol. 481, no. 1, pp. 7–16, 2011.

[4] Y.-G. Choi, S. Yeo, Y.-M. Hong, and S. Lim, "Neuroprotective changes of striatal degeneration-related gene expression by acupuncture in an MPTP mouse model of Parkinsonism: microarray analysis," *Cellular and Molecular Neurobiology*, vol. 31, no. 3, pp. 377–391, 2011.

[5] C. Tan, J. Wang, W. Feng, W. Ding, and M. Wang, "Preliminary correlation between warm needling treatment for knee osteoarthritis of deficiency-cold syndrome and metabolic functional genes and pathways," *Journal of Acupuncture and Meridian Studies*, vol. 3, no. 3, pp. 173–180, 2010.

[6] L.-H. Jiang and L.-L. Wang, "Gene chips-aided analysis on the profiles of hippocampal whole-genome expression in depression rats following electroacupuncture treatment," *Zhen Ci Yan Jiu*, vol. 35, no. 2, pp. 83–89, 2010.

[7] M. S. Hong, H.-K. Park, J.-S. Yang et al., "Gene expression profile of acupuncture treatment in 1-methyl-4-phenyl-1,2, 3,6-tetrahydropyridine-induced Parkinson's disease model," *Neurological Research*, vol. 32, supplement 1, pp. S74–S78, 2010.

[8] S.-H. Sohn, S. K. Kim, E. Ko et al., "The genome-wide expression profile of electroacupuncture in DNP-KLH immunized mice," *Cellular and Molecular Neurobiology*, vol. 30, no. 4, pp. 631–640, 2010.

[9] S. K. Kim, J. Y. Park, B. H. Koo et al., "Adenoviral gene transfer of acetylcholinesterase T subunit in the hypothalamus potentiates electroacupuncture analgesia in rats," *Genes, Brain and Behavior*, vol. 8, no. 2, pp. 174–180, 2009.

[10] H.-S. Shiue, Y.-S. Lee, C.-N. Tsai, Y.-M. Hsueh, J.-R. Sheu, and H.-H. Chang, "DNA microarray analysis of the effect on inflammation in patients treated with acupuncture for allergic rhinitis," *Journal of Alternative and Complementary Medicine*, vol. 14, no. 6, pp. 689–698, 2008.

[11] X.-Y. Wang, X.-L. Li, S.-Q. Hong, Y.-B. Xi-Yang, and T.-H. Wang, "Electroacupuncture induced spinal plasticity is linked to multiple gene expressions in dorsal root deafferented rats," *Journal of Molecular Neuroscience*, vol. 37, no. 2, pp. 97–110, 2009.

[12] Y.-Z. Gao, S.-Y. Guo, Q.-Z. Yin, T. Hisamitsu, and X.-H. Jiang, "An individual variation study of electroacupuncture analgesia in rats using microarray," *The American Journal of Chinese Medicine*, vol. 35, no. 5, pp. 767–778, 2007.

[13] L.-P. Yang, M.-C. Wang, W.-G. Liu, and M.-Q. Wang, "Effects of warming-needle therapy on gene expression pathways in the patient with knee osteoarthritis of deficiency-cold syndrome," *Zhongguo Zhen Jiu*, vol. 27, no. 9, pp. 677–680, 2007.

[14] M. Li and Y. Zhang, "Modulation of gene expression in cholesterol-lowering effect of electroacupuncture at Fenglong acupoint (ST40): a cDNA microarray study," *International Journal of Molecular Medicine*, vol. 19, no. 4, pp. 617–629, 2007.

[15] Y. Chae, H.-J. Park, D.-H. Hahm, S.-H. Yi, and H. Lee, "Individual differences of acupuncture analgesia in humans using cDNA microarray," *Journal of Physiological Sciences*, vol. 56, no. 6, pp. 425–431, 2006.

[16] H. G. . Wu, H. R. Liu, C. Zhao et al., "Study on differentially expressed genes of ulcerative colitis in the rat treated by herbs-partitioned moxibustion," *Zhongguo Zhen Jiu*, vol. 25, no. 5, pp. 359–365, 2005.

[17] C. Keun Kim, S. C. Gi, D. O. Sang et al., "Electroacupuncture up-regulates natural killer cell activity: identification of genes altering their expressions in electroacupuncture induced up-regulation of natural killer cell activity," *Journal of Neuroimmunology*, vol. 168, no. 1-2, pp. 144–153, 2005.

[18] J.-C. Guo, H.-M. Gao, J. Chen et al., "Modulation of the gene expression in the protective effects of electroacupuncture against cerebral ischemia: a cDNA microarray study," *Acupuncture and Electro-Therapeutics Research*, vol. 29, no. 3-4, pp. 173–186, 2004.

[19] J. Ko, S. N. Doe, H. L. Young et al., "cDNA microarray analysis of the differential gene expression in the neuropathic pain and electroacupuncture treatment models," *Journal of Biochemistry and Molecular Biology*, vol. 35, no. 4, pp. 420–427, 2002.

[20] J.-H. Kim, H.-K. Kim, Y.-I. Park et al., "Moxibustion at ST36 alleviates pain in complete Freund's adjuvant-induced arthritic rats," *The American Journal of Chinese Medicine*, vol. 34, no. 1, pp. 57–67, 2006.

[21] L. Qi, H. R. Liu, T. Yi et al., "Warming moxibustion relieves chronic visceral hyperalgesia in rats: relations to spinal dynorphin and orphanin-FQ system," *Evidence-Based Complementary and Alternative Medicine*, vol. 2013, Article ID 920675, 10 pages, 2013.

[22] H. Yamashita, Y. Ichiman, and Y. Tanno, "Changes in peripheral lymphocyte subpopulations after direct moxibustion," *The American Journal of Chinese Medicine*, vol. 29, no. 2, pp. 227–235, 2001.

[23] Y.-Y. Kung, F.-P. Chen, and S.-J. Hwang, "The different immunomodulation of indirect moxibustion on normal subjects and patients with systemic lupus erythematosus," *The American Journal of Chinese Medicine*, vol. 34, no. 1, pp. 47–56, 2006.

[24] G. S. Choi, J. B. Han, J. H. Park et al., "Effects of moxibustion to zusanli (ST36) on alteration of natural killer cell activity in rats," *The American Journal of Chinese Medicine*, vol. 32, no. 2, pp. 303–312, 2004.

[25] J.-B. Han, S.-D. Oh, K.-S. Lee et al., "The role of the sympathetic nervous system in moxibustion-induced immunomodulation in rats," *Journal of Neuroimmunology*, vol. 140, no. 1-2, pp. 159–162, 2003.

[26] E.-H. Zhou, H.-R. Liu, H.-G. Wu et al., "Down-regulation of protein and mRNA expression of IL-8 and ICAM-1 in colon tissue of ulcerative colitis patients by partition-herb moxibustion," *Digestive Diseases and Sciences*, vol. 54, no. 10, pp. 2198–2206, 2009.

[27] E.-H. Zhou, X.-M. Wang, G.-H. Ding et al., "Suspended moxibustion relieves chronic visceral hyperalgesia and decreases hypothalamic corticotropin-releasing hormone levels," *World Journal of Gastroenterology*, vol. 17, no. 5, pp. 662–665, 2011.

[28] S. Chen and S.-X. Ma, "Nitric oxide in the gracile nucleus mediates depressor response to acupuncture (ST36)," *Journal of Neurophysiology*, vol. 90, no. 2, pp. 780–785, 2003.

[29] C. Stein, M. J. Millan, and A. Herz, "Unilateral inflammation of the hindpaw in rats as a model of prolonged noxious stimulation: alterations in behavior and nociceptive thresholds," *Pharmacology Biochemistry and Behavior*, vol. 31, no. 2, pp. 445–451, 1988.

[30] Y. Guo, H. Guo, L. Zhang et al., "Genomic analysis of anti-hepatitis B virus (HBV) activity by small interfering RNA and lamivudine in stable HBV-producing cells," *Journal of Virology*, vol. 79, no. 22, pp. 14392–14403, 2005.

[31] T. A. Patterson, E. K. Lobenhofer, S. B. Fulmer-Smentek et al., "Performance comparison of one-color and two-color platforms within the MicroArray Quality Control (MAQC) project," *Nature Biotechnology*, vol. 24, no. 9, pp. 1140–1150, 2006.

[32] J.-Q. Fang, E. Aoki, A. Seto, Y. Yu, T. Kasahara, T. Hisamitsu et al., "Influence of moxibustion on collagen-induced arthritis in mice," *In Vivo*, vol. 12, no. 4, pp. 421–426, 1998.

[33] C. M. Pearson and F. D. Wood, "Studies of arthritis and other lesions induced in rats by the injection of mycobacterial adjuvant. VII. Pathologic details of the arthritis and spondylitis," *The American Journal of Pathology*, vol. 42, pp. 73–95, 1963.

[34] C. M. Pearson, B. H. Waksman, and J. T. Sharp, "Studies of arthritis and other lesions induced in rats by injection of mycobacterial adjuvant. V. Changes affecting the skin and mucous membranes. Comparison of the experimental process with human disease," *The Journal of Experimental Medicine*, vol. 113, no. 3, pp. 485–510, 1961.

[35] Z. L. Tang, X. G. Song, F. Q. Zang et al., "Study on the action mechanism of moxibustion in anti-inflammation and immunoregulation in rheumatoid arthritis rats," *Acupuncture Research*, vol. 28, no. 4, pp. 292–298, 2003.

[36] Y. . Shi and S. L. Zhou, "Effect of zusanli (ST36) acupoint on nerve-endocrine-immune network," *Journal of Jiangxi College of Traditional Chinese Medicine*, vol. 15, no. 2, pp. 37–39, 2003.

[37] J. C. Simon, "Skin as an immune organ," *Medizinische Monatsschrift für Pharmazeuten*, vol. 18, no. 11, pp. 316–319, 1995.

[38] J. K. Salmon, C. A. Armstrong, and J. C. Ansel, "The skin as an immune organ," *Western Journal of Medicine*, vol. 160, no. 2, pp. 146–152, 1994.

[39] L. Misery, "The neuro-immuno-cutaneous system (NICS)," *Pathologie Biologie*, vol. 44, no. 10, pp. 867–874, 1996.

[40] J. D. Bos and M. L. Kapsenberg, "The skin immune system: progress in cutaneous biology," *Immunology Today*, vol. 14, no. 2, pp. 75–78, 1993.

[41] L. Misery, "The neuro-immuno-cutaneous system and ultraviolet radiation," *Photodermatology Photoimmunology and Photomedicine*, vol. 16, no. 2, pp. 78–81, 2000.

[42] F. O. Nestle, P. Di Meglio, J.-Z. Qin, and B. J. Nickoloff, "Skin immune sentinels in health and disease," *Nature Reviews Immunology*, vol. 9, no. 10, pp. 679–691, 2009.

[43] Y. Shi and S. L. Zhou, "Effect of Zusanli (ST36) Acupoint on nerve-endocrine-immune network," *Journal of Jiangxi College of Traditional Chinese Medicine*, vol. 15, no. 2, pp. 37–39, 2003.

[44] J. W. Li, J. M. Liu, Y. Y. Xiong, and S. Y. Xiang, "Advance in research on nerve-endocrine-immune network of rheumatoid arthritis mediated by acupuncture," *Traditional Chinese Medical Research*, vol. 19, no. 3, pp. 57–60, 2006.

[45] C. Jen-Hwey, "How does moxibustion possibly work?" *Evidence-Based Complementary and Alternative Medicine*, vol. 2013, Article ID 198584, 8 pages, 2013.

Hindawi Publishing Corporation
Evidence-Based Complementary and Alternative Medicine
Volume 2013, Article ID 294091, 9 pages
http://dx.doi.org/10.1155/2013/294091

Research Article

Effect of Electroacupuncture Intervention on Expression of CGRP, SP, COX-1, and PGE2 of Dorsal Portion of the Cervical Spinal Cord in Rats with Neck-Incision Pain

Li-na Qiao,[1] Jun-ying Wang,[2] Yong-sheng Yang,[1] Shu-ping Chen,[2] Yong-hui Gao,[2] Jian-liang Zhang,[2] and Jun-ling Liu[2]

[1] *Department of Biochemistry and Molecular Biology, Institute of Acu-Moxibustion, China Academy of Chinese Medical Sciences, 16 Nanxiaojie Street, Dongzhimennei, Beijing 100700, China*
[2] *Department of Physiology, Institute of Acu-Moxibustion, China Academy of Chinese Medical Sciences, 16 Nanxiaojie Street, Dongzhimennei, Beijing 100700, China*

Correspondence should be addressed to Jun-ling Liu; 13521898023@163.com

Received 3 June 2013; Accepted 19 July 2013

Academic Editor: Yong-Qing Yang

The present study was aimed to determine if cervicospinal substance P (SP) and its neurokinin-1 receptor (NK-1R), calcitonin gene-related peptide (CGRP), cyclooxygenase-1 (COX-1), and prostaglandin E2 (PGE2) were involved in electroacupuncture (EA) analgesia in neck-incision pain rats. EA intervention was applied to bilateral Futu (LI18), Hegu (LI4)-Neiguan (PC6), and Zusanli (ST36)-Yanglingquan (GB34) for 30 min. Cervicospinal SP and CGRP immunoactivity was detected by immunofluorescence technique, NK-1R and COX-1 protein and mRNA expression levels were determined using Western blot and real-time PCR, respectively, and PGE2 content was measured using ELISA. Outcomes indicated that EA of EA-LI18 and LI4-PC6 (not ST36-GB34) significantly suppressed neck-incision induced decrease of thermal pain threshold ($P < 0.05$). EA stimulation of LI18 and LI4-PC6 markedly inhibited neck-incision induced upregulation of SP and CGRP immunoactivity, NK-1 R and COX-1 mRNA and protein expression levels, as well as the increase of PGE2 content in the dorsal cervicospinal cord ($P < 0.05$). These findings showed that LI18 and LI4-PC6 EA stimulation-induced downregulation of SP, CGRP, NK-1R, COX-1, and PGE2 levels in the dorsal cervicospinal cord may contribute to their effects in relieving neck-incision pain. This study highlights the targets of EA intervention for reducing post-thyroid-surgery pain for the first time.

1. Introduction

Postoperative pain in patients undergoing thyroidectomy generally lasts for hours or days in spite of being moderate in severity and different in duration for the types of diseases [1]. In the treatment of this type of postoperative pain, oral administration of opioids (about 90% of the patients) and nonopioid adjuncts is the optimized choice currently [2]. However, these drugs may worsen anesthetics-induced nausea, vomiting, and other side effects [3] and the analgesic effect of these drugs is not always effective [4].

Therefore, a multimodal approach combining various analgesics with a nonpharmacological strategy is necessary for providing adequate postoperative pain control. Acupuncture, a component of traditional Chinese medicine, has been used to treat pain for millennia, and accumulating evidence indicates the efficacy of acupuncture for postoperative analgesia [5–10]. It has been demonstrated that the analgesic effect of acupuncture is related to its functions in upregulating plasma beta-endorphin level in patients undergoing colonoscopy [6], breast radical carcinoma operation [11], and in activating peripheral opioid pathway in a mouse model of postoperative pain [12]. It has been well documented from clinical practice of acupuncture analgesia and anesthesia that Futu (LI18) and Hegu (LI4)-Neiguan (PC6) are effective acupoints for thyroid surgery [13–16]. But there have been no

research reports about acupuncture intervention for relieving postthyroidectomy pain till now. In the past several years, our research group investigated the spinal mechanism of electroacupuncture (EA) therapy underlying pain relief of thyroid surgery. Our findings showed that the analgesic effect of EA of Futu (LI18) and Hegu (LI4)-Neiguan (PC6) for neck-incision pain is closely associated with its actions in upregulating 5-HT 2A receptor (5-HT2AR) mRNA and protein, glial cell derived neurotrophic factor (GDNF), and its receptor GDNF family receptor alpha-1 (GFR alpha-1) gene expression [17, 18], and in downregulating expression levels of intracellular cAMP mRNA and cAMP response element binding protein (CREB) mRNA in the cervical spinal cord (C1–C4) [19].

However, the pathogenesis of postoperative pain is very complex, including both peripheral and central neuronal changes, cellular and molecular activities, ectopia, sensitization of nociceptors, phenotypic switching, structural plasticity, disinhibition, and neuroinflammation [20–22]. Neuronal cells in the superficial layers of the spinal dorsal horn play an important role in the development and maintenance of hyperalgesia. Various mediators released from the central terminals of the primary sensory neurons contribute to this process. Among them, the excitatory amino acid glutamate, calcitonin gene related peptide (CGRP), substance P (SP), brain-derived neurotrophic factor (BDNF) and somatostatin, and so forth. Proinflammatory cytokines, chemokines, and so forth produced and released from nonneuronal cells (predominantly immune and glial cells) are also important mediators for persistent pain and all are capable of changing the response properties of central pain signaling neurons [23, 24]. Among the factors, SP, one of the neurotransmitters released from the primary nociceptive afferent endings in the dorsal horn of the spinal cord and postsynaptically binds to NK (1)-receptors [25]. CGRP, an important molecule in the spinal nociceptive processing and ensuring response from primary afferents in the spinal dorsal horn, and PGE2, the main product of cyclooxygenases (COX) and a crucial mediator for inflammatory pain sensitization via promoting synaptic transmission within the spinal cord dorsal horn [26], also contribute to the spinal pain processing network. Therefore, the present study was designed to observe their changes in the cervical spinal cord after neckincision and electroacupuncture (EA) intervention, so as to study the mechanism of acupuncture therapy underlying relieving thyroid surgery-induced pain.

2. Material and Methods

2.1. Animals and Grouping. Adult male Wistar rats (200–250 g), purchased from Beijing Union Medical College, were acclimatized to standard laboratory conditions (about 12 h alternate light-dark cycle) of our institute's environment first for a week and were given free access to standard chow pellet diet and water. All protocols were approved by the Institute of Acu-moxibustion, China Academy of Chinese Medical Sciences, and accorded to the Guidelines for Laboratory Animal Care and Use of the Chinese Ministry of Science and Technology. The rats were randomly assigned to 5 experimental groups: control, model, Futu (LI18), Hegu (LI4)-Neiguan (PC6), and Zusanli (ST36)-Yanglingquan (GB34), with 8 rats in each group.

2.2. Thyroid Area Incision Surgery. After detecting the baseline thermal pain threshold, the rat's neck-incision pain model was established by making a 1.5 cm longitudinal incision along the midline of the neck under isoflurane (1-2% in oxygen) inhalational anesthesia using a table-top Isoflurane anesthesia unit (VME, Matrix Company, USA), followed by repeated blunt dissection stimulation of the bilateral sternohyoideus around the thyroid gland regions for 5 min with a pair of forceps. The incision was then sutured in layers.

2.3. Measurement of Thermal Pain Threshold. The thermal pain threshold of the neck-incision area was measured 30 min before surgery, 4 h after surgical incision procedures and post-EA using a tail-flick apparatus (Model 37360, Tail Flick Unit, UGO Basile, Italy). The heat intensity was set to 25 units, and the cut-off time was set to 30 s to prevent tissue damage. The latency of escape was recorded automatically when the rat swiftly moved its neck from the heat source. Each rat was tested 3 times, with a 3–5 minutes' interval between tests.

2.4. Electroacupuncture Stimulation. Four hours after neck-incision, under light anesthesia with isoflurane (0.5–1% in oxygen) via a nose cone of a table-top Isoflurane anesthesia unit, the rats of the 3 electroacupuncture (EA) treatment groups were administrated with EA stimulation following insertion of filiform needles (Gauge-32, made by Suzhou Acu-moxibustion Products Factory, China) into bilateral Futu (LI18), Hegu (LI4), Neiguan (PC6), Zusanli (ST36), and Yanglingquan (GB34), respectively. With reference to the descriptions about LI18 in the human body, the rat's LI18 is located between the sternal branch and the clavicular branch of the sternocleidomastoid muscle, at the middle of the sternocleidomastoid muscle and on the horizontal level of the 4th cervical vertebra. In the rat, LI4 is located between the 1st and 2nd metacarpal bones; PC6, about 3 mm to the wrist transverse stripe on the axopetal end; ST36, about 5 mm inferior to the capitulum fibulae and posterior-lateral to the hindlimb knee joint; and GB34, about 5 mm superior-lateral to ST36 [27].

After insertion, the needle handles were connected to a HANS EA Apparatus (Hans-100A, Jisheng Medical Technology, Co., Ltd., Nanjing, China) for stimulating the abovementioned acupoints with duration of 30 min, frequency of alternative 2 Hz and 15 Hz (2/15 Hz), and electric current strength of 1 mA for the first 15 min and 2 mA for the rest 15 min. Animals of the control group and model group were treated with the same anesthesia and other procedures but without EA stimulation.

2.5. Tissue Preparation. After the EA treatment and for immunofluorescence staining, rats were deeply anesthetized with a mixture solution of 20% urethane (420 mg/kg) and 1.5% chloralose (50 mg/kg, 1 : 2, 6 mL/kg, i.p.) and transcardiacly perfused through the ascending aorta with normal saline (250 mL), followed by 200 mL of 4% paraformaldehyde

(Yili Fine Chemical Co., Ltd., Beijing, China) in 0.1 M phosphate buffer saline (PBS, pH 7.4). The upper segments of the cervical spinal cord (C2–C5) were removed and placed in the same fixative (4°C) overnight and then kept in 0.1 M sodium phosphate buffer (pH 7.4) containing 30% sucrose for 24 h.

For Western blot and quantitative real-time PCR analysis, the rats, deeply anesthetized with the same anesthetics mentioned above, were killed for collecting dorsal part of the cervical spinal cord (C2–C5, semisection along the longitudinal plane) on an ice plate after the EA treatment, kept in liquid nitrogen or stored in −80°C for mRNA and protein extraction later.

2.6. Immunofluorescence Assay. The spinal cord tissue was sectioned on a freezing microtome at 40 μm for immunofluorescence double-labeling. Free-floating tissue sections were placed in 0.01 M PBS, washed with PBS Tween-20 (PBST) three times, incubated in 1 N HCL for 20 min and in 3% H_2O_2 in distilled water for 15 min, and blocked with 5% goat serum for 30 min at room temperature to block the unspecific staining, respectively. The sections were incubated with a mixture solution of primary antibodies: calcitonin-gene-related peptide (CGRP, diluted 1 : 500, C8198, Sigma, USA) and substance P (SP, 1 : 1000, Santa Cruz Biotechnology Inc., USA) for 36–48 h at 4°C, washed three times with phosphate buffered saline (PBS), and then incubated in the secondary antibodies, goat anti-rabbit IgG conjugated Alexa Fluor 561 (Invitrogen, red fluorescence, diluted 1 : 300) and goat anti-mouse IgG conjugated Alexa Fluor 488 (Invitrogen, green fluorescence, diluted 1 : 300) on a rocking bed (away from light) for 2 h under room temperature, respectively.

For control staining, primary antibody was omitted. The tissue sections were mounted on glass slides, washed four more times with running water, dried under room temperature and away from light, and sealed with coverslips at last. The analysis was performed using a light microscope Olympus AX70 with an objective magnification of 40x and software analySIS Pro 3.1. Visualization was performed with avidin-biotin complex method. Images of the spinal cord slices were acquired using confocal microscope (FV1000, Olympus, Japan). Laser channels used were 488 nm excitation and 561 nm excitation. And the fluorescence intensity was measured by Adobe Photoshop 6.0 (Adobe Systems, San Jose, CA, USA).

2.7. Western Blotting Analysis. Total protein was extracted from the tissue in RIPA lysis buffer (containing protease and phosphatase inhibitor mixtures (Roche)) by using a tissue homogenizer, followed by clearing tissue debris by centrifugation at 13000 rpm at 4°C for 20 min. Twenty micrograms of protein was loaded per lane and separated by 5% or 8% SDS-PAGE gel electrophoresis, then, transferred onto PVDF membranes. Blocking was carried out in 3% bovine serum albumin (BSA, Amresco, USA) solution for 30 min at room temperature. The membranes were incubated with primary antibody rabbit anti-NK-1R (diluted 1 : 2000, BS2632, Bioworld, USA), or rabbit anti-COX-1 (diluted 1 : 2000, 5153-1, Epitomics, USA) overnight at 4°C and with secondary antibody (1 : 20000 dilution of goat anti-rabbit Immunoglobulin G) conjugated to horseradish peroxidase (Jackson, ImmunoResearch Laboratories, West Grove, PA, USA) for 1 h at room temperature on the following day. Immunoblotting signal was detected by ECL (enhanced chemiluminescence) on chemiluminescent films. For densitometric analyses, the blots were scanned and quantified using TotalLab Quant analysis software (TotalLab Limited, England), and the result was expressed as the ratio of target gene immunoreactivity to β-actin immunoreactivity.

2.8. Quantitative Real-Time PCR. Total RNA was extracted with Trizol (CW0581, CWbio. Co. Ltd, Beijing, China), and then reversely transcribed with cDNA Synthesis Kit (CW0744, CWbio. Co. Ltd, Beijing, China). The reverse transcribed products were amplified. The primer sequences used were as follows: NK-1R: forward 5′-GAGCATCCCAACAGGACTTAT-3′, reverse 5′-ATGGTAGCGGTCAGAGGAGT-3′; COX-1: forward 5′-TCCTACATGGGATGACGAGC-3′, reverse 5′-GGTTGCGATACTGGAACTGG-3′; β-actin: forward 5′-GGAGATTACTGCCCTGGCTCCTA-3′, reverse 5′-GACTCATCGTACTCCTGCTTGCTG-3′.

Quantitative real-time (QRT)-PCR was performed in 96-well plates using the QRT-PCR detection systems (AB7500, Applied Biosystem, USA). Three different biological replicates for each sample were performed. All the cDNA samples were amplified in triplicate from the same RNA preparation and the mean value was calculated. Each reaction included 2 μL of cDNA, 10 μL of REALSYBRMixture (2x), 0.8 μL (10 μmol/μL) of both forward and reverse primers, and 7.2 μL of PCR-grade water, equating to a final volume of 20 μL. PCR was performed under the following conditions: 10 min at 95°C, followed by 40 cycles of 15 s at 95°C, and 60 s at 60°C. Then, the fluorescence acquisition after each cycle was performed. Finally, a dissociation curve was generated by increasing temperature from 65°C to 95°C in order to verify primer specificity. All samples for each reference gene were run on the same plate to avoid between-ran variations. The relative expression was calculated in accordance with the $\Delta\Delta$Ct method. Relative mRNA levels were expressed as $2^{-\Delta\Delta Ct}$ values.

2.9. Enzyme-Linked Immunosorbent Assay (ELISA). The cervical spinal cord (C2–C5, semitransection) tissue specimen (1 g), added with 5 mL of homogenization buffer (0.1 M phosphate, pH 7.4, containing 1 mM EDTA and 10 μM indomethacin), was homogenized at 5500 rpm for 20 s using a polytron homogenizer (PT1200, Switzerland), and then centrifuged at 4°C and 10,000 rpm for 10 min using a centrifuger (Eppendorf Centrifuge 5430, Germany). The supernatant (50 μL) from each sample was added to a PGE2 assay plate for determining PGE2 levels by enzyme immunoassay (prostaglandin-E2-Monoclonal Enzyme immunoassay Kit, 2A-514010-96, Cayman, USA) according to the manufacture's protocols. A microplate reader (Multiskan MK3, Thermo, USA) at a wavelength of 410 nm was used to detect PGE2 contents, and data were computerized with Excel. The measurements were made in duplicate, and the results were expressed in pg/mg.

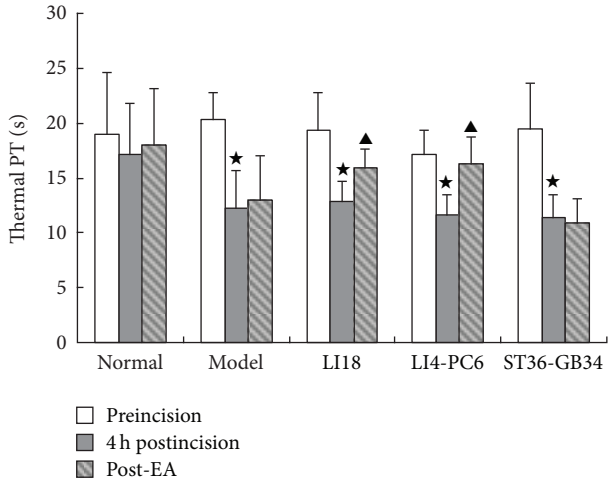

Figure 1: Effect of EA stimulation of Futu (LI18), Hegu (LI4)-Neiguan (PC6), and Zusanli (ST36)-Yanglingquan (GB34) on thermal pain thresholds (PT) in rats with neck incision pain ($n = 8$ in each group). Pain thresholds were measured at the time-points of pre-incision, 4 h post incision, and post-EA, and data are expressed as mean ± SD. $^{*}P < 0.05$, compared with the normal group; $^{\blacktriangle}P < 0.05$, compared with the model group (after neck incision).

2.10. Statistical Analysis. The data collected in the present study were expressed as mean ± standard deviation (Mean ± SD) and analyzed by two-way repeated measures ANOVA, followed by post hoc test for least significant difference (LSD) to determine differences between two groups. $P < 0.05$ was considered statistically significant.

3. Results

3.1. Effects of EA on Thermal Pain Threshold. Before neck-incision, the rats' thermal pain thresholds had no significant differences among the normal, model, LI18, LI4-PC6, and ST36-GB34 groups ($P > 0.05$). Four hours after the incision, the pain thresholds were significantly decreased ($P < 0.05$). Following EA stimulation of LI18 and LI4-PC6, the pain thresholds were considerably increased ($P < 0.05$), while that of EA of ST36-GB34 had no marked changes in comparison with the model group ($P > 0.05$, Figure 1).

3.2. Effects of EA on the Immunoreactivity of SP and CGRP in Spinal Dorsal Horn. Results of immunofluorescence staining showed that SP and CGRP immunoreaction (IR)-positive products were densely distributed in the superficial layer of dorsal horns of the cervical spinal cord, particularly 4 h after neck incision (Figure 2(a)). In comparison with the normal control group, the fluorescence intensity of both SP and CGRP IR-positive products in the cervicospinal cord were significantly increased in the model group (Figures 2(b) and 2(c), $P < 0.05$), suggesting an increase of immunoactivity of SP and CGRP after neck incision. Following EA intervention, the immunoactivity levels of spinal CGRP in the LI18 group and LI4-PC6 group, and SP in the LI18 group were significantly decreased ($P < 0.05$). No apparent changes of both SP and CGRP immunoactivity were found in the ST36-GB34 group in comparison with the model group ($P > 0.05$).

3.3. Effects of EA on Expression of NK-1R mRNA and Protein in Dorsal Spinal Cord. Compared with the normal group, the relative expression levels of NK-1R mRNA and protein in the dorsal cervical spinal cord were significantly increased in the model group ($P < 0.05$, Figures 3(a) and 3(b)). Following EA intervention, the expression levels of both NK-1R mRNA and protein in the LI18 group, and NK-1R mRNA in the LI4-PC6 group were considerably lower than those in the model group ($P < 0.05$). No significant differences were found between ST36-GB34 and model groups in the expression levels of NK-1R mRNA and protein ($P > 0.05$). The effects of EA of LI18 were apparently superior to those of EA of ST36-GB34 in downregulating the expression of NK-1 mRNA and protein ($P < 0.05$).

3.4. Effects of EA Intervention on Expression of COX-1 mRNA and Protein in Dorsal Spinal Cord. In comparison with the normal group, the expression levels of COX-1 mRNA and protein in the cervical spinal cord were significantly increased in the model group ($P < 0.05$, Figures 4(a) and 4(b)). After EA intervention, the expression levels of COX-1 mRNA and protein were obviously downregulated in the LI18 and LI4-PC6 groups ($P < 0.05$). No significant changes were found in COX-1 mRNA and protein expression in the ST36-GB34 group compared with the model group ($P > 0.05$).

3.5. Effects of EA on PGE2 Content in the Cervical Spinal Cord. In comparison with the normal control group, PGE2 content of the cervical spinal cord in the model group was significantly increased 4 h after neck incision ($P < 0.05$, Figure 5). Following EA interventions of LI18 and LI4-PC6, spinal PGE2 levels in the LI18, LI4-PC6, and ST36-GB34 groups were considerably decreased ($P < 0.05$), having no significant differences among the three groups ($P > 0.05$).

4. Discussion

In the present report, we characterized for the first time changes of the expression of CGRP, NK-1R, and COX-1 mRNA and proteins and PGE2 level in the cervical spinal cord in neck-incision pain rats. Results of this study showed that, 4 hours after neck incision and repeated mechanical stimulation (for miming thyroidectomy), the regional thermal pain threshold was significantly decreased. At the same time, the immunoactivity of both SP and CGRP in the superficial layers of the cervical spinal dorsal horns, the expression levels of NK-1R mRNA and protein, COX-1 mRNA and protein, and PGE2 content of the cervical dorsal spinal cord tissue were considerably increased in rats with neck-incision pain. The behavioral pain reactions, immunoactivity of SP, and the expression of NK-1R mRNA and protein and COX-1 mRNA and protein of the present study were identical to the results of our past studies using conventional immunohistochemistry in the same rat model [28] and similar study in postsurgery rats [29]. Among the indexes, spinal COX-1 expression change was the same to Zhu and colleagues' results

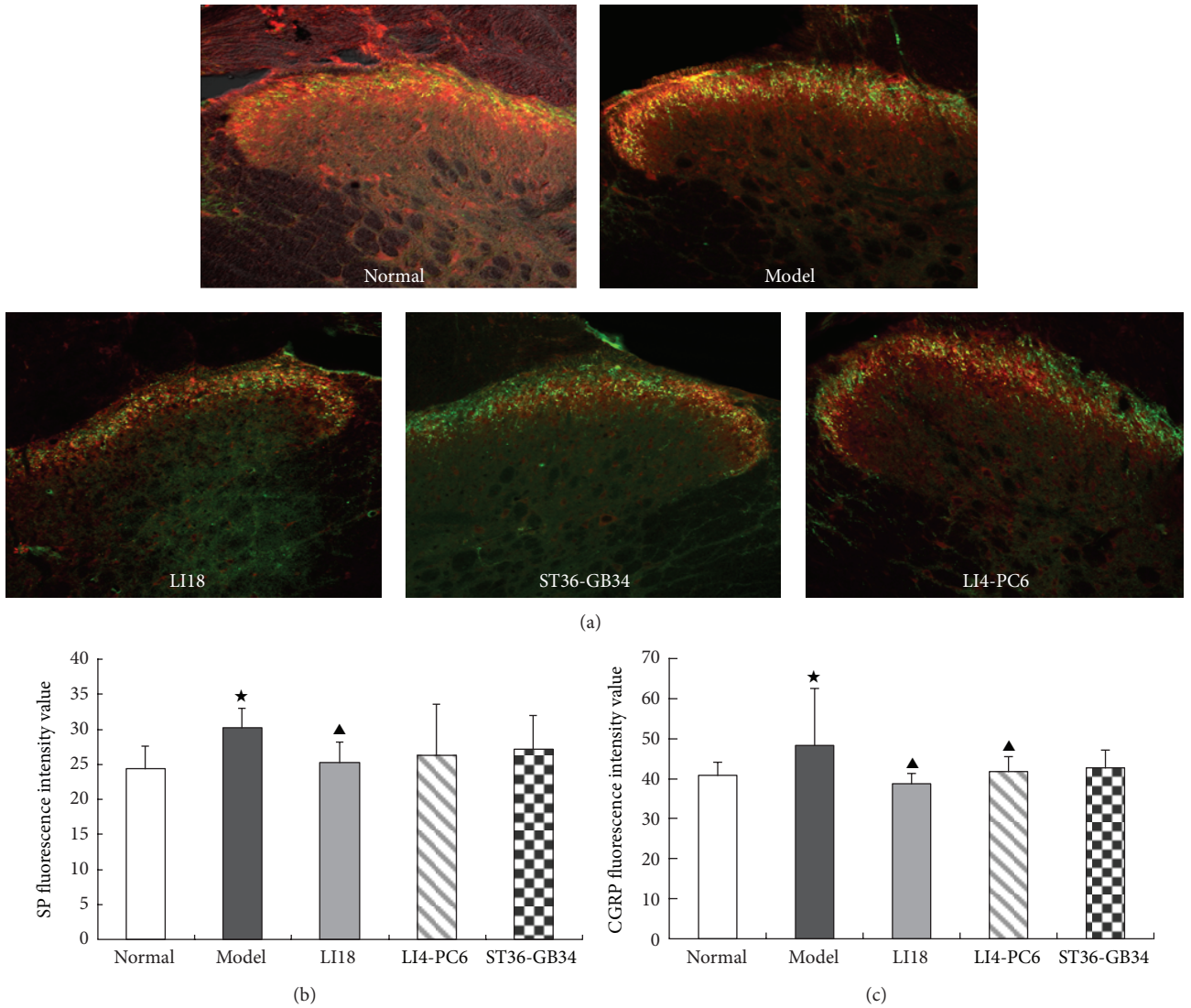

Figure 2: Effect of EA stimulation of different acupoints on the immunoactivity of SP and CGRP in the rat's cervical spinal cord 4 h after neck incision ($n = 6$ in each group). (a) Representative confocal microscopic photos of immunofluorescence double staining showing SP and CGRP immunoreaction (IR) positive products (green for SP and red for CGRP) in the cervical spinal cord in the 5 groups. (b) and (c) Histograms showing the mean fluorescence intensity of SP-IR positive products (b) and CGRP-IR positive products (c) in the 5 groups. Data are expressed as the mean ± SD (ANOVA, followed by LSD post hoc test); $^{\star}P < 0.05$, compared with the normal control group; $^{\blacktriangle}P < 0.05$, compared with the model group.

about COX-1 immunoactivity change of the lumbar spinal cord determined by using immunohistochemistry [30] and the validated role of COX-1 in spinal hypersensitivity by intrathecal injection of preferring inhibitor, ketorolac, and the specific inhibitor SC-560 of COX-1 in paw-incision model [31].

It has been demonstrated that SP and CGRP coexist to a large extent (70%) in terminals of the primary afferent neurons in the dorsal horn of the spinal cord [32], and released in response to peripheral noxious stimuli [33]. Therefore, SP and CGRP (proinflammatory neuropeptides) immunoactivity was obviously increased following neck-incision and local mechanical stimulation in the present study. Simultaneously, spinal NK-1R mRNA and protein expression levels were also upregulated after neck incision.

Studies have showed that NK-1R is present on approximately 80% of lamina 1 neurons that project to various brain regions [34] and NK-1R on lamina I neurons activated signal transduction pathways and low-threshold (T-type) voltage-gated calcium channels synergistically and facilitated calcium-dependent long-term potentiation (LTP) at synapses from nociceptive nerve fibers. This may be the cellular mechanism of lamina I neurons in spinal dorsal horn expressing NK-1 receptor for SP mediated abnormal pain sensitivity under conditions of inflammation, trauma, or nerve injury [35].

Yaksh and colleagues [36] held that the postoperative hypersensitivity process results partially from a complex cascade starting with the release of SP and glutamate, followed by activation of spinal NK-1 and NMDA receptors. Among

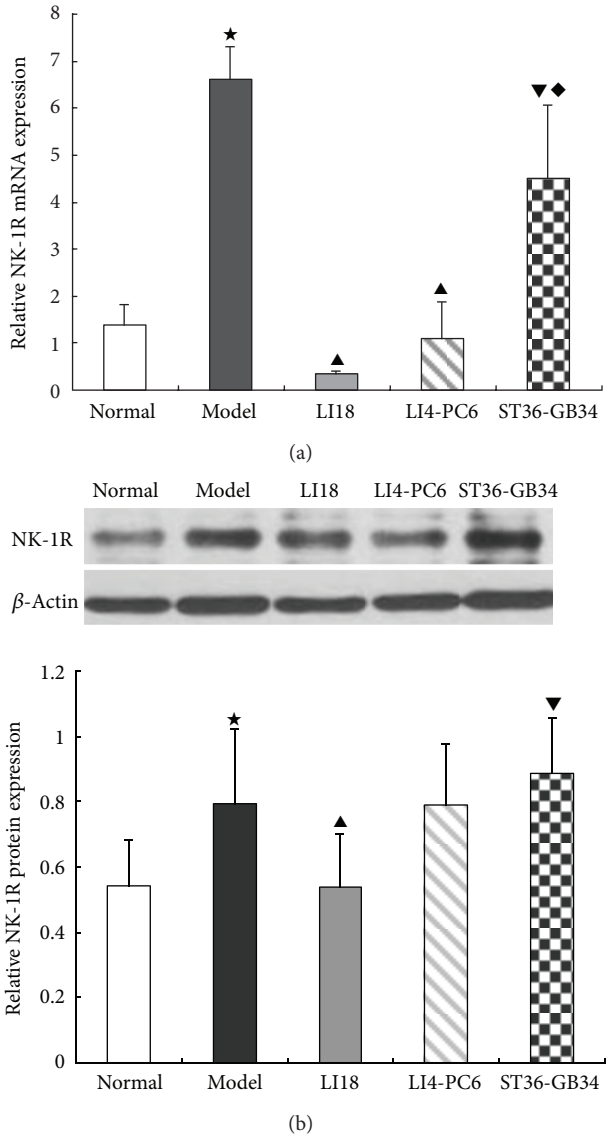

Figure 3: Effect of EA stimulation of different acupoints on the relative expression levels of NK-1R mRNA (a) and protein (b) in the cervical spinal cord 4 h after neck incision in rats. Data are expressed as mean ± SD ($n = 7$), (ANOVA, followed by LSD post hoc test). $^{\star}P < 0.05$, compared with the normal group, $^{\blacktriangle}P < 0.05$, compared with the model group; $^{\blacktriangledown}P < 0.05$, compared with the LI18 group, $^{\blacklozenge}P < 0.05$, compared with the LI4-PC6 group.

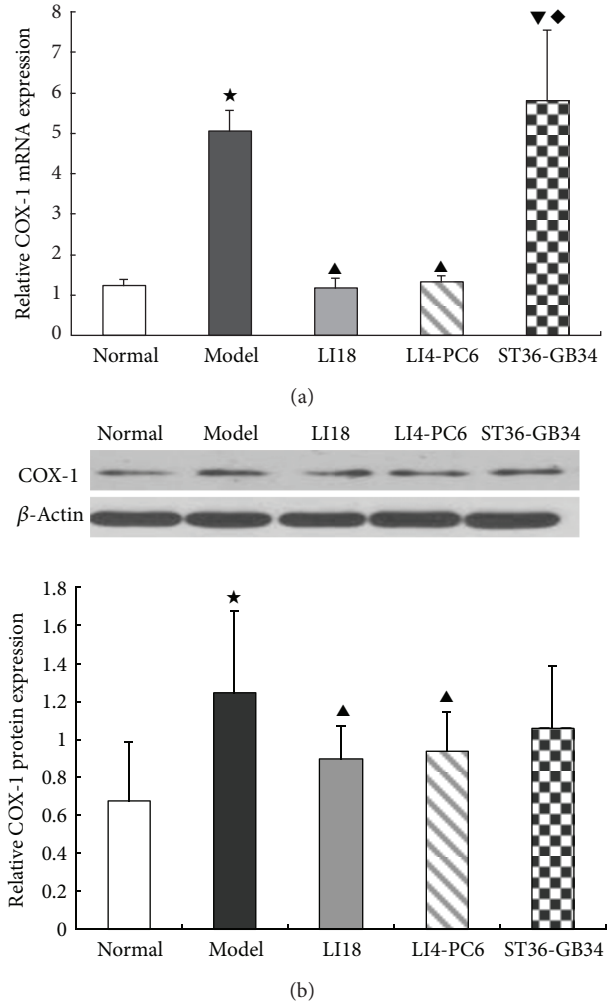

Figure 4: Effect of EA stimulation of different acupoints on COX-1 mRNA (a) and protein (b) expression 4 h after neck incision in rats. Data are expressed as mean ± SD ($n = 7$), (ANOVA, followed by LSD post hoc test); $^{\star}P < 0.05$, compared with the normal group, $^{\blacktriangle}P < 0.05$, compared with the model group; $^{\blacktriangledown}P < 0.05$, compared with the LI18 group; $^{\blacklozenge}P < 0.05$, compared with the LI4-PC6 group.

several elements, this cascade activates spinal phospholipases and generates prostanoids by COX activity, leading to spinal prostanoid release. Further studies have shown that nerve or tissue injury is associated not only with increases in NK-1 receptor density, but also with increases in NK-1 gene expression; thus, persistent activation of SP-containing primary afferent neurons might increase transcription of the NK-1 receptor mRNA and enhance the expression of NK-1 receptor protein [37], which is consistent to our observations in the present study. A cAMP response element (CRE) site occurs within the promoter region of the NK-1 receptor gene which has a CREB binding site [38]. CGRP is a transmembrane signaling molecule that increases cAMP levels and cAMP (CRE)-dependent gene expression, and also increases the levels of NK-1R mRNA in spinal neurons, indicating that CGRP regulates the expression of NK-1R via a pathway involving activation of the transcription factor, (CREB) [39]. Moreover, we have demonstrated that in formalin injection induced neck pain rats, the expression levels of cervical spinal NMDA receptor 2B subunit mRNA and its phosphorylated protein were markedly upregulated [40], but if the NMDA R is involved in neck-incision induced pain processing or not, it needs further study.

It was demonstrated that NK-1 receptors are not only expressed in neurons, but also in astrocytes and microglia which have a high affinity for SP, and more importantly, SP and NK-1 receptor interactions elicit activation of signal transduction pathways in both cell types and can initiate

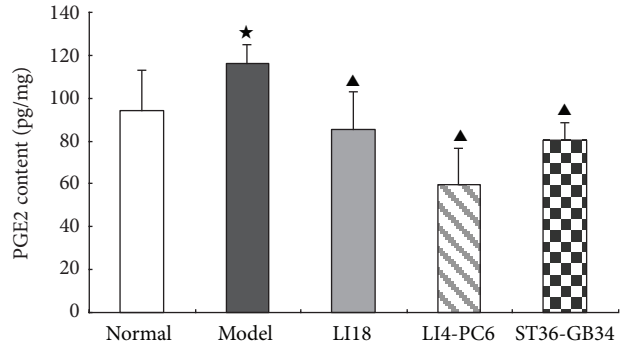

Figure 5: Effect of EA stimulation of different acupoints on prostaglandin E2 (PGE2) content in the dorsal spinal cord (C2–C5) 4 h after neck incision in rats. Data are expressed as mean ± SD ($n = 8$), (ANOVA, followed by LSD post hoc test). $^{*}P < 0.05$, compared with the normal group, $^{\blacktriangle}P < 0.05$, compared with the model group. The level of PGE2 in the cervical spinal cord was determined using an ELISA kit.

or augment pain responses [41, 42]. SP can also stimulate secretion of TNF-alpha from macrophages from which IL-1β was found to increase the production of SP and PGE2 in a number of neurons and glial cells [43, 44]. Prostaglandins (PGs), including PGD-2, PGE-2, PGF-2 alpha, and PGI-2 and known to be produced by cyclooxygenase (COX), catalyze their synthesis from arachidonic acid [45] and potentiate release of excitatory amino acids, SP, CGRP, and nitric oxide to enhance excitation and synaptic transmission of pain signals in the spinal cord [46].

COX has two forms of COX-1 and COX-2 which are constitutively expressed in the spinal cord. Double labeling studies showed that 96% of COX-1 immunoreactive cells are colocalized with microglia and 98% of COX-2 immunoreactive cells colocalized with neurons [47]. COX-1 expression was upregulated in microglia within hours after surgical incision [48–50] or thoracic muscle deep incision [51], and COX-2 played a prominent role in inflammatory pain [52–54]. These results indicate that SP, NK-1R, CGRP, COX-1, and PGE-2 in the spinal cord are all involved in postsurgery pain including neck-incision pain of the present study. Both neurons and glia cells in the cervical spinal cord are probably complicated with the neck-incision pain processing. However, the detailed interaction situations of the cervicospinal neurons and glia cells in inducing postincision pain need studying in the future.

In addition, findings of the present study showed that following EA intervention of LI18 (at the neck) and LI4-PC6 (at the forelimb), the thermal pain thresholds were obviously upregulated, while EA stimulation of ST36-GB34 (at the hindlimb) had no apparent effect on the decreased pain threshold in neck-incision pain rats. Correspondingly, EA of LI18 and LI4-PC6 could effectively suppress neck-incision induced upregulation of expression of NK-1 mRNA, COX-1 mRNA and protein, and PGE2 content in the upper-cervical spinal cord. However, EA stimulation of ST36-GB34 had no apparent effect on SP and CGRP immunoactivity, NK-1R mRNA and protein, and COX-1 mRNA and protein expression levels in the cervical spinal cord. It suggests that the effects of EA stimulation of the three acupoints or acupoint groups in resisting pain reaction and suppressing incision-induced upregulation of spinal NK-1 mRNA and COX-1 mRNA and protein are mainly via homosegmental nerve reflex pathway. But, why the content of spinal PGE-2 was also downregulated after EA of ST36-GB34, the reason was not clear and the result needs being confirmed further.

The results of EA analgesia and spinal SP expression are basically identical to those in our past studies [17, 28, 55] and changes of spinal PGE-2 after EA intervention are similar to those of other studies in reducing spinal PGE-2 levels in inflammatory pain rats [56, 57]. Up to now, we have not found any studies on the involvement of spinal CGRP, NK-1R mRNA and protein and COX-1 mRNA and protein in postsurgery pain. However, viewing from the known mechanisms of pain processing, we do not think that changes of these indexes are not expectable under EA analgesia. Moreover, EA analgesia might also involve its favorable regulation on the communication or interaction between neurons and glia cells in the spinal cord in neck-incision pain rats.

In conclusion, findings of the present study show that SP, CGRP, NK-1R, COX-1, and PGE2 in the cervicospinal cord play an important role in pain processing after neck incision in the rat. EA stimulation of LI18 and LI4-PC6 can effectively suppress neck-incision-induced sensory hypersensitivity by downregulating expression levels of spinal SP, CGRP, NK-1 mRNA, COX-1 mRNA and protein, and PGE2 content in the cervicospinal cord. These results highlight the targets of EA therapy for reducing post-thyroid-surgery pain. The exact mechanisms of EA underlying regulation of cross-talk of spinal neurons and gliacytes will be researched in the coming days.

Conflict of Interests

The authors declare that there was no conflict of interests.

Authors' Contribution

Experiments were finished by Li-na Qiao, Jun-ying Wang, Yong-sheng Yang, Shu-ping Chen, and Yong-hui Gao and Jian-liang Zhang. The present paper was written by Li-na Qiao and revised by Jun-ling Liu. Li-na Qiao and Jun-ying Wang equally contributed to this paper.

Acknowledgments

The present study was subsidized by the Special Project of Chinese Medicine (973) of the National Basic Research Program of China (nos. 2007CB512505 and 2013CB531904), the Chinese National Natural Science Foundation (nos. 90709031, 30973796, 81273830, and 81202762), and Independent Research Project of China Academy of Chinese Medical Sciences (Z02015).

References

[1] J. L. Apfelbaum, C. Chen, S. S. Mehta, and T. J. Gan, "Postoperative pain experience: results from a national survey suggest

postoperative pain continues to be undermanaged," *Anesthesia and Analgesia*, vol. 97, no. 2, pp. 534–540, 2003.

[2] M. Ayman, G. Materazzi, M. Bericotti, R. Rago, and Y. P. Nidal, "Bupivacaine 0.5% versus ropivacaine 0.75% wound infiltration to decrease postoperative pain in total thyroidectomy, a prospective controlled study," *Minerva Chirurgica*, vol. 67, no. 6, pp. 511–516, 2003.

[3] A. Barros, C. P. Vale, F. C. Oliveira et al., "Dexamethasone effect on postoperative pain and tramadol requirement after thyroidectomy," *Pharmacology*, vol. 91, no. 3-4, pp. 153–157, 2013.

[4] H. R. Ryu, J. Lee, J. H. Park et al., "A comparison of postoperative pain after conventional open thyroidectomy and transaxillary single-incision robotic thyroidectomy: a prospective study," *Annals of Surgical Oncology*, vol. 20, no. 7, pp. 2279–2284, 2013.

[5] S. Sertel, S. Herrmann, H. J. Greten et al., "Additional use of acupuncture to NSAID effectively reduces post-tonsillectomy pain," *European Archives of Oto-Rhino-Laryngology*, vol. 266, no. 6, pp. 919–925, 2009.

[6] Y.-F. Ni, J. Li, B.-F. Wang et al., "Effects of electroacupuncture on bispectral index and plasma beta-endorphin in patients undergoing colonoscopy," *Zhen Ci Yan Jiu*, vol. 34, no. 5, pp. 339–343, 2009.

[7] M. El-Rakshy, S. C. Clark, J. Thompson, and M. Thant, "Effect of intraoperative electroacupuncture on postoperative pain, analgesic requirements, nausea and sedation: a randomised controlled trial," *Acupuncture in Medicine*, vol. 27, no. 1, pp. 9–12, 2009.

[8] R. Oliveira and W. A. Prado, "Anti-hyperalgesic effect of electroacupuncture in a model of post-incisional pain in rats," *Brazilian Journal of Medical and Biological Research*, vol. 33, no. 8, pp. 957–960, 2000.

[9] L. Lao, S. Bergman, P. Langenberg, R. H. Wong, and B. Berman, "Efficacy of Chinese acupuncture on postoperative oral surgery pain," *Oral Surgery, Oral Medicine, Oral Pathology, Oral Radiology, and Endodontics*, vol. 79, no. 4, pp. 423–428, 1995.

[10] L. E. F. Coura, C. H. U. Manoel, R. Poffo, A. Bedin, and G. A. Westphal, "Randomised, controlled study of preoperative eletroacupuncture for postoperative pain control after cardiac surgery," *Acupuncture in Medicine*, vol. 29, no. 1, pp. 16–20, 2011.

[11] J.-M. Yu, P.-S. Qu, H. Fan, Z. Wang, Y.-B. Jin, and F. Tao, "Observation on the analgesic effect of transcutaneous electrical acupoint stimulation for breast radical carcinoma operation," *Zhen Ci Yan Jiu*, vol. 35, no. 1, pp. 43–46, 2010.

[12] D. F. Martins, F. Bobinski, L. Mazzardo-Martins et al., "Ankle joint mobilization decreases hypersensitivity by activation of peripheral opioid receptors in a mouse model of postoperative pain," *Pain Medicine*, vol. 13, no. 8, pp. 1049–1058, 2012.

[13] Y. H. Li, W. H. Ma, X. Q. Gao et al., "Comparison of the efficacy of acupuncture-assisted anesthesia with different frequency stimulation for thyroid surgery," *Guangdong Medical Journal*, vol. 29, no. 8, pp. 1257–1260, 2008.

[14] Y.-Q. Gao, Q. Jia, J. Yang, J.-L. Liu, and J.-H. Shi, "Analysis on the superiority of compound acupuncture anesthesia for thyroid ablation," *Zhen Ci Yan Jiu*, vol. 34, no. 6, pp. 410–420, 2009.

[15] C. J. Zhang, F. Yang, and M. Li, "Effect of electroacupuncture combined with cervical plexus block on stress responses in patients undergoing thyroid surgery," *Zhen Ci Yan Jiu*, vol. 38, no. 1, pp. 1–8, 2013.

[16] P. Z. Wang, J. L. Zhao, S. An, and A. H. Yao, "Application of local injection of anesthetics at Futu (LI18) to thyroid surgery," *Journal of Changchun College of Traditional Chinese Medicine*, vol. 16, no. 1, pp. 25–26, 2000.

[17] L.-N. Qiao, Y.-S. Yang, J.-Y. Wang et al., "Effects of electroacupuncture at "Futu" (LI 18), etc. on expression of spinal 5-HT 1 AR mRNA, 5-HT 2 AR mRNA and protein in rats with neck incision pain," *Zhen Ci Yan Jiu*, vol. 36, no. 6, pp. 391–396, 2011.

[18] S. J. Wang, L. H. Tan, and J. L. Liu, "Effect of electroacupuncture at different acupoints on expression of cervico-spinal GDNF and BDNF and their receptor genes in neck-incision pain rats," *Zhen Ci Yan Jiu*, vol. 37, no. 5, pp. 351–356, 2012.

[19] D. Lin, Y. Kan, L. N. Qiao et al., "Effects of electroacupuncture at "Futu" (LI 18), etc. on pain threshold and cervico-spinal mGlu receptor 5/cAmp/CREB signaling in rats with neck incision pain," *Zhen Ci Yan Jiu*, vol. 37, no. 3, pp. 191–196, 2012.

[20] T. J. Brennan, "Pathophysiology of postoperative pain," *Pain*, vol. 152, supplement 3, pp. S33–S40, 2011.

[21] R. Deumens, A. Steyaert, P. Forget et al., "Prevention of chronic postoperative pain: cellular, molecular, and clinical insights for mechanism-based treatment approaches," *Progress in Neurobiology*, vol. 104, pp. 1–37, 2013.

[22] J. V. Berger, L. Knaepen, S. P. M. Janssen et al., "Cellular and molecular insights into neuropathy-induced pain hypersensitivity for mechanism-based treatment approaches," *Brain Research Reviews*, vol. 67, no. 1-2, pp. 282–310, 2011.

[23] S. Pezet, M. Malcangio, and S. B. McMahon, "BDNF: a neuromodulator in nociceptive pathways?" *Brain Research Reviews*, vol. 40, no. 1–3, pp. 240–249, 2002.

[24] S. B. McMahon, W. B. J. Cafferty, and F. Marchand, "Immune and glial cell factors as pain mediators and modulators," *Experimental Neurology*, vol. 192, no. 2, pp. 444–462, 2005.

[25] S. H. Sindrup, A. Graf, and N. Sfikas, "The NK1-receptor antagonist TKA731 in painful diabetic neuropathy: a randomised, controlled trial," *European Journal of Pain*, vol. 10, no. 6, pp. 567–571, 2006.

[26] H. U. Zeilhofer, "The glycinergic control of spinal pain processing," *Cellular and Molecular Life Sciences*, vol. 62, no. 18, pp. 2027–2035, 2005.

[27] Z. R. Li, *Experimental Acupuncturolog*, Traditional Chinese Medicine Publishing House, Beijing, China, 2003.

[28] L.-N. Qiao, J.-Y. Wang, S.-P. Chen, Y.-H. Gao, Y.-S. Yang, and J.-L. Liu, "Effects of electroacupuncture at "Futu" (LI 18) on the immunoactivity of substance P, 5-HT 1 AR, etc. of the cervical spinal dorsal horn in rats with neck incision pain," *Zhen Ci Yan Jiu*, vol. 35, no. 2, pp. 91–98, 2010.

[29] G. Saxler, J. Brankamp, M. von Knoch, F. Löer, G. Hilken, and U. Hanesch, "The density of nociceptive SP- and CGRP-immunopositive nerve fibers in the dura mater lumbalis of rats is enhanced after laminectomy, even after application of autologous fat grafts," *European Spine Journal*, vol. 17, no. 10, pp. 1362–1372, 2008.

[30] X. Zhu, M. A. Vincler, R. Parker, and J. C. Eisenach, "Spinal cord dynorphin expression increases, but does not drive microglial prostaglandin production or mechanical hypersensitivity after incisional surgery in rats," *Pain*, vol. 125, no. 1-2, pp. 43–52, 2006.

[31] X. Zhu, D. R. Conklin, and J. C. Eisenach, "Preoperative inhibition of cyclooxygenase-1 in the spinal cord reduces

postoperative pain," *Anesthesia and Analgesia*, vol. 100, no. 5, pp. 1390–1393, 2005.

[32] M. M. Tuchscherer and V. S. Seybold, "A quantitative study of the coexistence of peptides in varicosities within the superficial laminae of the dorsal horn of the rat spinal cord," *Journal of Neuroscience*, vol. 9, no. 1, pp. 195–205, 1989.

[33] C. R. Morton and W. D. Hutchison, "Release of sensory neuropeptides in the spinal cord: studies with calcitonin gene-related peptide and galanin," *Neuroscience*, vol. 31, no. 3, pp. 807–815, 1989.

[34] K. M. Al-Khater, R. Kerr, and A. J. Todd, "A quantitative study of spinothalamic neurons in laminae I, III and IV in lumbar and cervical segments of the rat spinal cord," *Journal of Comparative Neurology*, vol. 511, no. 1, pp. 1–18, 2008.

[35] H. Ikeda, B. Heinke, R. Ruscheweyh, and J. Sandkühler, "Synaptic plasticity in spinal lamina I projection neurons that mediate hyperalgesia," *Science*, vol. 299, no. 5610, pp. 1237–1240, 2003.

[36] T. L. Yaksh, X.-Y. Hua, I. Kalcheva, N. Nozaki-Taguchi, and M. Marsala, "The spinal biology in humans and animals of pain states generated by persistent small afferent input," *Proceedings of the National Academy of Sciences of the United States of America*, vol. 96, no. 14, pp. 7680–7686, 1999.

[37] B. K. Taylor and K. E. McCarson, "Neurokinin-1 receptor gene expression in the mouse dorsal horn increases with neuropathic pain," *Journal of Pain*, vol. 5, no. 2, pp. 71–76, 2004.

[38] N. P. Gerard, L. A. Garraway, R. L. Eddy Jr. et al., "Human substance P receptor (NK-1): organization of the gene, chromosome localization, and functional expression of cDNA clones," *Biochemistry*, vol. 30, no. 44, pp. 10640–10646, 1991.

[39] V. S. Seybold, K. E. McCarson, P. G. Mermelstein, R. D. Groth, and L. G. Abrahams, "Calcitonin gene-related peptide regulates expression of neurokinin1 receptors by rat spinal neurons," *Journal of Neuroscience*, vol. 23, no. 5, pp. 1816–1824, 2003.

[40] Y.-H. Gao, S.-P. Chen, J.-Y. Wang, L.-N. Qiao, Q.-L. Xu, and J.-L. Liu, "Effects of electroacupuncture at different acupoints on the pain behavior and NMDA receptor 2 B subunit mRNA and protein expression and phosphorylation level in the cervical spinal cord in rats with thyroid regional pain," *Zhen Ci Yan Jiu*, vol. 34, no. 6, pp. 376–382, 2009.

[41] I. Marriott, "The role of tachykinins in central nervous system inflammatory responses," *Frontiers in Bioscience*, vol. 9, pp. 2153–2165, 2004.

[42] S. Tumati, T. M. Largent-Milnes, A. I. Keresztes et al., "Tachykinin NK1 receptor antagonist co-administration attenuates opioid withdrawal-mediated spinal microglia and astrocyte activation," *European Journal of Pharmacology*, vol. 684, no. 1–3, pp. 64–70, 2012.

[43] K. Miyano, N. Morioka, T. Sugimoto, S. Shiraishi, Y. Uezono, and Y. Nakata, "Activation of the neurokinin-1 receptor in rat spinal astrocytes induces Ca^{2+} release from IP_3-sensitive Ca^{2+} stores and extracellular Ca^{2+} influx through TRPC3," *Neurochemistry International*, vol. 57, no. 8, pp. 923–934, 2010.

[44] A. P. Jeanjean, S. M. Moussaoui, J.-M. Maloteaux, and P. M. Laduron, "Interleukin-1β induces long-term increase of axonally transported opiate receptors and substance P," *Neuroscience*, vol. 68, no. 1, pp. 151–157, 1995.

[45] A. Schweizer, U. Feige, A. Fontana, K. Müller, and C. A. Dinarello, "Interleukin-1 enhances pain reflexes. Mediation through increased prostaglandin E2 levels," *Agents and Actions*, vol. 25, no. 3-4, pp. 246–251, 1988.

[46] H. Vanegas and H.-G. Schaible, "Prostaglandins and cycloxygenases in the spinal cord," *Progress in Neurobiology*, vol. 64, no. 4, pp. 327–363, 2001.

[47] A. Ebersberger, B. D. Grubb, H. L. Willingale, N. J. Gardiner, J. Nebe, and H.-G. Schaible, "The intraspinal release of prostaglandin E2 in a model of acute arthritis is accompanied by an up-regulation of cyclo-oxygenase-2 in the spinal cord," *Neuroscience*, vol. 93, no. 2, pp. 775–781, 1999.

[48] D. G. Ririe, H. M. Prout, and J. C. Eisenach, "Effect of cyclooxygenase-1 inhibition in postoperative pain is developmentally regulated," *Anesthesiology*, vol. 101, no. 4, pp. 1031–1035, 2004.

[49] X. Zhu, D. Conklin, and J. C. Eisenach, "Cyclooxygenase-1 in the spinal cord plays an important role in postoperative pain," *Pain*, vol. 104, no. 1-2, pp. 15–23, 2003.

[50] M. Prochazkova, T. Dolezal, J. Sliva, and M. Krsiak, "Different patterns of spinal cyclooxygenase-1 and cyclooxygenase-2 mRNA expression in inflammatory and postoperative pain," *Basic and Clinical Pharmacology and Toxicology*, vol. 99, no. 2, pp. 173–177, 2006.

[51] J. S. Kroin, M. Takatori, J. Li, E.-Y. Chen, A. Buvanendran, and K. J. Tuman, "Upregulation of dorsal horn microglial cyclooxygenase-1 and neuronal cyclooxygenase-2 after thoracic deep muscle incisions in the rat," *Anesthesia and Analgesia*, vol. 106, no. 4, pp. 1288–1295, 2008.

[52] J.-J. Wang, G.-J. Chen, W. Chen, J. Du, A.-L. Luo, and Y.-G. Huang, "Analgesic effect of calpain inhibitor ALLN on the zymosan-induced paw inflammatory pain and its effect on the expression of cyclooxygenase-2 in the spinal dorsal horn," *Zhongguo Yi Xue Ke Xue Yuan Xue Bao*, vol. 34, no. 1, pp. 25–31, 2012.

[53] H. J. Jeong, S. H. Lee, S. Y. Cho et al., "Roles of serotonergic and adrenergic receptors in the antinociception of selective cyclooxygenase-2 inhibitor in the rat spinal cord," *Korean Journal of Pain*, vol. 24, no. 4, pp. 179–184, 2011.

[54] T. L. Yaksh, D. M. Dirig, C. M. Conway, C. Svensson, Z. D. Luo, and P. C. Isakson, "The acute antihyperalgesic action of nonsteroidal, anti-inflammatory drugs and release of spinal prostaglandin E2 is mediated by the inhibition of constitutive spinal cyclooxygenase-2 (COX-2) but not COX-1," *Journal of Neuroscience*, vol. 21, no. 16, pp. 5847–5853, 2001.

[55] Y. H. Gao, S. P. Chen, J. Y. Wang et al., "Effects of electroacupuncture of "Futu" (LI 18), etc. on pain behavior and expression of GABA receptor subunit genes in cervical spinal cord in rats with thyroid regional pain," *Zhen Ci Yan Jiu*, vol. 37, no. 2, pp. 93–98, 2012.

[56] J.-H. Lee, K.-J. Jang, Y.-T. Lee, Y.-H. Choi, and B.-T. Choi, "Electroacupuncture inhibits inflammatory edema and hyperalgesia through regulation of cyclooxygenase synthesis in both peripheral and central nociceptive sites," *The American Journal of Chinese Medicine*, vol. 34, no. 6, pp. 981–988, 2006.

[57] W.-L. Mi, Q.-L. Mao-Ying, Q. Liu, X.-W. Wang, Y.-Q. Wang, and G.-C. Wu, "Synergistic anti-hyperalgesia of electroacupuncture and low dose of celecoxib in monoarthritic rats: involvement of the cyclooxygenase activity in the spinal cord," *Brain Research Bulletin*, vol. 77, no. 2-3, pp. 98–104, 2008.

Hindawi Publishing Corporation
Evidence-Based Complementary and Alternative Medicine
Volume 2013, Article ID 801457, 11 pages
http://dx.doi.org/10.1155/2013/801457

Review Article

Roles of Chlorogenic Acid on Regulating Glucose and Lipids Metabolism: A Review

Shengxi Meng,[1] Jianmei Cao,[1,2] Qin Feng,[1] Jinghua Peng,[1] and Yiyang Hu[1,3]

[1] *Institute of Liver Diseases, Shuguang Hospital Affiliated to Shanghai University of Traditional Chinese Medicine, 528 Zhangheng Road, Pudong, Shang hai 201203, China*
[2] *Shanghai University of Traditional Chinese Medicine, 1200 Cailun Road, Pudong, Shanghai 201203, China*
[3] *E-Institute of Traditional Chinese Internal Medicine of Shanghai Municipal Education Commission, 1200 Cailun Road, Pudong, Shanghai 201203, China*

Correspondence should be addressed to Yiyang Hu; yyhuliver@163.com

Received 24 May 2013; Revised 9 July 2013; Accepted 12 July 2013

Academic Editor: Yong-Qing Yang

Intracellular glucose and lipid metabolic homeostasis is vital for maintaining basic life activities of a cell or an organism. Glucose and lipid metabolic disorders are closely related with the occurrence and progression of diabetes, obesity, hepatic steatosis, cardiovascular disease, and cancer. Chlorogenic acid (CGA), one of the most abundant polyphenol compounds in the human diet, is a group of phenolic secondary metabolites produced by certain plant species and is an important component of coffee. Accumulating evidence has demonstrated that CGA exerts many biological properties, including antibacterial, antioxidant, and anticarcinogenic activities. Recently, the roles and applications of CGA, particularly in relation to glucose and lipid metabolism, have been highlighted. This review addresses current studies investigating the roles of CGA in glucose and lipid metabolism.

1. Introduction

Intracellular glucose and lipid metabolic homeostasis is very vital for maintaining the basic life activities of a cell or an organism. In terms of cytology, intracellular glucose and lipid metabolic disorders are the basis of a variety of metabolic diseases. Glucose and lipid metabolic disorders are closely related with the occurrence and progression of diabetes, obesity, hepatic steatosis, cardiovascular disease, and cancer [1]. The complications of glucose and lipid metabolic disorders will impose a significant burden on health care systems all over the world. However, medical therapeutic options are not only limited, but also associated with unwanted side effects [2–4]. Therapies with novel mechanisms of action to combat glucose and lipid metabolic disorders would therefore have significant medical and economic impacts.

Chlorogenic acid (CGA) (Figure 1), one of the most abundant polyphenol compounds in the human diet, is a group of phenolic secondary metabolites produced by certain plant species and an important component of coffee. It has been reported that coffee had the highest concentration of polyphenols among the beverages analyzed [5, 6]. The major polyphenol in coffee is CGA. Chlorogenic acid (CGA) is an ester formed from cinnamic acids and quinic acid and is also known as 5-O-caffeoylquinic acid (5-CQA) (IUPAC numbering) or 3-CQA (pre-IUPAC numbering) [7]. The most common form of CGA is 5-caffeoylquinic acid (5-CQA) (Figure 2). Accumulating evidence has demonstrated that CGA exhibits many biological properties, including antibacterial, antioxidant, and anticarcinogenic activities, particularly hypoglycemic and hypolipidemic effects [8–14]. CGA has been recently claimed to modulate glucose and lipid metabolism *in vivo* in both healthy and genetically metabolic disordered conditions [14–16].

Recently, the roles and the applications of CGA, particularly in relation to glucose and lipid metabolism, have been highlighted in both biological and medical fields [17–21]. It will possibly, we think, become a research focus or a trend of medicine and pharmacology in the near future. A review of the roles and applications of CGA in glucose and

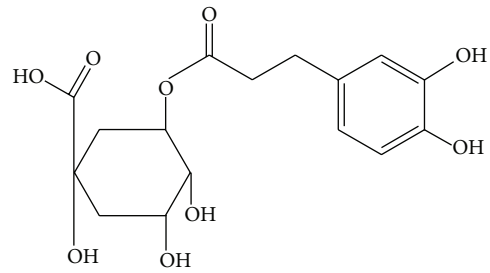

Figure 1: Chemical structure of chlorogenic acid (CGA).

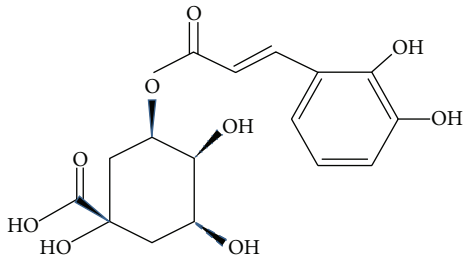

Figure 2: Chemical structure of 5-O-cafeoylquinic acid (chlorogenic acid).

lipid metabolism is consequently urgent and vital to assist in further research.

2. Effects on Glucose Metabolism

2.1. Hypoglycemic and Antidiabetic Effect. Regular consumption of coffee has been associated with a lower risk of type 2 diabetes mellitus (T2DM), and this has been replicated across sexes, geographical locations, and obesity levels [22–28]. CGA is major bioactive compound in coffee that may provide health benefits. For example, it is reported that daily consumption of 3 to 4 cups of decaffeinated coffee containing high contents of CGA significantly reduced the risk for T2DM by 30% [29].

Chlorogenic acid (CGA) is a novel insulin sensitizer that potentiates insulin action similar to the therapeutic action of metformin [30]. Chlorogenic acid (CGA) at a dose of 5 mg/kg body weight exerts antidiabetic potential in streptozotocin (STZ) (45 mg/kg b.w.) nicotinamide induced diabetic rats [31–33].

Bassoli et al. (2008) analysed the effects of CGA on hepatic glucose output, blood glucose levels, and glucose tolerance. It was found that CGA did promote a significant reduction in the plasma glucose peak in the oral glucose tolerance test, most likely by attenuating intestinal glucose absorption, indicating a possible role for CGA as a glycaemic index lowering agent and highlighting it as a compound of interest for reducing the risk of developing T2DM [12].

CGA exerts its antidiabetic effects on stimulating glucose uptake in both insulin-sensitive and insulin-resistant adipocytes. The potency of CGA to stimulate 2-[N-(7-nitrobenz-2-oxa-1,3-diazol-4-yl)amino]-2-deoxy-d-glucose(2-NBDG) uptake was comparable to the antidiabetic drug rosiglitazone [34]. Moreover, CGA, unlike thiazolidinedione (TZD) or insulin, does not induce obesity or other side effects.

It was reported that CGA ingestion significantly reduced early fasting glucose and insulin responses in overweight men during an OGTT [35]. Clinical trials have also testified that CGA is able to lower the glycemic impact of foods and chronically lower background blood glucose levels of T2DM [36].

2.2. Stimulation of Insulin Secretion. CGA has been described as a potential antidiabetic agent. Using *in vitro* studies, Tousch et al. [37] (2008) reported that CGA increased glucose uptake in L6 muscular cells, an effect only observed in the presence of stimulating concentrations of insulin. In addition it was found that CGA stimulates insulin secretion from the INS-1E insulin-secreting cell line and rat islets of Langerhans. Clinical trials have also testified that CGA in coffee is able to modulate glucose uptake and gastrointestinal hormone and insulin secretion in humans [38].

2.3. Improving Glucose Tolerance and Insulin Resistance. Insulin resistance is a major obstacle in the diabetes treatment and is often accompanied by hyperglycemia, hyperinsulinemia, and hyperlipaemia in obesity-induced type 2 diabetic patients, which is also regarded as one of the risk factors leading to a series of complications, such as nephropathy, retinopathy, myocardial infarction, and neuropathy [39]. CGA has been shown to act as an active principle in glucose metabolism regulation [40, 41]. CGA is capable of improving glucose tolerance and insulin resistance in obese (*fa*/*fa*) Zucker rats, suggesting that CGA may be a promising candidate for the development of antidiabetic agents [13]. Liang et al. [42] also found that, compared to model group (mice were administrated with high-fat emulsion by gastric perfusion), CGA interference group (mice were administrated with high-fat emulsion and CGA (20 mg·kg^{-1} body weight)) had better glucose tolerance, higher insulin sensitivity index (ISI), and lower HOMA-IR index. And the contents of TG, TC, and LDL-C in serum were decreased in the CGA interference group.

3. Effects on Lipid Metabolism

3.1. Lowering Serum and Hepatic CG and TG Levels. Hypercholesterolemia is a major risk factor for the development of cardiovascular disease and nonalcoholic fatty liver disease. CGA are hypoglycemic agents and may affect lipid metabolism. Rodriguez de Sotillo and Hadley [14] investigated the effects of CGA *in vivo*, by using obese, hyperlipidemic, and insulin resistant (*fa*/*fa*) Zucker rats. The authors reported that CGA did not promote sustained hypoglycemia, but significantly lowered the postprandial peak response to a glucose challenge when compared to the same group of rats before CGA treatment. In CGA-treated rats, fasting plasma cholesterol and triacylglycerol concentrations significantly decreased by 44% and 58%, respectively, as did liver triacylglycerols concentrations (24%). There were no statistical differences ($P > 0.05$) in adipose triacylglycerol concentrations. Significant differences ($P < 0.05$) in the plasma, liver,

and spleen concentration of selected minerals were found in CGA-treated rats. This study suggested that *in vivo* CGA improves glucose tolerance, decreases various plasma and liver lipids, and improves mineral pool distribution.

3.2. Reducing LDL Oxidation Susceptibility and Decreasing LDL-Cholesterol and MDA Levels. It is currently believed that oxidative modification of low-density lipoproteins (LDL) by free radicals is a key early event in the pathogenesis of atherosclerosis. The rapid uptake of oxidatively modified LDL via a scavenger receptor leads to the formation of foam cells. Oxidized LDL also has a number of other atherogenic properties [43]. Chlorogenic acid may favorably affect cardiovascular risk status by modestly reducing LDL oxidation susceptibility and decreasing LDL-cholesterol and malondialdehyde (MDA) levels. Chlorogenic acid, active compound in coffee, inhibits oxidation of LDL *in vitro* and may therefore protect against cardiovascular disease [44, 45].

3.3. Inhibiting Fat Absorption and Activating Fat Metabolism in the Liver. Shimoda et al. [46] (2006) testified that CGA, caffeine, and other polyphenolic compounds in green coffee bean extract (GCBE) act to suppress body weight gain and visceral fat accumulation in mice. The authors reported that CGA is possibly effective against weight gain and fat accumulation by inhibition of fat absorption and activation of fat metabolism in the liver. And oral administration of CGA (30 and 60 mg/kg/day) for 14 days dramatically reduced the level of hepatic TG in mice. The suppressive effect of CGA on hepatic TG accumulation was more potent than that of GCBE.

3.4. Improvement of Obesity-Related Hormones Levels. Cho et al. [47] (2010) investigated the efficacy of CGA on altering body fat in high-fat diet (37% calories from fat) induced obese mice compared to caffeic acid. The authors found that CGA significantly lowered body weight, visceral fat mass and plasma leptin, and insulin levels compared to the high-fat control group. CGA also lowered triglyceride (in plasma, liver, and heart) and cholesterol (in plasma, adipose tissue, and heart) concentrations. Chlorogenic acid significantly inhibited fatty acid synthase, 3-hydroxy-3-methylglutaryl CoA reductase, and acyl-CoA cholesterol acyltransferase activities, while they increased fatty acid beta-oxidation activity and peroxisome proliferator-activated receptors alpha expression in the liver compared to the high-fat group. The authors' results suggested that CGA can improve body weight, lipid metabolism, and obesity-related hormones levels in high-fat fed mice.

3.5. Alterations in Lipids, Lipoproteins, and Enzymes Involved in Lipid Metabolism. Diabetes mellitus is associated with dyslipidemia which is a significant risk factor for cardiovascular complications. Karthikesan et al. [48] evaluated the effects of CGA on alterations in lipids, lipoproteins, and enzymes involved in lipid metabolism in STZ-nicotinamide-(NA-) induced T2DM rats. The authors found that there was a significant increase in the concentrations of plasma and tissue (liver and kidney) lipids, cholesterol, triglycerides (TGs), free fatty acids (FFAs) and phospholipids (PLs), and low density and very low-density lipoproteins (LDL and VLDL), respectively, and a decrease in the concentration of high-density lipoproteins (HDL) in STZ administered diabetic rats. In addition, the activity of 3-hydroxy 3-methylglutaryl coenzyme A (HMG-CoA) reductase increased significantly in the liver and kidney whereas the activities of lipoprotein lipase (LPL) and lecithin cholesterol acyl transferase (LCAT) were decreased significantly in the plasma of diabetic rats. Administration of CGA remarkably reduced the STZ-induced changes in lipids, lipoproteins, and lipid metabolising enzymes in diabetic rats. The author's results indicate that CGA can potentially ameliorate lipid abnormalities in experimental T2DM.

3.6. Inhibiting Lipids' Absorption and Transformation, Inhibiting Cholesterol's Intestinal Absorption and Hepatic Biosynthesis. Li et al. [49] (2012) observed the effects of CGA on key enzyme activities in lipid metabolism and explored its antihyperlipidemia mechanism. The authors studied the lipid-lowering effect and mechanism of CGA by observing the influence on the formation of cholesterol micelles and on the inhibition of 3-hydroxy-3-methylglutaryl-CoA (HMG-CoA) reductase from normal pig liver as well as pancreatic lipase *in vitro*. The authors found that CGA has strong inhibitory effects on cholesterol micelles formation and has stronger inhibitory potency on HMG-CoA reductase than simvastatin. In addition, CGA also has a stronger inhibition on the activity of pancreatic lipase. The mechanism of CGA in reducing blood lipids was most likely associated with the inhibition of absorption and transformation of lipids and with the inhibition of intestinal absorption and hepatic biosynthesis of cholesterol.

3.7. Improvement of Antioxidant Activities. Wang et al. [50] (2012) investigated the effect of CGA on lipid metabolism of hyperlipidemia mice. It was found that the contents of serum TC, TG, LDL-C levels, and liver TC were significantly lower. Furthermore, malondialdehyde (MDA) contents in serum and liver were decreased, and activities of antioxidant enzymes were increased. Arteriosclerosis index (AI) was also lower than that of the model group. The results indicated that CGA could effectively reduce the blood and liver lipid accumulation and regulate lipid metabolism by improving their antioxidant activities. Furthermore, the group at the dose of 50 mg/kg CGA showed the best effect among all groups.

4. Mechanism of Action

4.1. Improvement of Cellular Mechanisms. *In vivo* studies have confirmed that CGA can improve glucose tolerance and mineral pool distribution in obese Zucker rats [14]. The significant decrease in postprandial blood glucose concentrations may be attributed to an improved sensitivity to insulin [51]. Impaired glucose tolerance and insulin resistance have been associated with differences in the hepatic mRNA expression of the spliced variants of the insulin receptor at exon 11. Spliced variants of the insulin receptor have not been studied in obese Zucker rats. Thus, Rodriguez de Sotillo et al. [15]

(2006) studied the *in vivo* effect of CGA on plasma insulin concentrations in a glucose tolerance test. It was found that in the CGA-treated group, areas under the curve (AUC) for blood glucose and plasma insulin improved, and the protein and DNA concentrations in the liver increased. There were no significant differences between groups for the hepatic G-6-Pase activity. The insulin receptor exon 11 (+) and the exon 11 (−) variants were expressed in the liver of Zucker (fa/fa) rats without significant changes. It is consequently suggested that CGA may improve some cellular mechanisms that are stimulated by insulin.

4.2. Inhibition of the Activity of α-Glucosidase. Zheng et al. [52] (2007) examined the inhibitory effect of CGA on the postprandial blood glucose concentration in rats. It was reported that CGA inhibited the activities of α-amylase and α-glucosidase and reduced the postprandial blood glucose concentration. Chlorogenic acid (CGA), as well as acarbose, strongly inhibited the activity of α-glucosidase and reduced the postprandial blood glucose concentration. It was reported that CGA suppresses postprandial hyperglycemia by inhibiting α-glucosidase and that its action resembles that of currently available α-glucosidase inhibitors such as acarbose, miglitol, and voglibose [53, 54]. Matsui et al. described that CGA inhibits rat intestinal α-glucosidase in a noncompetitive manner [55].

In particular, CGA has been implicated to be responsible for anti-hyperglycemic effects in humans [56]. McCarty [57] had reported that the consumption of coffee by humans reduced the rise of plasma glucose concentrations in a tolerance test. It suggested that CGA may exert an antagonistic effect on glucose transport. Experiments with everted gut sac have showed that CGA inhibits the uptake of glucose from the rat intestine. Their results suggested that CGA may inhibit α-glucosidase by the attenuation of glucose transport in a synergistic manner.

4.3. Alteration of GIP Concentrations. Chlorogenic acid (CGA) may inhibit intestinal glucose uptake *in vitro*. Furthermore, CGA is thought to stimulate the secretion of glucagon-like peptide-1 (GLP-1), which is known to have a beneficial effect on the response to glucose in pancreatic beta cells [58]. To elucidate the mechanisms by which CGA acts to mediate blood glucose response *in vivo*, Tunnicliffe et al. [59] (2011) investigated Sprague-Dawley rats that were catheterized and gavage-fed a standardized meal administered with or without CGA in a randomized crossover design separated by a 3-day washout period. It was found that the total area under the curve (AUC) for blood glucose was significantly attenuated in rats fed with CGA ($P < 0.05$). In contrast, no differences in plasma insulin nor nonesterified fatty acids, and gastric emptying were observed. Plasma glucose-dependent insulinotropic peptide (GIP) response was blunted in rats fed with CGA, with a lower peak concentration and AUC up to 180 min postprandially ($P < 0.05$). There were no changes in GLP-1 secretion in either the *in vivo* or *in vitro* studies. It was demonstrated that CGA treatment resulted in beneficial effects on blood glucose response, with alterations seen in GIP concentrations. In view of the widespread consumption and availability of coffee, CGA may be a viable preventative tool for T2DM.

4.4. Activation of AMPK. AMP activated protein kinase (AMPK) is a master sensor and regulator of cellular energy balance [60]. It is activated by various pharmacological, pathological, and metabolic stressors such as metformin, thiazolidinediones, hypoxia and exercise. Activation of AMPK leads to translocation of GLUT4 from intracellular membranes to plasma membranes, thus increasing glucose transport [61].

Prabhakar and Doble [62] (2009) revealed that CGA stimulated glucose transport in myotubes via increasing expression of GLUT4 and PPAR-γ transcript. Subsequently, Ong et al. [63] (2012) investigated the role of CGA in the regulation of glucose transport in skeletal muscle isolated from db/db mice and L6 skeletal muscle cells. The results showed that CGA stimulated glucose transport in L6 myotubes in a dose- and time-dependent manner. In addition, it was demonstrated for the first time that CGA stimulates glucose transport in skeletal muscle via the activation of AMPK. In the following year, Ong et al. [18] further investigated the effects of CGA on glucose tolerance, insulin sensitivity, hepatic gluconeogenesis, lipid metabolism, and skeletal muscle glucose uptake in $Lepr^{db/db}$ mice. It was found that in $Lepr^{db/db}$ mice, acute treatment with CGA lowered AUC glucose in an OGTT. Chronic administration of CGA inhibited hepatic G-6-Pase expression and activity, attenuated hepatic steatosis, and improved lipid profiles and skeletal muscle glucose uptake, which in turn improved fasting glucose level, glucose tolerance, insulin sensitivity, and dyslipidemia in $Lepr^{db/db}$ mice. Furthermore the results of this study showed that CGA activated AMPK, leading to subsequent beneficial metabolic effects, such as suppression of hepatic glucose production and fatty acid synthesis. Inhibition and knockdown of AMPK abrogated these metabolic alterations. It suggested that CGA can improve glucose and lipid metabolism via the activation of AMPK (Figure 3).

4.5. Inhibition of HMG CoA Reductase. Gebhardt [64] demonstrated that CGA can indirectly yet efficiently inhibit β-hydroxy-β-methyl glutaric acyl coenzyme A reductase (HMG CoA reductase) in primary cultured rat hepatocytes and inhibit the synthesis of cholesterol.

4.6. Strengthening the Activity of CPT. Chlorogenic acid is able to strengthen the activity of carnitine palmitoyl transferase (CPT), a fatty acid oxidation speed limit enzyme, and promote the oxidation of fatty acid. This suggests a possible way for CGA involvement with lipid metabolism [65].

4.7. Inhibition of G-6-Pase Expression. In previous studies, many beneficial effects of CGA on the metabolism of glucose have been noted, with the possibility of improved systemic glucose control [66]. One of the dominant mechanisms is thought to be delayed absorption in the small intestine through the inhibition of glucose-6-phosphate translocase and reduction of the sodium gradient driven apical glucose transport [67].

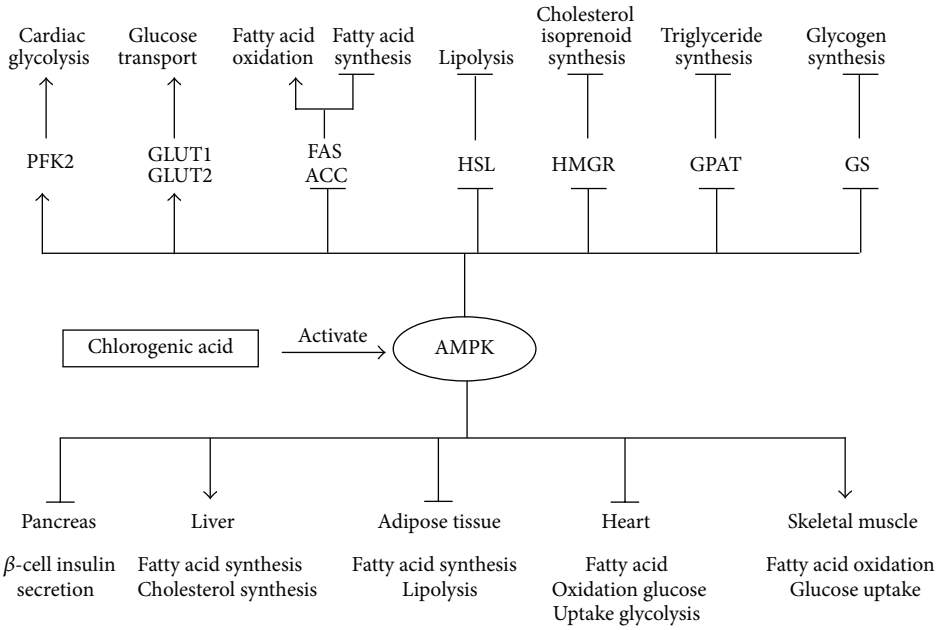

Figure 3: Chlorogenic acid regulates glucose and lipid metabolism via activating AMPK signal pathway.

Chlorogenic acid (CGA) has been shown to affect glucose metabolism [12, 34, 68, 69]. It has been shown to delay glucose absorption in the intestine through inhibition of G-6-pase translocase and reduction of the sodium gradient-driven apical glucose transport [68]. It was reported that CGA inhibited approximately 40% of glucose-6-phosphatase (G-6-Pase) activity in the microsomal fraction of hepatocytes [12]. Thus, CGA can decrease hepatic glucose output through inhibition of the activity of G-6-Pase [62, 66–68].

Chlorogenic acid (CGA) lowers the blood glucose concentrations and inhibits G-6-Pase, the two main metabolic pathways responsible for the release of glucose from the liver [36, 67, 70–72]. Previous experimental data shows that CGA promotes the uptake of glucose by liver cells and regulates the overproduction of glucose by inhibiting G-6-Pase; thereby, CGA controls glycemic status in T2DM patients [73]. In a 1997 study, Arion et al. [68] investigated the interactions of CGA and 2-hydroxy-5-nitrobenzaldehyde (HNB) with the components of the rat hepatic G-6-Pase system. Both CGA and HNB are competitive inhibitors of G-6-Pase hydrolysis in intact microsomes with Ki values of 0.26 mm and 0.22 mm, respectively. The authors revealed that CGA is the most specific T1 (the G-6-Pase transporter) inhibitor, and that CGA may selectively inhibit hepatic G-6-Pase, which is a rate-limiting enzyme involved in gluconeogenesis.

Chlorogenic acid (CGA) is a novel insulin sensitizer that potentiates insulin action similar to the therapeutic action of metformin [30]. In contrast, CGA reduces blood glucose level by directly inhibiting G-6-Pase activity with the related effects of hepatic glycogenolysis [36] and gluconeogenesis [74]. Andrade-Cetto and Wiedenfeld [75] (2001) examined hypoglycemic effects of CGA in STZ-induced diabetic rats. No statistical difference between CGA and glyburide in the hypoglycemic effect after 3 hours was observed. The mechanism may be related to inhibition of glucose-6-phosphate displacement enzymes and glucose absorption. Wang et al. [69] (2012) investigated the effects of CGA on hepatic G-6-pase, skeletal muscle GLUT4 expression, blood glucose and lipid levels in STZ-induced diabetic rats. It was found that CGA exerted effects on improving blood glucose, TG, TC, insulin sensitivity, downregulating expression of G-6-pase and upregulating mRNA levels of GLUT4. Consequently the authors demonstrated that CGA may ameliorate the changes of glucose metabolism, lipid metabolism, insulin sensitivity, hepatic G-6-pase expression, and skeletal muscle GLUT4 expression in STZ-included SD diabetic rats.

CGA has hypoglycemic and hypolipidemic functions, and can relieve the mouse insulin resistance development significantly by down-regulating the expression of G-6-Pase mRNA and up-regulating GLUT-4 transcript [42].

4.8. Upregulation of Expression of Hepatic PPAR-α. Zhang et al. [17] (2011) examined the effect of CGA on disordered glucose and lipid metabolism in *db*/*db* mice and its mechanism. They found that the mRNA expression level of G-6-Pase, the key enzyme that catalyzes the final step of glycogenolysis and gluconeogenesis, was significantly downregulated in db/db-CGA group when compared with db/db-CON group. Both the mRNA level and the protein expression levels of PPAR-α were significantly upregulated in db/db-CGA group compared with the db/db-CON group. The results of this study demonstrated that CGA improves the disordered glucose/lipid metabolism in *db*/*db* mice, which is speculated to be related with its role in modulating the adipokines secretion, upregulating expression of hepatic PPAR-α, and inhibiting expression of G-6-Pase (Figure 4).

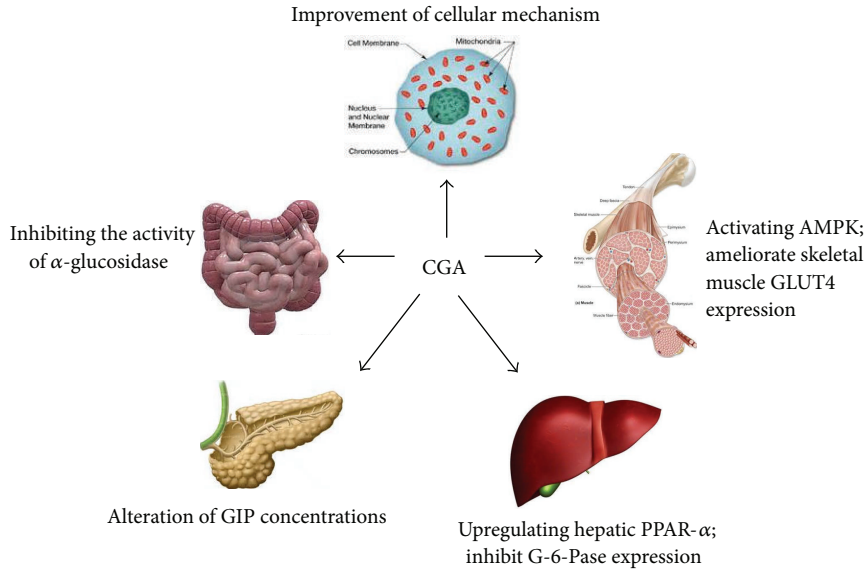

Figure 4: Chlorogenic acid's possible mechanism of action of regulating glucose and lipid metabolism.

Li et al. [76] (2009) investigated the effects of CGA on glucose and lipid metabolism under a high-dietary fat burden explored the possible role of peroxisome proliferator-activated receptor-alpha (PPAR-alpha) in these effects. It was found that CGA treatment significantly elevated the level of mRNA and protein expression in hepatic PPAR-α. The authors' results indicated that CGA may modify glucose and lipids metabolism, which may be attributed to PPAR-α facilitated lipid clearance in the liver and improved insulin sensitivity.

Wan et al. [19] (2013) investigated the hypocholesterolemic effects of the dietary consumption of CGA by monitoring plasma lipid profile in Sprague-Dawley rats. The authors found that CGA markedly altered the increased plasma total cholesterol and low-density lipoprotein but decreased HDL induced by a hypercholesterolemic diet with a dose-dependent improvement on both atherogenic index and cardiac risk factor. Lipid depositions in the liver were attenuated significantly in hypercholesterolemic animals supplemented with CGA. It is consequently postulated that hypocholesterolemic effect is the primary beneficial effect given by CGA, which leads to further secondary beneficial effects such as atheroscleroprotective, cardioprotective, and hepatoprotective functions. It suggested that the hypocholesterolemic functions of CGA are most likely due to the increase in fatty acid utilization in the liver via the upregulation of peroxisome proliferation-activated receptor α mRNA.

Li [77] (2007) found that CGA can increase the activity of animals' hepatic lipase in the liver, the activity of PPARα, β, and γ in the liver, and PPARγ in visceral fat in various extents. PPARs are members of the nuclear receptor superfamily that play a key role in regulating glucolipid metabolism. It was demonstrated that CGA may regulate glucolipid metabolism by activating PPARs *in vivo* in rats. Thus, CGA may regulate glucolipid metabolism by a variety of mechanisms interactively.

From previous as are stated, it has been testified and reported that CGA is able to exert vital roles on regulation of glucose and lipid metabolic disorders (Table 1), which are closely associated with the occurrence and progression of diabetes, obesity, hepatic steatosis, cardiovascular disease, and cancer. And increasing evidence shows that CGA will be exhibiting more potency in glucose and lipid metabolism in the near future. To our excitement, from diverse aspects, some mechanisms of actions of CGA are being elucidated, which will be beneficial to treat some diseases associated with glucose and lipid metabolic disorders.

5. Future Research Direction and Prospects

Present population epidemiological and animal studies suggest that CGA, which *in vivo* can regulate glucose and lipid metabolism and improves insulin sensitivity, may be capable of preventing and treating obesity, diabetes mellitus, and metabolic syndrome. However, this needs to be verified through the intervention studies of large-scale populations. Dose-response relationship and mechanisms of action of CGA's beneficial effects require further research and testification. Based on the study concerning the bioactivity of CGA and glucose and lipid metabolism, individuals may be guided to adopt a healthy diet, adjust dietary structure, and increase intake of natural plant ingredients, in order to prevent the occurrence and progression of chronic diseases.

6. Conclusion

Accumulating research and studies, related with the role of CGA on glucose and lipid metabolism, have been conducted. While progress has been made, the mechanism on glucose and lipid metabolism has not yet been conclusively elucidated. The side effects of CGA have not yet been investigated comprehensively. Further research is required

Table 1: Summary of studies of CGA on glucose and lipid metabolism.

Study (references)	Year	*In vivo*/ *in vitro*	Animal experiment		Clinical trial	Findings	Mechanism of action
			Animal/cell	Disease model			
Karthikesan et al. [31]	2010	*In vivo*	STZ-NA-induced diabetic rats	T2DM	—	Hypoglycemic and antidiabetic effects	—
Karthikesan et al. [32]	2010	*In vivo*	STZ-NA-induced T2DM adult Wistar rats	T2DM	—	hypoglycemic and antidiabetic effects	—
Pari et al. [33]	2010	*In vivo*	STZ-NA-induced T2DM adult Wistar rats	T2DM	—	hypoglycemic and antidiabetic effects	—
Bassoli et al. [12]	2008	*In vitro*	Liver perfusion	—	—	Reduction in the plasma glucose peak in the oral glucose tolerance test	—
Alonso-Castro et al. [34]	2008	*In vitro*	3T3-F442A murine adipocytes		—	Exerting antidiabetic effects on stimulating glucose uptake in both insulin-sensitive and insulin-resistant adipocytes	—
van Dijk et al. [35]	2009	—	—	—	Overweight men	Reducing early fasting glucose and insulin responses in overweight men during an OGTT	—
Ahrens and Thompson [36]	2013	—	—	—	T2DM patients	Lowering the glycemic impact of foods and lowering background blood glucose levels of T2DM	—
Tousch et al. [37]	2008	*In vitro*	L6 muscular cells		—	Stimulation of insulin secretion	—
Johnston et al. [38]	2003	—	—	—	Healthy fasted volunteers	Stimulation of insulin secretion	—
Liang et al. [42]	2013	*In vivo*	Mouse induced by high fat emulsion	Insulin resistance	—	Improvement of glucose tolerance and insulin resistance	—
Rodriguez de Sotillo and Hadley [14]	2002	*In vivo*	(fa/fa) Zucker rats	T2DM	—	Lowering serum and hepatic CG and TG levels	—
Shimoda et al. [46]	2006	*In vivo*	Male ddy mice	—	—	Inhibiting fat absorption and activating fat metabolism in the liver	—
Cho et al. [47]	2010	*In vivo*	High-fat diet induced-obese mice	T2DM	—	Improvement of obesity-related hormones levels	—
Karthikesan et al. [48]	2010	*In vivo*	STZ-NA induced diabetic rats	T2DM	—	Alterations in lipids, lipoproteins, and enzymes involved in lipid metabolism	—
Wang et al. [50]	2012	*In vivo*	Mice induced by high-fat diet	T2DM	—	Improvement of antioxidant activities	—
Rodriguez de Sotillo et al. [15]	2006	*In vivo*	Obese Zucker (fa/fa) rats	T2DM	—	Improvement of glucose tolerance and mineral pool distribution	Improvement of cellular mechanisms
Zheng et al. [52]	2007	*In vivo*	Kud:Wistar rats	—	—	Reducing the postprandialblood glucose concentration	Inhibiting the activity of α-glucosidase
Tunnicliffe et al. [59]	2011	*In vivo*	Male Sprague-Dawley rats	T2DM	—	Attenuating AUC for blood glucose	Alteration of GIP concentrations

Table 1: Continued.

Study (references)	Year	Animal experiment			Clinical trial	Findings	Mechanism of action
		In vivo/ *in vitro*	Animal/cell	Disease model			
Ong et al. [63]	2012	*In vivo* *In vitro*	db/db mice L6 skeletal muscle cells	T2DM	—	Stimulating glucose transport in L6 myotubes in a dose- and time-dependent manner	Activation of AMPK
Ong et al. [18]	2013	*In vivo* *In vitro*	Lepr db/db mice Hepatoma HepG2	T2DM	—	Attenuating hepatic steatosis, improving lipid profiles and skeletal muscle glucose uptake, glucose tolerance, insulin sensitivity, and dyslipidemia	Activation of AMPK
Gebhardt [64]	1998	*In vitro*	Primary cultured rat hepatocytes	—	—	—	Inhibiting HMG CoA reductase and inhibiting the synthesis of cholesterol
Frank et al. [65]	2003	*In vivo*	Sprague-Dawley rats	—	—	—	Strengthening the activity of carnitine palmitoyl transferase (CPT)
Arion et al. [68]	1997	*In vitro*	Rat hepatic cells	—	—	—	CGA is the most specific T1 (the G-6-Pase transporter) inhibitor, and may inhibit hepatic G-6-Pase
Wang et al. [69]	2012	*In vivo*	Chemical-induced diabetic rats	T2DM	—	Exerting effects on improving blood glucose, TG, TC, and insulin sensitivity	Downregulating expression of G-6-pase and upregulating mRNA levels of GLUT4
Zhang et al. [17]	2011	*In vivo*	db/db mice	T2DM	—	Improvement of the disordered glucose/lipid metabolism	Upregulating expression of hepatic PPAR-α
Li et al. [76]	2009	*In vivo*	Golden hamsters fed on high-fat diet	T2DM	—	Modifying glucose and lipids metabolism	Upregulating expression of hepatic PPAR-α
Wan et al. [19]	2013	*In vivo*	Sprague-Dawley rats induced with a high-cholesterol diet	Hyperlipidemia	—	Altering the increased plasma total cholesterol and low-density lipoprotein but decreased HDL induced by a hypercholesterolemic diet with a dose-dependent improvement	Upregulating expression of hepatic PPAR-α

STZ: streptozotocin; NA: nicotinamide; CPT: carnitine palmitoyl transferase; HMG CoA reductase: β-hydroxy-β-methyl glutaric acyl coenzyme A reductase.

to elucidate both the short- and long-term effects of CGA on glucose and lipid metabolism. It is hoped that research concerning the mechanism of action of CGA on glucose and lipid metabolism will be developed in the future, and that information on the potential clinical applications of CGA will increase.

Abbreviations

AUC:	Areas under the curve
AOM:	Azoxymethane
b.w.:	Body weight
CaA:	Caffeic acid
CGA:	Chlorogenic acid
CH:	Cholesterol
CRA:	Chicoric acid
FFA:	Free fatty acid
GCE:	Green coffee bean extract
G-6-PASE:	Glucose-6-phosphatase
GIP:	Glucose-dependent insulinotropic peptide
HBV:	Hepatitis B virus
HDL:	High-density lipoprotein
HHQ:	Hydroxyhydroquinone
HOMA-IR:	Homeostasis model assessment for insulin resistance
MAPKs:	Mitogen-activated protein kinases
MMP:	Matrix metalloproteinase
NA:	Nicotinamide
NF-kappaB:	Nuclear transcription factor κB
ROS:	Reactive oxygen species
STZ:	Streptozotocin
TC:	Total cholesterol
TG:	Triacylglycerols
T2DM:	Type 2 diabetes mellitus
THC:	Tetrahydrocurcumin
TZD:	Thiazolidinedione.

Authors' Contribution

Shengxi Meng and Jianmei Cao contributed equally to this work.

Acknowledgment

This project was supported by the National Natural Science Foundation of China (no. 81173404).

References

[1] P. G. Kopelman, "Obesity as a medical problem," *Nature*, vol. 404, no. 6778, pp. 635–643, 2000.

[2] H. Ben-Ami, P. Nagachandran, A. Mendelson, and Y. Edoute, "Drug-induced hypoglycemic coma in 102 diabetic patients," *Archives of Internal Medicine*, vol. 159, no. 3, pp. 281–284, 1999.

[3] H. Yki-Järvinen, "Thiazolidinediones," *New England Journal of Medicine*, vol. 351, no. 11, pp. 1106–1158, 2004.

[4] A. M. Lincoff, K. Wolski, S. J. Nicholls, and S. E. Nissen, "Pioglitazone and risk of cardiovascular events in patients with type 2 diabetes mellitus: a meta-analysis of randomized trials," *Journal of the American Medical Association*, vol. 298, no. 10, pp. 1180–1188, 2007.

[5] M. R. Olthof, P. C. H. Hollman, M. B. Katan et al., "Chlorogenic acid and caffeic acid are absorbed in humans," *Journal of Nutrition*, vol. 131, no. 1, pp. 66–71, 2001.

[6] M. N. Clifford, "Chlorogenic acids and other cinnamates—nature, occurrence and dietary burden," *Journal of the Science of Food and Agriculture*, vol. 79, no. 3, pp. 362–372, 1999.

[7] M. N. Clifford, "Chlorogenic acids and other cinnamates—nature, occurrence, dietary burden, absorption and metabolism," *Journal of the Science of Food and Agriculture*, vol. 80, no. 7, pp. 1033–1043, 2000.

[8] Y. Kono, K. Kobayashi, S. Tagawa et al., "Antioxidant activity of polyphenolics in diets. Rate constants of reactions of chlorogenic acid and caffeic acid with reactive species of oxygen and nitrogen," *Biochimica et Biophysica Acta—General Subjects*, vol. 1335, no. 3, pp. 335–342, 1997.

[9] H. Kasai, S. Fukada, Z. Yamaizumi, S. Sugie, and H. Mori, "Action of chlorogenic acid in vegetables and fruits as an inhibitor of 8-hydroxydeoxyguanosine formation *in vitro* and in a rat carcinogenesis model," *Food and Chemical Toxicology*, vol. 38, no. 5, pp. 467–471, 2000.

[10] M. D. dos Santos, M. C. Almeida, N. P. Lopes, and G. E. P. de Souza, "Evaluation of the anti-inflammatory, analgesic and antipyretic activities of the natural polyphenol chlorogenic acid," *Biological and Pharmaceutical Bulletin*, vol. 29, no. 11, pp. 2236–2240, 2006.

[11] R. Feng, Y. Lu, L. L. Bowman, Y. Qian, V. Castranova, and M. Ding, "Inhibition of activator protein-1, NF-κB, and MAPKs and induction of phase 2 detoxifying enzyme activity by chlorogenic acid," *Journal of Biological Chemistry*, vol. 280, no. 30, pp. 27888–27895, 2005.

[12] B. K. Bassoli, P. Cassolla, G. R. Borba-Murad et al., "Chlorogenic acid reduces the plasma glucose peak in the oral glucose tolerance test: effects on hepatic glucose release and glycaemia," *Cell Biochemistry and Function*, vol. 26, no. 3, pp. 320–328, 2008.

[13] F.-L. Hsu, Y.-C. Chen, and J.-T. Cheng, "Caffeic acid as active principle from the fruit of Xanthium strumarium to lower plasma glucose in diabetic rats," *Planta Medica*, vol. 66, no. 3, pp. 228–230, 2000.

[14] D. V. Rodriguez de Sotillo and M. Hadley, "Chlorogenic acid modifies plasma and liver concentrations of: cholesterol, triacylglycerol, and minerals in (fa/fa) Zucker rats," *Journal of Nutritional Biochemistry*, vol. 13, no. 12, pp. 717–726, 2002.

[15] D. V. Rodriguez de Sotillo, M. Hadley, and J. E. Sotillo, "Insulin receptor exon 11+/- is expressed in Zucker (fa/fa) rats, and chlorogenic acid modifies their plasma insulin and liver protein and DNA," *Journal of Nutritional Biochemistry*, vol. 17, no. 1, pp. 63–71, 2006.

[16] P. Nicasio, L. Aguilar-Santamaría, E. Aranda, S. Ortiz, and M. González, "Hypoglycemic effect and chlorogenic acid content in two Cecropia species," *Phytotherapy Research*, vol. 19, no. 8, pp. 661–664, 2005.

[17] L.-T. Zhang, C.-Q. Chang, Y. Liu, and Z.-M. Chen, "Effect of chlorogenic acid on disordered glucose and lipid metabolism in db/db mice and its mechanism," *Acta Academiae Medicinae Sinicae*, vol. 33, no. 3, pp. 281–286, 2011 (Chinese).

[18] K. W. Ong, A. Hsu, and B. K. Tan, "Anti-diabetic and anti-lipidemic effects of chlorogenic acid are mediated by ampk activation," *Biochemical Pharmacology*, vol. 85, no. 9, pp. 1341–1351, 2013.

[19] C. W. Wan, C. N. Wong, W. K. Pin et al., "Exhibits cholesterol lowering and fatty liver attenuating properties by up-regulating the gene expression of PPAR-α," *Phytotherapy Research*, vol. 27, no. 4, pp. 545–551, 2013.

[20] Z. Z. Huang and C. Q. Chang, "Advances of study on glucose and lipids metabolism of chlorogenic acid regulating," *Journal of Hygiene Research*, vol. 37, no. 5, pp. 637–639, 2008 (Chinese).

[21] R. Gao, Y. N. Lin, G. Liang, and Y. Gao, "Absorption and metabolism of chlorogenic acid," *Chinese Journal of Experimental Traditional Medical Formulae*, vol. 18, no. 10, pp. 316–319, 2012 (Chinese).

[22] E. E. Agardh, S. Carlsson, A. Ahlbom et al., "Coffee consumption, type 2 diabetes and impaired glucose tolerance in Swedish men and women," *Journal of Internal Medicine*, vol. 255, no. 6, pp. 645–652, 2004.

[23] W.-Y. Lin, F. Xaiver Pi-Sunyer, C.-C. Chen et al., "Coffee consumption is inversely associated with type 2 diabetes in Chinese," *European Journal of Clinical Investigation*, vol. 41, no. 6, pp. 659–666, 2011.

[24] M. A. Pereira, E. D. Parker, and A. R. Folsom, "Coffee consumption and risk of type 2 diabetes mellitus: an 11-year prospective study of 28 812 postmenopausal women," *Archives of Internal Medicine*, vol. 166, no. 12, pp. 1311–1316, 2006.

[25] E. Salazar-Martinez, W. C. Willett, A. Ascherio et al., "Coffee consumption and risk for type 2 diabetes mellitus," *Annals of Internal Medicine*, vol. 140, no. 1, pp. 1–I17, 2004.

[26] J. Tuomilehto, G. Hu, S. Bidel, J. Lindström, and P. Jousilahti, "Coffee consumption and risk of type 2 diabetes mellitus among middle-aged finnish men and women," *Journal of the American Medical Association*, vol. 291, no. 10, pp. 1213–1219, 2004.

[27] R. M. van Dam, "Coffee consumption and risk of type 2 diabetes, cardiovascular diseases, and cancer," *Applied Physiology, Nutrition and Metabolism*, vol. 33, no. 6, pp. 1269–1283, 2008.

[28] R. M. van Dam and E. J. M. Feskens, "Coffee consumption and risk of type 2 diabetes mellitus," *The Lancet*, vol. 360, no. 9344, pp. 1477–1478, 2002.

[29] R. Huxley, C. M. Y. Lee, F. Barzi et al., "Coffee, decaffeinated coffee, and tea consumption in relation to incident type 2 diabetes mellitus: a systematic review with meta-analysis," *Archives of Internal Medicine*, vol. 169, no. 22, pp. 2053–2063, 2009.

[30] M. F. McCarty, "A chlorogenic acid-induced increase in GLP-1 production may mediate the impact of heavy coffee consumption on diabetes risk," *Medical Hypotheses*, vol. 64, no. 4, pp. 848–853, 2005.

[31] K. Karthikesan, L. Pari, and V. P. Menon, "Combined treatment of tetrahydrocurcumin and chlorogenic acid exerts potential antihyperglycemic effect on streptozotocin-nicotinamide-induced diabetic rats," *General Physiology and Biophysics*, vol. 29, no. 1, pp. 23–30, 2010.

[32] K. Karthikesan, L. Pari, and V. P. Menon, "Protective effect of tetrahydrocurcumin and chlorogenic acid against streptozotocin-nicotinamide generated oxidative stress induced diabetes," *Journal of Functional Foods*, vol. 2, no. 2, pp. 134–142, 2010.

[33] L. Pari, K. Karthikesan, and V. P. Menon, "Comparative and combined effect of chlorogenic acid and tetrahydrocurcumin on antioxidant disparities in chemical induced experimental diabetes," *Molecular and Cellular Biochemistry*, vol. 341, no. 1-2, pp. 109–117, 2010.

[34] A. J. Alonso-Castro, A. C. Miranda-Torres, M. M. González-Chávez, and L. A. Salazar-Olivo, "Cecropia obtusifolia Bertol and its active compound, chlorogenic acid, stimulate 2-NBDglucose uptake in both insulin-sensitive and insulin-resistant 3T3 adipocytes," *Journal of Ethnopharmacology*, vol. 120, no. 3, pp. 458–464, 2008.

[35] A. E. van Dijk, M. R. Olthof, J. C. Meeuse, E. Seebus, R. J. Heine, and R. M. van Dam, "Acute effects of decaffeinated coffee and the major coffee components chlorogenic acid and trigonelline on glucose tolerance," *Diabetes Care*, vol. 32, no. 6, pp. 1023–1025, 2009.

[36] M. J. Ahrens and D. L. Thompson, "Effect of Emulin on blood glucose in type 2 diabetics," *Journal of Medicinal Food*, vol. 16, no. 3, pp. 211–215, 2013.

[37] D. Tousch, A.-D. Lajoix, E. Hosy et al., "Chicoric acid, a new compound able to enhance insulin release and glucose uptake," *Biochemical and Biophysical Research Communications*, vol. 377, no. 1, pp. 131–135, 2008.

[38] K. L. Johnston, M. N. Clifford, and L. M. Morgan, "Coffee acutely modifies gastrointestinal hormone secretion and glucose tolerance in humans: glycemic effects of chlorogenic acid and caffeine," *American Journal of Clinical Nutrition*, vol. 78, no. 4, pp. 728–733, 2003.

[39] A. S. Attele, Y.-P. Zhou, J.-T. Xie et al., "Antidiabetic effects of *Panax ginseng* berry extract and the identification of an effective component," *Diabetes*, vol. 51, no. 6, pp. 1851–1858, 2002.

[40] P. Nicasio, L. Aguilar-Santamaría, E. Aranda, S. Ortiz, and M. González, "Hypoglycemic effect and chlorogenic acid content in two Cecropia species," *Phytotherapy Research*, vol. 19, no. 8, pp. 661–664, 2005.

[41] U. J. Jung, M.-K. Lee, Y. B. Park, S.-M. Jeon, and M.-S. Choi, "Antihyperglycemic and antioxidant properties of caffeic acid in db/db mice," *Journal of Pharmacology and Experimental Therapeutics*, vol. 318, no. 2, pp. 476–483, 2006.

[42] X. C. Liang, W. Meng, Y. L. Zhong et al., "Effects of chlorogenic acid on mouse insulin resistance development induced by high fat emulsion," *Chinese Pharmacological Bulletin*, vol. 29, no. 5, pp. 654–658, 2013 (Chinese).

[43] J. L. Goldstein, Y. K. Ho, S. K. Basu, and M. S. Brown, "Binding site on macrophages that mediates uptake and degradation of acetylated low density lipoprotein, producing massive cholesterol deposition," *Proceedings of the National Academy of Sciences of the United States of America*, vol. 76, no. 1, pp. 333–337, 1979.

[44] G. S. Yukawa, M. Mune, H. Otani et al., "Effects of coffee consumption on oxidative susceptibility of low-density lipoproteins and serum lipid levels in humans," *Biochemistry (Moscow)*, vol. 69, no. 1, pp. 70–74, 2004.

[45] J. A. N. Laranjinha, L. M. Almeida, and V. M. C. Madeira, "Reactivity of dietary phenolic acids with peroxyl radicals: antioxidant activity upon low density lipoprotein peroxidation," *Biochemical Pharmacology*, vol. 48, no. 3, pp. 487–494, 1994.

[46] H. Shimoda, E. Seki, and M. Aitani, "Inhibitory effect of green coffee bean extract on fat accumulation and body weight gain in mice," *BMC Complementary and Alternative Medicine*, vol. 6, article 9, 2006.

[47] A.-S. Cho, S.-M. Jeon, M.-J. Kim et al., "Chlorogenic acid exhibits anti-obesity property and improves lipid metabolism in high-fat diet-induced-obese mice," *Food and Chemical Toxicology*, vol. 48, no. 3, pp. 937–943, 2010.

[48] K. Karthikesan, L. Pari, and V. P. Menon, "Antihyperlipidemic effect of chlorogenic acid and tetrahydrocurcumin in rats subjected to diabetogenic agents," *Chemico-Biological Interactions*, vol. 188, no. 3, pp. 643–650, 2010.

[49] W. N. Li, Y. D. Han, Y. H. Liu et al., "Effects of Chlorogenic acid extract from leaves of Eucommia ulmoides on key enzyme activities in lipid metabolism," *Traditional Chinese Drug Research and Clinical Pharmacology*, vol. 23, no. 1, pp. 30–33, 2012 (Chinese).

[50] J. H. Wang, Y. L. Liu, C. L. Li et al., "Effect of chlorogenic acid extracted from Eucommia Ulmoides Oliv on hyperlipemia of mice induced by high fat diet," *Science and Technology of Food Industry*, no. 15, pp. 360–362, 2012 (Chinese).

[51] Y. Ebina, L. Ellis, and K. Jarnagin, "The human insulin receptor cDNA: the structural basis for hormone-activated transmembrane signalling," *Cell*, vol. 40, no. 4, pp. 747–758, 1985.

[52] Y. N. Zheng, K. Liu, G. Y. Jia et al., "Effect of hot-water extract of coffee seeds on postprandial blood glucose concentration in rats," *Chinese Pharmaceutical Journal*, vol. 42, no. 1, pp. 32–35, 2007 (Chinese).

[53] A. D. Mooradian and J. E. Thurman, "Drug therapy of postprandial hyperglycaemia," *Drugs*, vol. 57, no. 1, pp. 19–29, 1999.

[54] J. R. Gavin III, "Pathophysiologic mechanisms of postprandial hyperglycemia," *American Journal of Cardiology*, vol. 88, no. 6A, pp. 4H–8H, 2001.

[55] T. Matsui, I. A. Ogunwande, K. J. M. Abesundara, and K. Matsumoto, "Anti-hyperglycemic potential of natural products," *Mini-Reviews in Medicinal Chemistry*, vol. 6, no. 3, pp. 349–356, 2006.

[56] E. Sondheimer, "On the distribution of caffeic acid and the chlorogenic acid isomers in plants," *Archives of Biochemistry and Biophysics*, vol. 74, no. 1, pp. 131–138, 1958.

[57] M. F. McCarty, "Nutraceutical resources for diabetes prevention—an update," *Medical Hypotheses*, vol. 64, no. 1, pp. 151–158, 2005.

[58] K. L. Johnston, M. N. Clifford, and L. M. Morgan, "Coffee acutely modifies gastrointestinal hormone secretion and glucose tolerance in humans: glycemic effects of chlorogenic acid and caffeine," *American Journal of Clinical Nutrition*, vol. 78, no. 4, pp. 728–733, 2003.

[59] J. M. Tunnicliffe, L. K. Eller, R. A. Reimer, D. S. Hittel, and J. Shearer, "Chlorogenic acid differentially affects postprandial glucose and glucose-dependent insulinotropic polypeptide response in rats," *Applied Physiology, Nutrition and Metabolism*, vol. 36, no. 5, pp. 650–659, 2011.

[60] B. B. Kahn, T. Alquier, D. Carling, and D. G. Hardie, "AMP-activated protein kinase: ancient energy gauge provides clues to modern understanding of metabolism," *Cell Metabolism*, vol. 1, no. 1, pp. 15–25, 2005.

[61] E. J. Kurth-Kraczek, M. F. Hirshman, L. J. Goodyear, and W. W. Winder, "5' AMP-activated protein kinase activation causes GLUT4 translocation in skeletal muscle," *Diabetes*, vol. 48, no. 8, pp. 1667–1671, 1999.

[62] P. K. Prabhakar and M. Doble, "Synergistic effect of phytochemicals in combination with hypoglycemic drugs on glucose uptake in myotubes," *Phytomedicine*, vol. 16, no. 12, pp. 1119–1126, 2009.

[63] K. W. Ong, A. Hsu, and B. K. H. Tan, "Chlorogenic acid stimulates glucose transport in skeletal muscle via AMPK activation: a contributor to the beneficial effects of coffee on diabetes," *PLoS ONE*, vol. 7, no. 3, Article ID e32718, 2012.

[64] R. Gebhardt, "Inhibition of cholesterol biosynthesis in primary cultured rat hepatocytes by artichoke (Cynara scolymus L) extracts1," *Journal of Pharmacology and Experimental Therapeutics*, vol. 286, no. 3, pp. 1122–1128, 1998.

[65] J. Frank, A. Kamal-Eldin, A. Razdan, T. Lundh, and B. Vessby, "The dietary hydroxycinnamate caffeic acid and its conjugate chlorogenic acid increase vitamin E and cholesterol concentrations in Sprague-Dawley rats," *Journal of Agricultural and Food Chemistry*, vol. 51, no. 9, pp. 2526–2531, 2003.

[66] J. Y. Shin, J. Sohn, and K. H. Park, "Chlorogenic acid decreases retinal vascular hypermeability in diabetic rat model," *Journal of Korean Medical Science*, vol. 28, no. 4, pp. 608–613, 2013.

[67] A. W. Herling, D. Schwab, H.-J. Burger et al., "Prolonged blood glucose reduction in mrp-2 deficient rats (GY/TR-) by the glucose-6-phosphate translocase inhibitor S 3025," *Biochimica et Biophysica Acta—General Subjects*, vol. 1569, no. 1–3, pp. 105–110, 2002.

[68] W. J. Arion, W. K. Canfield, F. C. Ramos et al., "Chlorogenic acid and hydroxynitrobenzaldehyde: new inhibitors of hepatic glucose 6-phosphatase," *Archives of Biochemistry and Biophysics*, vol. 339, no. 2, pp. 315–322, 1997.

[69] Y. Wang, L. Huang, Y. L. Zhong et al., "Effects of three kinds of dietary polyphenolyphenols on glucose and lipid metabolism in chemical-induced diabetic rats," *Acta Nutrimenta Sinica*, vol. 34, no. 6, pp. 572–575, 2012.

[70] A. W. Herling, H.-J. Burger, G. Schubert, H. Hemmerle, H.-L. Schaefer, and W. Kramer, "Alterations of carbohydrate and lipid intermediary metabolism during inhibition of glucose-6-phosphatase in rats," *European Journal of Pharmacology*, vol. 386, no. 1, pp. 75–82, 1999.

[71] H. Hemmerle, H.-J. Burger, P. Below et al., "Chlorogenic acid and synthetic chlorogenic acid derivatives: novel inhibitors of hepatic glucose-6-phosphate translocase," *Journal of Medicinal Chemistry*, vol. 40, no. 2, pp. 137–145, 1997.

[72] C. Simon, A. W. Herling, G. Preibisch, and H.-J. Burger, "Upregulation of hepatic glucose 6-phosphatase gene expression in rats treated with an inhibitor of glucose-6-phosphate translocase," *Archives of Biochemistry and Biophysics*, vol. 373, no. 2, pp. 418–428, 2000.

[73] R. A. DeFronzo, E. Ferrannini, D. C. Simonson et al., "Fasting hyperglycemia in non-insulin-dependent diabetes mellitus: contributions of excessive hepatic glucose production and impaired tissue glucose uptake," *Metabolism: Clinical and Experimental*, vol. 38, no. 4, pp. 387–395, 1989.

[74] T. H. van Dijk, F. H. van der Sluijs, C. H. Wiegman et al., "Acute inhibition of hepatic glucose-6-phosphatase does not affect gluconeogenesis but directs gluconeogenic flux toward glycogen in fasted rats. A pharmacological study with the chlorogenic acid derivative S4048," *Journal of Biological Chemistry*, vol. 276, no. 28, pp. 25727–25735, 2001.

[75] A. Andrade-Cetto and H. Wiedenfeld, "Hypoglycemic effect of Cecropia obtusifolia on streptozotocin diabetic rats," *Journal of Ethnopharmacology*, vol. 78, no. 2-3, pp. 145–149, 2001.

[76] S.-Y. Li, C.-Q. Chang, F.-Y. Ma, and C.-L. Yu, "Modulating effects of chlorogenic acid on lipids and glucose metabolism and expression of hepatic peroxisome proliferator-activated receptor-α in golden hamsters fed on high fat diet," *Biomedical and Environmental Sciences*, vol. 22, no. 2, pp. 122–129, 2009.

[77] S. Y. Li, *Study of Chlorogenic Acid on Influence of Lipid Metabolism, Glucose Metabolism and Atherosclerosis and Its Mechanism in High Fat Diet*, Peking University, Beijing, China, 2007, (Chinese).

Hindawi Publishing Corporation
Evidence-Based Complementary and Alternative Medicine
Volume 2013, Article ID 643403, 6 pages
http://dx.doi.org/10.1155/2013/643403

Research Article

Specificity of Sensory and Motor Neurons Associated with BL40 and GB30 in the Rat: A Dual Fluorescent Labeling Study

Jingjing Cui,[1] Lijuan Ha,[2] Xinlong Zhu,[1] Fuchun Wang,[2] Xianghong Jing,[1] and Wanzhu Bai[1]

[1] *Institute of Acupuncture and Moxibustion, China Academy of Chinese Medical Sciences, Beijing 100700, China*
[2] *Changchun University of Chinese Medicine, Changchun 130117, China*

Correspondence should be addressed to Wanzhu Bai; wanzhubaisy@hotmail.com

Received 5 June 2013; Accepted 23 July 2013

Academic Editor: Yong-Qing Yang

The purpose of this study is to investigate the specific innervations on "Weizhong" (BL40) and "Huantiao" (GB30) by using a dual neural tracing technique. After Alexa Fluor 488 and 594 conjugates of cholera toxin subunit B (AF488/594-CTB) were, respectively, injected into BL40 and GB30 in the same rat, the labeled sensory and motor neurons were examined in the rat's dorsal root ganglia (DRGs) and spinal cord at thoracic (T) and lumbar (L) segments with a laser scanning confocal microscope. In the cases of BL40 injection, AF488-CTB labeled sensory and motor neurons were located in L_{2-6} DRGs and on the mediolateral part of spinal ventral horn from L_3 to L_5 segments, respectively. By contrast, in the cases of GB30 injection, AF594-CTB labeled sensory and motor neurons were distributed in T_{13}–L_6 DRGs and on the anterolateral part of spinal ventral horn from L_1 to L_5 segments, respectively. These results indicate that the sensory and motor neurons associated with BL40 and GB30 are located in different spinal segments and regions in the nervous system, providing the neuroanatomical evidence to serve the specificity of acupoints.

1. Introduction

Both "Weizhong" (BL40) and "Huantiao" (GB30) are commonly used for acupuncture treatment on lumbar and lower limb disorders [1–3], which could be traced back to "A Verse on the Twelve Heaven-Star Points" compiled by Ma Danyang in Song dynasty, showing its important historical position in acupuncture treatment. Although BL40 and GB30 play active roles in treating common ailments, such as sciatica, lumbar intervertebral disc herniation, and muscle strain [1–3], the underlying mechanism for their effectiveness remains unclear. Recent studies suggest that the effect of acupuncture is highly correlated with the activation of the nervous system [4–8]. Thus, to understand the neural properties of different acupoints may play a pivotal role in exploring the mechanism of acupuncture. In line with this kind of studies, how to apply an effective approach for further investigating the specific innervations on different acupoints is an important task to know the specificity of acupoints.

Since neural tracing technique was introduced into the acupuncture research, it has opened a new field to understand the neural properties of acupoints at the cellular level, especially the sensory and motor innervation on acupoints [9–11]. As a new generation of sensitive tracer [12, 13], Alexa Fluor 488 and 594 conjugates of cholera toxin subunit B (AF488/594-CTB) have been proven to be a potential approach in morphological study on the neural properties of acupoints [14, 15]. In order to reveal the characteristics of the neurons related to different acupoints, in this study, BL40 and GB30 were, respectively, labeled AF488/594-CTB in rats. By using this neural tracing technique, the distribution of the sensory and motor neurons associated with BL40 and GB30 could be revealed, which should benefit the understanding of the specificity of acupoints from the perspective of neuroanatomy.

2. Material and Methods

2.1. Subjects. Four adult male Sprague Dawley rats (6-7 weeks old, weight 225 ± 25 g) at clean level were used in the present study. Experimental animals were provided by the Institute of Laboratory Animal Sciences, Chinese Academy of Medical

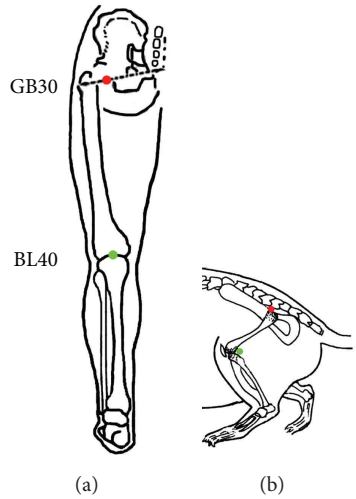

Figure 1: Illustration of the acupoints of Huantiao (GB30, red) and Weizhong (BL40, green) in human (a) and rat (b).

Sciences. The license number is SCKX (JUN) 2007-004. All animals were housed in a 12 h light/dark cycle with controlled temperature and humidity and allowed free access to food and water. The handling and care of experimental animals conformed to the regulations provided by the National Institutes of Health Guide for the Care and Use of Laboratory Animals [16].

2.2. Research Protocol

2.2.1. Microinjection of AF488/594-CTB. Injection was performed on both BL40 and GB30 in the same rat. Based on the classification of traditional Chinese medicine, BL40 belongs to the bladder meridian of foot Taiyang and GB30 is located on the gallbladder meridian of foot Shaoyang. The AF488/594-CTB (Invitrogen-Molecular Probes, Eugene, OR, USA) were used as tracers to, respectively, determine the distribution of neurons related to BL40 and GB30. According to the principle of comparative anatomy, BL40 is located at the midpoint of the popliteal crease, and GB30 is situated at the junction of the lateral 1/3 and medial 2/3 of the line connecting the prominence of greater trochanter of femur with the sacral hiatus on the rat, corresponding to BL40 and GB30 on the human body (Figure 1). Under anesthesia with isoflurane (Litian, Jiupai Pharmaceutical Co. Ltd, Hebei, China) controlled by small animal anesthesia machine (VMR, Matrx, Midmark, USA), 8 μL of 0.1% AF488/594-CTB were, respectively, injected into BL40 and GB30 on the left side with 10 μL Hamilton syringe. The depth of injection was 4-5 mm. In order to prevent leakage of solution, the needle was kept for 1 min after injection and then slowly pulled out. When the rats awoke from anesthesia, they were put back in their cages.

2.2.2. Perfusion. Three days (72 h) after injection, the rats were deeply anaesthetized by ether and transcardially perfused with 150 mL of 0.9% saline immediately followed by 300 mL of 4% paraformaldehyde in 0.1 M phosphate buffered solution (PB, pH 7.4). After perfusion, dorsal root ganglia (DRGs) and spinal cord from thoracic (T) 10 to lumbar (L) 6 segments were dissected out and put into the same fixative solution about 2–4 h, then changed into 25% sucrose PB (0.1 M, pH 7.4) at 4°C, and allowed to sink. The tissue on injection site was also dissected out for observing the local diffusion of tracers. The level of spinal segments was determined cytoarchitecturally, referred as to *The Rat Brain in Stereotaxic Coordinates* [17].

2.2.3. Section. Serial sagittal sections of DRGs and transverse sections of spinal cord were cut at a thickness of 40 μm on a freezing microtome (Thermo, Microm International GmbH, Germany). All sections were collected in order in a six-hole Petri dish with in 0.1 M PB (pH 7.4) and then stored in the refrigerator at 4°C.

Before observation, the sections were mounted on the microscope slides and coverslipped with 50% glycerin to improve visualization of labeling.

2.2.4. Observation. The tissue samples were observed and recorded with a laser scanning confocal microscope (FV1000, Olympus Co., Tokyo, Japan). Digital images were then processed with Adobe Photoshop CS2 (Adobe Systems, San Jose, CA, USA).

2.2.5. Statistical Analysis. Data was expressed as mean ± standard deviation and processed with the statistical software SPSS 16.0.

3. Results

The labeled sensory and motor neurons with AF488/594-CTB were located ipsilaterally on the injection side, in which AF488-CTB labeling was demonstrated in fluorescent green, and AF594-CTB was shown in fluorescent red (Figure 2). The neurons associated with BL40 and GB30 were distributed separately on the thoracic and lumbar DRGs and spinal cord. No neural labeling was observed above the level of spinal cord. The segmental and regional distribution of the sensory and motor neurons associated with BL40 and GB30 was summarized in Figure 3.

3.1. Sensory Innervation. In the cases of BL40 injection, the AF488-CTB labeled sensory neurons were detected in L_2–L_6 DRGs with high concentration in L_5 DRGs (Figures 2(A) and 3). By contrast, in the cases of GB30 injection, the AF594-CTB labeled sensory neurons were detected in the T_{13}–L_6 DRGs with high concentration in L_4 DRGs (Figures 2(A1) and 3). No double labeled sensory neurons were detected (Figure 2(A2)). In the four rats, a total of 538 AF488-CTB labeled sensory neurons (BL40) and 866 AF594-CTB labeled sensory neurons (GB30) were counted in the DRGs and arranged in order at different segments (Figure 4).

According to the size of soma diameter, the labeled sensory neurons were assigned to three classes: the large one (soma diameter > 50 μm), the medium one (soma diameter between 30 μm and 50 μm), or the small one

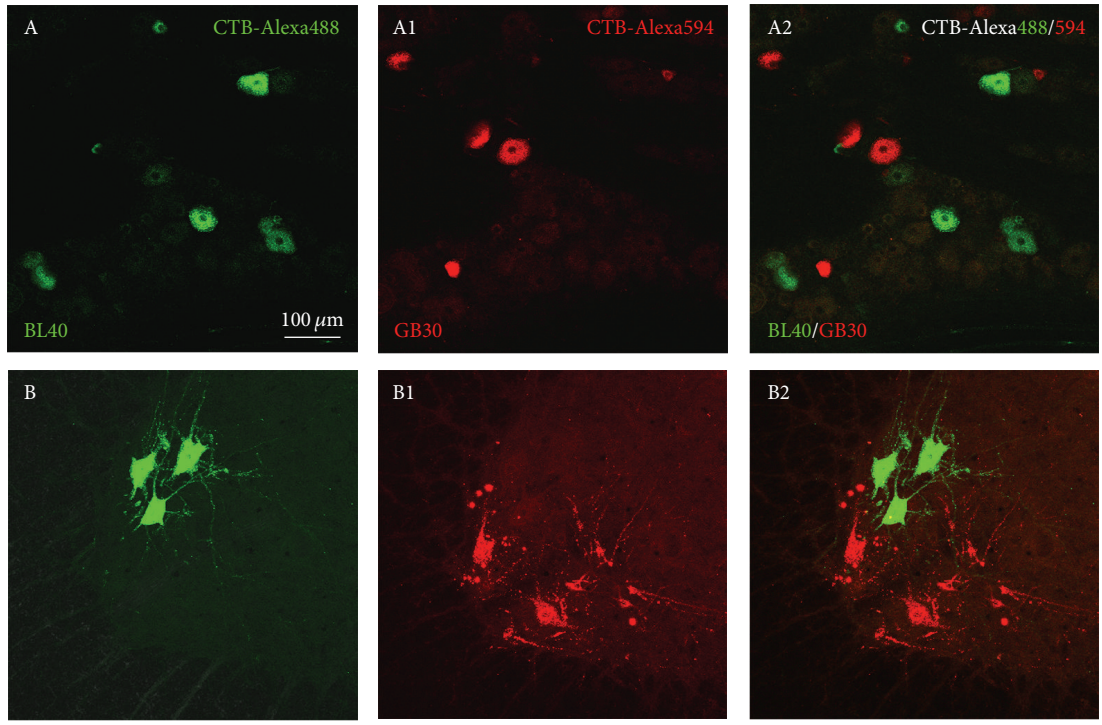

Figure 2: Representative sections from lumbar 4 dorsal root ganglion (DRG) and spinal cord showing the distribution of the labeled sensory neurons in DRG (A–A2) and motor neurons in spinal ventral horn (B–B2) after respective injection of AF488-CTB and AF594-CTB into BL40 and GB30 in the same rat. A, B: AF488-CTB labeled sensory (A) and motor (B) neurons related to BL40; A1, B1: AF594-CTB labeled sensory (A1) and motor (B1) neurons related to GB30; A2, B2: merged photo from A and A1(A2), B and B1(B2). Scale bar for all photos shown in A.

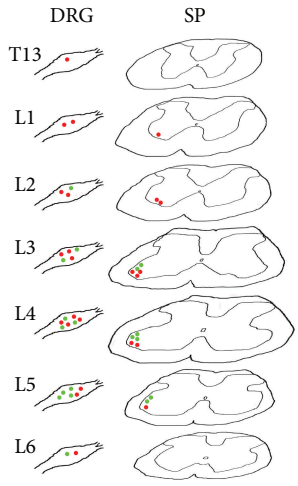

Figure 3: A series of line drawings through seven levels of dorsal root ganglia (DRGs) and approximately equal levels of spinal cord (SP) from thoracic (T) 13 to lumbar (L) 6 spinal segments showing the segmental and regional distribution of the sensory and motor neurons associated with BL40 (green) and GB30 (red), respectively.

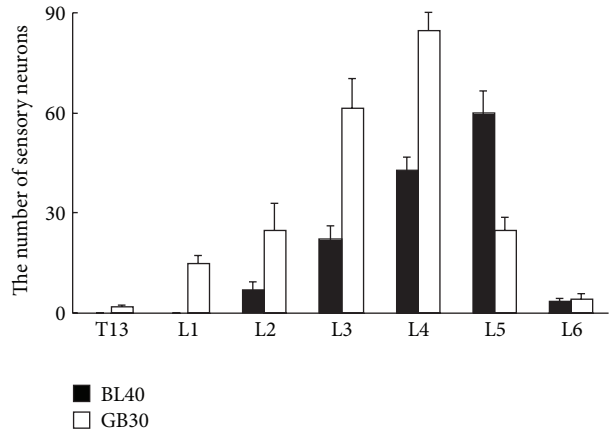

Figure 4: The average number of the AF488-CTB and AF594-CTB labeled sensory neurons in the DRGs ranging from thoracic (T) 13 to lumbar (L) 6 segments (mean ± standard deviation, $n = 4$), in which the sensory neurons associated with BL40 were distributed from L2 to L6 segments and those of GB30 distributed from T13 to L6.

(soma diameter < 30 μm) [18]. In both BL40 and GB30 injections, the small- and medium-sized sensory neurons each represented over 40% of the labeled neurons (Table 1).

3.2. Motor Innervation. In the cases of BL40 injection, the AF488-CTB labeled motor neurons were distributed on the mediolateral part of spinal ventral horn from L_3 to L_5 segments and concentrated at L_4 segment (Figures 2(B) and 3). By contrast, in the cases of GB30 injection, the AF594-CTB

Table 1: Numbers and proportions of large-, medium-, and small-sized sensory neurons associated with BL40 and GB30 in the DRGs (number (%)).

Sensory neurons in the DRGs	BL40	GB30
Large-sized neuron	58 (10.78%)	149 (17.21%)
Medium-sized neuron	222 (41.26%)	357 (41.22%)
Small-sized neuron	258 (47.96%)	360 (41.57%)

labeled motor neurons were distributed on the anterolateral part of spinal ventral horn from L_1 to L_5 segments with high concentration at L_3 segment (Figures 2(B1) and 3). No double labeled motor neurons were observed (Figure 2(B2)). Because there is no distinct boundary among the different spinal segments, the figures were shown at approximate segment of spinal cord, and the labeled motor neurons were not counted separately.

According to the size of soma diameter, the labeled motor neurons were divided into two classes: the large one (soma diameter > 25 μm) or the small one (soma diameter ≤ 25 μm), belonging to α and γ motor neurons, respectively [19]. The approximate 60 transverse sections from spinal cord were counted on every rat, resulting in a total of 136 AF488-CTB labeled motor neurons (BL40) and 174 AF594-CTB labeled motor neurons (GB30). The large- and small-sized motor neurons, respectively, represented 98.53% (134/136) and 1.47% (2/136) in the cases of BL40 injection and 92.53% (161/174) and 7.47% (13/174) in the cases of GB30 injection.

In addition, around the injection site, AF488-CTB and AF594-CTB were diffused in the muscles and subcutaneous tissues, but the scope of local diffusion was not over 1 mm from the center of injection site.

4. Discussion

By using a dual fluorescent labeling technique with AF488/594-CTB, we successfully revealed that the sensory and motor neurons associated with BL40 and GB30 were distributed separately in DRGs and spinal cord in rats, in which the segmental and regional arranged neurons closely correspond with individual acupoint, providing the neuroanatomical evidence to serve the specificity of acupoints.

4.1. Technical Considerations. Recently, AF488/594-CTB are increasingly used for tracing the neural pathway in neuroscience research [12, 13]. Our recent studies also suggested that the technique of AF488/594-CTB is a proper choice to investigate the neural properties of different acupoints [14, 15]. Compared with tracers previously used in this field, such as propidium iodide (PI) and bisbenzimide (Bb) [20–22], the main advantages of AF488/594-CTB are their sensitivity and fluorescence persistence. Because the spectral range of specific fluorescent materials carried by AF488/594-CTB is concentrated and corresponds with the stimulating lights of a laser scanning confocal microscope, its neural labeling is more easily observed and identified without disturbance of nonspecific fluorescence labeling as observed with that of PI and Bb labeling [20–22]. Although it does not need complex staining processes to detect neural labeling of AF488/594-CTB like that of Horseradish Peroxidase (HRP) [11], it should be noted that AF488/594-CTB are only limited to the application of retrograde labeling the sensory and motor neurons in the tracing study and cannot be used for labeling transganglionic axonal terminals like that of HRP. Nevertheless, the present results provided sufficient evidence to propose that AF488/594-CTB are a suitable couple for dual fluorescent labeling in morphological research of acupuncture.

4.2. Distribution of Sensory and Motor Neurons. Previous topographic studies have shown that BL40 and GB30 are highly correlated with the tibial nerve and sciatic nerve, respectively, at the level of gross anatomy [23, 24]. However, at the cellular level, we still do not know the distribution of the sensory and motor neurons associated with both acupoints in the nervous system. In this study, we demonstrated that neurons related to BL40 and GB30 were distributed in a definite segmental and regional pattern, in which the sensory and motor neurons associated with GB30 distributed more extensively and higher than those of BL40 about one or two segments in DRGs and spinal ventral horn (Figure 3). Although with a part of segmental overlap, there were no dual labeled neurons in the present study. Thus it could be concluded that BL40 and GB30 received innervations from different sensory and motor neurons. In addition, the motor neurons related to BL40 and GB30 were distributed in the mediolateral and anterolateral regions of spinal ventral horn, respectively. This regional arrangement also supports the idea that the innervations on different acupoints originate from different neurons.

It has been shown that peripheral areas on the body correlate orderly with the nervous system, which was named somatotopic organization [25–27]. Without exception, as a point of peripheral areas, every acupoint has its own corresponding neurons in the nervous system. Considering the distances from BL40 and GB30 to the truck of body, it is clear that the closer to the body trunk the acupoint is, the higher the neurons associated with the corresponding acupoint situate in the spinal segment. Similar results were also demonstrated in our previous observations on the acupoints of "Taixi" (KI3), "Chengshan" (BL 57), "Jinggu" (BL64), and "Dazhong" (KI4) [11, 14, 15]. Through these neural tracing studies on the different acupoints, we can speculate the innervations on acupoints according to their locations on the proximal, mid, and distal parts of hindlimb. Therefore, from the perspective of neuroanatomy, this study increases our understanding of the regular connections between the different acupoints and the nervous system.

4.3. The Subtype of Sensory and Motor Neurons. Large-, medium-, and small-sized sensory neurons were simultaneously labeled in both cases of BL40 and GB30 injections, which roughly correspond to Aα/Aβ-, Aδ-, and C-fibers, respectively [18, 28]. These three types of sensory neurons may play different roles in the processing of signals transmission due to their electrophysiological properties [29–31]. It was suggested that Aα/Aβ-type fibers transmit messages of tactile sensation and proprioception, while Aδ- and C-type fibers

relay messages of nociception and thermal sensation [29–31]. Since different kinds of sensory neurons directly innervate the acupoints, it may be an important implication for further considering roles of these subtype neurons in the process of acupuncture stimulation. Besides the different kinds of sensory neurons, both α and γ motor neurons also participate in innervation on the BL40 and GB30. It should be another important consideration on the neural properties of different acupoints. Although we only provided the neuroanatomical evidence of BL40 and GB30 in this study, these results have served as a source of inspiration for investigating the specificity of acupoints at the cellular level.

4.4. The Significance for Clinical Practice. The relative specificity of acupoints is an important issue in the clinical treatment. To understand the neural properties of BL40 or GB30 should be of benefit for us to select proper one for acupuncture treatment according to the patient's symptoms. Given that the neurons associated with BL40 and GB30 concentrate on different spinal segments, we suggest that when the lumbar disorder occurred on L_4, GB30 was recommended as main acupoint, while if it occurred on L_5, BL40 was recommended. We can also simultaneously select both GB30 and BL40 to treat the ailment involving multiple spinal segments. Although this implication was supported by the perspective of neural pathway from the different acupoints to the nervous system, it remains to be verified in clinical practice.

5. Conclusion

In summary, we successfully demonstrated the specificity of distribution and subtype of the sensory and motor neurons associated with BL40 and GB30 in the rat by using a dual fluorescent labeling technique with AF488/594-CTB. These results suggest that regular connections between the different acupoints and the nervous system should be an important consideration during the acupuncture treatment.

Acknowledgments

This study was funded by the National Natural Science Foundation of China (Project no. 81072759) and the National Basic Research Program of China (973 Program, no. 2010CB530507; no. 2011CB505201) and the Self-Selected Research Program from China Academy of Chinese Medical Sciences (no. 2009Z02024).

References

[1] R. Q. Gao, "168 cases of acupuncturing Huantiao and Weizhong on sciatica," *Hebei Journal of Traditional Chinese Medicine*, vol. 24, no. 1, p. 41, 2002.

[2] R. Zou, Y. Xu, and H. Zhang, "Evaluation on analgesic effect of electroacupuncture combined with acupoint-injection in treating lumbar intervertebral disc herniation," *China Journal of Orthopaedics and Traumatology*, vol. 22, no. 10, pp. 759–761, 2009.

[3] M. Hu and R. Zhang, "Clinical observation on warming-promotion acupuncture for lumbar muscle strain," *Chinese Acupuncture & Moxibustion*, vol. 31, no. 7, pp. 622–624, 2011.

[4] Z. Zhao, "Neural mechanism underlying acupuncture analgesia," *Progress in Neurobiology*, vol. 85, no. 4, pp. 355–375, 2008.

[5] C. Y. Chen, R. S. Chern, M. H. Liao, Y. H. Chang, J. Y. C. Hsu, and C. H. Chien, "The possible neuronal mechanism of acupuncture: morphological evidence of the neuronal connection between groin A-shi point and uterus," *Evidence-Based Complementary and Alternative Medicine*, vol. 2013, Article ID 429186, 13 pages, 2013.

[6] S. X. Ma, "Neurobiology of acupuncture: toward CAM," *Evidence-Based Complementary and Alternative Medicine*, vol. 1, no. 1, pp. 41–47, 2004.

[7] S. Uchida and H. Hotta, "Acupuncture affects regional blood flow in various organs," *Evidence-Based Complementary and Alternative Medicine*, vol. 5, no. 2, pp. 145–151, 2008.

[8] Z. Zhang, X. Wang, and G. M. McAlonan, "Neural acupuncture unit: a new concept for interpreting effects and mechanisms of acupuncture," *Evidence-Based Complementary and Alternative Medicine*, vol. 2012, Article ID 429412, 23 pages, 2012.

[9] Z. L. Tao, Z. P. Zhang, L. P. Wang, C. H. Li, and B. Z. Wen, "The segmentation of the afferent neurons of the area of 'Zusanli'," *Acupuncture Research*, vol. 8, no. 2, pp. 136–140, 1983.

[10] S. Y. Xi and Z. L. Tao, "Afferent fibers of the points of three Yang channels of the foot in the lower limbs projected to the spinal cord and medulla oblongata," *Acupuncture Research*, no. 2, pp. 130–134, 1983.

[11] J. Jiang, W. Bai, L. Zhang, X. Jing, and Z. Jin, "Segmental and regional innervation of acupoint "Taixi" (KI 3) area in the rat: a horseradish peroxidase method study," *Acupuncture Research*, vol. 35, no. 1, pp. 27–36, 2010.

[12] W. L. Conte, H. Kamishina, and R. L. Reep, "Multiple neuroanatomical tract-tracing using fluorescent Alexa Fluor conjugates of cholera toxin subunit B in rats," *Nature Protocols*, vol. 4, no. 8, pp. 1157–1166, 2009.

[13] J. A. Christianson, R. Liang, E. E. Ustinova, B. M. Davis, M. O. Fraser, and M. A. Pezzone, "Convergence of bladder and colon sensory innervation occurs at the primary afferent level," *Pain*, vol. 128, no. 3, pp. 235–243, 2007.

[14] X. Zhu, W. Bai, F. Wu, J. Jiang, and X. Jing, "Neuroanatomical characteristics of acupoint "Chengshan" (BL 57) in the rat: a cholera toxin subunit B conjugated with Alexa Fluor 488 method study," *Acupuncture Research*, vol. 35, no. 6, pp. 433–437, 2010.

[15] J. Cui, X. Zhu, C. Ji, X. Jing, and W. Bai, "Neuroanatomical basis of clinical joint application of "Jinggu" (BL 64, a source-acupoint) and "Dazhong" (KI 4, a Luo-acupoint) in the rat: a double-labeling study of cholera toxin subunit B conjugated with Alexa Fluor 488 and 594," *Acupuncture Research*, vol. 36, no. 4, pp. 262–267, 2011.

[16] National Research Council, *Guide for the Care and Use of Laboratory Animals*, National Academic Press, Washington, DC, USA, 1996.

[17] G. Paxinos and C. Watson, *The Rat Brain in Stereotaxic Coordinates*, Academic Press, San Diego, Calif, USA, 1998.

[18] J. M. Caffrey, D. L. Eng, J. A. Black, S. G. Waxman, and J. D. Kocsis, "Three types of sodium channels in adult rat dorsal root ganglion neurons," *Brain Research*, vol. 592, no. 1-2, pp. 283–297, 1992.

[19] R. R. Roy, A. Matsumoto, H. Zhong, A. Ishihara, and V. R. Edgerton, "Rat α- and γ-motoneuron soma size and succinate dehydrogenase activity are independent of neuromuscular activity level," *Muscle and Nerve*, vol. 36, no. 2, pp. 234–241, 2007.

[20] C. G. Tong, S. Z. Gu, H. Q. Yi, C. Q. Guo, X. R. Xiang, and B. Xu, "Research on the specific pathways connecting stomach and its Back-Shu and Front-Mu points by using fluorescent double labeling method," *Shanghai Journal of Acupuncture and Moxibustion*, vol. 22, no. 5, pp. 16–19, 2003.

[21] J. L. Zhang, S. P. Chen, and J. L. Liu, "Research on the connection pathway between "Tianquan" (PC 2) of the "Pericardium Meridian" and the heart in the cat," *Acupuncture Research*, vol. 27, no. 2, pp. 124–129, 2002.

[22] L. Zhang, J. Jiang, Z. Jin, and J. Liu, "Afferent nerve connection among "Hegu" (LI4), "Neiguan" (PC6), "Futu" (LI18) and thyroid gland region: fluorescent double labelling method," *Acupuncture Research*, vol. 35, no. 6, pp. 438–442, 2010.

[23] H. R. Cui, X. F. Lou, K. Y. Dai, S. W. Hu, S. H. Jiang, and X. D. Yang, "Topographic research of Weizhong Acupoint (BL40) and its clinical significance," *Journal of Wenzhou Medical College*, vol. 37, no. 3, pp. 224–226, 2007.

[24] W. X. Qiu, S. X. Duan, L. P. Hou et al., "Anatomical research of Huantiao Acupoint (GB30) and the sciatic nerve," *Journal of Clinical Acupuncture and Moxibustion*, vol. 15, no. 4, pp. 57–58, 1999.

[25] C. Rivero-Melian, "Organization of hindlimb nerve projections to the rat spinal cord: a choleragenoid horseradish peroxidase study," *The Journal of Comparative Neurology*, vol. 364, no. 4, pp. 651–663, 1996.

[26] C. Molander and G. Grant, "Laminar distribution and somatotopic organization of primary afferent fibers from hindlimb nerves in the dorsal horn. A study by transganglionic transport of horseradish peroxidase in the rat," *Neuroscience*, vol. 19, no. 1, pp. 297–312, 1986.

[27] Y. Takahashi, T. Chiba, M. Kurokawa, and Y. Aoki, "Dermatomes and the central organization of dermatomes and body surface regions in the spinal cord dorsal horn in rats," *Journal of Comparative Neurology*, vol. 462, no. 1, pp. 29–41, 2003.

[28] A. A. Harper and S. N. Lawson, "Conduction velocity is related to morphological cell type in rat dorsal root ganglion neurones," *Journal of Physiology*, vol. 359, pp. 31–46, 1985.

[29] T. L. Yaksh and D. L. Hammond, "Peripheral and central substrates involved in the Rostrad transmission of nociceptive information," *Pain*, vol. 13, no. 1, pp. 1–85, 1982.

[30] A. A. Harper and S. N. Lawson, "Electrical properties of rat dorsal root ganglion neurones with different peripheral nerve conduction velocities," *Journal of Physiology*, vol. 359, pp. 47–63, 1985.

[31] P. J. Waddell and S. N. Lawson, "Electrophsyiological properties of subpopulations of rat dorsal root ganglion neurons in vitro," *Neuroscience*, vol. 36, no. 3, pp. 811–822, 1990.

Hindawi Publishing Corporation
Evidence-Based Complementary and Alternative Medicine
Volume 2013, Article ID 547837, 9 pages
http://dx.doi.org/10.1155/2013/547837

Research Article

Specific Link between Lung and Large Intestine: A New Perspective on Neuropeptide Secretion in Lung with Herbal Laxative Stimulation

Xiang-Gen Zhong, Feng-Jie Zheng, Yu-Hang Li, Hong Xu, Qian Wang, Yu-Chao Liu, Miao Liu, Ruo-Han Wu, Yu-Shan Gao, Shu-Jing Zhang, Jin-Chao Zhang, Tian-Yu Zhang, and Si-Hua Gao

School of Preclinical Medicine, Beijing University of Chinese Medicine, Beijing 100029, China

Correspondence should be addressed to Yu-Hang Li; liyuhang@bucm.edu.cn and Si-Hua Gao; gaosihua1216@163.com

Received 7 June 2013; Accepted 19 July 2013

Academic Editor: Yong-Qing Yang

Background. To investigate the specific link between lung and large intestine. *Methods*. Rat COPD-like model was prepared. Mirabilite or Chinese rhubarb was administrated intragastrically to stimulate the large intestine. Histological analysis of lung inflammation was assessed. The tissues levels of SP, VIP, NK1R, VIPR1, and VIPR2 were measured by using ELISA kits. In addition, mouse model of allergic asthma was prepared. Mirabilite was administrated intragastrically to stimulate the large intestine. Airway responsiveness and lung inflammation were assessed. The tissues levels of SP, VIP, NKA, NKB, NK1R, VIPR1, and VIPR2 were measured by using ELISA kits. *Results*. Stimulating the intestine with Mangxiao or Dahuang, SP, NK-1R, VIP, VIPR1, and VIPR2 were significantly increased in intestine tissues of rats with COPD and mice with asthma. Meanwhile, the SP and NK1R were significantly decreased, while VIP, VIPR1, and VIPR2 were significantly increased in lung tissues. An abnormal secretion of SP and VIP can be observed in other tissues; however, no marked changes were found in the receptors. The NKA and NKB levels were similar in lung tissues of mice with asthma among groups. *Conclusions*. Stimulating intestine with Mangxiao or Dahuang can specifically regulate the secretion of SP, VIP, and the receptors in lung tissues.

1. Introduction

Traditional Chinese medicine (TCM) is characterized by its unique system of therapies and theories. The theory of exterior-interior correlation between the lung and large intestine is one of the most important components of the TCM Zang-Fu theory, which has been widely applied in TCM clinical practice, particularly in the treatments of the lung-intestine diseases, such as COPD and asthma [1]. Over thousands of years, TCM doctors have been continuously exploring the practical implication and application of the theory. They found that the significance of the theory is demonstrated in the explanation of lung and large intestine physiological functions.

Recent studies have proved the relationship between lung and large intestine from various perspectives, such as embryonic development, lymph circulation, mucosal immunity, micro ecology, and inflammatory harass [2, 3]. However, this exterior-interior relationship between lung and large intestine still has not been completely explicated. Further research on this theory from a biological point of view is necessary, which we believe might provide new valuable references for the treatment strategies for lung-intestine diseases.

Relaxing the bowels with laxative is one of the common treating methods for lung diseases based on the theory of exterior-interior correlation between lung and large intestine. Our previous studies found that Chinese Rhubarb (Dahuang) could not only effectively improve the intestinal obstruction in COPD patients and rats with COPD but also effectively improve the dyspnea and gas exchange function [4, 5], and this effect was related to the changes of neuropeptide levels in the blood [6]. Therefore, we hypothesized that stimulus of intestinal track, like herbal laxatives (osmotic or stimulant),

Table 1: SP levels in lung, large intestine, stomach, kidney, spleen, heart, brain, and liver tissues of COPD-like rats (pg/ug, mean ± SD).

Groups	n	Lung	Large intestine	Stomach	Kidney	Spleen	Heart	Brain	Liver
Control group	6	0.78 ± 0.07	14.54 ± 3.53	10.51 ± 3.36	102.15 ± 10.67	1.78 ± 0.69	23.50 ± 6.29	2.93 ± 1.64	113.47 ± 9.16
Model group (LPS + cigarette)	7	1.49 ± 0.37*	9.07 ± 2.06*	22.10 ± 4.25*	101.10 ± 24.63	2.35 ± 0.48	15.96 ± 3.25*	7.59 ± 1.60*	130.71 ± 24.02
Mangxiao group (LPS + cigarette + Mangxiao)	6	0.99 ± 0.28$^\#$	16.93 ± 2.21$^\#$	6.51 ± 3.78$^\#$	66.34 ± 7.79$^\#$	2.09 ± 0.54	16.13 ± 5.42	2.97 ± 1.55$^\#$	348.79 ± 15.19$^\#$
Dahuang group (LPS + cigarette + Dahuang)	8	0.78 ± 0.21$^\#$	15.35 ± 3.35$^\#$	16.12 ± 7.33$^\#$	104.48 ± 9.35	2.53 ± 0.23	10.01 ± 3.35$^\#$	2.76 ± 1.10$^\#$	144.93 ± 23.53

Means labeled with superscripts were significantly different. $^*P < 0.05$ versus control group, $^\#P < 0.05$ versus model group.

Table 2: VIP levels in lung, large intestine, stomach, kidney, spleen, heart, brain, and liver tissues of COPD-like rats (pg/ug, mean ± SD).

Groups	n	Lung	Large intestine	Stomach	Kidney	Spleen	Heart	Brain	Liver
Control group	6	1.06 ± 0.30	18.99 ± 7.81	19.02 ± 5.26	212.97 ± 29.65	8.90 ± 2.29	34.68 ± 8.01	0.42 ± 0.13	201.58 ± 8.95
Model group (LPS + cigarette)	7	0.51 ± 0.20*	8.24 ± 2.36*	20.42 ± 5.87	209.95 ± 43.53	9.19 ± 1.99	32.08 ± 7.85	0.30 ± 0.12*	220.40 ± 15.72
Mangxiao group (LPS + cigarette + Mangxiao)	6	0.86 ± 0.15$^\#$	12.58 ± 2.45$^\#$	10.41 ± 2.94$^\#$	183.00 ± 35.58	3.09 ± 1.10$^\#$	21.24 ± 5.59$^\#$	0.20 ± 0.01$^\#$	671.90 ± 81.16$^\#$
Dahuang group (LPS + cigarette + Dahuang)	8	0.96 ± 0.42$^\#$	12.08 ± 3.29$^\#$	21.66 ± 7.38	221.89 ± 51.60	8.45 ± 1.28	33.04 ± 9.45	0.21 ± 0.06$^\#$	245.28 ± 49.94

Means labeled with superscripts were significantly different. $^*P < 0.05$ versus control group, $^\#P < 0.05$ versus model group.

may affect the secretion of certain specific neuropeptides (factors linked with lung performance) in lung tissue, which is similar to the inner meridians collaterals between lung and large intestine. In order to confirm this hypothesis, we conducted the following study.

2. Materials and Methods

2.1. Preparation of Herbs. Mangxiao and Dahuang were purchased from a traditional Chinese medicinal store (Tongrentang) in Beijing, China, and were authenticated by Professor Yue-qi Wang, Basic Theory and Key Technology Research Center, Beijing University of Chinese Medicine. Mangxiao is an osmotic laxative, acting on large intestine, and its effective ingredient is sodium sulfate [7]. Dahuang is a stimulant laxative, acting on large intestine, and its main effective ingredient is phenolphthalein [7]. According to the dose-equivalence equation between rats and humans (9 g/d) [8], the dose of Mangxiao and Dahuang for rats was 1.5 g/kg, and the dose of Mangxiao for mice was 1.0 g/kg. Mangxiao or Dahuang decoction was prepared in accordance with conventional TCM decocting methods, respectively [9, 10]. Quality was controlled with high-performance liquid chromatography (HPLC) and ion chromatography [11, 12]. The herbs were nontoxic, which were evaluated by animals liver and kidney function, and so on (data not shown).

2.2. Experimental Animals. Male Wistar rats (230 ± 20 g) and female BALB/c mice (20 ± 2 g) were obtained from Bei Jing Vital River Laboratories (VRL) Co., Ltd. (Beijing, China), and maintained in the Animal Center, Beijing University of Chinese Medicine, for 1 week prior to the experiments. Animals were maintained in plastic cages at 23°C ± 1°C with free access to water. They were kept on a 12-hour light-dark cycle. All experimental procedures were performed in accordance with the guidelines of the Animal Care and Ethics Committee of Beijing University of Chinese Medicine.

2.3. Rat COPD-Like Model and Herb Administration. Rat COPD-like model was prepared by cigarette smoking and lipopolysaccharides (LPS, Sigma, St. Louis, MO, USA) stimuli, as previously described [13]. Briefly, on the 1st and 14th days, 200 μL LPS (1 mg/mL in normal saline) was administered intratracheally. On days 2–28, rats were confined in an airtight plexiglass container (60 cm × 50 cm × 40 cm) for 1 hour twice daily, which was full of cigarette smoke at a concentration of about 5% (v/v). Rats were randomized into 4 groups, the treatment was performed as follows: control group received room air, intratracheal normal saline instillation, and intragastric administration of water on days 22–28; model group received cigarette smoking, intratracheal LPS instillation, and intragastric administration of water on days 22–28; Mangxiao group received cigarette smoking, intratracheal LPS instillation, and intragastric administration of Mangxiao decoction on days 22–28; Dahuang group received cigarette smoking, intratracheal LPS instillation, and intragastric administration of Dahuang decoction on days 22–28.

Table 3: NK1R levels in lung, large intestine, stomach, heart, and brain tissues of COPD-like rats (pg/ug, mean ± SD).

Groups	n	Lung	Large intestine	Stomach	Heart	Brain
Control group	6	4.49 ± 0.58	101.33 ± 48.03	116.31 ± 20.12	98.67 ± 22.51	51.24 ± 8.11
Model group (LPS + cigarette)	7	6.43 ± 0.82*	44.86 ± 11.73*	125.80 ± 34.06	106.92 ± 20.47	24.98 ± 14.33*
Mangxiao group (LPS + cigarette + Mangxiao)	6	4.40 ± 1.57$^\#$	42.05 ± 13.33	40.06 ± 19.45$^\#$	84.60 ± 20.39	24.97 ± 7.99
Dahuang group (LPS + cigarette + Dahuang)	8	3.29 ± 0.75$^\#$	73.20 ± 12.10$^\#$	108.59 ± 31.91	106.70 ± 21.23	20.99 ± 7.11

Means labeled with superscripts were significantly different. $^*P < 0.05$ versus control group, $^\#P < 0.05$ versus model group.

Table 4: VIPR1 levels in lung, large intestine, stomach, and brain tissues of COPD-like rats (pg/ug, mean ± SD).

Groups	n	Lung	Large intestine	Stomach	Brain
Control group	6	3.08 ± 0.45	647.83 ± 86.18	101.83 ± 12.12	52.62 ± 14.00
Model group (LPS + cigarette)	7	1.76 ± 0.43*	253.17 ± 41.75*	64.60 ± 9.77*	45.76 ± 8.31
Mangxiao group (LPS + cigarette + Mangxiao)	6	2.44 ± 0.80	230.44 ± 43.62	66.26 ± 9.02	41.01 ± 11.15
Dahuang group (LPS + cigarette + Dahuang)	8	3.29 ± 1.74$^\#$	323.27 ± 66.17$^\#$	67.75 ± 8.76	42.40 ± 11.90

Means labeled with superscripts were significantly different. $^*P < 0.05$ versus control group, $^\#P < 0.05$ versus model group.

2.4. Mouse Model of Allergic Asthma and Herb Administration. Sensitization and challenge of mice were performed as previously described [14], with some modifications. Briefly, mice were immunized via intraperitoneal injection of 100 μg chicken OVA (grade V; Sigma, St. Louis, MO, USA) and 4 mg aluminum hydroxide (Thermo, Rockford, IL, USA) suspended in 0.1 mL saline on days 0 and 14. On days 22, 23, and 24, mice were challenged with aerosolized 3% (w/v in PBS) OVA solution for 30 min using an ultrasonic nebulizer (YC-Y800, Yadu Corp., Beijing, China). Mice were randomly divided into 3 groups, the treatment was performed as follows: control group and model group received intragastric administration of water on days 17–23; Mangxiao group received intragastric administration of Mangxiao decoction on days 17–23. Animals were sacrificed 48 h after the last challenge.

2.5. Assessment of Respiratory Resistance in Mouse Model of Allergic Asthma. Airway high reactivity (AHR) as an indicator of decline in lung function was detected in 24 hrs after the final exposure to aerosol by using an AniRes 2005 Lung Function system (Bestlab 2.0, Beijing, China) according to manufacturer's instructions. Anesthesia was induced by intraperitoneal injection of 95 mg/kg pentobarbital sodium. A connection was made by a computer-controlled ventilator *via* a cannula that had been implanted surgically in the trachea. The respiratory rate and the time ratio of expiration/inspiration were preset at 90/min and 1.5 : 1, respectively. Each mouse inhaled increasing doses of methacholine (MCH, Sigma, USA) ranging from 0 to 0.2 mg/kg body weight for 5 min while staying inside the whole-body plethysmograph, and AHR was recorded and assessed by indexes of expiratory resistance (R_e).

2.6. Histological Analysis of Lung Inflammation in Rat Model of COPD and Mouse Model of Allergic Asthma. For staining with H&E, lungs were inflated and fixed with 10% buffered formalin. Samples were embedded in paraffin, then sectioned (4 μm), and stained with H&E.

2.7. Measurement of SP and VIP in the Lung, Large Intestine, Stomach, Kidney, Spleen, Heart, Brain, and Liver Tissues in Model of COPD and Allergic Asthma. After the serum sample collection, lung, large intestine, stomach, kidney, spleen, heart, brain, and liver tissues were rinsed in ice cold phosphate-buffered saline (PBS: pH 7.5), then dried, and weighed. Afterwards, the tissues were homogenized by using a glass homogenizer on ice, with 10 mL/g of ice cold PBS. Next, homogenates were centrifuged at 5000 ×g, for 5 min at 4°C, and supernatants were collected for detection. The tissue levels of SP and VIP were measured by using enzyme-linked immuno sorbent assay (ELISA) kits according to manufacturer's instructions (Cusabio).

2.8. Measurement of NK1R, VIPR1, and VIPR2 in Lung, Large Intestine, Stomach, And So On Tissues in Model of COPD and Allergic Asthma. After the serum sample collection, lung, large intestine, stomach, heart, and brain tissues were rinsed in ice cold phosphate-buffered saline. Then, the rinsed tissues were homogenized in 1 mL PBS and stored overnight at −20°C. After two freeze-thaw cycles, the tissues were performed to break the cell membranes, the homogenates were centrifuged at 5000 ×g, for 5 minutes at 4°C, and the supernatants were collected for detection.

Levels of NK1R in the tissues of lung, large intestine, stomach, heart, and brain, VIPR1 and VIPR2 levels in the tissues of lung, large intestine, stomach, and brain of COPD

Table 5: VIPR2 levels in lung, large intestine, stomach, and brain tissues of COPD-like rats (pg/ug, mean ± SD).

Groups	n	Lung	Large intestine	Stomach	Brain
Control group	6	16.84 ± 3.18	152.97 ± 62.04	132.55 ± 12.57	66.96 ± 3.34
Model group (LPS + cigarette)	7	11.97 ± 2.19*	84.93 ± 22.24*	114.45 ± 31.26	58.10 ± 13.29
Mangxiao group (LPS + cigarette + Mangxiao)	6	19.04 ± 3.91$^{\#}$	95.52 ± 14.27	98.16 ± 51.85	53.44 ± 7.89
Dahuang group (LPS + cigarette + Dahuang)	8	16.14 ± 3.17$^{\#}$	75.71 ± 8.75	119.63 ± 28.01	67.89 ± 18.69

Means labeled with superscripts were significantly different. $^{*}P < 0.05$ versus control group, $^{\#}P < 0.05$ versus model group.

Table 6: SP levels in lung, large intestine, stomach, kidney, spleen, heart, brain, and liver tissues of asthma mice (pg/mg, $n = 6$, mean ± SD).

Groups	Lung	Large intestine	Stomach	Kidney	Spleen	Heart	Brain	Liver
Control group	5.92 ± 0.58	3.08 ± 0.26	2.98 ± 1.03	1.80 ± 0.54	2.78 ± 0.52	3.47 ± 0.40	2.48 ± 0.60	1.62 ± 0.32
Model group (OVA)	7.27 ± 1.76*	1.74 ± 0.26*	3.10 ± 0.75	1.89 ± 0.44	2.25 ± 0.28	2.13 ± 0.24*	2.08 ± 0.61	0.99 ± 0.13*
Mangxiao group (OVA + Mangxiao)	5.29 ± 2.37$^{\#}$	2.49 ± 0.73$^{\#}$	4.01 ± 0.99$^{\#}$	1.88 ± 0.28	2.38 ± 0.65	2.05 ± 0.72	2.13 ± 0.24	0.78 ± 0.22

Means labeled with superscripts were significantly different. $^{*}P < 0.05$ versus control group, $^{\#}P < 0.05$ versus model group.

rats, and levels of NK1R, VIPR1, and VIPR2 in the tissues of lung, large intestine, stomach, and heart of allergic asthma mice were measured by using a commercial ELISA kit, following the manufacturer's instructions (Cusabio).

2.9. Measurement of NKA and NKB in Lung, Large Intestine, Stomach, Kidney, Spleen, Heart, Brain, and Liver Tissues in Model of Allergic Asthma. Levels of NKA and NKB in lung, large intestine, stomach, kidney, spleen, heart, brain, and liver tissues were measured by using a commercial ELISA kit, following the manufacturer's instructions (Cusabio).

2.10. Statistical Analysis. Data were expressed as mean values ± standard deviation. Statistical comparisons were performed by using one-way analysis of variance. Significant levels were set at $P < 0.05$.

3. Results

3.1. Effects of Mangxiao or Dahuang on SP and VIP Levels in Lung, Large Intestine, Stomach, Kidney, Spleen, Heart, Brain, and Liver Tissues of COPD-Like Rats. Compared with the control group, the levels of SP in lung, stomach, and brain tissues were significantly increased, while the levels of SP in large intestine and heart tissues were decreased in the model group ($P < 0.05$). Compared with the model group, the levels of SP in lung, stomach, and brain tissues were significantly decreased, while the level of SP in large intestine tissue were increased in Mangxiao group and Dahuang group (Table 1).

The levels of VIP in lung, large intestine, and brain tissues in the model group were notably lower than that in the control group ($P < 0.05$). However, intervention with Mangxiao or Dahuang significantly increased the levels of VIP in lung and large intestine tissues while reducing the levels of VIP in brain tissue compared with the model group ($P < 0.05$) (Table 2).

3.2. Effects of Mangxiao or Dahuang on NK1R, VIPR1, and VIPR2 Levels in Lung, Large Intestine, Stomach Heart, and Brain Tissues of COPD-Like Rats. Compared with the control group, the level of NK1R in lung tissues was distinctively increased, while the levels of NK1R in large intestine and brain tissues were decreased in the model group. Intervention with Mangxiao or Dahuang significantly reduced the level of NK1R in lung tissue ($P < 0.05$) compared with the model group (Table 3).

The levels of VIPR1 and VIPR2 in lung and large intestine tissues in the model group were significantly lower than that in the control group. Intervention with Mangxiao or Dahuang increased the levels of VIPR1 and VIPR2 in lung tissues, compared with the model group, while the levels of VIPR1 and VIPR2 in stomach and brain tissues had no obvious changes (Tables 4 and 5).

3.3. Effects of Mangxiao on SP and VIP Levels in Lung, Large Intestine, Stomach, Kidney, Spleen, Heart, Brain, and Liver Tissues of OVA Allergic Asthma Mice. Compared with the control group, a considerable increase in the level of SP in lung tissues and a decrease in the levels in large intestine, heart, and liver tissues were observed in the model group. Intervention with Mangxiao markedly lowered the level of SP in lung tissues and increased the levels of SP in large intestine and stomach tissues (Table 6).

Compared with the control group, the levels of VIP in lung, large intestine, heart, and brain tissues were reduced significantly ($P < 0.05$), and the level of VIP in stomach tissues was increased obviously in the model group. Intervention with Mangxiao increased the level of VIP in lung, large intestine, and heart tissues while lowering the level of VIP in stomach tissues compared with that in the model group (Table 7).

3.4. Effects of Mangxiao on of NK1R, VIPR1, and VIPR2 Levels in Lung, Large Intestine, Stomach, and Heart Tissues of OVA Allergic Asthma Mice. Compared with the control group, the level of NK1R in lung and stomach tissues was up ($P < 0.05$), while the levels of NK1R in large intestine and heart tissues

Table 7: VIP levels in lung, large intestine, stomach, kidney, spleen, heart, brain, and liver tissues of asthma mice (pg/mg, $n = 6$, mean ± SD).

Groups	Lung	Large intestine	Stomach	Kidney	Spleen	Heart	Brain	Liver
Control group	5.84 ± 0.35	2.10 ± 0.36	3.22 ± 0.35	1.53 ± 0.27	1.90 ± 0.27	2.74 ± 0.84	2.10 ± 0.31	1.23 ± 0.17
Model group (OVA)	4.04 ± 0.26*	1.43 ± 0.28*	3.80 ± 0.11*	1.50 ± 0.18	2.15 ± 0.30	1.27 ± 0.35*	1.53 ± 0.30*	0.96 ± 0.15
Mangxiao group (OVA + Mangxiao)	5.09 ± 0.60#	1.95 ± 0.35#	3.26 ± 0.50#	1.76 ± 0.20	1.96 ± 0.25	2.16 ± 0.54#	1.56 ± 0.38	1.16 ± 0.39

Means labeled with superscripts were significantly different. *$P < 0.05$ versus control group, #$P < 0.05$ versus model group.

Table 8: NK1R levels in lung, large intestine, stomach, and heart tissues of OVA allergic asthma mice (pg/ug, $n = 6$, mean ± SD).

Groups	Lung	Large intestine	Stomach	Heart
Control group	0.96 ± 0.19	1.16 ± 0.23	6.80 ± 2.36	29.11 ± 5.28
Model group (OVA)	1.18 ± 0.19*	1.38 ± 0.32	9.40 ± 1.13*	35.38 ± 10.05
Mangxiao group (OVA + Mangxiao)	0.97 ± 0.13#	1.86 ± 0.27#	10.84 ± 1.38	35.60 ± 13.06

All values are expressed as mean ± SD. Means labeled with superscripts were significantly different. *$P < 0.05$ versus control group, #$P < 0.05$ versus model group.

had no distinct changes in the model group mice. Compared with the model group, the level of NK1R in lung tissues reduced obviously, while the level of NK1R in large intestine tissues increased sharply in the Mangxiao group (Table 8).

Compared with the control group, the levels of VIPR1 and VIPR2 in lung tissue were significantly lower ($P < 0.05$). Intervention with Mangxiao visibly increased ($P < 0.05$) the level of VIPR1 in lung tissues compared with the model group (Tables 9 and 10).

3.5. Effects of Mangxiao on NKA and NKB Levels in Lung, Large Intestine, Stomach, Kidney, Spleen, Heart, Brain, and Liver Tissues of OVA Allergic Asthma Mice. The levels of NKA and NKB in lung, large intestine, stomach, kidney, and spleen tissues were similar between the control group and the model group ($P > 0.05$). Compared with the control group, levels of NKA in heart and liver tissues and level of NKB in brain tissues went down significantly ($P < 0.05$). However, the levels of NKA in large intestine and NKB levels in lung, large intestine, stomach, and spleen tissues were reduced in Mangxiao group (Tables 11 and 12).

3.6. Effect of Mangxiao or Dahuang on Inflammation in Lung Tissues of COPD-Like Rats. As the results of hematoxylin-eosin staining shown in Figure 1, the lung tissue of control group had normal alveolar structure and no inflammatory infiltration and exudates. The model group showed basic pulmonary pathological changes of COPD, the bronchial epithelium presented with degeneration, necrosis, and shedding, and intrabronchial presented with exudation. The bronchial wall was thickening and surrounded by pulmonary bullae. Compared with the model group, after treatment of Mangxiao or Dahuang, the pathological changes of lung tissue were alleviated, which presented with mild congestion and pulmonary interstitial inflammation (Figure 1).

3.7. Comparison of Airway Effect in Mice. After excitation by different concentrated MCH, airway resistance changes are displayed in Figure 2. Compared with the control group, when the MCH concentration was 0.0125 mg/kg, 0.025 mg/kg, 0.05 mg/kg, 0.1 mg/kg, and 0.2 mg/kg, respectively, the airway resistance in the model group mice went up distinctively (10.03 ± 2.63 versus 5.06 ± 2.38, 18.05 ± 4.38 versus 8.09 ± 4.52, 21.21 ± 0.57 versus 10.91 ± 1.98, 30.66 ± 7.67 versus 13.47 ± 1.52, and 104.15 ± 35.23 versus 22.66 ± 3.81); compared with the model group, when the MCH concentration was 0.05 mg/kg, 0.1 mg/kg, and 0.2 mg/kg, respectively, airway resistance decreased significantly in mice of Mangxiao group (12.55 ± 5.97, 20.39 ± 7.53, and 38.84 ± 18.28) (Figure 2).

3.8. Effect of Mangxiao on Inflammation in Lung Tissue of OVA Allergic Asthma Mice. Hematoxylin-eosin staining displayed that alveolar epithelial cells arranged orderly, alveolar walls had structure integrity, no hyperemia, hemorrhage, or inflammatory cell infiltration were present in the control group. However, OVA-challenged lung tissues displayed bronchial epithelial cells which arranged disorderly. Compared to the control group, part of epithelium damage and infiltration of inflammatory cells into the airway were observed around the bronchi, bronchioles, and alveoli. Moreover, the majority of leukocytes were eosinophils and lymphocytes. Infiltration of inflammatory leukocytes in OVA-challenged mice treated with Mangxiao was significantly attenuated, compared with that in OVA-challenged mice (Figure 3).

4. Discussion

This study explored the specific link between lung and large intestine. Rat COPD-like model was prepared by cigarette smoking and LPS stimuli. Intragastric administration of Mangxiao (an osmotic laxative) or Dahuang (a stimulant laxative) was to stimulate the large intestine. Mouse model of allergic asthma was prepared by ovalbumin (OVA) sensitization and challenge. Intragastric administration of Mirabilite was to stimulate the large intestine. The tissue (including lung, and large intestine) levels of neuropeptides

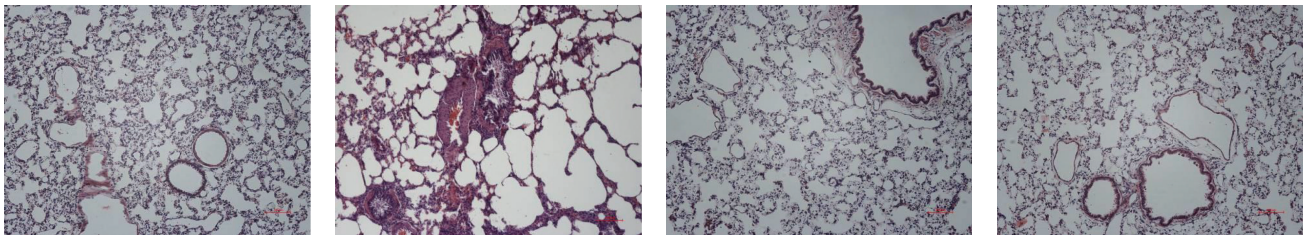

(a) (b) (c) (d)

Figure 1: The effects of Mangxiao or Dahuang on COPD-like rats' lung histopathology (H&E stain ×100). Histological examination of lung tissues was performed 48 h after the final administration. Lung tissues were fixed, sectioned at 4 μm thickness, and stained with H&E solution. (a) Control group: received room air, intratracheal normal saline instillation, and intragastric administration of water. (b) Model group (LPS + cigarette): received cigarette smoking, intratracheal LPS instillation, and intragastric administration of water. (c) Mangxiao group (LPS + cigarette + Mangxiao): received cigarette smoking, intratracheal LPS instillation, and intragastric administration of Mangxiao (1.5 g/kg) decoction. (d) Dahuang group (LPS + cigarette + Dahuang): received cigarette smoking, intratracheal LPS instillation, and intragastric administration of Dahuang (1.5 g/kg) decoction.

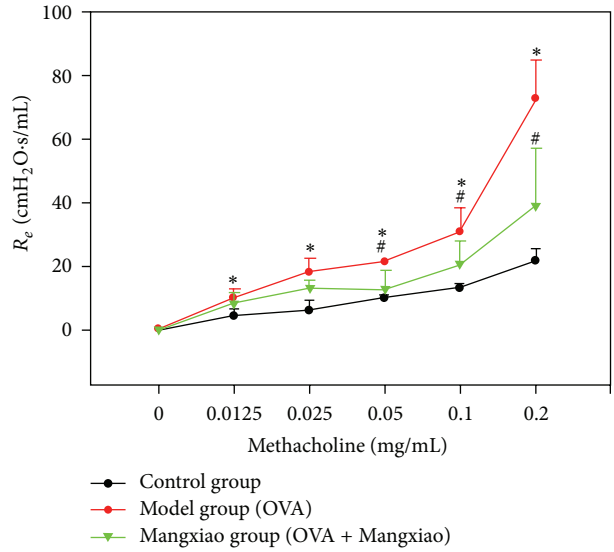

Figure 2: The development of airway hyperresponsiveness analysis (mean ± SD, $n = 5$). All values are expressed as mean ± SD. Means labeled with superscripts were significantly different. $^{*}P < 0.05$ versus control group, $^{\#}P < 0.05$ versus model group (OVA).

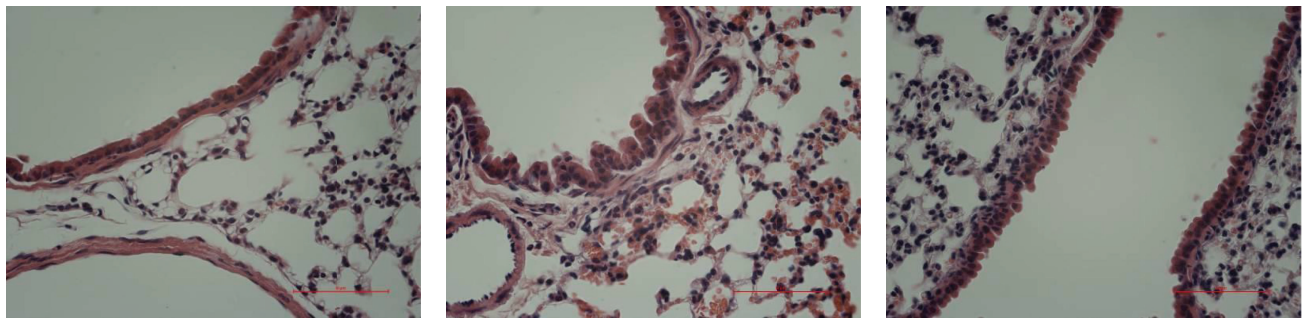

(a) (b) (c)

Figure 3: The effects of Mangxiao on mice's lung histopathology (H&E stain ×400). Histological examination of lung tissues was performed 48 h after the final OVA challenge. Lung tissues were fixed, sectioned at 4 μm thickness, and stained with H&E solution. (a) Control group, (b) model group (OVA): OVA-sensitized/-challenged mice, and (c) Mangxiao group (OVA + Mangxiao): Mangxiao (1 g/kg) + OVA-sensitized/-challenged mice.

Table 9: VIPR1 levels in lung, large intestine, stomach, and heart tissues of asthma mice (pg/ug, $n = 6$, mean ± SD).

Groups	Lung	Large intestine	Stomach	Heart
Control group	5.72 ± 0.62	1.06 ± 0.13	2.67 ± 0.85	7.59 ± 3.89
Model group (OVA)	3.93 ± 0.47*	0.73 ± 0.15*	3.15 ± 0.68	7.26 ± 3.10
Mangxiao group (OVA + Mangxiao)	5.26 ± 0.65#	0.96 ± 0.11#	10.089 ± 4.78#	8.46 ± 0.54

Means labeled with superscripts were significantly different. *$P < 0.05$ versus control group, #$P < 0.05$ versus model group.

Table 10: VIPR2 levels in lung, large intestine, stomach, and heart of asthma mice (pg/ug, $n = 6$, mean ± SD).

Groups	Lung	Large intestine	Stomach	Heart
Control group	1.47 ± 0.19	1.18 ± 0.17	2.84 ± 1.09	16.59 ± 8.78
Model group (OVA)	1.11 ± 0.41*	1.22 ± 0.48	6.00 ± 1.30*	24.32 ± 13.55
Mangxiao group (OVA + Mangxiao)	1.43 ± 0.15	1.32 ± 0.19	5.85 ± 3.04	29.57 ± 17.12

Means labeled with superscripts were significantly different. *$P < 0.05$ versus control group, #$P < 0.05$ versus model group.

and the receptors, such as SP, VIP, NKA, NKB, NK1R, VIPR1, and VIPR2, were measured by using ELISA kits. The findings indicate that stimulating intestine with Mangxiao or Dahuang can specifically regulate the secretion of SP, VIP, and the receptors in lung tissues. These findings provide a new perspective to interpret the TCM theory of exterior-interior correlation between lung and large intestine.

The theory of exterior-interior correlation between the lung and large intestine was first recorded in *Huang Di Nei Jing* (the Yellow Emperor's Canon of Internal Medicine) and became one of the basic theories of TCM. The theory posits that the specific link between lung and large intestine is meridians. Since the lung meridian of Hand-Taiyin and the large intestine meridian of Hand-Yang ming are a pair of interior-exterior meridians, there is a very close connection between the lung and the large intestine. That is to say, they interact with each other physically and interfere with each other pathologically, such as lung diseases could affect the large intestine [15, 16] and vice versa [17–19]. It has been proved that relaxing intestine by laxative can be very helpful in treating a number of lung diseases including asthma, bronchitis, pneumonia, pleural effusion, pulmonary heart disease, adult respiratory distress syndrome (ARDS), and chronic obstructive pulmonary disease (COPD).

The theory of exterior-interior correlation between the lung and large intestine suggests that they connect with each other directly by meridians, and the connection between the lung meridian and the large intestine meridian is further strengthened by collaterals and branches of the two meridians [20]. The circulation of meridians and meridian points are the physiological basis of acupuncture effects [21]. Some scholars have found that the neural anatomy could be the basis of acupuncture effects and acupuncture stimulation acts on the nerves which could lead to the excretion of substance P, vasoactive intestinal peptide, neuropeptide Y, and so on [22–24]. The finding suggests that peptidergic nerve and neural peptides might play an important role in the exterior-interior correlation between meridians and organs.

Mangxiao and Dahuang, as an osmotic laxative and a stimulant laxative, respectively, have been used in TCM clinical practice for nearly 2000 years. Both of them have an intense effect on contracting the intestinal smooth muscle and increasing peristalsis [25–27], so they are widely prescribed in treating COPD, asthma, and exacerbations or attack other pulmonary diseases. Here, we assumed that herbs like Mangxiao and Dahuang could generate stimuli by stimulating the intestinal tract. Then, enteric nerves receive the stimuli and transmit them to lung through some neural pathways in the body, which ultimately creates a biological effect on regulating lung tissue neuropeptide, such as SP, VIP, and their receptors.

Our findings indicate that by stimulating the large intestine by Mangxiao or Dahuang in rats with COPD, the levels of SP in lung, stomach, and brain tissues and the level of NK1R in lung were reduced. The levels of SP and NK1R in large intestine tissue were increased after stimulating by Dahuang. The levels of VIP in lung and large intestine tissues and VIPR1 and VIPR2 in lung tissue were increased. The level of VIP in brain tissue was reduced. Stimulating the large intestine by Mangxiao in mice with asthma significantly reduced the levels of SP and NK1R in lung tissues but increased the levels of SP and NK1R in large intestine tissues. The levels of VIP in lung, large intestine, and heart tissues and VIPR1 in lung tissues were increased. The levels of NKA and NKB in lung and large intestine tissues of mice with asthma were similar between the control and the model groups.

The results confirmed that after stimulating the large intestine by Mangxiao or Dahuang, SP, NK1R, VIP, VIPR1, and VIPR2 were all significantly increased in large intestine tissue of rats with COPD and mice with asthma. At the same time, the SP and NK1R were markedly decreased, while VIP, VIPR1, and VIPR2 became much higher in lung tissue. Abnormal secretion of SP and VIP could be observed in other organs such as stomach tissues of rats or heart and stomach tissues of mice; however, the receptors did not change obviously, while the NKA and NKB levels were similar in lung tissues of mice with asthma among groups. It indicates that stimulating large intestine with Mangxiao or Dahuang can specifically regulate the secretion of SP, VIP, and the receptors in lung tissues. Our findings provide some new lines of evidence to interpret the theory of exterior-interior correlation between the lung and large intestine.

Table 11: NKA levels in lung, large intestine, stomach, kidney, spleen, heart, brain, and liver tissues of asthma mice (pg/mg, $n = 6$, mean ± SD).

Groups	Lung	Large intestine	Stomach	Kidney	Spleen	Heart	Brain	Liver
Control group	0.88 ± 0.23	0.27 ± 0.06	0.39 ± 0.08	0.24 ± 0.03	0.30 ± 0.05	0.41 ± 0.05	0.26 ± 0.06	0.17 ± 0.03
Model group (OVA)	0.87 ± 0.07	0.28 ± 0.06	0.37 ± 0.06	0.21 ± 0.05	0.27 ± 0.06	0.30 ± 0.03*	0.25 ± 0.03	0.14 ± 0.01*
Mangxiao group (OVA + Mangxiao)	0.75 ± 0.09	0.19 ± 0.05#	0.30 ± 0.02	0.24 ± 0.04	0.30 ± 0.04	0.29 ± 0.05	0.25 ± 0.05	0.15 ± 0.03

Means labeled with superscripts were significantly different. * $P < 0.05$ versus control group, # $P < 0.05$ versus model group.

Table 12: NKB levels in lung, large intestine, stomach, kidney, spleen, heart, brain, and liver tissues of asthma mice (pg/mg, $n = 6$, mean ± SD).

Groups	Lung	Large intestine	Stomach	Kidney	Spleen	Heart	Brain	Liver
Control group	2.97 ± 0.36	1.16 ± 0.35	1.48 ± 0.08	0.80 ± 0.24	1.02 ± 0.22	0.64 ± 0.26	1.02 ± 0.14	0.27 ± 0.09
Model group (OVA)	2.81 ± 0.64	1.33 ± 0.43	1.55 ± 0.34	0.68 ± 0.15	0.87 ± 0.22	0.43 ± 0.24	0.72 ± 0.13*	0.23 ± 0.06
Mangxiao group (OVA + Mangxiao)	2.07 ± 0.45#	0.22 ± 0.08#	0.62 ± 0.21#	0.76 ± 0.12	0.55 ± 0.20#	0.75 ± 0.24	0.84 ± 0.16	0.27 ± 0.06

Means labeled with superscripts were significantly different. * $P < 0.05$ versus control group, # $P < 0.05$ versus model group.

In conclusion, we have found some new lines of evidence which suggest that a signal conditioning way of *Meridian - nerve - neuropeptide* between lung and large intestine does exist. Because of the complexity of the nervous system and the neural signal transmission, we still need to do further and deeper researches to find out specific nerves and specific ways that associate with the neuropeptide secretion. However, the theory of central neural circuits, proposed by academician Zhang in the research of the mechanism of acupuncture analgesia, may point out a direction for future researches [28].

Conflict of Interests

The authors declare that they have no conflict of interests.

Authors' Contributions

Xiang-Gen Zhong and Feng-Jie Zheng have equally contributed to this paper. Yu-Hang Li and Si-Hua Gao contributed to the conception and design of the study. Xiang-Gen Zhong and Feng-Jie Zheng analysed the data and drafted the paper. All by-line authors read and approved the final paper.

Acknowledgments

This study was funded by China National key basic research plan (no. 2009CB522704). The authors are grateful to The Ministry of Science and Technology of the People's Republic of China for funding this study. Thanks to Professor Yong Qing Yang, Shanghai Research Institute of Acupuncture and Meridian, Yueyang Hospital, Shanghai University of Traditional Chinese Medicine, for the presentation of the guide.

References

[1] P. Liu, P. Wang, D. Z. Tian, J. Liu, G. Chen, and S. Liu, "Study on traditional Chinese medicine theory of lung being connected with large intestine," *Journal of Traditional Chinese Medicine*, vol. 32, no. 3, pp. 482–487, 2012.

[2] J. X. Ni and S. H. Gao, "Understanding the viscera-related theory that the lung and large intestine are exterior-interiorly related," *Journal of Traditional Chinese Medicine*, vol. 32, no. 2, pp. 293–298, 2012.

[3] Y. Liu and X. Y. Wang, "Pulmonary-intestinal crosstalk in the pathological process of COPD and IBD: a perspective from the lung and the large intestine being interior-exteriorly related theory," *World Journal of Gastroenterology*, vol. 21, no. 10, pp. 886–893, 2013.

[4] R. Wu, Z. Fengjie, Y. Li et al., "Modified Dachengqi decoction combined with conventional treatment for treating acute exacerbation of chronic obstructive pulmonary disease: a systematic review based on randomized controlled trials," *Evidence-Based Complementary and Alternative Medicine*, vol. 2013, Article ID 323715, 8 pages, 2013.

[5] Y. H. Li, X. G. Zhong, X. Jia et al., "Influences of relaxing large intestine therapy on lung function and blood gas in rat model of chronic obstructive pulmonary diseases," *Journal of Beijing University of Traditional Chinese Medicine*, vol. 33, no. 7, pp. 452–455, 2010.

[6] X. M. Li and L. Brown, "Efficacy and mechanisms of action of traditional Chinese medicines for treating asthma and allergy," *Journal of Allergy and Clinical Immunology*, vol. 123, no. 2, pp. 297–306, 2009.

[7] P. Cheng, "Pharmacology of traditional Chinese medicine," in *National Planning in Higher Institutions of Chinese Medicine Textbooks*, pp. 141–145, China Press of Traditional Chinese Medicine, Beijing, China, 9th edition, 2012.

[8] X. Shuyun, B. Rulian, and C. Xiu, *Methodology of Pharmacological Experiment*, People's Medical Publishing House, Beijing, China, 1991.

[9] T. Liu, L. L. Yang, L. Zou et al., "Chinese medicine formula Linggui zhugan decoction improves beta-oxidation and metabolism of fatty acid in high-fat-diet-induced rat model of fatty liver disease," *Evidence-Based Complementary and Alternative Medicine*, vol. 2013, Article ID 429738, 9 pages, 2013.

[10] H. Kashtan, R. C. Gregoire, W. R. Bruce, K. Hay, and H. S. Stern, "Effects of sodium sulfate on fecal pH and proliferation of

colonic mucosa in patients at high risk for colon cancer," *Journal of the National Cancer Institute*, vol. 82, no. 11, pp. 950–952, 1990.

[11] X. Yuan, J. F. Gao, J. Cao et al., "Study on HPLC fingerprint of anthraquinones in rhizoma of rhubarb," *Natural Product Research*, no. 24, pp. 36–40, 2012.

[12] S. Gan, X. G. Shi, T. Han, and C. Q. Wu, "Determination of sodium sulfate in medicinal mirabilite by ion chromatography," *China Pharmaceuticals*, vol. 21, no. 14, pp. 39–40, 2012.

[13] Y. H. Li, F. J. Zheng, Y. Huang, X. G. Zhong, and M. Z. Guo, "Synergistic anti-inflammatory effect of Radix Platycodon in combination with herbs for cleaning-heat and detoxification and its mechanism," *Chinese Journal of Integrative Medicine*, vol. 19, no. 1, pp. 29–35, 2013.

[14] R. Marino, T. Thuraisingam, P. Camateros et al., "Secretory leukocyte protease inhibitor plays an important role in the regulation of allergic asthma in mice," *Journal of Immunology*, vol. 186, no. 7, pp. 4433–4442, 2011.

[15] T. V. Gavrish, "Dysbioses of the oral cavity and intestines and immune reactivity in of adolescent bronchial asthma patients," *Zhurnal Mikrobiologii Epidemiologii i Immunobiologii*, no. 6, pp. 74–77, 2001.

[16] N. Powell, B. Huntley, T. Beech, W. Knight, H. Knight, and C. J. Corrigan, "Increased prevalence of gastrointestinal symptoms in patients with allergic disease," *Postgraduate Medical Journal*, vol. 83, no. 977, pp. 182–186, 2007.

[17] J. G. Douglas, C. F. McDonald, M. J. Leslie, J. Gillon, G. K. Crompton, and G. J. R. McHardy, "Respiratory impairment in inflammatory bowel disease: does it vary with disease activity?" *Respiratory Medicine*, vol. 83, no. 5, pp. 389–394, 1989.

[18] N. Songür, Y. Songür, M. Tüzün et al., "Pulmonary function tests and high-resolution CT in the detection of pulmonary involvement in inflammatory bowel disease," *Journal of Clinical Gastroenterology*, vol. 37, no. 4, pp. 292–298, 2003.

[19] B. B. Ceyhan, S. Karakurt, H. Cevik, and M. Sungur, "Bronchial hyperreactivity and allergic status in inflammatory bowel disease," *Respiration*, vol. 70, no. 1, pp. 60–66, 2003.

[20] B. Liu, J. Wang, and J. P. Zhao, "Intermediate structure of the interior-exterior relationship between lung and large intestine," *Zhongguo Zhen Jiu*, vol. 31, no. 4, pp. 363–365, 2011.

[21] T. T. Ma, S. Y. Yu, Y. Li et al., "Randomised clinical trial: an assessment of acupuncture on specific meridian or specific acupoint versus sham acupuncture for treating functional dyspepsia," *Alimentary Pharmacology and Therapeutics*, vol. 35, no. 5, pp. 552–561, 2012.

[22] Y. Guangfu, L. Chuanyou, C. Fuyuan et al., "Influence of electroacupuncture at Quchi and Binao points on substance P and neuropeptide Y immunoreaetive nerves at Renzhong, Heliao and Chengjiang in rat," *Acta Universitatis Medicinae Tongji*, vol. 26, no. 4, pp. 267–270, 1997.

[23] Q. Y. Ma, C. C. Pan, K. M. Wang et al., "Research on connection pathway between channels and viscera and its relation with neuropeptide-like substances," *Acupuncture Research*, vol. 25, no. 2, pp. 117–120, 2000.

[24] M. Silberstein, "Do acupuncture meridians exist? Correlation with referred itch (mitempfindung) stimulus and referral points," *Acupuncture in Medicine*, vol. 30, no. 1, pp. 17–20, 2012.

[25] M. Yu, Y. L. Luo, J. W. Zheng et al., "Effects of rhubarb on isolated gastric muscle strips of guinea pigs," *World Journal of Gastroenterology*, vol. 11, no. 17, pp. 2670–2673, 2005.

[26] Z. Q. Lei, *Chinese Medicine*, Shanghai Science and Technology Press, Shanghai, China, 2001.

[27] M. Doui, H. Ando, C. Goi, N. Kakiuchi, and M. Mikage, "Herbological studies on combination of rhubarb and mirabilite," *Yakushigaku Zasshi*, vol. 45, no. 2, pp. 106–111, 2010.

[28] X. T. Zhang, "Integration of the role of the thalamus in the process of acupuncture analgesia," *Scientia Sinica Mathematio*, no. 1, pp. 28–52, 1973.

Hindawi Publishing Corporation
Evidence-Based Complementary and Alternative Medicine
Volume 2013, Article ID 982095, 8 pages
http://dx.doi.org/10.1155/2013/982095

Research Article

Effects of Acupuncture on 1-Chloro-2,4-dinitrochlorobenzene-Induced Atopic Dermatitis

Ji-Yeun Park,[1,2] Hi-Joon Park,[1] You Yeon Choi,[3] Mi Hye Kim,[3] Seung-Nam Kim,[1,2] and Woong Mo Yang[3]

[1] *Studies of Translational Acupuncture Research (STAR), Acupuncture and Meridian Science Research Center (AMSRC), Kyung Hee University, 26 Kyungheedae-ro, Dongdaemun-gu, Seoul 130-701, Republic of Korea*
[2] *Department of Korean Medical Science, Graduate School of Korean Medicine, Kyung Hee University, Seoul 130-701, Republic of Korea*
[3] *Department of Prescriptionology, College of Korean Medicine, Kyung Hee University, 26 Kyungheedae-ro, Dongdaemun-gu, Seoul 130-701, Republic of Korea*

Correspondence should be addressed to Hi-Joon Park; acufind@khu.ac.kr and Woong Mo Yang; wmyang@khu.ac.kr

Received 16 May 2013; Revised 3 July 2013; Accepted 5 July 2013

Academic Editor: Yong-Qing Yang

Though the effects of acupuncture in atopic dermatitis have been proven in clinical studies, its mechanism remains unclear. In this study, we investigate the effectiveness and mechanism of action for acupuncture treatment on the LI11 meridian point for treatment of allergic contact dermatitis. BALB/c mice received 1-chloro-2,4-dinitrobenzene (DNCB) application to induce skin inflammation. Acupuncture treatment on LI11 significantly inhibited cutaneous hyperplasia, serum IgE levels, and expression of proinflammatory cytokine (IL-4, IL-8, and TNF-α) mRNA and NF-κB, ERK1/2, JNK, and p38 proteins. Acupuncture treatment of local points also inhibited cutaneous hyperplasia and serum IgE levels; however, it was not effective in regulating proinflammatory cytokines and proteins. In addition, LI11 treatment is more effective at reducing serum IgE levels and pro-inflammatory cytokines and proteins than local point treatment. These results suggest that acupuncture treatment is effective in alleviating allergic contact dermatitis by reducing pro-inflammatory cytokines and proteins.

1. Introduction

Allergic contact dermatitis (ACD) is a chronic inflammatory skin disease presenting with cutaneous hyperreactivity that progresses due to the activation of inflammatory cells related to various allergic immune responses [1]. Although the etiology and pathology of ACD are not fully understood, previous studies suggest that typical symptoms of ACD are predominantly caused by allergen-specific T-helper (Th) 1/2 cell dysregulation, leading to immunoglobulin E (IgE) production [2, 3] and the accumulation of proinflammatory mediators [4].

The incidence of ACD has increased dramatically, especially in industrialized countries, and it now affects up to 20% of children and 3% of adults worldwide [5]. Until recently, ACD has been treated with medications such as steroid therapy and immunosuppressive agents. However, these pharmacological therapies may cause various side effects [6]. Thus, the use of less toxic alternative therapies, including acupuncture and herbal preparations, is increasing for the treatment of ACD [7–9].

Acupuncture is a nonpharmacologic technique widely used in the treatment of pain [10–12], wounds, and various skin diseases such as inflammation [13–15]. In several studies, acupuncture has been shown to reduce experimental itch, allergen-induced basophil activation, and eczema in atopic dermatitis [16–19]. Though the therapeutic efficacy of acupuncture in the treatment of atopic dermatitis has been proven in clinical studies [17, 18], its mechanism of action remains poorly understood.

In the present study, we employed a 1-chloro-2,4-dinitrobenzene- (DNCB-) induced model of ACD in mice.

Table 1: Primer sequences.

Target gene	Primer	Sequence (5′-3′)	Amplicon size (bp)
IL-8	F	5′-TGTGGGAGGCTGTGTTTGTA-3′	151
	R	5′-ACGAGACCAGGAGAAACAGG-3′	
IL-4	F	5′-TCATCGGCATTTTGAACGAG-3′	399
	R	5′-CCCATACTTTAGGAAGACACGGATT-3′;	
IL-1β	F	5′-CTC TAG ACC ATG CTA CAG AC-3′	291
	R	5′-TGG AAT CCA GGG GAA ACA CTG-3′	
TNF-α	F	5′-GGT GCA ATG CAG AGC CTT CC-3′	173
	R	5′-CAG TGA TGT AGC GAC AGC CTG G-3′	
GAPDH	F	5′-GGC ATG GAC TGT GGT CAT GA-3′	376
	R	5′-TTC ACC ACC ATG GAG AAG GC-3′	

To evaluate the effects of acupuncture on ACD, we investigated changes in histology, total IgE serum levels, and mRNA expression of pro-inflammatory cytokines. In addition, the expression of NF-κB and MAPKs (ERK1/2, JNK, and p38) was measured in the dorsal skin by western blot.

2. Materials and Methods

2.1. Animals and Treatment. BALB/c mice (7-week-old females) were purchased from Japan SLC, Inc. (Hamamatsu, Japan). Both animal care and the study protocol were conducted according to the guidelines of the Committee on Care and Use of Laboratory Animals of Kyung Hee University (KHUASP (SE)-12-020). The mice were maintained for 10 days in pathogen-free conditions before the start of the experiment. Mice were kept at a constant temperature (23°C) and humidity (55%) with a 12 h light/dark cycle, and they were provided with a laboratory diet and water *ad libitum*. After the 10-day adaptation period, mice were assigned to one of four groups (each, $n = 5$): *NOR* (normal group, mice treated with vehicle); *DNCB* (negative control group, mice sensitized with DNCB); *MP* (meridian point, mice sensitized with DNCB and treated at meridian point LI11); and *LP* (local point, mice sensitized with DNCB and treated at local points surrounding the lesion).

For induction of ACD-like skin disorders, DNCB was applied onto the mouse dorsal skin. The dorsal skin region of mice in all groups was shaved with an electric razor in preparation for each experimental cutaneous application. Induction of ACD was achieved by topical application of 100 μL 1% DNCB in 4 : 1 (v/v) acetone/olive oil solution (A/O) once daily to the shaved dorsal skin. These procedures were repeated for 3 days (days 0–2) and followed by a period of no treatment for 5 days (days 3–7). In the second challenge, the LP and MP groups were treated with acupuncture 3 h prior to the application of 0.5% DNCB (days 8–16). Mice in the control group for ACD received vehicle treatment alone (A/O, 4 : 1) without DNCB treatment. Following challenge for 7 days, the mice were sacrificed on day 17 of the experiment. Skin tissues from the backs of the mice were excised and subjected to histological examination, and blood was collected in heparinized tubes from cardiac puncture. All experiments were performed blindly.

2.2. Histological Examination. The dorsal skin (1 × 0.5 cm) was removed and fixed in 10% paraformaldehyde (Sigma, St. Louis, MO, USA). Fixed tissues were embedded in paraffin for 24 h and serially sectioned to a thickness of 4 μm for histological analysis. Tissue sections were stained with hematoxylin and eosin (H&E) and examined for general morphology. To assess epidermal and dermal hyperplasia in all four groups, all tissue samples were examined and photographed in a blinded fashion. Images were captured using the Leica Application Suite (LAS; Leica Microsystems, Buffalo Grove, IL, USA) and viewed at ×100 magnification.

2.3. Measurement of Total Serum IgE Levels. Blood samples were collected from the mice after sacrifice, and serum samples were obtained by centrifugation (14,000 ×g, 30 min). Total serum IgE levels of three group ($n = 5$) were measured three times repeatedly by an enzyme-linked immunosorbent assay (ELISA) kit (Cat. no. KT-401; Kamiya Biomedical, Seattle, WA, USA) following the manufacturer's instructions.

2.4. Detection of mRNA Expression by Reverse Transcription Polymerase Chain Reaction (RT-PCR). To determine cytokine gene expression in the dorsal skin, reverse-transcription PCR was performed. Total RNA was extracted from the dorsal skin using TRIzol Reagent (Invitrogen Corp., Carlsbad, CA, USA) following the manufacturer's instruction and quantified by determining the OD at 260 nm. Prepared cDNAs were amplified using commercially available cDNA synthesis kits (Invitrogen Corp., Carlsbad, CA, USA) according to the manufacturer's recommendations. Thermocycler conditions consisted of an initial step at 4°C for 5 min, followed by a step at 45°C for 60 min and 40 cycles of a subsequent 2-step PCR program at 95°C for 5 min. Amplification of cDNA was conducted with Taq polymerase (Promega) and primers specific for tumor necrosis factor- (TNF-) α, interleukin- (IL-) 1β, IL-4, IL-8, and GAPDH mRNA. The primers used for amplification were synthesized using Primer Express Software (Applied Biosystems), and the sequences of the primers used in this study are shown in Table 1. The PCR cycles consisted of denaturation at 94°C for 30 s, annealing at 58°C for 30 s, and extension at 72°C for 45 s for 30 cycles. PCR products were separated by electrophoresis through a 2% agarose gel, stained with ethidium bromide, and

then detected using UV light. For semiquantitative analysis of PCR bands, the density of each band was measured with a computer imaging device and accompanying software (Bio-Rad, Hercules, CA, USA).

2.5. Detection of Protein Expression by Western Blot Analysis. Western blotting was performed to study pro-inflammatory protein expression. Frozen skin tissues were homogenized in cytoplasmic lysis buffer (10 mM HEPES, pH 7.9, 10 mM KCl, 0.1 mM EDTA, 0.1 mM EGTA, 1 mM DTT, 0.15% Nonidet P-40, 50 mM β-glycerophosphate, 10 mM NaF, and 5 mM Na_3VO_4) containing a protease inhibitor cocktail (Roche, Indianapolis, IN, USA) and centrifuged at 500 rpm for 5 min. After removing the supernatant, the sunken pellet (nuclear pellet) was added to nuclear lysis buffer (20 mM HEPES, pH 7.9, 400 mM NaCl, 1 mM EDTA, 1 mM EGTA, 1 mM DTT, 0.50% Nonidet P-40, 50 mM β-glycerophosphate, 10 mM NaF, and 5 mM Na_3VO_4) containing protease inhibitor cocktail and then homogenized for 15 min on ice. Nuclear protein was centrifuged at 12,000 ×g for 15 min at 4°C to determine NF-κB levels. MAPKs (extracellular signal-regulated kinase (ERK), Jun NH2-terminal kinase (JNK), and p38 MAPK) levels were confirmed from whole extracts. Each group of skin tissues was homogenized on ice for 15 min in RIPA buffer (50 mM Tris-HCl, pH 7.4, 1% Nonidet P-40, 0.5% sodium deoxycholate, and 150 mM NaCl) containing protease inhibitor cocktail. The resultant homogenate was centrifuged at 10,000 ×g for 30 min at 4°C, and the supernatant was collected for whole protein extraction. The protein concentration was measured using a protein assay reagent (Bio-Rad, Hercules, CA, USA), and 30 μg of protein was denatured with SDS buffer. Samples were separated on a 10% SDS-polyacrylamide gel, and the proteins were then electrotransferred to a polyvinylidene fluoride (PVDF) membrane. The immunoblot was incubated overnight in blocking solution (5% skim milk) at 4°C, followed by a 4 h incubation in monoclonal anti-NF-κB, ERK1/2, JNK, or p38 (Cell Signaling, CA, USA). Blots were washed two times with TBS-T and incubated with anti-rabbit alkaline phosphatase-conjugated secondary antibody (Santa Cruz Biotechnology Inc., CA, USA) for 2 h at room temperature. The proteins were then visualized using an enhanced chemiluminescence (ECL) detection reagent (Amersham Pharmacia, Piscataway, NJ, USA). The relative band density was determined using a computerized densitometry system and normalized to the β-actin signal from a blot developed under similar conditions.

2.6. Statistical Analysis. GraphPad Prism 5 software (GraphPad Software Inc., San Diego, CA, USA) was used for the statistical analysis. All data are expressed as the mean ± standard deviation (SD). Significance was determined using one-way ANOVA with the Newman-Keuls post hoc test. In all analyses, $P < 0.05$ indicated statistical significance.

3. Results

3.1. Effects of Acupuncture on Histological Changes. We examined whether acupuncture treatment affected the interrupted skin barrier in ACD using H&E staining. The average epidermal thickness of the dorsal skin was 32.58 ± 6.55 μm in the normal group, 120 ± 15.83 μm in the DNCB group, 87.16 ± 12.38 μm in the LP group, and 76.30 ± 10.34 μm in the MP group. Additionally, the average dermal thickness of the dorsal skin was 243.36 ± 15.37 μm in the normal group, 660.97 ± 67.89 μm in the DNCB group, 447.27 ± 38.55 μm in the LP group, and 427.94 ± 19.89 μm in the MP group. The skin was significantly thicker in DNCB-treated mice than in the normal group. Compared to the DNCB group, MP-treated mice displayed significantly reduced skin thickening and hyperplasia ($P < 0.001$). LP-treated mice also showed reduced skin thickening compared to the DNCB group ($P < 0.001$), although not to the extent of that observed in the MP group, which displayed the least amount of thickening among the groups (Figures 1(c)–1(e)).

3.2. Effects of Acupuncture on Serum IgE Levels. Total IgE serum levels were measured to assess the effects of acupuncture treatment on DNCB-induced mice. The DNCB group showed increased IgE levels (328.87 ± 25.13 ng/mL, $P < 0.001$) compared to the normal control group (46.95 ± 2.5 ng/mL). DNCB-mediated enhancement of serum IgE levels was significantly reduced in the MP-treated group (186.37 ± 3.23 ng/mL, $P < 0.001$) and the LP-treated group (232.47 ± 5.93 ng/mL, $P < 0.001$) compared to the DNCB group. In addition, IgE levels of the MP group were significantly reduced compared to the LP group ($P < 0.01$) (Figure 2).

3.3. Effects of Acupuncture on Cytokine Levels. RT-PCR was performed to measure the expression levels of pro-inflammatory cytokine (IL-8, TNF-α, and IL-1β) and Th2 cytokine (IL-4) mRNA in the dorsal skin. Expression of IL-4, IL-8, TNF-α, and IL-1β mRNA was induced by DNCB treatment (5.05 ± 1.25, 155.04 ± 22.49, 110.67 ± 11.16, and 392.82 ± 70.59, resp.). IL-4, IL-8, and TNF-α mRNA expression was drastically downregulated in the dorsal skin of MP-treated mice (2.05 ± 0.35, 50.58 ± 16.87, and 21.21 ± 1.61, resp.) but not in the LP group (Figure 3). In addition, the level of IL-4, IL-8, and TNF-α mRNA was significantly reduced in the MP group compared to the LP group. Expression of IL-1β mRNA followed an expression pattern similar to that of the other cytokines in the treatment groups, but it was not statistically significant.

3.4. Effects of Acupuncture on NF-κB Expression in the Skin. To investigate the anti-inflammatory mechanism of acupuncture treatment in ACD-like disorders, the effects of acupuncture on activation of NF-κB, an important transcription factor that mediates the transcription of many pro-inflammatory cytokine genes, were examined by western blotting. MP and LP treatment significantly reduced the expression of NF-κB (MP: 260.02 ± 14.67, $P < 0.001$; LP: 556.87 ± 36.24, $P < 0.001$) compared to the DNCB group (826.82 ± 60.63). In addition, the MP group displayed greater anti-inflammatory efficacy than the LP group ($P < 0.001$) (Figure 4).

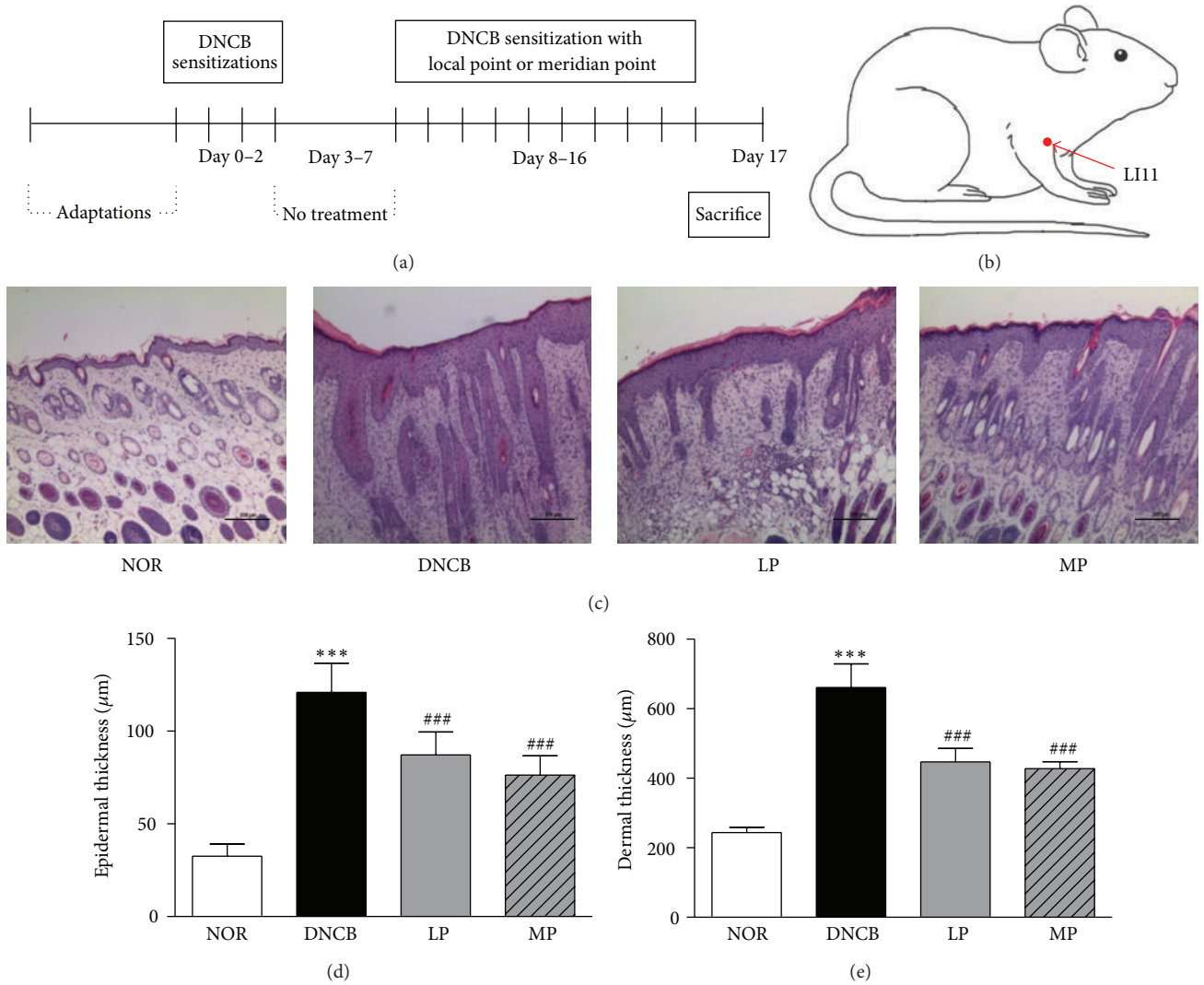

Figure 1: Experimental details and the result of histological analysis by H&E staining of epidermal and dermal hyperplasia. (a) Experimental schedule of DNCB sensitization and acupuncture treatment at the local and meridian points. (b) Location of the acupuncture point LI11 used in this study. LI11 is in the depression on the lateral end of the cubital crease, at the midpoint of the line connecting LU5 with the lateral epicondyle of the humerus. (c) Reduced thickening and hyperplasia after acupuncture treatment at local and meridian points in the epidermis and dermis. Scale bar: 200 μm. (d-e) The skin thickness of the DNCB group was significantly increased compared to the normal group. Acupuncture treatment at the local points and meridian points significantly reduced thickening and hyperplasia in the epidermis (d) and dermis (e) compared to the DNCB group. NOR: mice treated with vehicle; DNCB: mice sensitized with DNCB; LP: mice sensitized with DNCB and treated at local points around the lesion; MP: mice sensitized with DNCB and treated at meridian point, LI11. $^{***}P < 0.001$, compared to the NOR group; $^{###}P < 0.001$, compared to the DNCB group. One-way ANOVA followed by the Newman-Keuls test was performed for statistical analysis, and all data are presented as the mean ± S.D.

3.5. Effects of Acupuncture on Expression of MAPKs in the Skin. The DNCB group displayed increased expression of MAPK signaling proteins: p-ERK1/2, p-JNK, and p-p38 in the MAPK signaling pathway (946.89 ± 68.80, 305.89 ± 7.64, and 184.81 ± 24.64, resp.). MP treatment inhibited the upregulation of phosphorylation of ERK1/2, JNK, and p38 (299.95 ± 10.39, 161.66 ± 21.35, and 93.00 ± 20.04) compared with the DNCB group. In addition, the levels of p-ERK1/2 and p-38 in the LP group were not statistically different from, the DNCB group, whereas the change in expression of p-JNK was statistically significant. MP treatment reduced the levels of p-ERK1/2, p-JNK, and p-p38 more effectively than LP treatment (930.88 ± 77.37, 260.99 ± 21.77, and 201.35 ± 18.08, resp.) (Figure 5).

4. Discussion

Although acupuncture treatment has been increasingly used in atopic dermatitis, with several clinical studies demonstrating the effectiveness of acupuncture [17, 18], preclinical studies, especially in vivo studies, investigating the mechanism of

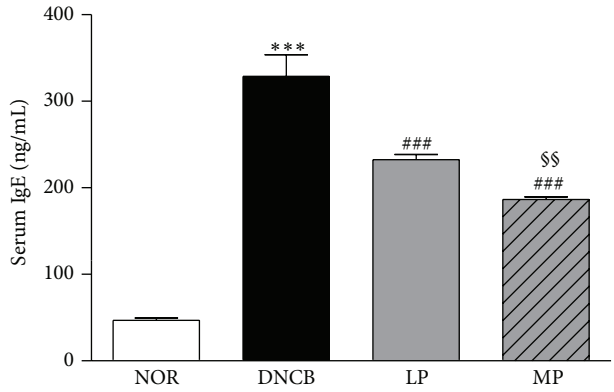

Figure 2: Suppression of serum IgE levels by acupuncture treatment. DNCB-mediated induction of IgE levels was significantly reduced in the MP and LP groups. IgE levels in the MP group were less than in the LP group. NOR: mice treated with vehicle; DNCB: mice sensitized with DNCB; LP: mice sensitized with DNCB and treated at local points around the lesion; MP: mice sensitized with DNCB and treated at meridian point LI11. $^{***}P < 0.001$, compared to the NOR group; $^{###}P < 0.001$, compared to the DNCB group. $^{§§}P < 0.01$, compared to the LP group. One-way ANOVA followed by the Newman-Keuls test was performed for statistical analysis, and all data are presented as the mean ± S.D.

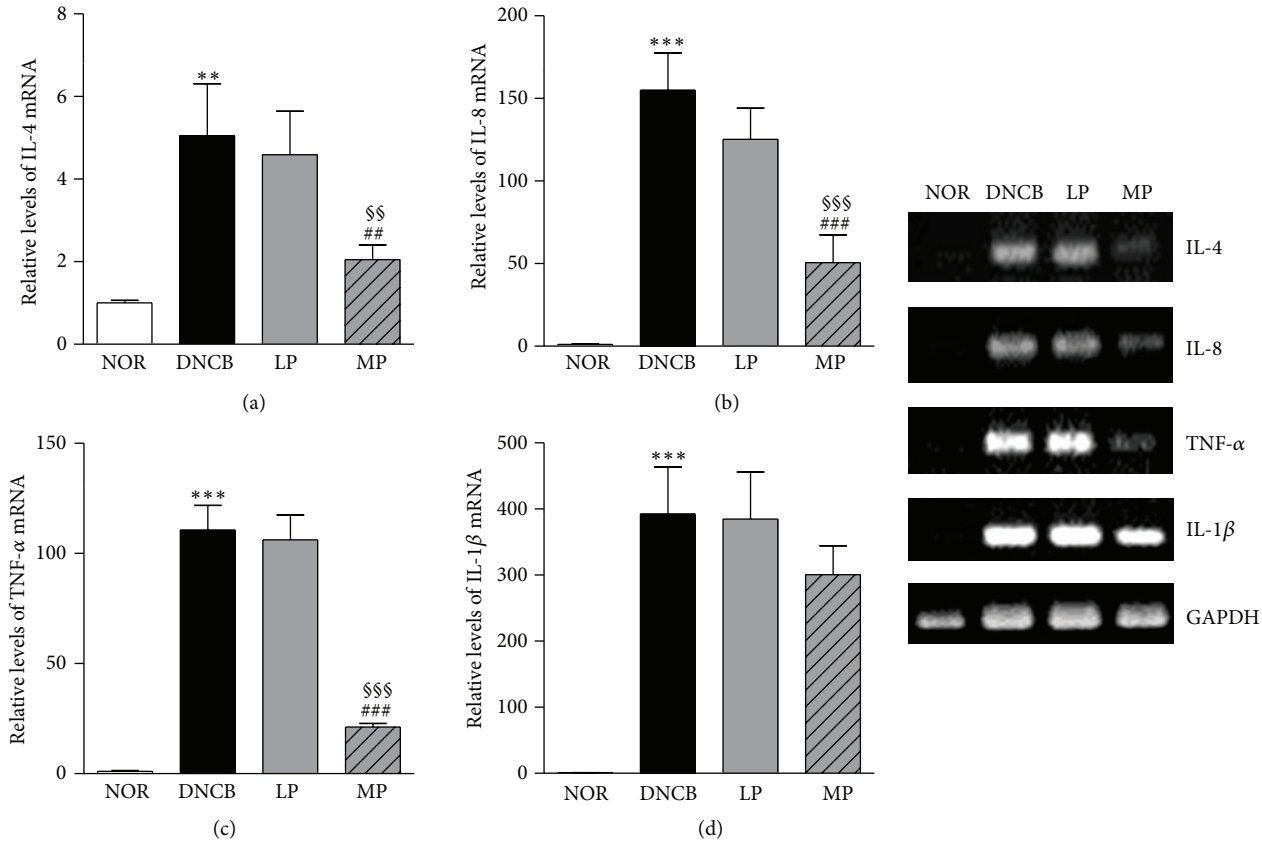

Figure 3: Effects of acupuncture treatment on production of cytokines. IL-4, IL-8, TNF-α, and IL-1β mRNA expression was increased significantly by DNCB sensitization. MP treatment significantly reduced IL-4, IL-8, and TNF-α expression. NOR: mice treated with vehicle; DNCB: mice sensitized with DNCB; LP: mice sensitized with DNCB and treated at local points around the lesion; MP: mice sensitized with DNCB and treated at meridian point LI11. $^{**}P < 0.01$, $^{***}P < 0.001$, compared to the NOR group; $^{##}P < 0.01$, $^{###}P < 0.001$, compared to the DNCB group; $^{§§}P < 0.01$, $^{§§§}P < 0.001$, compared to the LP group. One-way ANOVA followed by the Newman-Keuls test was performed for statistical analysis, and all data are presented as the mean ± S.D.

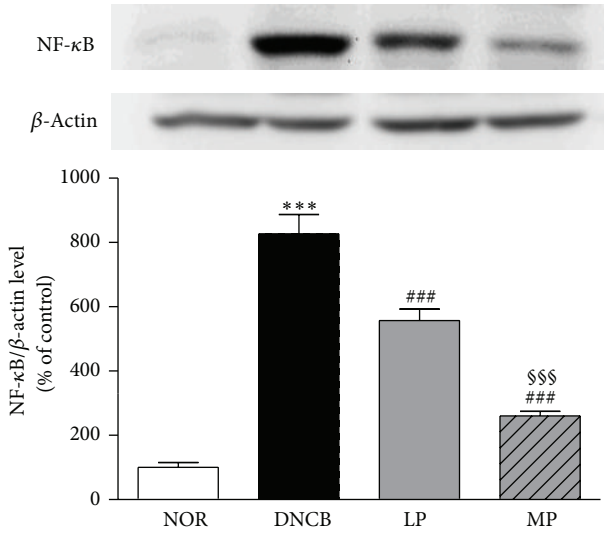

Figure 4: Suppression of NF-κB expression by acupuncture treatment. Increased expression of NF-κB was significantly reduced upon MP and LP treatment. The MP group showed reduced expression compared to the LP group. NOR: mice treated with vehicle; DNCB: mice sensitized with DNCB; LP: mice sensitized with DNCB and treated at local points around the lesion; MP: mice sensitized with DNCB and treated at meridian point LI11. $^{***}P < 0.001$, compared to the NOR group; $^{\#\#\#}P < 0.001$, compared to the DNCB group; $^{\S\S\S}P < 0.001$, compared to the LP group. One-way ANOVA followed by the Newman-Keuls test was performed for statistical analysis, and all data are presented as the mean ± S.D.

action for acupuncture are lacking. To the best of our knowledge, this is the first study to identify acupuncture-mediated anti-inflammatory mechanisms in atopic dermatitis.

Several methods for selecting acupuncture points to treat dermatitis exist. One method involves selection of meridian points at locations remote from the lesion, such as LI11 and LI4 [20, 21]. An alternative method selects local points around the lesion [14]. Among the meridian points, LI11 is known to have therapeutic effects on various skin diseases such as inflammation, pruritus, and urticaria [20–22]. In this study, we investigated the therapeutic effect of the LI11 meridian point compared to local points around the lesion to define potential differences of the effect based on the location of acupuncture treatment.

ACD is defined as inflammatory skin disease characterized by pruritic and eczematous skin lesions, extensive inflammatory cell infiltration, and release of pro-inflammatory mediators [23]. To evaluate the histological changes after MP treatment in DNCB-induced mice, dorsal skin sections were subjected to H&E staining. Hypertrophy and hyperkeratosis of the dermis and epidermis were observed in our DNCB-induced model. In contrast, the MP and LP groups displayed significant reductions in DNCB-induced hyperplasia of epidermal and dermal thickening. Though there was no significant difference between the MP and LP groups, the reduction of DNCB-induced hyperplasia and epidermal thickening was a little more pronounced in the MP group.

IgE expression was known to cause both acute and chronic phase skin inflammations. Therefore, the upregulation of total serum IgE is a hallmark of ACD [24]. In the present study, the concentration of total serum IgE was reduced in both MP- and LP-treated mice as compared to the DNCB group. Interestingly, meridian point acupuncture treatment is more effective in reducing allergic sensitization and the severity of ACD than local acupuncture treatment.

We next examined the effect of acupuncture treatment on cytokine responses. In the pathogenesis and progression of ACD, the regulation of inflammatory cytokine production is an essential step. Important roles of Th1 and Th2 cytokines have been confirmed in DNCB-induced allergic skin inflammation models by targeting deletions of these cytokines [25]. Generally, contact allergens have been associated with increases in the Th1 cytokines, INF-γ and TNF-α. In particular, TNF-α is an essential mediator of ACD [26]. TNF-α expression is increased after challenge with DNCB and only showed a significant reduction in MP treatment. Also, we showed that MP treatment decreased Th2 cytokine IL-4, which plays a central role in the promotion of an allergic inflammatory eosinophilic reaction in allergic diseases through IgE isotype switching [25]. Therefore, our results suggest that MP treatment can reduce serum IgE by suppressing the Th1 response as well as Th2. In addition, IL-8, a member of the chemokine family, is produced by various types of cells upon stimulation with inflammatory stimuli [27]. A pathological increase of cutaneous IL-1β is associated with edema formation, epidermal hyperproliferation, and contact atopic dermatitis in humans [27]. Our data showed that IL-8 and IL-1β expression is increased after challenge with DNCB and only showed a significant reduction of IL-8 reduction in MP treatment. Meanwhile, LP treatment did not affect any of the expression of pro-inflammatory cytokines. These results showed that acupuncture treatment on the LI11 meridian point is more effective in regulating pro-inflammatory, Th1 and Th2, cytokines than local point treatment.

Transcription factors of the NF-κB family have also been implicated in the arrest of proliferation and initiation of differentiation in epidermal keratinocytes [28]. Additionally, many studies have reported that the MAPK signaling cascade plays an essential role in the initiation of inflammatory responses [29]. In addition, activation of the MAPK signaling pathway ultimately results in direct or indirect phosphorylation and/or activation of NF-κB, as well as alterations in gene expression [30]. These findings indicate that the MAPK pathway could be an effective target for anti-inflammatory therapy. We confirmed that increased expression of NF-κB and MAPKs by DNCB treatment was subsequently reduced after MP treatment. The results suggest that MP treatment has anti-inflammatory effects by inhibiting pro-inflammatory activities. This anti-inflammatory effect of MP treatment might be produced through the systemic immune modulations which are connected to central nerve changes induced by acupuncture treatment [31–37]. We also found that LP treatment influenced regulating NF-κB and p-JNK. It might be mainly produced by local anti-inflammatory action of acupuncture stimulation [14]. Overall, effect of LP

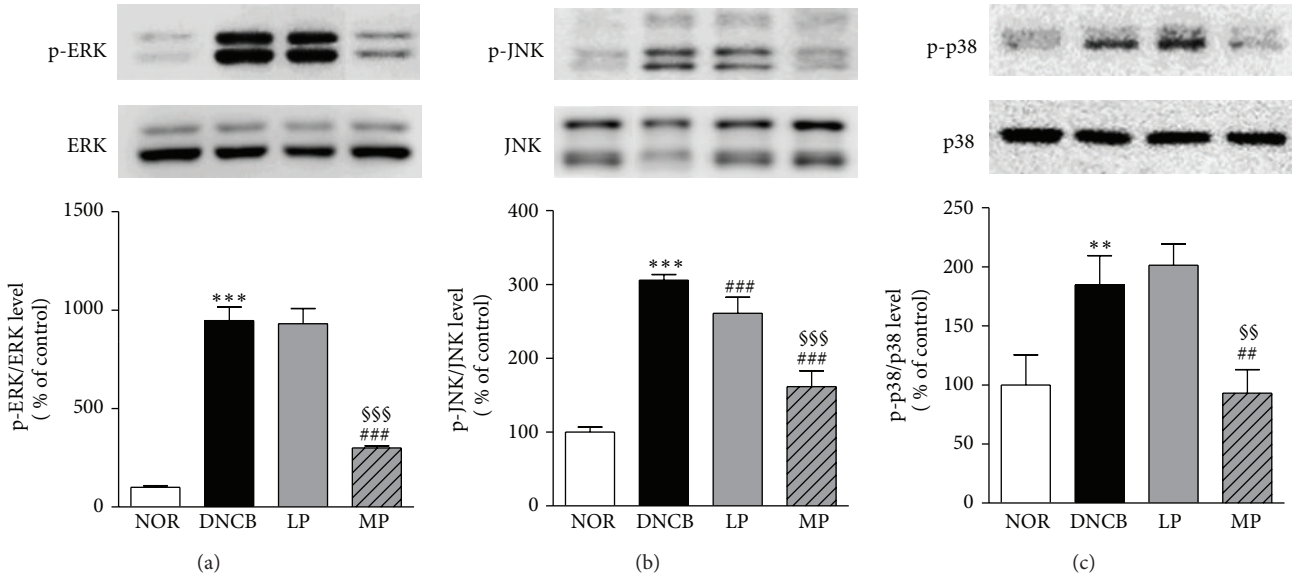

Figure 5: Suppression of MAP kinase expression by acupuncture at the meridian point LI11. Phosphorylation of ERK1/2, JNK, and p38 MAP kinases was significantly elevated by DNCB sensitization. Acupuncture treatment on the meridian point significantly suppressed the expression of MAP kinases. NOR: mice treated with vehicle; DNCB: mice sensitized with DNCB; LP: mice sensitized with DNCB and treated at local points around the lesion; MP: mice sensitized with DNCB and treated at meridian point LI11. $^{**}P < 0.01$, $^{***}P < 0.001$, compared to the NOR group; $^{\#\#}P < 0.01$, $^{\#\#\#}P < 0.001$, compared to the DNCB group; $^{\S\S}P < 0.01$, $^{\S\S\S}P < 0.001$, compared to the LP group. One-way ANOVA followed by the Newman-Keuls test was performed for statistical analysis, and all data are presented as the mean ± S.D.

treatment was less powerful than MP treatment and it did not affect pro-inflammatory cytokines and proteins. From these results, we suggest that MP treatment is more effective in regulating pro-inflammatory biomarkers speculated to be exerted by systemic modulation.

In summary, we demonstrated that acupuncture treatment on the LI11 meridian point is an effective means to reduce mouse dorsal skin hyperplasia and serum IgE levels in ACD, and these effects were mediated by regulating pro-inflammatory cytokines (IL-4, IL-8, and TNF-α) and proteins (NF-κB and MAPKs). In contrast, local point treatment was also effective in reducing dorsal skin thickness and serum IgE levels; however, it did not affect most of pro-inflammatory cytokines and proteins, which indicates that the therapeutic effect of local stimulation in ACD might be produced by pathways other than pro-inflammatory pathways. These results demonstrate that acupuncture may be a useful treatment for the treatment of ACD. Further investigation would be necessary to clarify its molecular mechanisms of action.

Acknowledgment

This research was supported by the Basic Science Research Program through the National Research Foundation of Korea (NRF) funded by the Ministry of Education, Science and Technology (no. 2005-0049404).

References

[1] M. Vocanson, A. Hennino, M. Cluzel-Tailhardat et al., "CD8+ T cells are effector cells of contact dermatitis to common skin allergens in mice," *Journal of Investigative Dermatology*, vol. 126, no. 4, pp. 815–820, 2006.

[2] J. A. Woodfolk, "T-cell responses to allergens," *Journal of Allergy and Clinical Immunology*, vol. 119, no. 2, pp. 280–294, 2007.

[3] M. Uehara, R. Izukura, and T. Sawai, "Blood eosinophilia in atopic dermatitis," *Clinical and Experimental Dermatology*, vol. 15, no. 4, pp. 264–266, 1990.

[4] Y. Y. Choi, M. H. Kim, J. H. Kim et al., "Schizonepeta tenuifolia inhibits the development of atopic dermatitis in mice," *Phytotherapy Research*, vol. 27, no. 8, pp. 1131–1135, 2013.

[5] F. Schultz Larsen, "The epidemiology of atopic dermatitis," *Monographs in Allergy*, vol. 31, pp. 9–28, 1993.

[6] J. del Rosso and S. F. Friedlander, "Corticosteroids: options in the era of steroid-sparing therapy," *Journal of the American Academy of Dermatology*, vol. 53, no. 1, pp. S50–S58, 2005.

[7] T. Schäfer, A. Riehle, H.-E. Wichmann, and J. Ring, "Alternative medicine in allergies—prevalence, patterns of use, and costs," *Allergy*, vol. 57, no. 8, pp. 694–700, 2002.

[8] S. Boneberger, R. A. Rupec, and T. Ruzicka, "Complementary therapy for atopic dermatitis and other allergic skin diseases: facts and controversies," *Clinics in Dermatology*, vol. 28, no. 1, pp. 57–61, 2010.

[9] M. Yeom, S. H. Kim, B. Lee et al., "Oral administration of glucosylceramide ameliorates inflammatory dry-skin condition in chronic oxazolone-induced irritant contact dermatitis in the mouse ear," *The Journal of Dermatological Science*, vol. 67, no. 2, pp. 101–110, 2012.

[10] B. M. Berman, H. H. Langevin, C. M. Witt, and R. Dubner, "Acupuncture for chronic low back pain," *The New England Journal of Medicine*, vol. 363, no. 5, pp. 454–461, 2010.

[11] A. J. Vickers, A. M. Cronin, A. C. Maschino et al., "Acupuncture for chronic pain: individual patient data meta-analysis,"

Archives of Internal Medicine, vol. 172, no. 19, pp. 1444–1453, 2012.

[12] C. H. M. Woollam and A. O. Jackson, "Acupuncture in the management of chronic pain," *Anaesthesia*, vol. 53, no. 6, pp. 593–595, 1998.

[13] T. F. Su, Y. Q. Zhao, L. H. Zhang et al., "Electroacupuncture reduces the expression of proinflammatory cytokines in inflamed skin tissues through activation of cannabinoid CB2 receptors," *European Journal of Pain*, vol. 16, no. 5, pp. 624–635, 2012.

[14] J.-A. Lee, H. J. Jeong, H.-J. Park, S. Jeon, and S.-U. Hong, "Acupuncture accelerates wound healing in burn-injured mice," *Burns*, vol. 37, no. 1, pp. 117–125, 2011.

[15] S. I. Park, Y. Y. Sunwoo, Y. J. Jung et al., "Therapeutic effects of acupuncture through enhancement of functional angiogenesis and granulogenesis in rat wound healing," *Evidence-Based Complementary and Alternative Medicine*, vol. 2012, Article ID 464586, 10 pages, 2012.

[16] F. Salameh, D. Perla, M. Solomon et al., "The effectiveness of combined Chinese herbal medicine and acupuncture in the treatment of atopic dermatitis," *Journal of Alternative and Complementary Medicine*, vol. 14, no. 8, pp. 1043–1048, 2008.

[17] F. Pfab, J. Huss-Marp, A. Gatti et al., "Influence of acupuncture on type i hypersensitivity itch and the wheal and flare response in adults with atopic eczema—a blinded, randomized, placebo-controlled, crossover trial," *Allergy*, vol. 65, no. 7, pp. 903–910, 2010.

[18] F. Pfab, M.-T. Kirchner, J. Huss-Marp et al., "Acupuncture compared with oral antihistamine for type i hypersensitivity itch and skin response in adults with atopic dermatitis—a patient- and examiner-blinded, randomized, placebo-controlled, crossover trial," *Allergy*, vol. 67, no. 4, pp. 566–573, 2012.

[19] F. Pfab, G. I. Athanasiadis, J. Huss-Marp et al., "Effect of acupuncture on allergen-induced basophil activation in patients with atopic eczema: a pilot trial," *Journal of Alternative and Complementary Medicine*, vol. 17, no. 4, pp. 309–314, 2011.

[20] K. C. Lee, A. Keyes, J. R. Hensley et al., "Effectiveness of acupressure on pruritus and lichenifi cation associated with atopic dermatitis: a pilot trial," *Acupuncture in Medicine*, vol. 30, no. 1, pp. 8–11, 2012.

[21] C.-Y. Chou, C. Y. Wen, M.-T. Kao, and C.-C. Huang, "Acupuncture in haemodialysis patients at the Quchi (LI11) acupoint for refractory uraemic pruritus," *Nephrology Dialysis Transplantation*, vol. 20, no. 9, pp. 1912–1915, 2005.

[22] M. A. C. C. O. K. O. M. Colleges, *Details of Meridians & Acupoints (Volume I): A Guidebook for College Students*, Eui Bang Publishing Co, Wonju, Republic of Korea, 2009.

[23] N. Morar, S. A. G. Willis-Owen, M. F. Moffatt, and W. O. C. M. Cookson, "The genetics of atopic dermatitis," *Journal of Allergy and Clinical Immunology*, vol. 118, no. 1, pp. 24–34, 2006.

[24] S. H. Arshad and S. Holgate, "The role of IgE in allergen-induced inflammation and the potential for intervention with a humanized monoclonal anti-IgE antibody," *Clinical and Experimental Allergy*, vol. 31, no. 9, pp. 1344–1351, 2001.

[25] C. A. Akdis, M. Akdis, T. Bieber et al., "Diagnosis and treatment of atopic dermatitis in children and adults: European Academy of Allergology and Clinical Immunology/American Academy of Allergy, Asthma and Immunology/PRACTALL consensus report," *The Journal of Allergy and Clinical Immunology*, vol. 118, no. 1, pp. 152–169, 2006.

[26] S. E. Anderson, P. D. Siegel, and B. J. Meade, "The LLNA: a brief review of recent advances and limitations," *Journal of Allergy*, vol. 2011, Article ID 424203, 10 pages, 2011.

[27] A. Harada, N. Sekido, T. Akahoshi, T. Wada, N. Mukaida, and K. Matsushima, "Essential involvement of interleukin-8 (IL-8) in acute inflammation," *Journal of Leukocyte Biology*, vol. 56, no. 5, pp. 559–564, 1994.

[28] C. S. Seitz, Q. Lin, H. Deng, and P. A. Khavari, "Alterations in NF-κB function in transgenic epithelial tissue demonstrate a growth inhibitory role for NF-κB," *Proceedings of the National Academy of Sciences of the United States of America*, vol. 95, no. 5, pp. 2307–2312, 1998.

[29] H. Adwanikar, F. Karim, and R. W. Gereau IV, "Inflammation persistently enhances nocifensive behaviors mediated by spinal group I mGluRs through sustained ERK activation," *Pain*, vol. 111, no. 1-2, pp. 125–135, 2004.

[30] L. Y. Guo, T. M. Hung, K. H. Bae et al., "Anti-inflammatory effects of schisandrin isolated from the fruit of Schisandra chinensis Baill," *European Journal of Pharmacology*, vol. 591, no. 1–3, pp. 293–299, 2008.

[31] N. Goldman, M. Chen, T. Fujita et al., "Adenosine A1 receptors mediate local anti-nociceptive effects of acupuncture," *Nature Neuroscience*, vol. 13, no. 7, pp. 883–888, 2010.

[32] Z.-L. Guo, A. R. Moazzami, S. Tjen-A-Looi, and J. C. Longhurst, "Responses of opioid and serotonin containing medullary raphe neurons to electroacupuncture," *Brain Research*, vol. 1229, pp. 125–136, 2008.

[33] F. J. Zijlstra, I. van den Berg-de Lange, F. J. P. M. Huygen, and J. Klein, "Anti-inflammatory actions of acupuncture," *Mediators of Inflammation*, vol. 12, no. 2, pp. 59–69, 2003.

[34] M. T. Cabioglu and B. E. Cetin, "Acupuncture and immunomodulation," *The American Journal of Chinese Medicine*, vol. 36, no. 1, pp. 25–36, 2008.

[35] S. K. Kim and H. Bae, "Acupuncture and immune modulation," *Autonomic Neuroscience: Basic and Clinical*, vol. 157, no. 1-2, pp. 38–41, 2010.

[36] C. Libert, "Inflammation: a nervous connection," *Nature*, vol. 421, no. 6921, pp. 328–329, 2003.

[37] E.-T. Hahm, J.-J. Lee, W.-K. Lee, H.-S. Bae, B.-I. Min, and Y.-W. Cho, "Electroacupuncture enhancement of natural killer cell activity suppressed by anterior hypothalamic lesions in rats," *NeuroImmunoModulation*, vol. 11, no. 4, pp. 268–272, 2004.

Hindawi Publishing Corporation
Evidence-Based Complementary and Alternative Medicine
Volume 2013, Article ID 452948, 15 pages
http://dx.doi.org/10.1155/2013/452948

Research Article

Mechanisms Underlying the Antiproliferative and Prodifferentiative Effects of Psoralen on Adult Neural Stem Cells via DNA Microarray

You Ning,[1] Jian-Hua Huang,[1] Shi-Jin Xia,[2] Qin Bian,[1] Yang Chen,[1] Xin-Min Zhang,[1] Jing-Cheng Dong,[1] and Zi-Yin Shen[1]

[1] *Institute of Integrated Traditional Chinese Medicine and Western Medicine, Huashan Hospital, Fudan University, Shanghai 200031, China*
[2] *Shanghai Institute of Geriatrics, Huadong Hospital, Fudan University, Shanghai 200031, China*

Correspondence should be addressed to Zi-Yin Shen; ziyinshen@126.com

Received 21 March 2013; Accepted 28 April 2013

Academic Editor: Yong Qing Yang

Adult neural stem cells (NSCs) persist throughout life to replace mature cells that are lost during turnover, disease, or injury. The investigation of NSC creates novel treatments for central nervous system (CNS) injuries and neurodegenerative disorders. The plasticity and reparative potential of NSC are regulated by different factors, which are critical for neurological regenerative medicine research. We investigated the effects of Psoralen, which is the mature fruit of *Psoralea corylifolia L.*, on NSC behaviors and the underlying mechanisms. The self-renewal and proliferation of NSC were examined. We detected neuron- and/or astrocyte-specific markers using immunofluorescence and Western blotting, which could evaluate NSC differentiation. Psoralen treatment significantly inhibited neurosphere formation in a dose-dependent manner. Psoralen treatment increased the expression of the astrocyte-specific marker but decreased neuron-specific marker expression. These results suggested that Psoralen was a differentiation inducer in astrocyte. Differential gene expression following Psoralen treatment was screened using DNA microarray and confirmed by quantitative real-time PCR. Our microarray study demonstrated that Psoralen could effectively regulate the specific gene expression profile of NSC. The genes involved in the classification of cellular differentiation, proliferation, and metabolism, the transcription factors belonging to Ets family, and the hedgehog pathway may be closely related to the regulation.

1. Introduction

Adult neural stem cells (NSCs) in the adult nervous system serve as a common source of all neural cells, including neurons, astrocytes, and oligodendrocytes [1]. NSCs persist throughout life in the subgranular zone (SGZ) and the subventricular zone (SVZ) [2] to replace mature cells that are lost during turnover, disease, or injury. NSCs remain relatively quiet under normal circumstances [3]. However, various stimuli, such as blood anoxia, trauma, and oxidative stress, initiate the proliferation and differentiation of NSC [4]. NSCs continually self-renew and expand the pool of undifferentiated cells during early stages. These actively proliferating NSC create neurons and subsequently differentiate into astrocytes and oligodendrocytes. Neurons are the functional components of the nervous system, and they are responsible for information processing and transmission. In contrast, astrocytes and oligodendrocytes are collectively known as glia and play supporting roles that are essential for the proper functioning of the nervous system. Astrocytes have become the focus of brain function research in recent years. Mouse brain astrocytes modulate the excitation of inhibitory neurons and inhibit the general activity of surrounding neurons to prevent the overexcitation of neurons in the nerve ring [5]. Neurons cannot produce an enhanced response without the help of astrocytes [6]. This long-term neuronal reaction is the basis of learning and memory. Astrocytes may aid neurons in the production of this enhanced response for a few hours or several days. Astrocytes may play an important role in brain functional activities.

The plasticity and reparative potential of NSC is regulated by various factors, such as neurotransmitters, growth factors,

and other extrinsic factors [7]. Therefore, the factors that control the balance between NSC proliferation and differentiation are critical for neurological regenerative medicine research.

Recent evidence suggests that Chinese traditional medicines protect neural cells, improve the ability to resist the damage, and induce NSC proliferation and differentiation [8]. Notably, some herbs may be involved in the maintenance of NSC, but others induce neurogenesis or astrogenesis. The literature [9] suggests that astragaloside as the main active components in astragalus (Huang-Qi in Chinese) significantly promotes the proliferation of NSCs in vitro. Another evidence [10] has established that the combination of BDNF and salidroside can promote the NSCs in the epileptic brain tissues that differentiate into GABA neurons. Therefore, the use of Chinese medicine and its effective ingredients in NSC research generates a novel direction in nerve regeneration research and demonstrates great potential for the curing of diseases of the central nervous system.

Psoralens are the linear isomers of the furocoumarin family. Psoralen is extracted from the mature fruit of *Psoralea corylifolia L.* (Bu-Gu-Zhi in Chinese) and exhibit photosensitizing effects and various biological activities. Psoralen is commonly used in combination with long wavelength ultraviolet light for the treatment of a variety of skin diseases, such as psoriasis, vitiligo, cutaneous T-cell lymphoma, pemphigus vulgaris, systemic sclerosis, and systemic lupus erythematosus [11–15]. Varying degrees of remission of these diseases occur after Psoralen treatment. The ability of Psoralen to modulate the proliferation and differentiation of cultured cells in vitro, including epidermal cells [16], vascular smooth muscle cells [17], bladder carcinoma cells [18], mucoepidermoid carcinoma cells [19], mammary cancer cells [20], and osteoblasts [21], has been investigated. Psoralen induces transformation from the G1 phase to the S phase or the G2 phase in osteoblasts, which suggests that these compounds effectively regulate progenitor and stem cells.

A series of experiments were performed to examine the role of Psoralen on the proliferation, multidirectional differentiation of NSC. Microarray libraries were generated from the Psoralen-treated NSC to systematically analyze the transcript profile of Psoralen-treated NSC and gain insight into the underlying molecular mechanisms.

2. Materials and Methods

2.1. Animals. Pregnant Kunming female mice were maintained in the animal facility of the Public Health Center of Fudan University. All procedures were approved by the Animal Care and Use Committee of Fudan University in accordance with the guidelines for animal use of the National Institutes of Health.

2.2. NSC Preparation and Culture. Neurosphere culture was performed as described previously [22] with some modifications. Mouse embryos at embryonic day 14 (E14) were collected from timed-pregnant Kunming mice and placed in D-PBS (Invitrogen, CA, USA). The forebrain neuroepithelium was removed from the embryos under a dissection microscope. The resultant tissue was dissociated by mechanical dissociation into a single-cell suspension using a small-bore, fire-polished Pasteur pipette. The cells were filtered through a sterile nylon mesh and washed twice with a DMEM/F12 medium (Invitrogen, CA, USA) containing 100 units/mL penicillin and 100 μg/mL streptomycin. The number of viable cells was determined by trypan blue staining. Neurosphere culture was initiated by seeding the cells at a density of 1×10^5 to 2×10^5 viable cells/mL in the basal medium supplemented with 20 ng/mL human recombinant fibroblast growth factor-2 (hrFGF2, Invitrogen, CA, USA), 20 ng/mL human recombinant endothelial growth factor (hrEGF, Invitrogen, CA, USA), and Stempro NSC supplement (Invitrogen, CA, USA). The surface of the culture dishes was coated with Poly-D lysine (PDL) (10 mg/mL, Millipore, USA) to prevent cell attachment.

2.3. Neurosphere Formation Assay. Cells were plated under clonal conditions at 5 cells/μL in 96-well plate (0.1 mL/well) in serum-free DMEM/F12 medium containing 20 ng/mL hrFGF-2 (Invitrogen, CA, USA), Stempro NSC supplement (Invitrogen, CA, USA), 100 units/mL penicillin and 100 μg/mL streptomycin. The next day, various concentrations (10 nM, 50 nM, and 100 nM) of Psoralen (Yousi Biotechnology, Shanghai, China; purity above 99% HPLC) were added to each well. The total number of spheres that formed in each well was quantified after 8 d. Only colonies >40 μm in diameter were counted as neurospheres. Neurosphere size was determined by measuring the diameters of individual neurospheres under light microscopy, and it is expressed as a volume (assuming a spherical shape). The consecutive second, third, or fourth passages were used to determine neurosphere formation.

2.4. Cell Proliferation Assay. Cell proliferation was based on the incorporation of EdU and its subsequent detection by a fluorescent azide through a Cu(I)-catalyzed [3 + 2] cycloaddition reaction ("click" chemistry) as described previously [23]. In brief, single NSCs were grown in 96-well plates in DMEM/F12 medium containing 20 ng/mL hrFGF-2 and hrEGF (Invitrogen, CA, USA), Stempro NSC supplement (Invitrogen, CA, USA), 100 units/mL penicillin, and 100 μg/mL streptomycin. EdU was added to the culture media in a final concentration of 10 μM for 3 h. Cells were fixed in formaldehyde and penetrated with 0.5% Triton X-100. The cells were stained during a 30 min incubation with 100 mM Tris, 0.5 mM $CuSO_4$, 10 μM Alexa 594-azide, and 50 mM ascorbic acid. Cells were counterstained with 4′-6-diamidino-2-phenylindole (DAPI). The cells were washed and imaged using fluorescence microscopy.

2.5. Differentiation Assay. Single NSCs were plated at a density of 5000 cells/well in 10 μg/mL PDL-coated 96-well culture dishes (Corning, NY, USA) and incubated for 3 d in a differentiation medium of DMEM/F12 containing 1% fetal bovine serum (Invitrogen, CA, USA), Stempro NSC supplement (Invitrogen, CA, USA), 100 units/mL penicillin, and

100 μg/mL streptomycin. The cells were harvested 3 d later for Western blot and immunocytochemical analyses.

2.6. Western Blot Analysis. Cells cultured using the differentiation protocol were harvested and lysed in a buffer containing 50 mM HEPES-NaOH (pH 7.5), 100 mM KCl, 1% Triton X-100, 1% sodium deoxycholate, 0.1% sodium dodecyl sulfate, 1 mM EGTA, 1 mM dithiothreitol, 1 mM phenylmethylsulfonyl fluoride, 0.5% protease inhibitor cocktail (Sigma-Aldrich, MO, USA), 1 mM Na_3VO_4, 10 mM NaF, and 20 mM β-glycerophosphate. The resultant extracts were centrifuged at 14,000 g for 15 min at 4°C to obtain clear cell lysates. Protein concentrations were determined using the Biotime protein assay kit (Beyotime, Shanghai, China) with BSA as a standard. Equal amounts of 35 μg of proteins were loaded on a sodium dodecyl sulfate polyacrylamide gel and separated by electrophoresis. Separated proteins were transferred to nitrocellulose membranes (Amersham Biosciences, USA). The membranes were blocked with 5% (w/v) skim milk in phosphate-buffered saline containing 0.1% Tween 20 and blotted with antibodies for glial fibrillary acidic protein (GFAP) (1 : 500; Chemicon, USA) and β-tubulin III (TuJ1) (1 : 200, Chemicon, USA) followed by incubation with appropriate sets of secondary HRP-conjugated goat anti-mouse or rabbit antibodies (1 : 5000; Jackson ImmunoResearch, USA). Immunoreactive bands were visualized with ECL reagents (Biyotime, Shanghai, China).

2.7. Immunocytochemistry. The cells cultured using the differentiation protocol were fixed for 20 min in 4% paraformaldehyde, blocked in 1% BSA and 0.1% Triton X-100, washed with PBS, incubated for 30 min with 0.3% H_2O_2 to inhibit endogenous peroxidases, and blocked for 1 h using 3% BSA in PBS/0.1% Triton X-100. The following primary antibodies were incubated for 2 hours at room temperature: monoclonal rabbit anti-GFAP (1 : 500; Chemicon, USA), mouse anti-TuJ1 (diluted 1 : 200; Chemicon, USA), and rabbit antinestin (1 : 1000, Chemicon, USA). Secondary Alexa-conjugated 594 F(ab)′2 goat anti-rabbit antibody and 488 Alexa-conjugated goat anti-mouse IgG (H + L) (1 : 1000; Invitrogen, USA) were added for 1.5 h in PBS in 1% BSA and 0.1% Triton X-100. The cells were counterstained with DAPI. The number of immunoreactive cells in each well was quantified using fluorescent microscopy.

2.8. Microarray and Data Analysis. The cells cultured using the differentiation protocol for 3 days were harvested and lysed in TRIzol Reagent (Invitrogen, USA). Total RNA was isolated using the Qiagen RNeasy kit (Qiagen) in accordance with the manufacturer's protocol. The isolated RNA was subject to a quality control test. RNA from each sample was used for cDNA synthesis followed by the labeling of the cDNA with Cy3. The labeled cDNA samples were submitted to NimbleGen and hybridized to Mouse Gene Expression 12x135K Arrays (Roche NimbleGen, 05543797001) that represent 44,170 mouse genes. The single-color NimbleGen arrays were scanned using a GenePix 4000B microarray scanner. The data were extracted from the scanned images using NimbleScan v2.5 Software. Expression data were normalized through quantile normalization, and the Robust Multichip Average (RMA) algorithm was included in the NimbleScan software. The Probe level (∗_norm_RMA.pair) files and Gene level (∗_RMA.calls) files were generated after normalization. All gene level files were imported into Agilent GeneSpring GX software (version 11.5.1) for further analysis.

2.9. Quantitative Real-Time PCR. Total RNA from cells was extracted using TRIzol reagent (Invitrogen, USA). One microgram of total RNA was reverse transcribed using the Advantage RT-for-PCR kit (Qiagen, Valencia, CA). Freshly transcribed cDNA was used for quantitative real-time PCR using SYBR Green (Bio-Bad, Hercules, CA). The primers for each gene were designed using the online tool, Primer3 (http://frodo.wi.mit.edu/), and the sequences are listed in supplementary Table 1. PCR was performed using a Rotor-Gene real-time DNA amplification system (Corbett Research, Sydney, Australia) as described in our previous study [24].

2.10. Bioinformatic Analysis. Differentially expressed genes ($P < 0.05$) between the control and Psoralen-treated groups were functionally annotated via the functional annotation tool, Database for Annotation, Visualization, and Integrated Discovery (DAVID) (http://david.abcc.ncifcrf.gov/), which was developed within the Gene Ontology Consortium [25]. The KEGG pathways of the differentially expressed genes between the control and Psoralen-treated groups were also matched using the DAVID functional annotation tool.

The key regulatory processes of the Psoralen effect were analyzed using the Gene Ontology (GO) Tree Machine (http://bioinfo.vanderbilt.edu/webgestalt/) [26]. The directed acyclic graph (DAG) was generated automatically by the GO Tree Machine for the input gene sets, which was created to identify the most important GO categories and suggest their potential biological importance.

Transcription factors are of great significance for cellular differentiation and proliferation. The online tool, oPOSSUM (http://www.cisreg.ca/oPOSSUM/), was used for the analysis of transcription factor binding sites of differentially expressed genes [27].

2.11. Statistical Analysis. All data were expressed as the means ± SD. The statistical significance was calculated using One-way ANOVA (analysis of variance) followed by the least significant difference (LSD) test for post hoc analysis. The significance level was defined as $P < 0.05$. The number of replicated experiments is indicated in the results section or the figure legends.

3. Results

3.1. Psoralen Inhibited Neurosphere Formation. Neurosphere formation demonstrates the self-renewal ability of NSC when single NSC are plated at a very low cell density. NSC formed neurospheres of various sizes in our growth culturing conditions with diameters ranging from 20 μm to greater than 100 μm (Figure 1(a)). These neurospheres exhibited positive

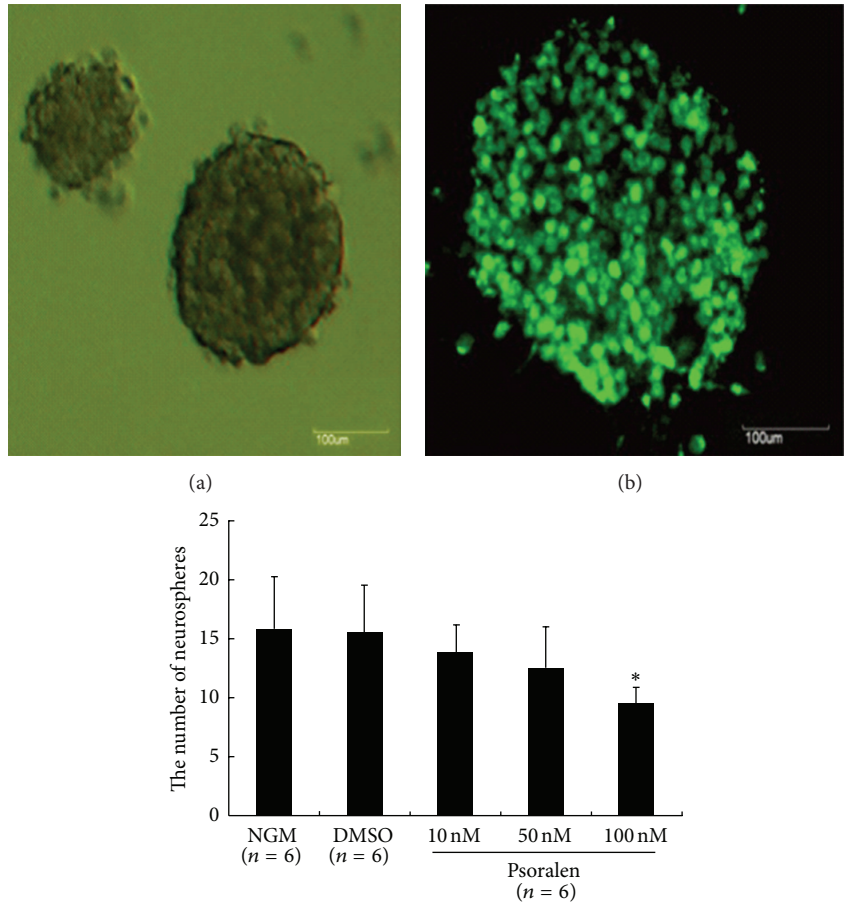

Figure 1: Effects of Psoralen on neurosphere formation of neural stem cells in vitro. Single NSCs at a density of 500 cells/well were cultured in normal growth medium (NGM) containing DMEM/F12 supplemented with hrFGF for 7 days to form various size of neurospheres (a). The neurospheres expressed NSC marker nestin (b). Single NSCs were exposed to NGM, DMSO (0.1%), and 10, 50, 100 nM Psoralen dissolved in DMSO (0.1%), respectively. Psoralen caused a significant decrease in frequency of neurosphere formation (c). Scale bars: 100 μm. Results were expressed as mean ± S.D. of six independent experiments. $^{*}P < 0.05$ versus NGM.

nestin staining (NSC marker), which suggests the presence of NSC and/or neural progenitor cells (Figure 1(b)). We calculated the frequency of neurosphere formation in the presence or absence of Psoralen. The control group formed 15.75 ± 4.43 ($n = 6$) neurospheres from the initially seeded 500 hundred cells (frequency of approximately 3.15%). The solvent (DMSO) did not alter the frequency of neurosphere formation (15.5 ± 3.99, $n = 6$). The neurosphere frequencies for the low (10 nM), middle (50 nM), and high (100 nM) concentrations of Psoralen were 13.91 ± 2.17, 12.56 ± 3.41, 9.43 ± 1.53 ($n = 6$), respectively. The high Psoralen concentration (100 nM) significantly decreased the neurosphere formation of NSC compared to control ($P < 0.05$) (Figure 1(c)).

3.2. Psoralen Inhibited NSC Proliferation. The decrease in neurosphere formation may have been due to a compromised cell proliferation of NSC. Therefore, we investigated NSC proliferation in the presence of Psoralen using EdU incorporation, which identifies cells in the S phase of the cell cycle. The ratio of EdU-positive cells to total cells was 18.8 ± 3.2% ($n = 4$) in the control group. The incorporation of EdU into NSC decreased significantly in the presence of 100 nM Psoralen (12.6 ± 0.8%, $n = 4$; $P < 0.05$ versus control) (Figures 2(a), 2(b), and 2(c)).

3.3. Psoralen Induced the Differentiation of NSC to Astrocytes. Single cells were cultured in a monolayer on PDL-coated dishes in serum without growth factors for 48 h. Immunochemistry revealed that 43.93 ± 6.21% ($n = 4$) of cells in the control group were GFAP-positive (Figure 3(a)) and 18.45 ± 4.6% ($n = 4$) of cells were TuJ1-positive (Figure 3(b)), which suggests multi-potential NSC. The percentage of TuJ1-positive cells did not change after Psoralen treatment ($P > 0.05$ versus control) (Figure 3(c)), but the percentage of GFAP-positive cells significantly increased to 54.32 ± 6.33% ($n = 4$; $P < 0.05$ versus control) (Figure 3(d)). Western blotting analyses of total cell lysates in the Psoralen-treated or untreated cells revealed an increase in GFAP expression.

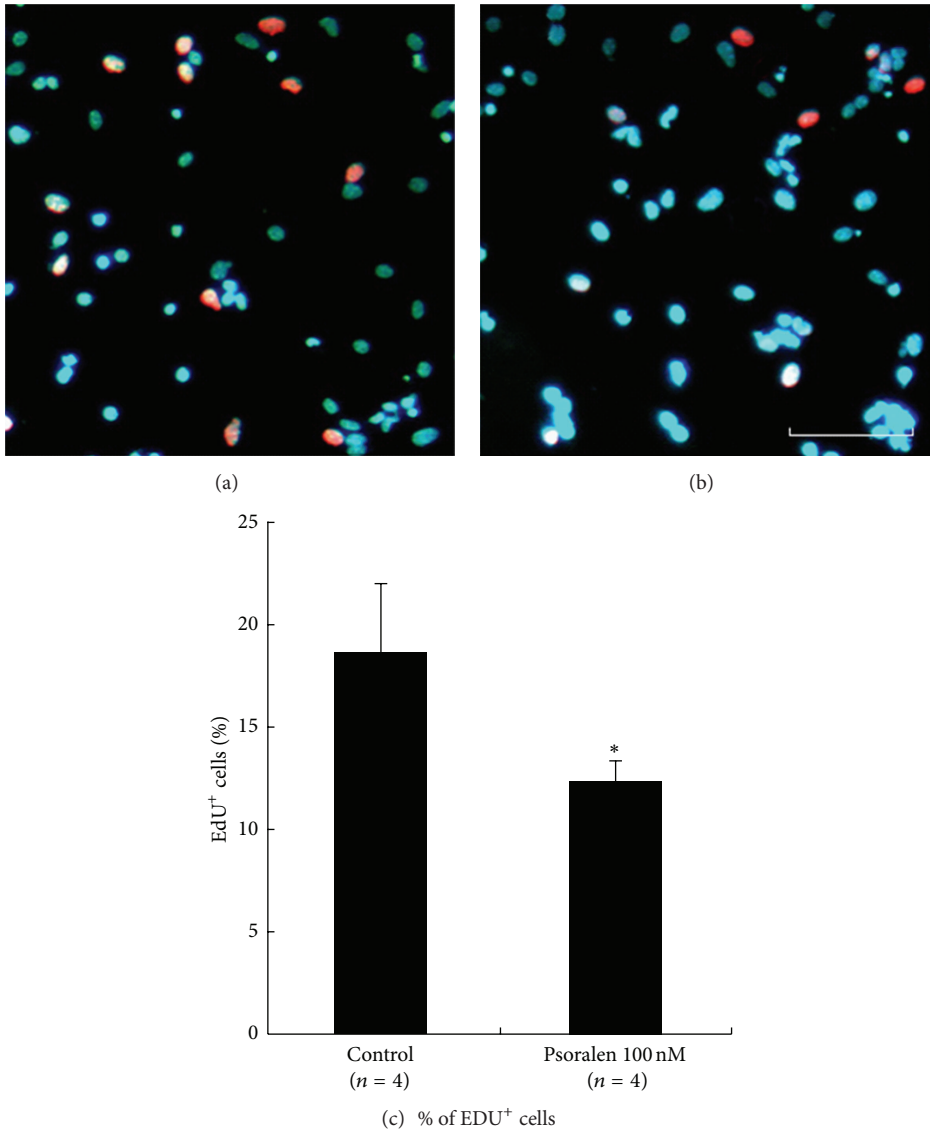

Figure 2: Effects of Psoralen on the proliferation of NSC. Single NSCs were plated at a density of 5000 cells per well in PDL-coated 96-well plate for 12 h. Then, cells were subjected to 10 nM EdU for 2 h, followed by addition of 100 nM OA (b) or not (a). Then Edu immunofluorescence analysis was performed. The cell nuclei were counterstained with DAPI. The percentage of EdU-positive cells in total of 1000 cells was calculated. As a result, Psoralen significantly inhibited the DNA incorporation (c). Scale bars: 100 μm. Results were expressed as mean ± S.D. from four independent experiments. $^{*}P < 0.05$ versus control.

The expression of TuJ1 protein, a neuron-specific marker, was slightly decreased (Figure 3(f)). These results suggested that Psoralen induces the differentiation of NSC to astrocytes.

3.4. Microarray and Data Analysis. We screened the differential expression of genes that were induced by Psoralen using the microarray technique. A total of 129 genes were upregulated by Psoralen by more than 1.5-fold compared to the control group ($P < 0.05$), and 146 genes were downregulated by more than 1.5-fold ($P < 0.05$).

3.5. Confirmation of Differentially Expressed Genes Using Quantitative Real-Time PCR. We confirmed the mRNA expression of CREM, Kit1, Shh, TBX1, Bcl2l11 using quantitative real-time PCR, and these genes were chosen based on the gene function after bioinformatic analyses. The results were a highly consistent with the DNA microarray measurements (Figure 4). CREM (cAMP responsive element modulator) encodes a ZIP transcription factor that binds to the cAMP-responsive element in many viral and cellular promoters. Kit1 (Kit ligand), otherwise known as Stem cell factor or Steel factor, is a growth factor important for the survival, proliferation, and differentiation of hematopoietic stem cells and other progenitor cells. Shh (Sonic hedgehog) is a secreted protein that is required to establish patterns of cellular growth and differentiation within ventral regions of the developing CNS. TBX1 (T-box-1) plays an important role in developmental processes. The fourth gene encodes Bcl2l11 (BCL2-like 11, apoptosis facilitator), regulates, and contributes to programmed cell death and apoptosis. The expression profiles

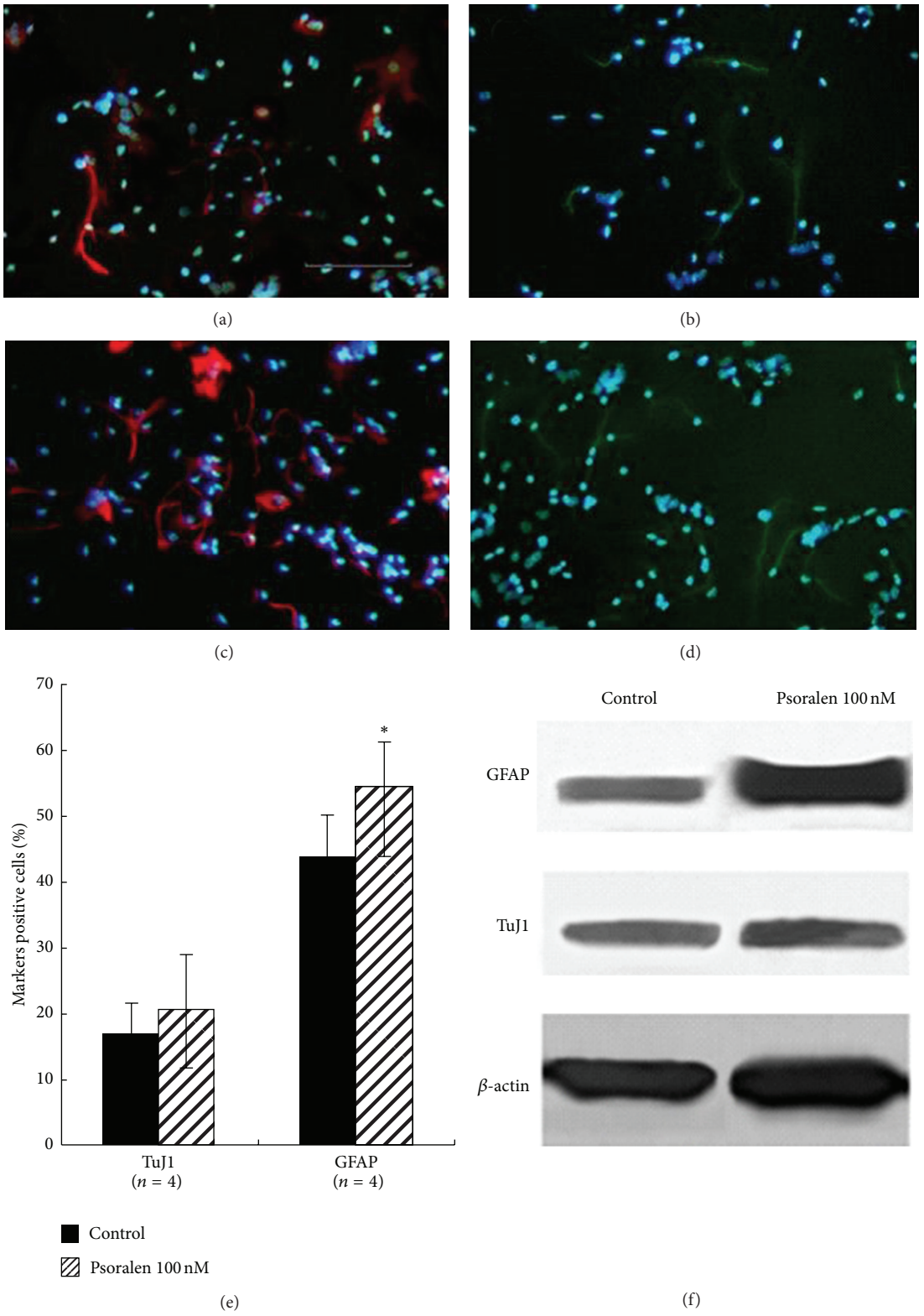

FIGURE 3: Effects of Psoralen on the differentiation of NSC. Single NSCs were seeded at a density of 50 cells/μL in PDL-coated 96-well plate in differentiation medium for 48 h without Psoralen (a, b) or with 100 nM Psoralen (c, d). Cells were subjected to primary antibodies of GFAP, TuJ1 and corresponding secondary antibodies and visualized with Alexa-conjugated 594 F(ab)′2 goat anti-rabit antibody and 488 Alexa-conjugated goat anti mouse IgG (H + L). The ratio of GFAP, TuJ1-positive cells against DAPI-stained cells was calculated. Psoralen significantly increased the GFAP-positive cells and decreased the TuJ1-positive cells (e). The same cells were performed using Western blotting. Psoralen significantly increased the GFAP, decreased the TuJ1 protein expression (f). Scale bars: 100 μm. Results were expressed as mean ± S.D. from three independent experiments. $^{*}P < 0.05$ versus control.

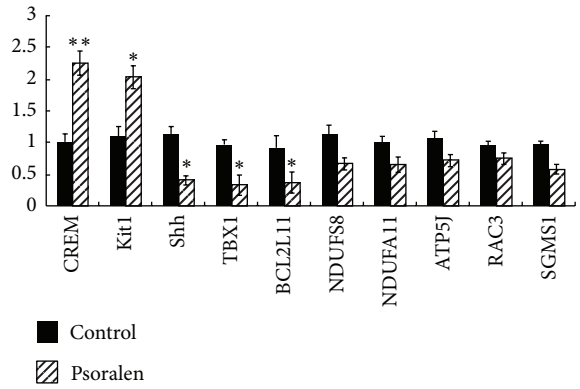

Figure 4: The expression profiles of these representative genes including CREM, Kit1, Shh, TBX1, and Bcl2l11 were confirmed by quantitative real-time PCR, which validates our data. Our data sets could be used for further bioinformatic analyses.

of these representative genes using quantitative real-time PCR analysis corresponded to the microarray profiles, which validates our data.

3.6. Comparisons of the DAVID Gene Functional Classification. A total of 276 known genes with different genebank accession numbers were assigned to the data sets using the DAVID Functional Annotation Tool for the functional annotation of the differentially expressed genes. The 261 system-recognized genes were functionally classified into 7 groups using the default settings (medium classification stringency), and the corresponding enrichment scores were greater than 1. These groups included "apoptosis" (12 genes), "regulation of apoptosis" (11 genes), "multicellular organism reproduction" (10 genes), "cellular protein catabolic process" (9 genes), "epidermis development" (4 genes), "cell differentiation" (3 genes), and "regulation of cell cycle process" (3 genes). The details of the differentially expressed genes are listed in Table 1.

3.7. DAG Analysis of Gene Categories. DAG visualized enriched gene categories. Ten GO categories were enriched after Psoralen treatment, including "establishment of cell polarity" (2 genes), "myotube differentiation" (2 genes), "positive regulation of angiogenesis" (2 genes), "glycolipid metabolic process" (2 genes), "regulation of pigmentation during development" (2 genes), "negative regulation of DNA metabolic process" (2 genes), "microtubule polymerization or depolymerization" (2 genes), "telomere organization" (2 genes), "mesenchymal cell development" (3 genes), and "neural crest cell differentiation" (3 genes). The details of the differentially expressed genes are listed in Table 2.

3.8. Identification of KEGG Pathways. KEGG pathway analysis was assigned using the DAVID annotation tool to reveal the functional roles of the differentially expressed genes. Twenty-nine KEGG pathways were matched to the differentially expressed tags of the two groups, such as "Hedgehog signaling pathway", "Oxidative phosphorylation", and "Wnt signaling pathway". The details of the differentially expressed genes are listed in Table 3. The Hedgehog signaling pathway is a key regulator of animal development, and it also plays an important role in the development of adult NSC. Oxidative phosphorylation is an important metabolic pathway for cellular respiration, glycolysis, and the Krebs cycle. The Wnt signaling pathway plays a key role in cellular differentiation, apoptosis, and development.

3.9. Identification of Transcription Factor Binding Sites. oPOSSUM is a web-based system for the detection of overrepresented transcription factor binding sites in the promoters of gene sets [27]. A total of 171 transcription factors were identified in this study, including the gene families of "Ets" "BetaBetaAlpha-zinc finger," "TATA-binding," "Helix-Loop-Helix," and "Hormone-nuclear Receptor". The details of the differentially expressed genes are listed in Table 4. The transcription factor, Sfpi1_1(PU.1), targeted 139 genes, which may encode an ETS-domain transcription factor that is critical for the determination of cell lineage and the regulation of differentiation versus stem cell proliferation [28]. Recent research indicates that Sfpi1_1 controls dendritic cell development in a dose-dependent manner [29].

4. Discussion

NSCs open a new way of treatment of the injured central nervous system and neurodegenerative disorders. Potential uses of NSC in repair include transplantation to repair missing cells and the activation of endogenous cells to provide "self-repair." Before the full potential of NSC can be realized, we need to know what controls their proliferation and differentiation. Precise control of proliferation and differentiation of multipotent NSC is crucial for proper development of the nervous system. Chinese herb extracts as effective factors regulating the self-renewal and differentiation capacity of NSC have been widely studied [8]. Psoralen can modulate the proliferation and differentiation of a variety of stem cells through different mechanisms [19–21].

In the present study, single cells derived from dissected neural tissue form floating balls of cells, termed neurospheres, when plated under nonadherent, permissive conditions [30]. These highly heterogeneous structures contain neural stem cells, more restricted progenitors, and differentiated progeny. The more restricted progenitors and differentiated progeny exhibit limited proliferation capacity, and these cells only form very small neurospheres. However, the neural stem cells demonstrate strong self-renewal and generate neurospheres in continuous passages. The self-renewal potential of cells within neurosphere cultures may be investigated by the dissociation of single cells that must be plated at a density at which a single cell gives rise to a single neurosphere. This process is termed clonal analysis. Single cells that are plated under medium to high cell densities permit the adherence of cells or small neurospheres to each other, and these structures combine to form larger neurospheres [31, 32]. Clonal analysis is impossible in this situation, and the true proliferative capacity of stem cells cannot be properly determined. However, drug-screening assays do not require that

Table 1: The list of the differentially expressed tags of DAVID gene functional classification.

Functional annotation clustering	Gene number	Gene bank accession	Description
Apoptosis	12	BC058175	BCL2-like 11 (apoptosis facilitator)
		AK144648	CASP2 and RIPK1 domain containing adaptor with death domain
		AK186862	Cytokine-induced apoptosis inhibitor 1
		AK049134	Ectodysplasin A2 isoform receptor
		AK010878	Hypothetical protein LOC100233175
		AK041961	Kit ligand
		XM_001476612	Predicted gene 15753, Sp110 nuclear body protein
		BC016606	Proteasome (prosome, macropain) assembly chaperone 2, similar to Clast3 protein
		BC063087	Sonic hedgehog
		AK082974	Sphingomyelin synthase 1
		BC027335	Tectonic family member 3
		AK183781	Zinc finger, DHHC domain containing 16
Regulation of apoptosis	11	BC058175	BCL2-like 11 (apoptosis facilitator)
		AK144648	CASP2 and RIPK1 domain containing adaptor with death domain
		AK186862	Cytokine-induced apoptosis inhibitor 1
		BC080315	Glutamate receptor, metabotropic 7
		BC152841	Heat shock protein 1B, heat shock protein 1A, heat shock protein 1-like
		AK010878	Hypothetical protein LOC100233175
		AK041961	Kit ligand
		AK160757	Microphthalmia-associated transcription factor
		XM_001476612	Sp110 nuclear body protein
		BC016606	Proteasome (prosome, macropain) assembly chaperone 2; similar to Clast3 protein
		AK082974	Sphingomyelin synthase 1
Multicellular organism reproduction	10	BC058175	BCL2-like 11 (apoptosis facilitator)
		AK086849	*beta*-1,4-N-Acetyl-galactosaminyl transferase 1
		AY738720	cAMP responsive element modulator
		BC152841	Heat shock protein 1B, heat shock protein 1A, heat shock protein 1-like
		AK160943	Heterogeneous nuclear ribonucleoprotein L-like, glutathione peroxidase 4
		AK041961	Kit ligand
		AK078529	Neuralized homolog 1A (Drosophila); similar to neuralized 1
		XM_001474694	Rik protein
		BC115962	Germ cell-less homolog 1
		BC061175	Testis-specific serine kinase 2
Cellular protein catabolic process	9	BC058593	SUMO1/sentrin specific peptidase 7
		AK053749	WW domain containing E3 ubiquitin protein ligase 2
		BC040367	Ligand of numb-protein X 1
		BC128498	Myosin, heavy polypeptide 9, nonmuscle
		BC115962	Germ cell-less homolog 1
		XM_001474694	Rik protein
		XM_354829	Seven in absentia homolog 3 (Drosophila)
		BC059027	Similar to midline 1, midline 1
		BC026983	Ubiquitin specific peptidase 39

Table 1: Continued.

Functional annotation clustering	Gene number	Gene bank accession	Description
Epidermis development	4	BC152326	Involucrin, RIKEN cDNA 1110019C06 gene
		BC148438	Small proline-rich protein 2E, small proline-rich protein 2F, Small proline-rich protein 2I
		BC156163	Small proline-rich protein 2H
		BC063087	Sonic hedgehog
Cell differentiation	3	AK041961	Kit ligand
		AF349658	Similar to T-box 1; T-box 1
		BC063087	Sonic hedgehog
Regulation of cell cycle process	3	AK018243	ZW10 homolog (Drosophila), centromere/kinetochore protein
		BC016606	Proteasome (prosome, macropain) assembly chaperone 2, similar to Clast3 protein
		AK003451	Timeless interacting protein

Table 2: The list of the differentially expressed tags of DAG analysis of gene categories.

Categories	Gene bank accession	Description
Establishment of cell polarity	17886	Myosin, heavy polypeptide 9, nonmuscle
	20423	Sonic hedgehog
Myotube differentiation	17886	Myosin, heavy polypeptide 9, nonmuscle
	20423	Sonic hedgehog
Positive regulation of angiogenesis	14461	GATA binding protein 2
	12394	Runt-related transcription factor 1
Glycolipid metabolic process	14421	*beta*-1,4-N-Acetyl-galactosaminyl transferase 1
	12916	cAMP responsive element modulator
Regulation of pigmentation during development	12125	BCL2-like 11 (apoptosis facilitator)
	17311	Kit ligand
Negative regulation of DNA metabolic process	66131	Timeless interacting protein
	72836	Protection of telomeres 1B
Microtubule polymerization or depolymerization	17318	Midline 1
	17997	Neural precursor cell expressed, developmentally downregulated gene 1
Telomere organization	15511	Heat shock protein 1B
	72836	Protection of telomeres 1B
Mesenchymal cell development	21380	T-box 1
	20423	Sonic hedgehog
	17311	Kit ligand
Neural crest cell differentiation	21380	T-box 1
	20423	Sonic hedgehog
	17311	Kit ligand

each neurosphere derived from a single stem or progenitor cell. A low plating cell density of 5000 cells/mL or 1000 cells/mL is sufficient to measure the self-renewal of neural stem cells [33, 34].

We plated single cells at a density of 5000 cells/mL in 100 μL/well in a 96-well plate. Approximately 5% of the plated single cells reformed neurospheres, which is consistent with previous studies. Psoralen significantly inhibited neurosphere formation with maximum effects at 100 nM. This Psoralen-induced decrease in neurosphere formation may be derived from the compromised proliferation of NSC. Therefore, we investigated NSC proliferation in the presence of Psoralen using an EdU incorporation assay. Psoralen significantly reduced EdU incorporation. These results suggested that Psoralen inhibits the self-renewal of NSC through the inhibition of proliferation.

NSCs generally and gradually exit the cell cycle when they enter the process of differentiation. The length of the neural

Table 3: The list of the differentially expressed tags of matched KEGG pathway analysis.

KEGG pathways	Gene number matched	Gene bank accession	Description
MAPK signaling pathway	5	BC119041	RAS-related C3 botulinum substrate 3
		BC052705	Dual specificity phosphatase 8
		BC152841	Heat shock protein 1B
		BC006037	Mitogen-activated protein kinase kinase kinase kinase 3
		BC054533	Protein kinase, cAMP dependent, catalytic, beta
Pathways in cancer	5	BC119041	RAS-related C3 botulinum substrate 3
		AK041961	Kit ligand
		AK160757	Microphthalmia-associated transcription factor
		AK155262	Runt-related transcription factor 1
		BC063087	Sonic hedgehog
Spliceosome	4	AK040680	Cell division cycle 40 homolog (yeast)
		BC152841	Heat shock protein 1B
		BC004793	Poly(rC) binding protein 1
		BC026983	Ubiquitin specific peptidase 39
Axon guidance	4	AK089130	Eph receptor A5
		BC119041	RAS-related C3 botulinum substrate 3
		AK171860	Actin-binding LIM protein 1
		AK053689	Netrin G1
Hedgehog signaling pathway	3	AK149310	Casein kinase 1, gamma 1
		BC054533	Protein kinase, cAMP dependent, catalytic, beta
		BC063087	Sonic hedgehog
Viral myocarditis	3	BC119041	RAS-related C3 botulinum substrate 3
		BC128498	Myosin, heavy polypeptide 9, nonmuscle
		BC156199	v-abl Abelson murine leukemia viral oncogene homolog 2
Melanogenesis	3	AK041961	Kit ligand
		AK160757	Microphthalmia-associated transcription factor
		BC054533	Protein kinase, cAMP dependent, catalytic, beta
Oxidative phosphorylation	3	AK078484	ATP synthase
		XM_895878	NADH dehydrogenase (ubiquinone) 1 alpha subcomplex 11
		AK149674	NADH dehydrogenase (ubiquinone) Fe-S protein 8
Cytokine-cytokine receptor interaction	3	AK049134	Ectodysplasin A2 isoform receptor
		AY221616	Interleukin 15 receptor, alpha chain
		AK041961	Kit ligand
Cysteine and methionine metabolism	2	AK085987	5-Methyltetrahydrofolate-homocysteine methyltransferase
		BC094469	Mercaptopyruvate sulfurtransferase
Prion diseases	2	BC152841	Heat shock protein 1B
		BC054533	Protein kinase, cAMP dependent, catalytic, beta
SNARE interactions in vesicular transport	2	AK030538	Vesicle transport through interaction with t-SNAREs homolog 1A
		BC086925	Vesicle-associated membrane protein 5
Adherens junction	2	AK137694	LIM domain only 7
		BC119041	RAS-related C3 botulinum substrate 3
Gap junction	2	AK031305	Guanylate cyclase 1, soluble, alpha 3
		BC054533	Protein kinase, cAMP dependent, catalytic, beta
Systemic lupus erythematosus	2	BC152885	Histone H4
		K02799	Complement C4 precursor

Table 3: Continued.

KEGG pathways	Gene number matched	Gene bank accession	Description
Vascular smooth muscle contraction	2	AK031305	Guanylate cyclase 1, soluble, alpha 3
		BC054533	Protein kinase, cAMP dependent, catalytic, beta
Natural killer cell mediated cytotoxicity	2	BC119041	RAS-related C3 botulinum substrate 3
		AY860969	Natural killer cell receptor Ly49C
Parkinson's disease	2	AK078484	ATP synthase
		AK149674	NADH dehydrogenase (ubiquinone) Fe-S protein 8
Tight junction	2	BC002003	Claudin 1
		BC128498	Myosin, heavy polypeptide 9, non-muscle
Ubiquitin mediated proteolysis	2	AK053749	WW domain containing E3 ubiquitin protein ligase 2
		BC059027	Midline 1
Insulin signaling pathway	2	BC054533	Protein kinase, cAMP dependent, catalytic, beta
		AK172276	Regulatory associated protein of MTOR, complex 1
Wnt signaling pathway	2	BC119041	RAS-related C3 botulinum substrate 3
		BC054533	Protein kinase, cAMP dependent, catalytic, beta
Purine metabolism	2	AK031305	Guanylate cyclase 1, soluble, alpha 3
		AK036090	Phosphodiesterase 8B
Alzheimer's disease	2	AK078484	ATP synthase
		AK149674	NADH dehydrogenase (ubiquinone) Fe-S protein 8
Chemokine signaling pathway	2	BC010478	Hemopoietic cell kinase
		BC054533	Protein kinase, cAMP dependent, catalytic, beta
Huntington's disease	2	AK078484	ATP synthase
		AK149674	NADH dehydrogenase (ubiquinone) Fe-S protein 8
Regulation of actin cytoskeleton	2	BC119041	RAS-related C3 botulinum substrate 3
		BC128498	Myosin, heavy polypeptide 9, non-muscle
Neuroactive ligand-receptor interaction	2	AK050472	Gastric inhibitory polypeptide receptor
		BC080315	Glutamate receptor, metabotropic 7
Olfactory transduction	2	BC104278	Olfactory receptor 1173
		BC054533	Protein kinase, cAMP dependent, catalytic, beta

progenitor cell cycle is directly coupled to cell fate choices because factors that shorten the cell cycle inhibit differentiation divisions, but factors that lengthen the cell cycle promote differentiation divisions. We also investigated the effect of Psoralen on NSC differentiation. Psoralen increased the percentage of GFAP-positive cells, but the percentage of TuJ1-positive cells was not altered. Psoralen increased GFAP protein expression on Western blots, but it did not influence TuJ1 protein expression. Our experiment demonstrated that Psoralen strongly induced the differentiation of NSC into astrocytes.

A cluster analysis was performed on these differentially expressed genes using DAVID bioinformatics resources. DAVID functional classification suggested that Psoralen primarily altered the expression of genes involved in differentiation, proliferation, apoptosis, and catabolism. The DAG analysis suggested that the effect of Psoralen on neural stem cells is a biological process that impacts the metabolism of DNA, sugar, and lipids and regulates cellular proliferation, split polarization, and differentiation.

There are several genes of interest in the DAVID and DAG classification, including BCL2-like 11, Kit ligand, and Sonic hedgehog, which were confirmed by our previous quantitative real-time PCR test. BCL2-like 11 protein is encoded by a gene in the BCL-2 protein family, which play important roles in the regulation of neuronal and lymphocytic apoptosis. BCL-2 deficiency does not affect neuronal numbers in the cerebellum [35], but this protein has been implicated in hippocampal neuronal protection in a seizure model [36]. BCL-2-deficient mice exhibit relatively normal development of the nervous system, but BCL-2 is important for the postnatal maintenance of specific neuronal subsets, including facial motor neurons and dorsal root ganglia [37]. Kit ligand, also known as stem cell factor (SCF), steel factor (SLF) and mast cell growth factor (MGF), is as 30-kDa glycoprotein with broad activity in various tissues [38]. Kit ligand regulates the development of cellular lineage by expressing c-kit, which affects proliferation and maturation [38, 39]. Kit signaling in the CNS influences oligodendrocyte precursors prior to differentiation towards a myelinated phenotype [39]. Greater

Table 4: The list of the differentially expressed tags of matched transcription factor binding sites.

Transcription factor	Gene family	Target gene (>70 hits)
Sfpi1_1	Ets	139
Elf3_1	Ets	131
Zfp105_1	Beta-Beta-Alpha-zinc finger	114
Tbp_1	TATA binding	110
Foxj1_1	Forkhead	100
Sox12_1	High-mobility group	95
Tcfap2a_1	Helix-Loop-Helix	94
Zic2_2	Beta-Beta-Alpha-zinc finger	93
Irf3_1	IRF	92
Foxj3_2	Forkhead	91
Zic3_2	Beta-Beta-Alpha-zinc finger	89
Sox11_1	High-mobility group	89
Sox4_1	High-mobility group	86
Klf7_1	Beta-Beta-Alpha-zinc finger	85
Arid5a_1	Arid	83
Ehf_1	Ets	83
Sox11_2	High-mobility group	80
Sox18_1	High-mobility group	80
Osr1_2	Beta-Beta-Alpha-zinc finger	79
Sox5_1	High-mobility group	79
Sp4_1	Beta-Beta-Alpha-zinc finger	77
Zscan4_2	Beta-Beta-Alpha-zinc finger	76
Tcfap2e_1	Helix-Loop-Helix	76
Egr1_2	Beta-Beta-Alpha-zinc finger	75
Foxl1_2	Forkhead	75
Foxa2_1	Forkhead	75
Tcfap2c_1	Helix-Loop-Helix	75
Sox14_2	High-mobility group	75
Smad3_1	MH1	75
Sox17_1	High-mobility group	74
Hic1_2	Beta-Beta-Alpha-zinc finger	73
Sox21_2	High-mobility group	72
Zic1_2	Beta-Beta-Alpha-zinc finger	71
Tcf1_2	Homeo	71
Zfp740_1	Beta-Beta-Alpha-zinc finger	70

than 93% of nestin-positive NSC from the embryonic rat cortex express Kit ligand [40]. Kit ligand is a survival factor for NSPCs during the early stages of differentiation [41]. The Sonic hedgehog (Shh) gene is one of a homolog gene of Hedgehog (hh) [42]. Shh gene plays an important role in the development of the mammary glands, prostate, lung, hair, nervous system, and other organs. Shh regulates the development of the neural system, especially the proliferation and differentiation of neural stem cells [43, 44]. Shh is a positive regulator of adult hippocampal neural stem cell proliferation, and it may participate in injury remodeling.

We further searched the possible transcription factor binding sites existing in the upstream sequences of differentially expressed genes. Consequently, 139 genes differentially expressed were predicted to have transcription factor binding sites for Sfpi1, a member of the Ets family. The common character of Ets factors was highly conserved and the DNA binding domain can combine with specific gene sequence to regulate the expression and function of target gene by being involved in cell proliferation, differentiation, apoptosis, and mesenchymal-epithelial interactions [45, 46]. ETs could be involved in many physiological and pathological processes. A large number of researches showed that Ets transcription factors play an important regulation role in the development, tumor invasion, and metastasis of amphibians, birds and mammals [47].

Sfpi1, also called PU.1, belongs to the SpI subfamily of the Ets family. The transcription factors Sfpi2, Sfpi3 also belong to the same family. These members all showed the existence of the Ets structure domain in the C-terminal of the protein and an acid transcription activation structure domain in the N-terminal. Literature study reported that this kind of structure played an important role in the differentiation process of a variety of cells. The changes of the expression quantity of the transcription factors played a decisive role in adjusting the differentiation direction of stem cells [48]. Sfpi1 was highly expressed in myeloid cells but not in lymphocyte. It functioned in the early state of differentiation in granulocyte, red blood cells, and megakaryocyte, and it suppressed red blood cell differentiating to red blood cells. Studies [28] have shown that a high level of Sfpi1 could cause differentiation of macrophage but not proliferation of progenitor cells. In embryogenesis process, lack of Sfpi1 could lead to development delay [49, 50]. In recent years, study [29] showed that Sfpi1 also played an essential role in differentiation of dendritic cells. Based on bioinformatical analysis and the literature review, we thought that Sfpi1 may mediate the effects of Psoralen.

The KEGG pathway analysis demonstrated that the effects of Psoralen on neural stem cells were closely related to the Hedgehog signaling pathway, Wnt signaling pathways, MAPK, spliceosomes, axon guidance, oxidative phosphorylation, adherens junction, gap junction, and tight junction. The matched Hedgehog signaling pathway is of interest, which is crucial for the generation and maintenance of both embryonic and adult stem cells. This pathway regulates spinal dorsal-ventral plasticity and the multizone of neural precursor cell proliferation and differentiation in the developing nervous system. Hedgehog signaling pathway also plays a key role in the regulation of neural progenitor cell growth [51]. Granule cell precursor proliferation in the cerebellum requires Hedgehog signaling [52]. Hedgehog signaling may regulate the self-renewal of progenitor cells in the SVZ, hippocampus, olfactory bulb, and other brain areas [51, 53]. The downstream target gene of the Hedgehog pathway, BMI1, regulates central and peripheral nervous system progenitor cell self-renewal [54]. The oligodendrocyte generation of glial precursor cells and the subsequent differentiation into mature

oligodendrocytes require Hedgehog signaling in $SHH^{(-/-)}$ mutants [55]. Cell proliferation and differentiation culture conditions in the NSC clones express mRNA of the functional Shh receptor, PTCH, and Shh (5~50 nmol/L) in vitro promotes the proliferation of fetal rat spinal cord in primary and passaged neural stem cells in a dose-dependent manner. This activation is also observed in quiescent adult neural stem cells in which the Hedgehog signal pathway stimulates continuous proliferation and differentiation [56].

Recently, Crosstalk of Hedgehog with other critical signaling pathways has been mentioned. Hedgehog and Wnt pathways resulted in opposite proliferative outcomes of neural stem/progenitor cells, and Sfrp-1 and Gli3 contributed to this negative cross-regulation [57]. But Hedgehog and Notch signaling could cooperate to regulate neurogenic divisions of neocortical progenitors. The transcription factors Hes1 and Blbp were possibly the key molecules in the Hh/Notch coregulation of corticogenesis [58].

In conclusion, our study demonstrated the antiproliferative and prodifferentiative effects of Psoralen on NSC. The microarray study demonstrated that the gene expression profile of NSC could be specifically regulated by Psoralen. The genes involved in the classification of cellular differentiation, proliferation, and metabolism, the transcription factors belonging to Ets family, and the hedgehog pathway may play important roles in the regulation process, which need further studies.

Authors' Contribution

You Ning and Jian-Hua Huang share first authorship of this paper.

Conflict of Interests

The authors declare no financial or commercial conflict of interest.

Acknowledgments

This work was supported by the National Basic Research Program in China (no. 2010CB530402) and the National Natural Science Foundation of China (no. 81202745, and no. 31171129).

References

[1] F. H. Gage, "Mammalian neural stem cells," *Science*, vol. 287, no. 5457, pp. 1433–1438, 2000.

[2] C. M. Zhao, W. Deng, and F. H. Gage, "Mechanisms and functional implications of adult neurogenesis," *Cell*, vol. 132, no. 4, pp. 645–660, 2008.

[3] S. Lugert, O. Basak, P. Knuckles et al., "Quiescent and active hippocampal neural stem cells with distinct morphologies respond selectively to physiological and pathological stimuli and aging," *Cell Stem Cell*, vol. 6, no. 5, pp. 445–456, 2010.

[4] H. I. Kornblum, "Introduction to neural stem cells," *Stroke*, vol. 38, no. 2, pp. 810–816, 2007.

[5] J. M. Zhang, H. K. Wang, C. Q. Ye et al., "ATP released by astrocytes mediates glutamatergic activity-dependent heterosynaptic suppression," *Neuron*, vol. 40, no. 5, pp. 971–982, 2003.

[6] Y. Yang, W. Ge, Y. Chen et al., "Contribution of astrocytes to hippocampal long-term potentiation through release of D-serine," *Proceedings of the National Academy of Sciences of the United States of America*, vol. 100, no. 25, pp. 15194–15199, 2003.

[7] C. T. Leung, P. A. Coulombe, and R. R. Reed, "Contribution of olfactory neural stem cells to tissue maintenance and regeneration," *Nature Neuroscience*, vol. 10, no. 6, pp. 720–726, 2007.

[8] W. Wang, W. Huang, and H. Ai, "Proliferation and differentiation of adult neural stem cell induced by traditional Chinese medicine in brain," *Chinese Journal of Rehabilitation Theory and Practice*, vol. 13, no. 1, pp. 26–28, 2007.

[9] L. J. Chai, P. R. Zhong, Z. H. Zhou, X. Y. Wang, T. Ishida, and Y. J. Zhang, "Proliferation effects of astragaloside on neural atem cells in vitro," *Chinese Pharmacological Bulletin*, vol. 26, no. 5, pp. 670–673, 2010.

[10] M. He, M. L. Liu, K. X. Wang et al., "Investigation of the directed differentiation of neural stem cells after brain-derived neurotrophic factor, salidroside and neural stem cells transplanted into epileptic rat brain," *Chinese Journal of Clinical Neurosciences*, vol. 20, no. 2, pp. 181–187, 2012.

[11] D. Bethea, B. Fullmer, S. Syed et al., "Psoralen photobiology and photochemotherapy: 50 years of science and medicine," *Journal of Dermatological Science*, vol. 19, no. 2, pp. 78–88, 1999.

[12] J. Llano, J. Raber, and L. A. Eriksson, "Theoretical study of phototoxic reactions of psoralens," *Journal of Photochemistry and Photobiology A*, vol. 154, no. 2-3, pp. 235–243, 2003.

[13] S. S. Yones, R. A. Palmer, T. M. Garibaldinos, and J. L. M. Hawk, "Randomized double-blind trial of treatment of vitiligo: efficacy of psoralen-UV-A therapy versus narrowband-UV-B therapy," *Archives of Dermatology*, vol. 143, no. 5, pp. 578–584, 2007.

[14] C. Querfeld, S. T. Rosen, T. M. Kuzel et al., "Long-term follow-up of patients with early-stage cutaneous T-cell lymphoma who achieved complete remission with psoralen plus UV-A monotherapy," *Archives of Dermatology*, vol. 141, no. 3, pp. 305–311, 2005.

[15] R. S. Stern, "Psoralen and ultraviolet a light therapy for psoriasis," *The New England Journal of Medicine*, vol. 357, no. 7, pp. 682–690, 2007.

[16] A. B. Santamaria, D. W. Davis, D. X. Nghiem et al., "p53 and Fas ligand are required for psoralen and UVA-inducedapoptosis in mouse epidermal cells," *Cell Death and Differentiation*, vol. 9, no. 5, pp. 549–560, 2002.

[17] K. L. March, B. L. Patton, R. L. Wilensky, and D. R. Hathaway, "8-methoxypsoralen and longwave ultraviolet irradiation are a novel antiproliferative combination for vascular smooth muscle," *Circulation*, vol. 87, no. 1, pp. 184–191, 1993.

[18] T. E. Keane, J. A. Petros, B. Velimirovich, K. T. Yue, and S. D. Graham, "Methoxypsoralen phototherapy of transitional cell carcinoma," *Urology*, vol. 44, no. 6, pp. 842–846, 1994.

[19] J. Z. Wu, Z. Q. Situ, W. Wang, J. Chen, and B. Liu, "Antitumor activity of psoralen on mucoepidermoid carcinoma cell line MEC-1," *Chinese Medical Journal*, vol. 105, no. 11, pp. 913–917, 1992.

[20] S. Wu, Z. Zhang, and J. Zhao, "An experimental study on antitumor activity of psoralen on mammary cancer cell line EMT6 in vitro and in vivo," *China Journal of Chinese Materia Medica*, vol. 23, no. 5, pp. 303–305, 1998.

[21] D. Z. Tang, F. Yang, Z. Yang et al., "Psoralen stimulates osteoblast differentiation through activation of BMP signaling," *Biochemical and Biophysical Research Communications*, vol. 405, no. 2, pp. 256–261, 2011.

[22] B. A. Reynolds and S. Weiss, "Clonal and population analyses demonstrate that an EGF-responsive mammalian embryonic CNS precursor is a stem cell," *Developmental Biology*, vol. 175, no. 1, pp. 1–13, 1996.

[23] A. Salic and T. J. Mitchison, "A chemical method for fast and sensitive detection of DNA synthesis in vivo," *Proceedings of the National Academy of Sciences of the United States of America*, vol. 105, no. 7, pp. 2415–2420, 2008.

[24] Q. Bian, J. H. Huang, Q. Q. Liang et al., "The osteogenetic effect of astragaloside IV with centrifugating pressure on the OCT-1 cells," *Pharmazie*, vol. 66, no. 1, pp. 63–68, 2011.

[25] G. J. Dennis, B. T. Sherman, D. A. Hosack et al., "DAVID: database for annotation, visualization, and integrated discovery," *Genome Biology*, vol. 4, no. 5, article P3, 2003.

[26] B. Zhang, D. Schmoyer, S. Kirov, and J. Snoddy, "GOTree Machine (GOTM): a web-based platform for interpreting sets of interesting genes using Gene Ontology hierarchies," *BMC Bioinformatics*, vol. 5, article 16, 2004.

[27] S. J. H. Sui, J. R. Mortimer, D. J. Arenillas et al., "oPOSSUM: identification of over-represented transcription factor binding sites in co-expressed genes," *Nucleic Acids Research*, vol. 33, no. 10, pp. 3154–3164, 2005.

[28] G. U. Gangenahalli, P. Gupta, D. Saluja et al., "Stem cell fate specification: Role of master regulatory switch transcription factor PU.1 in differential hematopoiesis," *Stem Cells and Development*, vol. 14, no. 2, pp. 140–152, 2005.

[29] S. Carotta, A. Dakic, A. D'Amico et al., "The transcription factor PU.1 controls dendritic cell development and Flt3 cytokine receptor expression in a dose-dependent manner," *Immunity*, vol. 32, no. 5, pp. 628–641, 2010.

[30] B. A. Reynolds and S. Weiss, "Generation of neurons and astrocytes from isolated cells of the adult mammalian central nervous system," *Science*, vol. 255, no. 5052, pp. 1707–1710, 1992.

[31] I. Singec, R. Knoth, R. P. Meyer et al., "Defining the actual sensitivity and specificity of the neurosphere assay in stem cell biology," *Nature Methods*, vol. 3, no. 10, pp. 801–806, 2006.

[32] S. Jessberger, G. D. Clemenson, and F. H. Gage, "Spontaneous fusion and nonclonal growth of adult neural stem cells," *Stem Cells*, vol. 25, no. 4, pp. 871–874, 2007.

[33] J. P. Saxe, H. Wu, T. K. Kelly et al., "A phenotypic small-molecule screen identifies an orphan ligand-receptor pair that regulates neural stem cell differentiation," *Chemistry and Biology*, vol. 14, no. 9, pp. 1019–1030, 2007.

[34] M. Nagao, M. Sugimori, and M. Nakafuku, "Cross talk between Notch and growth factor/cytokine signaling pathways in neural stem cells," *Molecular and Cellular Biology*, vol. 27, no. 11, pp. 3982–3994, 2007.

[35] Q. A. Liu and H. Shio, "Mitochondrial morphogenesis, dendrite development, and synapse formation in cerebellum require both Bcl-w and the glutamate receptor $\delta 2$," *PLoS Genetics*, vol. 4, no. 6, Article ID e1000097, 2008.

[36] B. Murphy, M. Dunleavy, S. Shinoda et al., "Bcl-w protects hippocampus during experimental status epilepticus," *The American Journal of Pathology*, vol. 171, no. 4, pp. 1258–1268, 2007.

[37] D. J. Veis, C. M. Sorenson, J. R. Shutter, and S. J. Korsmeyer, "Bcl-2-deficient mice demonstrate fulminant lymphoid apoptosis, polycystic kidneys, and hypopigmented hair," *Cell*, vol. 75, no. 2, pp. 229–240, 1993.

[38] L. K. Ashman, "The biology of stem cell factor and its receptor C-kit," *International Journal of Biochemistry and Cell Biology*, vol. 31, no. 10, pp. 1037–1051, 1999.

[39] K. Jin, X. O. Mao, Y. Sun, L. Xie, and D. A. Greenberg, "Stem cell factor stimulates neurogenesis in vitro and in vivo," *Journal of Clinical Investigation*, vol. 110, no. 3, pp. 311–319, 2002.

[40] A. Erlandsson, J. Larsson, and K. Forsberg-Nilsson, "Stem cell factor is a chemoattractant and a survival factor for CNS stem cells," *Experimental Cell Research*, vol. 301, no. 2, pp. 201–210, 2004.

[41] Y. Sun, K. Jin, J. T. Childs, L. Xie, X. O. Mao, and D. A. Greenberg, "Vascular endothelial growth factor-B (VEGFB) stimulates neurogenesis: evidence from knockout mice and growth factor administration," *Developmental Biology*, vol. 289, no. 2, pp. 329–335, 2006.

[42] X. Zhu, S. Bidlingmaier, R. Hashizume, C. D. James, M. S. Berger, and B. Liu, "Identification of internalizing human single-chain antibodies targeting brain tumor sphere cells," *Molecular Cancer Therapeutics*, vol. 9, no. 7, pp. 2131–2141, 2010.

[43] A. M. Kenney and D. H. Rowitch, "Sonic hedgehog promotes G1 cyclin expression and sustained cell cycle progression in mammalian neuronal precursors," *Molecular and Cellular Biology*, vol. 20, no. 23, pp. 9055–9067, 2000.

[44] C. G. Feijóo, M. G. Oñate, L. A. Milla, and V. A. Palma, "Sonic hedgehog (Shh)-Gli signaling controls neural progenitor cell division in the developing tectum in zebrafish," *European Journal of Neuroscience*, vol. 33, no. 4, pp. 589–598, 2011.

[45] T. Hsu, M. Trojanowska, and D. K. Watson, "Ets proteins in biological control and cancer," *Journal of Cellular Biochemistry*, vol. 91, no. 5, pp. 896–903, 2004.

[46] V. I. Sementchenko and D. K. Watson, "Ets target genes: past, present and future," *Oncogene*, vol. 19, no. 55, pp. 6533–6548, 2000.

[47] I. G. Maroulakou and D. B. Bowe, "Expression and function of Ets transcription factors in mammalian development: a regulatory network," *Oncogene*, vol. 19, no. 55, pp. 6432–6442, 2000.

[48] S. Zhu, S. Barshow, J. Wildonger, L. Y. Jan, and Y. N. Jan, "Ets transcription factor Pointed promotes the generation of intermediate neural progenitors in Drosophila larval brains," *Proceedings of the National Academy of Sciences of the United States of America*, vol. 108, no. 51, pp. 20615–20620, 2011.

[49] A. L. Brass, A. Q. Zhu, and H. Singh, "Assembly requirements of PU.1-Pip (IRF-4) activator complexes: inhibiting function in vivo using fused dimers," *EMBO Journal*, vol. 18, no. 4, pp. 977–991, 1999.

[50] R. P. DeKoter and H. Singh, "Regulation of B lymphocyte and macrophage development by graded expression of PU.1," *Science*, vol. 288, no. 5470, pp. 1439–1441, 2000.

[51] K. Lai, B. K. Kaspar, F. H. Gage, and D. V. Schaffer, "Sonic hedgehog regulates adult neural progenitor proliferation in vitro and in vivo," *Nature Neuroscience*, vol. 6, no. 1, pp. 21–27, 2003.

[52] R. Machold, S. Hayashi, M. Rutlin et al., "Sonic hedgehog is required for progenitor cell maintenance in telencephalic stem cell niches," *Neuron*, vol. 39, no. 6, pp. 937–950, 2003.

[53] R. J. Wechsler-Reya, "Analysis of gene expression in the normal and malignant cerebellum," *Recent Progress in Hormone Research*, vol. 58, pp. 227–248, 2003.

[54] A. V. Molofsky, R. Pardal, T. Iwashita, I. K. Park, M. F. Clarke, and S. J. Morrison, "Bmi-1 dependence distinguishes neural stem cell self-renewal from progenitor proliferation," *Nature*, vol. 425, no. 6961, pp. 962–967, 2003.

[55] S. Oh, X. Huang, and C. Chiang, "Specific requirements of sonic hedgehog signaling during oligodendrocyte development," *Developmental Dynamics*, vol. 234, no. 3, pp. 489–496, 2005.

[56] S. Ahn and A. L. Joyner, "In vivo analysis of quiescent adult neural stem cells responding to Sonic hedgehog," *Nature*, vol. 437, no. 7060, pp. 894–897, 2005.

[57] C. Borday, P. Cabochette, K. Parain, and M. Perron, "Antagonistic cross-regulation between Wnt and Hedgehog signalling pathways controls post-embryonic retinal proliferation," *Development*, vol. 139, no. 19, pp. 3499–3509, 2012.

[58] R. K. Dave, T. Ellis, M. C. Toumpas et al., "Sonic hedgehog and notch signaling can cooperate to regulate neurogenic divisions of neocortical progenitors," *PLoS ONE*, vol. 6, no. 2, Article ID e14680, 2011.

Hindawi Publishing Corporation
Evidence-Based Complementary and Alternative Medicine
Volume 2013, Article ID 830714, 7 pages
http://dx.doi.org/10.1155/2013/830714

Research Article

Biofeedback Therapy Combined with Traditional Chinese Medicine Prescription Improves the Symptoms, Surface Myoelectricity, and Anal Canal Pressure of the Patients with Spleen Deficiency Constipation

Yi-Bo Yao, Yong-Qing Cao, Xiu-Tian Guo, Jin Yi, Hong-Tao Liang, Chen Wang, and Jin-Gen Lu

Department of Anorectal Surgery, Longhua Hospital Affiliated to Shanghai University of Traditional Chinese Medicine, 725 South Wanping Road, Shanghai 200030, China

Correspondence should be addressed to Jin-Gen Lu; longhuadoctor_jin@163.com

Received 31 May 2013; Accepted 5 July 2013

Academic Editor: Yong-Qing Yang

In order to observe the clinical therapeutic effects of Yiqi Kaimi Prescription and biofeedback therapy on treating constipation with deficiency of spleen qi, the 30 cases in the control group were given oral administration of Yiqi Kaimi Prescription, in combination with anus-lifting exercise; the 30 cases in the treatment group were given biofeedback therapy on the basis of the afore mentioned methods for the control group. The TCM symptom scores and anorectal pressures before and after treatment were observed and evaluated. There were significant differences in TCM symptom scores, anorectal pressure, and clinical recovery rate before and after treatment. In the treatment group, the total recovery rate was 86.66%, while in the control group it was 50%; there were significant differences between the two groups ($P < 0.01$). Yiqi Kaimi Prescription coupled with biofeedback therapy is clinically effective for treating constipation with deficiency of spleen qi, and thus this method is applicable for functional constipation with deficiency of spleen qi.

1. Introduction

Constipation, defined as having a bowel movement less than three times a week or the necessity of using laxatives more than three times a week [1], is a common problem with high prevalence and greatly affects the life quality of people [2]. The prevalence rates were 22.6% for constipation in the primary care clinic of the United States [3]. The prevalence of constipation was 14.1%–27% in the different ages of women in Australia [4]. In Asia, the chronic constipation affects 15% of Sri Lankan school children and adolescents [5]. It is also reported that up to 30% of preschool children in the eastern district of Hong Kong had constipation [6]. The prevalence of constipation of China is about 6%, which is substantially lower than that in the western countries [7]. However, a survey on people who were above 60 in Tianjin and Xi'an revealed that the incidence of chronic constipation reached 7.3%~20.39% [8]. With the aging of society, quickening pace of the modern life and the influencing of improper life habits (e.g., lack of fiber in food, irregular defecation, and subjective inhibition of desire for defecation), the incidence rate of this disease is increasing year by year.

Symptoms of constipation include infrequency of spontaneous defecation, difficulty initiating or completing bowel movement, rectal bleeding, pain, abdominal distention, and faecal incontinence [9]. It is known that the constipation was associated with multiple complications such as faecal impaction and bowel perforation [10]. The occurrence of constipation was related to many factors, so a single therapy will not achieve satisfactory effects. The chronic constipation may be caused by the diet deficient in fiber and fluids. It is reported that the moderate physical activity and increasing fiber intake were associated with substantial reduction in the prevalence of constipation in women [11]. However,

the function of fiber in a diet for the chronic constipation was controversial. Although some patients may be helped by a fiber-rich diet, many patients with more severe constipation get worse symptoms when increasing dietary fiber intake [12]. There was also no evidence that constipation can successfully be treated by increasing fluid intake unless there is evidence of dehydration [13]. Functional limitations such as immobility and lack of exercise were other important reasons. A cross-sectional survey supported the notion that those who undertake more physical activity do have a lesser incidence of constipation [14]. The symptom of constipation was also a common adverse effect of many medications including analgesics, antidepressant drugs, iron salts, nonsteroidal anti-inflammatory drugs, and opiates. It is reported that factors other than opioid dose and physical functioning may be more important in contributing to constipation [15]. The afore-mentioned study suggested that the combination of many methods or therapies provides more possibilities for the diagnosis and cure.

TCM syndrome differentiation is of unique advantage, and hence it is widely accepted and applied in treating digestive tract diseases, which collect and analyze symptoms and signs to evaluate the overall conditions and to classify the pattern of maladjustment through determining the nature and location of the maladjustment [16]. It is reported that patients in the active treatment groups (standard and individualized Chinese herbal medicine) had significant improvement in bowel symptom scores when compared with patients in the placebo group [17]. The result of a systematic review suggested that traditional Chinese medicine interventions appear to be useful to manage constipation [18]. However, a research of European and Asian demonstrated that there was no clear consensus as to whether complementary therapies were beneficial, although the symptoms of many patients with inflammatory bowel disease were improved [19]. In general, the effects of traditional Chinese medicine therapy in treating the digestive system diseases were still controversial and need more well-designed studies.

Biofeedback, as a nonmedicinal and noninvasive therapy, has no side effects and can be used repeatedly, so it is regarded as the first choice for the clinical treatment of functional constipation. It is widely recognized that oral administration of Chinese medicine in combination with biofeedback therapy can be very effective for functional constipation. Our study aims at investigating the clinical therapeutic effects of Yiqi Kaimi Prescription and biofeedback therapy on treating constipation with deficiency of spleen qi, which could provide evidence for biofeedback therapy with traditional Chinese medicine prescription in treating diseases.

2. Methods

2.1. Clinical Data. The 60 patients were diagnosed as functional constipation at the department of proctology from June 2009 to May 2011. The two groups included 27 males and 33 females, averaging 40.28 ± 11.40 years old. There were no significant differences between the groups in gender, age, disease course, and scores ($P > 0.05$). The constipation symptoms of patients were determined by the Rome III diagnostic criteria [20]. The TCM diagnostic criteria for deficiency of spleen qi syndrome include the primary symptoms and secondary symptoms. The primary symptoms were dry stools resembling chestnuts, with desire for defecation yet without strength to complete it, shortness of qi, and pale tongue. The secondary symptoms were whitish complexion, lassitude with weakened qi, weary limbs with reluctance to speak, and weak pulse. Patients with 3 items of the primary symptoms or 2 items of the primary symptoms plus 2 items of the secondary symptoms could be determined.

2.2. Treatment Methods. The two groups were given Yiqi Kaimi Prescription before the treatment. The Yiqi Kaimi Prescription was composed of the Raw Astragalus (30 g), Atractylodes (15 g), Aitrus Aurantium (12 g), Almond (12 g), Radix Rehmanniae (15 g), and Rngelica (15 g). It was taken orally twice a day, and four weeks made up a disease course. Before the treatment, the anorectal pressure was measured. The treatment group was given oral Yiqi Kaimi Prescription in combination with biofeedback treatment as well as anorectal muscle electrical testing. The control group was given oral Yiqi Kaimi Prescription in combination with anus-lifting exercise.

The specific procedures and main indexes of anorectal pressure test were as follows. The urine and feces were evacuated before the test. And the whole process should be explained in detail to the patient. At first, put a pressure-measurement tube into the anus at 6 cm in depth, and then tell the patient to imitate the effort to defecate, which lasted for 5~10 seconds. After 5 seconds of rest, ask the patient to contract his anus for 5~10 seconds; then adjust the depth of the tube to 2 cm, and tell the patient to rest for 30~60 seconds; afterwards repeat the previous procedures; use a syringe to rapidly inject 10 mL of gas into the anus at the 2 cm position, then discharge the gas 1 or 2 seconds later, and meanwhile observe the pressure difference and if the pressure curve would present double phase waves; inflate 50 mL of gas into the saccule and at the same time tell the patient to imitate the effort to defecate, which should last for 5~10 seconds; after 30~60 seconds of rest, inflate the saccule with a syringe slowly and evenly, and meanwhile record the initial feels, initial pressing and intense pressuring, of the patients.

For specific procedures of biofeedback, The patient should lie on his or her back and bend the body until the upper half and the lower half formed a 120° angle, and then the doctor put the measuring electrode of the biofeedback equipment into the anus and conducted Glazer assessment (test when relaxing the anus for 60 seconds, rapidly contracting it for 5 times/relaxing for 10 seconds, contracting for 10 seconds/relaxing for 10 seconds, persistently contracting for 60 seconds, and posterior baseline for 60 seconds).

Above 2 uv at the vagina and above 4 uv at the anus when relaxing, first carry out pelvic floor muscle multimedia training, electrostimulation on the pelvic floor nerves and muscles, myoelectricity triggering electric stimulation, and template Kegel training. If the pelvic floor muscles contract rapidly and the index is lower than 37.5 at the vagina and lower than 70 uv at the anus, yet there is no increase of resting value, the electrostimulation on the pelvic floor nerves and

Table 1: The score before and after treatment.

	Treatment group		Control group	
	Before	After	Before	After
Difficult defecation	2.06 ± 0.37	1.06 ± 0.58*#	2.07 ± 0.37	1.10 ± 0.30*
Fecal character	2.07 ± 0.42	0.79 ± 0.38*#	2.10 ± 0.45	1.34 ± 0.45*#
Defecation time (min)	2.10 ± 0.30	0.96 ± 0.18*#	1.87 ± 0.58	1.21 ± 0.41#
Endless and dilatation felling	2.03 ± 0.31	1.57 ± 0.50*#	1.90 ± 0.54	1.17 ± 0.38#
Frequency	2.14 ± 0.48	0.86 ± 0.48*	2.10 ± 0.45	0.82 ± 0.43*
Abdominal distension	2.17 ± 0.46	0.87 ± 0.35*#	1.90 ± 0.55	1.53 ± 0.51#

Data were shown as mean ± SD ($n = 30$). Statistical comparisons were made by the Student's t-test. * indicates $P < 0.05$, compared to that of before; # Indicates $P < 0.05$, compared to that of control.

muscles, myoelectricity triggering electric stimulation, and template kegel training should be carried out first once a day and 20 min a time for 3 treatment courses; anorectal muscle electrical testing was performed every six days; a treatment course includes 10 days. The changes of TCM symptoms after treatment and retest of the anorectal pressure will be observed.

2.3. Therapeutic Criteria. The therapeutic criteria for constipation are made according to the Guiding Principles for Clinical Research of New Traditional Chinese Medicines stipulated by China's Ministry of Health in 1993 [21].

2.4. Statistical Analysis. The comparisons of curative rate and disappearance rate of positive transmission test were analyzed by X^2 test. The clinical symptom scores and life quality scores were processed by t-test or analysis of variance.

3. Results

In this study, it was found that patients with deficiency of spleen qi cannot be simply diagnosed as slow transmission constipation (STC). The weakened intestinal motive power was often accompanied by uncoordinated contraction of the pelvic floor muscles and interferences of psychological factors during defecation. Before the treatment, the survey on the age and gender baselines of the patients found that the average onset age of the patients with deficiency of spleen qi was 40.28 ± 11.40 years old. Constipation with deficiency of spleen qi was common in old people, and females account for a large proportion, which may be due to the influence of menopause and hormone levels.

The results showed that the constipation symptoms, such as difficult defecation, endless and dilatation felling, and abdominal distension, had been significantly improved ($P < 0.05$; see Table 1). The defecation time was also significantly shortened after treatment from 2.1 min to 0.96 min, which had a significant difference when compared to that of the control ($P < 0.05$). After biological feedback therapy, the anorectal muscle electricity of patients in the treatment group was significantly improved ($P < 0.05$); at the same time, anorectal muscle electricity continues to rise in the six-time detection; the fast flick voltage and intermittent and continuous contraction voltages were significantly elevated, which suggested that the strength has been significantly improved. The change of the resting muscle electricity was not obvious, which suggested that the impact of the biofeedback treatment on the pelvic floor muscle was weak. However, the resting muscle electricity of the 30 patients in the treatment group was tested every 6 days. The result showed that the pelvic floor muscles get more training; the myo-electrical value and the muscle endurance were significantly improved at the same time (see Figure 1). Meanwhile, after biofeedback therapy combined with traditional Chinese medicine prescription, the fast flick voltage, and intermittent contraction voltages, continuous contraction voltages of 14 patients with clinical recovery were greatly improved after 3 medical courses. However, the fast flick voltage, intermittent contraction voltages, and continuous contraction voltages of 4 patients with ineffectiveness were not significantly changed, which may be related to the change of myoelectricity within 30% (see Figure 2).

The resting pressure of the internal sphincter, pressure of the external anal sphincter, and maximum systolic pressure significantly increased to some degree ($P < 0.05$; see Table 2). The contradictory contraction of the pelvic floor muscles during defecation was addressed; some patients had improved rectal sensory function, coordination between the rectum's motive power and the relaxation of the anus, and establishment of correct defecation. In both groups, there was no significant difference in the initial threshold values before and after treatment ($P > 0.05$). In the treatment group, there was significant difference in the maximum threshold values before and after treatment ($P < 0.05$). This indicated that biofeedback can improve the rectal sensory function; there was marked change in the treatment group after the treatment, indicating that the anus-lifting exercise lacks an effective nervous feedback-circuit training mechanism. Without regular and quantized training, the therapeutic effects were often unsatisfactory. However, in the treatment group, the biofeedback treatment coupled with electric stimulation can effectively improve the sensibility of the lower portion of the rectum, which may be due to the reparation of damaged nerves. However, the sample size of the study was small; the relationships among the conditions of the pelvic floor electromyography, the symptoms, and the anorectal pressure functional change were still unclear and need further research.

Table 2: The rectum pressure before and after treatment.

	Treatment group		Control group	
	Before	After	Before	After
Anal rest pressure	38.23 ± 13.14	53.70 ± 10.07*#	30.90 ± 14.90	39.23 ± 10.45#
Maximum systolic pressure	100.48 ± 22.55	128.83 ± 23.38*#	88.97 ± 20.45	95.53 ± 12.19#
Rectal initial threshold	39.73 ± 9.26	35.76 ± 5.50	37.43 ± 6.67	36.53 ± 5.30
Rectal maximum threshold	246.47 ± 46.50	225.13 ± 42.71*#	218.83 ± 52.50	219.93 ± 45.80

Data were shown as mean ± SD ($n = 30$). *indicated $P < 0.05$, compared to that of the control, #Indicated $P < 0.05$, compared to that of the before treatment.

Table 3: The comparison of the clinical effects.

Groups	Cases	Total effective rate	Clinical recovery rate	Excellent effectiveness rate	Effectiveness rate	Ineffectiveness rate
Treatment group	30	26 (86.66%)	14 (46.7%)	8 (26.66%)	4 (13.33%)	4 (13.33%)
Control group	30	15 (50.00%)	2 (6.66%)	5 (16.67%)	8 (26.66%)	15 (50.00%)

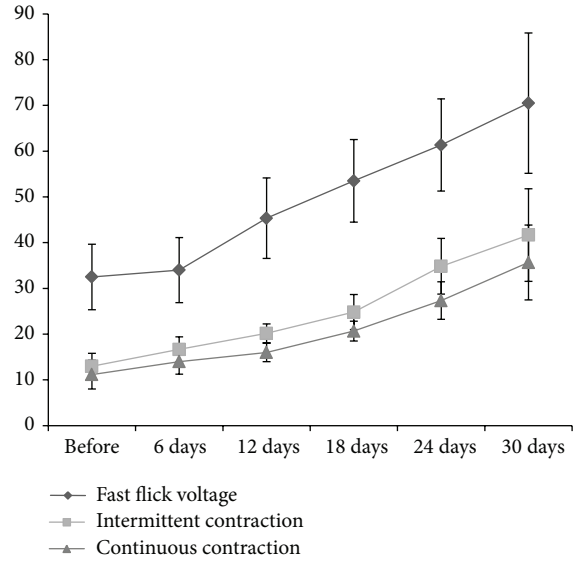

Figure 1: The trends of fast flick voltage, intermittent contraction, and continuous contraction within 30 days in the treatment group. The anorectal muscle electricity of patients in the treatment group continued to rise in the six-time detection, including the fast flick voltage and intermittent and continuous contraction voltages, which suggested that the strength has been significantly improved.

In general, the total effective rate of the treatment group was 86.66% (26 cases; see Table 3), the clinical recovery rate was 46.7% (14 cases), the excellent effectiveness rate was 26.66% (8 cases), the effectiveness rate was 13.33% (4 cases), and the ineffectiveness rate was 13.33% (4 cases).

4. Discussion

According to Rome III, functional constipation can be divided into three types: slow transmission constipation (STC), outlet obstructive constipation (OOC), and mixed pattern constipation [22]. Clinically the symptoms of functional constipation were various, which may differentiate STC from OOC. However, the treatment with clear target received unsatisfactory effects. Some patients had atypical symptoms of STC or OOC, long histories of drug reliance, and too many accompanying diseases and symptoms, which affected the diagnosis and treatment of constipation. The disease differentiation and syndrome differentiation of TCM had a unique advantage in the treatment of constipation. The diagnosis was made through examining the symptoms and signs of the patients as well as the anorectal pressure and made by combining TCM disease differentiation and syndrome differentiation [23]. After the diagnosis, the disease can be treated by traditional Chinese medicine coupled with modern therapeutics, and the effects were often satisfactory.

TCM had a unique advantage in treating functional constipation [24]. It approached the disease from overall regulation, emphasized on the root cause, and treated it in view of time, locality, and individuality [25]. Flexible in medication, it took into account both the primary and the secondary aspects and treated the disease and syndrome simultaneously, thus fully playing the role of individualized treatment. Biofeedback training was a new psychological treatment developed on the basis of behavior therapy [26]. It was based on Kegel training and aimed at directing the patient to correctly exercise the pelvic floor muscles, hence changing the measurable physiological parameters, strengthening the contracting function of the pelvic floor muscles, and achieving the best effects for excises of pelvic floor muscles [27]. The main symptoms of patients with spleen deficiency constipation were the decrease of both the intestinal motility and the anal sphincter muscle power, un-coordination of the pelvic floor muscle movement. The prescription was able to regulate the qi activity, improve intestinal motility, and promote the power of anal sphincter muscle. On the other hand, biofeedback therapy could improve the pelvic floor muscle movement through the enhancement of the anal sphincter muscle strength, which improved the symptoms of spleen deficiency constipation.

The disease location of constipation was in the large intestine, but it was also closely related to the viscera, channels, qi, blood, fluids, and emotions. It was controlled by the spleen, so if the spleen qi was sufficient, the defecation will

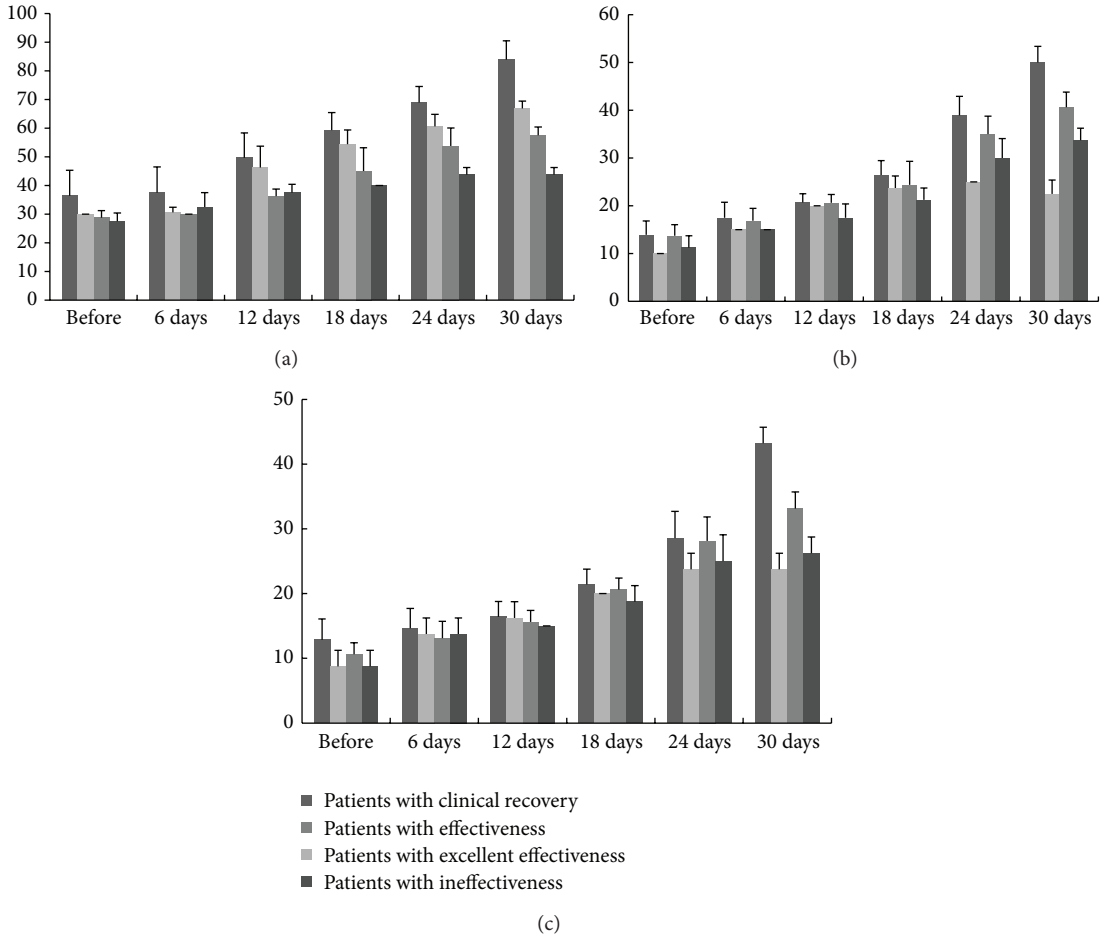

Figure 2: The comparison of the fast flick voltage, intermittent contraction voltages, and continuous contraction voltages among the groups of patients with clinical recovery, patients with excellent effectiveness, patients with effectiveness, and patients with ineffectiveness. (a) The trends of the fast flick voltage among the 4 groups. (b) The trends of the intermittent contraction voltages among the 4 groups. (c) The trends of the continuous contraction voltages among the 4 groups.

be normal; if the spleen qi was deficient, the transportation will be abnormal, or the qi transformation will be inadequate, leading to malfunction of transformation and, eventually, constipation. The root of constipation (deficiency of spleen pattern) was qi stagnation and/or spleen deficiency, and the branch was accumulation of heat. Unsmooth flow of qi leaded to the obstruction of the large intestine, or deficiency of qi failed to promote transportation, also leading to constipation. Qi deficiency and qi stagnation were often mixed and inter-promoted, thus making the disease more refractory. In brief, unsmooth qi transformation, stagnated qi movements, and insufficient qi and fluid were the fundamental causes of this disease.

Deficient spleen qi failed to promote transportation, so the intestinal movements and transportation of water and food will slow down, leading to prolonged retaining of food dregs in the intestinal tract and excessive absorption of water, characterized by dry, hard stools like chestnuts. The dysfunction of the spleen and stomach in digestion gives rise to abnormal ascending of food essences and abnormal descending of turbid things, and consequently the promoting ability of the intestines will be weakened. The spleen and stomach were the prenatal foundation, so their malfunction will cause disordered circulation of qi and blood in the whole body, marked by whitish complexion, lassitude with weakened qi, weary limbs with reluctance to speak, weak pulse, and decreased muscle strength, as well as asynchrony of abdominal muscle strength and pelvic floor muscle group in varying degrees.

Yiqi Kaimi Prescription was effective for constipation due to deficiency of spleen qi [28]. It used Raw Astragalus and Atractylodes as the monarch herbs and used Aitrus Aurantium and Almond to regulate qi so as to dredge both the upper orifices and lower ones and promote the transportation of the large intestine. If coupled with a small quantity of Radix Rehmanniae, they can moisten the intestinal tract, nourish the middle energizer, and regulate qi activity. Once the qi was replenished, it will regain its original abilities, break the stagnations, and remove the obstructions. Through nourishing qi, ascending the clear, and descending the turbid, as well as steaming the fluids, the yin will be nourished, so will the fluids. The fluids and qi were interchanged and

mutually moistened. All of these factors worked together so as to effectively improve the intestinal motive power and restore the transportation of the stomach and intestines.

The anorectal pressures before and after the treatment were measured. Although the technique cannot give a direct view of the structural disorder of the gastrointestinal tract, it can objectively describe the functional disorder of the gastrointestinal tract [29]. It was one of the main methods which can reveal whether the constipation was due to structural disorder or due to functional disorder and a way to classify chronic constipation. It can also help us understand, quantize, and evaluate the defecation function of the anal canal and rectum, thus providing pathological and physiological foundations for the researches into anorectal disorders such as abnormal defecation [30]. The changes of sensory threshold value also played a critical role in the occurrence and development of constipation [31]. It can provide objective foundation for the contradictory contraction of the anus and abdominal muscles and therefore guide clinical treatment. Patients with constipation due to deficiency of spleen qi often had anal laxity and relatively low resting pressure of the internal sphincter, pressure of the external anal sphincter, and maximum squeezing pressure. When making an effort to defecate, the patients may present with inadequate increase of rectal pressure, weak abdominal strength, and contradictory contraction of anal sphincter, though such occasions are rare. There was also a slight increase of the initial sensory threshold value of the rectum, initial defecation threshold value, and maximum toleration value of the rectum. Besides, in patients with constipation due to spleen deficiency, there may be damages of the internal motor nerves, which require further studies for confirmation.

For some patients with colon transportation disturbances without apparent symptoms of outlet obstruction, their situations can also be improved through biofeedback treatment [32]. This indicated that biofeedback can promote defecation at the same time of improving anorectal sensibility. However, the effects of placebo and psychological factors cannot be excluded. The patients in the control group performed anus-lifting exercise, yet without effective guidance and electric stimulation. The effect was not obvious, and the effect of the treatment group was far better than that of the control group. Traditional Chinese medicine coupled with biofeedback treatment can effectively improve the intestinal motive power, with marked improvement of TCM symptoms and alleviation of exhaust gas and abdominal distension. Biofeedback treatment was used to actively train the contraction of pelvic floor muscles so as to strengthen them, improve their supportive force and prevent prolapse and slackness of the pelvic floor. It can display the muscular electric activities by electrodes inserted into the rectum or abdomen. The physiological signals in these positions can be amplified and transformed into visible ones such as sound, lights, and graphs, which will be fed back to the patients. The patients trained themselves on the basis of these signals, and gradually developed conditioned reflex, and learned to voluntarily control the contraction of pelvic floor muscles. For patients with reduced sensitivity, the stimulation will be increased mainly by stimulus wave produced by microcurrent, which changed the central nervous system indirectly and regulated the pelvic floor nervous system. In this study, the treatment group received three courses of biofeedback treatment in addition to traditional Chinese medicine.

Multipattern combined treatment of functional constipation was of great significance. Constipation cannot be explained by monism, so medication should be combined with biofeedback so as to regulate the intestinal motive power and strengthen the coordination of pelvic floor muscle groups. The clinical therapeutic effects were often satisfactory.

Conflict of Interests

There is no financial or commercial conflict of interests.

Authors' Contribution

Yi-Bo Yao and Yong-Qing Cao contributed equally to this work.

Acknowledgments

This work was supported by the Shanghai Municipal Health Bureau (no. ZYSNXD-CC-HPGC-JD-002) and National Natural Science Foundation of China (81273763).

References

[1] C. J. M. Böhmer, J. A. J. M. Taminiau, E. C. Klinkenberg-Knol, and S. G. M. Meuwissen, "The prevalence of constipation in institutionalized people with intellectual disability," *Journal of Intellectual Disability Research*, vol. 45, no. 3, pp. 212–218, 2001.

[2] V. Garrigues, C. Gálvez, V. Ortiz, M. Ponce, P. Nos, and J. Ponce, "Prevalence of constipation: agreement among several criteria and evaluation of the diagnostic accuracy of qualifying symptoms and self-reported definition in a population-based survey in Spain," *American Journal of Epidemiology*, vol. 159, no. 5, pp. 520–526, 2004.

[3] V. Loening-Baucke, "Prevalence rates for constipation and faecal and urinary incontinence," *Archives of Disease in Childhood*, vol. 92, no. 6, pp. 486–489, 2007.

[4] P. Chiarelli, W. Brown, and P. McElduff, "Constipation in Australian women: prevalence and associated factors," *International Urogynecology Journal and Pelvic Floor Dysfunction*, vol. 11, no. 2, pp. 71–78, 2000.

[5] S. Rajindrajith, N. M. Devanarayana, C. Adhikari, W. Pannala, and M. A. Benninga, "Constipation in children: an epidemiological study in Sri Lanka using Rome III criteria," *Archives of Disease in Childhood*, vol. 97, no. 1, pp. 43–45, 2012.

[6] K. S. Ip, W. T. K. Lee, J. S. H. Chan, and B. W. Y. Young, "A community-based study of the prevalence of constipation in young children and the role of dietary fibre," *Hong Kong Medical Journal*, vol. 11, no. 6, pp. 431–436, 2005.

[7] Y.-F. Zhao, X.-Q. Ma, R. Wang et al., "Epidemiology of functional constipation and comparison with constipation-predominant irritable bowel syndrome: the Systematic Investigation of Gastrointestinal Diseases in China (SILC)," *Alimentary Pharmacology and Therapeutics*, vol. 34, no. 8, pp. 1020–1029, 2011.

[8] P. D. R. Higgins and J. F. Johanson, "Epidemiology of constipation in North America: a systematic review," *American Journal of Gastroenterology*, vol. 99, no. 4, pp. 750–759, 2004.

[9] L. R. Schiller, "Constipation and fecal incontinence in the elderly," *Gastroenterology Clinics of North America*, vol. 30, no. 2, pp. 497–515, 2001.

[10] C. Dennison, M. Prasad, A. Lloyd, S. K. Bhattacharyya, R. Dhawan, and K. Coyne, "The health-related quality of life and economic burden of constipation," *PharmacoEconomics*, vol. 23, no. 5, pp. 461–476, 2005.

[11] L. Dukas, W. C. Willett, and E. L. Giovannucci, "Association between physical activity, fiber intake, and other lifestyle variables and constipation in a study of women," *American Journal of Gastroenterology*, vol. 98, no. 8, pp. 1790–1796, 2003.

[12] S. A. Müller-Lissner, M. A. Kamm, C. Scarpignato, and A. Wald, "Myths and misconceptions about chronic constipation," *American Journal of Gastroenterology*, vol. 100, no. 1, pp. 232–242, 2005.

[13] R. D. Lindeman, L. J. Romero, H. C. Liang, R. N. Baumgartner, K. M. Koehler, and P. J. Garry, "Do elderly persons need to be encouraged to drink more fluids?" *Journals of Gerontology A*, vol. 55, no. 7, pp. M361–M365, 2000.

[14] S. Müller-Lissner, A. Rykx, R. Kerstens, and L. Vandeplassche, "A double-blind, placebo-controlled study of prucalopride in elderly patients with chronic constipation," *Neurogastroenterology and Motility*, vol. 22, no. 9, pp. 991–998, 2010.

[15] M. Bennett and H. Cresswell, "Factors influencing constipation in advanced cancer patients: a prospective study of opioid dose, dantron dose and physical functioning," *Palliative Medicine*, vol. 17, no. 5, pp. 418–422, 2003.

[16] W.-Y. Jiang, "Therapeutic wisdom in traditional Chinese medicine: a perspective from modern science," *Trends in Pharmacological Sciences*, vol. 26, no. 11, pp. 558–563, 2005.

[17] A. Bensoussan, N. J. Talley, M. Hing, R. Menzies, A. Guo, and M. Ngu, "Treatment of irritable bowel syndrome with Chinese herbal medicine: a randomized controlled trial," *Journal of the American Medical Association*, vol. 280, no. 18, pp. 1585–1589, 1998.

[18] L.-W. Lin, Y.-T. Fu, T. Dunning et al., "Efficacy of traditional Chinese medicine for the management of constipation: a systematic review," *Journal of Alternative and Complementary Medicine*, vol. 15, no. 12, pp. 1335–1346, 2009.

[19] G. A. Moody, J. A. Eaden, P. Bhakta, K. Sher, and J. F. Mayberry, "The role of complementary medicine in European and Asian patients with inflammatory bowel disease," *Public Health*, vol. 112, no. 4, pp. 269–271, 1998.

[20] D. A. Douglas, *ROME III—the Functional Gastrointestinal Disorder*, Degnon Associates, Inc., 2006.

[21] Ministry of Health of the People's Republic of China, "The clinical research guiding principles of new drug of the traditional Chinese medicine," p. 41, 1993.

[22] A. E. Bharucha, A. Wald, P. Enck, and S. Rao, "Functional anorectal disorders," *Gastroenterology*, vol. 130, no. 5, pp. 1510–1518, 2006.

[23] Y. Feng, Z. Wu, X. Zhou, Z. Zhou, and W. Fan, "Knowledge discovery in traditional Chinese medicine: state of the art and perspectives," *Artificial Intelligence in Medicine*, vol. 38, no. 3, pp. 219–236, 2006.

[24] M. S. Lee, T.-Y. Choi, J.-E. Park, and E. Ernst, "Effects of moxibustion for constipation treatment: a systematic review of randomized controlled trials," *Chinese Medicine*, vol. 5, article 28, 2010.

[25] G. Maciocia, *The Foundations of Chinese Medicine: A Comprehensive Text for Acupuncturists and Herbalists*, Elsevier Churchill Livingstone, 2005.

[26] V. Ricca, G. Castellini, E. Mannucci et al., "Comparison of individual and group cognitive behavioral therapy for binge eating disorder. A randomized, three-year follow-up study," *Appetite*, vol. 55, no. 3, pp. 656–665, 2010.

[27] S. S. C. Rao, "Constipation: evaluation and treatment of colonic and anorectal motility disorders," *Gastroenterology Clinics of North America*, vol. 36, no. 3, pp. 687–711, 2007.

[28] Y. Zou, X. Zheng, and S. Dai, "Effect of Zhi Zhu decoction on substance P and vasoactive intestine peptide expression in the colon of spleen-deficiency constipation mice," *Journal of New Chinese Medicine*, vol. 43, no. 1, p. 128, 2011.

[29] D. Wingate, M. Hongo, J. Kellow, G. Lindberg, and A. Smout, "Disorders of gastrointestinal motility: towards a new classification," *Journal of Gastroenterology and Hepatology*, vol. 17, no. 1, pp. S1–S14, 2002.

[30] A. E. Bharucha, J. G. Fletcher, B. Seide, S. J. Riederer, and A. R. Zinsmeister, "Phenotypic variation in functional disorders of defecation," *Gastroenterology*, vol. 128, no. 5, pp. 1199–1210, 2005.

[31] J. Wang, M.-H. Luo, Q.-H. Qi, and Z.-L. Dong, "Prospective study of biofeedback retraining in patients with chronic idiopathic functional constipation," *World Journal of Gastroenterology*, vol. 9, no. 9, pp. 2109–2113, 2003.

[32] S. S. C. Rao, "Constipation: evaluation and treatment of colonic and anorectal motility disorders," *Gastrointestinal Endoscopy Clinics of North America*, vol. 19, no. 1, pp. 117–139, 2009.

Hindawi Publishing Corporation
Evidence-Based Complementary and Alternative Medicine
Volume 2013, Article ID 198282, 12 pages
http://dx.doi.org/10.1155/2013/198282

Research Article

Moxibustion Inhibits the ERK Signaling Pathway and Intestinal Fibrosis in Rats with Crohn's Disease

Xiaomei Wang,[1] Yuan Lu,[2] Luyi Wu,[2] Chen Zhao,[1] Chunbin Song,[2] Shuguang Yu,[3] Baixiao Zhao,[4] Tianping Zhao,[2] Huirong Liu,[2] Chuanzi Dou,[2] Yingying Zhang,[2] and Huangan Wu[1,2]

[1] *Yueyang Hospital of Integrated Traditional Chinese and Western Medicine, Shanghai University of Traditional Chinese Medicine, Shanghai 200437, China*
[2] *Key Laboratory of Acupuncture-Moxibustion and Immunological Effects, Shanghai University of Traditional Chinese Medicine, Shanghai 200030, China*
[3] *Laboratory of Experimental Acupuncture of College of Acumox and Tuina, Chengdu University of Traditional Chinese Medicine, Chengdu 610075, China*
[4] *School of Acupuncture-Moxibustion and Tuina, Beijing University of Chinese Medicine, Beijing 100029, China*

Correspondence should be addressed to Huangan Wu; wuhuangan@126.com

Received 27 May 2013; Accepted 2 July 2013

Academic Editor: Yong-Qing Yang

Intestinal fibrosis is the main pathological process in Crohn's disease (CD); acupuncture and moxibustion can inhibit the process of fibrosis in CD rats, but the regulatory mechanism remains unknown. The present study observed the effect of moxibustion on the extracellular signal-regulated kinase (ERK) signaling pathway in the CD rat. The result shows that the phosphorylation of the Ras, Raf-1, MEK-1, and ERK-1/2 proteins and the expression of the corresponding mRNAs in the colon tissue of CD rat were significantly higher than the normal control group. Both treatments with mild moxibustion and with herb-separated moxibustion significantly reduced the expression of the Ras, Raf-1, MEK-1, and ERK-1/2 proteins and Ras and Raf-1 mRNA. MEK-1 and ERK-1/2 mRNA expression in each treatment group showed a downward trend, and the ERK-1/2 mRNA levels were significantly lower in the mild moxibustion group. It indicates that Ras, Raf-1, MEK-1, and ERK-1/2 are involved in the process of intestinal fibrosis in CD rats. Moxibustion can downregulate the abnormal expression of colonic Ras, Raf-1, MEK-1, and ERK-1/2 protein and mRNA levels in CD intestinal fibrosis in rats. Moxibustion may play a role in the treatment of CD intestinal fibrosis by regulating ERK signaling pathway.

1. Introduction

Crohn's disease (CD) is an agnogenic, chronic, and nonspecific granulomatous inflammatory disease of the intestine [1]. The histological features of CD are characterized by transmural inflammation, lymphangiectasia, and lymphatic and fibrous tissue hyperplasia. CD is more common in Europe and the USA than in other countries. The annual incidence in Europe and the USA is 5–10 per 100,000 persons, and the prevalence is 50–100 per 100,000 persons [2]. The incidence of CD in Asia is lower than in Western countries, although the incidence in China has noticeably increased in recent years [3, 4].

Under the pathological conditions of the chronic and recurring inflammation of CD, collagen decomposition is limited, and the continuously increasing deposition of collagen fibers results in excessive scar tissue, which promotes the hardening of the intestinal wall and luminal stenosis. Therefore, local intestinal function is impaired [5]. The results of impaired intestinal function range from the loss of intestinal wall compliance, severe abdominal pain, anorexia, and diarrhea to priming fistula formation and even increasing the possibility of malignant transformation, in which disease duration is persistent and refractory [6]. Studies have shown [7, 8] that early mild intestinal fibrosis can be reversed, which has great significance for slowing disease. At present,

the basis of therapy for CD intestinal fibrosis is long-term anti-inflammatory treatment. However, although they may reduce inflammation, anti-inflammatory treatments do not reduce fibrous stenosis. Therefore, an understanding of the pathogenesis of CD intestinal fibrosis and the discovery of effective prophylactic measures with fewer side effects are urgently needed in this field.

Intestinal fibrosis is a complicated pathological process in which many cell types, cytokines, and signaling pathways participate, including the extracellular signal-regulated kinase (ERK) signaling pathway, which has become a popular topic of current study. ERK, including ERK1 and ERK2, is one of the mitogen-activated protein kinase (MAPK) signaling pathways. The ERK1/2-MAPK signaling pathway is a cascade that is related to the pathological fibrosis of multiple diseases [9]. An activated Ras-Raf-MEK-ERK pathway promotes fibrosis and plays an important role in TGF-β-mediated type I collagen expression, extracellular matrix (ECM) production, and myofibroblast formation [10, 11].

Preliminary studies have shown that medicine-separated moxibustion can significantly inhibit the process of fibrosis in CD rats [12, 13], but the regulatory mechanism underlying this process remains to be further explored. In this study, a CD intestinal fibrosis rat model was prepared by the Morris method [14]. EnVision immunohistochemistry and qPCR were used to measure the levels of Ras, Raf, MEK, and ERK proteins and mRNA expression in colon tissues to explore the key signaling molecules involved in the regulation of CD intestinal fibrosis in rats and reveal the mechanisms underlying the effects of moxibustion on CD intestinal fibrosis.

2. Materials and Methods

2.1. Experimental Animals. A total of 60 male Sprague-Dawley (SD) rats with a body weight of 180 ± 20 g were provided by the Experimental Animal Center at the Shanghai University of Traditional Chinese Medicine. All of the rats were kept for one week at room temperature after receipt. The rats that behaved normally with respect to feeding, drinking, and other behaviors were included in the experiment. This study received permission from the Ethics Committee in Yueyang Hospital, which is affiliated with Shanghai University of Traditional Chinese Medicine, China. All protocols were performed in strict accordance with *the Guidance Suggestions for the Care and Use of Laboratory Animals*, formulated by the Ministry of Science and Technology of the People's Republic of China [15].

2.2. Grouping and Model Establishment. A total of 60 SD rats were randomly divided into a normal group of 12 rats and a model group of 48 rats. A 2,4,6-trinitrobenzene sulfonic acid (TNBS) (Sigma Co., St. Louis, USA) enema of 5% TNBS and 50% ethanol was prepared at a 2 : 1 ratio. The rats in each group were fasted but not deprived of water for 48 h. The rats in the model group were anesthetized by the intraperitoneal injection of 2% sodium pentobarbital (China Langchem Inc., Shanghai, China) at a dose of 20 mg/kg and were vertically inverted to introduce 100 mg/kg TNBS by rectal infusion once per 7 days for a total of four treatments, whereas the normal group was not treated. To validate the model, the distal colons from one rat in the normal group and two rats in the model group were examined by visual observation and H&E staining. After the success of the model was confirmed, the 44 rats were randomly assigned to a model group, a mild moxibustion group, a herb-separated moxibustion group, and an EA group, with 11 rats per group. Two rats died during the modeling process, and one rat from the model group and one rat from the mild moxibustion group died during the course of treatment.

2.3. Treatment

NC Group. No treatment.

MC Group. TNBS enema only, no treatment.

MM Group. A TNBS enema was administered, and the ST25 (bilateral) and RN6 acupuncture points were located. A moxa stick (Nanyang Hanyi Moxa Co., Ltd. China) 5 mm in diameter was lit and placed at points at a distance of 1-2 cm from the ST25 and RN6 acupuncture points. Moxibustion was performed for 10 min per point per treatment, once a day for a total of seven treatments.

HSP Group. A TNBS enema was administered, and the ST25 (bilateral) and RN6 acupuncture points were located. Aconite, cinnamon, salvia, and other drugs were milled into a powder and mixed with rice wine to form a paste. The paste was then pressed into a medicinal cake, 5 mm in diameter and 3 mm in thickness. A moxa cone was formed from 90 mg of refined moxa. Two moxa cones were used for moxibustion for each point per day, and a total of seven moxibustion treatments were performed for 7 days.

EA Group. A TNBS enema was administered, and the ST25 (bilateral) and RN6 acupuncture points were located. Needles (Suzhou Huatuo Co., Ltd. Suzhou, China) 0.25 mm in diameter and 25 mm in length were inserted to a depth of 3-4 mm and connected to an LD202H Han electroacupuncture apparatus (Beijing Huawei Co., Ltd. Beijing, China). The RN6 and bilateral ST25 acupuncture points were stimulated alternately by a continuous wave of 0.3 ms pulse width, 100 Hz frequency, and 1 mA current once a day for 10 min, with continuous treatment for 7 days.

2.4. Specimen Collection. Following treatment, the rats were fasted for 24 h with access to water and were then anesthetized by intraperitoneal injection of 2% sodium pentobarbital at a dose of 50 mg/kg. The anesthetized rats were then surgically sectioned to remove approximately 6 cm of the distal colon. The mesenterium was then cut longitudinally and rinsed with 4°C saline. The mucosal injury was visually examined and evaluated using a gross injury score [16, 17]. Two pieces of tissue with obvious lesions were removed, of which one was transferred to liquid nitrogen until testing, and the other was fixed in a 10% neutral formaldehyde solution.

2.5. Detection of Collagen Fibers in the Rat Colon. Masson trichrome staining was used to detect collagen fibers in

Table 1: The sequence of the forward primer and reverse primer used for fluorescent quantitative PCR assays.

Name	Primer sense	Sequence (5′→3′)	Amplification product (bp)
GAPDH	Forward	5′-CCGAGGGCCCACTAAAGG-3′	116 bp
	Reverse	5′-GCTGTTGAAGTCACAGGAGACAA-3′	
Ras	Forward	5′-TGGTGGGCAACAAGTGTGAC-3′	181 bp
	Reverse	5′-GGGTTCAGTTTCCGCAGTTTATG-3′	
Raf-1	Forward	5′-CAGGAGCACAAAGGTAAGAAAGC-3′	201 bp
	Reverse	5′-GCCACAAGTCTGACATCGAAATC-3′	
MEK-1	Forward	5′-AATATGTCAGGTTCAAGGAAAGGAC-3′	169 bp
	Reverse	5′-AGGTAAGGACGAAGCCACAAG-3′	
ERK-1/2	Forward	5′-TATATACATTCAGCTAATGTTCTGC-3′	169 bp
	Reverse	5′-TCTACCTGCAGCTGGAACCTCTC-3′	

the rat colon. Green staining was interpreted as collagen, mucus, and cartilage; red staining denotes muscle and nerve fibers; and black indicates nuclei.

2.6. EnVision Plus Immunohistochemical Detection of Ras, Raf, MEK, and ERK-1/2 in Colonic Tissue. Fixed tissues were conventionally deparaffinized in water and washed three times for 3 min in 0.01 M PBS, pH 7.4. The tissue samples were heated and allowed to equilibrate to room temperature for 20 min and then washed three times in PBS for 3 min. To inhibit endogenous peroxidase, the samples were treated with 0.3% H_2O_2 at room temperature for 20 min and then rinsed three times with PBS for 3 min. The tissue samples were incubated in 20% normal goat serum at room temperature for 30 min and then with one drop of the appropriately diluted primary antibody (Santa Cruz Bio Inc., Santa Cruz, USA) at 4°C for 18 h. The tissues were washed three times with PBS for 3 min, mixed with one drop of Envision reagent (HRP-M), and incubated in a humidified chamber for 30 min at 37°C. After washing three times with PBS for 3 min, the assay was developed in 0.04% DAB and 0.3% H_2O_2 for 8–12 min, then washed in water, stained with hematoxylin for 1 min, and bathed in hot water for 3 sec to allow the blue color to develop. Finally, the tissue sections were dried and mounted with a neutral resin. All the samples were analyzed by a Motic Med 6.0 image analysis system (Motic Group Co., Ltd.). Three fields were randomly selected, the positive target value of the integral optical density was calculated under an optical microscope (Olympus Co., Ltd.) at 200x magnification.

2.7. qPCR Detection of Ras, Raf, MEK, and ERK-1/2 mRNA Levels in Colonic Tissues. The total RNA was extracted from colon tissue samples. The cDNA was synthesized by reverse transcription (RT) according to the qPCR kit (Shanghai Daweike Bio Inc., Shanghai, China) instructions and amplified by PCR according to the kit instructions (Table 1). The following cycling conditions were used: RT at 37°C for 1 h, 95°C for 5 min to inactivate the MMLV RT enzyme, 50°C for 2 min, 95°C for 5 min, and 40 cycles of 95°C for 15 sec and 60°C for 45 sec.

2.8. Statistical Analysis. SPSS 18.0 statistical software (SPSS Inc., Chicago, USA) was used for statistical analysis. The measurement data are presented as the mean ± SD. For normally distributed data, one-way analysis of variance (ANOVA) was applied. The least significant difference method (LSD) was used for the homogeneity of variance, and Games-Howell was used to compare the differences between groups for the heterogeneity of variance; A value of $P < 0.05$ was considered statistically significant. The nonparametric Mann-Whitney U-test was used for abnormal distributions.

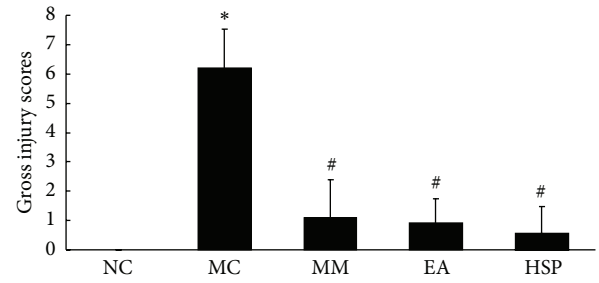

Figure 1: The gross injury scores of the colon tissue in each rat group. NC: normal control group, MC: model control group, MM: mild moxibustion, EA: electroacupuncture, and HSM: herb-separated moxibustion. $^{*}P < 0.01$ versus NC; $^{\#}P < 0.01$ versus MC.

3. Results

3.1. Gross Injury in the Colon Tissue of Rat. When the colonic tissues were observed by visual inspection, the rats in the normal group exhibited a uniformity of colon bowel and intestinal wall, a smooth colonic mucosa surface, clear vascular texture, no bleeder, and no erosion or ulcers. The model group exhibited partial intestinal canal stenosis or intestinal wall thicken and harden, fuzzy vascular texture, edematous colonic mucosa, serious congestion, erosion, and different size, shape, and depth ulcer formation. After treatments, there were lacked smooth colonic mucosa surface, edematous colonic mucosa and erosion in both MM and EA group, and lacked smooth colonic mucosa surface with no obvious erosion and ulcer in HPM group.

As shown in Figure 1, the gross injury score of the colonic tissue in the NC group was significantly higher than the MC group ($P < 0.01$). After treatment, the scores were lower in

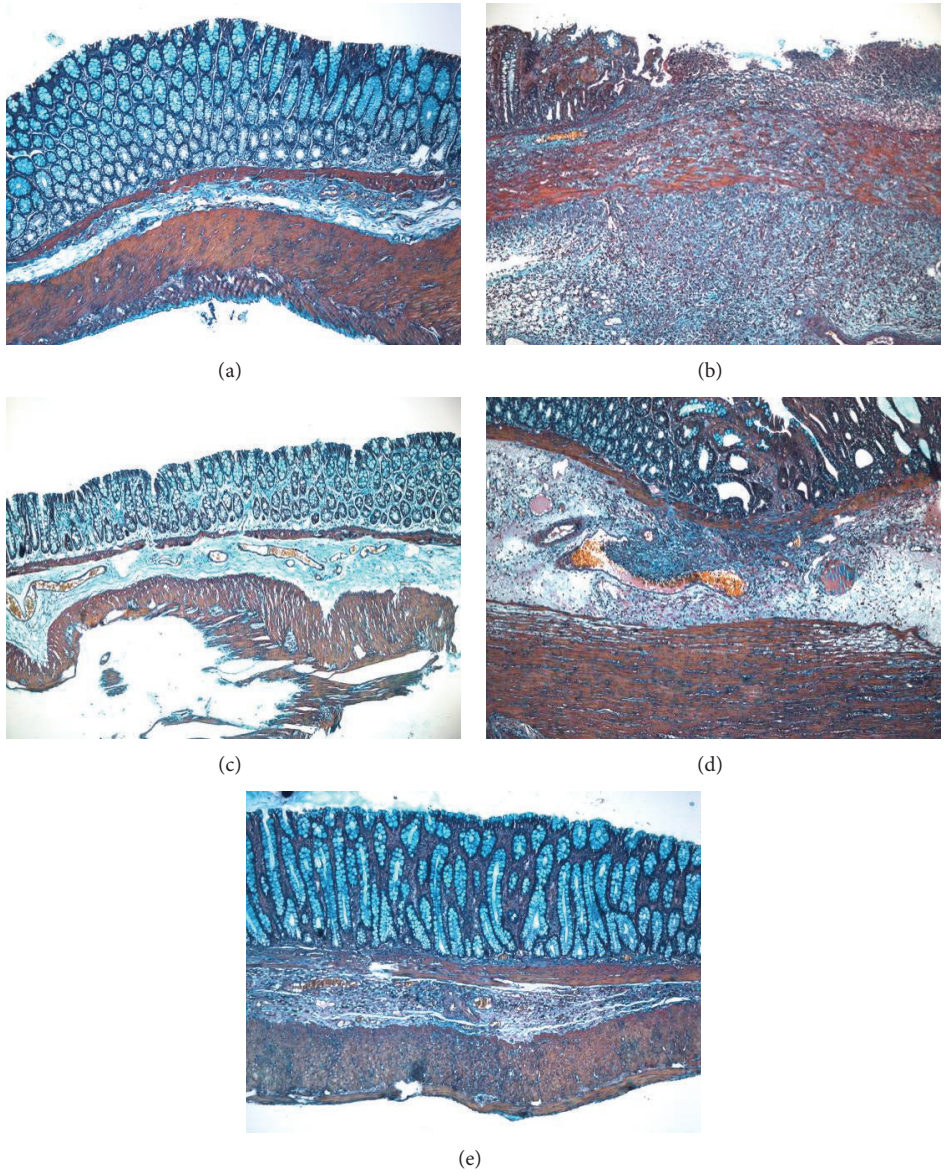

Figure 2: Expression of collagen fibers in the colon tissue of rat. Masson trichrome staining method, ×100. (a) Normal; (b) Crohn's disease; (c) mild moxibustion; (d) electroacupuncture; (e) herb-separated moxibustion.

both the HPM group, MM group, and the EA group ($P < 0.01$). It suggests that these treatments are able to improve the tissue damage of CD.

3.2. Expression of Collagen Fibers in the Colon Tissue of Rat. As shown in Figure 2, Masson trichrome staining revealed that in the MC group, a large number of collagen fibers were present in the mucosa, muscularis mucosa, submucosa, and muscularis of the rat colon, with a disordered arrangement. In the MM group and the HSM group, there were small numbers of collagen fibers in the colonic lamina propria and submucosa at the original ulcer-healing location, which was less severe compared with that of the model group. In the EA group, there were a small number of collagen fibers in the mucosa, submucosa, muscularis, and serosa of the rat colon, and the effect was less severe than in the MC group.

3.3. Ras Expression in the Colonic Mucosa of Rat. As shown in Figures 3 and 4, the phosphorylation of Ras protein in the rat colon was significantly higher in the MC group than in the NC group ($P < 0.01$). Ras protein expression was significantly reduced ($P < 0.01$) to normal levels after acupuncture treatment.

Figure 5 indicates that Ras mRNA expression in the MC group was higher than that in the NC group ($P < 0.01$) and that HSM effectively reduced the Ras mRNA levels in the rat colon ($P < 0.05$), whereas there was no significant difference between the EA group and the NC group.

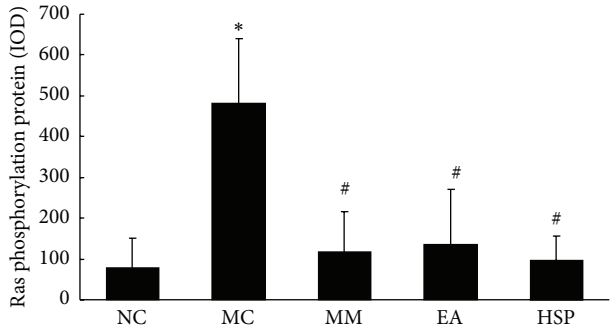

Figure 3: The integral optical density (IOD) of Ras phosphorylation in each rat group. NC: normal control group, MC: model control group, MM: mild moxibustion, EA: electroacupuncture, and HSM: herb-separated moxibustion. $^{*}P < 0.01$ versus NC; $^{\#}P < 0.01$ versus MC.

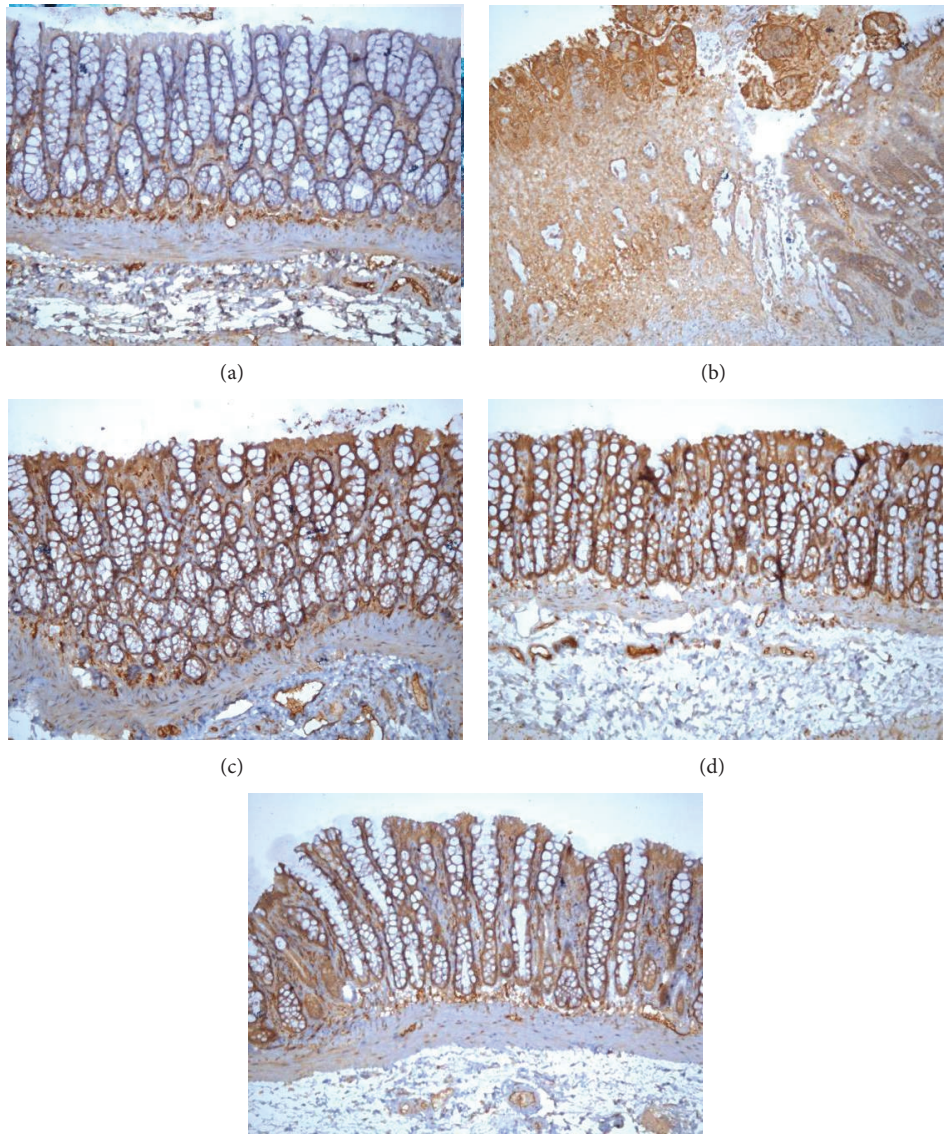

Figure 4: Expression of phosphorylated Ras protein in the colonic mucosa of rat. The phosphorylation of Ras protein was expressed in epithelial cells and lymphocyte in the colonic mucosa of rats. EnVision Plus method, ×200. (a) Normal; (b) Crohn's disease; (c) mild moxibustion; (d) electroacupuncture; (e) herb-separated moxibustion.

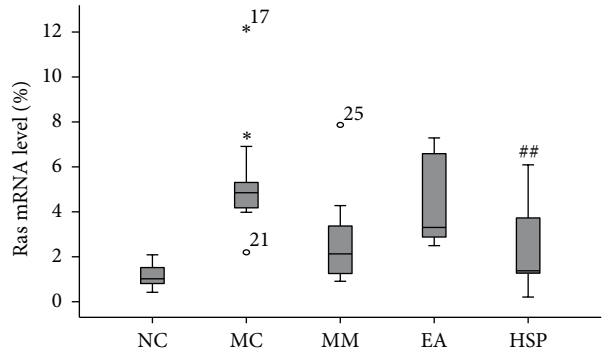

Figure 5: The Ras mRNA levels in the rat colon. NC: normal control group, MC: model control group, MM: mild moxibustion, EA: electroacupuncture, and HSM: herb-separated moxibustion. $^{*}P < 0.01$ versus NC; $^{\#\#}P < 0.05$ versus MC.

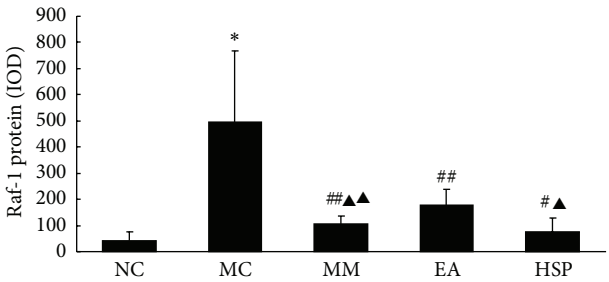

Figure 6: The IOD of Raf-1 protein expression in rat colon. NC: normal control group, MC: model control group, MM: mild moxibustion, EA: electroacupuncture, and HSM: herb-separated moxibustion. $^{*}P < 0.01$ versus NC; $^{\#\#}P < 0.05$, $^{\#}P < 0.01$ versus MC; $^{\blacktriangle\blacktriangle}P < 0.05$, $^{\blacktriangle}P < 0.01$ versus EA.

3.4. The Raf-1 Expression in the Colonic Mucosa of Rat. As shown in Figures 6 and 7, the Raf-1 protein expression in the colonic tissue of the MC group was significantly higher than in the NC group ($P < 0.01$) and that the Raf-1 protein expression in the colon was reduced to varying degrees after acupuncture treatment ($P < 0.05$ or $P < 0.05$).

The results in Figure 8 show that the Raf-1 mRNA levels in the MC group were significantly higher than in the NC group ($P < 0.01$) and that MM and HSM treatments significantly reduced rat colon Raf-1 mRNA levels ($P < 0.05$), whereas EA treatment did not significantly affect rat colon Raf-1 mRNA levels.

3.5. The MEK-1 Expression in the Colonic Mucosa of Rat. As shown in Figures 9 and 10, the MEK-1 protein expression in the colonic tissue of the MC group was significantly higher than in NC rats ($P < 0.01$), and MEK-1 protein expression was significantly reduced in each group after acupuncture treatment ($P < 0.01$), although the levels were still higher than normal levels ($P < 0.01$).

The results in Figure 11 show that the MEK-1 mRNA levels in the model group were significantly higher than those in the NC group ($P < 0.01$) and that MM, HSM, and EA treatment reduced MEK-1 mRNA levels, although there was no statistically significant difference between the treatment and no treatment groups or among the treatment groups.

3.6. The ERK-1/2 Expression in the Colonic Mucosa of Rat. As shown in Figures 12 and 13, the phosphorylation of ERK-1/2 significantly increased in the MC group compared with the NC group ($P < 0.01$) and that the levels of phosphorylated ERK-1/2 proteins were significantly reduced after the MM and HSM treatments ($P < 0.01$).

The results in Figure 14 show that the ERK-1/2 mRNA expression in the MC group was significantly higher than that in the NC group ($P < 0.01$) and that ERK-1/2 mRNA expression was significantly lower in the MM group after acupuncture treatment compared with the MC group ($P < 0.05$).

4. Discussion

Extracellular signal-regulated kinase (ERK), a member of the mitogen-activated protein kinase (MAPK) family, plays an important biological role in transmitting signals from surface receptors to the nucleus. The ERK1/2 pathway is the most thoroughly researched pathway in the ERK family and plays a role in a wide range of cellular functions, including regulating meiosis, mitosis, and anaphase processes in different cells. A variety of stimulating factors, such as growth factors, cytokines, viruses, G protein-coupled receptor ligands, and oncogenes, can activate the ERK1/2 pathway [18]. The ERK signaling pathway is a Ras-Raf-MEK-ERK pathway. Phosphorylation-activated ERK1/2 translocates from the cytoplasm to the nucleus and thereby mediates the transcriptional activation of Elk-1, ATF, NF-κB, AP-1, and c-fos, which in turn regulate cell proliferation and differentiation, the maintenance of cell shape, the construction of the cytoskeleton, apoptosis, and the malignant transformation of cells, among other biological functions.

One of the features of CD is the transformation of smooth muscle cells into fibroblasts and/or myofibroblasts [8]. This abundance of fibroblasts and myofibroblasts increases the expression of type I collagen mRNA and produces collagen tissue within the muscle [19]. There are a large number of fibroblast cells and type I, III, IV, and V collagen transcripts in the small intestines of CD patients [20], which produce more ECM, including collagen, elastin, and glycoproteins that are deposited intramurally to produce a thickening of the intestinal wall [10]. Based on a large number of experimental reports, the ERK-1/2 signaling pathway appears to participate in myofibroblast proliferation, differentiation, and collagen production [10, 11, 21–25], extracellular matrix synthesis [26, 27], smooth muscle cell proliferation and apoptosis [28], and the migration of vascular smooth muscle cells [29]. Inhibiting the expression and activity of ERK can inhibit the proliferation of vascular smooth muscle cells [30] to reduce the accumulation of ECM [31]. Therefore, it is inferred that the ERK-1/2 signaling pathway may induce the activation and proliferation of CD intestinal myofibroblasts and their transformation into muscle fiber cells. Additionally, the ERK-1/2 signaling pathway may regulate the proliferation and apoptosis of smooth muscle cells.

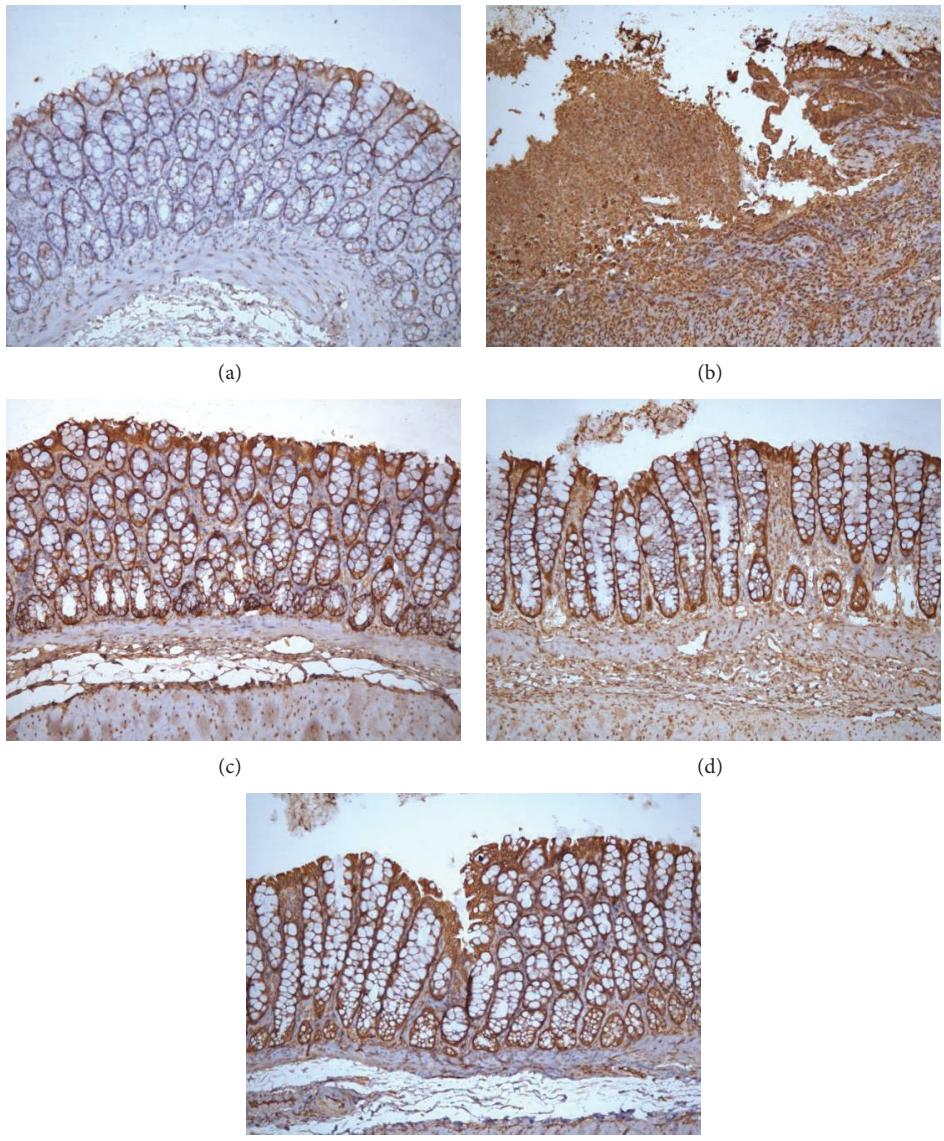

Figure 7: Expression of Raf-1 protein in the colonic mucosa of rat. The Raf-1 protein was expressed in epithelial cells in the colonic mucosa of rats. EnVision Plus method, ×200. (a) Normal; (b) Crohn's disease; (c) mild moxibustion; (d) electroacupuncture; and (e) herb-separated moxibustion.

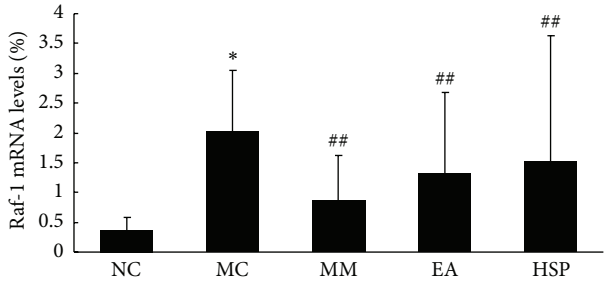

Figure 8: The Raf-1 mRNA levels in the rat colon. NC: normal control group, MC: model control group, MM: mild moxibustion, EA: electroacupuncture, and HSM: herb-separated moxibustion. $^{*}P < 0.01$ versus NC; $^{\#\#}P < 0.05$ versus MC.

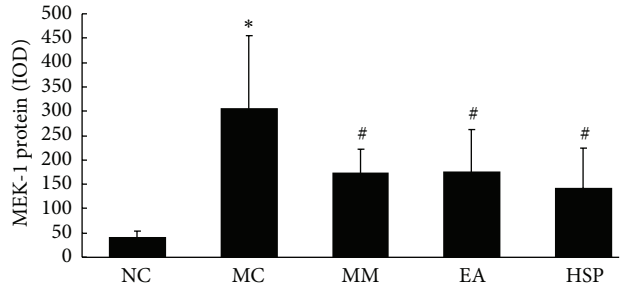

Figure 9: The IOD of MEK-1 protein expression in the rat colon. NC: normal control group, MC: model control group, MM: mild moxibustion, EA: electroacupuncture, and HSM: herb-separated moxibustion. $^{*}P < 0.01$ versus NC; $^{\#}P < 0.01$ versus MC.

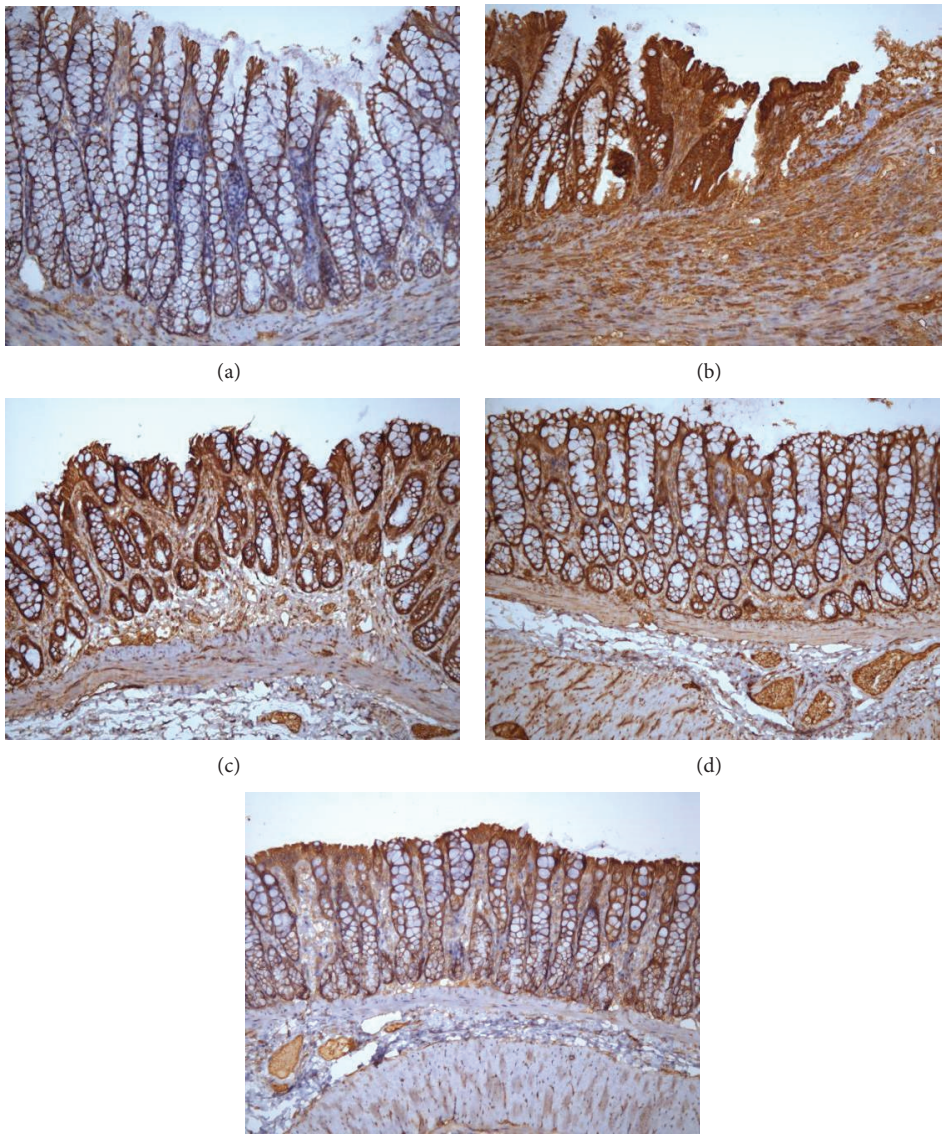

Figure 10: Expression of MEK-1 protein in the colonic mucosa of rat. The MEK-1 protein was expressed in epithelial cells in the colonic mucosa of rats. EnVision Plus method, ×200. (a) Normal; (b) Crohn's disease; (c) mild moxibustion; (d) electroacupuncture; and (e) herb-separated moxibustion.

As an upstream protein in the Raf-MEK-ERK pathway, Ras is the product of the proto-oncogene *c-ras*. A variety of stimulating factors, particularly growth factors (e.g., PDGF, EGF, TNF, and PKC activators as well as Src family members) can activate Ras, which further activates Raf-1. Activated Raf-1 then activates MEK and ERK downstream [32, 33] to initiate the MAPK pathway. Raf-1 protein kinase is widely expressed in various types of cells [34]. Ras and Raf-1 often exist in the form of complexes. Ras, the upstream activator protein, can translocate Raf from the cytoplasm to the plasma membrane, where the latter is activated. However, the mechanism by which Raf is activated remains unclear, although it may include phosphorylation [35]. All that is known is that Raf activation is related to its phosphorylation on Ser/Thr residues [33]. Recent studies have shown that Raf-1 protein kinase may be a point of crosstalk with other signaling pathways. This protein may participate in a variety of biological processes in signal transduction, including its own regulation, by interacting with other signaling molecules or via reciprocal regulation.

The MAPK kinases include MEK1 (MKK1) and MEK2 (MKK2). MEK1 and MEK2 are the central links in the MAPK pathway. The activated upstream Raf-1 protein kinase can combine with MEK1 and 2 and doubly phosphorylate Tyr and Thr, its two regulatory sites, to activate ERK [36]. MEKs are not only ERK activators but may also relocalize the activated ERKs to the nucleus or other active sites to further phosphorylate downstream substrates [37].

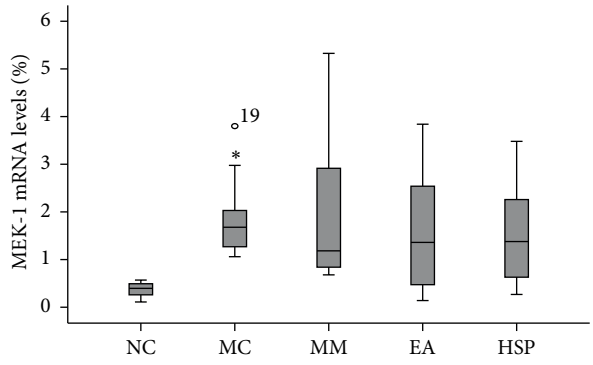

Figure 11: The MEK-1 mRNA levels in the rat colon. NC: normal control group, MC: model control group, MM: mild moxibustion, EA: electroacupuncture, and HSM: herb-separated moxibustion. $^{*}P < 0.01$ versus NC.

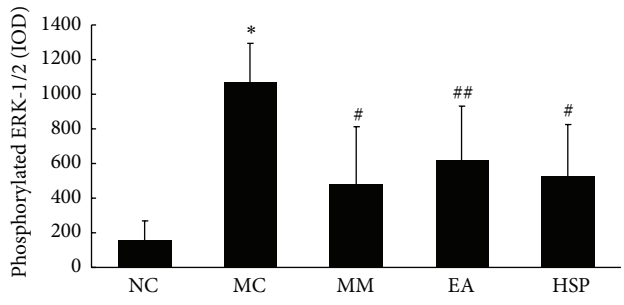

Figure 12: The IOD of phosphorylated ERK-1/2 levels in the rat colon. NC: normal control group, MC: model control group, MM: mild moxibustion, EA: electroacupuncture, and HSM: herb-separated moxibustion. $^{*}P < 0.01$ versus NC; $^{\#\#}P < 0.05$, $^{\#}P < 0.01$ versus MC.

The upstream kinase MEK1 is a dual-specificity enzyme. Activated MEK1 can phosphorylate ERK1 and ERK2. There is evidence that the Tyr residues of ERK1 and 2 are phosphorylated before the Thr residues, both intracellularly and extracellularly [38]. ERK translocates into the nucleus by forming a homodimer of phosphorylated ERK and phosphorylated or unphosphorylated ERK [39]. ERK is evenly distributed in quiescent cells, but when the cells are stimulated by serum, persistently activated ERK can partially translocate into the nucleus, whereas transiently activated ERK cannot relocalize. Activated ERKs accumulate in the nucleus and then phosphorylate the corresponding transcription factors, which drive expression of specific gene products. Because of the difference in nuclear localization, transiently activated (or low-activity) ERK and persistently activated (or high-activity) ERK cause cells to express genes at a different quality or quantity, resulting in different biological effects [40–43].

The ERK1-ERK2-MAPK pathway incorporates a mechanism for inactivation after activation, which can prevent excessive activation-induced adverse consequences. At the same time, the inactivated kinase is prepared for the next activation. The mechanisms of inhibition of this pathway include the following: (1) the activation of ERK1/2-MAPK is the result of the phosphorylation cascade and can be inactivated by dephosphorylation by the corresponding phosphatases; (2) Raf-1 is the direct substrate of PKA, which can phosphorylate Ser43 of c-Raf, an inhibitory phosphorylation site in the N-terminus of Raf that interacts with Ras, and the phosphorylation of this site can inhibit the binding between RasGTP and the N-terminus of Raf, which blocks the activation of ERK; (3) the phosphatase PP2 can inactivate MEK and ERK via dephosphorylation; (4) activated ERK phosphorylates Sos and Raf while ERK dephosphorylation inactivates them, thereby generates negative feedback regulation of the pathway. Therefore, the study of the mechanism by which acupuncture regulates the expression of ERK upstream receptors, the phosphorylation of ERK cascade members, the targets of downstream signal transduction, and the potential impact of other signaling pathways on this pathway is necessary to confirm acupuncture as an antifibrotic treatment.

Our experiments studied the regulation of Ras, Raf, MEK, and ERK protein and gene expression by acupuncture in CD intestinal fibrosis in the rat colon. Our results show that the mRNA levels of Ras, Raf-1, MEK-1, and ERK-1/2 were significantly increased in CD rat intestinal tissue and that the expression of p-Ras, Raf-1, MEK-1, and p-ERK-1/2 proteins in intestinal epithelial cells were also significantly increased. These results suggest that the activity of the ERK pathway in CD intestinal fibrosis process was altered. Medicine-separated moxibustion mild moxibustion, and electroacupuncture treatments could effectively downregulate the expression of p-Ras, Raf-1, MEK-1, and p-ERK-1/2, but different inhibitory effects on Ras, Raf-1, MEK-1, and ERK-1/2 mRNA levels were shown in ERK pathway activity changes. In this discussion, we propose the following: (1) medicine-separated moxibustion, mild moxibustion, and electroacupuncture can inhibit CD intestinal fibrosis by regulating ERK pathway activity; and (2) the acupuncture-induced inhibition of p-Ras, Raf-1, MEK-1, and p-ERK-1/2 expression may be the key elements in the treatment's inhibition of CD intestinal fibrosis. At present, most reports regarding the role of acupuncture in the regulation of the ERK signaling pathway have focused on EA, such as EA model rats. After EA on the Dazhui (DU14) and Baihui (DU20) acupuncture points, the number of ERK-positive striatal cells increased significantly in the cerebral cortex, and ERK protein expression was increased in rats with damaged neurons after cerebral ischemia and reperfusion; therefore, EA can increase ERK pathway activity [44, 45]. After the EA treatment of gastric mucosa-injured rats, the phosphorylation levels of ERK in gastric mucosal cells from extracted serum were significantly increased and were significantly different between the serum of the normal rats and that of the model rats. These observations suggest that ERK may be involved in signal transduction in the EA stimulation at acupoints of stomach meridian of foot yangming, repairing gastric mucosal injury [46], and that EA had an analgesic effect by downregulating p-ERK expression levels in the dorsal horn of the spinal cord of rats with adjuvant arthritis [47]. The previous reports have demonstrated that EA can regulate the ERK signal transduction pathway. The results of our experiments show that medicine-separated moxibustion

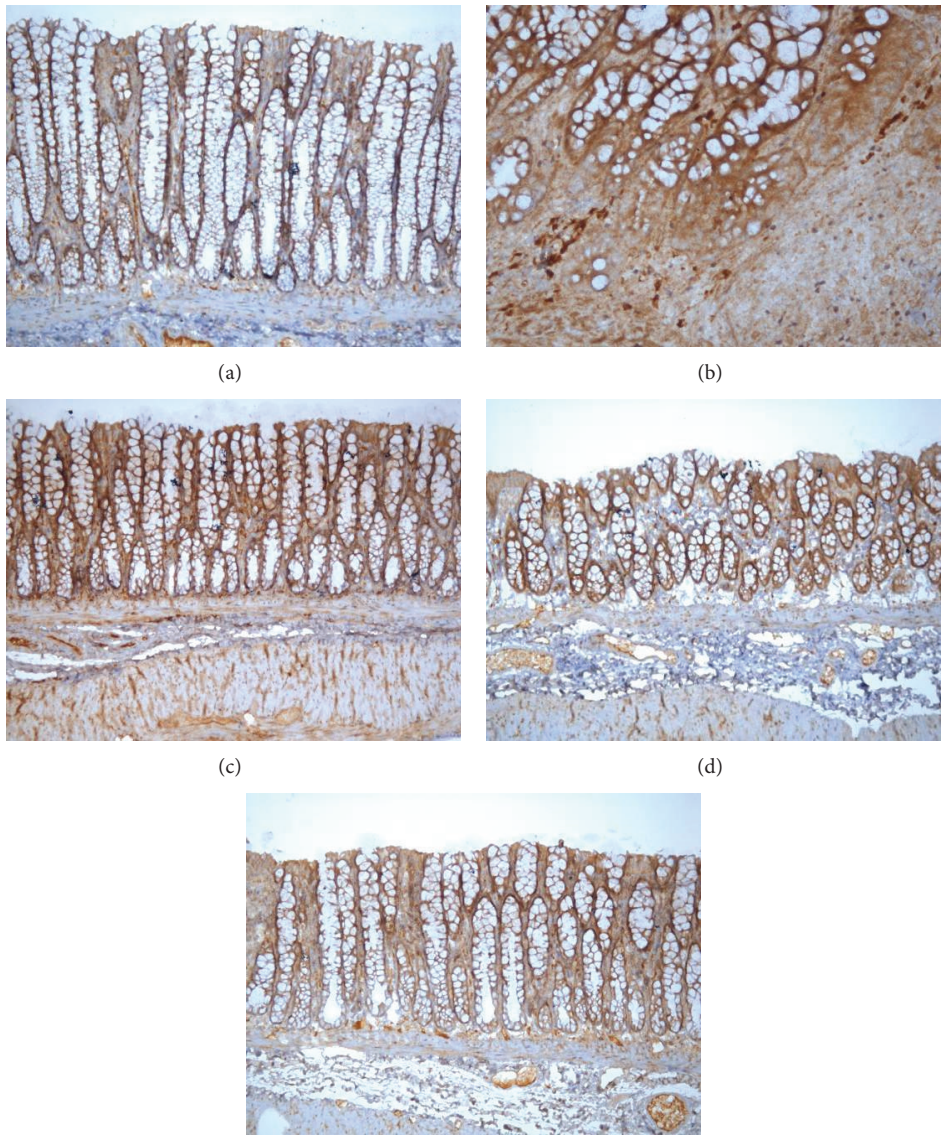

Figure 13: Expression of phosphorylated ERK-1/2 protein in the colonic mucosa of rat. The phosphorylation of ERK-1/2 protein was expressed in epithelial cells and lymphocyte in the colonic mucosa of rats. EnVision Plus method, ×200. (a) Normal; (b) Crohn's disease; (c) mild moxibustion; (d) electroacupuncture; and (e) herb-separated moxibustion.

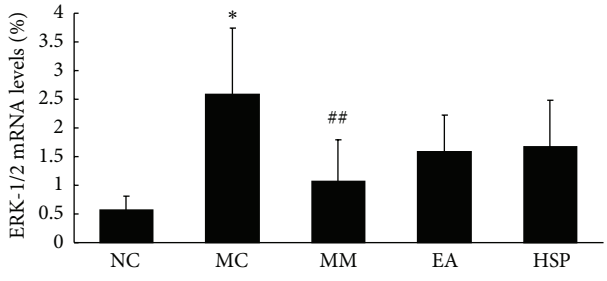

Figure 14: The ERK-1/2 mRNA levels in the rat colon. NC: normal control group, MC: model control group, MM: mild moxibustion, EA: electroacupuncture, and HSM: herb-separated moxibustion. $^{*}P < 0.01$ versus NC; $^{\#\#}P < 0.05$ versus MC.

and mild moxibustion can also regulate the ERK signal transduction pathway and inhibit Ras and Raf-1 better than EA. The functional mechanisms underlying these observations need to be explored further.

Abbreviations

CD: Crohn's disease
NC: Normal control group
MC: Model control group
EA: Electroacupuncture
MM: Mild moxibustion
HSM: Herb-separated moxibustion
ST25: Tianshu acupoint

RN6: Qihai acupoint
ERK: Extracellular signal-regulated kinase
MAPK: Mitogen-activated protein kinase
TNBS: 2,4,6-Trinitrobenzene sulfonic acid.

Acknowledgments

The authors thank Professor Shuhui Jiang for technical assistance and the support of the National Natural Science Foundation of China (no. 81173331) and National Basic Research Program of China (973 program, no. 2009CB522900). Xiaomei Wang and Yuan Lu have the same right.

References

[1] G. Manning, D. B. Whyte, R. Martinez, T. Hunter, and S. Sudarsanam, "The protein kinase complement of the human genome," *Science*, vol. 298, no. 5600, pp. 1912–1934, 2002.

[2] C. Mowat, A. Cole, A. Windsor et al., "Guidelines for the management of inflammatory bowel disease in adults," *Gut*, vol. 60, no. 5, pp. 571–607, 2011.

[3] Inflammatory Bowel Disease Co-operation Group, Chinese Society of Gastroenterology, "Chinese consensus on diagnosis and treatment standard of inflammatory bowel disease," *Chinese Journal of Gastroenterology*, vol. 12, no. 8, pp. 490–494, 2007.

[4] J. J. Zheng, X. S. Zhu, Z. Huangfu, Z. X. Gao, Z. R. Guo, and Z. Wang, "Crohn's disease in mainland China: a systematic analysis of 50 years of research," *Chinese Journal of Digestive Diseases*, vol. 6, no. 4, pp. 175–181, 2005.

[5] M. Dai and B. M. Li, "Research progress in mechanisms of intestinal fibrosis in Crohn's disease," *Shijie Huaren Xiaohua Zazhi*, vol. 17, no. 11, pp. 1117–1121, 2009.

[6] O. Grip, J. Malm, B. Veress, A. Bjartell, S. Lindgren, and A. Egesten, "Increased presence of cells containing transforming growth factor alpha (TGF-α) in ulcerative colitis, both during active inflammation and in remission," *European Journal of Gastroenterology and Hepatology*, vol. 12, no. 7, pp. 761–766, 2000.

[7] I. E. Koutroubakis, E. Petinaki, P. Dimoulios et al., "Serum laminin and collagen IV in inflammatory bowel disease," *Journal of Clinical Pathology*, vol. 56, no. 11, pp. 817–820, 2003.

[8] S. Speca, I. Giusti, F. Rieder, and G. Latella, "Cellular and molecular mechanisms of intestinal fibrosis," *World Journal of Gastroenterology*, vol. 18, no. 28, pp. 3635–3661, 2012.

[9] Y. F. Song, J. H. Hong, and L. M. Xu, "TGF-β 1/ERK pathways and its inhibitors and fibrosis," *Chinese Journal of Clinical Hepatology*, vol. 21, no. 2, pp. 125–127, 2005.

[10] H. C. Huang, M. Yang, J. Z. Li, and H. Y. Wang, "Connective tissue growth factor promotes the proliferation of myofibroblast through Erk-1/2 signaling pathway," *National Medical Journal of China*, vol. 85, no. 19, pp. 1322–1326, 2005.

[11] L. P. Guo, H. C. Huang, and J. Z. Li, "Hypoxia induces myofibroblast formation and stimulates production of collagen I in myofibroblasts through ERK1/2 pathway," *Chinese Journal of Pathophysiology*, vol. 24, no. 12, pp. 2428–2432, 2008.

[12] H. R. Liu, X. P. Ma, T. P. Zhao, and H. G. Wu, "The adjustment of acupuncture on colon collagen synthesis and TGF-β mRNA expression in Crohn's disease rat," *Journal of Anhui Traditional Chinese Medical College*, vol. 24, no. 4, pp. 25–30, 2005.

[13] X. P. Ma, C. P. An, H. G. Wu et al., "Herbs-partitioned moxibustion and electro-acupuncture effects on transforming growth factor-beta 1, connective tissue growth factor, collagen type I and fibronectin expression in the colon of Crohn' s disease rats," *Journal of Clinical Rehabilitative Tissue Engineering Research*, vol. 12, no. 20, pp. 3853–3858, 2008.

[14] G. P. Morris, P. L. Beck, M. S. Herridge, W. T. Depew, M. R. Szewczuk, and J. L. Wallace, "Hapten-induced model of chronic inflammation and ulceration in the rat colon," *Gastroenterology*, vol. 96, no. 3, pp. 795–803, 1989.

[15] The Ministry of Science and Technology of the People's Republic of China, Guidance Suggestions for the Care and Use of Laboratory Animals, 2006.

[16] J. D. Butzner, R. Parmar, C. J. Bell, and V. Dalal, "Butyrate enema therapy stimulates mucosal repair in experimental colitis in the rat," *Gut*, vol. 38, no. 4, pp. 568–573, 1996.

[17] X. M. Wang, Y. Lu, L. Y. Wu et al., "Moxibustion inhibits interleukin-12 and tumor necrosis factor alpha and modulates intestinal flora in rat with ulcerative colitis," *World Journal of Gastroenterology*, vol. 18, no. 46, pp. 6826–6835, 2012.

[18] J. B. Pucilowska, K. K. McNaughton, N. K. Mohapatra et al., "IGF-I and procollagen α1(I) are coexpressed in a subset of mesenchymal cells in active Crohn's disease," *American Journal of Physiology*, vol. 279, no. 6, pp. G1307–G1322, 2000.

[19] M. Gharaee-Kermani, B. Hu, S. H. Phan, and M. R. Gyetko, "Recent advances in molecular targets and treatment of idiopathic pulmonary fibrosis: focus on TGFβ signaling and the myofibroblast," *Current Medicinal Chemistry*, vol. 16, no. 11, pp. 1400–1417, 2009.

[20] E. M. Zimmermann, L. Li, Y. T. Hou, M. Cannon, G. M. Christman, and K. N. Bitar, "IGF-I induces collagen and IGFBP-5 mRNA in rat intestinal smooth muscle," *American Journal of Physiology*, vol. 273, no. 4, pp. G875–G882, 1997.

[21] L. J. Zhang, Q. Li, P. Chen et al., "Mediating effect of extracellular signal-regulated kinase 1/2 in PDGF-induced proliferation and collagen synthesis of cultured rat cardiac fibroblasts," *Chinese Journal of Anatomy*, vol. 13, no. 4, p. 223, 2007.

[22] M. Tang, W. Zhang, H. Lin, H. Jiang, H. Dai, and Y. Zhang, "High glucose promotes the production of collagen types I and III by cardiac fibroblasts through a pathway dependent on extracellular-signal-regulated kinase 1/2," *Molecular and Cellular Biochemistry*, vol. 301, no. 1-2, pp. 109–114, 2007.

[23] H. Y. Dai, Z. M. Ge, and Y. H. Li, "Effect of urotensin II on proliferative potential and phosphorylation of extracellular signal-regulated kinase 1/2 adventitial fibroblasts from spontaneously hypertensive rat," *Acta Academiae Medicinae Sinicae*, vol. 28, no. 6, pp. 776–780, 2006.

[24] I. Fuentes-Calvo, A. M. Blázquez-Medela, N. Eleno, E. Santos, J. M. López-Novoa, and C. Martínez-Salgado, "H-Ras isoform modulates extracellular matrix synthesis, proliferation, and migration in fibroblasts," *American Journal of Physiology*, vol. 302, no. 4, pp. C686–C697, 2012.

[25] Y. W. Ma, G. T. Bai, and M. X. Zhang, "Studies on signal transduction pathway induced by fibronectin in human embryonic lung fibroblasts," *Shanxi Medical Journal*, vol. 38, no. 7, pp. 587–589, 2009.

[26] J. H. Jang and C. P. Chung, "Fibronectin-mediated adhesion rescues cell cycle arrest induced by fibroblast growth factor-1 by decreased expression of P21CIP/WAF in human chondrocytes," *In Vitro Cellular and Developmental Biology*, vol. 41, no. 5-6, pp. 126–129, 2005.

[27] B. Zhu, Y. J. Wang, C. F. Zhu et al., "Triptolide inhibits extracellular matrix protein synthesis by suppressing the Smad2

but not the MAPK pathway in TGF-β1-stimulated NRK-49F cells," *Nephrology Dialysis Transplantation*, vol. 25, no. 10, pp. 3180–3191, 2010.

[28] J. Bai, X. S. Liu, Y. J. Xu, M. Xie, and W. Ni, "Effects of extracellular signal regulated kinase signaling pathway on cell cycle of airway smooth muscle cells in asthmatic rats," *Chinese Journal of Respiratory and Critical Care Medicine*, vol. 9, no. 1, pp. 23–27, 2010.

[29] S. Matsusaka and I. Wakabayashi, "Enhancement of vascular smooth muscle cell migration by urotensin II," *Naunyn-Schmiedeberg's Archives of Pharmacology*, vol. 373, no. 5, pp. 381–386, 2006.

[30] Y. Chen, Z. Dai, Y. M. Liu et al., "Inhibitory effects of CGRP on vascular smooth muscle cell proliferation: role of caveolae/caveolin-1/ERK1/2 signal pathway," *Progress in Biochemistry and Biophysics*, vol. 40, no. 5, pp. 445–453, 2013.

[31] W. L. Wu, A. Q. Zhang, Q. Yin, and W. H. Gan, "Effects of ERK signal pathway on extracellular matrix synthesis of rat mesangial cells treated with PDGF-BB," *ACTA University Medicinalis Nanjing*, vol. 27, no. 10, pp. 1126–1129, 2007.

[32] L. S. Steelman, W. H. Chappell, S. L. Abrams et al., "Roles of the Raf/MEK/ERK and PI3K/PTEN/Akt/mTOR pathways in controlling growth and sensitivity to therapy-implications for cancer and aging," *Aging*, vol. 3, no. 3, pp. 192–222, 2011.

[33] W. Kolch, "Meaningful relationships: the regulation of the Ras/Raf/MEK/ERK pathway by protein interactions," *Biochemical Journal*, vol. 351, no. 2, pp. 289–305, 2000.

[34] D. Matallanas, M. Birtwistle, D. Romano et al., "Raf family kinases: old dogs have learned new tricks," *Genes and Cancer*, vol. 2, no. 3, pp. 232–260, 2011.

[35] C. S. Mason, C. J. Springer, R. G. Cooper, G. Superti-Furga, C. J. Marshall, and R. Marais, "Serine and tyrosine phosphorylations cooperate in Raf-1, but not B-Raf activation," *The EMBO Journal*, vol. 18, no. 8, pp. 2137–2148, 1999.

[36] R. J. Fiddes, P. W. Janes, S. P. Sivertsen, R. L. Sutherland, E. A. Musgrove, and R. J. Daly, "Inhibition of the MAP kinase cascade blocks heregulin-induced cell cycle progression in T-47D human breast cancer cells," *Oncogene*, vol. 16, no. 21, pp. 2803–2813, 1998.

[37] S. T. Eblen, J. K. Slack, M. J. Weber, and A. D. Catling, "Rac-PAK signaling stimulates extracellular signal-regulated kinase (ERK) activation by regulating formation of MEK1-ERK complexes," *Molecular and Cellular Biology*, vol. 22, no. 17, pp. 6023–6033, 2002.

[38] M. Cargnello and P. P. Roux, "Activation and function of the MAPKs and their substrates, the MAPK-activated protein kinases," *Microbiology and Molecular Biology Reviews*, vol. 75, no. 1, pp. 50–83, 2011.

[39] A. V. Khokhlatchev, B. Canagarajah, J. Wilsbacher et al., "Phosphorylation of the MAP kinase ERK2 promotes its homodimerization and nuclear translocation," *Cell*, vol. 93, no. 4, pp. 605–615, 1998.

[40] R. H. Chen, C. Sarnecki, and J. Blenis, "Nuclear localization and regulation of erk- and rsk-encoded protein kinases," *Molecular and Cellular Biology*, vol. 12, no. 3, pp. 915–927, 1992.

[41] S. Traverse, K. Seedorf, H. Paterson, C. J. Marshall, P. Cohen, and A. Ullrich, "EGF triggers neuronal differentiation of PC12 cells that overexpress the EGF receptor," *Current Biology*, vol. 4, no. 8, pp. 694–701, 1994.

[42] T. T. Nguyen, J. C. Scimeca, C. Filloux, P. Peraldi, J. L. Carpentier, and E. Van Obberghen, "Co-regulation of the mitogen-activated protein kinase, extracellular signal-regulated kinase 1, and the 90-kDa ribosomal S6 kinase in PC12 cells. Distinct effects of the neurotrophic factor, nerve growth factor, and the mitogenic factor, epidermal growth factor," *Journal of Biological Chemistry*, vol. 268, no. 13, pp. 9803–9810, 1993.

[43] I. Dikic, J. Schlessinger, and I. Lax, "PC12 cells overexpressing the insulin receptor undergo insulin-dependent neuronal differentiation," *Current Biology*, vol. 4, no. 8, pp. 702–708, 1994.

[44] M. H. Shen, Z. R. Li, X. R. Xiang, W. M. Niu, and C. B. Zhang, "Effect of electro-acupuncture on ERK protein expression of MCAO rats," *Journal of Clinical Acupuncture and Moxibustion*, vol. 23, no. 7, pp. 62–63, 2007.

[45] M. H. Shen, Z. R. Li, X. R. Xiang, W. M. Niu, and C. B. Zhang, "Involvement of extracellular regulated protein kinase signal transduction pathway in electroacupuncture-induced improvement of ischemic cerebral injury in rats with cerebral ischemia reperfusion," *Acupuncture Research*, vol. 32, no. 6, pp. 368–372, 2007.

[46] Z. B. Yang, J. Yan, and S. X. Yi, "Up-regulation of the ERK phosphorylation in gastric mucosal cell by the serum of rats treated with electroacupuncture at stomach meridian acupoints," *Basic & Clinical Medicine*, vol. 29, no. 2, pp. 135–138, 2009.

[47] C. L. Wang, S. X. Wang, and W. Gong, "Changes in phosphatized ERK in the spinal dorsal horn in adjuvant arthritis rats during electroacupuncture of Jiaji points for analgesia," *Shanghai Journal of Acupuncture and Moxibustion*, vol. 24, no. 12, pp. 33–35, 2005.

Hindawi Publishing Corporation
Evidence-Based Complementary and Alternative Medicine
Volume 2013, Article ID 695641, 9 pages
http://dx.doi.org/10.1155/2013/695641

Research Article

An In Vivo and In Vitro Evaluation of the Mutual Interactions between the Lung and the Large Intestine

Lei-Miao Yin, Guang-Quan Zhang, Xing-Ke Yan, Yu Wang, Yu-Dong Xu, and Yong-Qing Yang

Shanghai Research Institute of Acupuncture and Meridian, Shanghai University of Traditional Chinese Medicine, Shanghai 200030, China

Correspondence should be addressed to Yong-Qing Yang; yyq@shutcm.edu.cn

Received 25 May 2013; Accepted 28 June 2013

Academic Editor: Xiang-Yu Hou

One of the most important theories of the traditional Chinese medicine is the exterior-interior relationship between the lung and the large intestine; so far, little direct experimental evidence has been reported to support such relationship. Here we for the first time investigated the mutual interactions between the lung and the large intestine by examining the relevancies between the pulmonary functions and the rectal resting pressure in the rat models of asthma and constipation. We also evaluated the effects of the lung homogenate and the large intestine homogenate on the isolated large intestine muscle strip and the isolated tracheal spiral, respectively. Our results showed that the pulmonary resistance and pulmonary compliance were closely related to the rectal resting pressure in the asthmatic rat model, while the rectal resting pressure was much correlated with the pulmonary resistance in the rat model of constipation. Moreover, it was shown that the lung homogenate could specifically contract the isolated large intestine muscle strip. Overall, this study provided new lines of evidence for the theory and highlighted the potential application in the treatment of the corresponding diseases.

1. Introduction

The theory of the "exterior-interior relationship between the lung and the large intestine" originates from the Yellow Emperor's Classic of Internal Medicine (Huang Di Nei Jing), which is one of the most important governing principles of traditional Chinese medicine in the clinical application [1]. According to the theory, the lung meridian communicates with the large intestine meridian, which creates an exterior-interior relationship and influences each other specifically [2]. The lung diseases affect the condition of the large intestine except for the symptoms of nose and throat, while the disturbances of the large intestine could cause the pulmonary and bronchial dysfunctions. The lung is the essential respiration organ while the large intestine absorbs water and passes the wastes out of the body; obviously the two organs are anatomically separated; however, there are several aspects of evidence for the special relationship between the lung and the large intestine in both physiology and pathology.

The possibility of the mutual interaction between the lung and the large intestine was demonstrated by the same origin, the interactive pathophysiologic relationship, and the common effectors molecules. From the developmental point of view, the foregut was the common developmental structure of the lung and the large intestine, which suggested that there were similar regulations in the critical biological processes, such as the cellular apoptosis, mutations, communication, proliferation, and differentiation [3, 4]. Besides, the structures of bronchus and intestine were both characterized by the columnar epithelia with goblet cells and submucosal glands, which provided a basis for the development of inflammatory changes in both bronchus or bowel diseases under the same circumstance [5].

In the normal condition, the lung maintains the movement and gas emission of the large intestine by respiratory movement, while the large intestine assisted the lung to conduct proper breathing function [6]. In pathological conditions, the disorders of the lung and the large intestines

can affect each other. The epidemiological survey showed that lung and large intestine cancers were closely associated with the industrialization and the related factors [7]. Large intestine carcinoma is usually accompanied by cough and shortness of breath because of endo-bronchial metastases [8]. Alveolar leakage and airway inflammation were found during intestinal ischemia by using laser confocal microscope [9]. Similarly, the intestinal permeability was increased in children with asthma [10]. It is reported that 28.5% of patients with inflammatory bowel diseases had abnormal pulmonary function tests, and 22% of patients had small airway obstruction or bronchiectasis via high-resolution CT screening [11]. The gut-derived factors contributed to burn-induced lung injury and were related to subsequent respiratory failure [12]. In multiple organ dysfunction syndrome (MODS), the digestive tract symptoms often appeared after acute lung injury [13]. The activation of neutrophils in blood released a large number of enzymes and cytokines and caused inflammatory reaction in both lung and large intestine [14], which suggested that active components in the blood circulation and lymphokinesis may contribute to the relationship between the two organs.

A serial of common effector molecules were found in various pathophysiologic conditions in both lung and intestine, such as pulmonary surfactants family, vasoactive intestinal peptide, pulmonary thromboxane A2, sIgA (soluble immunoglobulin A), and cholecystokinin. The pulmonary surfactants played a key role in the evolution of air breathing [15]; however, intestinal surfactants had an earlier origin which could perform a variety of functions after the secretion of enterocyte [16, 17]. It is reported that the pulmonary surfactant proteins A and D were expressed in both pulmonary and gastrointestinal epitheliums [17], which extended the concept of intestinal surfactant and underlined its close relationships with pulmonary surfactant [18, 19]. It is recognized that the onset of asthma and airway responsiveness were closely associated with decrease of vasoactive intestinal peptide (VIP), which influenced the endogenous oxidant/antioxidant balance and the relaxation of the intestine [20]. Through the release of pulmonary thromboxane A2 (TxA2), intestinal reperfusion induced pulmonary vaso-constriction and increased pulmonary microvascular permeability [21]. After intestinal ischemia and reperfusion, the release of nitric oxide (NO) from the pulmonary vascular endothelium and the airway smooth muscle contraction were impaired, which may contribute to the respiratory failure [22]. The trefoil factor family domain peptides (TFF), responsible for the protection and repair of the intestinal epithelium, were expressed much higher in respiratory tract than in colon tissue and found to be closely associated with lung function [23]. Pathogenic effector Th17 cells were considered to be the common pathogenetic basis in both intestinal and respiratory tracts [24].

The above-mentioned facts provided preliminary scientific evidence for the close relationship between the two organs; however, direct experimental proofs are still lacking. Our study aims to investigate the mutual interactions between the lung and the large intestine by examining the relevancies between the pulmonary functions and the rectal resting pressure in the rat models of asthma and constipation, evaluate the effects of the lung homogenate and the large intestine homogenate on the isolated large intestine muscle strip and the isolated tracheal spiral, respectively, which could provide not only solid experimental evidence for the special relationship between lung and large intestine but also clues for solving complex clinical problems.

2. Method

2.1. Animals. Male Sprague-Dawley (SD) rats (4 weeks old, 110–130 g, SLAC Laboratory Animal Co. Ltd., Shanghai, China) were raised in a pathogen-free rodent facility and provided with food and water *ad libitum*. Rats were kept in animal facilities approved by the Shanghai Committee for Accreditation of Laboratory Animal, and the animal experiment conformed to the regulations of the State Science and Technology Commission.

2.2. The Rat Model of Asthma. Rats were randomly divided into two groups ($n = 8$ each): control and asthmatic model groups. The protocol of SD rat model of asthma was described as previously [25]. Briefly, rats were sensitized with 1 mg ovalbumin (OVA) precipitated with 10 mg of aluminum hydroxide gel in 1 mL normal saline with intraperitoneal injection. The sensitized rats were challenged two weeks later with 1 mL/kg of 5% OVA in normal saline by injection into the external jugular vein over 10 s. Control rats were sensitized and challenged with normal saline instead of OVA.

2.3. The Rat Model of Constipation. Rats were randomly divided into two groups ($n = 8$ each): control and constipation model groups. The protocol of rat model of constipation was modified from Shan et al. [26]. Briefly, after fasting for 24 h with free access to water, rats were treated with compound diphenoxylate (10 mg/kg body weight, once a day, for four days) in 1 mL normal saline through intragastric administration, and the time of first defecation with the charcoal meal was recorded. Number and weight of feces were recorded 12 h after the administration. Control rats were treated with normal saline instead of compound diphenoxylate.

2.4. Measurements of the Pulmonary Functions and the Rectal Resting Pressure. When measuring the pulmonary function, a rat under anesthesia was placed on a wood plate in the supine position. A heater was controlled pneumotachograph which connected to a differential pressure transducer (600D-011, AutoTran, USA) was gently inserted into the trachea, and the tidal flow was determined. To measure transpulmonary pressure, a water-filled tube which coupled to a pressure transducer (PT14MX, Jialong Teaching Equipment, Shanghai) was inserted into the esophagus to the level of the midthorax. The pneumotachograph tidal flow signal was integrated with time to obtain tidal volume, which was continuously recorded for 30 min. The measurement of rectal resting pressure was modified from Hancock [27]. The tube (diameter = 2.5 mm) with a balloon at the front end was inserted slowly into anus for 3.5 cm, which connected with

pressure transducer (PT14MX, Jialong Teaching Equipment, Shanghai). Twenty min after the tube insertion, rectal resting pressure was recorded by the SMUP-B biological signal analysis system for 30 min.

2.5. The Preparation of the Tissue Homogenates. After rats were sacrificed, the lung (including trachea), heart, small intestine (total ileum), and large intestine (total colon) were taken out quickly and respectively. After washing with normal saline and removal of fat, the tissues were weighed and mixed with normal saline at the ratio of 1 : 4. By using electric glass homogenizer machine in ice bath, the tissues were turned into homogenates. After centrifugation at 3500 r/min for 20 min, the supernatants were kept. The protein concentrations of the homogenates of the lung, heart, large intestine and small intestine, were all adjusted to 5 mg/mL, BSA (5 mg/mL) and normal saline were served as control.

2.6. The Preparation of the Tracheal Spiral and the Large Intestine Muscle Strip. The trachea and large intestine were immediately removed after the sacrifice of rats. The adherent connective tissue and fat on the surface were all removed, and the tissues were put into a Petri dish full of Krebs'-Henseleit (KH) solution (NaCl 118.0 mmol/L; KCl 4.7 mmol/L; $CaCl_2$ 2.5 mmol/L; $MgSO_4$ 1.2 mmol/L; $NaHCO_3$ 25.0 mmol/L; KH_2PO_4 1.2 mmol/L; glucose 10.0 mmol/L). A tracheal segment (approximately 20 mm in length from thyroid cartilage to bifurcation of tracheas) was isolated and then suspended in a 80 mL organ bath by two stainless-steel wires (0.3 mm diameter). The 2.5 cm long large intestine was quickly cut (20 mm away from the lower end of the cecum). One end was fixed to the bottom of the organ bath, whereas the other was connected to the pressure transducer (PT14MX, Jialong Teaching Equipment, Shanghai) for the measurement of isometric tension. The tracheal spiral and the large intestine muscle strip were set up vertically under a tension of 1.5 g, which were maintained in the KH solution. The organ bath was kept at $37.0 \pm 0.5^{\circ}$C and continuously gassed with 95% O_2 and 5% CO_2. The measurement of the isometric tension was recorded, and the tension changed in 10 min was analyzed. Each tracheal spiral and large intestine muscle strip were used only one time.

2.7. Data Analysis. All data are expressed as the mean ± SD. The Student's t-test was used to analyze the significance of the pulmonary resistance, the pulmonary compliance, and the rectal resting pressure between the two groups in vivo. The relationship between two variables was identified by the linear regression analysis. One-way ANOVA (analysis of variance) followed by the least significant difference (LSD) test for post hoc analysis was used to analyze the significance of tension among the different groups in vitro. The P value that was lower than 0.05 was considered significant.

3. Results

3.1. The Pulmonary Functions Were Closely Related to Rectal Resting Pressure in the Rat Models of Asthma and Constipation. There was no significant relationship between rectal resting pressure and pulmonary resistance in the control rat within 30 min ($r = -0.032$, $P > 0.05$), and there was also no significant relationship between rectal resting pressure and pulmonary compliance within 30 min ($r = -0.050$, $P > 0.05$). In asthmatic rat, the pulmonary resistance was significantly increased at 3–7 min ($P < 0.05$, Table 1); the pulmonary compliance was significantly decreased at 3–10 min ($P < 0.05$), which suggested the successful establishment of asthma model. There was a significant difference in the rectal resting pressure at 2 min between the asthmatic model and the control group ($P < 0.05$). Three to seven min after OVA challenge, the rectal resting pressure was decreased and had a negative relationship with pulmonary resistance within 30 min ($r = -0.423$, $P < 0.05$). Meanwhile, the rectal resting pressure has a positive relationship with pulmonary compliance within 30 min ($r = 0.711$, $P < 0.05$), which demonstrated that the changes of the pulmonary resistance and pulmonary compliance were closely associated with the level of the rectal resting pressure in the asthmatic model.

Twelve h after compound diphenoxylate administration, the number of stool of rats was significantly decreased by 77.23% when compared to that of the control group ($P < 0.05$). The weight of stool was significantly decreased in rats in the group of compound diphenoxylate administration by 76.01% ($P < 0.05$), which suggested the successful establishment of the constipation model. There was no significant difference in the rectal resting pressure between the constipation model and the control group in 10 min ($P > 0.05$), although the rectal resting pressure of the constipation rats had a tendency to decrease. The pulmonary resistance had a tendency to increase ($P > 0.05$) but had no significant relationship with the rectal resting pressure within 30 min ($r = 0.063$, $P > 0.05$). However, the pulmonary compliance of the constipation model was significantly decreased at 1-2, 4–7, and 9-10 min ($P < 0.05$, Table 2) and had a significant positive relationship with the rectal resting pressure within 30 min ($r = 0.663$, $P < 0.05$), which suggested that the constipation and the breath difficulty happened at the same time, and the change of the pulmonary compliance was closely associated with the level of the rectal resting pressure in the constipation model.

3.2. Measurements of the Isometric Tensions. The different levels of the acetyl choline (Ach) were used to test the contractive effect on the isolated large intestine muscle strip and the isolated tracheal spiral, and the 70%–75% of the maximal contractile response was chosen and examined in order to avoid the maximum of the concentration response and allow for adequate extension [28]. In the study, the addition of 0.02 mg/L and 20 mg/L Ach produced 70%–75% of the maximum contraction of the isolated large intestine muscle strip and the isolated tracheal spiral, respectively, which suggested the successful establishment of the in vitro testing system and demonstrated that the sensitivity of isolated large intestine muscle strip was about 1000 times higher than that of the isolated tracheal spiral.

Different volumes of the tissue homogenates were added separately into the bath of the large intestine muscle strip,

Table 1: The pulmonary compliance, the pulmonary resistance, and the rectal resting pressure of the control and asthmatic model of rats.

Items	Groups	Min 1	Min 2	Min 3	Min 4	Min 5	Min 6	Min 7	Min 8	Min 9	Min 10
Pulmonary compliance (mL/kPa)	Control	−0.030 ± 0.001	−0.026 ± 0.001	−0.006 ± 0.001	−0.040 ± 0.001	−0.047 ± 0.001	0.020 ± 0.001	0.030 ± 0.002	−0.021 ± 0.001	−0.100 ± 0.002	−0.040 ± 0.002
	Asthma	−0.300 ± 0.007	−0.620 ± 0.010	−0.867 ± 0.010*	−0.806 ± 0.009*	−0.862 ± 0.010*	−0.866 ± 0.009*	−0.809 ± 0.009*	−0.713 ± 0.007*	−0.809 ± 0.010*	−0.788 ± 0.010*
Pulmonary resistance (kPa/mL/s)	Control	−0.001 ± 0.001	−0.001 ± 0.002	−0.001 ± 0.002	−0.001 ± 0.002	−0.002 ± 0.002	−0.001 ± 0.005	−0.001 ± 0.004	−0.001 ± 0.004	0.001 ± 0.008	0.001 ± 0.007
	Asthma	0.012 ± 0.012	0.029 ± 0.029	0.112 ± 0.033$^{\#}$	0.186 ± 0.028$^{\#}$	0.109 ± 0.029$^{\#}$	0.082 ± 0.030$^{\#}$	0.060 ± 0.017$^{\#}$	0.018 ± 0.015	0.014 ± 0.010	0.008 ± 0.006
Rectal resting pressure (kPa)	Control	−0.050 ± 0.142	−0.114 ± 0.107	−0.075 ± 0.149	−0.049 ± 0.070	−0.018 ± 0.147	−0.076 ± 0.115	−0.028 ± 0.113	−0.009 ± 0.093	−0.026 ± 0.177	0.022 ± 0.108
	Asthma	0.197 ± 0.401	0.013 ± 0.108$^{\&}$	−0.032 ± 0.099	−0.062 ± 0.107	−0.058 ± 0.130	−0.047 ± 0.107	−0.075 ± 0.157	−0.008 ± 0.116	−0.046 ± 0.196	−0.096 ± 0.169

Data were shown as mean ± SD ($n = 8$). The values of pulmonary resistance in the table were expressed as differential values subtracted from the corresponding baseline values. Statistical comparisons were made by the Student's t-test. $^{*}P < 0.05$, compared to control; $^{\#}P < 0.05$, compared to control; $^{\&}P < 0.05$, compared to control.

Table 2: The pulmonary compliance, the pulmonary resistance, and the rectal resting pressure of control and constipation model of rats.

Items	Groups	Min 1	Min 2	Min 3	Min 4	Min 5	Min 6	Min 7	Min 8	Min 9	Min 10
Pulmonary compliance (mL/kPa)	Control	0.083 ± 0.021	0.080 ± 0.017	0.080 ± 0.016	0.081 ± 0.017	0.077 ± 0.020	0.080 ± 0.016	0.080 ± 0.018	0.074 ± 0.022	0.077 ± 0.018	0.084 ± 0.020
	Constipation	0.059 ± 0.007*	0.057 ± 0.007*	0.065 ± 0.015	0.058 ± 0.006*	0.059 ± 0.005*	0.059 ± 0.007*	0.059 ± 0.006*	0.058 ± 0.005	0.059 ± 0.006*	0.058 ± 0.006*
Pulmonary resistance (kPa/mL/s)	Control	0.096 ± 0.018	0.095 ± 0.016	0.096 ± 0.016	0.097 ± 0.015	0.097 ± 0.015	0.112 ± 0.043	0.098 ± 0.017	0.095 ± 0.020	0.088 ± 0.010	0.086 ± 0.008
	Constipation	0.093 ± 0.012	0.093 ± 0.014	0.096 ± 0.017	0.098 ± 0.018	0.098 ± 0.019	0.094 ± 0.017	0.096 ± 0.019	0.095 ± 0.017	0.096 ± 0.017	0.096 ± 0.015
Rectal resting pressure (kPa)	Control	0.072 ± 0.099	0.067 ± 0.092	0.048 ± 0.027	0.051 ± 0.023	0.063 ± 0.068	0.048 ± 0.017	0.077 ± 0.082	0.082 ± 0.078	0.102 ± 0.127	0.068 ± 0.073
	Constipation	0.019 ± 0.020	0.052 ± 0.066	0.055 ± 0.072	0.034 ± 0.046	0.069 ± 0.071	0.053 ± 0.073	0.042 ± 0.070	0.089 ± 0.101	0.056 ± 0.069	0.029 ± 0.047

Data were shown as mean ± SD ($n = 8$). The values of pulmonary resistance in the table were expressed as differential values subtracted from the corresponding baseline values. Statistical comparisons were made by the Student's t-test. $^*P < 0.05$, compared to control.

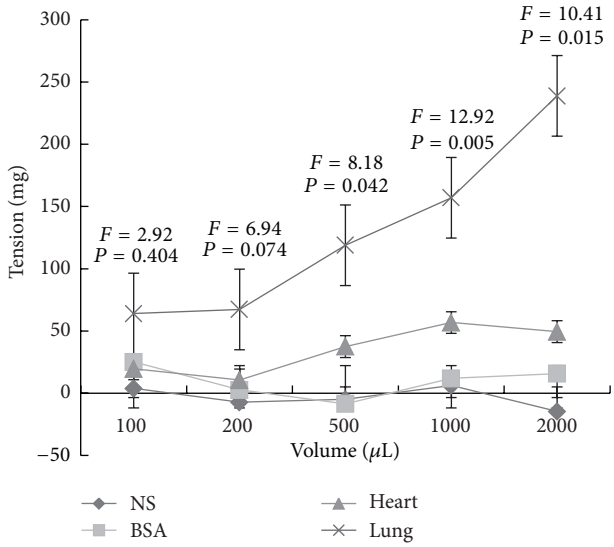

Figure 1: The effects of the lung homogenate, the heart homogenate, BSA, and normal saline on the isolated large intestine muscle strip. The addition of 100, 200, 500, 1000, and 2000 μL of the 5 mg/mL lung homogenate, heart homogenate, BSA, and normal saline into the in vitro testing system of the isolated large intestine muscle strip. The addition of the lung homogenate could significantly contract the isolated large intestine muscle strip at the volume of 500, 1000, and 2000 μL ($P < 0.05$).

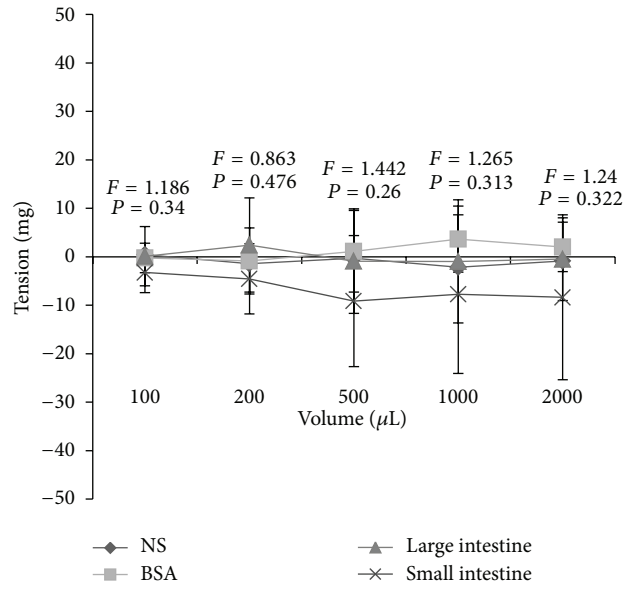

Figure 2: The effects of the large intestine homogenate, the small intestine homogenate, BSA, and normal saline on the isolated tracheal spiral. The addition of the 100, 200, 500, 1000, and 2000 μL of the 5 mg/mL large intestine homogenate, small intestine homogenate, BSA, and normal saline had no significant effects ($P > 0.05$) on the isolated tracheal spiral.

and, with the increase of the volume, the contraction response was recorded. The addition of the 100, 200, 500, 1000, and 2000 μL of the 5 mg/mL heart homogenate, BSA, and normal saline had no significant effects on the isolated large intestine muscle strip ($P > 0.05$, Figure 1); however, the addition of 500, 1000, and 2000 μL of the 5 mg/mL lung homogenate could significantly contract the isolated large intestine muscle strip ($P < 0.05$), which demonstrated the special effect of lung homogenate on the isolated large intestine muscle strip. In the group of 500 and 1000 μL addition, the tension induced by the lung homogenate was 3.1 and 2.8 times greater than that of the heart homogenate ($P < 0.05$). In the group of 2000 μL addition, the tension induced by the lung homogenate was the maximal and 4.8 time greater than that of the heart homogenate ($P < 0.05$).

The addition of the 100, 200, 500, 1000, and 2000 μL of the 5 mg/mL large intestine homogenate, small intestine homogenate, BSA, and normal saline had no significant effects ($P > 0.05$, Figure 2) on the isolated tracheal spiral, which may be due to the low sensitivity of the isolated tracheal spiral.

4. Discussion

The data showed that the pulmonary resistance and pulmonary compliance were closely related to the rectal resting pressure in asthmatic rat model, and the rectal resting pressure was closely associated with pulmonary resistance in the rat model of constipation. The lung homogenate could specifically contract the isolated large intestine muscle strip in vitro. These results suggested that the lung and large intestine had a specific relationship between each other, which may provide clues for a further study.

The common active proteins and the corresponding receptors, such as sIgA and cholecystokinin, may account for the underlying mechanism of lung and large intestine mutual interaction. sIgA exists specifically in both lung and intestinal tissues and is considered to be the common mucosal immune molecules base [29]. The polymeric immunoglobulin receptors for IgA were also found expressed in lung, bronchi, gut, and so on, which was involved not only in the antigen-antibody complex recognition but also in various signal transduction under different conditions [30]. Another important neuropeptide cholecystokinin (CCK), which is expressed in the gastrointestinal nervous system, was now found widely distributed in trachea and alveoli [31]. CCK played a role in protecting gastric mucosa and stimulating the digestion of nutrition, and now totally two types of CCK receptors have been identified [32]. Recent studies have reported that the sIgA and CCK and their corresponding receptors may be closely associated with the specific relationship between the lung and large intestine. It is reported that the CCK2 receptor with retention of intron 4 (CCK2Ri4sv) was now a marker of specific gastrointestinal and lung tumors [33]. In CCR3 knockout mice model, the eosinophil recruitment in the lung was decreased while the number of intraepithelial mast cells was increased in the trachea after OVA sensitization and allergen challenge [34]. Study demonstrated that the expression of CCK receptors and cytokine productions on peripheral blood and bronchoalveolar lavage fluid (BALF) in asthma patients were significantly increased [35]. Modern

research has confirmed that both the lung and large intestine were endocrine organs and could synthesize a serial of active substances when receiving signals from the internal and external environments. Ovalbumin (OVA) is widely used as a reference allergen to induce allergic asthma, which can cause the imbalance of CD4+ T lymphocytes, secretion of cytokines, and immune inflammation [36]. In our rat model of OVA-induced asthma, the expressions of immune-related proteins, like sIgA and CCK, could be changed in asthmatic lung; meanwhile the corresponding receptors were subsequently altered in the large intestine; in this way the pathological condition of lung may influence the status of large intestine and vice versa.

The intestine muscle strip is frequently used as an evaluation tool for the intestinal smooth muscle function, and the behavior of the intestines varies among different species. It is showed that the 0.01 mg/L Ach evoked the contraction of human colon [37], which was two times more sensitive than that of the rat intestine. The level of 0.03 mg/L Ach caused the contraction of the longitudinal muscle strip which was obtained from guinea pig ileum [38]. It is reported that 0.1–10 mg/L Ach contracted the longitudinal and circular muscle strips of rabbit while 0.1 mg/L atropine blocked the effect of 10 mg/L Ach [39]. In our large intestine muscle strip of rat, the level of 0.02 mg/L Ach caused about 70%–75% of the maximum contraction, and this data was consistent with the previous studies, which provided a suitable testing system for the in vitro research.

A serial of pharmacological agents have been tested in the model of the intestine muscle strip. It is reported that the 10–50 μm ATP transmural stimulation caused relaxations of the rat duodenum and ileum [40]. Exogenous addition of 20 ng/mL IL-6 increased the contraction of the circular muscle strip of colon and suggested that the contraction induced by IL-6 may be due to the acting on the gut's nervous system [41]. As an antagonist of the muscarinic receptors, MB327 showed a fully reversible smooth muscle relaxing effect at lower concentrations in a rat jejunum smooth muscle model [42]. In our in vitro study, the addition of the lung homogenate contracted specially the isolated large intestine muscle strip, which suggested that the lung homogenate might contain active proteins that could bind to the corresponding receptors in the large intestine and carried out biological functions. Besides, it is also known that the interstitial cells, such as smooth muscle cells and the interstitial cell of Cajal (ICC), could release Ach by transmural stimuli and the activation of the cholinergic fibers [43, 44]. In our study, the addition of tissue homogenates may induce a small amount of Ach release of the large intestine and lead to the contraction. The study provided a foundation for further research, and, if a specific protein and receptor could be well identified in the future, it may contribute to the medical science and well reflect the biological value of traditional Chinese medicine.

5. Conclusion

In the current study, we showed that the changes of the pulmonary functions were closely related to the rectal resting pressure in the rat models of asthma and constipation, and the lung homogenate could significantly contract the large intestine muscle strip. It provided new lines of evidence for the "exterior-interior relationship between the lung and the large intestine" and highlighted the use of this theory in the treatment of the corresponding diseases in the future.

Conflict of Interests

The authors have declared that no competing interests exist.

Authors' Contribution

Lei-Miao Yin and Guang-Quan Zhang contributed equally to this work.

Acknowledgments

This work was supported by the National Natural Science Foundation of China (nos. 81001548, 81173341, 81173332, and 81202753) and Shanghai Rising-Star Program (12QA-1403000).

References

[1] G. Maciocia, *The Foundations of Chinese Medicine*, Churchill Livingstone, Edinburgh, UK, 2005.

[2] B. Liu, J. Wang, and J.-P. Zhao, "Intermediate structure of the interior-exterior relationship between lung and large intestine," *Zhongguo Zhen Jiu*, vol. 31, no. 4, pp. 363–365, 2011.

[3] S. Faure and P. de Santa Barbara, "Molecular embryology of the foregut," *Journal of Pediatric Gastroenterology and Nutrition*, vol. 52, no. 1, pp. S2–S3, 2011.

[4] A. M. Zorn and J. M. Wells, "Vertebrate endoderm development and organ formation," *Annual Review of Cell and Developmental Biology*, vol. 25, no. 1, pp. 221–251, 2009.

[5] T. Higenbottam, G. M. Cochrane, T. J. H. Clark, D. Turner, R. Millis, and W. Seymour, "Bronchial disease in ulcerative colitis," *Thorax*, vol. 35, no. 8, pp. 581–585, 1980.

[6] W. E. Arnould-taylor, *A Textbook of Anatomy and Physiology*, Nelson Thornes, Cheltenham, UK, 1998.

[7] M. Murata, K. Takayama, S. Fukuma et al., "A comparative epidemiologic study on geographic distributions of cancers of the lung and the large intestine in Japan," *Japanese Journal of Cancer Research*, vol. 79, no. 9, pp. 1005–1016, 1988.

[8] B. W. Carlin, J. H. Harrell II, L. K. Olson, and K. M. Moser, "Endobronchial metastases due to colorectal carcinoma," *Chest*, vol. 96, no. 5, pp. 1110–1114, 1989.

[9] H. Mitsuoka, T. Sakurai, N. Unno et al., "Intravital laser confocal microscopy of pulmonary edema resulting from intestinal ischemia-reperfusion injury in the rat," *Critical Care Medicine*, vol. 27, no. 9, pp. 1862–1868, 1999.

[10] Z. Hijazi, A. M. Molla, H. Al-Habashi, W. M. R. A. Muawad, A. M. Mollo, and P. N. Sharma, "Intestinal permeability is increased in bronchial asthma," *Archives of Disease in Childhood*, vol. 89, no. 3, pp. 227–229, 2004.

[11] D. Desai, S. Patil, Z. Udwadia, S. Maheshwari, P. Abraham, and A. Joshi, "Pulmonary manifestations in inflammatory bowel disease: a prospective study," *Indian Journal of Gastroenterology*, vol. 30, no. 5, pp. 225–228, 2011.

[12] L. J. Magnotti, D.-Z. Xu, Q. Lu, and E. A. Deitch, "Gut-derived mesenteric lymph: a link between burn and lung injury," *Archives of Surgery*, vol. 134, no. 12, pp. 1333–1341, 1999.

[13] E. D. Crouser and P. M. Dorinsky, "Gastrointestinal tract dysfunction in critical illness: pathophysiology and interaction with acute lung injury in adult respiratory distress syndrome/multiple organ dysfunction syndrome," *New Horizons*, vol. 2, no. 4, pp. 476–487, 1994.

[14] K. Brown, S. Brain, J. Pearson, J. Edgeworth, S. Lewis, and D. Treacher, "Neutrophils in development of multiple organ failure in sepsis," *The Lancet*, vol. 368, no. 9530, pp. 157–169, 2006.

[15] C. B. Daniels and S. Orgeig, "Pulmonary surfactant: the key to the evolution of air breathing," *News in Physiological Sciences*, vol. 18, no. 4, pp. 151–157, 2003.

[16] A. Turan, S. Gupta, and A. Mahmood, "Characteristics and physiological role of surfactant-like particles secreted by entrocytes," *Indian Journal of Experimental Biology*, vol. 44, no. 7, pp. 519–525, 2006.

[17] J. R. Bourbon and B. Chailley-Heu, "Surfactant proteins in the digestive tract, mesentery, and other organs: evolutionary significance," *Comparative Biochemistry and Physiology*, vol. 129, no. 1, pp. 151–161, 2001.

[18] S. Rubio, T. Lacaze-Masmonteil, B. Chailley-Heu, A. Kahn, J. R. Bourbon, and R. Ducroc, "Pulmonary surfactant protein A (SP-A) is expressed by epithelial cells of small and large intestine," *Journal of Biological Chemistry*, vol. 270, no. 20, pp. 12162–12169, 1995.

[19] Z. Lin and J. Floros, "Heterogeneous allele expression of pulmonary SP-D gene in rat large intestine and other tissues," *Physiological Genomics*, vol. 11, pp. 235–243, 2003.

[20] A. M. Szema, S. A. Hamidi, A. Koller, and D. W. Martin, "Vasoactive Intestinal Peptide Knockout (VIP KO) mouse model of sulfite-sensitive asthma: up-regulation of novel lung carbonyl reductase," *BMC Immunology*, vol. 12, article no. 66, 2011.

[21] R. H. Turnage, J. L. Lanoue, K. M. Kadesky, Y. Meng, and S. I. Myers, "Thromboxane A2 mediates increased pulmonary microvascular permeability after intestinal reperfusion," *Journal of Applied Physiology*, vol. 82, no. 2, pp. 592–598, 1997.

[22] C. Köksoy, M. A. Kuzu, H. Ergün, E. Demirpençe, and B. Zülfikaroglu, "Intestinal ischemia and reperfusion impairs vasomotor functions of pulmonary vascular bed," *Annals of Surgery*, vol. 231, no. 1, pp. 105–111, 2000.

[23] E. dos Santos Silva, M. Ulrich, G. Doring, K. Botzenhart, and P. Gott, "Trefoil factor family domain peptides in the human respiratory tract," *Journal of Pathology*, vol. 190, no. 2, pp. 133–142, 2000.

[24] C. T. Weaver, C. O. Elson, L. A. Fouser, and J. K. Kolls, "The Th17 pathway and inflammatory diseases of the intestines, lungs, and skin," *Annual Review of Pathology*, vol. 8, pp. 477–512, 2013.

[25] L.-M. Yin, G.-H. Jiang, Y. Wang et al., "Serial analysis of gene expression in a rat lung model of asthma," *Respirology*, vol. 13, no. 7, pp. 972–982, 2008.

[26] J. J. Shan, Y. Zhang, Y. L. Diao, W. S. Qu, and X. N. Zhao, "Effect of an antidiabetic polysaccharide from Inula japonica on constipation in normal and two models of experimental constipated mice," *Phytotherapy Research*, vol. 24, no. 11, pp. 1734–1738, 2010.

[27] B. D. Hancock, "Measurement of anal pressure and motility," *Gut*, vol. 17, no. 8, pp. 645–651, 1976.

[28] L.-M. Yin, H.-Y. Li, Q.-H. Zhang et al., "Effects of S100A9 in a rat model of asthma and in isolated tracheal spirals," *Biochemical and Biophysical Research Communications*, vol. 398, no. 3, pp. 547–552, 2010.

[29] B. Corthésy, "Roundtrip ticket for secretory IgA: role in mucosal homeostasis?" *Journal of Immunology*, vol. 178, no. 1, pp. 27–32, 2007.

[30] C. Pilette, Y. Ouadrhiri, V. Godding, J.-P. Vaerman, and Y. Sibille, "Lung mucosal immunity: immunoglobulin: a revisited," *European Respiratory Journal*, vol. 18, no. 3, pp. 571–588, 2001.

[31] F. Noble, S. A. Wank, J. N. Crawley et al., "International union of pharmacology. XXI. Structure, distribution, and functions of cholecystokinin receptors," *Pharmacological Reviews*, vol. 51, no. 4, pp. 745–781, 1999.

[32] M. Dufresne, C. Seva, and D. Fourmy, "Cholecystokinin and gastrin receptors," *Physiological Reviews*, vol. 86, no. 3, pp. 805–847, 2006.

[33] M. Körner, B. Waser, J. C. Reubi, and L. J. Miller, "CCK2 receptor splice variant with intron 4 retention in human gastrointestinal and lung tumours," *Journal of Cellular and Molecular Medicine*, vol. 14, no. 4, pp. 933–943, 2010.

[34] A. A. Humbles, B. Lu, D. S. Friend et al., "The murine CCR3 receptor regulates both the role of eosinophils and mast cells in allergen-induced airway inflammation and hyperresponsiveness," *Proceedings of the National Academy of Sciences of the United States of America*, vol. 99, no. 3, pp. 1479–1484, 2002.

[35] A. J. Morgan, F. A. Symon, M. A. Berry, I. D. Pavord, C. J. Corrigan, and A. J. Wardlaw, "IL-4-expressing bronchoalveolar T cells from asthmatic and healthy subjects preferentially express CCR3 and CCR4," *Journal of Allergy and Clinical Immunology*, vol. 116, no. 3, pp. 594–600, 2005.

[36] R. K. Kumar, C. Herbert, and P. S. Foster, "The "classical" ovalbumin challenge model of asthma in mice," *Current Drug Targets*, vol. 9, no. 6, pp. 485–494, 2008.

[37] D. J. Fishlock and A. G. Parks, "A study of human colonic muscle in vitro," *British Medical Journal*, vol. 2, no. 5358, pp. 666–667, 1963.

[38] W. D. Paton and M. A. Zar, "The origin of acetylcholine released from guinea-pig intestine and longitudinal muscle strips," *Journal of Physiology*, vol. 194, no. 1, pp. 13–33, 1968.

[39] M. Gallacher, B. R. Mackenna, and H. C. McKirdy, "Effects of drugs and of electrical stimulation on the muscularis mucosae of rabbit large intestine," *British Journal of Pharmacology*, vol. 47, no. 4, pp. 760–764, 1973.

[40] G. Burnstock, D. G. Satchell, and A. Smythe, "A comparison of the excitatory and inhibitory effects of non-adrenergic, non-cholinergic nerve stimulation and exogenously applied ATP on a variety of smooth muscle preparations from different vertebrate species," *British Journal of Pharmacology*, vol. 46, no. 2, pp. 234–242, 1972.

[41] L. Zhang, L. Hu, M. Chen, and B. Yu, "Exogenous interleukin-6 facilitated the contraction of the colon in a depression rat model," *Digestive Diseases and Sciences*, 2013.

[42] C. Koniger, F. Worek, H. Thiermann, and T. Wille, "Effect of MB327 and oximes on rat intestinal smooth muscle function," *Chemico-Biological Interactions*, vol. 204, no. 1, pp. 1–5, 2013.

[43] H. M. Cousins, F. R. Edwards, and G. D. S. Hirst, "Neuronally released and applied acetylcholine on the longitudinal muscle of the guinea-pig ileum," *Neuroscience*, vol. 65, no. 1, pp. 193–207, 1995.

[44] G. D. S. Hirst and S. M. Ward, "Interstitial cells: involvement in rhythmicity and neural control of gut smooth muscle," *Journal of Physiology*, vol. 550, no. 2, pp. 337–346, 2003.

Hindawi Publishing Corporation
Evidence-Based Complementary and Alternative Medicine
Volume 2013, Article ID 170910, 9 pages
http://dx.doi.org/10.1155/2013/170910

Research Article

Low Frequency Electroacupuncture Alleviated Spinal Nerve Ligation Induced Mechanical Allodynia by Inhibiting TRPV1 Upregulation in Ipsilateral Undamaged Dorsal Root Ganglia in Rats

Yong-Liang Jiang, Xiao-Hu Yin, Ya-Fang Shen, Xiao-Fen He, and Jian-Qiao Fang

Department of Neurobiology and Acupuncture Research, the Third Clinical Medical College, Zhejiang Chinese Medical University, Hangzhou 310053, China

Correspondence should be addressed to Jian-Qiao Fang; fangjianqiao7532@163.com

Received 25 May 2013; Accepted 24 June 2013

Academic Editor: Yong-Qing Yang

Neuropathic pain is an intractable problem in clinical practice. Accumulating evidence shows that electroacupuncture (EA) with low frequency can effectively relieve neuropathic pain. Transient receptor potential vanilloid type 1 (TRPV1) plays a key role in neuropathic pain. The study aimed to investigate whether neuropathic pain relieved by EA administration correlates with TRPV1 inhibition. Neuropathic pain was induced by right L5 spinal nerve ligation (SNL) in rats. 2 Hz EA stimulation was administered. SNL induced mechanical allodynia in ipsilateral hind paw. SNL caused a significant reduction of TRPV1 expression in ipsilateral L5 dorsal root ganglia (DRG), but a significant up-regulation in ipsilateral L4 and L6 DRGs. Calcitonin gene-related peptide (CGRP) change was consistent with that of TRPV1. EA alleviated mechanical allodynia, and inhibited TRPV1 and CGRP overexpressions in ipsilateral L4 and L6 DRGs. SNL did not decrease pain threshold of contralateral hind paw, and TRPV1 expression was not changed in contralateral L5 DRG. 0.001, 0.01 mg/kg TRPV1 agonist 6′-IRTX fully blocked EA analgesia in ipsilateral hind paw. 0.01 mg/kg 6′-IRTX also significantly decreased pain threshold of contralateral paw. These results indicated that inhibition of TRPV1 up-regulation in ipsilateral adjacent undamaged DRGs contributed to low frequency EA analgesia for mechanical allodynia induced by spinal nerve ligation.

1. Introduction

Neuropathic pain such as painful diabetic neuropathy, postherpetic neuralgia, trigeminal neuralgia, and poststroke pain is an intractable problem in clinical practice. It results from lesions or disease affecting the somatosensory nervous system either in the periphery or centrally and is characterized by spontaneous pain, allodynia, and hyperalgisea [1]. Up to now, the medication treatment of neuropathic pain is still unsatisfactory [2].

Abnormalities of channels or receptors in sensory nociceptors and dorsal root ganglia (DRG) are closely related to neuropathic pain [2, 3]. Transient receptor potential vanilloid type 1 (TRPV1), an important signal integrator in sensory nociceptors, plays a key role in neuropathic pain [4]. TRPV1 up-regulation contributes to mechanical allodynia and thermal hyperalgisea caused by various nerve injuries, while its antagonists can reverse the allodynia and hyperalgisea [5–7]. Furthermore, TRPV1 is coexpressed with various neuropeptides including calcitonin gene-related peptide (CGRP) in sensory ganglia and small sensory C and Aδ fibers [8, 9]. Activation of TRPV1 promotes CGRP release from nerve terminals [10, 11], which further aggravates neuropathic pain [12, 13].

Electroacupuncture (EA), a commonly used acupuncture method applying a pulsating electrical current to acupuncture needles for acupoints stimulation, has been widely adopted for pain relief for decades [14]. Accumulating evidence shows that EA is effective in relieving neuropathic pain under multiple conditions like painful diabetic neuropathy,

nerve ligation, injury, and chronic constriction [15–19]. A former study showed that EA with low frequency reduced nociceptive response and normalized TRPV1 abnormalities in hind paw skin and DRG induced by nerve growth factor injection in rats [20]. However, little is known about the effect of EA with low frequency on TRPV1 under neuropathic pain condition, and whether this effect contributes to its alleviation of neuropathic pain.

For this sake, the rat neuropathic pain model induced by right L5 spinal nerve ligation (SNL) was used in the current study. The effects of EA with low frequency on mechanical allodynia and the expressions of TRPV1 and CGRP in ipsilateral L4–6 and contralateral L5 DRGs were systematically examined. A block study using TRPV1 agonist was also performed to further ascertain the involvement of TRPV1 inhibition in neuropathic pain relief by low frequency EA.

2. Materials and Methods

2.1. Animal Preparation. Male Sprague-Dawley rats (180–200 g body weight) were obtained from SLAC Laboratory Animal Co. Ltd., Shanghai, China. Rats were housed in temperature-controlled animal cages (25 ± 1°C) under a 12 h light and 12 h dark cycle, with free access to food and water. All animals were treated in accordance with the regulations of the State Science and Technology Commission for the care and use of laboratory animals (State Science and Technology Commission Order no. 2, 1988).

2.2. Experimental Design. Two experiments were conducted: (1) effects of low frequency EA on allodynia-like behavior and profiles of TRPV1 and CGRP in DRGs of rats with SNL-induced neuropathic pain and (2) effects of TRPV1 receptor agonist 6′-iodoresiniferatoxin (6′-IRTX) on EA action. In experiment 1, rats were randomly divided into the following groups ($n = 8$ per group): normal, sham, SNL, and SNL + 2 Hz EA. In experiment 2, SNL-induced neuropathic pain rats were randomly divided into SNL + 2 Hz EA + vehicle, SNL + 2 Hz EA + 0.001 mg/kg 6′-IRTX, and SNL + 2 Hz EA + 0.01 mg/kg 6′-IRTX groups ($n = 8$ per group).

2.3. Spinal Nerve Ligation. L5 SNL was performed as previously described [21]. Briefly, rats were anesthetized with chloral hydrate (300 mg/kg, i.p.) and placed under a microsurgical apparatus in a prone position. A midline incision was made at the L3–S2 level, and the dorsal vertebral column from L4 to S2 was exposed. The right L6 transverse process was carefully removed, and then the right L5 spinal nerve was carefully isolated and then tightly ligated with a 6-0 silk thread. Sham-operated animals were subjected to the same surgical procedure except that the isolated L5 spinal nerve was not ligated.

2.4. EA Treatment. Acupuncture needles of 0.25 mm in diameter were inserted approximately 5 mm deep into the ipsilateral acupoints Zusanli (ST36, 5 mm lateral to the anterior tubercule of the tibia) and Kunlun (BL60, at the ankle joint level and between the tip of the external malleolus and tendo calcaneus). The ends of the needles were attached to a pair of electrodes from an electrical stimulator (LH-202H, Huawei Co. Ltd., China). EA (2 Hz, 2 mA, 0.4 ms pulse width) was administered for 30 minutes once every other day from day 3 to day 15 after surgery. Since the analgesic effects of the two acupoints are well documented [10, 21], we did not carry out sham acupuncture for control. Animals were awake and calmed by placing the heads in black hoods with no physical restraint during EA treatment. Rats were subject to the same calming procedure in normal, sham, and SNL groups.

2.5. Drug Delivery. In experiment 2, 1 mg/mL 6′-IRTX (Sigma, USA) solution was made by dissolving 6′-IRTX in a 95% ethanol mixture which was used as the vehicle control. 6′-IRTX was intraperitoneally injected (0.001 mg/kg, 0.01 mg/kg, resp.) in a volume of 1 mL by adding saline 10 minutes before EA treatment on day 15.

2.6. Behavioral Testing. All tests were performed by an experimenter blinded to the treatment groups. After habituation, paw withdrawal threshold to a von Frey-like filament was measured to assess mechanical allodynia using a Dynamic Plantar Aesthesiometer (Ugo Basile, Italy) on day 0 (base), 1, 3, and 30 min after EA treatment on day 3, 7, 11, and 15 after surgery. The steel rod was pushed against the hind paw with linear ascending force (0–50 g) until a strong and immediate withdrawal occurred. Paw withdrawal threshold (PWT) was determined as the mean of three consecutive tests with intervals of 30 sec.

2.7. Immunofluorescence. Rats were deeply anesthetized by an intraperitoneal injection of 10% (w/v) chloral hydrate (3.5 mL/kg) and transcardially perfused with 150 mL cold sterilized saline followed by 500 mL cold, fresh 4% (w/v) paraformaldehyde in 0.01 M phosphate-buffered saline (PBS, pH 7.4). Contralateral L5 and ipsilateral L4, L5, and L6 DRGs were harvested, postfixed in the same fixatives for 2 h, and then consecutively immersed in 15% (w/v) and 30% (w/v) sucrose solution overnight at 4°C. DRGs were embedded in OCT (Bayer Corp., Elkhart, IN), frozen, and then cut in 10 μm sections. Sections were mounted on glass slides, rinsed in PBS (pH 7.4), and blocked for 1 h at 37°C in 0.01 M PBS containing 5% (v/v) normal donkey serum and 0.3% (v/v) Triton X-100. Sections were incubated overnight at 4°C with a primary antibody (sheep anti-rat TRPV1, 1:4000; Abcam, USA) dissolved in PBS containing 0.3% (v/v) Triton X-100 and 5% (v/v) donkey serum. After being washed in PBS, sections were incubated for 1 h at 37°C with Alexa Fluor 594-conjugated donkey anti-sheep IgG (1:400; Jackson Immunoresearch, USA). After immunostaining, sections were rinsed in PBS and cover-slipped with 50% (v/v) glycerol and 2.5% (w/v) triethylenediamine (antifading agent) in 0.05 M PBS. Images were obtained using a fluorescence microscope (Olympus IX71; Olympus, Japan) equipped with Image-Pro Insight 8.0 software (Media Cybernetics, USA).

TRPV1-immunoreactive (IR) analysis was performed as previously described [22, 23]. The observer was blinded for

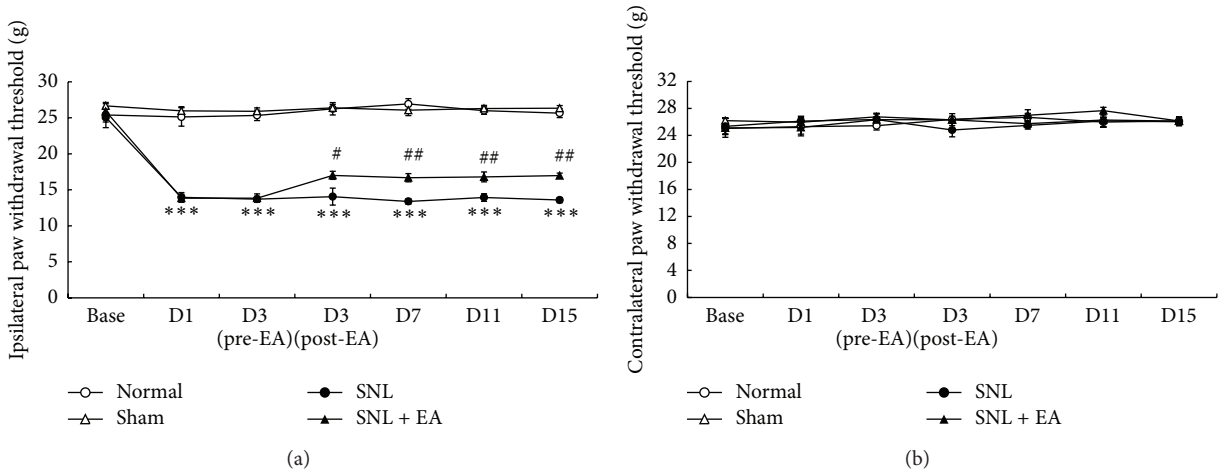

Figure 1: Effects of 2 Hz EA on bilateral paw withdrawal thresholds of rats subject to right L5 spinal nerve ligation. Data are presented as mean ± SEM, $n = 8$ per group. $^{***}P < 0.001$, SNL group versus normal group; $^{\#}P < 0.05$, $^{\#\#}P < 0.01$, SNL + EA group versus SNL group.

the treatment groups. DRG neurons with a clear nuclear profile were counted using Image-Pro Plus 6.0 (Media Cybernetics, USA). TRPV1-IR ratio was calculated by dividing the number of TRPV1-IR neurons by the total number of neurons in each section. The mean ratio was determined from three every tenth DRG sections for each DRG.

2.8. Western Blotting. Rats were deeply anesthetized by an intraperitoneal injection of 10% (w/v) chloral hydrate (3.5 mL/kg). Contralateral L5 and ipsilateral L4, L5, and L6 DRGs were harvested, sonicated on ice in RIPA Lysis Buffer (Beyotime, China) with an addition of protease inhibitor cocktail (Sangon Biotech, China), and centrifuged at 10,000x rpm for 10 min at 4°C, and then the supernatants were collected. Protein concentrations were determined by the bicinchoninic acid method. Protein extracts of animals in each group were equally pooled according to their concentrations. Samples were mixed with an equal volume of 2 × sample loading buffer and denatured by boiling at 100°C for 5 min. Proteins (30 μg/lane) were separated by an 8% SDS-PAGE gel for TRPV1 and 15% SDS-PAGE gel for CGRP and then transferred to 0.45 μm and 0.22 μm PVDF membranes, respectively (0.45 μm, Millipore, USA; 0.22 μm, Bio-Rad, USA). After being blocked in 0.01 M TBS with 0.1% Tween 20 and 5% dehydrated skim milk, the membranes were incubated overnight at 4°C with sheep anti-rat TRPV1 (1:2000; Abcam, USA), rabbit anti-rat CGRP (1:2000; Abcam, USA), or horseradish peroxidase-conjugated mouse anti-rat β-actin (1:10,000; Kangcheng, China). After being washed, the membrane for β-actin was visualized by chemiluminescence (ECL Plus; Amersham), while the membranes for TRPV1 and CGRP were incubated with the species-specific secondary antibodies for 2 h at room temperature and then washed and visualized by chemiluminescence (ECL Plus; Amersham, USA). Bands were detected by an Image Quant LAS 4000 system (Fujifilm, Japan) with Image Quant TL 7.0 software (GE Healthcare, USA). Three independent experiments were carried out for western blotting analysis. Target protein levels were normalized against β-actin levels and then expressed as relative fold changes compared to the normal control group [24, 25].

2.9. Statistical Analysis. All data were expressed as mean ± SEM. Statistical analysis was performed by one-way analysis of variance (ANOVA) followed by post hoc test of the least significant difference (LSD) for multiple comparisons. $P < 0.05$ was set as the level of statistical significance.

3. Results

3.1. EA Alleviated Mechanical Allodynia Induced by SNL. We first determined bilateral PWTs of rats to assess the extent of mechanical allodynia induced by SNL. Rats subjected to L5 SNL surgery developed mechanical allodynia in ipsilateral hind paw, as shown by a drastic reduction of ipsilateral PWLs on day 1, persisted to day 15 through the whole observation period (Figure 1(a)). 2 Hz EA significantly increased ipsilateral PWLs of rats subjected to SNL from day 3 after treatment, compared to the PWLs of SNL-controlled rats ($P < 0.05$, $P < 0.01$). Sham operation had no significant effect on ipsilateral PWLs during the whole period. Moreover, there was no significant difference in rats' contralateral PWTs among normal, sham-operated, SNL, and SNL + EA groups (Figure 1(b)).

3.2. EA Inhibited Ipsilateral Undamaged DRG TRPV1 Upregulation Resulted from SNL. To determine the contribution of TRPV1 to the mechanical allodynia resulted from SNL, we performed immunofluorescence study and western blotting analysis to test TRPV1 expressions and levels in ipsilateral L4, L5, and L6 and contralateral L5 DRGs of rats. Immunofluorescence showed that TRPV1 positive neurons were mainly small-to-medium DRG cells (20–50 μm; Figure 2). TRPV1 expression in ipsilateral L5 DRG in SNL group (7.0 ± 1.0%) was significantly reduced as compared to that in normal group (14.7 ± 2.8%, $P < 0.01$). No significant difference

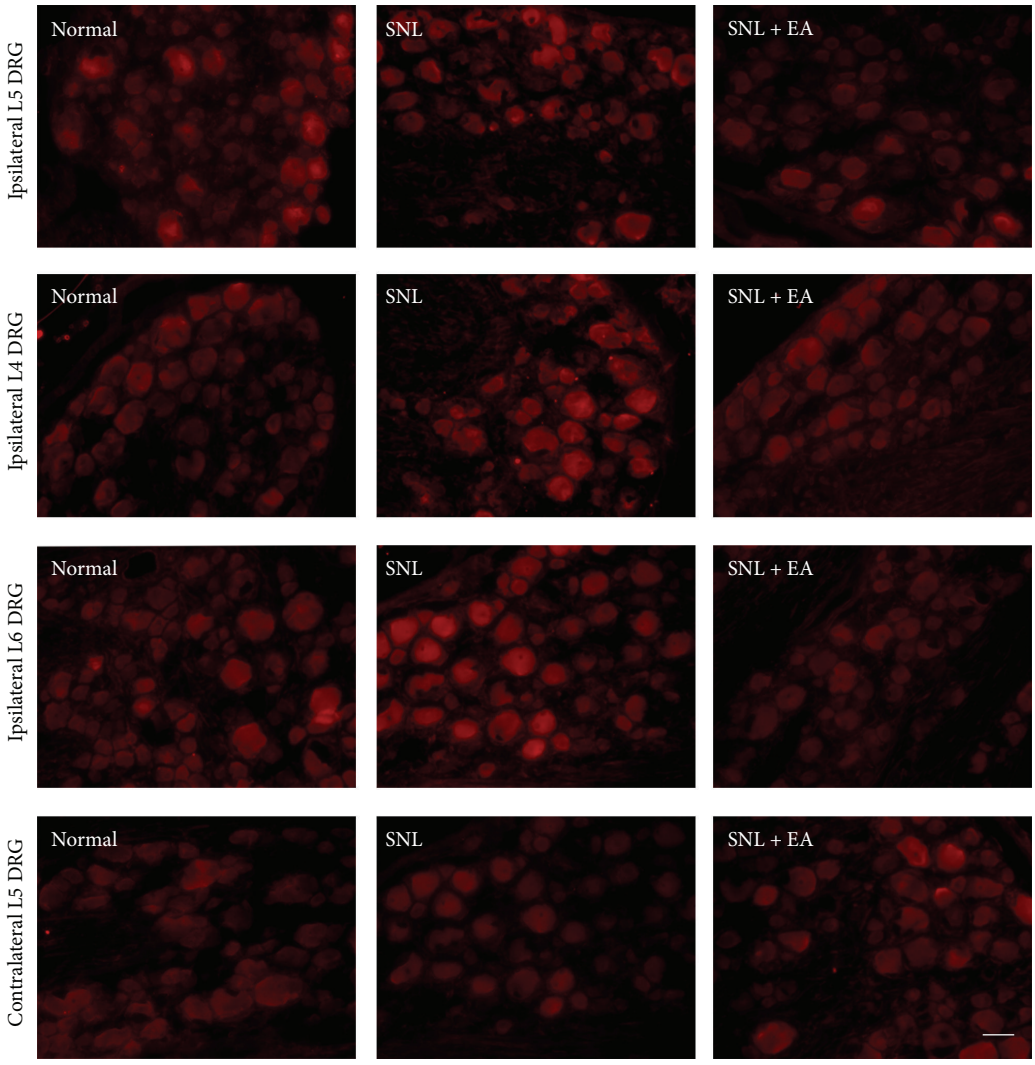

Figure 2: Immunofluorescence of TRPV1 expressions in ipsilateral L5, L4, and L6 and contralateral L5 DRGs in normal, SNL, and SNL + EA groups. TRPV1-IR is mainly seen in small-to-medium DRG neurons (20–50 μm). Scale bar, 50 μm for all.

of TRPV1 expression in ipsilateral L5 DRG was observed between SNL and SNL + EA groups. TRPV1 expressions in ipsilateral L4 and L6 DRGs in SNL group (18.1 ± 1.8%, 15.3 ± 1.0%) were significantly increased as compared to those in normal group (10.2 ± 1.3%, 9.4 ± 0.6%; $P < 0.001$, $P < 0.001$, resp.). The increases were inhibited by 2 Hz EA (7.3 ± 0.9%, 5.5 ± 0.7%; $P < 0.001$, $P < 0.001$, resp., compared to SNL group). Besides, there was no significant difference in TRPV1 expressions in rats' contralateral L5 DRG among normal, SNL, and SNL + EA groups.

The changes of TRPV1 protein levels as revealed by western blotting analysis were consistent with the changes of TRPV1 expressions. TRPV1 protein level in ipsilateral L5 DRG of rats in SNL group was significantly decreased as compared to that in normal group ($P < 0.01$), and no significant difference was found between SNL and SNL + EA groups (Figure 3(a)). TRPV1 levels in ipsilateral L4 and L6 DRGs in SNL group were significantly increased as compared to that in normal group ($P < 0.05$, $P < 0.05$, resp.). EA treatment with 2 Hz frequency fully inhibited SNL-induced increases of TRPV1 protein in ipsilateral L4 and L6 DRGs ($P < 0.001$, $P < 0.01$, resp., compared to SNL group) and even lower than normal TRPV1 levels ($P < 0.01$, $P < 0.05$, resp., compared to normal group; Figures 3(b) and 3(c)). No significant difference of TRPV1 levels in contralateral L5 DRG was observed in rats among normal, SNL, and SNL + EA groups (Figure 3(d)).

3.3. EA Inhibited Ipsilateral Undamaged DRG CGRP Upregulation Resulted from SNL. Since TRPV1 activation promotes CGRP release, which further strengthens TRPV1 role in pain sensation, we also performed western blotting analysis to detect CGRP protein levels. The changes of CGRP levels in ipsilateral DRGs were consistent with the changes of TRPV1 levels. CGRP protein level in ipsilateral L5 DRG in SNL group was significantly decreased as compared to that in normal group ($P < 0.05$), and no significant difference in CGRP protein level was found between SNL and SNL + EA groups

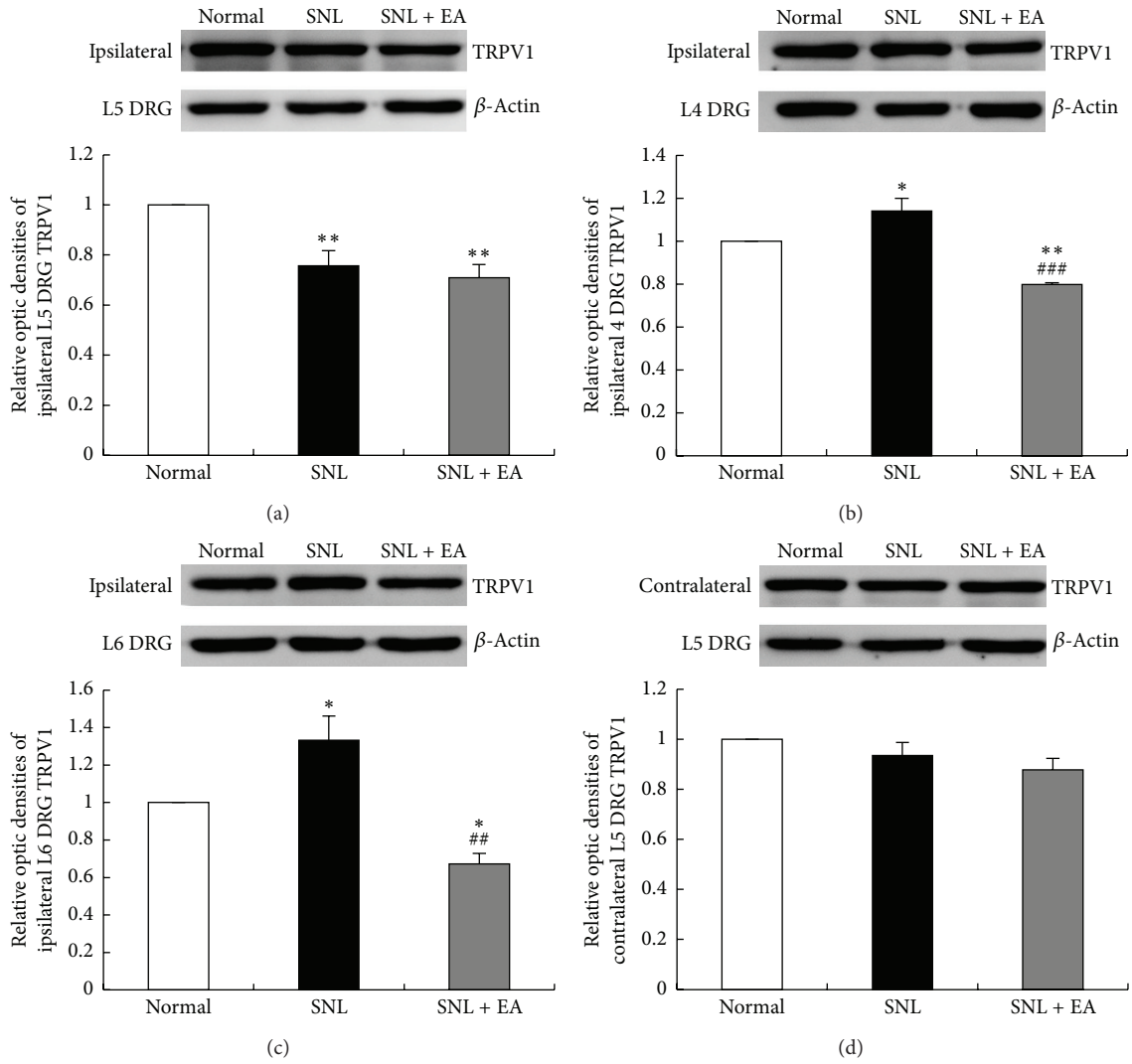

Figure 3: Western blotting analysis of TRPV1 levels in ipsilateral L5, L4, and L6 and contralateral L5 DRGs in normal, SNL, and SNL + EA groups. Results were expressed as relative fold changes as compared to normal group after normalization to β-actin. Data are presented as mean ± SEM of three independent experiments. $^{*}P < 0.05$, $^{**}P < 0.01$, SNL group or SNL + EA group versus normal group; $^{\#\#}P < 0.01$, $^{\#\#\#}P < 0.001$, SNL + EA group versus SNL group.

(Figure 4(a)). CGRP protein levels in ipsilateral L4 and L6 DRGs in SNL group were significantly increased as compared to that in normal group ($P < 0.05$, $P < 0.05$, resp.), and the increases of CGRP protein in these two DRGs were fully inhibited by 2 Hz EA ($P < 0.001$, $P < 0.01$, resp., compared to SNL group), with even lower expression in L4 DRG in SNL + EA group than that in normal group ($P < 0.01$; Figures 4(b) and 4(c)).

3.4. 6′-IRTX Blocked the Antiallodynic Effect of EA. To testify EA with 2 Hz frequency alleviated SNL-induced mechanical allodynia, at least in part, by inhibiting ipsilateral undamaged and adjacent DRG TRPV1 up-regulation, we performed block study via using TRPV1 ultrapotent agonist 6′-IRTX. Intraperitoneal injection of 0.001 and 0.01 mg/kg 6′-IRTX greatly reduced ipsilateral PWTs in EA-treated SNL rats ($P < 0.001$, $P < 0.001$, resp., compared to EA treatment-controlled group; Figure 5(a)). The two doses of injection blocked the antiallodynic effect of 2 Hz EA in ipsilateral hind paw, and 0.01 mg/kg 6′-IRTX was more potent than 0.001 mg/kg 6′-IRTX in counteracting 2 Hz EA action ($P < 0.05$). 0.001 mg/kg 6′-IRTX did not significantly change contralateral PWLs of SNL rats that received EA treatment, while 0.01 mg/kg 6′-IRTX significantly reduced contralateral PWL as compared to SNL + EA + vehicle and SNL + EA + 0.001 mg/kg 6′-IRTX groups ($P < 0.05$, $P < 0.05$, resp., Figure 5(b)).

4. Discussion

In the current study, the correlation of DRG TRPV1 with low frequency EA analgesia was for the first time investigated in rat neuropathic pain model induced by L5 SNL of the right

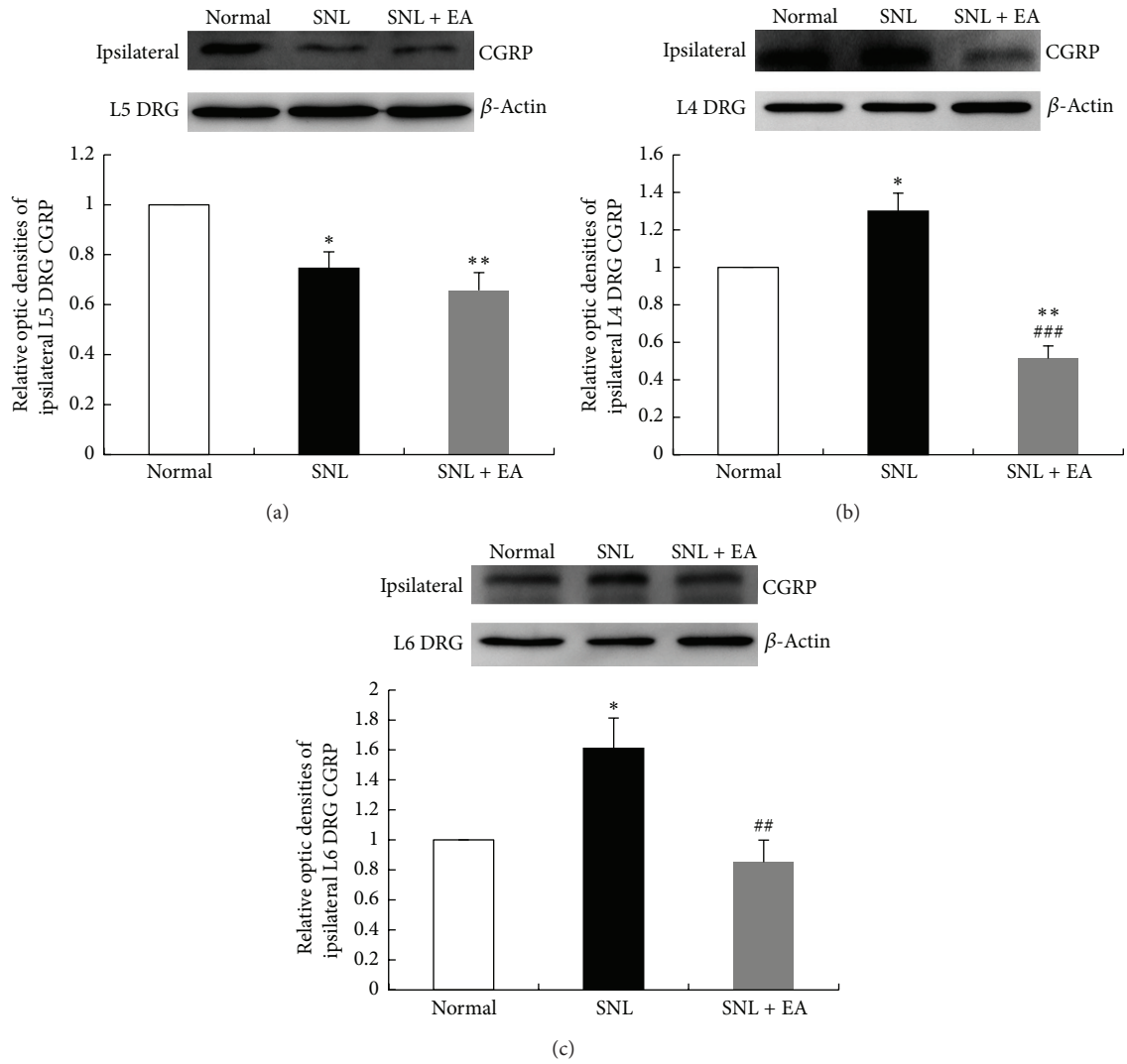

Figure 4: Western blotting analysis of CGRP levels in ipsilateral L5, L4, and L6 DRGs in normal, SNL, and SNL + EA groups. Results were expressed as relative fold changes as compared to normal group after normalization to β-actin. Data are presented as mean ± SEM of three independent experiments. $^{*}P < 0.05$, $^{**}P < 0.01$, SNL group or SNL + EA group versus normal group; $^{\#\#}P < 0.01$, $^{\#\#\#}P < 0.001$, SNL + EA group versus SNL group.

side. The rats' ipsilateral but not contralateral PWTs were decreased after SNL surgery. It was interesting to find that L5 SNL caused reductions of TRPV1 and CGRP in ipsilateral L5 DRG, but up-regulations in ipsilateral undamaged L4 and L6 DRGs. Low frequency EA alleviated mechanical allodynia and inhibited TRPV1 and CGRP upregulations. Furthermore, TRPV1 agonist 6′-IRTX fully blocked the antiallodynic effect of low frequency EA in ipsilateral hind paw.

Neuropathic pain may arise from nerve compression and trauma, diabetic neuropathy, chemotherapy-caused peripheral neuropathy, spinal cord injury stroke, and viral infections. Despite obvious differences in etiology, many of these pain conditions share common clinical phenomena: spontaneous pain together with allodynia and hyperalgisea [26, 27]. Nerve injury caused by SNL is a classic method to study neuropathic pain [28]. In the current study, rats subjected to L5 SNL developed prominent mechanical allodynia in ipsilateral hind paw. The signs of spontaneous pain such as guarding, licking, and lifting of ipsilateral hind paw were also observed. These results showed that neuropathic pain model was successfully made. Considering that mechanical allodynia was not further serious on day 3 after SNL surgery, we administered 2 Hz EA from day 3 and found that it effectively alleviated mechanical allodynia. Neuropathic pain relief by EA may be frequency specific. A former study showed that 2 Hz EA significantly attenuated hyperalgisea, whereas 120 Hz EA did not exert beneficial effect in diabetic neuropathic pain model [16]. The effectiveness of low frequency EA is also documented in other neuropathic pain models [17–19].

Changes in phenotype of primary sensory neurons following peripheral nerve injury contribute to allodynia and hyperalgisea in neuropathic pain [29]. TRPV1 is a member of TRP family channels which are ion channels that

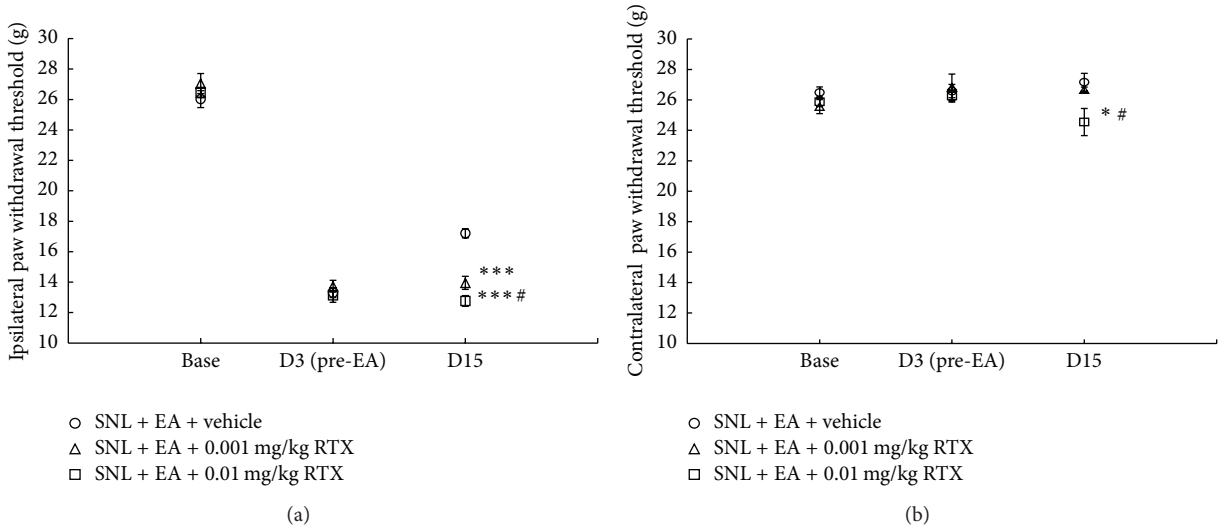

Figure 5: TRPV1 agonist 6′-IRTX blocked the antiallodynic effect of 2 Hz EA. 6′-IRTX was intraperitoneally injected 10 min before 2 Hz EA treatment on day 15. Data are presented as mean ± SEM, $n = 8$ per group. $^{*}P < 0.05$, $^{***}P < 0.001$, SNL + EA + 0.001 mg/kg 6′-IRTX group or SNL + EA + 0.01 mg/kg 6′-IRTX group versus SNL + EA + vehicle group; $^{\#}P < 0.05$, SNL + EA + 0.01 mg/kg 6′-IRTX group versus SNL + EA + 0.001 mg/kg 6′-IRTX group.

respond to mechanical, thermal, chemical, and many other stimuli coming from the extra- and intracellular milieu [30]. Activation of TRPV1 in sensory neurons results in pain perception. A former study showed that the enhanced TRPV1 function in injured sensory neurons by SNL was responsible for neuropathic pain [7]. In the present study, it was interesting to find that L5 SNL caused mechanical allodynia and resulted in an increase TRPV1 in the ipsilateral uninjured L4 and L6 DRGs but not in L5 DRG. It suggested that TRPV1 up-regulation in remaining adjacent undamaged sensory neurons may be also crucial to neuropathic pain. However, the reason why TRPV1 up-regulation could not be observed in injured sensory neurons by SNL needs to be further studied. The enhanced TRPV1 in ipsilateral L4 and L6 DRGs was fully inhibited by 2 Hz EA. Former studies also showed that analgesia produced by EA with low frequency was accompanied by inhibition of TRPV1 up-regulation in sensory neurons in diabetic neuropathic pain, nerve growth factor-induced hyperalgisea, and cancer-induced pain [15, 20, 31]. These findings suggest that inhibition of TRPV1 up-regulation in ipsilateral adjacent undamaged DRGs may be involved in alleviation of mechanical allodynia produced by 2 Hz EA.

Furthermore, we also carried out block study of 2 Hz EA analgesia by using TRPV1 ultrapotent agonist 6′-IRTX. TRPV1 agonist such as capsaicin can not only activate TRPV1 resulting in pain but also desensitize TRPV1 in a large dose leading to analgesia [32, 33]. A former study showed that systemic administration of RTX (0.1 mg/kg, i.p.) could lead to desensitization of TRPV1 resulting in abolishment of SNL-induced hyperalgisea in rats [33]. Thus, 6′-IRTX in smaller doses of 0.01 and 0.001 mg/kg were administered here to abrogate EA analgesia. A single intraperitoneal injection of 0.001 and 0.01 mg/kg 6′-IRTX on day 15 fully blocked the antiallodynic effect of 2 Hz EA in ipsilateral hind paw, which further supported the speculation mentioned above that 2 Hz EA alleviated neuropathic pain induced by SNL, at least in part, through inhibiting TRPV1 up-regulation.

Activation of TRPV1 can lead to the efferent release of proinflammatory neuropeptides [34]. CGRP is a pro-inflammatory neuropeptide implicated in a variety of painful conditions [35–37]. TRPV1-mediated release of CGRP contributes to TRPV1 role in pain sensation [10, 34]. We found that the variation of CGRP caused by SNL was consistent with that of TRPV1, with an increase in the adjacent intact L4 and L6 DRGs and a decrease in the injured L5 DRG. These results indicated interplay between TRPV1 and CGRP, which may further aggravate SNL-induced neuropathic pain. The increased CGRP was also inhibited by 2 Hz EA, which may result from the suppression of the increased TRPV1 and contribute to EA analgesia.

In conclusion, our data indicate that compensatory TRPV1 up-regulation in ipsilateral adjacent undamaged DRGs, with accompanied increased CGRP, may contribute to SNL-induced mechanical allodynia. EA with low frequency may alleviate SNL-induced mechanical allodynia through inhibiting TRPV1 up-regulation. Our study shows that EA with low frequency may be a useful approach for the management of neuropathic pain.

Conflict of Interests

There is no financial or commercial conflict of interests.

Acknowledgments

This study was supported by the Zhejiang Provincial Natural Science Foundation of China (LY12H27015, Z2100979), the National Natural Science Foundation of China (81072855),

and the Key Subject of State Administration of Traditional Chinese Medicine of China (Acupuncture and Moxibustion).

References

[1] R. Baron, A. Binder, and G. Wasner, "Neuropathic pain: diagnosis, pathophysiological mechanisms, and treatment," *The Lancet Neurology*, vol. 9, no. 8, pp. 807–819, 2010.

[2] R. Baron, "Mechanisms of disease: neuropathic pain. A clinical perspective," *Nature Clinical Practice Neurology*, vol. 2, no. 2, pp. 95–106, 2006.

[3] M. Takeda, Y. Tsuboi, J. Kitagawa, K. Nakagawa, K. Iwata, and S. Matsumoto, "Potassium channels as a potential therapeutic target for trigeminal neuropathic and inflammatory pain," *Molecular Pain*, vol. 7, article 5, 2011.

[4] E. Palazzo, L. Luongo, V. de Novellis, L. Berrino, F. Rossi, and S. Maione, "Moving towards supraspinal TRPV1 receptors for chronic pain relief," *Molecular Pain*, vol. 6, article 66, 2010.

[5] K. M. Walker, L. Urban, S. J. Medhurst et al., "The VR1 antagonist capsazepine reverses mechanical hyperalgesia in models of inflammatory and neuropathic pain," *Journal of Pharmacology and Experimental Therapeutics*, vol. 304, no. 1, pp. 56–62, 2003.

[6] Y. Kanai, E. Nakazato, A. Fujiuchi, T. Hara, and A. Imai, "Involvement of an increased spinal TRPV1 sensitization through its up-regulation in mechanical allodynia of CCI rats," *Neuropharmacology*, vol. 49, no. 7, pp. 977–984, 2005.

[7] D. Vilceanu, P. Honore, Q. H. Hogan, and C. L. Stucky, "Spinal nerve ligation in mouse upregulates TRPV1 heat function in injured IB4-positive nociceptors," *Journal of Pain*, vol. 11, no. 6, pp. 588–599, 2010.

[8] N. Bernardini, W. Neuhuber, P. W. Reeh, and S. K. Sauer, "Morphological evidence for functional capsaicin receptor expression and calcitonin gene-related peptide exocytosis in isolated peripheral nerve axons of the mouse," *Neuroscience*, vol. 126, no. 3, pp. 585–590, 2004.

[9] T. J. Price and C. M. Flores, "Critical evaluation of the colocalization between calcitonin gene-related peptide, substance P, transient receptor potential vanilloid subfamily type 1 immunoreactivities, and isolectin B4 binding in primary afferent neurons of the rat and mouse," *Journal of Pain*, vol. 8, no. 3, pp. 263–272, 2007.

[10] P. Nicoletti, M. Trevisani, M. Manconi et al., "Ethanol causes neurogenic vasodilation by TRPV1 activation and CGRP release in the trigeminovascular system of the guinea pig," *Cephalalgia*, vol. 28, no. 1, pp. 9–17, 2008.

[11] T. J. Price, M. D. Louria, D. Candelario-Soto et al., "Treatment of trigeminal ganglion neurons in vitro with NGF, GDNF or BDNF: effects on neuronal survival, neurochemical properties and TRPV1-mediated neuropeptide secretion," *BMC Neuroscience*, vol. 6, article 4, 2005.

[12] J. D. Richardson and M. R. Vasko, "Cellular mechanisms of neurogenic inflammation," *Journal of Pharmacology and Experimental Therapeutics*, vol. 302, no. 3, pp. 839–845, 2002.

[13] Y. Wang, Q. Guo, M. Wang, E. Wang, W. Zou, and J. Zhao, "Effect of intrathecal sufentanil and protein kinase C inhibitor on pain threshold and the expression of NMDA receptor/CGRP in spinal dorsal horn in rats with neuropathic pain," *Zhong Nan Da Xue Xue Bao Yi Xue Ban*, vol. 37, no. 8, pp. 783–789, 2012.

[14] J.-S. Han, "Acupuncture analgesia: areas of consensus and controversy," *Pain*, vol. 152, supplement, no. 3, pp. S41–S48, 2011.

[15] L. Manni, F. Florenzano, and L. Aloe, "Electroacupuncture counteracts the development of thermal hyperalgesia and the alteration of nerve growth factor and sensory neuromodulators induced by streptozotocin in adult rats," *Diabetologia*, vol. 54, no. 7, pp. 1900–1908, 2011.

[16] H. S. Hwang, E. J. Yang, S. M. Lee, S. C. Lee, and S. M. Choi, "Antiallodynic effects of electroacupuncture combined with MK-801 treatment through the regulation of p35/p25 in experimental diabetic neuropathy," *Experimental Neurobiology*, vol. 20, no. 3, pp. 144–152, 2011.

[17] R. Q. Sun, H. C. Wang, and Y. Wang, "Effect of electroacupuncture with different frequencies on neuropathic pain in a rat model," *Zhongguo Ying Yong Sheng Li Xue Za Zhi*, vol. 18, no. 2, pp. 128–131, 2002.

[18] K. K. Sun, H. P. Jung, J. B. Sang et al., "Effects of electroacupuncture on cold allodynia in a rat model of neuropathic pain: mediation by spinal adrenergic and serotonergic receptors," *Experimental Neurology*, vol. 195, no. 2, pp. 430–436, 2005.

[19] J. Yu, C. Zhao, and X. Luo, "The effects of electroacupuncture on the extracellular signal-regulated kinase 1/2/P2X3 signal pathway in the spinal cord of rats with chronic constriction injury," *Anesthesia and Analgesia*, vol. 116, no. 1, pp. 239–246, 2013.

[20] L. Aloe and L. Manni, "Low-frequency electro-acupuncture reduces the nociceptive response and the pain mediator enhancement induced by nerve growth factor," *Neuroscience Letters*, vol. 449, no. 3, pp. 173–177, 2009.

[21] S. H. Kim and J. M. Chung, "An experimental model for peripheral neuropathy produced by segmental spinal nerve ligation in the rat," *Pain*, vol. 50, no. 3, pp. 355–363, 1992.

[22] Y. L. Hsieh, C. L. Lin, H. Chiang, Y. S. Fu, J. H. Lue, and S. T. Hsieh, "Role of peptidergic nerve terminals in the skin: reversal of thermal sensation by calcitonin gene-related peptide in TRPV1-depleted neuropathy," *PLoS ONE*, vol. 7, no. 11, Article ID e50805, 2012.

[23] T. Shimizu, H. Toriumi, H. Sato et al., "Distribution and origin of TRPV1 receptor-containing nerve fibers in the dura mater of rat," *Brain Research*, vol. 1173, no. 1, pp. 84–91, 2007.

[24] J. Tang, Z. H. Li, S. N. Ge et al., "The inhibition of spinal astrocytic JAK2-STAT3 pathway activation correlates with the analgesic effects of triptolide in the rat neuropathic pain model," *Evidence-Based Complementary and Alternative Medicine*, vol. 2012, Article ID 185167, 13 pages, 2012.

[25] Y. L. Jiang, Y. Ning, Y. Y. Liu et al., "Effects of preventive acupuncture on streptozotocin-induced hyperglycemia in rats," *Journal of endocrinological investigation*, vol. 34, no. 10, pp. e355–361, 2011.

[26] M. Zimmermann, "Pathobiology of neuropathic pain," *European Journal of Pharmacology*, vol. 429, no. 1–3, pp. 23–37, 2001.

[27] R.-D. Treede, T. S. Jensen, J. N. Campbell et al., "Neuropathic pain: redefinition and a grading system for clinical and research purposes," *Neurology*, vol. 70, no. 18, pp. 1630–1635, 2008.

[28] T. Abuduhadeer, "Neuropathic pain intensity depends on the degree of peripheral nerve injury in the rat," *Journal of Nippon Medical School*, vol. 71, no. 6, pp. 399–407, 2004.

[29] M. Costigan, J. Scholz, and C. J. Woolf, "Neuropathic pain: a maladaptive response of the nervous system to damage," *Annual Review of Neuroscience*, vol. 32, pp. 1–32, 2009.

[30] C. Montell, L. Birnbaumer, and V. Flockerzi, "The TRP channels, a remarkably functional family," *Cell*, vol. 108, no. 5, pp. 595–598, 2002.

[31] Z. Zhang, C. Wang, G. Gu et al., "The effects of electroacupuncture at the ST36 (Zusanli) acupoint on cancer pain and transient receptor potential vanilloid subfamily 1 expression in walker 256 tumor-bearing rats," *Anesthesia and Analgesia*, vol. 114, no. 4, pp. 879–885, 2012.

[32] A. Szallasi and P. M. Blumberg, "Vanilloid (Capsaicin) receptors and mechanisms," *Pharmacological Reviews*, vol. 51, no. 2, pp. 159–211, 1999.

[33] T. King, C. Qu, A. Okun et al., "Contribution of afferent pathways to nerve injury-induced spontaneous pain and evoked hypersensitivity," *Pain*, vol. 152, no. 9, pp. 1997–2005, 2011.

[34] H. Xu, N. T. Blair, and D. E. Clapham, "Camphor activates and strongly desensitizes the transient receptor potential vanilloid subtype 1 channel in a vanilloid-independent mechanism," *Journal of Neuroscience*, vol. 25, no. 39, pp. 8924–8937, 2005.

[35] A. C. Raddant and A. F. Russo, "Calcitonin gene-related peptide in migraine: intersection of peripheral inflammation and central modulation," *Expert Reviews in Molecular Medicine*, vol. 13, article e36, 2011.

[36] J. M. Jimenez-Andrade, A. P. Bloom, J. I. Stake et al., "Pathological sprouting of adult nociceptors in chronic prostate cancer-induced bone pain," *Journal of Neuroscience*, vol. 30, no. 44, pp. 14649–14656, 2010.

[37] S. Hirsch, L. Corradini, S. Just, K. Arndt, and H. Doods, "The CGRP receptor antagonist BIBN4096BS peripherally alleviates inflammatory pain in rats," *Pain*, vol. 154, no. 5, pp. 700–707, 2013.

Hindawi Publishing Corporation
Evidence-Based Complementary and Alternative Medicine
Volume 2013, Article ID 894386, 11 pages
http://dx.doi.org/10.1155/2013/894386

Research Article

Inhibitory Effects of PC-SPESII Herbal Extract on Human Breast Cancer Metastasis

Xiu-Feng Wang, Jia Du, Tian-Ling Zhang, Qian-Mei Zhou, Yi-Yu Lu, Hui Zhang, and Shi-Bing Su

Research Center for Traditional Chinese Medicine Complexity System, Shanghai University of Traditional Chinese Medicine, 1200 Cailun Road, Pudong, Shanghai 201203, China

Correspondence should be addressed to Shi-Bing Su; shibingsu07@163.com

Received 13 March 2013; Accepted 28 April 2013

Academic Editor: Yong Qing Yang

Cancer metastasis is refractory to most forms of chemotherapy. Conventional and alternative drugs, such as Chinese herbal remedies, have been developed to target metastatic cancer cells. In this study, we investigated the effects of PC-SPESII, an herbal formulation, on the migration, invasion, and metastasis of an experimental human breast cancer cell line *in vivo* and *in vitro*. PC-SPESII suppressed pulmonary metastasis and tumor growth of MDA-MB-231 human breast cancer xenografts without affecting body weight, liver function, and kidney function. PC-SPESII also inhibited MDA-MB-231 cell migration and invasion *in vitro* in a dose-dependent manner. Based on ELISA analysis, secretion of MMP-2 and MMP-9, proteins associated with extracellular matrix degradation, was reduced in response to PC-SPESII treatment. Western blot analysis of whole-cell extracts revealed that the levels of proteolytic proteins associated with matrix and base membrane degradation (MMP-2, MMP-9, and uPA) were decreased and the levels of their endogenous inhibitors (TIMP1 and TIMP2) were increased. Moreover, the p38MAPK and SAPK/JNK signaling pathway, which stimulates proteolytic enzymes and matrix degradation, was inhibited by PC-PSESII. Remarkably, cotreatment with PC-PSESII and p38MAPK or SAPK/JNK inhibitors magnified the antimetastatic phenotype. Our results indicate that PC-PSESII impairs human breast cancer metastasis by regulating proteolytic enzymes and matrix dynamics through the p38MAPK and SAPK/JNK pathway.

1. Introduction

Breast cancer is the most common cancer among women, with 1.38 million cases diagnosed in 2008. Incidence rates of breast cancer vary by geographic region. They were highest in Europe and lowest in Africa and Asia [1], although the rates in China are rapidly increasing [2].

Metastasis is the major cause of death in cancer patients. It is a multifaceted process that results from coordinated events including cancer cell invasion, migration, and adhesion [3]. Degradation of extracellular matrix (ECM) and basement membrane (BM) by proteolytic enzymes and subsequent cancer invasion are the essential early steps of metastasis [4]. Matrix metalloproteinases (MMPs) and urokinase-type plasminogen activator (uPA) are the two important proteolytic enzymes that degrade the ECM and BM. Accordingly, expression of MMP-2, MMP-9, uPA, and uPA receptor (uPAR) is associated with increased tumor-cell invasion and metastasis in breast cancer [5, 6].

The functions of mitogen-activated protein kinase (MAPK) pathways are abundant in cancer cell progression. These pathways have been implicated in cell proliferation, differentiation, apoptosis, angiogenesis, and tumor metastasis [7]. In recent years, studies have shown that MAPK signaling is important for malignant tumor development. In early stages of metastasis, MAPK signaling pathways help regulate tumor cell adhesion, motility and degradation of ECM and BM [7–11].

Today, chemotherapy is the most frequently used treatment for breast cancer and other cancers. However, this method of treatment is not selective for cancer cells and often leads to the destruction of normal cells [12]. To compensate for the limitations and toxicity of chemotherapy, Chinese herbal medicines and other alternative strategies

are being developed. These agents are also being tested for their efficacy in preventing or suppressing metastasis. PC-SPESII, an herbal mixture, is made up of seven Chinese herbs (*Isatis indigotica, Glycyrrhiza glabra, Panax pseudoginseng, Rabdosia rubescens, Dendranthema morifolium, Scutellaria baicalensis,* and *Ganoderma lucidum*) [13]. This mixture contains 7 recognized and active antineoplastic compounds. A related mixture, PC-SPES, has an additional herb called saw palmetto. PC-SPES had been widely used for prostate cancer [14, 15] and PC-SPESII has been used in a phase I trial for prostate cancer [13]. The anticancer mechanisms of PC-SPES have been studied *in vitro* [16–21]. However, the inhibitory activities, if any, of PC-SPESII in the highly metastatic human breast cancer MDA-MB-231 cells have not been investigated.

In this study, we investigated the effects of PC-SPESII on migration, invasion, and metastasis of MDA-MB-231 cells and its molecular mechanisms of action. We found that PC-SPESII inhibits MDA-MB-231 cell migration, invasion, and metastasis. Furthermore, PC-SPESII regulates MMPs and uPA proteolytic enzymes via the p38MAPK and SAPK/JNK signaling pathway. Remarkably, PC-SPESII has no side effects.

2. Materials and Methods

2.1. Reagents. Matrigel, 3-(4, 5)-dimethylthiahiazo(-z-y1)-3, 5-di-phenytetrazoliumromide (MTT), was from Sigma (St. Louis, MO, USA). The antibodies against MMP-9, MMP-2, TIMP-1, TIMP-2, uPA, and uPAR were obtained from Santa Cruz Biotechnology (Santa Cruz, CA, USA). p38MAPK, p-p38MAPK, p-ERK1/2, p-SAPK/JNK, and SAPK/JNK antibodies were obtained from Cell Signaling Technology (Boston, MA, USA). The p38MAPK inhibitor SB203580 and the SAPK/JNK inhibitor SP600125 were obtained from Biomol (Philadelphia, PA, USA).

2.2. Drugs. PC-SPESII was obtained from Shanghai Zhong Yao BioTech Co., Ltd. (Shanghai, China). The following crude herbs, 1.0 g of Huangqin, 2.0 g of Daqingye, 1.0 g of Donglingcao, 0.5 g of Sanqi, 3.0 g of Lingzhi, 1.5 g of Juhua, and 0.5 g of Gancao, were made into PC-SPESII extract powder. The quality control and the standardization of each preparation of PC-SPESII is established and enforced strictly by Shanghai Zhong Yao BioTech Co., Ltd. To provide adequate quality control, the contents of major ingredients were measured on-line during the manufacturing processes (Table 1). The formulated PC-SPESII was subjected to high-performance liquid chromatography (HPLC) finger printing analysis in which the major peak was identified as the marker compound Baicalin (Figure 1).

320 mg of PC-SPESII powder was extracted with 70% ethanol as reported previously [16]. The ethanol extracts were kept at −20°C, and dilutions were made in the same culture media used for all *in vitro* studies. For *in vivo* studies, capsulated extracts were suspended in 1.5% CMC with 0.2% Tween 20 (Sigma, Chemical Co., St. Louis, MO, USA) as described previously [22].

Table 1: Quality control standardization for PC-SPESII.

Compounds (marker)	Refers to	Quality criterion (lowest amounts tolerated in 19 g of PC-SPESII crude extract)
Baicalin	Huangqin	15 mg
Indirubin	Daqingye	12 mg
Oridonin	Donglingcao	10 mg
Notoginsenoside	Sanqi	8 mg
Ganoderma lucidum polysaccharides	Lingzhi	1 mg
Chrysanthemum yellow ketone	Juhua	4 mg
Glycyrrhizic acid	Gancao	8 mg

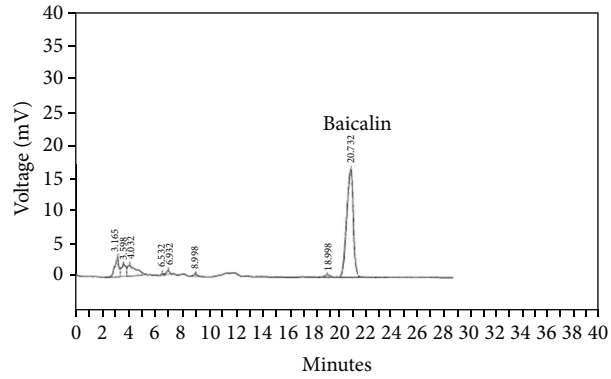

Figure 1: HPLC trace of the PC-SPESII extract. The major representative peaks of herbs in the formula are marked by their retention times. Baicalin represents one of markers listed in the PC-SPESII formula. The following HPLC conditions using a Discovery C18 analytical column (4.6 mm × 25 cm) were used: 100% methanol mobile phase at a flow rate of 1.0 mL/min and UV absorbance detected at 280 nm. Retention times of purified PC-SPESII are shown directly on this tracing.

2.3. Cell Culture. Human breast cancer MDA-MB-231 cells were obtained from American Type Culture Collection (Manassas, VA, USA) and were cultured in DMEM medium (Gibco, San Francisco, CA, USA) supplemented with 10% heat-inactivated (56°C, 30 min) fetal calf serum (PAA, A-4061, Pasching, Austria), 0.01 mg/mL insulin (Sigma, St. Louis, MO, USA), 2 mmol/L glutamine (Gibco, San Francisco, CA, USA), penicillin (100 U/mL), and streptomycin (100 μg/mL). The cell culture was maintained at 37°C with 5% CO_2 in a humidified atmosphere.

2.4. Human MDA-MB-231 Breast Cancer Xenograft Model Pulmonary Metastasis Assay. Female nude mice (6–8 weeks old) were purchased from the Laboratory Animal Center at Shanghai University of Traditional Chinese Medicine and housed in pathogen-free conditions throughout the duration of the experiment. Mice were given free access to commercial rodent feed and water. MDA-MB-231 cells (3×10^6, suspended

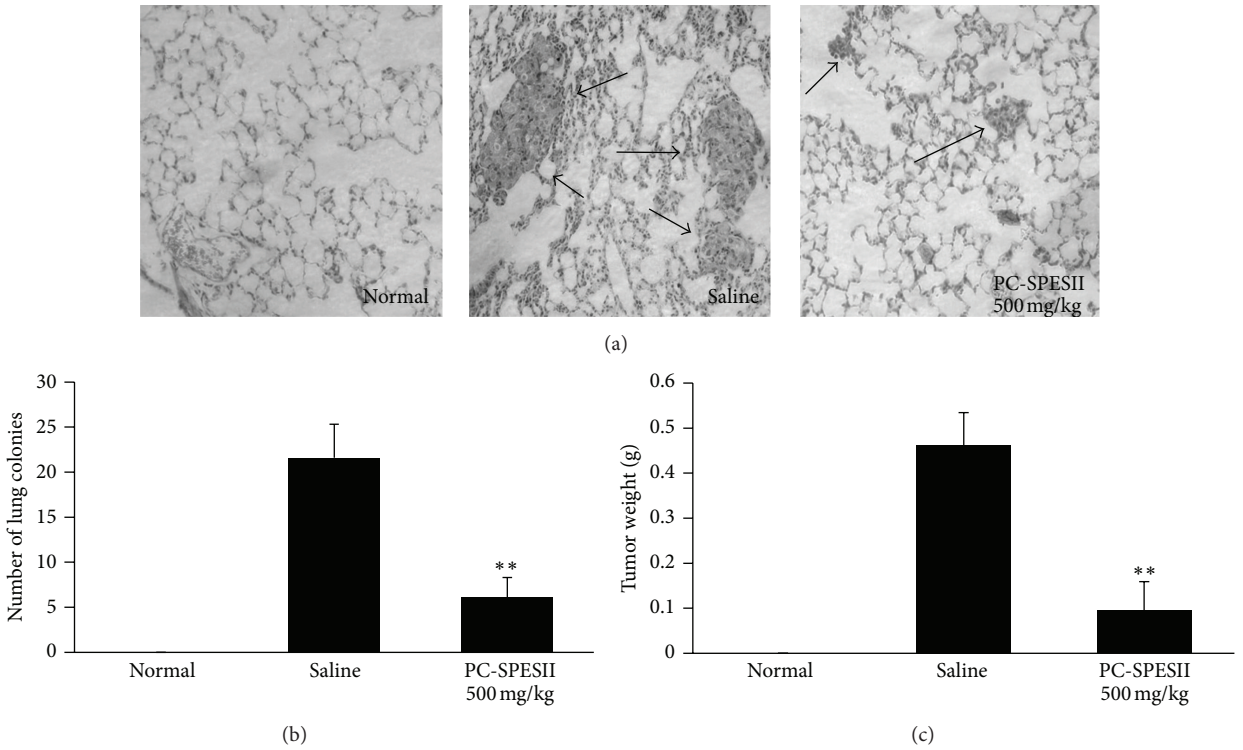

Figure 2: PC-SPESII inhibits pulmonary metastasis of MDA-MB-231 cells in Balb/c mice. Mice were divided into three experimental groups and were given drugs by oral gavage. The experiment was terminated 8 weeks after the initiation of therapy. Lungs were removed and fixed with Bouin's solution for 24 hours. Metastatic lesions on the lungs were counted under a dissecting microscope (100x magnification). (a) Histological appearances of representative lungs from normal, saline-treated, and PC-SPESII-treated mice are shown. (b) Quantification of metastatic lung nodules. (c) Tumor weights in grams of animals with different treatments were measured. $^{**}P < 0.01$ compared to the saline group.

in 100 μL of PBS) were injected into mammary fat pads of female athymic nude mice. One day after tumor cell inoculation, the mice were randomly divided into three groups ($n = 8$). In the treated group, 500 mg/kg of PC-SPESII was administered by oral gavage. Untreated groups were divided into a normal group and a model group (sham control) that were injected with physiological saline containing 1.5% CMC with 0.2% Tween 20. Body weight of each mouse was measured at different time points following tumor implantation. Mice were killed 2 months after tumor cell injection. The primary tumor of each mouse was weighed. The lungs were fixed with formalin. Thin sections were stained with hematoxylin and eosin. Five representative fields (at 100x magnification) for each group were photographed. The metastatic nodules of each field on the lungs were counted.

2.5. Kidney and Liver Function Tests. Blood was drawn from harvested eyeballs and centrifuged at 3000 rpm for 10 minutes to separate the serum. Glutamic oxalacetic transaminase (GOT/AST), glutamic pyruvic transaminase (GPT/ALT), serum creatinine (Cr), and blood urea nitrogen (BUN) were measured using the colorimeter testing kit (Kangcheng, Nanjing, China). Following the manufacturer's instructions, serum samples were measured at 510 nm, 510 nm, 510 nm, and 520 nm, respectively.

2.6. Cell Viability Assay. Cell viability was determined by MTT assay. MDA-MB-231 cells (5×10^4 cells/mL) were seeded in 96-well culture plates. After overnight incubation, MDA-MB-231 cells were treated with various concentrations of PC-SPESII. Following incubation, cell growth was measured at different time points after the addition of 20 μL MTT at 37°C for 4 h. Then, DMSO (150 μL) was added to dissolve the formazan crystals. Optical density (OD) was measured at 490 nm with an ELISA plate reader (BioTek, Winooski, VT, USA).

2.7. Wound Healing Migration Assay. The wound healing migration assay was performed as reported previously [23]. MDA-MB-231 cells were seeded at a density of $1\sim5 \times 10^5$ cells/well in 12-well culture plates and allowed to form a confluent monolayer. The layer of cells was then scraped with a 20–200 μL micropipette tip to create a ~1 mm wide wound. Cells were then washed twice with fresh medium and replaced with FBS-free medium containing indicated concentration of PC-SPESII. After incubation at 37°C for 24 h and 48 h, cells were washed with PBS, fixed with 4%

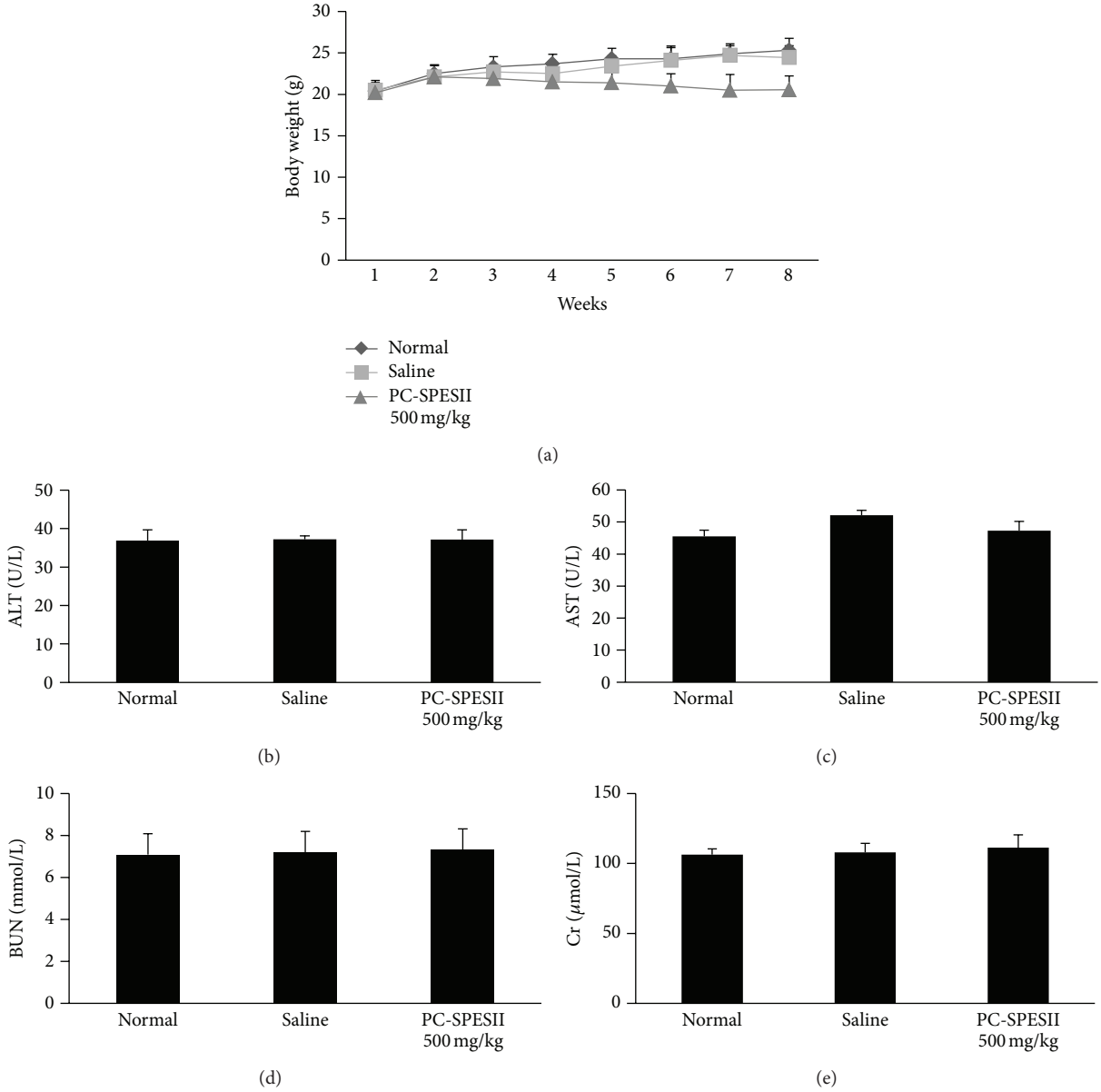

Figure 3: Effect of PC-SPESII on body weight, kidney function, and liver function in nude mice. Mice were treated with saline or PC-SPESII (500 mg/kg) for 8 weeks. (a) Body weights in grams of animals with different treatments were measured every week. (b) ALT, (c) AST, (d) BUN, (e) Cr and were measured using the colorimeter testing kit. According to the manufacturer's instructions, serum samples were measured at 510 nm, 510 nm, 510 nm, and 520 nm, respectively.

paraformaldehyde. Images of the wounds were captured at 0 h, 24 h, and 48 h after scraping at 100x magnification.

2.8. Migration and Invasion Assays. The *in vitro* cell migration and invasion assays were performed by using a Transwell chamber inserted with polyethylene terephthalate filter membrane containing 8 μm pores in 24-well plates (Corning, USA) as reported previously [24]. For cell invasion assays, the filter membranes were coated with Matrigel (30 μg, Sigma, USA). Cell migration assays did not require a coat of Matrigel in the upper chamber. Cells (1×10^5) suspended in 200 μL of serum-free medium were seeded onto the upper compartment of the Transwell chamber. The lower chamber was filled with medium containing chemoattractants (10% FBS for migration and invaded cancer cells) and various concentrations of PC-SPESII. After incubation for 24 h, the medium in the upper chamber was removed, and the filters were fixed with 70% ethanol for 10 min. The cells remaining on the upper surface of the filter membrane were then completely removed by wiping with a cotton swab, and the cells on the opposite surface of the filter membrane were stained with 0.5% Coomassie Brilliant Blue for 10 min. The migrated/invaded cells were then visualized and counted from six randomly selected fields (100x magnification) using an inverted microscope.

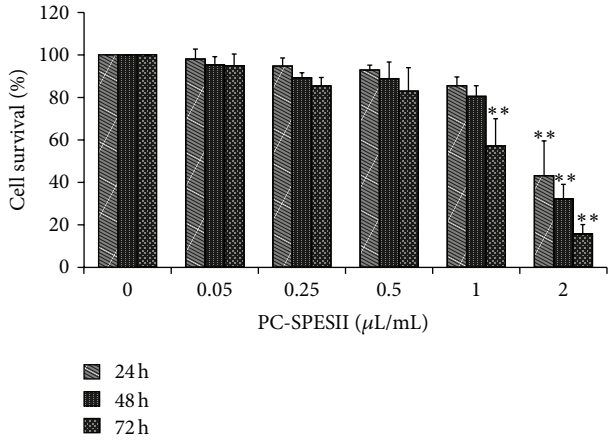

Figure 4: Effect of PC-SPESII on breast cancer cell viability. MTT assay was performed to measure cell survival (by percent) in response to PC-PSESII treatment. MDA-MB-231 cells were treated with the indicated amounts of PC-SPESII for 24, 48, or 72 hours. Results are presented as means ± SD of three independent experiments and SD are denoted by error bars ($^{**}P < 0.01$ compared to untreated control).

2.9. ELISA for Detection of Human MMP-2 and MMP-9 Protein Levels Secreted by Human Breast Cancer Cells. To measure human MMP-2 and MMP-9 secretion, MDA-MB-231 cells were treated with the indicated concentrations of PC-SPESII, and after 24 h the culture media was analyzed by ELISA using Human MMP-9 ELISA Kit from R&D Systems (Minneapolis, MN, USA) and Human MMP-2 ELISA Kit from RayBiotech. ELISA was done according to the instructions of the manufacturer. Each experiment was repeated three times.

2.10. Western Blot Analysis. Whole-cell lysate was loaded in each lane and separated by 10% or 8% SDS-PAGE. Protein expression was detected using primary antibody (1 : 1000~5000) and IRDye conjugated secondary antibody (1 : 10000~20000). Levels of MMP-2, MMP-9, TIMP-1, TIMP-2, uPA, uPAR, p38MAPK, p-p38MAPK, p-ERK1/2, p-SAPK/JNK, SAPK/JNL, and GAPDH were analyzed in this manner. Quantitative analysis of Western blotting was done using Alpha Ease FC (FluorChem FC2) software. Using the analysis tools, we calculated the density ratio of protein to GAPDH, the loading control.

2.11. Statistical Analyses. All data are expressed as means ± SD. Comparisons between groups were performed by Student's t-test and one-way analysis of variance (ANOVA). The level of significance was set at $P < 0.05$.

3. Results

3.1. PC-SPESII Inhibits In Vivo Pulmonary Metastasis of MDA-MB-231 Cells in Nude Mice. To determine whether PC-SPESII can inhibit human breast cancer metastasis, we examined the effects of PC-SPESII on spontaneous lung metastasis using MDA-MB-231 human breast cancer xenograftsin nude mice. Histological examination of the lung sections showed high levels of metastasized MDA-MB-231 cells in saline-fed mice (Figure 2(a)). The average number of tumor nodules was 21.60 ± 3.92 in the saline-treated group and 6.10 ± 2.33 in the PC-SPESII-treated group. These results indicated that PC-SPESII treatment significantly decreases tumor colonization in the lung compared with the saline group ($P < 0.01$; Figure 2(b)). Moreover, tumor weight was significantly inhibited in the PC-SPESII-treated group as shown in Figure 2(c) ($P < 0.01$). Together, these results strongly suggested that PC-SPESII can inhibit cancer metastasis and tumor growth.

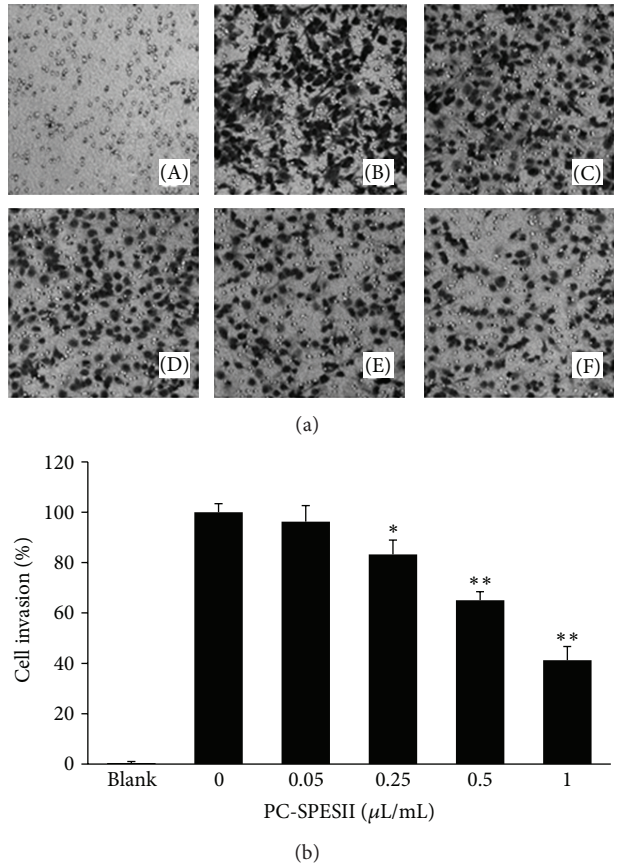

Figure 5: Effect of PC-SPESII on MDA-MB-231 cell invasion. (a) Transwell chamber was used for the invasion assay and images were taken at 200x magnification. The filter membranes were coated with Matrigel. MDA-MB-231 cells were treated with 0 (B), 0.05 (C), 0.25 (D), 0.5 (E), or 1 (F) μL/mL of PC-SPESII for 24 hours. No cells were seeded in (A). (b) Stand and error bars represent three independent experiments and each experiment was performed in triplicate ($^{*}P < 0.05$ and $^{**}P < 0.01$ compared to untreated control).

3.2. Side Effects of PC-SPESII in Nude Mice. In order to detect the potential side effects of PC-SPESII, we measured the body weight of mice every week. As shown in Figure 3(a), there were no significant differences in body weight among the three experimental groups ($P < 0.05$). We further tested the effects of PC-SPESII on liver and kidney functions. We did not detect significant changes on ALT (Figure 3(b)), AST (Figure 3(c)), BUN (Figure 3(d)), and Cr (Figure 3(e)) among

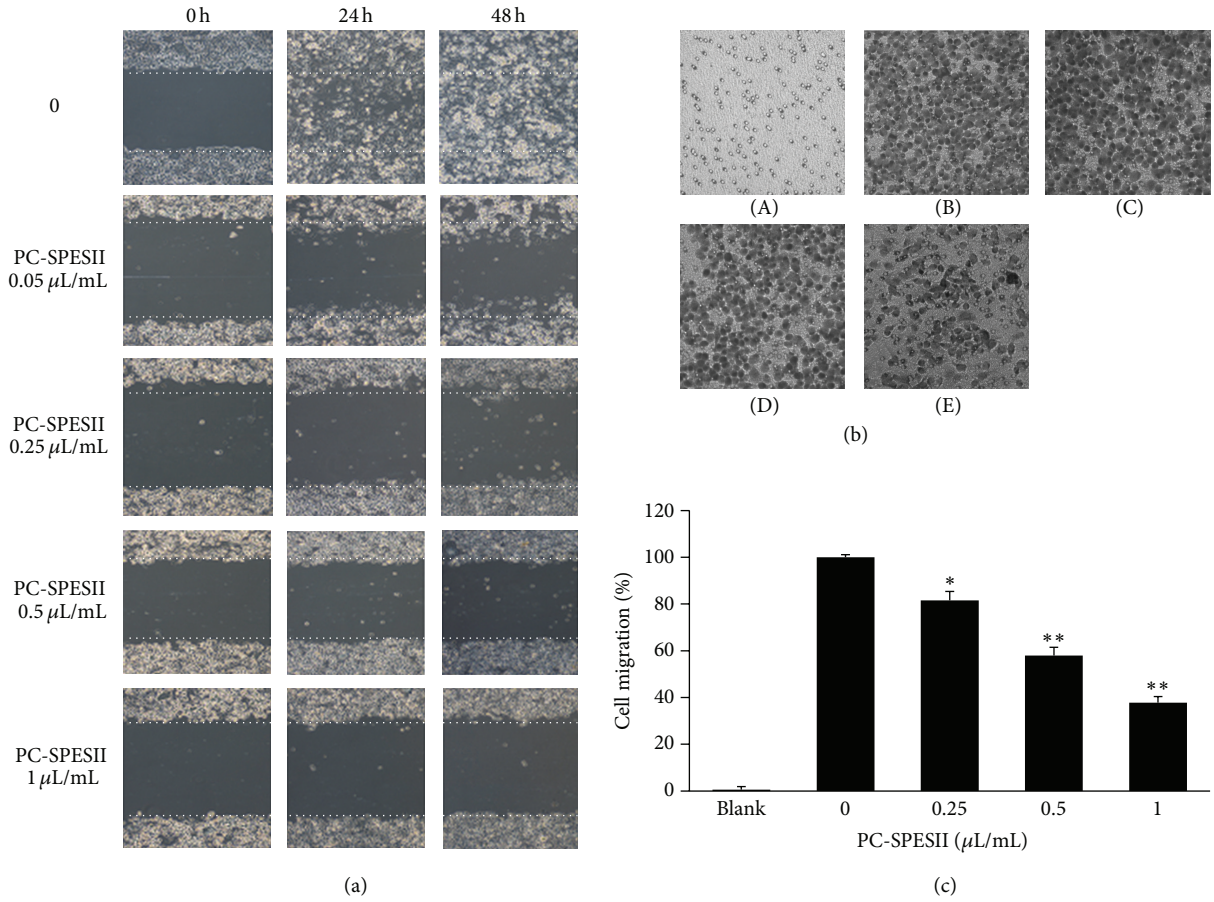

Figure 6: Effect of PC-SPESII on MDA-MB-231 cell migration. (a) Images of wound healing assays (100x magnification). Cells were seeded into 12-well cell culture plates, cultured in DMEM supplemented with 10% FBS, and allowed to grow to near confluence. Confluent monolayers were carefully wounded and the cellular debris was gently washed away with PBS. The wounded monolayer was reincubated in FBS-free DMEM containing 0, 0.25, 0.5, or 1 μL/mL of PC-SPESII for 24 or 48 hours. (b) Transwell chamber was performed for the migration assay (200x magnification). MDA-MB-231 cells were treated with 0 (B), 0.25 (C), 0.5 (D), or 1 (E) μL/mL of PC-SPESII for 24 hours during assay. No cells were seeded in (A). (c) Stand and error bars represent three independent experiments and each experiment was done in triplicate ($^{*}P < 0.05$ and $^{**}P < 0.01$ compared to untreated control).

the PC-SPESII-treated group, normal group, and saline group ($P < 0.05$), indicating that liver and kidney functions were normal after PC-PSESII treatment. Together, these results suggest that PC-SPESII has no side effects in mice.

3.3. Effect of PC-SPESII on Human Breast Cancer Cell Viability. In light of our findings *in vivo*, we further tested PC-SPESII *in vitro*. We first determined the effect of PC-SPESII on MDA-MB-231 cell viability by MTT assay. As shown in Figure 4, cell survival was inhibited after 72 h treatment with 1 μL/mL PC-PSESII. Doubling the dose to 2 μL/mL resulted in increased inhibition after 24 h, 48 h, and 72 h treatments. No significant differences were detected within 48 h at concentrations lower than 2 μL/mL compared with untreated cells. Therefore, to test the effects of PC-SPESII on human breast cancer cell invasion and migration without confounding effects from cytotoxicity, nonlethal concentrations (<2 μL/mL) and treatment times (<48 h) were used in subsequent experiments.

3.4. PC-SPESII Inhibits In Vitro Human Breast Cancer Cell Invasion. Metastasis consists of sequential steps involving cancer cell invasion and migration. To study whether PC-SPESII has anti-invasion effects, MDA-MB-231 cell invasion properties were analyzed by Matrigel coated Transwell chambers in the presence of PC-SPESII. Indeed, the number of cell invasions through the Matrigel coated filter was dose dependently reduced by PC-SPESII (Figure 5(a)). Compared with the control group, the number of invaded cells from PC-SPESII-treated (0.25, 0.5, and 1 μL/mL) samples was reduced by 17%, 35%, and 59% respectively ($P < 0.01$; Figure 5(b)). Thus, in addition to its inhibitory effect on cell viability at high concentrations, low concentrations of PC-SPESII inhibited the cell invasion potential of MDA-MB-231 cells *in vitro*. Notably, the inhibitory effects of PC-SPESII on cell invasion were not due to its cytotoxic effects because viability was barely affected at the concentration range tested (Figure 4).

3.5. PC-SPESII Inhibits In Vitro Human Breast Cancer Cell Migration. We next tested whether PC-SPESII can inhibit

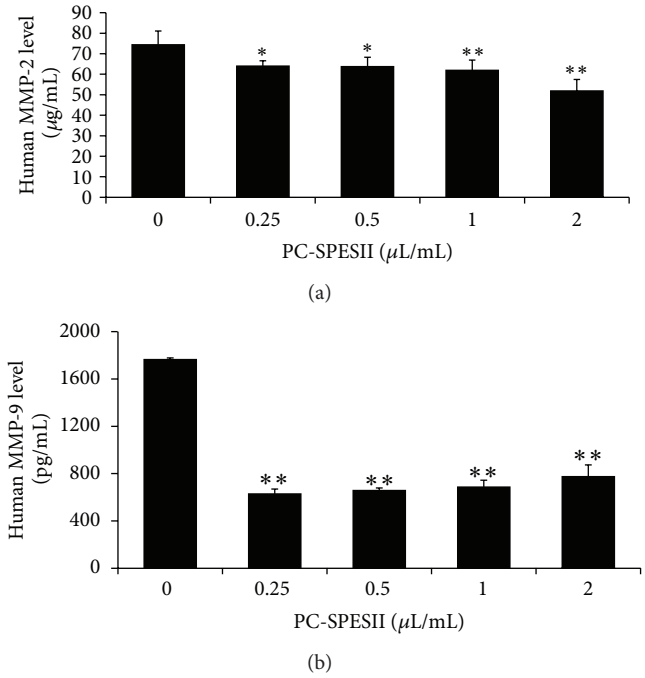

Figure 7: PC-SPESII reduces MMP-2 and MMP-9 extracellular secretion in MDA-MB-231 cells. MDA-MB-231 cells were treated for 24 h with the indicated concentrations of PC-SPESII. Then, each cell culture medium was collected and analyzed by ELISA using Human MMP-2 and MMP-9 ELISA Kit (a, b). ELISA was done according to the instructions from the manufacturer. Each experiment was repeated three times. $^{*}P < 0.05$ and $^{**}P < 0.01$ compared to untreated control.

the migration ability of MDA-MB-231 cells. We initially tested this by performing a wound-healing assay. Confluent cells were scraped with a sterilized tip and the remaining cells were allowed to migrate into the gap created in the absence or presence of PC-SPESII as shown in Figure 6(a). Remarkably, after 24 and 48 h incubation, the wound gap was wider in the PC-SPESII-treated (0.05, 0.25, 0.5, and 1 μL/mL) groups than the untreated group, indicating that PC-SPESII inhibits MDA-MB-231 cell motility.

To corroborate these findings, we tested the effect of PC-SPESII on MDA-MB-231 cell motility by the Transwell chamber assay. As expected from the wound-healing assay, the number of cells migrating to the lower chamber was reduced in response to PC-SPESII treatment in a concentration-dependent manner (Figure 6(b)). Compared to the untreated group, the number of migrated cells from PC-SPESII-treated (0.25, 0.5, and 1 μL/mL) groups was reduced by 19%, 42%, and 62%, respectively ($P < 0.01$; Figure 6(c)). Together, these data confirm that PC-SPESII inhibits MDA-MB-231 cell migration.

3.6. PC-SPESII Reduces MMP-2 and MMP-9 Secretion in MDA-MB-231 Cells. Degradation of extracellular matrix and basement membrane are very important steps in cancer invasion and metastasis. MMP-2 and MMP-9 are the two important proteolytic enzymes involved in this process. Here, we tested secretion levels of human MMP-2 and MMP-9 from MDA-MB-231 cells with or without PC-SPESII treatment. As shown in Figures 7(a) and 7(b), PC-SPESII significantly inhibited MMP-2 (0.25 and 0.5 μL/mL, $P < 0.05$; 1 μL/mL, $P < 0.01$) and MMP-9 ($P < 0.01$) secretion into the medium in a dose-dependent manner. This result suggests that PC-SPESII-dependent inhibition of breast cancer metastasis may involve the degradation of extracellular matrix and basement membrane.

3.7. PC-SPESII Regulates Proteolytic Enzymes. To determine whether proteolytic protein expression is regulated by PC-SPESII, cells were treated with or without PC-SPESII for 24 h and whole-cell extracts were analyzed by Western blotting. As shown in Figures 8(a) and 8(b), MMP-2, MMP-9, uPA, and uPAR levels were decreased by varying degrees in response to 1 μL/mL and other concentrations of PC-SPESII. Alternatively, TIMP-1 and TIMP-2 levels were significantly increased. Taken together, these data suggest that PC-SPESII-mediated inhibition of MDA-MB-231 cell migration, invasion, and metastasis is dependent on the degradation of extracellular matrix.

3.8. PC-SPESII Regulates Expression of Proteins Involved in the p38MAPK and SAPK/JNK Pathway. The MAPK and SAPK/JNK signaling pathway has been implicated in the regulation of various cellular processes including cancer cell metastasis. This pathway also regulates the expression of proteolytic proteins and ECM degradation. Thus, we tested the effect of PC-SPESII on MAPK levels and signaling by Western blotting. In response to PC-SPESII treatment, p38MAPK and SAPK/JNK expression were reduced while p-ERK1/2 expressions remained unchanged (Figures 8(c) and 8(d)). Phosphorylation of p38MAPK and SAPK/JNK was also reduced. The p38MAPK protein phosphorylated ratios were 0.59, 0.65, 0.55, and 1.60. The SAPK/JNK protein phosphorylated ratios were 0.90, 0.09, 0.02, and 0.01. These results confirmed that the signaling competency of these proteins was compromised.

We hypothesized that pharmacological inhibition of p38MAPK and SAPK/JNK signaling would recapitulate the phenotypes associated with PC-SPESII treatment. To test this, we treated MDA-MB-231 cells with the p38MAPK-specific inhibitor (SB203580) and the SAPK/JNK-specific inhibitor (SP600125) alone or in combination with PC-SPESII. Interestingly, inhibiting p38MAPK or SAPK/JNK mimicked the effects we described in PC-SPESII-treated cells (Figure 9), indicating that PC-SPESII acts on these signaling pathways. Since the inhibitors and PC-SPESII act on the same pathway, we reasoned that cotreatment would amplify their effects. Compared to cells treated with PC-SPESII alone, expression of MMP-9, uPA, TIMP-1, and TIMP-2 was further reduced in cells cotreated with PC-SPESII and SB203580 or SP600125 (Figures 9(a) and 9(b)). Next, we tested the effect of cotreatment on cell invasion by the Transwell chamber assay. Again, PC-SPESII and the two inhibitors combined to further reduce cell invasion (Figures 9(c) and 9(d)). Taken together, these results suggest that the anti-invasion effect

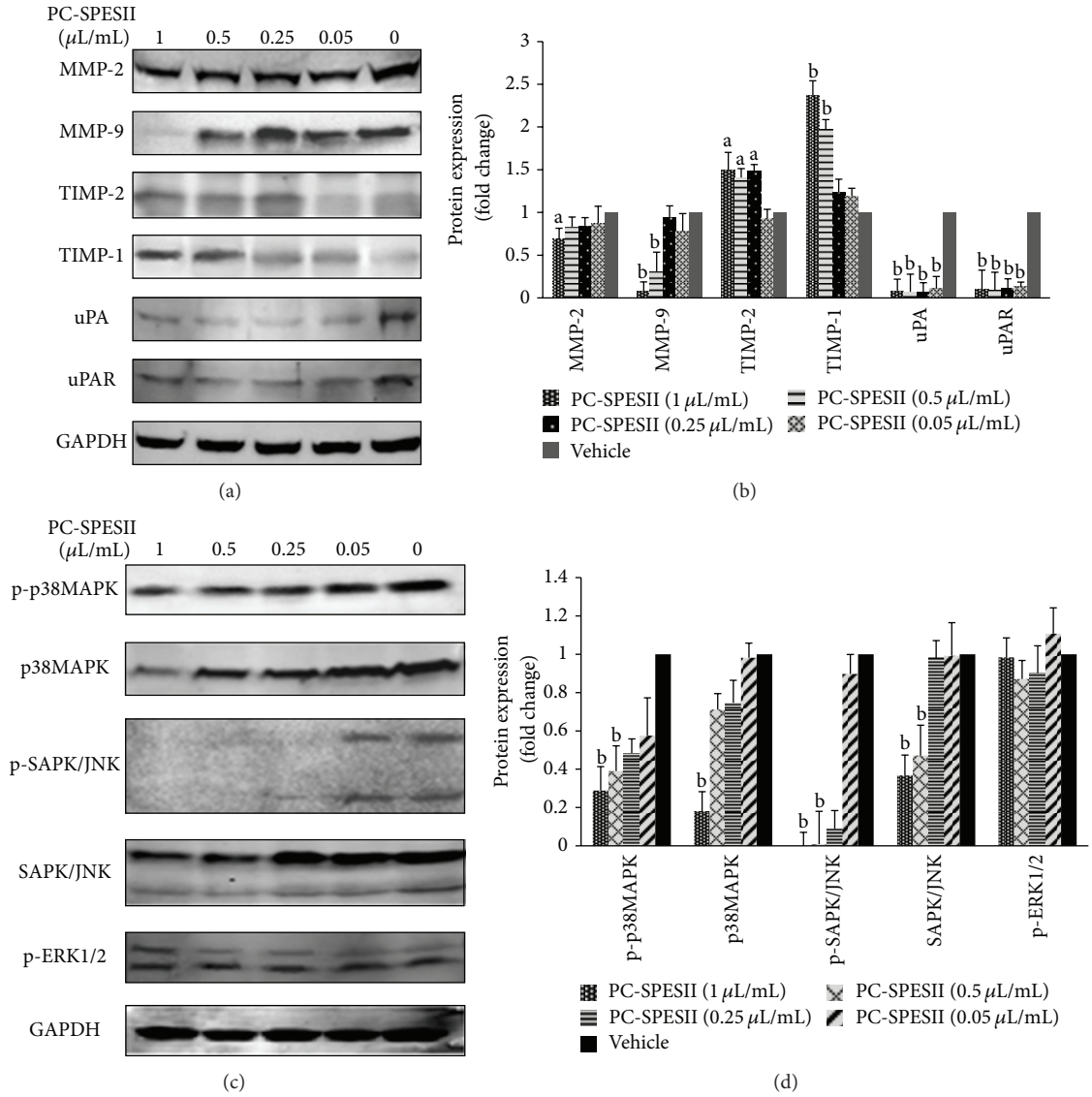

Figure 8: Changes in protein expression in response to PC-SPESII treatment. (a, c) MDA-MB-231 cells were treated with or without PC-SPESII for 24 h. Then Western blot analysis was performed using antibodies specific for MMP-2, MMP-9, uPA, uPAR, TIMP-1, TIMP-2, p38MAPK, p-p38MAPK, p-ERK1/2, p-SAPK/JNK, and SAPK/JNK. (b, d) The density ratio of proteins to GAPDH is shown as relative expression. Values are expressed in mean ± SD; three experiments were repeated with similar results. $^{a}P < 0.05$ and $^{b}P < 0.01$ compared to control.

of PC-SPESII acts through the p38MAPK and SAPK/JNK pathway in MDA-MB-231 cells.

4. Discussion

Most cancer patients do not die from local complications of their primary tumor growth, but rather from the development and spread of the tumor. Preventing and suppressing tumor invasion and metastasis is a promising means for decreasing the mortality of patients with malignant tumors. In recent years, studies performed on antitumor drugs are increasing. These include natural products that have been used as alternative treatments for treating certain cancers such as breast cancer [25, 26]. Despite the increased research in this field, there still remains a serious shortage of agents that target cancer cell metastasis [27].

This study focuses on the mechanism and antimetastatic effects of PC-PSESII, a Chinese herbal medicine. We demonstrated that PC-PSESII has high antimetastatic activity and low toxicity. Specifically, PC-PSESII suppressed pulmonary metastasis of human MDA-MB-231 breast cancer cells in nude mice. The average number of metastasized lung nodules and tumor weight in the PC-SPESII-treated group was significantly lower than in saline group (Figure 2). Despite its dramatic effects on cancer cell metastasis, PC-SPESII treatment did not alter body weight, kidney function, and liver function (Figure 3) *in vivo*. We also found concentration-dependent inhibition of MDA-MB-231 cell migration and invasion in

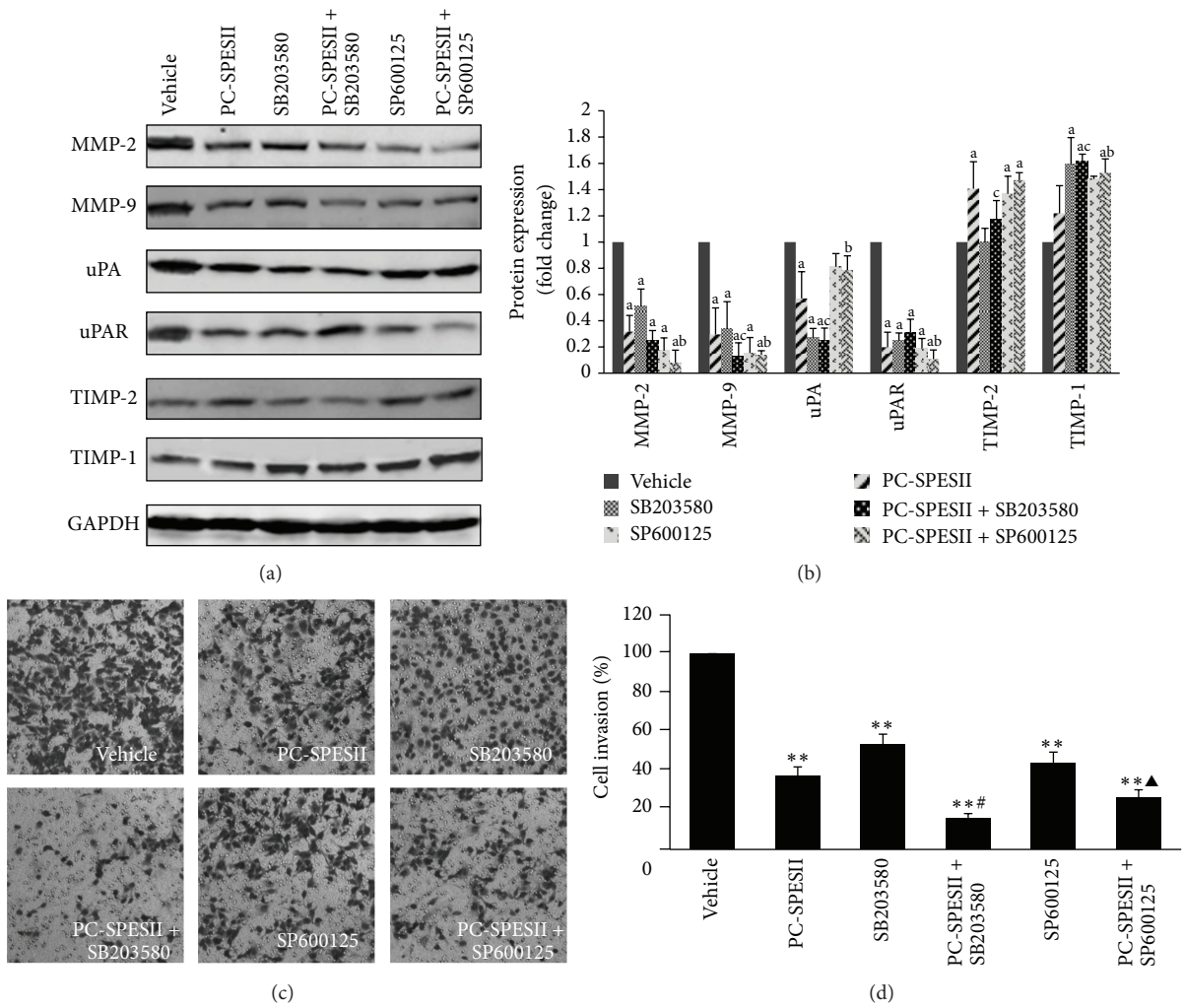

Figure 9: Protein expression and cell invasion after PC-SPESII treatment with or without p38MAPK and SAPK/JNK inhibitors. (a) MDA-MB-231 cells were treated with or without 1 μL/mL PC-SPESII, 15 μm/L SB203580, and 20 μm/L SP600125 in the indicated combinations for 24 h. Then, Western blot analysis was performed and stained for the indicated epitopes. (b) The density ratio of proteins to GAPDH is shown as relative expression. Values are expressed as mean ± SD. Three experiments were repeated with similar results. $^{a}P < 0.01$, $^{b}P < 0.05$, and $^{c}P < 0.05$ compared to control. (c, d) Transwell chamber was used for the invasion assay (100x magnification). The filter membranes were coated with Matrigel. Cells were treated according to the conditions in (a) for 24 h. Results are presented as mean ± SD of three independent experiments. $^{**}P < 0.01$ compared to control; $^{\#}P < 0.01$ and $^{\blacktriangle}P < 0.05$ compared to 1 μL/mL PC-SPESII treatment.

response to PC-SPESII *in vitro* (Figures 5 and 6). These results indicated that PC-SPESII has potent antimetastatic activity *in vivo* and *in vitro* with no side effects.

The ECM and BM are two barriers that hinder cancer cell invasion. The MMP family of zinc-dependent proteinases mediates ECM degradation. MMP-2 and MMP-9 are the key enzymes for type IV collagen degradation and are considered to be important for cancer invasion [28]. In cancer cells, MMP-2 and MMP-9 are controlled by their endogenous inhibitors TIMP-1 and TIMP-2 [29]. Therefore, decreasing MMP activity while increasing TIMP activity could inhibit cancer cell invasion and metastasis [30]. In order to investigate the mechanisms of the antimigration and anti-invasion effects of PC-SPESII, we examined the regulation of MMP and TIMP activity in MDA-MB-231 cells. Our data showed that PC-SPESII significantly inhibited MMP-2 and MMP-9 secretion (Figure 7) and expression and increased TIMP-1 and TIMP-2 levels (Figure 8(a)), consistent with its inhibitory effects on metastasis.

uPA is another important ECM proteinase. It is a serine protease that converts plasminogen to plasmin, which directly mediates cancer cell invasion by degrading matrix proteins such as collagen IV, fibronectin, and laminin or indirectly by activating MMP-2, MMP-3, MMP-9, and uPA [31]. It is well documented that overexpression of uPA in breast cancers is a strong indicator of poor prognosis. uPAR focuses uPA activity on the cell membrane, thus regulating cell surface-associated plasminogen proteolysis by uPA [32]. Thus, we studied the effects of PC-SPESII on uPA and uPAR in MAD-MB-231 cells. The results showed that PC-SPESII decreased uPA and uPAR expression (Figure 7(a)). Taken together, our data indicates that PC-PSESII exerts its effects

through regulating the balance between MMP and TIMP expression and decreasing uPA and uPAR expression *in vitro*.

The MAPK pathway is upstream of MMP activity and ECM degradation. It has been reported that the overexpression and phosphorylation of MEK and ERK may play an important role in the development of human breast cancer [33]. Tetraspanin CD9 activates p38MAPK, which induces MMP expression and activates JNK and c-Jun pathways in human melanoma cells [34]. Previous studies have shown that p38MAPK phosphorylation occurs in 20% of primary breast carcinomas and may be associated with poor outcomes in patients with lymph node-positive breast carcinoma [35]. P38MAPK could promote breast cancer progression by upregulating uPA expression, suggesting that phosphorylated p38MAPK and uPA expression could serve as biomarkers for breast cancer prognoses [20]. A natural product, Butein, inhibits the migration and invasion of SK-HEP-1 human hepatocarcinoma cells by suppressing the ERK, JNK, p38, and uPA signaling pathways [36]. Constitutive p38alpha MAPK activity is required for increased uPAR expression and matrix invasion by breast cancer cells [37]. Downstream from MAPK signaling, JNK activation helps regulate cancer cell invasion and expression of MMP-1, MMP-2, and MMP-9. Accordingly, inhibiting JNK decreases cancer cell invasion [38].

In this study, we confirmed that PC-SPESII functions by inhibiting the p38MAPK and SAPK/JNK pathway without altering ERK1/2 phosphorylation. In order to further assess the role of p38MAPK and SAPK/JNK in PC-SPESII treatment, MDA-MB-231 cells were treated with the p38MAPK-specific inhibitor, SB203580, and the SAPK/JNK-specific inhibitor, SP600125, alone or in combination with PC-SPESII. The results showed that the effects of PC-SPESII combined with inhibitors were significantly strengthened (Figures 9(a) and 9(b)), suggesting that PC-SPESII regulates the proteolytic enzyme via the p38MAPK and SAPK/JNK pathway in MDA-MB-231 cells.

5. Conclusion

PC-SPESII inhibits human breast cancer MDA-MB-231 cell migration, invasion, and metastasis through *in vitro* and *in vivo* studies. PC-PSESII regulates secretion and expression of proteolytic enzymes by targeting the p38MAPK and SPK/JNK pathway. The potent antimetastatic effect and low toxicity of PC-PSESII suggest that this Chinese herbal remedy has a high therapeutic potential for metastatic breast cancer.

Conflict of Interests

The authors declare that we have no financial and personal relationships with other people or organizations that can inappropriately influence their work; there is no potential conflict of interests include employment, consultancies, stock ownership, honoraria, paid expert testimony, patent applications and registrations, and grants or other funding.

Acknowledgments

This study was supported by the National Natural Science Funds (81073134), Leading Academic Discipline Project of Shanghai Municipal Education Commission (no. J50301), and E-institutes of Shanghai Municipal Education Commission (no. E03008).

References

[1] J. Ferlay, H. R. Shin, F. Bray et al., "GLOBOCAN 2008 v1.2, Cancer Incidence and Mortality Worldwide: IARC Cancer Base No. 10 [Internet]," International Agency for Research on Cancer, Lyon, France, 2010, http://globocan.iarc.fr/.

[2] R. G. Ziegler, W. F. Anderson, and M. H. Gail, "Increasing breast cancer incidence in China: the numbers add up," *Journal of the National Cancer Institute*, vol. 100, no. 19, pp. 1339–1341, 2008.

[3] M.-S. Kim, M.-K. You, D.-Y. Rhuy et al., "Loquat (Eriobotrya japonica) extracts suppress the adhesion, migration and invasion," *Nutrition Research and Practice*, vol. 3, no. 4, pp. 259–264, 2009.

[4] T. Bogenrieder and M. Herlyn, "Axis of evil: molecular mechanisms of cancer metastasis," *Oncogene*, vol. 22, no. 43, pp. 6524–6536, 2003.

[5] L. Liu, L. J. Liu, and P. Zhao, "Expressions and clinicopathological significance of matrix metalloproteinase-2,metalloproteinase-9 and E-cadherin in breast cancer tissues," *China Journal of Modern Medicine*, vol. 18, no. 21, pp. 3149–3151, 2008.

[6] M. M. Pacheco, I. N. Nishimoto, M. Mourão Neto, E. B. Mantovani, and M. M. Brentani, "Prognostic significance of the combined expression of matrix metalloproteinase-9, urokinase type plasminogen activator and its receptor in breast cancer as measured by Northern blot analysis," *International Journal of Biological Markers*, vol. 16, no. 1, pp. 62–68, 2001.

[7] M. Köbel, G. Pohl, W. D. Schmitt, S. Hauptmann, T.-L. Wang, and I.-M. Shih, "Activation of mitogen-activated protein kinase is required for migration and invasion of placental site trophoblastic tumor," *American Journal of Pathology*, vol. 167, no. 3, pp. 879–885, 2005.

[8] Y.-H. Zhou, X.-F. He, H. Gao, and Y.-F. Wang, "Mechanisms underlying the role of JNK signaling pathway in the invasion and metastasis of colon cancer cells," *World Chinese Journal of Digestology*, vol. 17, no. 21, pp. 2142–2146, 2009.

[9] J. Z. You, H. B. Wang, Z. W. Yang et al., "Signal transduction pathways involved in promotion of proliferation and migration via p-ERK in high metastasis potential breast cancer cells," *Chinese Journal of Biochemistry and Molecular Biology*, vol. 22, no. 12, pp. 1007–1012, 2006.

[10] Y.-C. Han, X.-X. Zeng, R. Wang, Y. Zhao, B.-L. Li, and M. Song, "Correlation of p38 mitogen-activated protein kinase signal transduction pathway to uPA expression in breast cancer," *Chinese journal of cancer*, vol. 26, no. 1, pp. 48–53, 2007.

[11] Y. C. Han, L. Y. Liu, D. X. Yang et al., "Increase of p-p38 and uPA expression in human breast cancer," *Basic & Clinical Medicin*, vol. 29, no. 2, pp. 170–173, 2009.

[12] S. Wang, Q. Liu, Y. Zhang et al., "Suppression of growth, migration and invasion of highly-metastatic human breast cancer cells by berbamine and its molecular mechanisms of action," *Molecular Cancer*, vol. 8, article 1476, p. 81, 2009.

[13] M. Shabbir, J. Love, and B. Montgometry, "Phase I trial of PC-Spes2 in advanced hormone refractory prostate cancer," *Oncology Reports*, vol. 19, no. 3, pp. 831–835, 2008.

[14] E. J. Small, M. W. Frohlich, R. Bok et al., "Prospective trial of the herbal supplement PC-SPES in patients with progressive prostate cancer," *Journal of Clinical Oncology*, vol. 18, no. 21, pp. 3595–3603, 2000.

[15] A. de la Taille, R. Buttyan, O. Hayek et al., "Herbal therapy PC-SPES: in vitro effects and evaluation of its efficacy in 69 patients with prostate cancer," *Journal of Urology*, vol. 164, no. 4, pp. 1229–1234, 2000.

[16] S. Chenn, "In vitro mechanism of PC SPES," *Urology*, vol. 58, no. 2, pp. 28–35, 2001.

[17] T.-C. Hsieh and J. M. Wu, "Mechanism of action of herbal supplement PC-SPES: elucidation of effects of individual herbs of PC-SPES on proliferation and prostate specific gene expression in androgen-dependent LNCaP cells," *International journal of oncology*, vol. 20, no. 3, pp. 583–588, 2002.

[18] S. Huerta, J. R. Arteaga, R. W. Irwin, T. Ikezoe, D. Heber, and H. P. Koeffler, "PC-SPES inhibits colon cancer growth in vitro and in vivo," *Cancer Research*, vol. 62, no. 18, pp. 5204–5209, 2002.

[19] M. J. Bonham, A. Galkin, B. Montgomery, W. Stahl, D. Agus, and P. S. Nelson, "Effects of the herbal extract PC-SPES on microtubule dynamics and paclitaxel-mediated prostate tumor growth inhibition," *Journal of the National Cancer Institute*, vol. 94, no. 21, pp. 1641–1671, 2002.

[20] X. Lu, J. Guo, and T.-C. Hsieh, "PC-SPES inhibits cell proliferation by modulating p21, cyclins D, E and B and multiple cell cycle-related genes in prostate cancer cells," *Cell Cycle*, vol. 2, no. 1, pp. 59–63, 2003.

[21] M. Schmidt, C. Polednik, P. Gruensfelder, J. Roller, and R. Hagen, "The effects of PC-Spes on chemosensitive and chemoresistant head and neck cancer cells and primary mucosal keratinocytes," *Oncology Reports*, vol. 21, no. 5, pp. 1297–1305, 2009.

[22] T. Kubota, J. Hisatake, Y. Hisatake et al., "PC-SPES: a unique inhibitor of proliferation of prostate cancer cells in vitro and in vivo," *Prostate*, vol. 42, pp. 163–171, 2000.

[23] X. Pan, H. Han, L. Wang et al., "Nitidine Chloride inhibits breast cancer cells migration and invasion by suppressing c-Src/FAK associated signaling pathway," *Cancer Letters*, vol. 313, no. 2, pp. 181–191, 2011.

[24] J. S. Rao, C. Gondi, C. Chetty, S. Chittivelu, P. A. Joseph, and S. S. Lakka, "Inhibition of invasion, angiogenesis, tumor growth, and metastasis by adenovirus-mediated transfer of antisense uPAR and MMP-9 in non-small cell lung cancer cells," *Molecular Cancer Therapeutics*, vol. 4, no. 9, pp. 1399–1408, 2005.

[25] Q.-M. Zhou, H. Zhang, Y.-Y. Lu, X.-F. Wang, and S.-B. Su, "Curcumin reduced the side effects of mitomycin C by inhibiting GRP58-mediated DNA cross-linking in MCF-7 breast cancer xenografts," *Cancer Science*, vol. 100, no. 11, pp. 2040–2045, 2009.

[26] Q.-M. Zhou, X.-F. Wang, X.-J. Liu, H. Zhang, Y.-Y. Lu, and S.-B. Su, "Curcumin enhanced antiproliferative effect of mitomycin C in human breast cancer MCF-7 cells in vitro and in vivo," *Acta Pharmacologica Sinica*, vol. 32, no. 11, pp. 1402–1410, 2011.

[27] M. J. Duffy, P. M. McGowan, and W. M. Gallagher, "Cancer invasion and metastasis: changing views," *Journal of Pathology*, vol. 214, no. 3, pp. 283–293, 2008.

[28] C. E. Brinckerhoff and L. M. Matrisian, "Matrix metalloproteinases: a tail of a frog that became a prince," *Nature Reviews Molecular Cell Biology*, vol. 3, no. 3, pp. 207–214, 2002.

[29] R. C. S. Figueira, L. R. Gomes, J. S. Neto, F. C. Silva, I. D. C. G. Silva, and M. C. Sogayar, "Correlation between MMPs and their inhibitors in breast cancer tumor tissue specimens and in cell lines with different metastatic potential," *BMC Cancer*, vol. 9, article 20, 2009.

[30] Z.-D. Wang, C. Huang, Z.-F. Li et al., "Chrysanthemum indicum ethanolic extract inhibits invasion of hepatocellular carcinoma via regulation of MMP/TIMP balance as therapeutic target," *Oncology Reports*, vol. 23, no. 2, pp. 413–421, 2010.

[31] D. Sliva, M. T. Rizzo, and D. English, "Phosphatidylinositol 3-kinase and NF-κB regulate motility of invasive MDA-MB-231 human breast cancer cells by the secretion of urokinase-type plasminogen activator," *The Journal of Biological Chemistry*, vol. 277, no. 5, pp. 3150–3157, 2002.

[32] K. Dano, N. Behrendt, N. Brunner, V. Ellis, M. Ploug, and C. Pyke, "The urokinase receptor. Protein structure and role in plasminogen activation and cancer invasion," *Fibrinolysis*, vol. 8, no. 1, pp. 189–203, 1994.

[33] Q. Yao, J.-R. Luo, J.-H. Chen et al., "Expression and activation of MAPK pathway signaling molecules in human breast cancer cell lines," *Chinese Journal of Cellular and Molecular Immunology*, vol. 20, no. 3, pp. 328–330, 2004.

[34] I.-K. Hong, Y.-M. Kim, D.-I. I. Jeoung, K.-C. Kim, and H. Lee, "Tetraspanin CD9 induces MMP-2 expression by activating p38 MAPK, JNK and c-Jun pathways in human melanoma cells," *Experimental and Molecular Medicine*, vol. 37, no. 3, pp. 230–239, 2005.

[35] F. J. Esteva, A. A. Sahin, T. L. Smith et al., "Prognostic Significance of Phosphorylated P38 Mitogen-Activated Protein Kinase and HER-2 Expression in Lymph Node-Positive Breast Carcinoma," *Cancer*, vol. 100, no. 3, pp. 499–506, 2004.

[36] C.-Y. Ma, W.-T. Ji, F.-S. Chueh et al., "Butein inhibits the migration and invasion of SK-HEP-1 human hepatocarcinoma cells through suppressing the ERK, JNK, p38, and uPA signaling multiple pathways," *Journal of Agricultural and Food Chemistry*, vol. 59, no. 16, pp. 9032–9038, 2011.

[37] S. Huang, L. New, Z. Pan, J. Han, and G. R. Nemerow, "Urokinase plasminogen activator/urokinase-specific surface receptor expression and matrix invasion by breast cancer cells requires constitutive p38α mitogen-activated protein kinase activity," *Journal of Biological Chemistry*, vol. 275, no. 16, pp. 12266–12272, 2000.

[38] G. Sekimoto, K. Matsuzaki, K. Yoshida et al., "Reversible Smad-dependent signaling between tumor suppression and oncogenesis," *Cancer Research*, vol. 67, no. 11, pp. 5090–5096, 2007.

Hindawi Publishing Corporation
Evidence-Based Complementary and Alternative Medicine
Volume 2013, Article ID 947075, 6 pages
http://dx.doi.org/10.1155/2013/947075

Research Article

The Efficacy Study on Si Ni San Freeze-Dried Powder on Sleep Phase in Insomniac and Normal Rats

Yuefeng Li,[1] Angguo Liu,[1] Ying Wang,[2] and Xingke Yan[1]

[1] *Department of Pharmacology of Chinese Materia Medica, Gansu University of Traditional Chinese Medicine, Lanzhou, Gansu 730000, China*
[2] *Department of Pharmacology, Dali University, Dali, Yunnan 671000, China*

Correspondence should be addressed to Xingke Yan; yanxingke@126.com

Received 15 January 2013; Revised 12 March 2013; Accepted 20 March 2013

Academic Editor: Yong Qing Yang

Objectives. To investigate the effect of Si Ni San freeze-dried powder (SNSP) on sleep phase in insomniac and normal rats, to identify its mode of action in improving sleep, and to provide a reliable method for determining pharmacodynamic material basis of Si-Ni-San on improving sleep. *Methods*. Rats were deprived of sleep by using the footplate electrical stimulator to record the rats' electroencephalogram (EEG) and electromyogram (EMG) by using polysomnography (PSG) and copy insomnia model by the method of electric stimulation. Analysis on EEG and EMG was carried out to observe the effects of SNSP on the sleep phase of insomniac and normal rats. *Results*. Rats were treated by intragastric administration (i.g.) consecutively for seven days. The results showed that the total sleep time was extended; meanwhile, SWS2 ($P < 0.01$) and REMS ($P < 0.05$) were mainly prolonged for both insomniac and normal rats. The dates implied SNSP could significantly improve sleep. *Conclusions*. SNSP could prolong SWS2 and REMS, the experimental reproducibility is good, and the dates indicate that SNSP has the sedative function. Study on the effects of SNSP on sleep phases provided a basis for the further studies on effective constituents and the pharmacodynamic mechanism of SNSP.

1. Introduction

With the accelerated pace of modern social life and work pressure, improving sleep quality has increasingly become the focus of attention. Sleep disturbance is a common disease and a variety of diseases' associated symptom. As necessary as sleep is for life, it is an important part of the body recovery, integration and consolidation of memories, indispensable part of health.

Sedative and hypnotic chemical drugs mainly decrease slow-wave sleep 2 (SWS2) and rapid-eye-movement sleep (REMS) and relatively increase slow-wave sleep 1 (SWS1) to prolong the total sleep time (TST). After repeated administration, addiction and dependence will appear. Moreover, many adverse effects such as abstinence symptoms and rebound phenomena will appear following drug withdrawal [1]. Traditional Chinese medicines have important effects in treating insomnia and have fewer side effects compared with chemical drugs. Si Ni San freeze-dry powder (SNSP) is considered a typical medicine.

Si Ni San was first recorded in Shang Han Lun by Zhang Zhongjing in Eastern Han Dynasty, and it consisted of four herbs that are bupleurum, white peony, immature bitter orange, and licorice. It is the basic prescriptions of traditional Chinese medicine (TCM) to alleviate Shaoyang and coordinate liver and spleen. Si Ni San can disperse pathogens, alleviate mental depression, sooth the liver, regulate the spleen, and exhaust the stagnation of qi and blood. In recent years, studies found that SNSP has a unique curative effect in sedative-hypnotic and raising the quality of sleep, after the experiment of sedative hypnotic pharmacodynamics of SNSP [2–5]. According to clinical data of traditional Chinese medicine, insomnia induced by stagnation of Liver-qi accounts for more than 80% of all insomnia patients. Therefore, we select a representative prescription Si Ni San with the function of relieving the depressed liver and harmonizing liver and spleen as the research objective and discuss its pharmacological effects on improving sleep. Compared with chemical drugs, Si Ni San has important effects in treating insomnia and has fewer side effects. Efficacy study on Si

Ni San of sleeping time of rats is carried out, which will provide a basic data for developing new traditional Chinese medicine drugs to improve sleep with high performance and low toxicity and provide information for the further studies on effective constituents and the effecting mechanism of Si Ni San.

The aim of this study is to verify the effect of SNSP on sleeping states of rats by recording the cortical electroencephalography (EEG) of insomniac rats and normal rats and calculating the total duration of each sleeping state, which will provide a reliable method for determining the pharmacodynamic material basis of Si Ni San on improving sleep.

2. Materials and Methods

2.1. Animals. This experiment was performed in the Department of Pharmacology of Chinese Materia Medica, Gansu University of Traditional Chinese Medicine from January 2008 to July 2011.

Male Wistar rats, weighing 220 ± 10 g, were purchased from the Experimental Animal Centre of Gansu University of Traditional Chinese Medicine. Before the study, the animals were acclimated for 5 to 7 days in temperature (20–22°C) and humidity (40–45%) controlled rooms with a 12 h light cycle. All experiments followed a protocol approved by the local Animal Ethics Committee and the local government.

2.2. Instruments. There are 16-channel physiological signal recorder (Stoelting Company, USA); electromagnetically shielded recording chamber; stereotaxic apparatus (Stoelting, USA); plexiglass boxes; footplate electrical stimulator (Lanzhou Research Institute of Electrical Instruments).

2.3. Reagents and Chemicals. Pentobarbital sodium (batch no. 080605) was purchased from Shanghai General Reagent Factory, Shanghai, China. It was prepared with distilled water to a 1% solution before use. Dental acrylic water (08-05-07) and dental acrylic cement (batch no. 09-07-02) were purchased from Gansu Dental Equipment Factory and benzylpenicillin sodium (batch no. A09078537) from the General Pharmaceutical Factory of the Gansu Pharmaceutical Group. Components of SNS, Bupleurum root, radix Paeoniae alba, bitter orange, and licorice were kindly authenticated by Dr. Chengyi Li, Professor of Pharmacognosy.

2.4. Methods

2.4.1. Preparation of Si Ni San Freeze-Dried Powder (SNSP). The mixture (580 g) of Bupleurum root, Radix Paeoniae Alba, bitter orange, and licorice was decocted for 30 min with boiling distilled water (equal to 10-fold the weight of the mixture) and then filtered. The drug residue was decocted for 20 min with boiling distilled water (equal to 6-fold the weight of the mixture) and then filtered. Filtrates from the two decoctions were put together, concentrated to the required volume, and prepared by freeze-drying processed Si Ni San freeze-dried powder. The constituents in Si Ni San freeze-dried powder were detected, and the four major ones of them (including paeoniflorin, naringin, hesperidin, and licorice acid) were quantified by HPLC (Figures 1 and 2, Table 1).

Table 1: The contents of five marker constituents in Si-Ni-San (freeze-dried powder) determined by 3D-HPLC.

Compound	Paeoniflorin	Naringin	Hesperidin	Licorice acid
Contents[a] (mg/g)	507.4 ± 0.03	167.5 ± 0.01	135.1 ± 0.02	136.6 ± 0.02

[a]Data expressed as mean ± SD ($n = 4$).

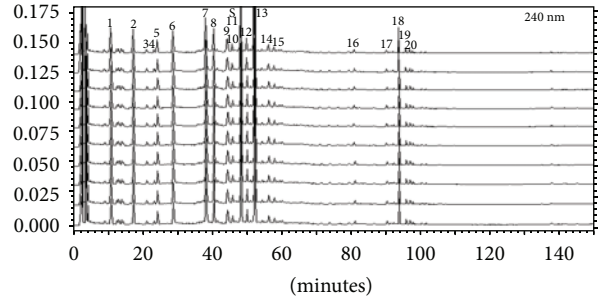

Figure 1: HPLC-FP of Si Ni San (freeze-dried powder).

2.4.2. Rat Sleep Phase Distinguishing Standard and Quantitative Analysis Index. Each 30 s is a segmented time, and the sleep-wake cycle of rats can be divided into four states [6–12] (Table 2) based on the wave form (Figure 3).

2.4.3. Implantation for EEG. After the animals were anesthetized with pentobarbital sodium (45 mg/kg) and fixed in the stereotaxic apparatus, the skull was exposed. Two screw electrodes (1 mm diameter) were implanted into the skull (AP-2, R2; AP+2, R2) as cortical electrodes, and another one was placed at the center of the frontal bone (AP+5, R0) as a ground electrode. The cortical electrodes must touch the dura, but not cut it. The electrodes were connected to a socket by leads, which were fixed on the skull with dental acrylic cement [13–16]. Postoperatively, rats were put into separate plexiglass boxes and housed in an electromagnetically shielded recording chamber under standard conditions of temperature (21 ± 2°C), humidity (40%–45%), lighting (7:00–21:00 h), and ventilation. Each rat was administered intraperitoneally with 45 000 U penicillin for three days and allowed to recover for seven days. Before testing, the EEG recording cable was connected to a socket for 5.5 h for habituation to the experimental conditions. During EEG recording, the behavior of the rats was observed using a video monitoring system.

2.4.4. Replication of Insomniac Model in Rats. On the 8th day after operation, the EEG signals of rats in a nonstressed state were recorded. Recording time lasted for 10 h from 08:00 to 18:00 h. The next day, animals were placed in separate plexiglass boxes (14 mm × 25 mm × 28 cm), on an electrified

Table 2: Sleeping states differentiation.

(a) Waking (W)	During W, EEG signals are different when rats are in different behavioral conditions, and there are two kinds of EEG signals: when rats are moving, climbing, exploring, or scanning, cortical EEG waves are predominantly theta rhythm (6–9 Hz) waves, and when rats are grooming or standing still, cortical EEG waves are predominantly low voltage waves with high frequency.
(b) SWS1 SWS2	When rats are lying, eyes closed, or sleeping, cortical EEG waves are predominantly high amplitude waves (0.5–5 Hz) with sleep spindles (10–15 Hz). During SWS1, high amplitude waves occupied less than 50% of the period. SWS2 is characterized by high amplitude waves with low frequency and also sleep spindles. High amplitude and low frequency waves occupied more than 50% of the period.
(c) Rapid eye-movement sleep (REMS)	REMS is characterized by theta waves which are not markedly different from W. Thus, REMS is determined according to the EEG signal together with the behavior of the rats. Because waking cannot transform into REMS directly, SWS must appear before REMS, while REMS can return to SWS or W directly. Generally, the duration of REMS is less than 3 min. Any separate state lasts for at least 20 s, and a period of 20 s is considered an analytic unit.
(d) TST	Total sleep time (TST) includes the SWS1, SWS2, and REMS.

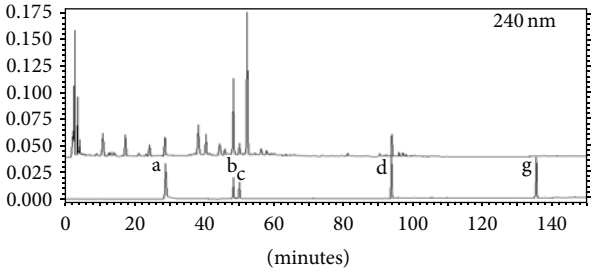

Figure 2: Contrast analysis of the HPLC chromatogram of Si Ni San (freeze-dried powder) and mixed standard substance a: peoniflorin, b: naringin, c: aurantiamarin, d: ammonium glycyrrhizinate salt, e: saikoside A, f: saikoside D, and g: enoxolone.

grid, through which electric shocks were delivered. The shock intensity was 0.5 mA, 1 Hz, and 18 ms long [7]. The electric shocks lasted for 30 s with a 30 min interval between sessions. At the same time, the EEG signals were recorded. After the test, the EEG and EMG were analyzed by the outcome measures of W, SWS1, SWS2, and REMS using the paired Student's *t*-test to check if the insomniac models were replicated successfully.

2.4.5. The Effect of Si Ni San Freeze-Dried Powder on Sleep Phase in Normal Rats. The animals were placed in a quiet laboratory, and the recording time lasted for 4.5 h from 09:30 to 14:00 h. Rats were housed under standard conditions of humidity (40%) and temperature (20°C). Rats' embedded recording electrodes were randomized into two groups, with fifteen rats in each group. Rats were ensured light and dark alternately for 12 h every day and allowed to recover for two days after operation. Rats were administrated with SNSP 5.0 g/kg (containing about paeoniflorin 43 mg, naringin 246 mg, hesperidin 19 mg, and licorice acid 20 mg) for seven consecutive days. Thirty min after the last administration, the EEG recording cable was connected to sixteen physiological signal recorders by a socket and a connecting line, and the sampling rate was 500.000 samples/sec. EEG and EMG signals of each rat were recorded for two days, and recording results were used averagely.

2.4.6. The Effect of Si Ni San Freeze-Dry Powder on Sleep Phase in Insomniac Rats. Rats' EEG and EMG signals were recorded in a nonstressed state on the 8th day after operation, recording under nonstress state of normal rat electroencephalogram (EEG) and electromyogram (EMG) signals. The tracing time was 9:30–17:30 for total 8 h. Nine am the next day, the same rats were given the same volume of distilled water by gavage again, and then the rats were placed in a cage electric gate at the bottom of insomnia stimulator; the rats' feet were bottom stimulated for 8 h. The impact strength was 0.5 mA, 15 ms wide, and 1 Hz, during stimulus EEG, and EMG recording line can automatically interrupt it. Electrical stimulation can be started by two adjustable timers automatically. Thus, each stimulus was 30 s with intervals of 30 min to cause rats' insomnia. Tracing time was from 9:30 to 17:30 after the end of the stimulation. EEG and EMG were analyzed after the test. Animals with the reduced SWS1, SWS2, and TST were used as the experimental mice. After three days, insomnia rats were administrated with SNSP 5.0 g/kg (containing about paeoniflorin 43 mg, naringin 246 mg, hesperidin 19 mg, and licorice acid 20 mg) for seven consecutive days. Thirty min after the last administration, the EEG and EMG signals of each rat in an electrically stimulated state were recorded for 8 h from 09:30 to 17:30 h. The variation characteristics of EEG were analyzed for pre- and poststimulation and different periods of administration.

2.4.7. Statistical Analysis. The first author analyzed the raw data statistically. All the results are analyzed with SPSS 17.0 using the paired Student's *t*-test.

3. Results

3.1. Analytical Results of the Effect of Si Ni San Freeze-Dry Powder on Sleep Phase in Normal Rats (Figure 4, Table 3). Results in Figure 4 and Table 3 were shown after rats were

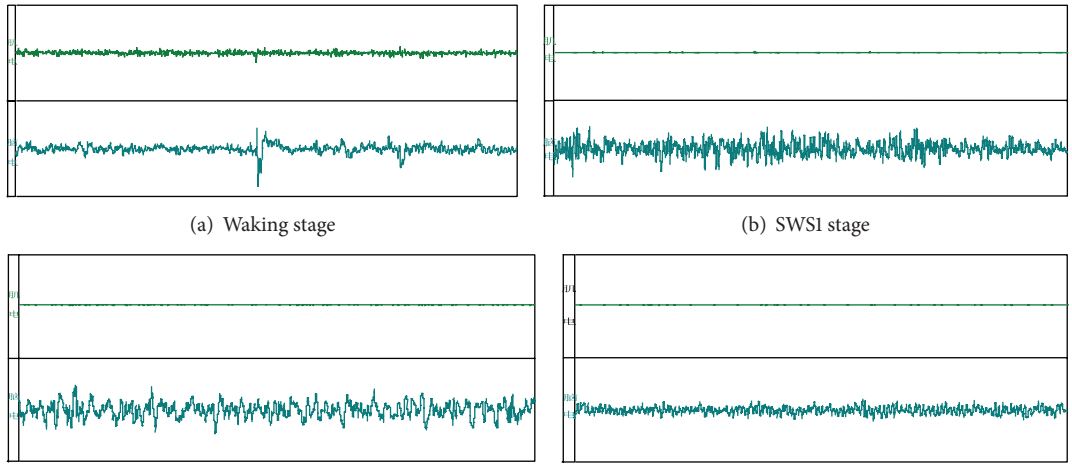

(a) Waking stage (b) SWS1 stage

(c) SWS2 stage (d) REMS stage

Figure 3: EMG and EEG of waking and sleep phase in freely moving rats.

Table 3: The effect of Si-Ni-San freeze-dry powder on sleep phase in normal rats ($\overline{x} \pm$ SD).

	n	W	SWS1	SWS2	SWS	REMS	TST (min)
BG	15	165.93 ± 23.75	83.77 ± 20.04	14.97 ± 14.61	100.27 ± 21.68	3.80 ± 3.95	104.07 ± 23.75
SNSP	15	133.70 ± 30.95**	100.40 ± 29.97	28.67 ± 18.06*	129.07 ± 29.82**	8.73 ± 7.12*	136.30 ± 30.95**
SNSD	15	125.83 ± 30.42	98.33 ±25.21	22.17 ± 15.09*	118.51 ± 24.33**	7.89 ± 6.35*	120.26 ± 35.47*
THS	15	131.52 ± 20.33	88.84 ± 21.03	15.85 ± 15.32	120.35 ± 21.25	6.55 ± 2.78*	125.11 ± 18.58*

** $P < 0.01$, * $P < 0.05$ versus BG: blank group; SNS: Si-Ni-San.
THS (melatonin) tui hei su (melatonin is a natural hypnotic substance that is deep within the brain-like echinacea size "the pineal gland secretion of an amine hormone, so some people call it the pineal gland"); SNSD Si-Ni-San decoction (SNSD: is hypnotic-sedative herbs).

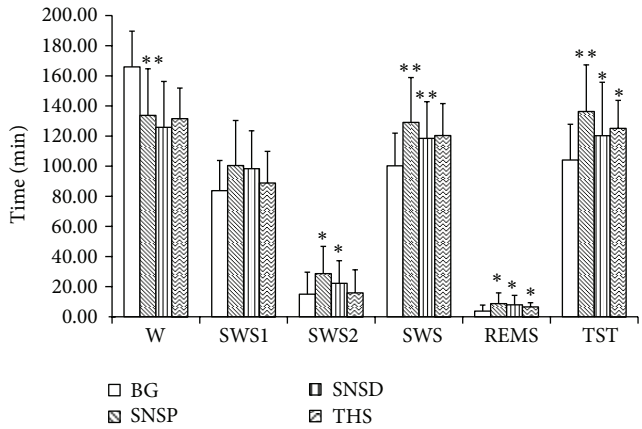

Figure 4: The effect of Si Ni San freeze-dry powder on sleep phase in normal rats.

administrated with SNSP 5.0 g/kg (containing about paeoniflorin 43 mg, naringin 246 mg, hesperidin 19 mg, and licorice acid 20 mg) for seven consecutive days. The time of the awakening of the normal rats' decreased significantly ($P < 0.01$), TST increased markedly ($P < 0.01$), SWS2 ($P < 0.05$), REMS ($P < 0.05$), and SWS increased, and SWS1 was not obviously affected. After the rats were administrated with SNSP for seven consecutive days, the effects of SNSP on prolonging the total sleeping time of mice were significantly stronger than those in the control group, and the effects of SNSP on prolonging the total sleeping time of mice were significantly stronger than those In the Si Ni San decoction (SNSD) and tui hei su (THS) groups.

3.2. Analytical Results of the Effect of Si Ni San Freeze-Dry Powder on Sleep Phase in Insomnia Rats (Figure 3, Table 2). Result in Figure 5 and Table 4 showed that significant differences were found for W, REMS SWS1, SWS2, and TST by comparing pre- with postshock (PrS and PS), indicating that the model was successful in replicating insomnia. The time of the awakening of insomniac rats decreased significantly ($P < 0.01$), but TST was significantly longer than preadministration with Si Ni San freeze-dried powder ($P < 0.01$), SWS2 increased markedly ($P < 0.01$), REMS increased significantly ($P < 0.05$), and SWS1 was not significantly longer than preadministration.

4. Discussion

So far, efficacy study on Si Ni San on sleeping time is limited to the clinical observation phase. In this study, research methods on the central nervous system pharmacology are used, and efficacy study on Si Ni San on sleeping time induced by

Table 4: The effect of Si-Ni-San freeze-dry powder on sleep phase in insomnic rats ($\overline{x} \pm$ SD).

	n	W	SWS1	SWS2	SWS	REMS	TST (min)
PrS	8	268.31 ± 44.02	161.88 ± 41.80	38.94 ± 15.63	199.56 ± 43.56	12.13 ± 5.13	211.69 ± 44.0
PS	8	380.63 ± 21.52**	83.13 ± 22.80**	12.06 ± 5.22**	95.19 ± 22.39**	4.19 ± 2.19**	99.38 ± 21.52**
PA	8	322.25 ± 41.61$^{\#\#}$	114.69 ± 46.97	34.13 ± 12.41$^{\#\#}$	148.81 ± 40.47$^{\#}$	8.94 ± 3.70$^{\#}$	157.75 ± 41.61$^{\#\#}$

$^{**}P < 0.01$, $^{*}P < 0.05$, versus PrS; $^{\#\#}P < 0.01$, $^{\#}P < 0.05$, versus PrS: pre-shock, PS: post-shock, PA: post-administration.

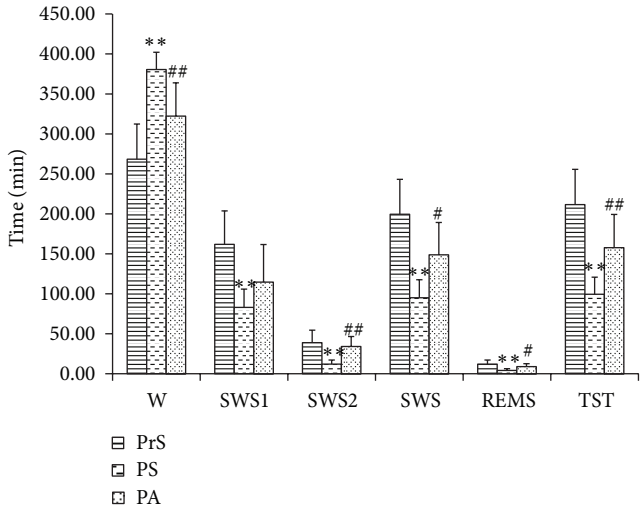

Figure 5: The effect of Si Ni San freeze-dry powder on sleep phase in insomniac rats.

pentobarbital sodium is carried out on mice, which elucidates its pharmacological effects on improving sleep.

The present study aimed to investigate the effect of SNSP at pre- and postshock (PrS and PS) on states of the sleep phase in insomniac Wistar rats using a modern experimental model. The effects of SNSP on prolonging the total sleeping time of rats were significantly stronger than those in the control group. The results showed that Si Ni San can increase markedly the sleeping time and also has a distinct pharmacological action in ameliorating insomnia as compared to synthetic drugs, because Si Ni San acts by extending SWS2 and REMS to increase the total sleeping time, and the effects of SNSP on prolonging the total sleeping time of mice were significantly stronger than those in the Si Ni San decoction (SNSD) and tui hei su (THS) groups. Si Ni San is likely to cause few side effects, and SNSP and SNSD could prolong the mouse sleeping time ($P < 0.01$), especially SNSP ($P < 0.01$), proving that SNSP has a very significant effect on insomnia treatments.

SNSP showed an internal role in improving sleep, which has been found in the cerebrospinal fluid component analysis studies. This explains that SNSP has some unique pharmacological effects on improving sleep role and has great advantages compared to synthetic drugs [1].

This study establishes the basis for clinical use of SNS and provides experimental evidence underlying its mechanism of action.

Abbreviations

SNSP: Si Ni San freeze-dried powder
SNSD: Si Ni San decoction
EEG: Electroencephalogram
EMG: Electromyogram
PSG: Polysomnography
SWS1: Slow-wave sleep 1
SWS2: Slow-wave sleep 2
TST: Total sleep time
REMS: Rapid-eye-movement sleep
TCM: Traditional Chinese medicine
THS: (Melatonin) tui hei su
BG: Blank group
PrS: Preshock
PS: Postshock
PA: Postadministration.

Acknowledgments

This work was supported by three grants from the National Natural Science Foundation (81073077), Ministry of Education, Science and Technology Key Project (212186), and Gansu Province Natural Science Foundation (1010RJZA212). The authors would like to thank the editor and the anonymous referees for the comments and checking the language of the paper.

References

[1] C. Dugovic, "Role of serotonin in sleep mechanisms," *Revue Neurologique*, vol. 157, no. 11, pp. S16–S19, 2001.

[2] K. Song and Y. Q. Mao, "Application of finger-print chromatogram on prescriptions of Chinese medicine," *Materia Medica*, vol. 13, no. 11, pp. 699–700, 2002.

[3] Y. F. Li, X. K. Yan, T. L. Li, and Y. X. Huang, "Studies on chemical components of lyophilized powder of Sini san," *Chinese Traditional and Herbal Drugs*, vol. 41, no. 8, pp. 854–859, 2010.

[4] Y. F. Li, Y. M. Su, and T. L. Li, "Pharmacodynamic material basis of sini powder for improving sleep," *Chinese Journal of Pharmacology and Toxicology*, vol. 43, no. 7, pp. 1361–1365, 2012.

[5] S. S. Liu, T. L. Li, and W. L. Zhu, "Sini bulk phase in the sleep insomnia rats that affect the mouth," *Chinese Medicine*, vol. 5, no. 15, pp. 19–36, 2008.

[6] C. Gottesmann, "The transition from slow-wave sleep to paradoxical sleep: evolving facts and concepts of the neurophysiological processes underlying the intermediate stage of sleep," *Neuroscience and Biobehavioral Reviews*, vol. 20, no. 3, pp. 367–387, 1996.

[7] P. Gauthier, C. Arnaud, G. Gandolfo, and C. Gottesmann, "Influence of a GABA(B) receptor antagonist on the sleep-waking cycle in the rat," *Brain Research*, vol. 773, no. 1-2, pp. 8–14, 1997.

[8] J. Zhang and M. Wang, "Sleep EEG studies," *Foreign Medical*, vol. 20, no. 2, pp. 65–68, 1997.

[9] M. Yoshimoto, H. Higuchi, M. Kamata, K. Yoshida, T. Shimizu, and Y. Hishikawa, "The effects of benzodiazepine (triazolam), cyclopyrrolone (zopiclone) and imidazopyridine (zolpidem) hypnotics on the frequency of hippocampal theta activity and sleep structure in rats," *European Neuropsychopharmacology*, vol. 9, no. 1-2, pp. 29–35, 1999.

[10] K. Saitou, Y. Kaneko, Y. Sugimoto, Z. Chen, and C. Kamei, "Slow wave sleep-inducing effects of first generation H1-antagonists," *Biological and Pharmaceutical Bulletin*, vol. 22, no. 10, pp. 1079–1082, 1999.

[11] L. Imeri, M. Mancia, and M. R. Opp, "Blockade of 5-hydroxytryptamine (serotonin)-2 receptors alters interleukin-1-induced changes in rat sleep," *Neuroscience*, vol. 92, no. 2, pp. 745–749, 1999.

[12] Y. Slisli and R. De Beaurepaire, "Interleukin-1β and calcitonin, but not corticotropin-releasing factor, alter sleep cycles when injected into the rat hypothalamic lateral paraventricular area," *Neuroscience Letters*, vol. 265, no. 1, pp. 29–32, 1999.

[13] H. Depoortere, "Some aspects of the polygraphic studies on sleep-wakefulness cycle in rat," *Waking and Sleeping*, vol. 4, no. 1, pp. 47–62, 1980.

[14] C. H. T. Dong and Z. H. J. Wang, "Animal models of human disease," *Beijing: People's Medical Publishing House*, pp. 348–358, 1982.

[15] X. M. Bao and S. Y. SHu, *Rat Brain Stereotaxic Atlas*, vol. 89, People's Health Publishing House, Beijing, China, 1991.

[16] X. Y. Tian and C. H. T. Dong, "Research on promoting sleep plant extract to adjust rats awakening-sleep cycle," *Brain and Nervous Diseases*, vol. 11, no. 1, pp. 36–38, 2003.

Hindawi Publishing Corporation
Evidence-Based Complementary and Alternative Medicine
Volume 2013, Article ID 393460, 10 pages
http://dx.doi.org/10.1155/2013/393460

Research Article

Electroacupuncture Inhibition of Hyperalgesia in Rats with Adjuvant Arthritis: Involvement of Cannabinoid Receptor 1 and Dopamine Receptor Subtypes in Striatum

Yin Shou,[1] Yang Yang,[1] Ming-Shu Xu,[2] Ying-Qian Zhao,[3] Lin-Bao Ge,[4,5] and Bi-Meng Zhang[1]

[1] *Shanghai First People's Hospital, School of Medicine, Shanghai Jiao Tong University, Shanghai 200080, China*
[2] *Neurobiology Laboratory of Brain Shanghai Research Institute of Acupuncture and Meridians, Shanghai 200030, China*
[3] *Shaanxi College of Traditional Chinese Medicine, Xianyang 712046, China*
[4] *Shanghai Research Institute of Qigong, Shanghai 200030, China*
[5] *Shanghai Research Center of Acupuncture and Meridians, Shanghai 201203, China*

Correspondence should be addressed to Bi-Meng Zhang; pjzhtiger08@yahoo.com.cn

Received 4 March 2013; Revised 28 April 2013; Accepted 10 May 2013

Academic Editor: Yong Qing Yang

Electroacupuncture (EA) has been regarded as an alternative treatment for inflammatory pain for several decades. However, the molecular mechanisms underlying the antinociceptive effect of EA have not been thoroughly clarified. Previous studies have shown that cannabinoid CB1 receptors are related to pain relief. Accumulating evidence has shown that the CB1 and dopamine systems sometimes interact and may operate synergistically in rat striatum. To our knowledge, dopamine D1/D2 receptors are involved in EA analgesia. In this study, we found that repeated EA at Zusanli (ST36) and Kunlun (BL60) acupoints resulted in marked improvements in thermal hyperalgesia. Both western blot assays and FQ-PCR analysis results showed that the levels of CB1 expression in the repeated-EA group were much higher than those in any other group ($P = 0.001$). The CB1-selective antagonist AM251 inhibited the effects of repeated EA by attenuating the increases in CB1 expression. The two kinds of dopamine receptors imparted different actions on the EA-induced CB1 upregulation in AA rat model. These results suggested that the strong activation of the CB1 receptor after repeated EA resulted in the concomitant phenomenon of the upregulation of D1 and D2 levels of gene expression.

1. Introduction

More than 40 disorders have been endorsed by the World Health Organization (WHO) as conditions that can benefit from acupuncture treatment. Acupuncture has been used for several years in the treatment of acute and chronic pain. Thus, of the 3975 acupuncture research articles that have been published from 1991 to 2009, 1647 (41%) focus on pain and analgesia [1]. According to the latest reports in the American journal of Nature Neuroscience, acupuncture has been found to cause the human body to release some natural painkillers [2]. In addition, arthritis-induced hyperalgesia and allodynia have been shown as suppressed by repeated EA in some animal experiments [3]. Several processes have been proposed to explain the EA effects, primarily the pain relief effects. One of the main processes of the pain relief effects is to stimulate the central nervous system to release neurotransmitters or neuromodulators, such as opioid peptides, serotonin, and noradrenaline, into muscles, spinal cord, and brain. These substances can either change the degree of pain scale or promote the release of some other chemicals, such as neurohormones, that influence the neuroimmune system [4]. Taken together, acupuncture analgesia involves a comprehensive course of multichannels, multilevels, and multilinks. Acupuncture signals and the pain transduction channels of the central nervous system have obvious overlapping parts, and thus, acupuncture may influence pain signal transduction in the central nervous

system [5]. In recent years, more and more studies have been conducted to discover the neurobiological mechanisms of acupuncture analgesia.

The endocannabinoid system is of great physiological significance in many aspects. In particular, endocannabinoids play an important role in pain modulation [6]. Earlier studies have demonstrated that the cannabinoid receptor system has therapeutic potential in curing inflammatory diseases, such as rheumatoid arthritis [7]. Electroacupuncture (EA) has been suggested by some researchers to be able to modulate neural responses by decreasing the release of gamma-aminobutyric acid in the brain, most likely through a presynaptic cannabinoid receptor 1 (CB1) mechanism [8]. Given the analgesic effects of EA and the importance of the endocannabinoid system in pain modulation, we hypothesized that the action of EA on inflammatory pain may be attributable to increases in the expression of the CB1 receptor. In order to verify this hypothesis, we established a complete Freund's adjuvant arthritis (AA) rat model and observed the effects of EA at the Zusanli (ST36) and Kunlun (BL60) acupoints on the arthritis and the expression of CB1. In addition, the paw withdrawing latency (PWL) of the AA rats in response to noxious heat was analyzed as an indicator of the thermal pain threshold (PT). We chose to observe the above acupoints because of their common use in acupuncture analgesia [9, 10]. Previous studies have shown that cannabinoid CB1 receptors of the rat corpus striatum, including the nucleus accumbens and caudate nucleus, interact with the dopamine system [11–13] and that dopamine D1/D2 receptors are involved in EA analgesia [14]. Therefore, we also monitored the cross-modulation between CB1 and dopamine D1 and D2 receptors in the analgesic effects of repeated EA.

2. Materials and Methods

2.1. Animals. 60 adult male Sprague-Dawley (SD) rats (age, 5 weeks old; weight, 180 ± 20 g; Shanghai Laboratory Animal Center, Chinese Academy of Sciences, Shanghai, China) were raised in groups of 4–6 per cage under controlled conditions (23 ± 1°C; relative humidity, 50% ± 10%, 12-h/12-h alternating light/dark cycles; and food and water ad libitum). All animals were handled with care to prevent infection and minimize stress. They all exhibited normal PWL values (8–11 s).

2.2. Environmental Adaptation and Grouping. 60 SD male rats were randomized into the following groups with 12 rats per group: sham model (injection of saline), model (injection of Complete Freund's Adjuvant (CFA) to induce arthritis), EA (injection of CFA followed by EA stimulation at ST36 and BL60), EA + AM251 (injection of CFA followed by EA stimulation at ST36 and BL60 and an injection of the CB1-selective antagonist AM251), and WIN55212-2 (injection of CFA followed by an injection of the potent cannabinoid receptor agonist WIN55212-2). At least one week before the experiment, all rats were habituated to a plastic chamber. All of the rats, except for the sham-model group, underwent AA model establishment on the 1st day, and they were taken for environmental adaptation on the 2nd day. On the 3rd day, the rats were subjected to PT measurements. After that, EA (2/100 Hz, 30 s, 1.0, −2.0, −3.0 mA) was applied to the "Zusanli" (ST 36) and "Kunlun" (BL 60) acupoints for 20 min, once every other day starting from the 4th day, for 4 sessions. The other groups of rats were maintained within the same small cages with five holes for their four limbs and their tail. On the 10th day, the rats in the relevant groups were intraperitoneally injected with AM251 (1 mg/kg) [15] or WIN55212-2 (2 mg/kg) [16]. The rest of the rats were intraperitoneally injected with an equal volume of 10% dimethyl sulfoxide according to their weight. One and a half hour later, all rats were decapitated, and specimen preparations were made after the last PT measurements. All animal experiments and protocols were approved by the Committee on the Ethics of Animal experiments of Shanghai University of Traditional Chinese Medicine (approval ID: 08001) and were conducted in accordance with the National Institutes of Health Guide for the Care and Use of Laboratory Animals and the International Association for the Study of Pain's (IASP) guidelines for pain research [17]. We conducted a randomized, controlled experiment with blinded evaluation and statistical analyses of the results. A flow chart of the study protocol is shown in the schematic diagram in Figure 1.

2.3. Reagents. Complete Freund's adjuvant (CFA) was used to induce inflammatory pain. The CB1-selective antagonist AM251 and the potent cannabinoid receptor agonist WIN55212-2 were used to interfere with the natural processes of the cannabinoid CB1 receptors. All of the above reagents were purchased from Sigma-Aldrich Co. LLC (St. Louis, MO, USA).

2.4. Instruments. An IITC Model 336GT paw/tail stimulator analgesia meter was purchased from IITC Life Science Inc. (Woodland Hills, CA, USA). Han's acupoint nerve stimulator LH202H was bought from Beijing Huawei Electronic Industry Development Co., Ltd (Beijing, China). The rodent brain matrix was purchased from Analytical Scientific Instruments (Richmond, CA, USA).

2.5. Induction of the AA Rat Model by CFA. The AA rat model was established on the 1st day of the experiment. It was induced as described previously [18]. Rats were anesthetized with 10% chloral hydrate (40 mg/kg, i. p.).The skin around the site of the injection was sterilized with 75% alcohol. A 25-gauge needle was inserted vertically to penetrate the skin and then turned distally to insert it into the left ankle articular cavity of the hind paw from the gap between the tendo calcaneus and the lateral malleolar fossa until an obvious decrease in resistance was felt. Then, a dose of 0.05 mL of CFA (1 mg/mL), which contained 0.05 mg of heat-killed and dried *Mycobacterium tuberculosis* in 85% paraffin oil and 15% mannide monooleate, was administered to this site. Rats in the sham group were injected with an equal volume of sterile normal saline instead of CFA. CFA is a strong and effective inflammation-inducing agent. It can induce obvious local inflammatory pain that lasts for a long period. A Complete

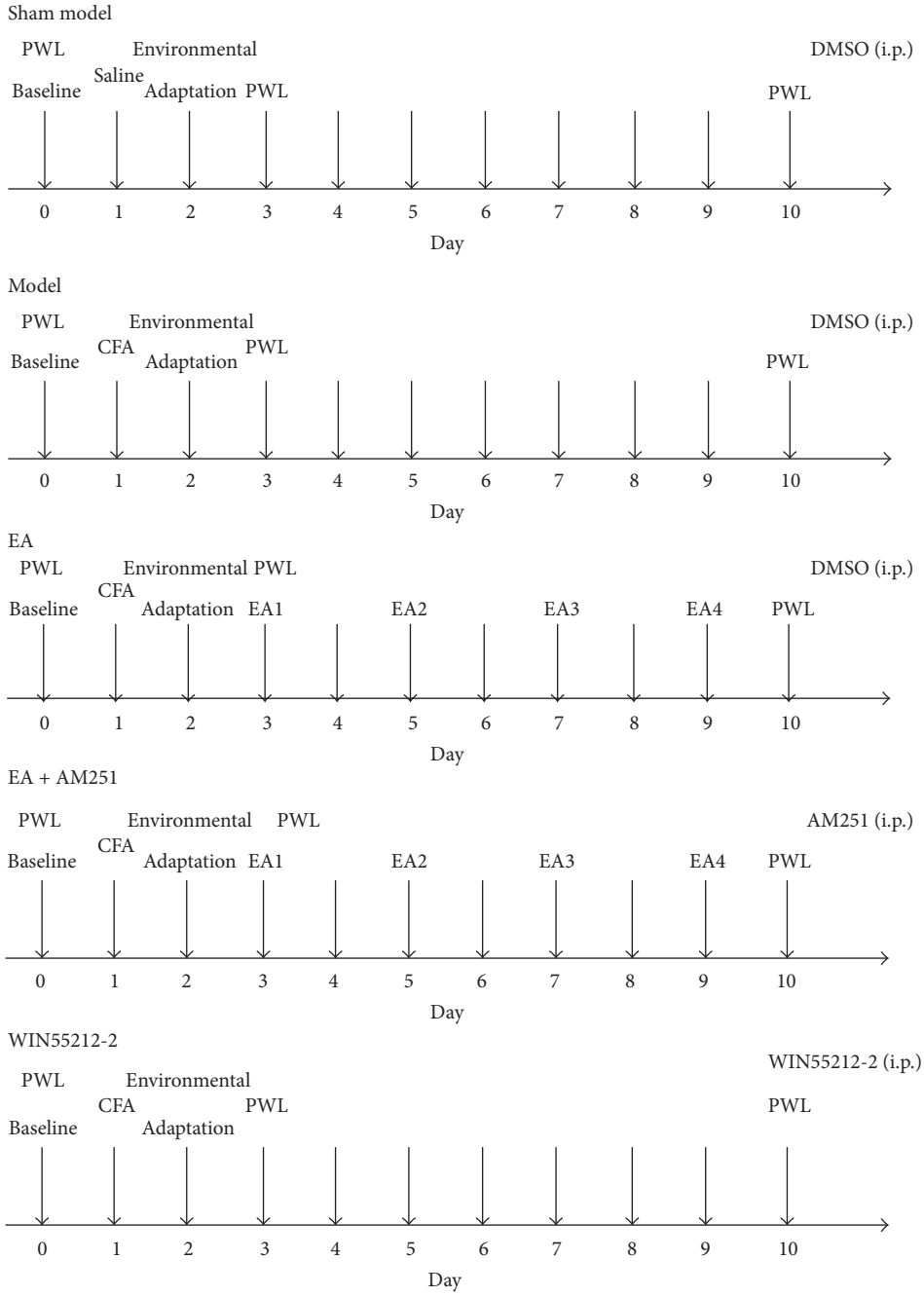

Figure 1: Experimental protocol: 60 rats were used with 12 rats each in 5 groups.

Freund's adjuvant arthritis (AA) model can better reflect the essence of pain and the analgesic courses. It is thought that the exaggerated pain results from peripheral sensitization due to an increase in the sensitivity of the nociceptive primary afferent neurons and central sensitization due to the hyperexcitability of nociceptive neurons in the central nervous system [19–22].

2.6. Blinded PWL Method. Thermal hyperalgesia was evaluated by measuring the latency of the PWL according to a previously described method [23]. The thermal stimulus was produced with the IITC model 336GT paw/tail stimulator analgesia meter. PWL was taken as an indicator of PT. An automatic 20 s cutoff was utilized to avoid tissue injury. Unrestrained and conscious rats were placed in the clear plastic chambers (12 × 12 × 18 cm) on an elevated surface, and they were allowed to habituate to the testing apparatus for 20 min. Then, the radiant heat that was produced by a strong light beam that was applied to the left hind paw near the toes. The time from onset of the radiant heat application to paw withdrawal was regarded as PWL. Each animal was tested three times with an interval of 15 min, and the average

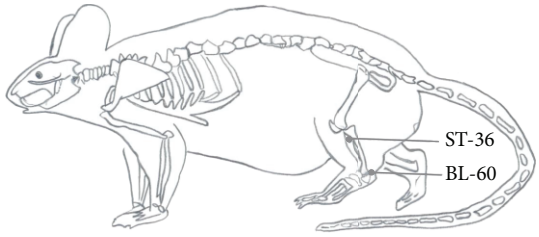

Figure 2: Schematic diagram indicating the selected acupoints, Kunlun (BL 60) and Zusanli (ST36), which correspond to the equivalent acupoints in humans.

was chosen as the baseline of PT. Those animals for which the baselines were higher than 11 s or lower than 8 s were excluded from the experiment. In addition, to control for potential bias, the investigators who performed the behavioral tests were blinded to the actual EA procedure.

2.7. EA Treatment. On the 3rd day, EA stimulation was performed. Sterilized disposable stainless-steel acupuncture needles (0.3 mm in diameter and 25 mm in length; Suzhou Medical Appliance Factory, Suzhou, China) were inserted to a depth of 7 mm into the left hind limb at ST36 and to a 2 mm insertion depth at BL60. As illustrated in Figure 2, Zusanli (ST36) is located 5 mm lateral and distal to the anterior tubercle of the tibia, and Kunlun (BL60) is located at the ankle joint level between the external malleolus and the tendo calcaneus in the hind limb. The needles that were inserted into the acupoints were connected to an EA stimulator. The stimuli were generated with a constant current programmed pulse generator and applied for 30 min. The electric stimuli were set to be square waves with a, 0.5 ms width, and a frequency of 2 or 100 Hz. The intensity was adjusted so that local muscle contractions were seen. Intensities of 1.0, 2.0, and 3.0 mA were applied for 10 min each. EA treatment was given every other day for 7 sessions in total. In order to examine the possible effects of EA, the other groups of rats were placed in the same apparatus, and they had needle insertions into the same acupoints. However, no electrical current was applied to these groups of rats [24].

2.8. Specimen Preparations. All rats were anesthetized and decapitated immediately after the PT measurements. The brains were removed from the skull and then transferred, ventral side up, to an ice-cold Rodent Brain Matrix with 0.5 mm spacing (this process required 1–1.5 min). The nucleus accumbens and striatum were taken from the adjacent slice that was approximately 2.0 mm to 1.5 mm anterior to the bregma with two thin, double-edged razor blades. Following the removal from the matrix, the 2.0 mm brain slices were placed flat onto an ice-cold dissection stage, and specific regions were dissected according to anatomical landmarks as described below. The brain tissues that were isolated from the right and left sides were rapidly frozen in liquid nitrogen and stored at −80°C [25–27].

2.9. Fluorescent Quantitative Reverse Transcription-Polymerase Chain Reaction (FQ-PCR) Analysis. Total RNA was prepared from treated frozen brain tissues that were treated with TRIzol extraction reagent (Shanghai UniBi Tec, Shanghai, China) and reverse transcribed with an M-MLV first-strand cDNA synthesis kit (Promega Corporation, Madison, WI, USA) and oligo(dT) primer, as recommended by the manufacturer. A 50 μL PCR reaction contained 10 μL of 5X Taq PCR Master Mix buffer, 0.5 μL of upstream primer, 0.5 μL of downstream primers, 0.5 μL of TaqMan fluorescence probe, 1 μL of taq polymerase, 0.5 μL of dNTPs, 32 μL ddH_2O, and 5 μL of first-strand cDNA. Quantitative PCR was performed with an iCycler iQ real-time PCR system (Bio-Rad Laboratories, Inc., Hercules, CA, USA). Amplified products were detected with SYBR Green PCR Master Mix (Toyobo Co., Ltd., Osaka, Japan). The sequences of the primer pairs that were specific for each gene are shown in Table 1. The PCR was initially denatured at 50°C for 2 min, which was followed by 40 PCR cycles of 95°C for 5 min, 95°C for 15 s, and 60°C for 45 s. The fold changes in expression were calculated relative to the expression of glyceraldehyde 3-phosphate dehydrogenase (GAPDH), which was used as an endogenous control for normalization. These mRNA levels were quantified by FQ-PCR based on TaqMan technology with the ABI PRISM 7500 Sequence Detection System (Life Technologies Corporation, Grand Island, NY, USA). Fluorescence was measured for each amplification cycle, and the data were analyzed with the $2^{-\Delta\Delta CT}$ method for the relative quantification of expression. Reactions were performed in duplicate [28].

2.10. Western Blot Analysis. The brain tissues were collected and stored for FQ-PCR. Each sample was weighed and homogenized in 100 mL of RIPA Lysis Buffer (Beyotime Institute of Biotechnology, Nanjing, China) containing 0.01 M Tris-HCl buffer (pH 7.6), 0.25 M sucrose, 0.1 M NaCl, 1 mM ethylenediaminetetraacetic acid, and 1 mM phenylmethyl sulfonyl fluoride at 4°C. The supernatant was centrifuged at after 12,000 rpm for 10 min and then examined with western blotting. The pellet was discarded, and the protein concentrations of the supernatant were determined with an Enhanced BCA Protein Assay Kit (Beyotime Institute of Biotechnology). In order to quantify the CB1 protein levels, 40 μg of total protein of each tissue was processed with 2x Tricine-SDS-PAGE loading buffer (Beyotime Institute of Biotechnology), separated on 10% gels with sodium dodecyl sulfate-polyacrylamide gel electrophoresis and then electrotransferred at 300 mA to Immun-Blot polyvinylidene fluoride membranes (EMD Millipore, Corporation, Billerica, MA, USA) for 1 h. Membranes were blocked in Tris-buffered saline with phosphate-buffered saline containing 5% nonfat dried milk and 0.1% Tween 20 for two hours at room temperature. The blocked membranes were incubated overnight at 4°C with the rabbit anti-cannabinoid CB1 receptor polyclonal antibody (1 : 250, Sigma-Aldrich Co, LLC), or the rabbit anti-GAPDH-horseradish peroxidase polyclonal antibody (1 : 4,000, Jingmei, Shanghai, China), which were diluted in Tris-Buffered Saline with Tween (TBST) containing 5% bovine serum albumin. Blots were washed

Table 1: Sequences of primers specific for real-time polymerase chain reaction analyses.

Target sequence	Sequence ($5' \rightarrow 3'$)	Size (bp)
Glyceraldehyde 3-phosphate dehydrogenase (GAPDH)	R: CGAGGGCCCACTAAAGG F: GCTGTTGAGTCACAGGAGCAA	116
Cannabinoid receptor 1 (CB1)	R: TATCGCAATAGTAATCGCTGTGTTG F: GTACATTCTCTGGAAGGCTCACA	182
Dopamine 1 receptor (D1)	R: GGGACTCCAACTCACTCTGC F: CTACATGGAGCCCGAGAAGC	187
Dopamine 2 receptor (D2)	R: GCCAACCTGAAGACACCACTC F: GGAAATGGAGATGCTGTCAAGC	159

extensively in TBST and incubated with goat anti-rabbit IgG that was conjugated to horseradish peroxidase (1 : 10,000, Immunology Consultants Laboratory, Inc., Portland, OR, USA) in TBST/1.25% bovine serum albumin for 1 h at room temperature. Immunocomplexes were visualized with enhanced chemiluminescence detection reagents (Beyotime Institute of Biotechnology) on X-ray films according to the manufacturer's protocol. The GAPDH band was used as an internal control. The relative intensities of each band on the western blots were measured with a computer-assisted imaging analysis system (Quantity One Software, Bio-Rad Laboratories, LTD., Hemel Hempstead, UK) and normalized to the intensity of the housekeeping gene GAPDH. The background in the films was subtracted from the optical density measurements. The experiments were repeated three times, and the values that were obtained for the relative intensities were subjected to statistical analysis [29–33].

2.11. Statistical Analysis. All data were analyzed with a commercial statistical program (SPSS 16.0 for Windows, IBM Corporation, Armonk, NY, USA). Descriptive statistics were expressed as mean ± (standard deviation (SD)). The normal distribution of the data was assessed with a Shapiro-Wilk test. One-way analysis of variance (ANOVA) tests and Wilcoxon W tests were used to evaluate the differences in PT and the levels of expression of CB1 and dopamine receptors among the groups. Post-hoc comparisons, if applicable, were performed with Least Significant Difference tests. Statistical significance was accepted with P values less than 0.05 [31, 34]. Our analyses showed that the blinding procedure was applied successfully. Thus, both the evaluations of the results and the statistical analyses were conducted in a blind fashion.

3. Results

3.1. Cumulative Effects of Repeated EA on AA Rat's Behavioral Hypersensitivity. Thermal hyperalgesia of the hind paw stably occurred one day after the CFA injection [21]. EA that was delivered to the ipsilateral hind limb at the "ST36" and "BL60" acupoints was given 4 times during the experiment. The baseline measures of PWL to radiant heat stimulation on the left ankle articular cavity of the hind paw did not differ between the model and sham-model groups prior to the intra-articular injection.

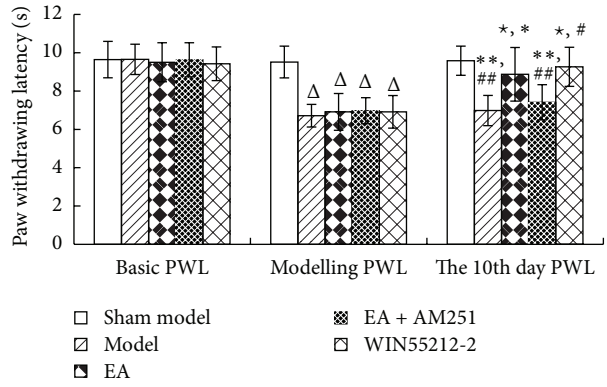

Figure 3: Paw withdrawing latency (PWL) values in the indicated groups. The data are presented as mean ± SD ($n = 12$). $^{\Delta}P < 0.01$ versus sham-model group at the same time-point. $^{\star}P < 0.01$ versus model group at the same time-point. $^{*}P < 0.01$ versus electroacupuncture (EA) group at modeling PWL. $^{\#}P < 0.01$ versus WIN55212-2 group at modeling PWL. $^{**}P < 0.01$ versus EA group at the same time-point. $^{\#\#}P < 0.01$ versus WIN55212-2 group at the same time-point.

Following the unilateral intra-articular injections of CFA, strong thermal hyperalgesia developed within 1 day, and it persisted for over 10 days [17] in the ipsilateral hind paw ($P = 0.00$).The PWL was prolonged after repeated EA ($P = 0.000$), while the analgesic effects of EA were attenuated after an injection of AM251 ($P = 0.001$). There was no significant difference in the analgesic effects between the WIN55212-2 group and the repeated EA groups ($P = 0.346$) (Figure 3).

3.2. Upregulation of the Cannabinoid CB1 Receptor Protein Levels of Expression in the Striatum. The results of the western blot analyses of the cannabinoid CB1 receptor protein levels demonstrated that there was no significant difference between the sham-model group and the model group ($P = 0.190$). The cannabinoid CB1 receptor protein levels were higher in the EA group than in the control group ($P = 0.001$). In addition, the CB1 receptor protein levels of the EA + AM251 group were notably lower than those in the repeated EA group ($P = 0.000$). There were no significant differences in the levels of protein expression of the CB1 receptor between the EA + AM251 group and the sham-model or the model groups ($P = 0.391$) (Figures 4 and 5).

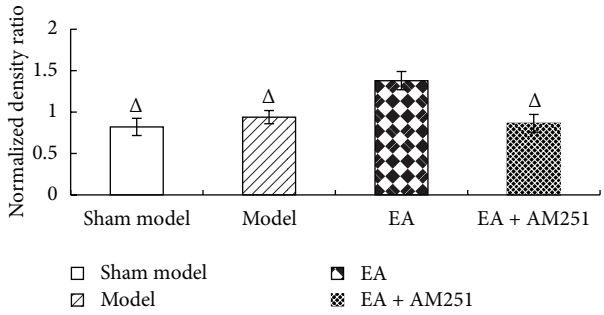

Figure 4: Normalized density ratio of CB1R and GAPDH in the nucleus accumbens and the caudate nucleus of each group (mean ± SD). $^{\Delta}P < 0.01$ versus EA group at the same time-point. CB1R, cannabinoid 1 receptor; GAPDH, glyceraldehyde 3-phosphate dehydrogenase.

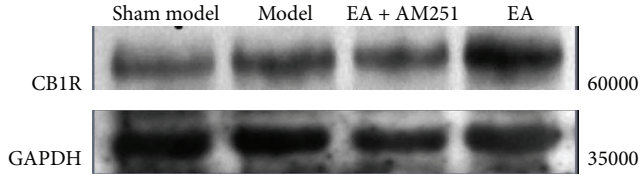

Figure 5: Comparison of the levels of expression of the CB1 receptor in the corpus striatum that were determined by western blot.

3.3. Enhanced Effects of Repeated EA on the Upregulation of CB1 mRNA Expression in the Striatum of AA Rats. The results of the FQ-PCR analyses further demonstrated that the intra-articular injection of CFA produced a marked increase in the levels of CB1 receptor mRNA in the corpus striatum ($P = 0.000$; $P = 0.000$; $P = 0.005$; $P = 0.000$). Most interestingly, repeated EA resulted in a profound enhancement of the upregulation in the levels of CB1 receptor mRNA in AA rats ($P = 0.001$). AM251 markedly reduced the EA-induced upregulation in the CB1 receptor mRNA levels ($P = 0.000$). No significant difference was detected between the EA + AM251 and the model group ($P = 0.319$). The CB1-selective antagonist AM251 inhibited the analgesic effects of repeated EA by reversing the increase in the levels of expression of the CB1 receptor, suggesting that CB1 receptor probably acts as an important mediator of the anti-inflammatory role of EA (Figure 6).

3.4. Increased Effects of Repeated EA on the Upregulation of D1 mRNA Levels in the Striatum of AA Rats. In order to observe whether the cross-modulation of the dopamine system and cannabinoid CB1 receptor influenced the analgesic effects of repeated EA, dopamine D1 and D2-mRNA levels were determined with FQ-PCR analyses. The results revealed that an intra-articular injection of CFA resulted in a significant enhancement of dopamine D1 mRNA expression in the corpus striatum ($P = 0.02$; $P = 0.000$; $P = 0.000$; $P = 0.000$). Following EA treatment, the levels of expression of the D1 receptor mRNA were markedly increased ($P = 0.000$). An

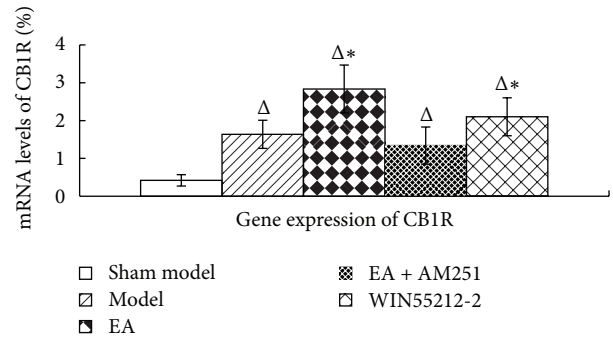

Figure 6: CB1 receptor gene expression in the corpus striatum in rats in the indicated groups. The data are presented as mean ± SD ($n = 5$). FQ-PCR, fluorescence quantitative-polymerase chain reaction. $^{\Delta}P < 0.05$ versus sham-model group at the same time-point. $^{*}P < 0.05$ versus EA + AM251 group at the same time-point.

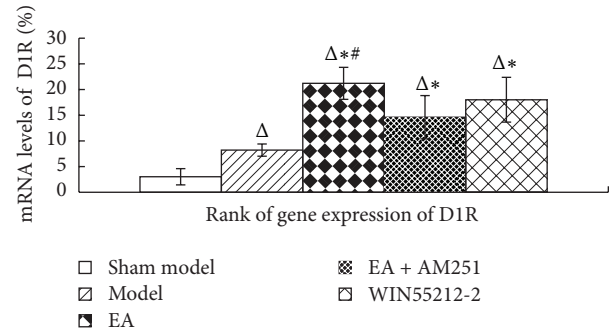

Figure 7: Rank of D1 receptor gene expression in the corpus striatum in the indicated groups. The data are presented as mean ± SD ($n = 5$). $^{\Delta}P < 0.05$ versus sham-model group at the same time-point. $^{*}P < 0.05$ versus model group at the same time-point. $^{\#}P < 0.05$ versus EA + AM251 group at the same time-point.

injection of AM251 resulted in a downregulation of the EA-induced effects ($P = 0.005$). Interestingly, there was no significant difference in the levels of D1 receptor mRNA expression between the repeated-EA group and the WIN55212-2 group ($P = 0.135$). Likewise, no significant difference was detected between the EA + AM251 and the WIN55212-2 groups ($P = 0.113$), indicating that AM251 had little impact on dopamine D1. In our experiment, different aspects of the changes in the expression of the dopamine D1 receptor and the cannabinoid CB1 receptor were observed. However, after an injection of WIN55212-2, D1 gene expression was significantly increased ($P = 0.000$), thus suggesting that, in the AA rat model, a strong activation of the CB1 receptor resulted in a significant change in the dopamine D1 receptor mRNA levels (Figure 7).

3.5. Increased Effects of Repeated EA on the Upregulation of D2 mRNA Levels in the Striatum of AA Rats. The changes in the dopamine D2 mRNA levels, which were similar to those of dopamine D1, were detected during FQ-PCR analyses. They showed that inflammatory pain resulted in a significant enhancement of the levels of dopamine D2 mRNA expression in the corpus striatum ($P = 0.000$; $P = 0.000$; $P = 0.000$;

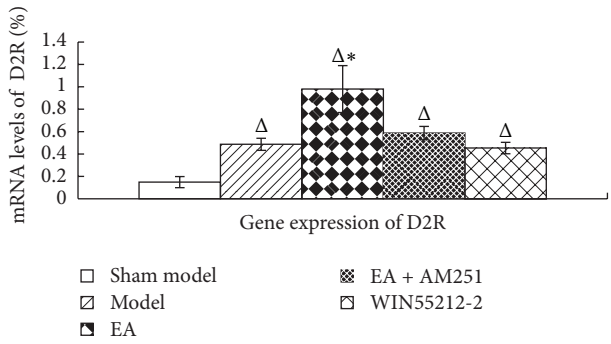

Figure 8: D2 receptor gene expression levels in the corpus striatum in the indicated groups. The data are presented as mean ± SD ($n = 5$). $^{\Delta}P < 0.001$ versus sham-model group at the same time-point. $^{*}P < 0.01$ versus model group at the same time-point.

$P = 0.000$). Likewise, the levels of expression of D2 receptor mRNA were markedly increased ($P = 0.000$) following EA treatment. Interestingly, there was no significant difference in the levels of D2 receptor mRNA expression between the WIN55212-2 and the model groups ($P = 0.624$). AM251 resulted in a downregulation of the EA-induced effects ($P = 0.000$). According to the changes in dopamine D2 mRNA levels, the effects of repeated EA analgesia were different from the analgesic effects of WIN55212-2 ($P = 0.000$). Furthermore, regarding their mRNA levels, the dopamine D2 receptor displayed much more activation than the dopamine D1 receptor did ($P = 0.000$ versus $P = 0.135$, resp.) (Figure 8).

4. Discussion

To the best of our knowledge, this is the first time that a scientific investigation has demonstrated a relationship between repeated EA and cannabinoid CB1 receptor levels in the corpus striatum. In the present study, we established an AA rat model and evaluated the effects of repeated EA stimulation on the experimental arthritis. Our data showed that intra-articular injections of CFA resulted in a robust enhancement of the levels of gene expression of cannabinoid receptors and dopamine D1 and D2 receptors, suggesting that these three receptors are involved in the process of arthritis-induced hyperalgesia and allodynia. After repeated EA treatment, these target genes displayed much higher levels of expression. Furthermore, the combination of repeated EA with the CB1-selective antagonist AM251 resulted in a marked decrease in mRNA levels, indicating that the effects of repeated EA might be associated with an upregulation of cannabinoid CB1 receptors and that EA acts on the cross-talk of the cannabinoid CB1 receptors and the dopamine systems in the striatum. In addition, the analgesia resulting from repeated EA was different from the analgesic effects of WIN55212-2, which is a potent cannabinoid receptor agonist. Most interestingly, the EA-induced up-regulation of the levels of D2 gene expression was much greater than that of the levels of D1 gene expression. However, it was observed that the strong activation of the CB1 receptor after repeated EA might lead to the concomitant phenomenon of an up-regulation of the levels of D1 and D2 gene expression in the AA rat model.

As a traditional Chinese medical technique, acupuncture has become very popular worldwide in the treatment of various illnesses. Our present data consistently indicated that repeated EA at acupoints, such as ST36 and BL60, could control inflammatory pain. Previous studies have also supported our results by showing that analgesic effects are exerted by EA stimulation at the ST36 and BL60 acupoints [9, 10, 35, 36].

Cannabinoid receptors are present not just in vertebrates but also in molluscs, leeches, and other invertebrate groups that have been evolutionarily separated for 500 million years [6]. The fact that natural selection has for so long conserved these receptors is an indication of their physiological importance. Cannabinoid actions in the central nervous system are confined to specific areas, most of which are involved in processing pain signals. One unproved but intriguing idea is that endocannabinoids may set the analgesic tone of the body, with the level of their production acting as a kind of pain thermostat. The use of acupuncture is controversial [37]. Numerous studies have indicated that EA stimulation is effective in relieving the pain of both somatic and visceral origin in humans and animals [38–40], and the ventrolateral column of the periaqueductal gray (PAG) may play a key role in the integration of the physiological responses to somatic and visceral pain [41]. Similar to previous studies, the posterior ventrolateral PAG is considered an important brain area for the antinociceptive effects of cannabinoids [6, 42, 43].

The functional interactions between endocannabinoid and dopaminergic systems may contribute to striatal signaling [44, 45]. CB1 receptors are colocalized with D1 or D2 receptors on the same population of striatal membranes, and they can interact at the level of G-protein/adenylyl cyclase signal transduction [46]. The endogenous cannabinoid system is involved in regulating striatal dopamine release [47]. The activation of postsynaptic dopamine receptors controls endocannabinoid mobilization by acting on presynaptic CB1 receptors and thus modulating glutamate release differently in glutamate terminals that project to D1 and D2 cells [48]. However, the endocannabinoid system is unlikely to directly affect dopamine release. Instead, it can modify dopamine transmission through transsynaptic mechanisms. These mechanisms involve gamma-aminobutyric acid (GABA) ergic and glutamatergic synapses, as well as converging signal transduction cascades of the cannabinoid and dopamine receptors. The dopamine and endocannabinoid systems exert mutual control on each other [49].

In the striatum, CB1 receptor activation has been shown to promote long-lasting changes in synaptic activity at both corticostriatal and striatonigral/pallidal synapses [50–52]. This activation also increases both the levels of extracellular dopamine and the activity of dopamine neurons [53, 54]. Cannabinergic signalling may lead to the release of dopamine, which can act through dopamine D1-like receptors as a negative feedback mechanism to counteract the effects of the activation of the cannabinoid CB1 receptor [49]. The elimination of dopamine D1 receptors has opposite effects on cannabinoid-mediated ERK1/2 signaling [55]. In

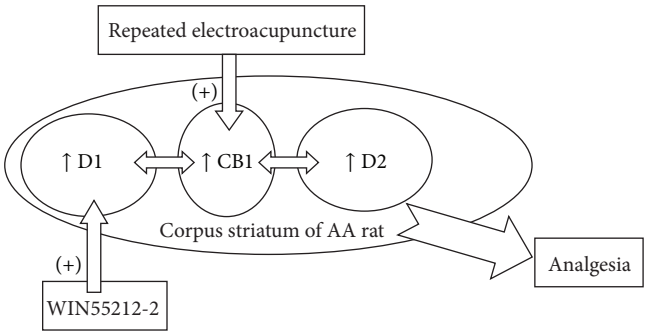

Figure 9: A hypothetical diagram illustrating the EA action that is mediated by CB1 in the adjuvant arthritis (AA) rat. The intra-articular injection of Complete Freund's adjuvant (CFA) promotes the expression of CB1, D1, and D2. EA stimulation at specific acupoints results in a much higher expression of these three receptors, but the CB1 receptor antagonist AM251 can reverse these antinociceptive effects. Compared to the action of WIN55212-2, EA mainly produces its effects by upregulating the cross-modulation of dopamine receptors and CB1 in the corpus striatum, while WIN55212-2, which is a potent CB1 receptor agonist, exerts its function on the relationship between CB1 and D1 for pain relief.

addition, dopaminergic signaling through dopamine D2-like receptors may lead to the up-regulation of cannabinergic signaling, which is likely to represent a negative feedback on dopaminergic signaling [49].

CB1 receptors that are located in the corpus striatum are involved in a number of biological processes, including analgesia [50], addiction [56], and motor deficits [46]. The corpus striatum has always been regarded as an active area that is related to EA analgesia [14]. Our results demonstrated that the CB1-selective antagonist AM251 could attenuate the analgesic effects of repeated EA by reversing the increased expression of the CB1 receptor, suggesting that the CB1 receptor plays an important role in EA analgesia. The two kinds of dopamine receptors have different influences on the EA-induced CB1 up-regulation in the AA rat model. The change in the EA-induced up-regulation of the levels of D2 gene expression was much greater than that of the D1 gene expression. It was also observed that the strong activation of the CB1 receptor after repeated EA might lead to the concomitant phenomenon of the up-regulation of the D1 and D2 levels of gene expression in the AA rat model. A hypothetical diagram of the anti-inflammatory actions of EA that are mediated by the cross-modulation of CB1 and the dopamine receptors in the AA rat model is shown in Figure 9.

In conclusion, our results indicated, for the first time, that EA treatment at Zusanli (ST36) and Kunlun (BL60) produced strong antinociceptive effects in rats with CFA-induced arthritis, at least partially, through an up-regulation in the levels of the cannabinoid CB1 receptor expression. The relationship between CB1 receptors and dopamine receptors may play a role in the analgesia that is associated with repeated EA. In addition, the analgesic effects of repeated EA were different from the analgesic effects of the CB1-selective agonist WIN55212-2. While WIN55212-2 exerted its function on the relationship between CB1 and D1 for pain relief, EA wields its effect by upregulating the cross-modulation of dopamine receptors and CB1 in the striatum. Thus, repeated EA analgesia had a more complex mechanism.

Authors' Contribution

Yin Shou and Yang Yang contributed equally to this paper.

Conflict of Interests

The authors declare they have no conflicts of interests with regard to this paper.

Acknowledgments

This project was supported by Grants from the National Basic Research Program of China (no. 2009CB522900), National Natural Science Foundation of China (no. 81001547), Shanghai Leading Academic Discipline Project (no. S30304), Shanghai Municipal Natural Science Foundation (no. 07DZ19722-5), and Shanghai Famous TCM academic research project (no. ZYSNXD-CC-MZY023).

References

[1] J. S. Han, "Acupuncture analgesia: areas of consensus and controversy," *Pain*, vol. 152, no. 3, pp. S41–S48, 2011.

[2] N. Goldman, M. Chen, T. Fujita et al., "Adenosine A1 receptors mediate local anti-nociceptive effects of acupuncture," *Nature Neuroscience*, vol. 13, no. 7, pp. 883–888, 2010.

[3] W. X. Li, Y. R. Huang, L. D. Lei et al., "Effects of electroacupuncture and manual acupuncture interventions on contents of serum inflammatory cytokines in rats with chronic adjuvant arthritis," *Zhen Ci Yan Jiu*, vol. 37, no. 4, pp. 271–276, 2012.

[4] K. Wang, R. Zhang, X. Xiang et al., "Differences in neural-immune gene expression response in rat spinal dorsal horn correlates with variations in electroacupuncture analgesia," *PLoS ONE*, vol. 7, no. 8, Article ID e42331, 2012.

[5] S. M. Wang, Z. N. Kain, and P. White, "Acupuncture analgesia: I. The scientific basis," *Anesthesia and Analgesia*, vol. 106, no. 2, pp. 602–610, 2008.

[6] I. Kaufmann, G. Schelling, C. Eisner et al., "Anandamide and neutrophil function in patients with fibromyalgia," *Psychoneuroendocrinology*, vol. 33, no. 5, pp. 676–685, 2008.

[7] D. Richardson, R. G. Pearson, N. Kurian et al., "Characterisation of the cannabinoid receptor system in synovial tissue and fluid in patients with osteoarthritis and rheumatoid arthritis," *Arthritis Research and Therapy*, vol. 10, no. 2, article R43, 2008.

[8] L. W. Fu and J. C. Longhurst, "Electroacupuncture modulates vlPAG release of GABA through presynaptic cannabinoid CB1 receptors," *Journal of Applied Physiology*, vol. 106, no. 6, pp. 1800–1809, 2009.

[9] C. P. Huang, H. N. Chen, H. L. Su et al., "Electroacupuncture reduces carrageenan- and CFA -Induced inflammatory pain accompanied by changing the expression of Nav1. 7 and Nav 1. 8, rather than Nav1. 9, in mice dorsal root ganglia," *Evidence-Based Complementary and Alternative Medicine*, vol. 2013, Article ID 312184, pp. 1–8, 2013.

[10] K. H. Chang, R. Won, I. Shim et al., "Effects of electroacupuncture at BL60 on formalin-induced pain in rats," *Evidence-Based*

Complementary and Alternative Medicine, vol. 2012, no. 1, pp. 1–7, 2012.

[11] C. Kortleven, L. C. Bruneau, and L. E. Trudeau, "Neurotensin inhibits glutamate-mediated synaptic inputs onto ventral tegmental area dopamine neurons through the release of the endocannabinoid 2-AG," *Neuropharmacology*, vol. 63, no. 6, pp. 983–991, 2012.

[12] M. A. EI Khoury, V. Gorgievski, L. Moutsimilli et al., "Interactions between the cannabinoid and dopaminergic systems: evidence from animal studies," *Prog Neuropsychopharmacol Biology Psychiatry*, vol. 38, no. 1, pp. 36–50, 2012.

[13] A. L. Terzian, F. Drago, C. T. Wotjak, and V. Micale, "The dopamine and cannabinoid interaction in the modulation of emotions and cognition: assessing the role of cannabinoid CB1 receptor in curons expressing dopamine D1receptors," *Frontiers in Behavioral Neuroscience*, vol. 5, p. 49, 2011.

[14] Y. Liang, C. X. Wang, J. Q. Fang et al., "Effect of pre-electroacupuncture at Zusanli(ST 36) on DA and 5-HT contents and their ratio in hypothalamus and striatum in exercise rats," *Zhongguo Zhen Jiu*, vol. 31, no. 12, pp. 1101–1105, 2011.

[15] K. A. B. Simão Da Silva, A. F. Paszcuk, G. F. Passos et al., "Activation of cannabinoid receptors by the pentacyclic triterpene α,β-amyrin inhibits inflammatory and neuropathic persistent pain in mice," *Pain*, vol. 152, no. 8, pp. 1872–1887, 2011.

[16] D. Kalbasi Anaraki, S. Sianati, M. Sadeghi et al., "Modulation by female sex hormones of the cannabinoid-induced catalepsy and analgesia in ovariectomized mice," *European Journal of Pharmacology*, vol. 586, no. 1–3, pp. 189–196, 2008.

[17] C. I. Svensson, M. Zattoni, and C. N. Serhan, "Lipoxins and aspirin-triggered lipoxin inhibit inflammatory pain processing," *Journal of Experimental Medicine*, vol. 204, no. 2, pp. 245–252, 2007.

[18] U. Heilborn, O. G. Berge, L. Arborelius, and E. Brodin, "Spontaneous nociceptive behaviour in female mice with Freund's complete adjuvant- and carrageenan-induced monoarthritis," *Brain Research*, vol. 1143, no. 1, pp. 143–149, 2007.

[19] J. I. Chung, S. Barua, B. H. Choi et al., "Anti-inflammatory effect of low intensity ultrasound (LIUS) on complete Freund's adjuvant -induced arthritis synovium," *Osteoarthritis and Cartilage*, vol. 20, no. 4, pp. 314–322, 2012.

[20] W. M. Li, K. M. Cui, N. Li et al., "Analgesic effect of electroacupuncture on complete Freund's adjuvant-induced inflammatory pain in mice: a model of antipain treatment by acupuncture in mice," *Japanese Journal of Physiology*, vol. 55, no. 6, pp. 339–344, 2005.

[21] S. Shan, M. Y. Qi-Liang, C. Hong et al., "Is functional state of spinal microglia involved in the anti-allodynic and anti-hyperalgesic effects of electroacupuncture in rat model of monoarthritis?" *Neurobiology of Disease*, vol. 26, no. 3, pp. 558–568, 2007.

[22] R. R. Ji and C. J. Woolf, "Neuronal plasticity and signal transduction in nociceptive neurons: implications for the initiation and maintenance of pathological pain," *Neurobiology of Disease*, vol. 8, no. 1, pp. 1–10, 2001.

[23] Y. Zhang, A. Li, J. Xin et al., "Involvement of spinal serotonin receptors in electroacupuncture anti-hyperalgesia in an inflammatory pain rat model," *Neurochemical Research*, vol. 36, no. 10, pp. 1785–1792, 2011.

[24] J. R. T. Silva, M. L. Silva, and W. A. Prado, "Analgesia induced by 2- or 100-Hz electroacupuncture in the rat tail-flick test depends on the activation of different descending pain inhibitory mechanisms," *Journal of Pain*, vol. 12, no. 1, pp. 51–60, 2011.

[25] K. Yoshimoto, Y. Watanabe, M. Tanaka et al., "Serotonin2c receptors in the nucleus accumbens are involved in enhanced alcohol-drinking behavior," *European Journal of Neuroscience*, vol. 35, pp. 1368–1380, 2012.

[26] J. Q. Ren, Y. Jiang, Z. Wang et al., "Prenatal l-DOPA exposure produces lasting changes in brain dopamine content, cocaine-induced dopamine release and cocaine conditioned place preference," *Neuropharmacology*, vol. 60, no. 2-3, pp. 295–302, 2011.

[27] S. K. Segall, A. G. Nackley, L. Diatchenko et al., "Comt1 genotype and expression predicts anxiety and nociceptive sensitivity in inbred strains of mice," *Genes, Brain and Behavior*, vol. 9, no. 8, pp. 933–946, 2010.

[28] A. F. Paszcuk, R. C. Dutra, K. Silva et al., "Cannabinoid agonists inhibit neuropathic pain induced by brachial plexus avulsion in mice by affecting glial cells and MAP Kinases," *PLOS ONE*, vol. 6, no. 9, Article ID e24034, 2011.

[29] W. L. Mi, Q. L. Mao-Ying, X. W. Wang et al., "Involvement of spinal neurotrophin-3 in electroacupuncture analgesia and inhibition of spinal glial activiation in rat model of monoarthritis," *The Journal of Pain*, vol. 12, no. 9, pp. 974–984, 2011.

[30] D. C. Choi, J. Y. Lee, Y. J. Moon, S. W. Kim, T. H. Oh, and T. Y. Yune, "Acupuncture-mediated inhibition of inflammation facilitates significant functional recovery after spinal cord injury," *Neurobiology of Disease*, vol. 39, no. 3, pp. 272–282, 2010.

[31] Y. D. Xu, J. M. Cui, Y. Wang et al., "Proteomic analysis reveals the deregulation of inflammation- related proteins in acupuncture treated rats with asthma onset," *Evidence- Based Complementary and Alternative Medicine*, vol. 2012, Article ID 850512, pp. 1–14, 2012.

[32] T. F. Su, L. H. Zhang, M. Peng et al., "Cannabinoid CB2 receptors contribute to upregulation of β-endorphin inflamed skin tissues by electroacupuncture," *Molecular Pain*, vol. 7, p. 98, 2011.

[33] J. Zhang, L. Chen, T. Su et al., "Electroacupuncture increases CB2 receptor expression on keratinocytes and infiltrating inflammatory cells in inflamed skin tissues of rats," *Journal of Pain*, vol. 11, no. 12, pp. 1250–1258, 2010.

[34] D. Groppetti, A. M. Pecile, P. Sacerdote et al., "Effectiveness of electroacupuncture analgesia compared with opioid administration in a dog model: a pilot study," *British Journal of Anaesthesia*, vol. 107, no. 4, pp. 612–618, 2011.

[35] Y. F. Chen, T. F. He, W. J. Yang, S. H. Zhang, C. Y. Zhang, and L. B. Li, "Electroacupuncture inhibits inflammation reaction by upregulating vasoactive intestinal peptide in rats with adjuvant-induced arthritis," *Evidence-Based Complementary and Alternative Medicine*, vol. 2011, Article ID 290489, 2011.

[36] Z. D. Zhang, C. S. Wang, G. Y. Gu et al., "The effects of electroacupuncture at the ST36(Zusanli) acupoint on Cancer pain and transient receptor potential vanilloid subfamily 1 expression in walker 256 tumor-bearing rats," *Anesthesia and Analgesia*, vol. 114, no. 4, pp. 879–885, 2012.

[37] J. Mooney, "Acupuncture review skepticism," *Pain*, vol. 152, no. 9, p. 2184, 2011.

[38] M. S. Lee and E. Ernst, "Acupuncture for pain: an overview of Cochrane reviews," *Chinese Journal of Integraive Medicine*, vol. 17, pp. 187–189, 2011.

[39] P. White, G. Lewith, P. Prescott, and J. Conway, "Acupuncture versus placebo for the treatment of chronic mechanical neck pain. A randomized, controlled trial," *Annals of Internal Medicine*, vol. 141, no. 12, 2004.

[40] K. M. Cui, W. M. Li, X. Gao, K. Chung, J. M. Chung, and G. C. Wu, "Electro-acupuncture relieves chronic visceral

hyperalgesia in rats," *Neuroscience Letters*, vol. 376, no. 1, pp. 20–23, 2005.

[41] K. A. Keay, "Convergence of deep somatic and visceral nociceptive information onto a discrete ventrolateral midbrain periaqueductal gray region," *Neuroscience*, vol. 61, no. 4, pp. 727–732, 1994.

[42] G. T. Dodd, A. A. Worth, D. J. Hodkinson et al., "Central functional response to the novel peptide cannabionid, hemopressin," *Neuropharmacology*, vol. 71, pp. 27–36, 2013.

[43] A. R. Wilson-Poe, M. M. Morgan, S. A. Aicher et al., "Distribution of CB1 cannabinoid receptors and their relationship with mu-opioid receptors in the rat periaqueductal gray," *Neuroscience*, vol. 213, pp. 191–200, 2012.

[44] A. B. Martín, E. Fernandez-Espejo, B. Ferrer et al., "Expression and function of CB1 receptor in the rat striatum: localization and effects on D1 and D2 dopamine receptor-mediated motor behaviors," *Neuropsychopharmacology*, vol. 33, no. 7, pp. 1667–1679, 2008.

[45] G. Navarro, S. Ferré, A. Cordomi et al., "Interactions between intracellular domains as key determinants of the quaternary structure and function of receptor heteromers," *Journal of Biological Chemistry*, vol. 285, no. 35, pp. 27346–27359, 2010.

[46] J. P. Meschler and A. C. Howlett, "Signal transduction interactions between CB1 cannabinoid and dopamine receptors in the rat and monkey striatum," *Neuropharmacology*, vol. 40, no. 7, pp. 918–926, 2001.

[47] M. G. Bossong, B. N. M. Van Berckel, R. Boellaard et al., "Δ9-tetrahydrocannabinol induces dopamine release in the human striatum," *Neuropsychopharmacology*, vol. 34, no. 3, pp. 759–766, 2009.

[48] V. M. Andre, C. Cepeda, D. M. Cummings et al., "Dopamine modulation of excitatory currents in the striatum is dictated by the expression of D1 or D2 receptors and modified by endocannabinoids," *European Journal of Neuroscience*, vol. 31, pp. 14–28, 2010.

[49] M. Van Der Stelt and V. Di Marzo, "The endocannabinoid system in the basal ganglia and in the mesolimbic reward system: implications for neurological and psychiatric disorders," *European Journal of Pharmacology*, vol. 480, no. 1–3, pp. 133–150, 2003.

[50] J. Ronesi and D. M. Lovinger, "Induction of striatal long-term synaptic depression by moderate frequency activation of cortical afferents in rat," *Journal of Physiology*, vol. 562, no. 1, pp. 245–256, 2005.

[51] G. L. Gerdeman, J. Ronesi, and D. M. Lovinger, "Postsynaptic endocannabinoid release is critical to long-term depression in the striatum," *Nature Neuroscience*, vol. 5, no. 5, pp. 446–451, 2002.

[52] A. C. Kreitzer and R. C. Malenka, "Endocannabinoid-mediated rescue of striatal LTD and motor deficits in Parkinson's disease models," *Nature*, vol. 445, no. 7128, pp. 643–647, 2007.

[53] E. D. French, "Δ9-Tetrahydrocannabinol excites rat VTA dopamine neurons through activation of cannabinoid CB1 but not opioid receptors," *Neuroscience Letters*, vol. 226, no. 3, pp. 159–162, 1997.

[54] G. Tanda, F. E. Pontieri, and G. Di Chiara, "Cannabinoid and heroin activation of mesolimbic dopamine transmission by a common μ1 opioid receptor mechanism," *Science*, vol. 276, no. 5321, pp. 2048–2050, 1997.

[55] T. L. Daigle, W. C. Wetsel, and M. G. Caron, "Opposite function of dopamine D1 and NMDA receptors in striatal cannabinoid-mediated signaling," *European Jouranl of Neuroscience*, vol. 34, no. 9, pp. 1378–1389, 2011.

[56] L. Adermark, S. Jonsson, M. Ericson et al., "Intermittent ethanol consumption depresses endocannabinoid-signaling in the dorsolateral striatum of rat," *Neuropharmacology*, vol. 61, no. 7, pp. 1160–1165, 2011.

Hindawi Publishing Corporation
Evidence-Based Complementary and Alternative Medicine
Volume 2013, Article ID 709865, 10 pages
http://dx.doi.org/10.1155/2013/709865

Research Article

Evaluation of the Wound Healing Potential of *Resina Draconis (Dracaena cochinchinensis)* in Animal Models

Huihui Liu,[1] Shaohui Lin,[2] Dan Xiao,[1] Xiao Zheng,[1] Yan Gu,[1] and Shanyu Guo[1]

[1] *Department of General Surgery, Ninth People's Hospital, Shanghai Jiao Tong University School of Medicine, Shanghai 200011, China*
[2] *Department of Geriatrics, Ninth People's Hospital, Shanghai Jiao Tong University School of Medicine, Shanghai 200011, China*

Correspondence should be addressed to Shanyu Guo; guoshyu@sina.com

Received 5 February 2013; Revised 7 April 2013; Accepted 8 April 2013

Academic Editor: Yong Qing Yang

Resina Draconis (RD) is a type of dragon's blood resin obtained from *Dracaena cochinchinensis* (Lour.) S.C. Chen (Yunnan, China). It has been used as a medicine since ancient times by many cultures. The ethanolic extract of *Resina Draconis* (RDEE) was evaluated for its wound-healing activity using excision and incision wound models in rats. Group I, the control group, was treated with ointment base. Group II, which served as a reference standard, was treated with moist exposed burn ointment (MEBO). Group III was treated with RDEE. The parameters observed were percentage of wound contraction, epithelialization period, tensile strength, histopathological studies, microvessel density (MVD), and the expression of vascular endothelial growth factor (VEGF) and transforming growth factor-β1 (TGF-β1). The group treated with RDEE showed significantly better wound contraction and better skin-breaking strength as compared with the control group. The results of histopathological examination, MVD, and the expression levels of growth factors supported the outcome of the wound models as well. The present study provided a scientific rationale for the traditional use of RD in the management of wounds.

1. Introduction

Skin healing is a complex process that involves inflammation, reepithelization, angiogenesis, granulation tissue formation, and deposition of interstitial matrix, beside other events carried out by different types of cells, such as keratinocytes, fibroblasts, inflammatory cells, and endothelial cells. There are three stages of the process of wound healing: inflammation, proliferation, and remodeling. The proliferative phase is characterized by angiogenesis, collagen deposition, granulation tissue formation, epithelization, and wound contraction. Angiogenesis involves new blood vessel growth from endothelial cells. In fibroplasia and granulation tissue formation, fibroblasts excrete collagen and fibronectin to form a new extracellular matrix. Subsequently epithelial cells crawl across the wound bed to cover it and the wound is contracted by myofibroblasts, which grip the wound edges and undergo contraction using a mechanism similar to that in smooth muscle cells. The final stage of wound healing is remodeling or maturation of the granulation tissue into mature connective tissue and/or scar. Alterations in any of these steps can lead to healing delay or even the inability to heal completely [1]. Current methods used to treat wounds include debridement, irrigation, antibiotics, tissue grafts, and proteolytic enzymes, which possess major drawbacks and unwanted side effects. The use of traditional medicinal remedies and plants in the treatment of burns and wounds is an important aspect of health management and at the same time is an effective way to provide cheaper healthcare options [2].

Since ancient times, people have used plants and preparations thereof to accelerate the wound-healing process [3]. Recently, the interest of using alternative therapies and natural remedies in wound management has rapidly increased. There are hundreds of medicinal plants that have long histories of curative properties against various diseases and ailments. However, their use is merely based on tradition, without any scientific evidence of their efficacy or knowledge about putative active compounds or their mode of actions. *Resina Draconis* is a red resin from tree stem of *Dracaena cochinchinensis* (Lour.) S.C. Chen, growing in Yunnan and Guangxi provinces in China, belonging to theLiliaceae family, *genus Dracaena*. It was discovered by Cai and Xu [4] in

1979 that it could serve as a substitute for Sanguis Draconis, a precious crude medicine recorded in the official Chinese pharmacopoeia named as "dragon's blood" [5]. In Chinese medicine, *Resina Draconis* is a major component of the well-known hemostatic preparation "Yun Nan Bai Yao," so, it is considered important for its potential application in Chinese medical practice. As a "panacea of blood activating" resin, RD has great medicinal value, and the main biological activity comes from phenolic compounds [6]. Pharmacological studies have showed that RD has positive effects on treatment of blood stasis syndrome, trauma, tumors, inflammation, gynecopathy, allergic dermatitis, and so on. It can promote blood circulation and serve as an antithrombotic, antioxidant, antiseptic, and anti-inflammation compound [7]. The ethanolic extracts of *Resina Draconis* possessed potential antithrombotic properties, affecting platelet aggregation and thus having anticoagulation activities [8]. All these studies indicate that *Resina Draconis* has enormous potential for further study.

It is well known that one kind of traditional Chinese medicine (TCM) usually contains a great number of components, which, all together, contribute to therapeutic effects. Despite that Chen et al. [9] have studied the wound-healing activity of dragon's blood (*Croton lechleri* sap), no scientific investigation is conducted on *Resina Draconis*'s wound-healing potential. Hence, in this study, we aimed to further investigate the wound-healing effects of RD using the excision and incision wound models, and to explore the possible mechanisms.

2. Materials and Methods

2.1. Preparation of Plant Extracts. Crude *Resina Draconis* was provided by the pharmacy department of No. 9 People's Hospital Affiliated to Shanghai Jiao Tong University School of Medicine. RD (30 g) was dissolved in absolute alcohol at room temperature for 48 h under shade and then was filtered. The solvent was concentrated under reduced pressure to ensure that no residual methanol was left behind furnishing a methanol extract. Normally, 4.57 g of dried powder can be obtained from 30 g of RD. The sample was stored at −80°C until used. The extract cream was formulated using ointment as the vehicle. The ointment consisted of propylene glycol : liquid paraffin (6 : 1) and applied topically onto the test animals. Extracts were prepared as 5% in the ointment.

2.2. Phytochemical Analysis. Preliminary phytochemical analysis was carried out using standard procedures to identify the constituents as described by Evans and Trease [10] and Harborne [11].

2.3. Experimental Animals. All study protocols were approved by the Shanghai Jiao Tong University Medical Center, Institutional Animal Care and Use Committee. Healthy Sprague-Dawley male rats weighing between 180 and 200 g were used. The rats were housed in polypropylene cage and maintained in standard laboratory conditions of temperature (22 ± 2°C) and light-dark cycle of 12 h : 12 h. They were maintained on standard pellet diet and provided with water *ad-libitum* throughout the experiment. At the end of the experiment the animals were sacrificed under anesthesia.

2.3.1. Excision Wound Model. The anesthetized rats were inflicted with excision wounds as described by Morton and Malone [12]. The dorsal fur of the animals was shaved with an electric clipper, and the area of the wound to be created was outlined on the back of the animals with methylene blue using a circular stainless steel stencil. A full thickness of the excision wound of circular area of 254 mm^2 and 2 mm depth was created along the markings with a surgical blade. The animals were randomly divided into 3 groups of 24 for each: Group I (control group) where animals were applied with simple ointment base [13]. Animals of Group II (standard group) were applied with a thin layer of moist exposed burn ointment (MEBO). Group III's (experimental group) animals were applied with a thin layer of the extract mixed with ointment. All vehicles were applied once daily, till the day of epithelization. The wound tissue was removed from control, MEBO, and RRDEE treated rats by sacrificing the animals on the 3rd, 7th, 11th, and 15th day after wound creation. Additionally, the rats of the three groups were maintained and treated as above for calculating of the rate of contraction and period of epithelialization.

2.3.2. Incision Wound Model. The animals were randomly divided into three groups of six. Two 6 cm long paravertebral incisions were made using surgical blade (No. 15) through the entire thickness of skin at a distance of about 2 cm from the midline on each side of the depilated back of the rat. After the incision, surgical sutures were applied to the parted skin at intervals of one centimeter. The wounds were left undressed then ointment base, MEBO, and RDEE ointment were applied daily up to 10 days. When wounds were cured thoroughly, the sutures were removed on day 10 and the tensile strength of cured wound skin was measured.

2.4. Measurement of Wound Contraction. Wound margin was traced after wound creation by using transparent paper and the area was measured by graph paper. Wound contraction was measured every two days interval throughout the monitoring period

$$\text{Wound contraction (100\%)} : = \frac{\text{Initial wound size} - \text{Specific day wound size}}{\text{Initial wound size}} \times 100\%. \quad (1)$$

2.5. Epithelialization Period. The epithelialization time was measured from the initial day to the day when the scab fell off from the wound surface exclusive of leaving a raw wound behind [14].

2.6. Measurement of Tensile Strength. The force required to open the healing action is known as the tensile strength.

It indicates how much the repaired tissue resists breaking under tension and may indicate in part the quality of the repaired tissue. The maximum load (tensile strength) tolerated by wounds was measured blindly on coded samples using a biomechanical analyzing instrument (Instron, Canton, MA, USA). Skin strips were stretched at a constant rate (1 mm/min) until disruption occurred. Wound breaking strength was expressed as the mean maximum level of tensile strength in newton (N) before separation of wounds.

2.7. Histopathological Studies. Granulation tissues from control and treatment groups were taken on the 3rd, 7th, 11th, and 15th day after wound creation. The specimens were formalin fixed and paraffin embedded according to the routine laboratorial techniques. Subsequently, serial 5 μm thick sections was obtained and stained with Masson-trichrome (for detection of collagen fibers) and hematoxylin and eosin (H&E) (for general morphological observations). Slides were examined qualitatively under a light microscope, for collagen formation, fibroblast proliferation, angiogenesis, and granulation tissue formation [1, 15].

2.8. CD31 Immunohistochemistry Analysis and Microvessel Density (MVD). Angiogenesis was assessed by CD31 (Epitomics, CA, USA) immunohistochemical in all the cases. Immunohistochemical staining was performed on paraffin sections using the SP method. After the sections were rinsed in distilled water, the endogenous peroxidase was inactivated with 3.0% hydrogen peroxide in distilled water for 10 minutes at room temperature. After rinsing the sections in phosphate-buffered saline (PBS, pH 7.4), the nonspecific binding site was blocked with 10% normal goat serum for 20 minutes at room temperature. The blocking serum was discarded, and then the primary antibodies were added directly. Rabbit anti-rat CD31 monoclonal antibody (Epitomics, CA, USA) was diluted to 1 : 500 in BSA. The sections were incubated with primary antibodies in a humid chamber at 4°C overnight. Sections were washed three times in phosphate buffer solution (PBS), and goat anti-rabbit polymer-peroxidase complex was added, and the sections were incubated for 30 minutes at room temperature. After rinsing with PBS, Streptavidin-horseradish peroxidase conjugate was added and the peroxidase activity was made visible with diaminobenzidine and counterstained with hematoxylin for 30 sec, then dehydrated, and mounted. Quantifications were performed by Image-Pro Plus 6.0 analysis system to calculate the integral optical density (IOD) of each field.

The microvessel density (MVD) was measured according to the method described by Zhen et al. [16]. Briefly, in areas of the most intense CD31 positive neovascularization, individual MVDs were made on a ×200 magnification field. Any endothelial cell or endothelial cell cluster was considered a single countable microvessel. MVD was expressed as the absolute number of microvessels per ×200 field for each case.

2.9. RNA Extraction and Quantitative Real-Time PCR. The expression patterns of TGF-β1 and VEGF of rat wound tissue on the 3rd, 7th, 11th, and 15th day after wound creation were analyzed by quantitative real-time PCR. Total RNA was extracted from the Granulation tissue sample with TRIzol (Invitrogen, Carlsbad, CA, USA) and then was further purified step using the RNeasy Mini Kit (Qiagen), in each case following the manufacturer's instructions. The concentration of the total RNA was detected. Total RNA (1 mg) in a 20 mL reaction volume was reverse transcribed into cDNA using the PrimeScript RT reagent kit (Takara, Dalian, China). Real-time PCR in 96-well optical plates was performed and analyzed with a Stratagene Mx3000P (Stratagene, La Jolla, CA, USA). The reactions were performed in a 20 mL volume using a SYBR Green reaction mix (Takara, Dalian, China) with 2 mL cDNA. The primers were: TGF-β1 forward: 5′-CGC AAC AAC GCA ATC TAT G-3′ and reverse: 5′-ACC AAG GTA ACG CCA GGA-3′; VEGF forward: 5′-TCA CCA AAG CCA GCA CAT AGG AGA-3′ and reverse: 5′-TTA CAC GTC TGC GGA TCT TGG ACA-3′; GAPDH forward: 5′-GAA CGG GAA GCT CAC TGG C-3′ and reverse: 5′-GCA TGT CAG ATC CAC AAC GG-3′. The thermal cycling consisted of denaturation for 30 sec at 95°C followed by 40 cycles of 30 sec at 95°C and 30 sec at 60°C. The threshold cycle (CT) values of target genes were normalized with GAPDH of the same sample and expressed as they were relative to controls.

2.10. Western Blot Analysis. Granulation tissues were homogenized in RIPA lysis buffer (150 mM NaCl, 1% Nonidet P-40, 0.1% SDS, 50 mM Tris-HCl pH 7.4, 1 mM EDTA, 1 mM PMSF, and 1 × Roche complete Mini Protease Inhibitor Cocktail). Protein concentration was determined using a BCA Protein Assay Kit. Equal amounts of protein were separated by 10% SDS gel electrophoresis (SDS-PAGE) under denaturing and nonreducing conditions and then transferred to a nitrocellulose membrane. The membrane was blocked with 5% nonfat milk in TBST at room temperature for 1 h and then incubated with anti-VEGF antibody (Abcam, UK, 1 : 200) at 4°C overnight. After washing in TBST, the blots were incubated with a horseradish-coupled secondary antibody. The signals were visualized using the enhancement system (ECL). GAPDH was used as the internal control and treated with the same protocol. The amount of proteins in gel slabs was quantified using a densitometer (Image Pro Plus 6.0 Media Cybernetics).

2.11. Statistical Analysis. The data were expressed as mean ± S.D. and performed using SPSS (Version19.0, Chicago, IL, USA). Significance was assessed by using the one-way ANOVA followed by t-test. Values were considered statistically significant when P value is less than 0.05.

3. Results

3.1. Phytochemical Analysis. The phytochemical analysis of the extract by qualitative method showed the presence of flavonoids, triterpenoids, steroids, cardiac glycosides, anthraquinones, carbohydrates, saponins, and phenols (Table 1).

3.2. Wound Contraction. Wound contraction is an essential process in healing that leads to wound closure. The rate

Table 1: Results of the phytochemical analysis of RD extract.

Constituents	Result
Cardiac glycosides	+
Flavonoids	+
Catechin tannins	−
Triterpenes	+
Carotenoids	−
Anthraquinones	+
Carbohydrates	+
Saponins	+
Phenols	+
Steroids	+

+: presence; −: absence.

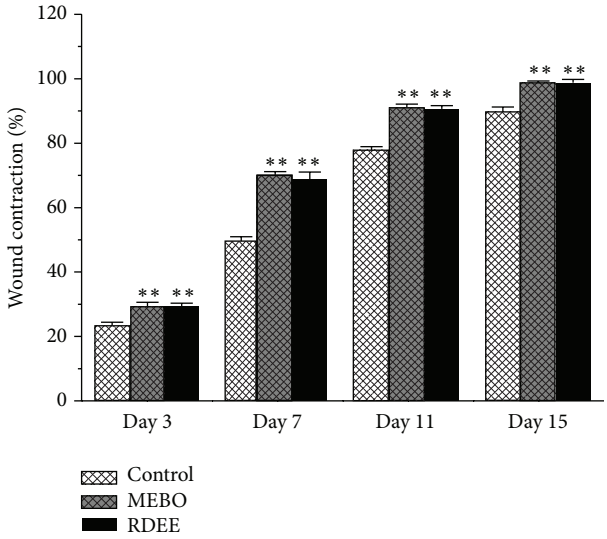

Figure 1: The rate of contraction in control, MEBO, and RDEE treated wound is shown here. Values are expressed as mean ± S.D. ($n = 6$ animals). $^{**}P < 0.01$, versus control.

of contraction of the control group, MEBO group, and the RDEE treated group wounds is shown in (Figure 1). The results revealed that treatment with RDEE and MEBO resulted in much faster contraction of wound ($P < 0.05$).

3.3. Epithelialization Time. The epithelialization time was measured from the first day. The epithelialization time was found to be significantly ($P < 0.05$) reduced in MEBO group and RDEE group as depicted in (Figure 2). Mean time to reepithelialization was 18.67 days (range, 18–20 days), control group; 14.16 days (range, 13–15 days), MEBO group; and 15.12 days (range, 14–16 days), RDEE group. There was no significant difference in the duration of wound healing between the groups treated with MEBO and RDEE; both healed by about 15 days. The control group, however, needed around 19 days to heal, about four days longer than the wound-healing time needed under MEBO and RDEE treatments.

3.4. Tensile Strength of Incision Wound Model. The results of the measurement of skin breaking strength on the 10th day

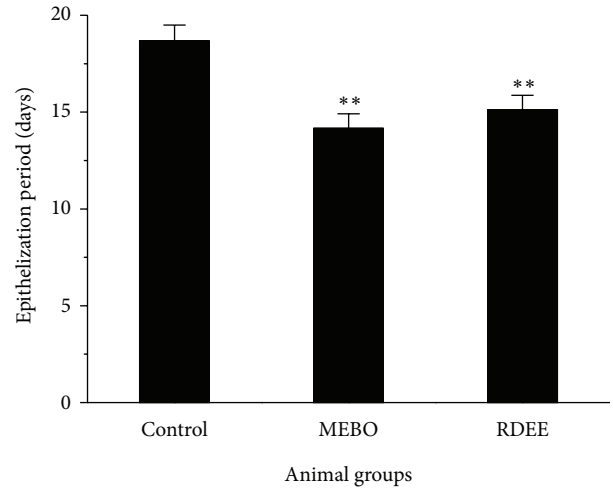

Figure 2: Period of epithelialization in control, MEBO, and RDEE treated wounds is shown. Values are expressed as mean ± S.D. ($n = 6$ animals). $^{**}P < 0.01$, versus control.

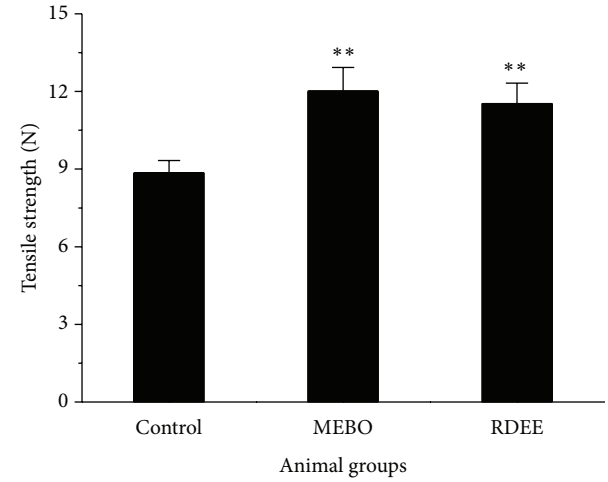

Figure 3: Tensile strength measurements of 10th day wound tissue of control, MEBO, and RDEE treated rats. Values are expressed as mean ± S.D. ($n = 6$ animals). $^{**}P < 0.01$, versus control.

after operation in incision wound-healing model were depicted in (Figure 3). A significant increase in the wound breaking strength (11.53 ± 0.79 N) was observed when compared with the controls (8.85 ± 0.48 N).

3.5. Histopathological Study. Histopathological examinations of the healed wounds are shown in Figures 4 and 5. Two types of stains were used, Hematoxylin and Eosin (H&E) stains and Masson-Trichrome stains for general morphology. H&E stains collagen fibers pale pink, cytoplasm purple, nuclei blue, and red blood cells cherry red. Masson-Trichrome stains collagen blue, while cytoplasm, red blood cells, and muscle are stained red and is typically used to assess the advancement of collagen deposition during the formation of granulation tissue and matrix remodeling [17]. The blue colour staining intensity corresponds to the relative quantity of collagen fiber

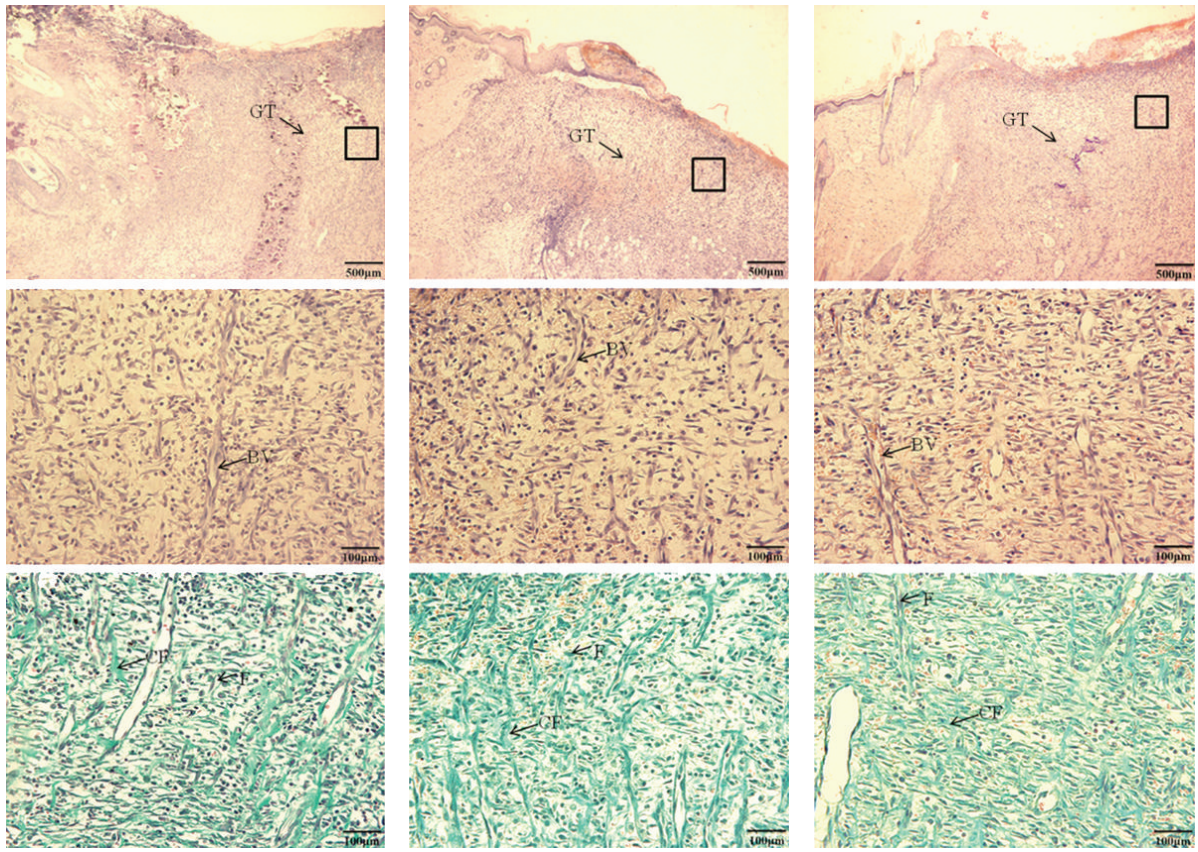

(a) (b) (c)

Figure 4: Photomicrograph of cutaneous wounds in rats at 7 days after wounding H&E stains. (a) Control group, (b) MEBO group, and (c) RDEE group. GT: granulation tissue; BV: blood vessel; F: fibroblasts cells; CF: collagen fibers.

deposit, which reflects the process of synthesis and degradation and remodeling [18]. Histological sections of granulation tissue from RDEE treated rats showed more proliferating blood capillaries, collagen fibres, and fibroblasts cells (Figure 4), which was similar to the effect of MEBO treated group 7 days after wound creation, when compared with the control group. On the 21st day after wound creation, all groups of experimental rats showed complete epithelialization of the wound area. Masson staining revealed that the collagen bundles were thicker, denser disorganized, and more abundant in the control groups. By contrast, collage fibers were decreased and more regularly ranged in the groups treated with MEBO and RDEE. Otherwise, we observed sebaceous gland in the center (Figure 5).

3.6. Immunohistochemistry Analysis and MVD. Vascular endothelial cells were detected using a mouse anti-rat CD31 monoclonal antibody. CD31 expression was mainly present in the cytoplasm and membrane of endothelial cell or cluster. Being different from the control group, condensed, short, and twisted blood vessels were observed in the RDEE treated group (Figure 6(a)). In quantitative analysis, the intensity of CD31 was increased as compared with the control group on the 3rd, 7th, and 11th day (Figure 6(b)). The microvessel density (MVD) of the RDEE treated wounds was significantly higher than that of the control group (Table 2).

3.7. Gene Expression Analysis. To investigate the molecular mechanism of RDEE-induced wound-healing activity, the expression levels of related genes were examined. TGF-β1 and VEGF are the major genes that are generally involved in wound healing. Following several days of treatment, a significant increase in expression of TGF-β1 and VEGF in the wound tissue of extract treated rats was noted, as compared with the control animals ($P < 0.05$). The results showed a day-dependent effect on TGF-β1 and VEGF mRNA expression. The mRNA expression levels of TGF-β1 of the three groups increased from day 3 after injury reaching pick levels at day 11 and then it declined constantly; the mRNA expression of VEGF was also increased from day 3 and correspondingly peaked at day 7 (Figures 7(a) and 7(b)). TGF-β1 and VEGF mRNA expression significantly correlated with the wound contraction.

3.8. Protein Levels by Western Blotting. We further examined the protein levels of VEGF in the granulation tissues of rats from the three groups by Western blotting. Western blot analysis showed an upregulated expression of VEGF in RDEE

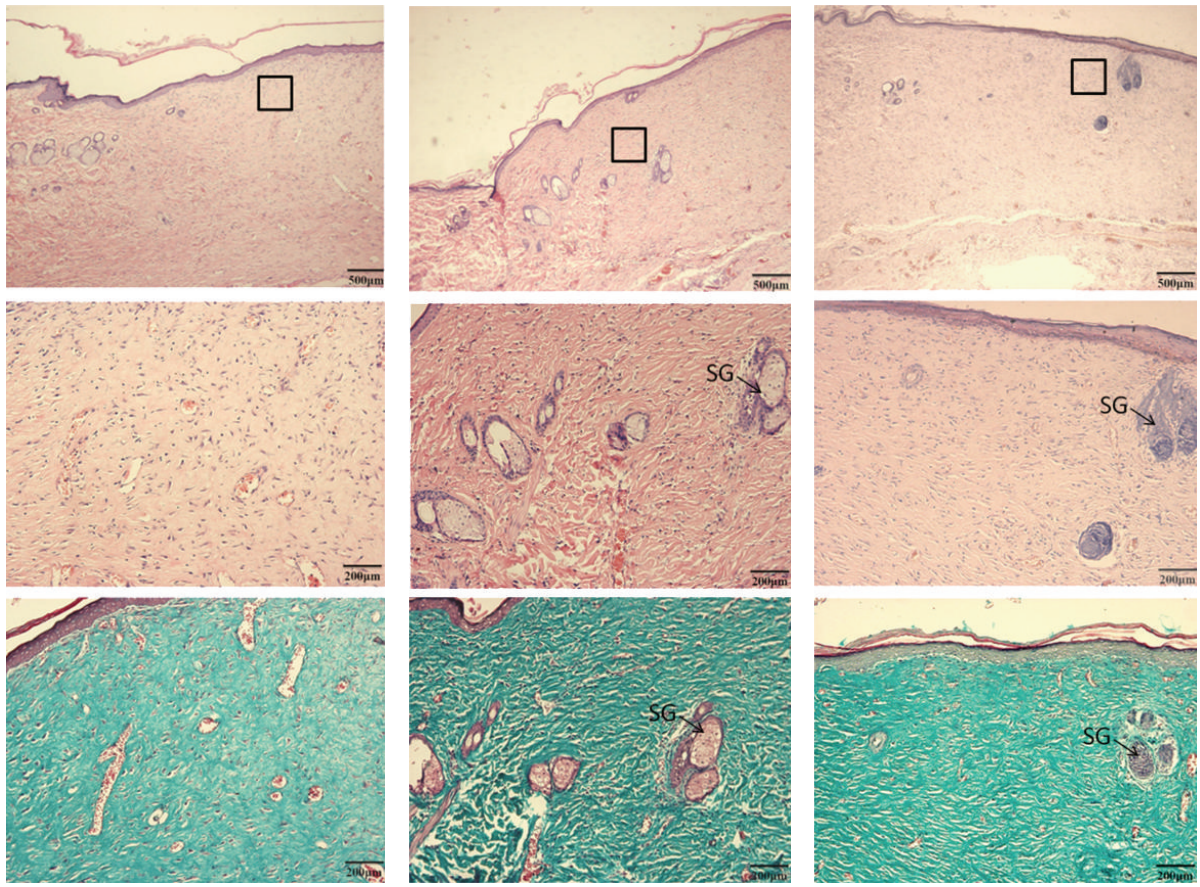

(a) (b) (c)

Figure 5: Photomicrograph showing histopathological changes of healed skin wounds on day 21 of postwounding (stained with hematoxylin-eosin and masson-trichrome). Collagen fibers were arranged more regularly and sparse than those of the scar tissue in the control group. (a) Control group, (b) MEBO group, and (c) RDEE group. SG: sebaceous gland.

Table 2: The comparison of MVD (mean ± S.D.) between each group.

Group	MVD (mean ± S.D.)			
	3 d	7 d	11 d	15 d
Control	20.00 ± 2.28	24.67 ± 4.50	46.00 ± 5.87	55.00 ± 4.05
MEBO	32.00 ± 3.35**	60.83 ± 3.54**	69.00 ± 3.58**	44.33 ± 4.13**
RDEE	35.33 ± 3.88**	62.50 ± 3.56**	72.33 ± 4.32**	51.50 ± 8.36

All values are expressed as the mean ± S.D. Means labeled with superscripts were significantly different. $^{**}P < 0.01$, versus control.

treated group as compared with the control group. On the 3rd, 7th, and 11th day after wound creation, the protein levels of VEGF were significantly increased in RDEE treated group ($P < 0.05$) (Figure 8(a)). Quantified protein level and the fold changes were shown in Figure 8(b).

4. Discussion

Wound healing is a complicated process. The aim of wound healing is to promote rapid wound closure and recover functional properties. Hence in this study, excision and incision wound models were used to evaluate the effects of RDEE on wound healing. The significant reduction in wound size and mean epithelization time as well as the higher expression of growth factors in the RDEE treated group as compared with those from vehicle group corroborate with the histopathological findings of increased epithelization activity, angiogenesis, and higher collagen fibers formation. These findings imply that RDEE promoted wound-healing activity via angiogenesis, collagen deposition, epithelization, and wound contraction.

Excisional and incisional wounds are the two main wound models in wound research which allowed the determination of the wound-healing phases. The excisional wound is found to be more suitable for histological evaluation due to the

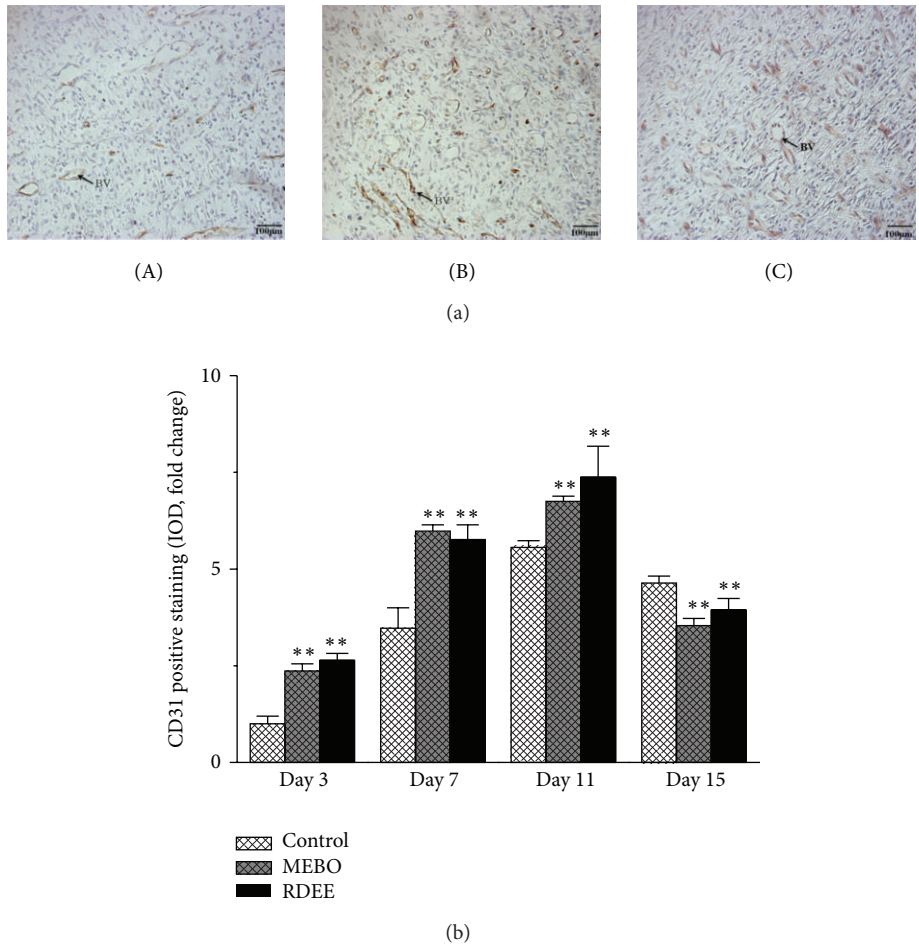

FIGURE 6: The histologic anti-rat CD31 staining of wound tissue samples. (a) Endothelial cells stained with the antibody were represented by brown colour. (A) Control group, (B) MEBO group, and (C) RDEE group. BV: blood vessel. (b) Quantitative analysis of the CD31 stain was calculated. All data were expressed as mean ± S.D. $^{**}P < 0.01$, versus control.

broader morphological changes occurring during the process of wound healing. Wound contraction is an essential process in healing which leads to wound closure. Thus, visible appearances and measurements of wound contraction become reliable parameters in macroscopic evaluation for wound healing [19]. This study showed that RDEE significantly stimulated the contraction of wounds as seen from the percentage of wound contraction (Figure 1). Reepithelialization is important, as it restores the integrity of the skin, making it less vulnerable to infection. The extract-treated animals showed a decreased time to epithelialization (Figure 2) compared with the control group. In incision wound, the increase in tensile strength of RDEE treated wounds may be due to the increase in collagen concentration and stabilization of the fibres [20]. Since incision wound treated with RDEE showed greater tensile strength, it might be speculated that it not only increased collagen synthesis per cell, but also aided in cross-linking of the protein. Histological analysis further revealed that topical application of RDEE significantly increased the fibroblast growth, collagen synthesis, and the healing process.

Histological evaluation showed that healing process of the wounded tissue in RDEE treated group was comparably close to the reference MEBO treated group, whereas significant difference was observed in negative control group. Granulation tissue primarily contains fibroblasts, collagen fibres, very less edema, and newly generated blood vessels, which were observed in RDEE treated group of animals (Figure 4). This histopathological observation provided additional evidence for the experimental wound-healing studies based on the contraction value of wound areas and the measurement of tensile strength. Enhanced healing activity has been attributed to increased collagen deposition and angiogenesis [21]. Collagen plays a central role in the healing of wounds, and it is a principal component of connective tissue and provides a structural framework for the regenerating tissue. Histopathological study showed better proliferation of collagen fibers in the RDEE group compared with the control group (Figure 4). In addition, the slim, defined, and well-organized collagen fibers in the RDEE treated group reinforce the improved quality of the final remodeling of the wound (Figure 5). Angiogenesis during wound repair serves the dual function of providing the nutrients required by supplying essential nutrients and oxygen to the wound site and promoting granulation tissue formation [22]. Histological evaluation

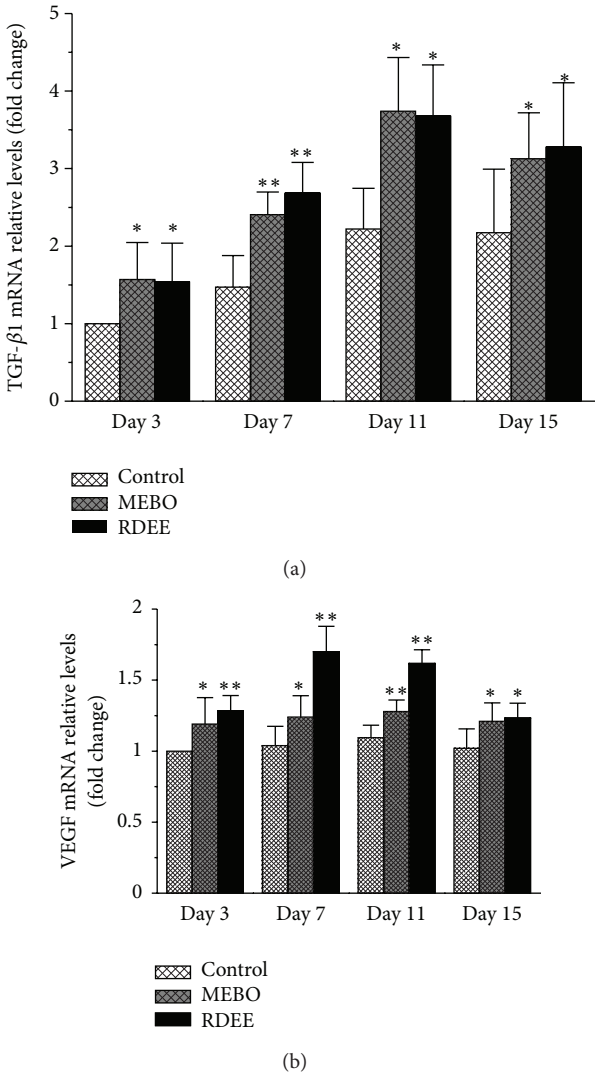

Figure 7: TGF-β1 and VEGF mRNA expression in cutaneous wounds. (a) TGF-β1; (b) VEGF. Normalization relative to GAPDH was performed. Results presented in bar graph are the mean ± S.D. $^{*}P < 0.05$, $^{**}P < 0.01$, versus control.

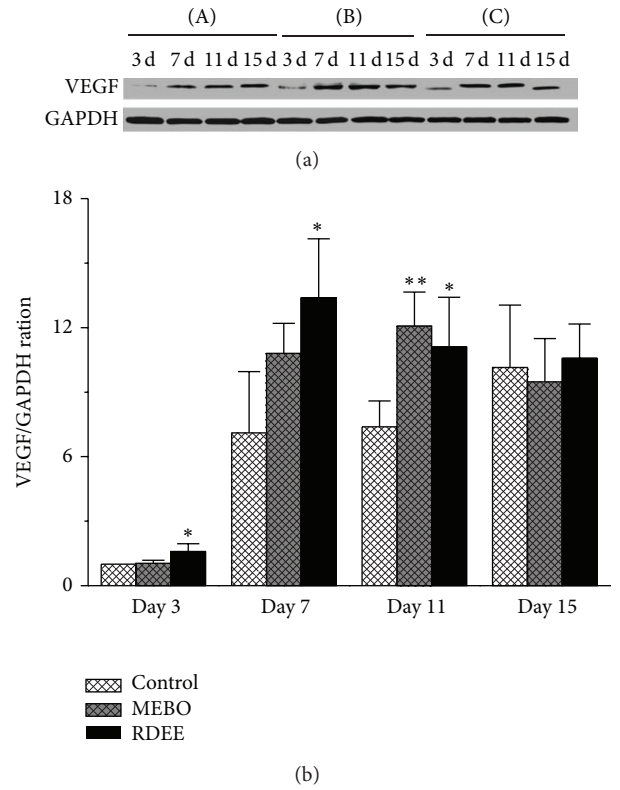

Figure 8: (a) Western blot results for vascular endothelial growth factor (VEGF) protein in the three groups. (b) Quantification of densitometry analysis of protein levels. All data were expressed as mean ± S.D. $^{*}P < 0.05$, $^{**}P < 0.01$, versus control.

showed an increase in the number of blood vessels in the granulation tissue of the rats treated with RDEE. Enhanced expression of CD31 as revealed through immunohistochemistry in RDEE treated group might be responsible for this activity. In the present study, the treatment group was found to increase angiogenesis as evidenced by MVD (Table 2).

Many types of cytokines and growth factors are responsible for inflammation, reepithelialization, the formation of granulation tissue, and neovascularization during the wound healing process [23]. Transforming growth factor beta is an important growth factor that regulates different cellular functions in all phases of wound healing. TGF-β1 produced by fibroblasts as a multifunctional cytokine acts on these cells [24] and enhances granulation tissue formation and collagen formation in wound-healing process [25]. TGF-β1 has also been reported to encourage wound contraction through its direct induction of alpha smooth muscle actin expression in fibroblasts [26]. Otherwise, VEGF appears to be a key factor in pathological situations such as tissue repair, which involves neovascularization and increased vascular permeability. VEGF improves angiogenesis during the process of wound healing by stimulating the migration of endothelial cells through the extracellular matrix [27]. VEGF also has been demonstrated to mediate angiogenic activity during the proliferative phase of wound healing [28]. In addition, VEGF mediates vascular hyperpermeability and promotes the secretion of active growth factors and cytokines necessary for wound repair [29]. The animals treated with RDEE significantly enhanced the expression of VEGF, which is the most potent angiogenic factor during wound healing, thereby, stimulating the formation of new blood vessels [30]. In the present study, our results showed that the expression of VEGF was significantly higher in the RDEE treated group and peaked on the 7th day (Figures 7(b) and 8).

The wound-healing property of RD may be attributed to the phytoconstituents present in the resina, and the quicker process of wound healing could be a function of either the individual or the additive effects of the phytoconstituents. In ethnopharmacological studies, the effects of dragon's blood on various biological activities, such as attenuate visceral nociception, antiviral, antibacterial, and antifungal have been reported [31, 32]. Our preliminary phytochemical screening

of ethanolic extract of RD showed the presence of flavonoids, triterpenoids, steroids, cardiac glycosides, anthraquinones, carbohydrates, saponins, and saponins (Table 1). Recent studies with other plant extracts have shown that phytochemical constituents such as flavonoids [33] and triterpenoids [34] are known to promote the wound-healing process mainly due to their astringent and antimicrobial properties, which appear to be responsible for wound contraction and increased rate of epithelization. Previous studies have revealed that the resin is rich in flavonoids, sterols, and terpenoids [35, 36]. Possibly, the wound-healing action of RD may probably be due to the presence of phytoconstituents in the plant or could be a function of either the individual or the additive effects of the phytoconstituents; however, further phytochemical studies are needed to isolate the active compound(s) responsible for these pharmacological activities.

5. Conclusion

We have shown that the RDEE facilitates wound healing in the experimental animal model. There is a need for further studies in order to isolate the active ingredients in the plant that are responsible for its biological activities and to elucidate the mechanisms of actions of these active ingredients.

Authors' Contribution

Huihui Liu and Shaohui Lin contributed equally to the paper, as joint first authors.

Acknowledgments

This study was supported by the Science and Technology Commission of Shanghai Municipality (no. 09DZ1970400). The authors sincerely thank Zhicheng Song and Xueyi Feng for their excellent technical assistance during this work.

References

[1] E. K. Akkol, U. Koca, I. Peşin, D. Yilmazer, G. Toker, and E. Yeşilada, "Exploring the wound healing activity of *Arnebia densiflora* (Nordm.) Ledeb. by *in vivo* models," *Journal of Ethnopharmacology*, vol. 124, no. 1, pp. 137–141, 2009.

[2] I. P. Süntar, E. K. Akkol, D. Yilmazer et al., "Investigations on the *in vivo* wound healing potential of *Hypericum perforatum* L," *Journal of Ethnopharmacology*, vol. 127, no. 2, pp. 468–477, 2010.

[3] M. Fronza, B. Heinzmann, M. Hamburger, S. Laufer, and I. Merfort, "Determination of the wound healing effect of Calendula extracts using the scratch assay with 3T3 fibroblasts," *Journal of Ethnopharmacology*, vol. 126, no. 3, pp. 463–467, 2009.

[4] X. Cai and Z. Xu, "Studies on the plant origin of Chinese Dragon's blood," *Acta Botanica Yunnanica*, vol. 1, pp. 1–9, 1979.

[5] C. P. Committee, *Pharmacopoeia of the People's Republic of China*, vol. 88, China Chemical Industry Press, Beijing, China, 2005.

[6] Z. Zhihong, W. Jinliang, and Y. Chongren, "Chemical constituents of Sanguis Draxonis made in China," *Zhong Cao Yao*, vol. 32, no. 6, pp. 484–486, 2001.

[7] C. S. Choy, C. M. Hu, W. T. Chiu et al., "Suppression of lipopolysaccharide-induced of inducible nitric oxide synthase and cyclooxygenase-2 by Sanguis Draconis, a dragon's blood resin, in RAW 264.7 cells," *Journal of Ethnopharmacology*, vol. 115, no. 3, pp. 455–462, 2007.

[8] N. Xin, Y. J. Li, Y. Li et al., "Dragon's Blood extract has antithrombotic properties, affecting platelet aggregation functions and anticoagulation activities," *Journal of Ethnopharmacology*, vol. 135, no. 2, pp. 510–514, 2011.

[9] Z. P. Chen, Y. Cai, and J. D. Phillipson, "Studies on the anti-tumour, anti-bacterial, and wound-healing properties of Dragon's blood," *Planta Medica*, vol. 60, no. 6, pp. 541–545, 1994.

[10] W. Evans and G. Trease, *Pharmacognosy*, Bailliere Tindal, London, UK, 1989.

[11] J. Harborne, "Methods of plant analysis," in *Phytochemical Methods*, vol. 132, 1973.

[12] J. J. Morton and M. H. Malone, "Evaluation of vulneray activity by an open wound procedure in rats," *Archives Internationales de Pharmacodynamie et de Therapie*, vol. 196, no. 1, pp. 117–126, 1972.

[13] A. Asif, G. Kakub, S. Mehmood, R. Khunum, and M. Gulfraz, "Wound healing activity of root extracts of *Berberis lyceum* Royle in rats," *Phytotherapy Research*, vol. 21, no. 6, pp. 589–591, 2007.

[14] A. N. Rashed, F. U. Afifi, and A. M. Disi, "Simple evaluation of the wound healing activity of a crude extract of *Portulaca oleracea* L. (growing in Jordan) in *Mus musculus* JVI-1," *Journal of Ethnopharmacology*, vol. 88, no. 2-3, pp. 131–136, 2003.

[15] G. J. Kaur and D. S. Arora, "Antibacterial and phytochemical screening of *Anethum graveolens*, *Foeniculum vulgare* and *Trachyspermum ammi*," *BMC Complementary and Alternative Medicine*, vol. 9, article 30, 2009.

[16] H. N. Zhen, X. Zhang, P. Z. Hu et al., "Survivin expression and its relation with proliferation, apoptosis, and angiogenesis in brain gliomas," *Cancer*, vol. 104, no. 12, pp. 2775–2783, 2005.

[17] L. Braiman-Wiksman, I. Solomonik, R. Spira, and T. Tennenbaum, "Novel insights into wound healing sequence of events," *Toxicologic Pathology*, vol. 35, no. 6, pp. 767–779, 2007.

[18] P. Aramwit and A. Sangcakul, "The effects of sericin cream on wound healing in rats," *Bioscience, Biotechnology and Biochemistry*, vol. 71, no. 10, pp. 2473–2477, 2007.

[19] P. Gal, R. Kilik, M. Mokry et al., "Simple method of open skin wound healing model in corticosteroid-treated and diabetic rats: standardization of semi-quantitative and quantitative histological assessments," *Veterinarni Medicina*, vol. 53, no. 12, pp. 652–659, 2008.

[20] A. L. Udupa, D. R. Kulkarni, and S. L. Udupa, "Effect of Tridax procumbens extracts on wound healing," *International Journal of Pharmacognosy*, vol. 33, no. 1, pp. 37–40, 1995.

[21] A. Shukla, A. M. Rasik, and B. N. Dhawan, "Asiaticoside-induced elevation of antioxidant levels in healing wounds," *Phytotherapy Research*, vol. 13, no. 1, pp. 50–54, 1999.

[22] H. Roy, S. Bhardwaj, and S. Ylä-Herttuala, "Biology of vascular endothelial growth factors," *FEBS Letters*, vol. 580, no. 12, pp. 2879–2887, 2006.

[23] J. S. Lim and G. Yoo, "Effects of adipose-derived stromal cells and of their extract on wound healing in a mouse model," *Journal of Korean Medical Science*, vol. 25, no. 5, pp. 746–751, 2010.

[24] P. Y. Lee, S. Chesnoy, and L. Huang, "Electroporatic delivery of TGF-β1 gene works synergistically with electric therapy to enhance diabetic wound healing in db/db mice," *Journal of Investigative Dermatology*, vol. 123, no. 4, pp. 791–798, 2004.

[25] S. Werner, T. Krieg, and H. Smola, "Keratinocyte-fibroblast interactions in wound healing," *Journal of Investigative Dermatology*, vol. 127, no. 5, pp. 998–1008, 2007.

[26] A. Desmouliere, A. Geinoz, F. Gabbiani, and G. Gabbiani, "Transforming growth factor-β1 induces α-smooth muscle actin expression in granulation tissue myofibroblasts and in quiescent and growing cultured fibroblasts," *Journal of Cell Biology*, vol. 122, no. 1, pp. 103–111, 1993.

[27] S. Constantino Rosa Santos, C. Miguel, I. Domingues et al., "VEGF and VEGFR-2 (KDR) internalization is required for endothelial recovery during wound healing," *Experimental Cell Research*, vol. 313, no. 8, pp. 1561–1574, 2007.

[28] N. N. Nissen, P. J. Polverini, A. E. Koch, M. V. Volin, R. L. Gamelli, and L. A. DiPietro, "Vascular endothelial growth factor mediates angiogenic activity during the proliferative phase of wound healing," *American Journal of Pathology*, vol. 152, no. 6, pp. 1445–1452, 1998.

[29] C. J. Corral, A. Siddiqui, L. Wu, C. L. Farrell, D. Lyons, and T. A. Mustoe, "Vascular endothelial growth factor is more important than basic fibroblastic growth factor during ischemic wound healing," *Archives of Surgery*, vol. 134, no. 2, pp. 200–205, 1999.

[30] B. Romana-Souza, A. P. Nascimento, and A. Monte-Alto-Costa, "Propranolol improves cutaneous wound healing in streptozotocin-induced diabetic rats," *European Journal of Pharmacology*, vol. 611, no. 1–3, pp. 77–84, 2009.

[31] M. T. L. P. Peres, F. Delle Monache, A. B. Cruz, M. G. Pizzolatti, and R. A. Yunes, "Chemical composition and antimicrobial activity of *Croton urucurana* Baillon (Euphorbiaceae)," *Journal of Ethnopharmacology*, vol. 56, no. 3, pp. 223–226, 1997.

[32] L. A. Gurgel, J. J. C. Sidrim, D. T. Martins, V. C. Filho, and V. S. Rao, "*in vitro* antifungal activity of dragon's blood from *Croton urucurana* against dermatophytes," *Journal of Ethnopharmacology*, vol. 97, no. 2, pp. 409–412, 2005.

[33] H. Tsuchiya, M. Sato, T. Miyazaki et al., "Comparative study on the antibacterial activity of phytochemical flavanones against methicillin-resistant *Staphylococcus aureus*," *Journal of Ethnopharmacology*, vol. 50, no. 1, pp. 27–34, 1996.

[34] M. Scortichini and M. P. Rossi, "Preliminary *in vitro* evaluation of the antimicrobial activity of terpenes and terpenoids towards *Erwinia amylovora* (Burrill) Winslow et al," *Journal of Applied Bacteriology*, vol. 71, no. 2, pp. 109–112, 1991.

[35] A. Vachalkova, L. Novotny, M. Nejedlikova, and V. Suchy, "Potential carcinogenicity of homoisoflavonoids and flavonoids from Resina sanguinis draconis (*Dracaena cinnabari* Balf.)," *Neoplasma*, vol. 42, no. 6, pp. 313–316, 1995.

[36] M. Masaoud, J. Schmidt, and G. Adam, "Sterols and triterpenoids from *Dracaena cinnabari*," *Phytochemistry*, vol. 38, no. 3, pp. 795–796, 1995.

Hindawi Publishing Corporation
Evidence-Based Complementary and Alternative Medicine
Volume 2013, Article ID 429738, 9 pages
http://dx.doi.org/10.1155/2013/429738

Research Article

Chinese Medicine Formula Lingguizhugan Decoction Improves Beta-Oxidation and Metabolism of Fatty Acid in High-Fat-Diet-Induced Rat Model of Fatty Liver Disease

Tao Liu,[1] Li-Li Yang,[1] Lu Zou,[1] Dong-Fei Li,[2] Hong-Zhu Wen,[1] Pei-Yong Zheng,[1] Lian-Jun Xing,[1] Hai-Yan Song,[1] Xu-Dong Tang,[3,4] and Guang Ji[1,4]

[1] *Institute of Digestive Diseases, Longhua Hospital, Shanghai University of Traditional Chinese Medicine, Shanghai 200032, China*
[2] *Shanghai East Hospital, Tongji University, Shanghai 200120, China*
[3] *Xiyuan Hospital of China Academy of Chinese Medical Sciences, Beijing 100091, China*
[4] *E-Institute of Shanghai Municipal Education Commission, Shanghai University of Traditional Chinese Medicine, Shanghai 201203, China*

Correspondence should be addressed to Xu-Dong Tang; txdly@sina.com.cn and Guang Ji; jiliver@vip.sina.com

Received 21 March 2013; Accepted 11 April 2013

Academic Editor: Yong Qing Yang

Lingguizhugan decoction (LGZG), a classic traditional Chinese medicine (TCM) formula, has been used to treat obesity and hyperlipidemia in recent years, but the related mechanisms underlying the regulation of lipid metabolism by LGZG are not clear yet. Here, we reported the effectiveness and possible mechanisms of LGZG on rats with fatty liver disease induced by high-fat diet (HFD). Our results demonstrated that LGZG significantly attenuated HFD-induced fatty liver disease, as measured by body weight, liver index, epididymal fat pad-body weight ratio (EFP/BW), liver injury, and hepatic triglycerides (TG) probably through increasing serum thyroid hormone levels, improving beta-oxidation (via modulation of TRβ1 and CPT1A expression), metabolism and transport (through modulation of SREBP-1c, ACSL and ApoB100 expression) of fatty acid. In addition, we discovered the herbal combination with the properties of warming yang to relieve water retention in the formula and proposed the biological basis of LGZG conventional effect via further study on disassembled formula. This study, for the first time, revealed the mechanisms through which LGZG regulates lipid metabolism. Furthermore, our study suggested that it might be feasible to understand the scientific implications of TCM from the perspective of classic formulas' conventional efficacy.

1. Introduction

Lingguizhugan (LGZG) decoction is an ancient Chinese herbal formula from a classic clinical book of traditional chinese Medicine (TCM) titled *Jingui Yaolue* for the treatment of diseases caused by phlegm-fluid retention. It is recorded that conditions with phlegm and fluid retention should be modulated by drugs with warm nature, and the specific formula is Lingguizhugan decoction. LGZG is a typical formula established under the therapeutic principle of warming yang to relieve water retention, indicated for phlegm and fluid retention. In the past decade, LGZG has also been applied to diseases with the feature of phlegm and fluid retention, such as chronic congestive heart failure (CHF). A metaanalysis including 280 patients concluded that LGZG increased clinical benefits of inotropes, diuretics and vasodilators therapy in CHF [1]. Furthermore, in animal studies, LGZG was found to improve cardiac function and cardiac endocrine function in rabbit models of CHF [2], reduce serum Ang II, ET-1, TNF-α, and IL-1β levels, retard adverse ventricular remodeling, and reduce overexpression of cytokines in rat models of CHF [3]. Moreover, LGZG was found to restrain the weight gain caused by antipsychotic medications without any obvious side effect [4], suggesting that LGZG may bring benefits for metabolic

syndrome (MS), which is regarded as having the properties of phlegm and fluid retention in TCM. LGZG also demonstrated clinical benefits for hemorheology in hyperlipidemic rats, indicating that it might also be an alternative choice for hyperlipidemia treatment [5, 6]. Taken together, it is of great significance to explore the effect and possible mechanisms of LGZG on nonalcoholic fatty liver disease (NAFLD), the hepatic component of MS with a high prevalence.

Our research team has been working in the field of NAFL treatment with TCM for more than two decades. Our epidemiological evidence [7] indicated that the crucial TCM pathogenesis of NAFL was phlegm and fluid retention, which was primarily caused by spleen-yang deficiency. Furthermore, we found that Warming Yang to Relieve Water Retention eliminated hepatic fat accumulation in NAFL patients [8]. Our previous study has compared the effectiveness of three different classic formulae on hepatic steatosis (as measured by hepatic triglycerides) in HFD-induced rat models of NAFL. These formulae were rooted in three different therapeutic principles, that was, tonifying Qi for spleen invigoration, warming yang for qi activation, and warming yang to relieve water retention. Finally the results demonstrated that LGZG effectively reduced hepatic triglycerides (TG) [9]. Therefore, investigating the mechanisms underlying the effect of LGZG on NAFL will provide another treatment option for NAFL and help us understand the scientific connotation of TCM therapeutic principle Warming Yang to Relieve Water Retention in NAFL treatment.

2. Materials and Methods

2.1. Drug Preparation and Diet. LGZG comprises four Chinese herbs: *Poria* (20 g), *Ramulus Cinnamomi* (15 g), *Rhizoma Atractylodis Macrocephalae* (15 g), and *Radix Glycyrrhizae* (10 g). The dosage is determined according to the text book of *The Hndouts of Jingui Yaolue* [10]. All herbs were purchased from Longhua Hospital affiliated to Shanghai University of TCM. Herbal decoction was prepared in accordance with conventional TCM decocting methods, briefly, (1) place all herbs in a cooking pot (porcelain) with 500 mL water; (2) boil the herbs with highest heat after 30 minutes of soak; (3) reduce heat and simmer for 20 minutes; (4) transfer the liquid by filtration; (5) add water and boil the remaining, and then repeat (3) and (4) one more time to make a second dose of medicine; (6) mix the two doses in a glass pot. The final concentrated decoction is 100 mL (pure solution). Quality was control under high-performance liquid chromatography (HPLC) as previously described [11], and details were shown in Supplement 1 (see Supplementary Material available online at http://dx.doi.org/10.1155/2013/429738). LGZG was administered at a dose of 10 mL/kg/d (pure solution), which was approximately 7 times of the standard dose in practice, according to the dose-equivalence equation between rats and humans [12]. Meanwhile, the following formulas were prepared based on the herbal combination rule: Lingguizhugan Decoction without *Ramulus Cinnamomi* (LZG, *Poria*, *Rhizoma Atractylodis Macrocephalae*, *Radix Glycyrrhizae*), Lingguizhugan Decoction without *Poria* (GZG, *Ramulus Cinnamomi*, *Atractylodis Macrocephalae*, *Radix Glycyrrhizae*), Lingguizhugan Decoction without *Rhizoma Atractylodis Macrocephalae* and *Radix Glycyrrhizae* (LG, *Poria*, *Ramulus Cinnamomi*). Methods used in decoction and quality control were the same as that used in LGZG, and equal doses were administered. Ordinary diet and HFD (consists of 10% lard oil, 2% cholesterol, and 88% STD) were obtained from Shanghai Si-Lai-Ke Experimental Animal Ltd. (Shanghai, China).

2.2. Animals and Interventions. SPF animals (male Wistar rats, 130 g ± 10 g) were obtained from Shanghai Si-Lai-Ke Experimental Animal Ltd. (Shanghai, China). Rats were housed in an SPF, temperature- (24°C ± 2°C) and humidity-controlled (55%± 10%) room with a 12-hour light-dark cycle (commencing with light at 08:00) in the experiment center, Longhua Hospital affiliated to Shanghai University of TCM. Animals were randomized into 6 groups: normal group, model group, LGZG group, LZG group, GZG group, and LG group ($n = 8$).

Studies began after an acclimation period of 1 week. Rats in the normal group were fed with ordinary diet, while the rats in the other groups were fed with HFD. Food and drinking water/herbal decoction were supplied ad libitum. Treatment lasted 5 weeks, and drug concentration was titrated every other day according to the daily liquid intake of animals.

Five weeks later, the animals were sacrificed under pentobarbital sodium (2%, 5.5 mL/kg) anesthesia following a 12-hour fast. Blood samples were collected in serum tubes from the abdominal aorta. Two samples (1.0 cm × 1.0 cm × 0.2 cm) from the identical lobe and position in the liver were obtained and then fixed in 10% neutral-buffered formalin. The remaining liver was stored at −80°C until use.

All animal procedures were approved by the Animal Experiment Ethics Committee of Shanghai University of TCM.

2.3. Pathology. Liver samples were fixed in 10% formalin for 48 hours and then routinely processed to paraffin. Sections which cut on a microtome at a thickness of 4 μm were stained with hematoxylin and eosin (H & E), and then microscopic images were obtained.

2.4. Biochemical Analysis. Almandine aminotransferase (ALT), aspartate aminotransferase (AST), triglyceride (TG), total cholesterol (TC), high-density lipoprotein cholesterol (HDL-C), and low-density lipoprotein Cholesterol (LDL-C) were measured with auto analyzer (HITACHI 7170, Japan).

TG concentration was assayed using kits obtained from Nanjing Jiancheng Bioengineering Institute following the manufacturers' instructions. 200 mg liver tissues were obtained and snipped into small pieces. These tissues were placed in 3 mL of ethanol-acetone mixture (v : v = 1 : 1), homogenized on ice at 10000–20000 rpm/min for 20 seconds (repeat 2-3 times), and then stored at 4°C overnight. In the next day, samples were centrifuged at 3000 rpm/min for 20 minutes at 4°C to obtain the supernatant.

3,5,3-Triiodothyronine (T3), free triiodothyronine (FT3), total thyroxine (T4), and free thyroxine (FT4) were measured with Roche Diagnostics GmbH (E170, Roche Diagnostics GmbH, Mannheim, Germany).

2.5. Real-Time PCR for mRNA Analysis. TRβ1, CPT1A, SREBP-1c, ApoB100, and ACSL mRNA levels were determined by real-time PCR. Primers were designed using the Primer premier 5.0 software (Table 1).

Quantitative measurement was performed using the Premix Ex Taq kit (TakaRa) according to the manufacturer's instructions on Applied Biosystems StepOne Plus Sequence Detection System. The real-time cycler conditions were as follows: first denaturated at 95°C for 30 sec and then amplified with 40 cycles (each cycle was denaturation at 95°C for 5 s and annealing/extension at 60°C for 30 min). Product purity was confirmed by dissociation curve analysis. Gene expression was quantified relative to the values of the control group after adjusting for β-actin by the $2^{-\Delta\Delta CT}$ method as described previously [13].

2.6. Protein Isolation and Western Blotting. Three liver samples of each group were homogenized in liquid nitrogen, and whole-cell protein was extracted by using lysate buffer containing proteinase inhibitor (complete ULTRA Tablets, minipore). Protein concentration was quantified spectrophotometrically (Bioiek H4) by using BSA protein assay kit (thermo). Protein samples were separated by PAGE using 10% SDS-polyacrylamide gels. Samples were transferred to polyvinylidene fluoride membrane (Immobilon-P transfer membrane, Millipore) and blocked with 5% milk. The membrane was incubated with a mouse anti-TRβ1 primary antibody (1 : 100, Santa Cruz) for 1.5 h at room temperature followed by the secondary antibody (against mouse, Cell Signaling) for 1 h at room temperature. The primary antibodies including rabbit anti-CPT1A (1 : 500, proteintech), and mouse anti-SREBP-1 (1 : 250, abcam), rabbit anti-ACSL (1 : 500, proteintech), mouse anti-beta-actin (1 : 1000, abcam) were similar. Lastly, each protein band was detected using enhanced chemiluminescence (ECL, Millipore). The densitometric values were measured with Gel-Pro Analyzer.

2.7. Statistical Analysis. Data were expressed as mean ± SD and were analyzed by one-way analysis of variance (ANOVA), LSD-*t*, or Games-Howell as appropriate. The statistical significance was defined as two-sided P value of <0.05. Statistical analyses were performed using SPSS 16.0 software (SPSS, Chicago, USA).

3. Results

3.1. Rats' Body Weight, Liver Index, and Epididymal Fat Pad-Body Weight Ratio (EFP/BW) Were Reduced by LGZG. Body weight, liver index, and EFP/BW in model group were significantly higher than that in normal group ($P < 0.05$). All four formulas decreased liver index and EFP/BW compared to model group, though statistical significance was only detected in LGZG and LG groups ($P < 0.05$). This effect was not significantly different between LZG and GZG groups ($P > 0.05$, Table 2).

3.2. Hepatic Injury and TG Were Improved by LGZG. Histological analysis showed that, in normal group (Figure 1(a)), the central vein (CV) was surrounded by hepatocytes arranged radially in plates, and the blue-stained nucleus was located in the centre of the cell. In model group (Figure 1(b)), hepatocytes were not only disordered with loosed cytoplasm and ballooning degeneration but also abundant marked lipid droplets and vacuolation presented; the blue-stained nucleus was located in the border of the cell. In LZG (Figure 1(d)) and ZGZ groups (Figure 1(e)), they were similar to that in the model group. On the contrary, in LGZG (Figure 1(c)) and LG (Figure 1(f)) groups, the lipid droplets were obviously reduced comparing with the model group, and the hepatocytes arrangement improved. LGZG effect was superior than LG.

The level of hepatic TG (Figure 1(g)) in model group was significantly higher than that in normal group ($P < 0.05$). A trend of decrease was seen in LZG and GZG groups comparing with model group ($P > 0.05$), while significant reduction was found in LGZG and LG groups ($P < 0.05$); moreover, LGZG effect was superior to LG group.

3.3. Serum Transaminases and Lipid Levels Were Reduced by LGZG. Serum AST in model group was significantly higher than that in normal group ($P < 0.05$), and significant reduction was detected in LGZG, GZG, and LG groups comparing with model group ($P < 0.05$), while no improvement was seen in LZG group ($P > 0.05$). However, serum ALT levels were similar between normal, model, and treating groups.

Serum HDL in model group was significantly lower than that in normal group ($P < 0.05$), while no significant difference was detected for TG. TG levels were significantly reduced in LGZG and LG groups comparing to model group ($P < 0.05$). Serum TC levels in model group were significantly higher than that in normal group ($P < 0.05$), and TC level was significantly reduced in LGZG and LG groups ($P < 0.05$), while no striking decrease was found in LZG and GZG groups ($P > 0.05$, Table 3).

3.4. Serum THs Were Increased by LGZG. Serum FT3, T4, and FT4 levels in model group were significantly lower than that in normal group ($P < 0.05$), while only a trend of reduction was found for T3 level ($P > 0.05$). T3, FT3, T4, and FT4 levels were significantly increased in LGZG and LG groups, compared with model group ($P < 0.05$). T4 level was significantly increased in GZG group ($P < 0.05$), but GZG treatment showed no effect on T3, FT3, and FT4 levels ($P > 0.05$). LZG treatment had no effect on all THs ($P > 0.05$, Table 4).

3.5. LGZG Improved Fatty Acid Beta-Oxidation via Regulation of TRβ1 and CPT1A Expression. The gene and protein expression of thyroid hormone receptor β1 (TRβ1) and carnitine palmitoyltransferase-1A (CPT1A) from the liver tissue in Model group were significantly lower than that in normal group ($P < 0.05$) (Figures 2(a) and 2(b)). LGZG, GZG, and LG treatments significantly improved the mRNA and protein expression of TRβ1 and CPT1A ($P < 0.05$), while no such effect was found in LZG group ($P > 0.05$). LGZG effect on mRNA expression of TRβ1 was superior to other groups.

Table 1: List of primers.

Gene	Forward primer	Reverse primer	Probe	NCBI RS*
TRβ1	AATGGGGAAATGGCAGGAC	AAGACATCAGCAGGACGGC	CAGGGCAACCTCCGTGTCATCC	NM_012672.2
CPT1A	ATCACTGGTGTGTTCCCCG	GATCTTTGCGATCATGCCC	ATGGATGAAATCACACCCACCACCA	NM_031559.2
SREBP-1c	GCCATCGACTACATCCGCTT	CAGGTCTTTCAGTGATTTGCTTTT	CAGCACAGCAACCAGAAACTCAAGCA	XM_213329
ApoB100	GCATTCTAACTGCCGAGGG	CAAATGGTTGTGCCGAAAAG	CCATTTAAGTTGGCATTGTGCTCACCA	NM_019287.2
ACSL	ATCTTCCCTGTGGTTCCGAG	TCTGACGATGCCACTGCG	CAAAATCCAACAGCCATCGCTTCAC	NM_012820.1
β-actin	AGGGAAATCGTGCGTGAC	CGCTCATTGCCGATAGTG	CTGTGCTATGTTGCCCTAGACTTC	NM_031144.2

*RS: reference sequence.

Table 2: The influence of LGZG decoction and its decomposed recipes on rats' body weight, liver index, and EFP/BW (mean ± SD).

Group	n	Body weight (gm)	Liver index (%)	EFP/BW (%)
Normal	8	323.25 ± 15.50	3.39 ± 0.11	0.101 ± 0.007
Model	8	341.13 ± 11.99*	4.44 ± 0.09*	0.139 ± 0.008*
LGZG	8	332.13 ± 17.47	4.21 ± 0.20#	0.119 ± 0.010#
LZG	8	344.75 ± 6.90	4.33 ± 0.11	0.129 ± 0.009
GZG	8	345.75 ± 13.14	4.33 ± 0.11	0.124 ± 0.016
LG	8	348.88 ± 17.23	4.27 ± 0.07#	0.121 ± 0.007#

*$P < 0.05$ versus normal group, #$P < 0.05$ versus model group.

3.6. LGZG Enhanced Metabolism and Transport of Fatty Acid through Modulation of SREBP-1c, ACSL, and ApoB100 Expression. The gene and protein expression of sterol regulatory element-binding protein 1c (SREBP-1c) from the liver tissue in model group were significantly higher than that in normal group (Figures 3(a) and 3(b)),while the treating groups reduced its expression significantly ($P < 0.05$).

Conversely, the gene and protein expression of long-chain acyl-CoA synthetase (ACSL) and apolipoprotein B100 (ApoB100) in model group were significantly lower than that in normal group ($P < 0.05$) (Figures 3(a), 3(c), and 3(d)); LGZG, LZG, and LG treatments significantly improved expression of ACSL and ApoB100 ($P < 0.05$), and LGZG was superior to LZG and LG groups; however, GZG treatment showed no such effect ($P > 0.05$).

4. Discussion

Lingguizhugan decoction (LGZG) is a classic TCM formula, which has been used to treat obesity and hyperlipidemia in recent years, but the related mechanisms by which LGZG regulates lipid metabolism is yet not clear. In this study, we demonstrated that LGZG significantly attenuated HFD-induced fatty liver disease, as measured by body weight, liver index, EFP/BW, liver injury, and hepatic TG. The possible mechanisms might include increasing serum THs and improving beta-oxidation (via modulation of TRβ1 and CPT1A expression), metabolism, and transport (through modulation of SREBP-1c, ACSL, and ApoB100 expression) of fatty acid. Our study, for the first time, revealed the mechanisms through which LGZG regulates lipid metabolism; furthermore, we discovered the herbal combination with the properties of warming yang to relieve water retention in the formula and proposed the biological basis of LGZG conventional effect via further study on disassembled formula. It is of great significance in understanding the classic formulas' conventional efficacy.

NAFL is characterized by the accumulation of TGs, which are formed from free fatty acids (FFA) and glycerol within the hepatocyte. There is a positive TG cycle between liver and adipose tissue in physiological conditions. It can only be exported from the liver in very low-density lipoprotein (VLDL) particles after incorporation into the apolipoprotein (ApoB100) because TG is liposoluble and insoluble in body (an aqueous environment). The ability of synthesizing TG in the liver is greater than that of synthesizing ApoB100 and package VLDL then as a result, NAFL commonly occurs in association with imbalance between production of TG and apolipoprotein synthesis.

FFA and glycerine are hydrolyzed by lipase from TG within the hepatocyte and then released into blood, and FFA generates energy via β-oxidation. FFA is firstly translated to activated acyl-CoA before the catabolic oxidation, and the latter one is freely soluble in water. Thus the metabolic activity of FFA is enhanced by catalyzing acyl-CoA synthetase (ACS).

Our results demonstrated that LGZG, LZG, and LG significantly increased hepatic ACSL (a major isoform of ACS in liver) and ApoB100 in rat models of NAFL. As these three formulas have a common herb *Poria* and the formula without *Poria* (GZG) showed no such effect, we suggested that *Poria* (which is sweet and tasteless in flavor, with a function of drain dampness with bland) is the key factor why a formula relieves water retention. *Poria* might function through promoting package of VLDL from TG, enhancing aqueous solubility and metabolic activity of fatty acid. The major biological basis of relieving water retention is the high expression of ACSL and ApoB100.

LGZG has the function of warming yang to relieve water retention, and there are similarities between TCM yang-warming and THs function. THs show great importance in metabolic regulation as they significantly promote energy metabolism and fat metabolism, and particularly they improve lipid mobilization, reduce fat storage, and accelerate fatty acid oxidation. Liver is an important target organ where THs execute its function by binding to thyroid hormone receptors (TRs) physiologically, and it also plays an important role in the synthesis, transformation, and inactivation of THs. TRβ1, a major isoform of TRs in liver, is the major modulator in T3 regulation of cholesterol metabolism which plays a key role in hepatic lipid metabolism [14, 15]. Preclinical studies have been conducted for TRβ1 receptor agonists and showed that they reduced plasma cholesterol and TG. In an animal

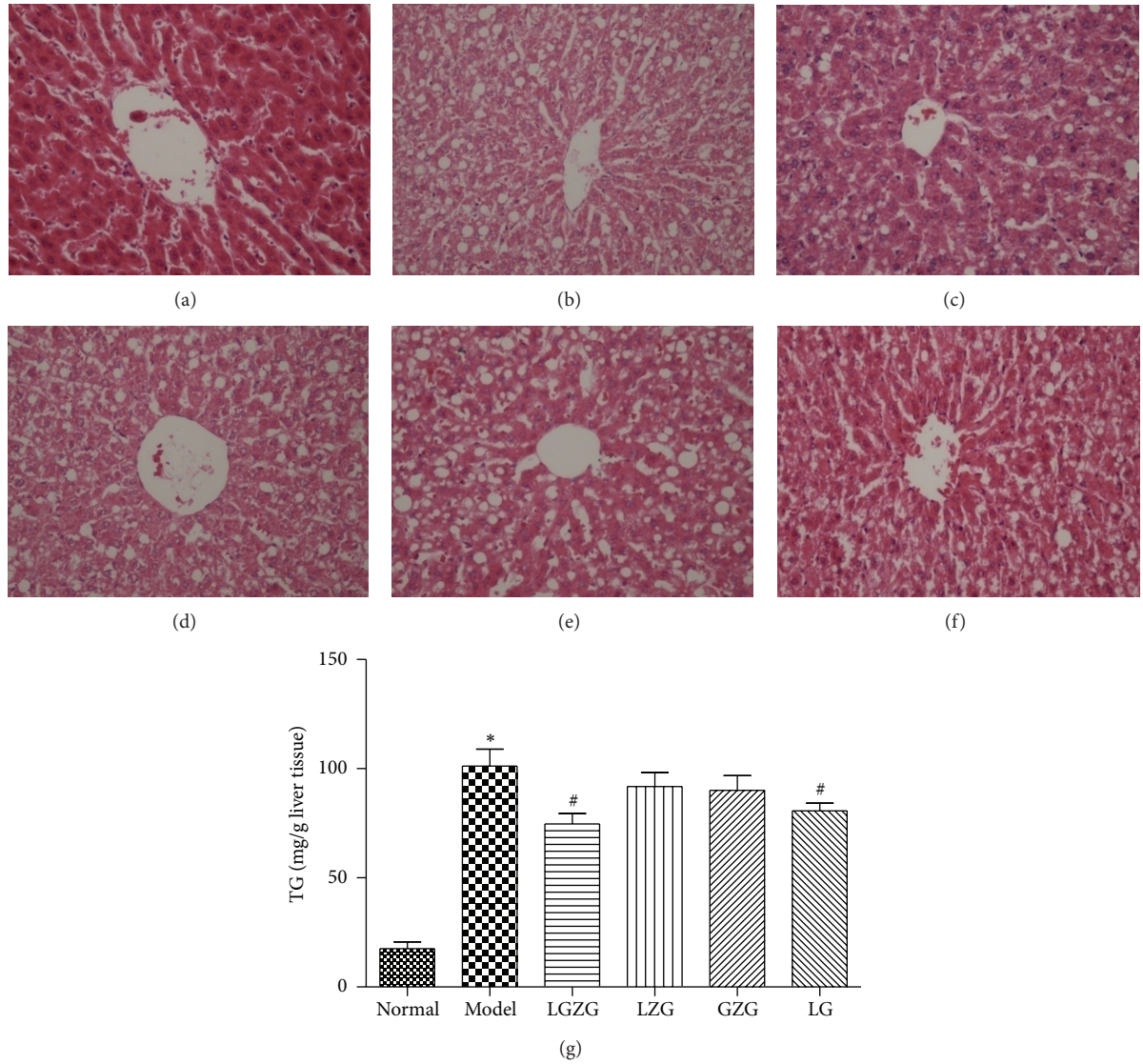

Figure 1: The influence of LGZG and its decomposed recipes on rats' histopathology (H&E stain ×200) and TG levels. (a) Normal group fed with chow diet; (b) model group fed with High-Fat Diet (HFD); (c) LGZG group fed with HFD and LGZG; (d) LZG group fed with HFD and LZG; (e) GZG group fed with HFD and GZG; (f) LG group fed with HFD and LG. (g) The influence of LGZG and its decomposed recipes on rats' hepatic TG. $^{*}P < 0.05$ versus normal group, $^{\#}P < 0.05$ versus model group.

study, a TRβ1 receptor agonist (M07811) was found to accelerate mitochondria fatty acid oxidation and alleviate hepatic steatosis [16].

Studies have demonstrated that TR regulated CPT1 expression by binding to TH-response elements (TRE) in the promoter regions of carnitine palmitoyltransferase-1 (CPT1), a rate-limiting enzyme in hepatic mitochondria fatty acid oxidation [17–20]. CPT1 expression is closely related to body fat percentage, and the gene expression is regulated at transcriptional level [21]. High-CPT1 expression is correlated with high decomposition of fatty acid, low body fat percentage, alleviated hepatic steatosis, and delayed occur of fatty liver [22]. Three isoforms of CPT1 are currently known: CPT1A, CPT1B, and CPT1C. CPT1A (liver isoform) is mainly expressed in liver, kidney, and pancreas, with the function of fatty acid β-oxidation regulation [23]. The CPT1A expression in NAFLD patients is reduced, and hepatic TG is reduced by increasing CPT1A expression [24]. Hepatic TG level is significantly increased while CPT1A activity is restrained [25]. Enhanced CPT1A activity is correlated with improved fatty acid β-oxidation, reduced injury caused by high FFA and TG, and increased TG secretion [26]. Another study has shown strong interaction between CPT1A and ACSL [27].

Hashimoto et al. [28] demonstrated that T3 significantly reduced mice SREBP-1c expression via TRβ1, and this suppression might be caused by TRs and LXR (from SREBP-1c) competition for a DNA binding site [29]. The expression of genes involved in lipid metabolism and glycometabolism is regulated by SREBP-1c, an isoform of sterol regulatory element binding proteins (SREBPs) in liver [30, 31]. Previous

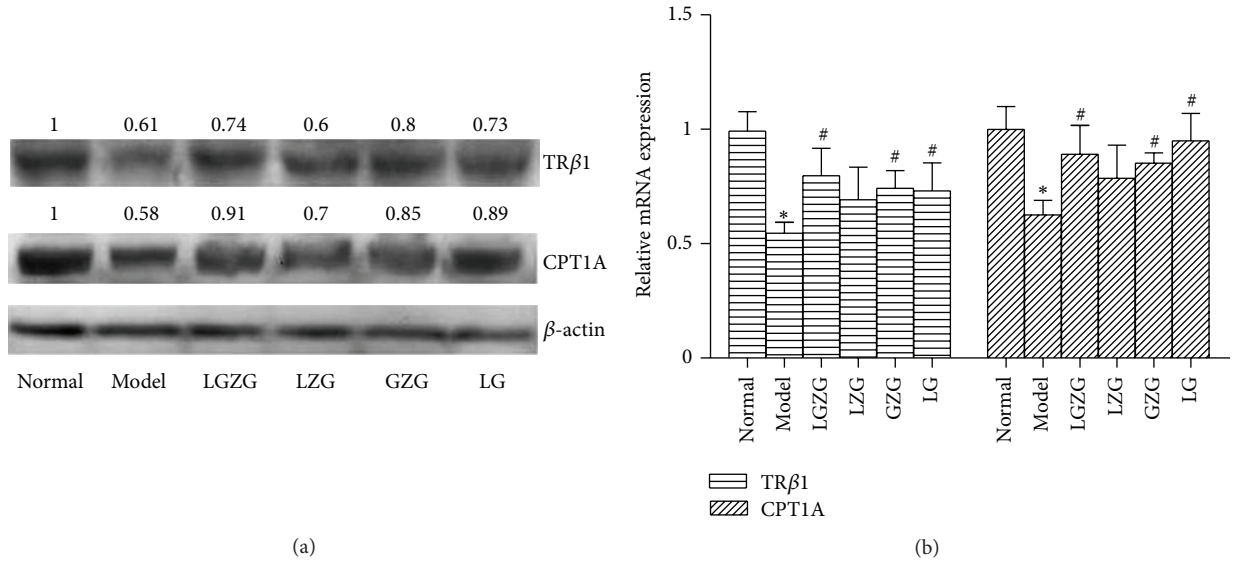

Figure 2: LGZG improved fatty acid beta-oxidation via regulation of TRβ1 and CPT1A expression. The relative mRNA and protein expression of TRβ1 and CPT1A were detected by real-time PCR and western blot. (a) The influence of LGZG and its decomposed recipes on the protein expression of hepatic TRβ1 and CPT1A; (b) the influence of LGZG and its decomposed recipes on the relative mRNA of hepatic TRβ1 and CPT1A (normalized by β-actin). $^{*}P < 0.05$ versus normal group, $^{\#}P < 0.05$ versus model group.

Table 3: The influence of LGZG decoction and its decomposed recipes on serum transaminases and lipid levels (mean ± SD).

Group	n	ALT (U/L)	AST (U/L)	TG (mmol/L)	TC (mmol/L)	HDL (mmol/L)	LDL (mmol/L)
Normal	8	41.83 ± 4.38	113.28 ± 21.51	1.31 ± 0.43	1.48 ± 0.10	1.39 ± 0.11	0.12 ± 0.02
Model	8	44.18 ± 3.83	128.64 ± 9.91*	1.24 ± 0.30	2.40 ± 0.22*	1.12 ± 0.10*	1.00 ± 0.19
LGZG	8	41.48 ± 3.10	105.41 ± 12.18$^{\#}$	0.60 ± 0.16$^{\#}$	2.00 ± 0.10$^{\#}$	1.03 ± 0.05$^{\#}$	0.94 ± 0.12
LZG	8	44.21 ± 3.56	118.10 ± 9.31	0.87 ± 0.13	2.18 ± 0.36	1.08 ± 0.08	1.00 ± 0.27
GZG	8	43.26 ± 4.60	103.90 ± 14.84$^{\#}$	0.94 ± 0.23	2.46 ± 0.24	1.09 ± 0.08	1.16 ± 0.22
LG	8	40.90 ± 4.48	105.44 ± 10.25$^{\#}$	0.55 ± 0.16$^{\#}$	2.04 ± 0.13$^{\#}$	1.03 ± 0.04$^{\#}$	0.96 ± 0.11

$^{*}P < 0.05$ versus normal group, $^{\#}P < 0.05$ versus model group.

study reported that SREBP-1c regulated synthesis and storage of TG in liver [32]. SREBP-1c overexpression can cause dyslipidaemia and lead to lipid accumulation and fatty liver. It was confirmed that hepatic fat content in ob/ob mice with a superimposed knockout of SREBP-1 was significantly lower than that in wide-type controls [33]. SREBP-1c regulates lipid synthesis via transcription regulation of hepatic lipase by changing its mRNA level. Our results demonstrated that LGZG, GZG, and LG significantly increased hepatic TRβ1 in rat models of NAFLD. As these three formulas have a common herb *Ramulus Cinnamomi* (with a function of warming yang for qi activation), while formula without *Ramulus Cinnamomi* (LZG) showed no such effect and all four formulas showed beneficial effect on CPT1A, we suggested that *Ramulus Cinnamomi* is the key factor why a formula warms yang for qi activation. *Ramulus Cinnamomi* might function through increasing THs, hepatic TRβ1, and CPT1A expression and enhancing fatty acid β-oxidation. Meanwhile, herbal combination (*Rhizoma Atractylodis Macrocephalae* and *Radix Glycyrrhizae*) with the property of fortifying the spleen and replenishing qi might strengthen this effect. The major biological basis to warm yang for qi activation is the high expression of TRβ1 and CPT1A.

In addition, our results demonstrated that LGZG and LG significantly reduced hepatic TG level in rat models of NAFLD, and formulas without *Poria* (diuresis) or R*amulus Cinnamomi* (yang-warming for qi activation) showed no such effect. Based on the theory of syndrome differentiation through formula and correspondence of prescription and syndrome, we proposed that water and dampness retention caused by spleen yang deficiency is the basic TCM pathogenesis of NAFLD, and warming yang to relieve water retention is an effective therapeutic principle in NAFLD preventionand treatment. This reflects the therapeutic idea rooted in *Jingui Yaolue*: *conditions with phlegm and fluid retention should be modulated by drugs with warming nature.* The combination of *Poria* and *Ramulus Cinnamomi* might be crucial in LGZG, which is established under the therapeutic principle of Warming Yang to Relieve Water Retention. This formula directly supports the idea that there is a harmonious combination of warming tonification and pathological accumulation elimination. The herbal combination of *Rhizoma*

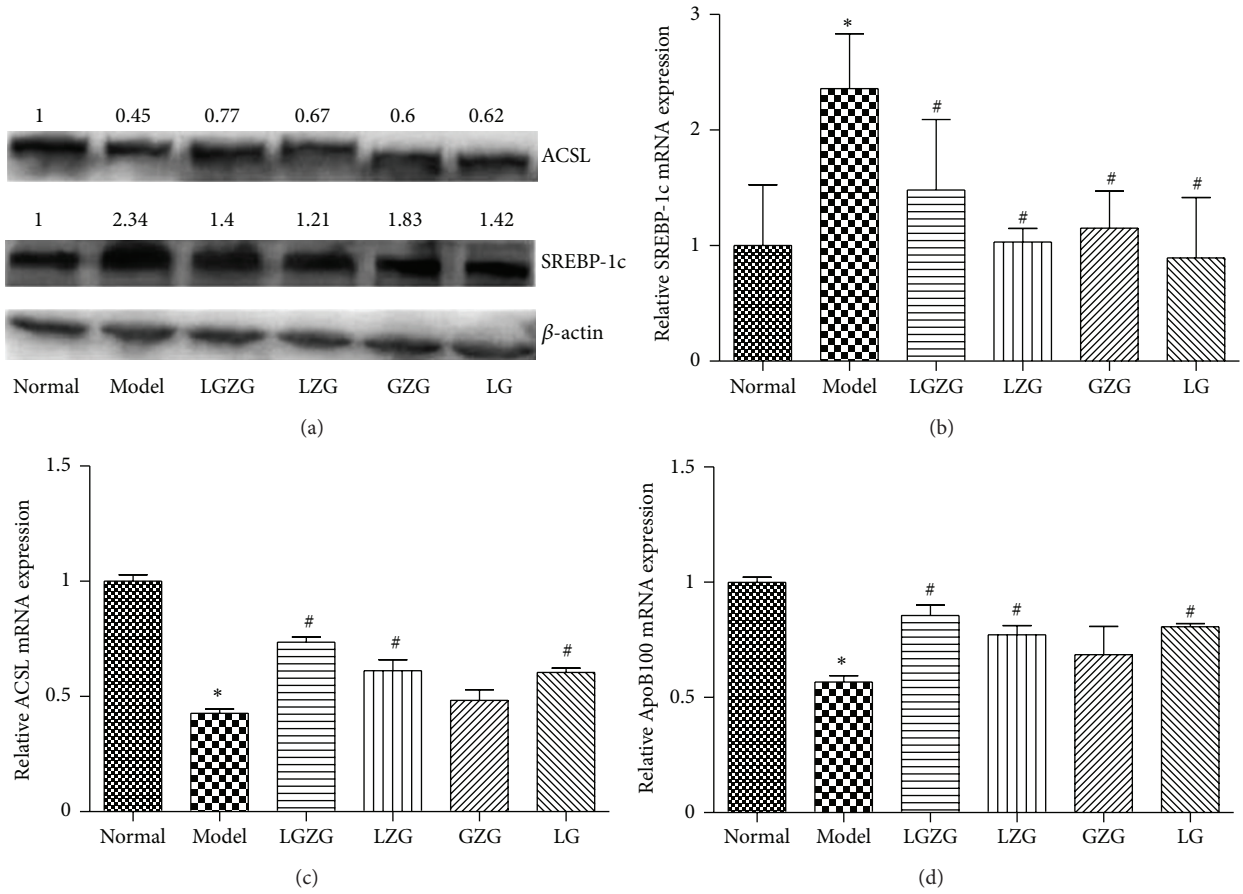

Figure 3: LGZG enhanced metabolism and transport of fatty acid through modulation of SREBP-1c, ACSL and ApoB100 expression. The relative mRNA and protein expression of SREBP-1c, ACSL, and ApoB100 were detected by real-time PCR and western blot. (a) The influence of LGZG and its decomposed recipes on the protein expression of hepatic SREBP-1c and ACSL; (b)–(d) the influence of LGZG and its decomposed recipes on the relative mRNA of hepatic SREBP-1c, ACSL, and ApoB100 (normalized by β-actin). $^{*}P < 0.05$ versus normal group, $^{\#}P < 0.05$ versus model group.

Table 4: The influence of LGZG decoction and its decomposed recipes on serum T3, FT3, T4, and FT4 (mean ± SD).

Group	n	T3 (nmol/L)	FT3 (nmol/L)	T4 (nmol/L)	FT4 (nmol/L)
Normal	8	1.02 ± 0.08	4.65 ± 0.61	73.59 ± 5.66	38.44 ± 2.12
Model	8	0.96 ± 0.08	4.06 ± 0.49*	54.97 ± 3.60*	28.38 ± 2.39*
LGZG	8	1.05 ± 0.06$^{\#}$	4.56 ± 0.39$^{\#}$	66.73 ± 2.58$^{\#}$	33.76 ± 1.88$^{\#}$
LZG	8	0.97 ± 0.07	4.04 ± 0.43	58.73 ± 4.67	30.31 ± 2.82
GZG	8	1.00 ± 0.10	4.48 ± 0.56	59.35 ± 3.05$^{\#}$	29.31 ± 1.66
LG	8	1.10 ± 0.05$^{\#}$	5.13 ± 0.30$^{\#}$	70.23 ± 4.10$^{\#}$	35.33 ± 1.93$^{\#}$

$^{*}P < 0.05$ versus normal group, $^{\#}P < 0.05$ versus model group.

Atractylodis Macrocephalae and *Radix Glycyrrhizae* enhances the effect of warming yang to relieve water retention.

In summary, our study confirmed that LGZG provided significant beneficial effect on HFD-induced rat models of NAFLD, and the mechanisms underlying the effect of LGZG may include increasing THs and improving fatty acid β-oxidation and metabolism. LGZG might be an alternative therapy for MS, such as NAFLD, based on the data from the present study. However, further clinical trials about LGZG efficacy and studies about other possible mechanisms are warranted.

Abbreviations

ACS: Acyl-CoA synthetase
ACSL: Long-chain acyl-CoA synthetase
ALT: Almandine aminotransferase
ApoB100: Apolipoprotein B100
AST: Aspartate aminotransferase
CPT1: Carnitine palmitoyltransferase-1
CPT1A: Carnitine palmitoyltransferase-1A
EFP/BW: Epididymal fat pad-bodyweight ratio
FT3: Free triiodothyronine

FT4: Free thyroxine
HDL-C: High-density lipoprotein cholesterol
LDL-C: Low-density lipoprotein cholesterol
NAFL: Nonalcoholic fatty liver
SREBP-1c: Sterol regulatory element-binding protein 1c
SREBPs: Sterol regulatory element binding proteins
TC: Total cholesterol
TG: Triglyceride
TRE: TH-response elements
TRs: Thyroid hormone receptors
TRβ1: Thyroid hormone receptorβ1
T3: 3,5,3–triiodothyronine
T4: Total thyroxine
VLDL: Very low-density lipoprotein.

Conflict of Interests

Tao Liu and Li-Li Yang have equally contributed to this paper. The authors report no conflict of interests.

Acknowledgments

This study was supported by the National Natural Science Foundation of China (81273727, 81202626, and 81202979), the Leading Academic Discipline Project, and Innovative Research Team in Universities from Shanghai Municipal Education Commission (J50305, E3008, ZYSNXD-CC-ZDYJ042, 2012JW35, and ZZszy12062).

References

[1] Q. Ming-Liang, M. Jing-Yuan, W. Jia-Ying, and W. Xian-Liang, "A Meta-analysis: effect of Linggui Zhugan or added formula on chronic heart failure," *Chinese Journal of Experimental Traditional Medical Formulae*, vol. 17, no. 16, pp. 243–247, 2011.

[2] G. Xiao-Yin, L. Xiao-Qiu, L. Xi-Qing, W. He-Wei, and T. Yan-Jing, "The effect of modification of Lingguizhugan decoction on serum arrial natriuretic factor and cardiac function of congestive heart failure disease of rabbits," *Journal of Emergency in Traditional Chinese Medicine*, vol. 15, no. 3, pp. 289–290, 2006.

[3] F. Hai-Yan, H. Jin-Ling, S. Fang-Fang et al., "Effects of Linggui Zhugan Decoction on levels of angiotensin II, endothelin-1, tumor necrosis factor-α and interleukin-1β in rats with chronic heart failure," *Journal of Anhui Traditional Chinese Medical College*, vol. 29, no. 2, pp. 53–55, 2010.

[4] G. A. Ding, G. H. Yu, S. C. Liang et al., "Jiawei lingguizhugan tang for obesity induced by psychoactive drugs," *Chinese Journal of Clinical Rehabilitation*, vol. 10, no. 43, pp. 46–48, 2006.

[5] Z. Qi, J. Yong, and C. Jian-Bin, "The experimental study on the influence of Lingguizhugan Decoction on the hemorheology in hyperlipidemic rats," *Journal of Chengdu Unversity of Tarditional Chinese Medicine*, vol. 26, no. 3, pp. 11–14, 2003.

[6] D. S. Chen, B. Ke, Y. J. Huang et al., "Effects of the modified linggui zhugan decoction (see text) combined with short-term very low calorie diets on glycemic control in newly diagnosed type 2 diabetics," *Journal of Traditional Chinese Medicine*, vol. 31, no. 3, pp. 185–188, 2011.

[7] H. F. Wei, T. Liu, L. J. Xing, P. Y. Zheng, and G. Ji, "Distribution pattern of traditional Chinese medicine syndromes in 793 patients with fatty liver disease," *Journal of Chinese Integrative Medicine*, vol. 7, no. 5, pp. 411–417, 2009.

[8] W. Miao, L. Tao, W. Hua-Feng, X. Lian-Jun, Z. Pei-Yong, and J. Guang, "Clinical study of "Jiangzhi Granule" and behavioral intervention for nonalcoholic fatty liver disease of phlegm and blood-stasis syndrome," *Shanghai Journal of Traditional Chinese Medicine*, vol. 44, no. 4, pp. 11–13, 2010.

[9] T. Liu, L.-L. Yang, L. Zhang, H.-Y. Song, D.-F. Li, and G. Ji, "Comparative study on the effects of different therapeutic methods in preventing and treating nonalcoholic fatty liver in rats," *Journal of Chinese Integrative Medicine*, vol. 10, no. 10, pp. 1120–1126, 2012.

[10] K. G. Li, *The Handouts of Jingui Yaolüe*, Shanghai Scientific and Technical Publishers, 1995.

[11] S. Zong-Hua, F. Dong, X.U. Jun-Bo, and B. Kai-Shun, "Study on the compatibility and therapeutical basis of composite herbal medicines of Lingguishugan Decoction," *Chinese Traditional Patent Medicine*, vol. 25, no. 5, pp. 132–137, 2003.

[12] C. X. Chen, *Pharmacology of Traditional Chinese Medicine*, Shanghai Scientific and Technical Publishers, Shanghai, China, 2006.

[13] K. J. Livak and T. D. Schmittgen, "Analysis of relative gene expression data using real-time quantitative PCR and the 2-$\Delta\Delta$CT method," *Methods*, vol. 25, no. 4, pp. 402–408, 2001.

[14] C. Pramfalk, M. Pedrelli, and P. Parini, "Role of thyroid receptor β in lipid metabolism," *Biochimica et Biophysica Acta*, vol. 1812, no. 8, pp. 929–937, 2011.

[15] H. Gullberg, M. Rudling, C. satló, D. Forrest, B. Angelin, and B. Vennstr*i*m, "Requirement for thyroid hormone receptor beta in T3 regulation of cholesterol metabolism in mice," *Molecular Endocrinology*, vol. 16, no. 8, pp. 1767–1777, 2002.

[16] E. E. Cable, P. D. Finn, J. W. Stebbins et al., "Reduction of hepatic steatosis in rats and mice after treatment with a liver-targeted thyroid hormone receptor agonist," *Hepatology*, vol. 49, no. 2, pp. 407–417, 2009.

[17] J. F. Louet, C. Le May, J. P. Pégorier, J. F. Decaux, and J. Girard, "Regulation of liver carnitine palmitoyltransferase I gene expression by hormones and fatty acids," *Biochemical Society Transactions*, vol. 29, no. 2, pp. 310–316, 2001.

[18] L. Napal, P. F. Marrero, and D. Haro, "An intronic peroxisome proliferator-activated receptor-binding sequence mediates fatty acid induction of the human carnitine palmitoyltransferase 1A," *Journal of Molecular Biology*, vol. 354, no. 4, pp. 751–759, 2005.

[19] H. M. Dann and J. K. Drackley, "Carnitine palmitoyltransferase I in liver of periparturient dairy cows: effects of prepartum intake, postpartum induction of ketosis, and periparturient disorders," *Journal of Dairy Science*, vol. 88, no. 11, pp. 3851–3859, 2005.

[20] K. G. Sim, J. Hammond, and B. Wilcken, "Strategies for the diagnosis of mitochondrial fatty acid β-oxidation disorders," *Clinica Chimica Acta*, vol. 323, no. 1-2, pp. 37–58, 2002.

[21] P. M. Barger and D. P. Kelly, "PPAR signaling in the control of cardiac energy metabolism," *Trends in Cardiovascular Medicine*, vol. 10, no. 6, pp. 238–245, 2000.

[22] G. Musso, R. Gambino, and M. Cassader, "Recent insights into hepatic lipid metabolism in non-alcoholic fatty liver disease (NAFLD)," *Progress in Lipid Research*, vol. 48, no. 1, pp. 1–26, 2009.

[23] L. Drynan, P. A. Quant, and V. A. Zammit, "Flux control exerted by mitochondrial outer membrane carnitine palmitoyltransferase over β-oxidation, ketogenesis and tricarboxylic acid cycle

activity in hepatocytes isolated from rats in different metabolic states," *Biochemical Journal*, vol. 317, no. 3, pp. 791–795, 1996.

[24] J. Chen, Z. Q. Xie, S. Ye, K. Wang, S. D. Wang, and Q. H. Zhang, "Effect of Ginkgo biloba extract (GBE50) on the metabolism of triglyceride in HepG2 cells," *Chinese Pharmacological Bulletin*, vol. 26, no. 7, pp. 961–964, 2010.

[25] R. L. Dobbins, L. S. Szczepaniak, B. Bentley, V. Esser, J. Myhill, and J. Denis McGarry, "Prolonged inhibition of muscle carnitine palmitoyltransferase-1 promotes intramyocellular lipid accumulation and insulin resistance in rats," *Diabetes*, vol. 50, no. 1, pp. 123–130, 2001.

[26] M. Stefanovic-Racic, G. Perdomo, B. S. Mantell, I. J. Sipula, N. F. Brown, and R. M. O'Doherty, "A moderate increase in carnitine palmitoyltransferase 1a activity is sufficient to substantially reduce hepatic triglyceride levels," *American Journal of Physiology, Endocrinology and Metabolism*, vol. 294, no. 5, pp. E969–E977, 2008.

[27] K. Lee, J. Kerner, and C. L. Hoppel, "Mitochondrial carnitine palmitoyltransferase 1a (CPT1a) is part of an outer membrane fatty acid transfer complex," *Journal of Biological Chemistry*, vol. 286, no. 29, pp. 25655–25662, 2011.

[28] K. Hashimoto, M. Yamada, S. Matsumoto, T. Monden, T. Satoh, and M. Mori, "Mouse sterol response element binding protein-1c gene expression is negatively regulated by thyroid hormone," *Endocrinology*, vol. 147, no. 9, pp. 4292–4302, 2006.

[29] Y. Y. Liu and G. A. Brent, "Thyroid hormone crosstalk with nuclear receptor signaling in metabolic regulation," *Trends in Endocrinology and Metabolism*, vol. 21, no. 3, pp. 166–173, 2010.

[30] J. D. Horton, N. A. Shah, J. A. Warrington et al., "Combined analysis of oligonucleotide microarray data from transgenic and knockout mice identifies direct SREBP target genes," *Proceedings of the National Academy of Sciences of the United States of America*, vol. 100, no. 21, pp. 12027–12032, 2003.

[31] H. Shimano, I. Shimomura, R. E. Hammer et al., "Elevated levels of SREBP-2 and cholesterol synthesis in livers of mice homozygous for a targeted disruption of the SREBP-1 gene," *Journal of Clinical Investigation*, vol. 100, no. 8, pp. 2115–2124, 1997.

[32] J. B. Kim, H. M. Wright, M. Wright, and B. M. Spiegelman, "ADD1/SREBP1 activates PPARgamma through the production of endogenous ligand," *Proceedings of the National Academy of Sciences of the United States of America*, vol. 95, no. 8, pp. 4333–4337, 1998.

[33] N. Yahagi, H. Shimano, A. H. Hasty et al., "Absence of sterol regulatory element-binding protein-1 (SREBP-1) ameliorates fatty livers but not obesity or insulin resistance in Lepob/Lepob mice," *Journal of Biological Chemistry*, vol. 277, no. 22, pp. 19353–19357, 2002.

Hindawi Publishing Corporation
Evidence-Based Complementary and Alternative Medicine
Volume 2013, Article ID 648054, 6 pages
http://dx.doi.org/10.1155/2013/648054

Research Article

A Meta-Analysis of Randomized Controlled Trials on Acupuncture for Amblyopia

Xingke Yan, Tiantian Zhu, Chongbing Ma, Anguo Liu, Lili Dong, and Junyan Wang

Department of Acupuncture and Moxibustion, Gansu University of Traditional Chinese Medicine, Dingxi Dong Road No. 35, Lanzhou 730000, China

Correspondence should be addressed to Xingke Yan; yanxingke@126.com

Received 11 January 2013; Revised 19 March 2013; Accepted 10 April 2013

Academic Editor: Xiang-Yu Hou

Objective. To assess the evidence of efficacy and safety of acupuncture for amblyopia and analyze the current situation of its clinical setting. *Methods*. We systemically searched Wanfang, Chongqing Weipu Database for Chinese Technical Periodicals (VIP), China National Knowledge Infrastructure (CNKI), and PubMed. Published randomized controlled trials (RCT) and controlled clinical trials (CCT) that evaluated the effect of acupuncture for amblyopia compared with conventional treatment were identified. The methodological quality of the included trials was assessed based on the Jadad scale. Data synthesis was facilitated using RevMan 5.1. *Results*. Fourteen trials involving 2662 participants satisfied the minimum criteria for meta-analysis. The evidence showed that the total effective rate of treatment within the group receiving acupuncture was higher than that in conventional group; there were statistically significant differences between groups (polled random effects model (RR) = 1.17, 95% confidence interval (1.11, 1.24), $Z = 5.56$, $P < 0.00001$). *Conclusion*. The total effective rate of acupuncture for amblyopia was significantly superior to conventional treatment, indicating that acupuncture was a promising treatment for amblyopia. However, due to the limited number of CCTs and RCTs, especially those of large sample size and multicenter randomized controlled studies that were quantitatively insufficient, we could not reach a completely affirmative conclusion until further studies of high quality are available.

1. Introduction

Amblyopia is a visual impairment (monocular or binocular) resulting from insufficient light stimulus entering eyes during congenital or critical period of visual development, depriving macula lutea of the opportunity of forming clear images, that is, so-called visual deprivation, and/or anisometropia leading to competition of clear image with fuzzy objects (binocular interaction abnormalities). Organic pathological changes cannot be found in general ophthalmologic examination, optical corrections ≤0.8 by cycloplegic retinoscopy correct [1]. Nowadays, available methods for amblyopia in clinical practice mainly include: patching, afterimage, synoptophore, visual physiological stimulation therapy, light therapy, He-Ne laser therapy, and L-dopa injection, all of which could achieve some therapeutic effect, but with a requirement for age. To older patients, the effect was not significant, and for children, the compliance was poor, therefore the effect was not satisfactory. In recent years, acupuncture as a popular treatment for amblyopia in clinical practice has various modalities. Its efficacy and safety have been evaluated in quite a few RCTs or CCTs. However, the quality of these reported RCTs or CCTs which investigated the efficacy of acupuncture on amblyopia have not been assessed systematically. Therefore, we conducted this meta-analysis (2001–2012) to provide the basic scientific evidence for clinical acupuncture practice.

2. Methods

Definitions of Randomized Controlled Trial (RCT) and Controlled Clinical Trial (CCT). We retrieved relevant RCTs and CCTs that are eligible for the inclusion according to the guidelines of International Cochrane Collaboration [2]. The clinical trial is defined as trial carried out on one or more patients, with concurrent comparison of two or more intervention measures. RCTs are those clinical studies in which subjects were assigned to different treatment groups using randomization allocation such as random number, computer-generated random sequences, tossing a coin, and draw

lots. CCTs (quasi-randomized studies) are those that do not strictly adhere to randomized methods of allocation, for example, allocation by order of admission, hospital registration number, date of birth, day of the week, or some other method that is not truly random, or clinical trials which randomization methods could not be identified.

2.1. Data Sources and Search Strategy. The literature search was performed by using the following databases: Chongqing Weipu Database for Chinese Technical Periodicals (VIP), Wanfang, China National Knowledge Infrastructure (CNKI), and PubMed (January 2001 to March 2012). There were no restrictions regarding the language of publication. All databases were across-retrieved to avoid missing. The key words used for the search were amblyopia AND (acupuncture OR moxibustion OR electroacupuncture OR auriculotherapy OR auricular application pressure). In addition, those articles that could not be obtained were screened manually and independently in Jilin Provincial Library until 12 March 2012 by two authors.

2.2. Study Selection. Studies were eligible only if they met the following criteria: (1) the clinical trials on acupuncture treatment for amblyopia are published in biomedical journals (January 2001 to March 2012); (2) the sample size of patients >10; (3) randomized or quasi-randomized study designs which contained the control group; (4) treatment and control groups were allocated according to the number of affected eyes; (5) with clear diagnosis and effect criteria; and (6) comparing acupuncture treatment with other modalities.

Trials were excluded if any of the following were identified. (1) If the type of articles were animal experiments, review articles, case reports or expert experience reports, conference papers, or dissertations. (2) If studies are comparing two different forms of acupuncture or point selection and formulating prescription. Articles that investigated acupuncture as adjunctive therapy were excluded as well.

2.3. Data Extraction and Management. Data on study characteristics were abstracted independently by the two authors using a standardized collection form, which includes first author, year of the study, sample size, randomization, blinding, baseline characteristics, diagnosis and effect criteria, study selection (inclusion and exclusion criteria), interventions, main outcome assessments, follow-up time, withdrawal, adverse effects, and literature provenance.

2.4. Methodological Quality Assessment. The methodological quality of retrieved articles was rated using the Jadad scale [3]. Any disagreements on study quality were resolved through reviewing the study and discussing the discrepancy. This scale consists of 4 criteria being: (1) random allocation of subjects and allocation concealment (two points for randomization scores. Studies that were described as randomized were given one point. A further point was given if the method of randomization was described and was appropriate, such as the use of a random numbers table); (2) except for intervention, the rest of measures being carried out in two groups were similar (between-group statistical comparisons); (3) blinding score (range 0~2). Studies that were described as double-blinded were given one point; a further point was given if blinding was appropriate, such as matched placebos; one point was deducted if blinding was inappropriate); and (4) if exclusion bias exists, in other words, whether there exist systematic differences in two groups on withdrawals (number and reasons of withdrawals for 0~1 point. If the number and reasons for withdrawals were described in the study, one point was given). The minimal and maximal scores for an included study were 1 and 5, respectively. We arbitrarily classified quality as high (score: 3–5) versus low (score: 0–2).

2.5. Data Synthesis and Analysis. Meta-analysis was conducted using RevMan 5.1 analyses software of the Cochrane Collaboration [4]. The method of analysis selected for this study was to calculate the risk ratio (RR) for each trial: and then conduct test for heterogeneity, the fixed effects models were used to combine effect size when better results of homogeneity presented ($P > 0.05$), on the contrary, using the random effects model. We selected RR as the effect size index and calculated the 95% confidence interval, where $P < 0.05$ was regarded as statistically significant.

3. Results

3.1. Study Characteristics. A total of 115 possible trials were identified, but only 14 satisfied the inclusion criteria, of which 101 were excluded in the screening process as they clearly did not meet the inclusion criteria. The English language literature search identified 10 articles, all of which were unavailable for this meta-analysis, while the Chinese literature search identified 105 articles, the title, abstract, and full text of which were reviewed and 14 full articles [5–18] were eligible for inclusion criteria. Because all articles were domestic periodicals, lingual bias existed in this study, and the published time was from 2001 to 2012. The methodological quality of each study is described in Table 1.

3.2. Quantitative Data Synthesis. Through comparisons of the overall effectiveness of acupuncture treatment for amblyopia in 14 papers [5–18], the extent of heterogeneity in trials was $X^2 = 37.91$, $P = 0.0003$. The random-effects models were used to combine effect. RR = 1.17 showed that the beneficial influence of the experimental factors on disease was significant. The 95% confidence interval was 1.11, 1.24, indicating that acupuncture treatment for amblyopia was effective. The test results of combined effect were $Z = 5.56$, $P < 0.00001$, showing that it was statistically significant in two groups (Figure 1). Just as Figure 1 depicted, diamond falling on the right side of the vertical line showed that comparison of treatment group with the control group was of statistically significant differences.

3.3. Publication Bias Analysis. We assessed publication bias using the funnel plot on studies comparing acupuncture for amblyopia with conventional treatment. When there is no

Table 1: The methodological quality of each study.

First author and date	Study design	Study selection			Methodology			Interventions		Baseline	Jadad score
		Diagnostic criteria	Inclusion/ exclusion criteria	Effect criteria	Randomization	Blinding	Adverse effects	Reports of withdrawal and follow-up	Treatment group	Control group	
Zhang (2001) [5]	RCT	Refer to criteria of [19]	None	Refer to criteria of [19]	Random and concurrent control	No	No	Duration of follow-up: 3 years, no withdrawal	Mainly used acupuncture	Mainly used the traditional treatment	Adequate	3
Xu (2005) [6]	CCT	Refer to criteria of [19]	None	Refer to criteria of [19]	Only random words	No	No	Duration of follow-up: 3 years, no withdrawal	Mainly used acupuncture	Mainly used the traditional treatment	Adequate	2
Lin (2007) [7]	CCT	Refer to criteria of [18]	None	Refer to criteria of [18]	Only random words	No	No	None	Mainly used acupuncture	Mainly used the traditional treatment	Adequate	2
Liu (2007) [8]	RCT	Refer to criteria of [19]	None	Refer to criteria of [19]	Random and concurrent control	No	No	Duration of follow-up: 3 years, no withdrawal	Mainly used acupuncture	Mainly used the traditional treatment	Adequate	3
Sun (2007) [9]	CCT	Refer to criteria of [20]	None	Refer to criteria of [20]	Only random words	No	No	Duration of follow-up: 1 years, no withdrawal	Mainly used auricular seed-pressing therapy	Mainly used the traditional treatment	No report	1
Ge (2009) [10]	CCT	Refer to criteria of [20]	None	Refer to criteria of [20]	Only random words	No	No	Duration of follow-up: 3 years, no withdrawal	Mainly used acupuncture	Mainly used the traditional treatment	Adequate	2
Li (2009) [11]	CCT	Only reports but not date	None	Only report but not date	Only random words	No	No	Duration of follow-up: 18 months, no withdrawal	Mainly used auricular seed-pressing therapy	Mainly used the traditional treatment	No report	1
Song (2009) [12]	CCT	Refer to criteria of [20]	Only report the inclusion criteria	Refer to criteria of *Ophthalmologist Must-Read* [21]	Only random words	No	No	Duration of follow-up: 3 years, no withdrawal	Mainly used auricular seed-pressing therapy	Mainly used the traditional treatment	Adequate	2
Zheng (2009) [13]	CCT	Refer to criteria of [20]	None	Refer to criteria of [20]	Simple random	No	No	Mention of follow-up, no withdrawal	Mainly used acupuncture	Mainly used the traditional treatment	Adequate	2

Table 1: Continued.

First author and date	Study design	Study selection			Methodology			Interventions			Baseline	Jadad score
		Diagnostic criteria	Inclusion/ exclusion criteria	Effect criteria	Randomization	Blinding	Adverse effects	Reports of withdrawal and follow-up	Treatment group	Control group		
Ge (2010) [14]	CCT	Refer to criteria of [20]	None	Refer to criteria of [20]	Only random words	No	No	Duration of follow-up: 3 years, no withdrawal	Mainly used acupuncture	Mainly used the traditional treatment	No report	1
Wu (2010) [15]	RCT	Refer to criteria of [20]	None	Refer to criteria of [20]	Block randomization and parallel control	No	No	None	Mainly used electrical plum-blossom needle	Mainly used the traditional treatment	Adequate	3
Gong (2011) [16]	RCT	Refer to criteria of [20]	Both	Refer to criteria of [20]	Table of random number	No	No	Duration of follow-up: 3 years, no withdrawal	Mainly used auricular seed-pressing therapy	Mainly used the traditional treatment	Adequate	3
Liao (2011) [17]	CCT	Refer to criteria of [20]	None	Refer to criteria of [20]	Only random words	No	No	Cases of withdrawal, no follow-up	Mainly used TCM heat-sensitive moxibustion	Mainly used the traditional treatment	Adequate	3
Wu (2011) [18]	RCT	Refer to criteria of [20]	Both	Refer to criteria of [20]	Block randomization and parallel control	No	No	Criteria of withdrawal, no follow-up	Mainly used electrical plum-blossom needle	Mainly used the traditional treatment	Adequate	4

Study or subgroup	Treatment Events	Total	Control Events	Total	Weight	Risk ratio M-H, random, 95% CI	Year
Qin Zhang 2001	327	341	305	340	13.0%	1.07 [1.02, 1.12]	2001
Lihua Xu 2005	45	48	32	41	5.8%	1.20 [1.01, 1.44]	2005
Aiyin Liu 2007	135	140	106	121	11.2%	1.10 [1.02, 1.19]	2007
Linping Sun 2007	82	84	52	66	8.0%	1.24 [1.09, 1.41]	2007
Jinglan Lin 2007	56	61	46	58	6.9%	1.16 [0.99 ,1.35]	2007
Wei Zheng 2009	75	76	67	75	10.7%	1.10 [1.02, 1.20]	2009
Qingrun Song 2009	47	48	36	43	7.5%	1.17 [1.02, 1.34]	2009
Fenglian Li 2009	48	52	44	52	7.4%	1.09 [0.95, 1.25]	2009
Huilin Ge 2009	49	58	29	50	3.4%	1.46 [1.12, 1.89]	2009
Lie Wu 2010	24	54	13	53	0.9%	1.81 [1.04, 3.17]	2010
Huilin Ge 2010	80	86	55	80	6.6%	1.35 [1.15, 1.59]	2010
Chaolan Miao 2011	57	67	31	55	3.6%	1.51 [1.17, 1.94]	2011
Lie Wu 2011	43	54	31	53	3.4%	1.36 [1.05, 1.77]	2011
Runlian Gong 2011	196	212	167	194	11.6%	1.07 [1.00, 1.15]	2011
Total (95% CI)		**1381**		**1281**	**100.0%**	**1.17 [1.11, 1.24]**	
Total events	1264		1014				

Heterogeneity: $\tau^2 = 0.01$; $\chi^2 = 37.91$, df = 13 ($P = 0.0003$); $I^2 = 66\%$

Test for overall effect: $Z = 5.56$ ($P < 0.00001$)

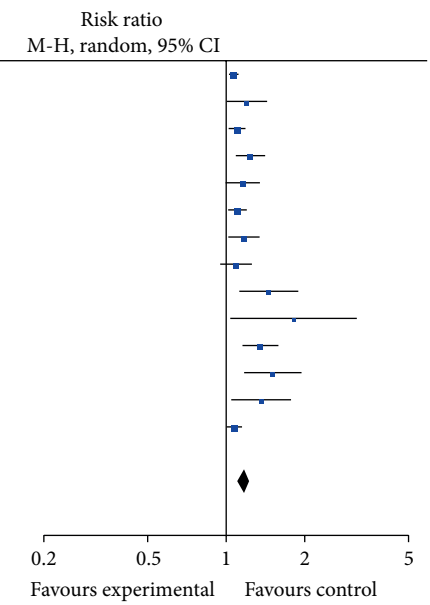

Figure 1: Meta-analysis of 14 trials (CI: confidence interval; *P*: *P*-value).

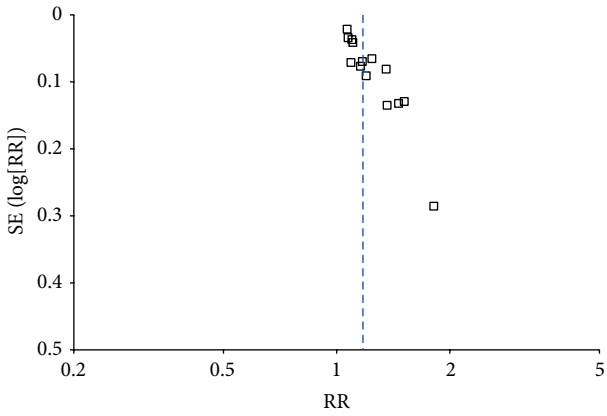

Figure 2: Funnel plot of publication bias analysis.

publication bias, points in funnel plot are almost matched. In this study points about the overall effect's comparison between groups presented asymmetry, suggesting the possibility of publication bias, which is shown in Figure 2. Although great efforts were made to retrieve all trials on the subject, we still could not exclude the possibility that studies with negative findings remain unpublished and parts of included studies were less relevant. In addition, language bias may exist because all included trials were published in Chinese. All in all, the total analysis displayed that publication bias, lingual bias, selection bias, and implementation bias in literatures included in the study may exist.

4. Discussion

4.1. Summary of Main Results. This study performed a meta-analysis to look at the overall effect of included RCTs or CCTs contribute to acupuncture treatment for amblyopia. The evidence suggested effect of acupuncture treatment for amblyopia was superior to conventional treatment. However, through analysis of included 14 trials, we found several problems of study design, including: (1) inadequate method of the randomization; only 6 out of 14 papers [5, 8, 13, 15, 16, 18] described the specific randomization and others were without specific descriptions. This may have resulted in poor comparability of the treatment and control groups; (2) no reports of blinding: blinding was mainly employed to avoid additional variables triggered by the subjective expectation of assessor and subjects and to ensure that the result was reliable. Blinding was not used in 14 trials. Therefore implementation bias may exist; (3) unclear expression of baseline characteristics. Five out of 14 papers [5, 8, 9, 11, 16] only referred to the comparability, even without reports of baseline characteristics, resulting in poor comparability and selection bias. The above results caused the low quality scores of literatures and only 6 papers [4, 7, 14–17] scored ≥3 points, indicating that the quality of literatures was disappointing.

4.2. Strengths and Weaknesses. The main findings of this meta-analysis were that effect of acupuncture treatment for amblyopia was superior to conventional treatment. However, there are several limitations to this meta-analysis. One limitation is the limited number of CCTs and RCTs, especially those of high quality, large samples size, and multicenter randomized controlled trails. Other issues are that inclusion and exclusion criteria were not uniform, no detailed reports of blinding, follow-up and withdrawal, few high-quality studies, only published articles, lingual limitation, and selection and implementation bias. So the efficacy of acupuncture for amblyopia has not been proven beyond reasonable doubt, and further randomized controlled trials with better study methodology are needed.

Acknowledgment

This study was supported in part by the National Natural Science Foundation of China (no. 81260560).

References

[1] J. Ge, *Ophthalmology*, The People's Medical Publishing House, Beijing, China, 2004.

[2] R. J. Alejandro, M. Michael, P. B. George et al., "Systematic reviews and meta-analyses on treatment of asthma: critical evaluation," *British Medical Journal*, vol. 320, no. 7234, pp. 537–540, 2000.

[3] A. R. Jadad, R. A. Moore, D. Carroll et al., "Assessing the quality of reports of randomized clinical trials: is blinding necessary?" *Controlled Clinical Trials*, vol. 17, no. 1, pp. 1–12, 1996.

[4] The Nordic Cochrane Centre, *Review Manager (RevMan)[Computer Program]. Version 5.0 For Windows*, The Cochrane Collaboration, Copenhagen, Denmark, 2009.

[5] Q. Zhang and W. Y. Wu, "Acupuncture with ear pressure treatment for 193 cases of children with amblyopia," *Shanghai Journal of Acupuncture and Moxibustion*, vol. 20, no. 2, pp. 26–27, 2001 (Chinese).

[6] L. H. Xu, Y. W. Guo, B. Zhang et al., "Varieties of acupuncture therapies combined with comprehensive training treatment for 29 cases of older children with amblyopia," *Journal of External Therapy of Traditional Chinese Medicine*, vol. 14, no. 3, pp. 40–41, 2005 (Chinese).

[7] J. L. Lin, "Comprehensive treatment of amblyopia in children: clinical observation of 75 cases," *Henan Traditional Chinese Medicine*, vol. 27, no. 11, pp. 64–65, 2007 (Chinese).

[8] A. Y. Liu, P. Luo, and S. Y. Zhang, "Comprehensive treatment of 108 cases of children with amblyopia," *China'S Naturopathy*, vol. 15, no. 8, pp. 56–57, 2007 (Chinese).

[9] L. P. Sun, X. Y. He, and Y. F. Li, "Clinical observation of auricular acupressure with self prescription of yi shen decoction as comprehensive treatment of amblyopia in children," *Public Medical-Forum Magazine*, vol. 11, no. 6, pp. 532–533, 2007 (Chinese).

[10] H. L. Ge and S. Q. Liu, "The curative effect observation of acupuncture treatment for intractable amblyopia," *World Journal of Integrated Traditional and Western Medicine*, vol. 4, no. 8, pp. 567–569, 2009 (Chinese).

[11] F. L. Li and L. N. Zhang, "Point by auricular pressure combined with foot reflexology treatment of strabismic amblyopia," *Journal of Changzhi Medical College*, vol. 23, no. 1, pp. 57–58, 2009 (Chinese).

[12] R. Q. Song, "The clinical observation of Aauricular-plaster with the decoction of chinese medicine in the treatment of amblyopia," *Chinese Modern Doctor*, vol. 47, no. 23, pp. 76–80, 2009 (Chinese).

[13] W. Zheng and D. Zhou, "The curative effect observation of acupuncture combined with amblyopia therapeutic instrument in the treatment of children with amblyopia," *Maternal and Child Health Care of China*, vol. 24, no. 12, pp. 1712–1713, 2009 (Chinese).

[14] H. L. Ge and S. Q. Liu, "Acupuncture treatment of 90 cases of children with amblyopia," *Guangming Journal of Chinese Medicine*, vol. 25, no. 11, pp. 2066–2077, 2010 (Chinese).

[15] L. Wu, G. L. Zhang, Y. X. Yang et al., "The short-term curative effect observation of Electric plum blossom needle treatment of amblyopia in children," *China Jouranl of Chinese Ophthalmology*, vol. 20, no. 6, pp. 338–340, 2010 (Chinese).

[16] R. L. Gong, "The curative effect observation of Auricular plaster therapy of amblyopia in children," *Chinese Acupuncture and Moxibustion*, vol. 31, no. 12, pp. 1081–1083, 2011 (Chinese).

[17] C. Y. Liao, R. X. Chen, Z. G. Pei et al., "The curative effect observation of Thermal moxibustion treatment of elder children with amblyopia," *China Journal of Traditional Chinese Medicine and Pharmacy*, vol. 26, no. 3, pp. 461–463, 2011 (Chinese).

[18] L. Wu, G. L. Zhang, Y. X. Yang et al., "Clinical study on electrical plum-blossom needle for treatment of amblyopia in children," *Chinese Journal of Integrated Traditional and Western Medicine*, vol. 31, no. 3, pp. 342–3433, 2011 (Chinese).

[19] National Amblyopia Prevention Study Group in 1987, "Prevention and treatment of children with amblyopia or strabismus," *Maternal and Child Health Care of China*, vol. 4, no. 1, p. 33, 1987.

[20] National Amblyopic and Strabismus children Prevention Study Group of Ophthalmologic Medcine in 1996, "The definition, classification and evaluation standard of effect of amblyopia," *Chinese Journal of Strabismus and Pediatric Ophthalmology*, vol. 4, no. 3, p. 97, 1996 (Chinese).

[21] L. T. Wang and L. Liu, *Ophthalmologist Must-Read*, People's Military Medical Press, Beijing, China, 1999.

Hindawi Publishing Corporation
Evidence-Based Complementary and Alternative Medicine
Volume 2013, Article ID 306712, 10 pages
http://dx.doi.org/10.1155/2013/306712

Research Article

Investigation of the Effect of Rice Wine on the Metabolites of the Main Components of Herbal Medicine in Rat Urine by Ultrahigh-Performance Liquid Chromatography-Quadrupole/Time-of-Flight Mass Spectrometry: A Case Study on *Cornus officinalis*

Gang Cao,[1,2,3] Hao Cai,[1,3] Xianke Yue,[2] Sicong Tu,[4] Baochang Cai,[1,2,3,5] and Zhiwei Xu[2]

[1] *Engineering Center of State Ministry of Education for Standardization of Chinese Medicine Processing, Nanjing University of Chinese Medicine, Nanjing 210023, China*
[2] *Research Center of TCM Processing Technology, Zhejiang Chinese Medical University, Hangzhou 310053, China*
[3] *National First-Class Key Discipline for Science of Chinese Materia Medica, Nanjing University of Chinese Medicine, Nanjing 210023, China*
[4] *Faculty of Medicine, University of New South Wales, Sydney, NSW 2031, Australia*
[5] *Nanjing Haichang Chinese Medicine Group Corporation, Nanjing 210061, China*

Correspondence should be addressed to Hao Cai; haocai_98@126.com and Baochang Cai; bccai@126.com

Received 4 February 2013; Revised 29 March 2013; Accepted 30 March 2013

Academic Editor: Yong Qing Yang

Ultrahigh-performance liquid chromatography-quadrupole/time-of-flight mass spectrometry (UPLC-QTOF/MS) was developed for rapid and sensitive analysis of the effect of rice wine on the metabolites of the main components of herbal medicine in rat urine. Using *Cornus officinalis* as a model of herbal medicine, the metabolite profiles of crude and processed (steaming the crude drug presteeped in rice wine) *Cornus officinalis* extracts in rat urine were investigated. The metabolites of *Cornus officinalis* were identified by using dynamic adjustment of the fragmentor voltage to produce structure-relevant fragment ions. In this work, we identified the parent compounds and metabolites of crude and processed *Cornus officinalis* in rats. In total, three parent compounds and seventeen new metabolites of *Cornus officinalis* were found in rats. The contents of the parent compounds and metabolites *in vivo* varied significantly after intragastric (i.g.) administration of aqueous extracts of crude and processed *Cornus officinalis*. Data from this study suggests that UPLC-QTOF/MS could be used as a potential tool for uncovering the effects of excipients found in the metabolites of the main components of herbal medicine, *in vivo*, to predict and discover the processing mechanisms of herbal medicine.

1. Introduction

The processing of Chinese materia medica is based on traditional Chinese medicine (TCM) and has undergone continual development and refinement for thousands of years. Traditional processing and treatment of TCM utilize a range of decoction pieces, with the aim of altering the nature of the medicine to accommodate different clinical dispensings and preparation requirements [1, 2]. During processing, fire and wine are utilized in heat and excipient treatments in many herbs, respectively [3]. The processing of Chinese materia medica with excipients has a long history and the efficacy of treatment can be enhanced by using a combination of excipient treatments. There is a close relationship between the nature of Chinese materia medica and excipient treatments, through the collaboration and regulatory roles of excipients. As a result, the inherent property of such medicine can be improved through these processes to improve its treatment efficacy, which is often achieved by heating the medicine and excipient together. Solid excipients are mainly

used to suppress the toxicity, while liquid excipients are used to enhance the treatment efficacy [4].

In processing TCM, wine is typically used as a gas component. It is believed that wine has the function of promoting blood circulation for removing obstruction in collaterals, strengthening the spleen and stomach, and removing foul odors [5, 6]. Through modern medicine, these therapeutic efficacies have been demonstrated as alcohol can dilate blood vessels to enhance cerebral blood flow, stimulate the central nervous system, and improve circulatory of the digestive system [7]. For processing TCM, rice wine is one of the most commonly used liquid excipients. Typically, rice wine is used for steeping, boiling, and steaming herbs, or making various pills and medicated wine [8]. Rice wine contains large amounts of proteins, carbohydrates, vitamins, organic acids, esters, and minerals [9]. During the saccharification and fermentation process of rice wine production, starch and protein are degraded into oligosaccharides, peptides, amino acids, and other ingredients that are readily absorbed by the human body, thus making rice wine a highly nutritious supplement. In addition, rice wine serves as a good organic solvent and has good solubility for a variety of chemical compounds and good tissue penetration capability. When the drugs are heated with wine, rice wine can change the property of medicine, lead the medicine uplink, and change the ups and downs of the Chinese medicine. It can also enhance drug efficacy and reduce foul taste and corrosion. Therefore, the processing of Chinese materia medica using rice wine offers many clinical benefits.

Dried sarcocarp of *Cornus officinalis* Sieb. et Zucc (Cornaceae) is a herbal medicine widely used in TCM for medical, food sanitation, and cosmetic purposes [10]. Clinically, it is used both in its crude herbal form and as a processed product [11]. While potent unprocessed, pharmaceutical processing may reduce toxicity or side efficacies, potentiate the beneficial effects, change the pharmacological properties, preserve active constituents, facilitate administration, improve flavor or eliminate unpleasant taste, and increase purity of herbal medicine [12, 13]. Extensive phytochemical and pharmacological studies of *Cornus officinalis* have isolated and characterized a total of 10 iridoids, most of which have been proven to have bioactive properties for the prevention and treatment of diabetic nephropathy and kidney deficiency, anti-inflammation, antivirus and antioxidation [14–16]. *Cornus officinalis*, after being stewed with yellow rice wine, has a stronger efficacy on nourishing kidneys, astringing semen, and reducing urination. It has been used diffusely for curing dizziness, coldness, pain in the waist, frequent micturition, enuresis, impotence, and prospermia [17]. Furthermore, *Cornus officinals* warmly dredges up the dint of wine and reduces its acidity.

Within the literature, the majority of studies examining drug metabolism have been based on studies in which the liver was used as the experimental organ [18]. It is now clear that kidney also plays a major role in drug metabolism, as drug compounds and metabolites are excreted into the urine. Although most pharmacokinetic parameters of iridoids, such as morroniside, loganin, and sweroside, in *Cornus officinals* have been investigated [19–21], there is no report of renal excretion of active constituents and metabolites of main components in crude *Cornus officinalis* and its processed form. The aim of our study was to examine whether the absorption and metabolism of active components in *Cornus officinalis* through renal excretion were altered after processing using rice wine. In the present study, we employed a new and rapid ultrahigh-performance liquid chromatography-quadrupole/time-of-flight mass spectrometry (UPLC-QTOF/MS) method to investigate the effect of rice wine on the metabolites of the main components of *Cornus officinalis* in rat urine.

2. Experimental

2.1. Materials, Chemicals, and Reagents. Crude *Cornus officinalis* was acquired from Henan suppliers and its processed form was treated according to the Chinese Pharmacopoeia (2010 eds.). HPLC grade acetonitrile and methanol were obtained from Merck (Darmstadt, Germany) and Fisher Scientific Corporation (Loughborough, UK), respectively. Deionized water was purified using the Milli-Q system (Millipore, Bedford, MA, USA) and HPLC grade formic acid was purchased from Honeywell Company (Morristown, NJ, USA). Loganin was purchased from the National Institute for the Control of Pharmaceutical and Biological Products (Beijing, China). Morroniside and sweroside were obtained from Shanghai Shangyi Biotechnology Co. Ltd. (Shanghai, China). HPLC analysis indicated that the purities of all reference compounds were greater than 98%. All remaining chemicals were of analytical grade and commercially available.

2.2. Instrumentation and UPLC-QTOF/MS Conditions. Chromatography was performed using an ACQUITY C_{18} BEH column (150 mm × 2.1 mm i.d., 1.7 μm) and CQUITYUPLC system (Waters Corp., Milford, MA, USA). The column was maintained at 40°C with a gradient elution of 0.1% formic acid in acetonitrile (solvent A) and 0.1% formic acid in water (solvent B) at 0–4.5 min (1–8.4% A), 4.5–8 min (8.4–9% A), 8–16 min (9–75% A), and 16-17 min (75–99% A). The flow rate was 0.45 mL/min, and 5 μL aliquot of each sample was injected into the column. The eluent was then introduced to the mass spectrometer directly, that is, without a split.

The eluent was introduced into the synapt high-definitionmass spectrometer (Waters Corp., Milford, MA, USA) analysis. The optimal conditions were as follows: capillary voltage of 2.5 kV, sampling cone voltage of 20 V, cone gas flow of 10 L/h, and desolvation gas flow of 700 L/h. The source and desolvation gas temperature were kept at 110 and 350°C, respectively. The data were collected and analyzed using Masslynx V 4.1 and MetaboLynx software. The mass spectrometric data were collected in full-scan mode; the *m/z* was from 100 to 1000 in positive and negative ions.

2.3. Preparation of Sample Solutions. 100 g of powdered *Cornus officinalis* and its processed samples were soaked in 200 mL of water for 2 h at room temperature and thereafter refluxed for 2 h, respectively. The filtrate was collected and the residues were then refluxed twice in 1000 mL of water

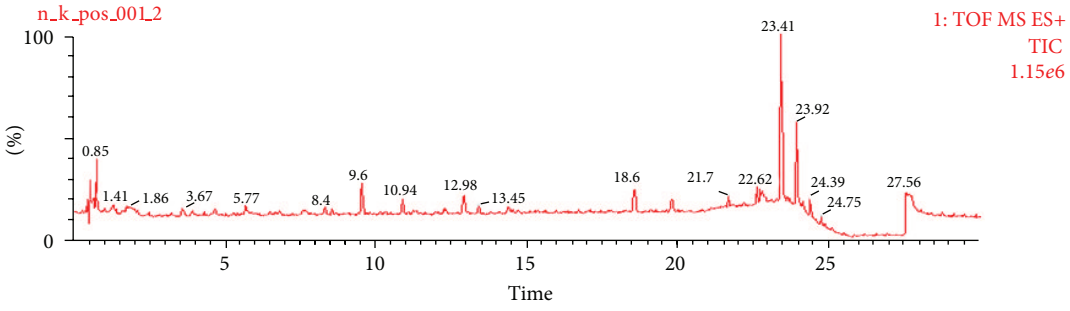

(a)

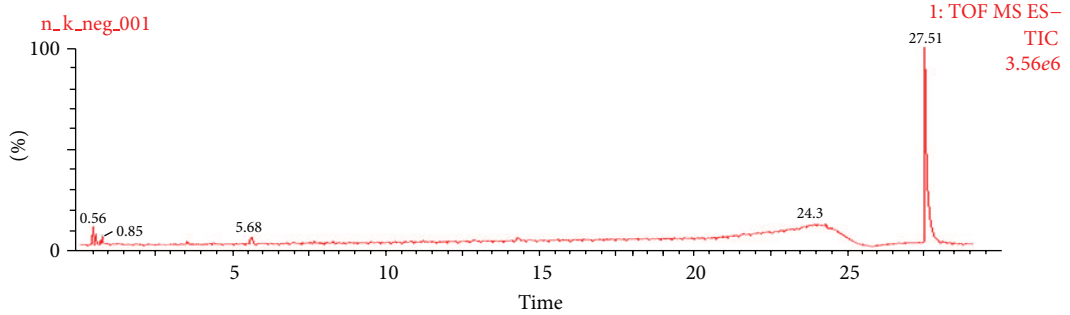

(b)

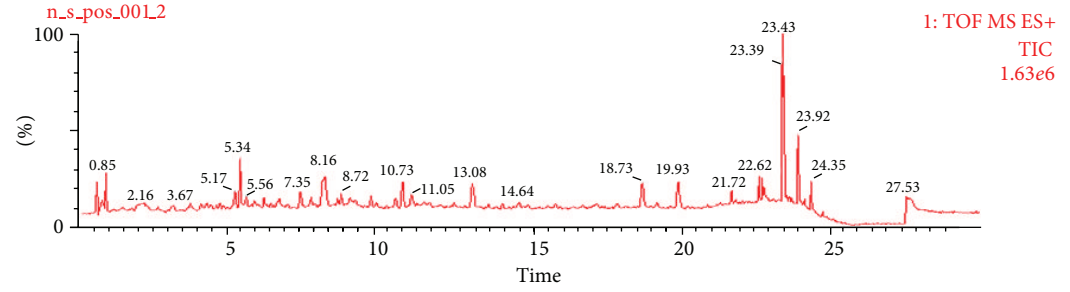

(c)

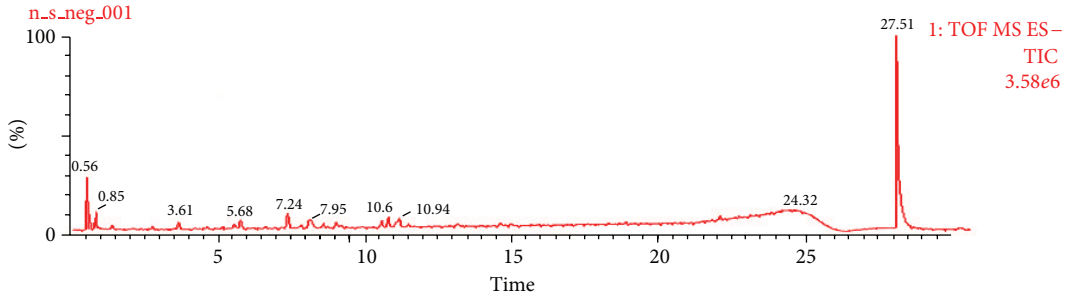

(d)

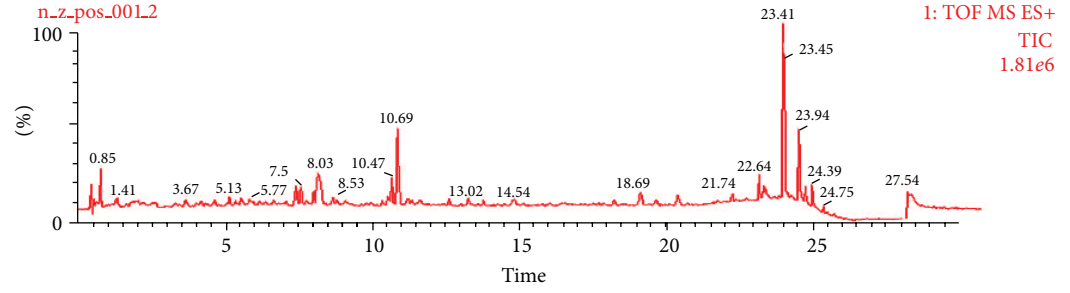

(e)

Figure 1: Continued.

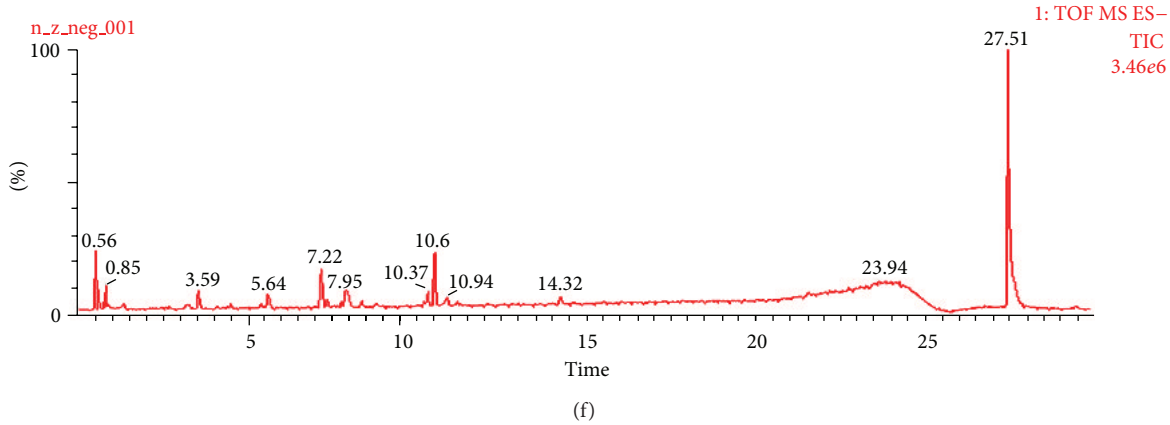

Figure 1: Total ion chromatograms of rat urine samples in positive and negative ion modes: (a) blank rat urine in positive mode; (b) blank rat urine in negative mode; (c) rat urine collected after administration of crude *Cornus officinalis* in positive mode; (d) rat urine collected after administration of crude *Cornus officinalis* in negative mode; (e) rat urine collected after administration of processed *Cornus officinalis* in positive mode; and (f) rat urine collected after administration of processed *Cornus officinalis* in negative mode.

for 1.5 h. The three filtrates were combined and evaporated to the final volume of 100 mL under reduced pressure at a temperature not exceeding 60°C.

2.4. Animals, Drug Administration, Biological Sample Collection, and Preparation. Fifteen male adult Sprague-Dawley rats weighing approximately 300 g were obtained from the Laboratory Animal Center of Zhejiang Academy of Medical Sciences (Zhejiang, China). Animals were acclimatized for at least 5 days with alternating 12 h dark/light cycles in a climate-controlled room with the temperature maintained at 22 ± 1°C, and a relative humidity of 60 ± 10%. Water and standard laboratory food were available ad libitum. All experiments were performed according to the guidelines for the care and use of animals as established by Zhe Jiang University.

The rats were equally divided into three groups (group A: crude *Cornus officinalis* group, $n = 5$; group B: processed *Cornus officinalis* group, $n = 5$; group C: control group, $n = 5$) and housed individually in metabolic cages for the collection of urine samples. The rats were fed with standard laboratory food as well as water, ad libitum, and acclimatized to the facilities for 1 week prior to the start of experiments. The animals were fasted overnight with free access to water before the test. Crude *Cornus officinalis* and its processed extracts were administered to each rat in groups A and B, respectively, by traditional oral gavage at a dose of 2 mL. Crude *Cornus officinalis* and its processed extracts were administered once daily for 1 week, while the equivalent volume of distilled water was orally administered to each rat in the control group (group C). Urine samples were collected after 1 week following administration. The volume of each sample was accurately measured and stored at −80°C for preservation.

For analysis preparation, urine samples (200 μL) were transferred to a 1.0 mL Eppendorf tube and acetonitrile (600 μL) was added. This mixture was vortex-mixed for 2 min and centrifuged at 4,000 rpm for 5 min. The supernatant was separated out and blowed dry with nitrogen at 40°C. The residue was then reconstituted in 100 μL acetonitrile and mixed to make final testing samples. A 5 μL aliquot of the final testing samples was injected into the UPLC-QTOF/MS system for analysis after centrifugation at 15,000 ×g for 15 min.

2.5. Data Processing. The mass data analysis was carried out using MetaboLynx and Masslynx V 4.1 (Waters Corp., Milford, MA, USA) for *in vivo* metabolite identification. The data was processed and mass full-scan raw data were collected through MSE acquisition. The UPLC-QTOF/MS data was detected and noise reduced in both the UPLC and MS domains, such that only true analytical peaks were further processed by the software (e.g., residual noise spikes were rejected).

3. Results and Discussion

3.1. UPLC-QTOF/MS Identification of the Main Active Components in Rat Urine. Iridoid glycosides and their metabolites are main components and active compounds in *Cornus officinalis*. In the current experiment, we expected that in addition to the major iridoid glycosides in *Cornus officinalis* extract, several metabolites would be detected in rat urine. From our results, we identified three iridoid glycosides in crude *Cornus officinalis* and its processed extracts, including morroniside, loganin, and sweroside, by comparing their retention times and MS data with established standards. The ion chromatograms of three iridoid glycosides and their metabolites are presented in Figure 1, and the monitored ions of each compound are listed in Table 1. The identification of each compound is outlined below.

3.2. Identification of Parent Compounds and Related Metabolites

3.2.1. Analysis of Parent Compound 1 and its Metabolites. Compound 1 showed an $[M+COOH]^-$ ion at m/z 451.1456.

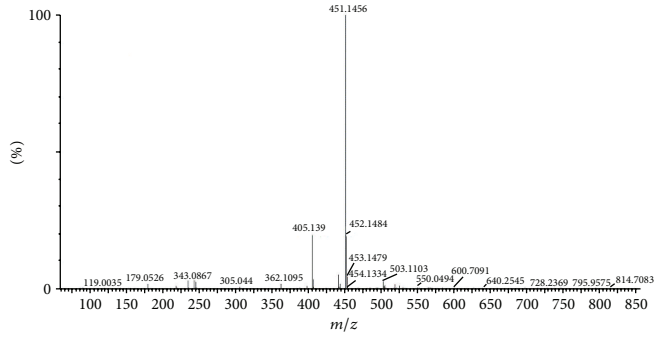

(a)

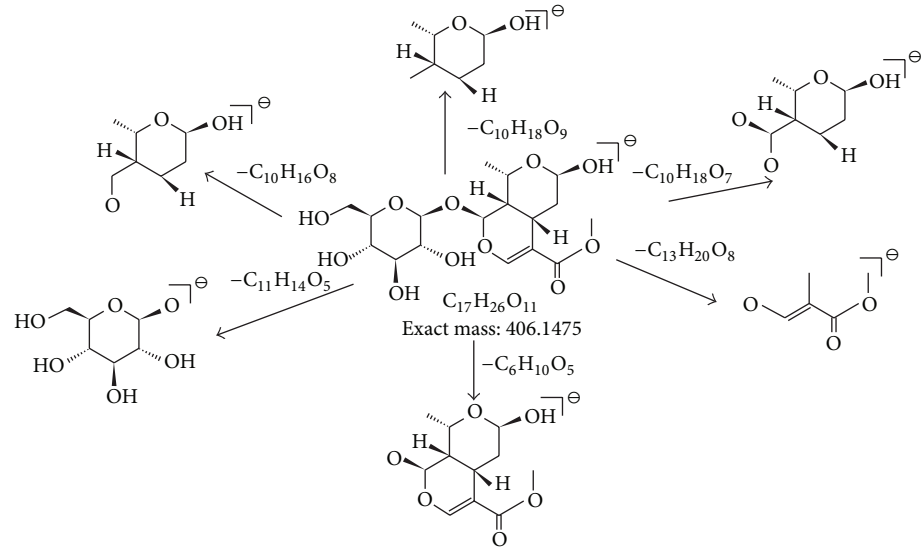

(b)

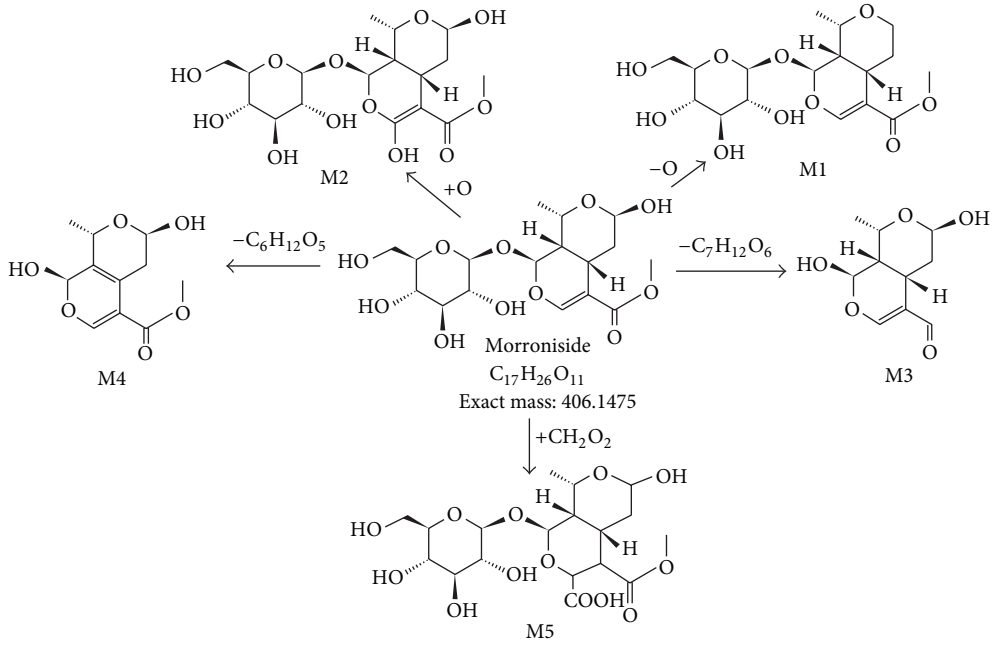

(c)

Figure 2: Proposed fragmentation pathways of morroniside and its metabolites from analysis of the rat urine samples: (a) accurate MS spectra of morroniside; (b) proposed fragmentation pathway of morroniside; and (c) proposed metabolic pathway of morroniside.

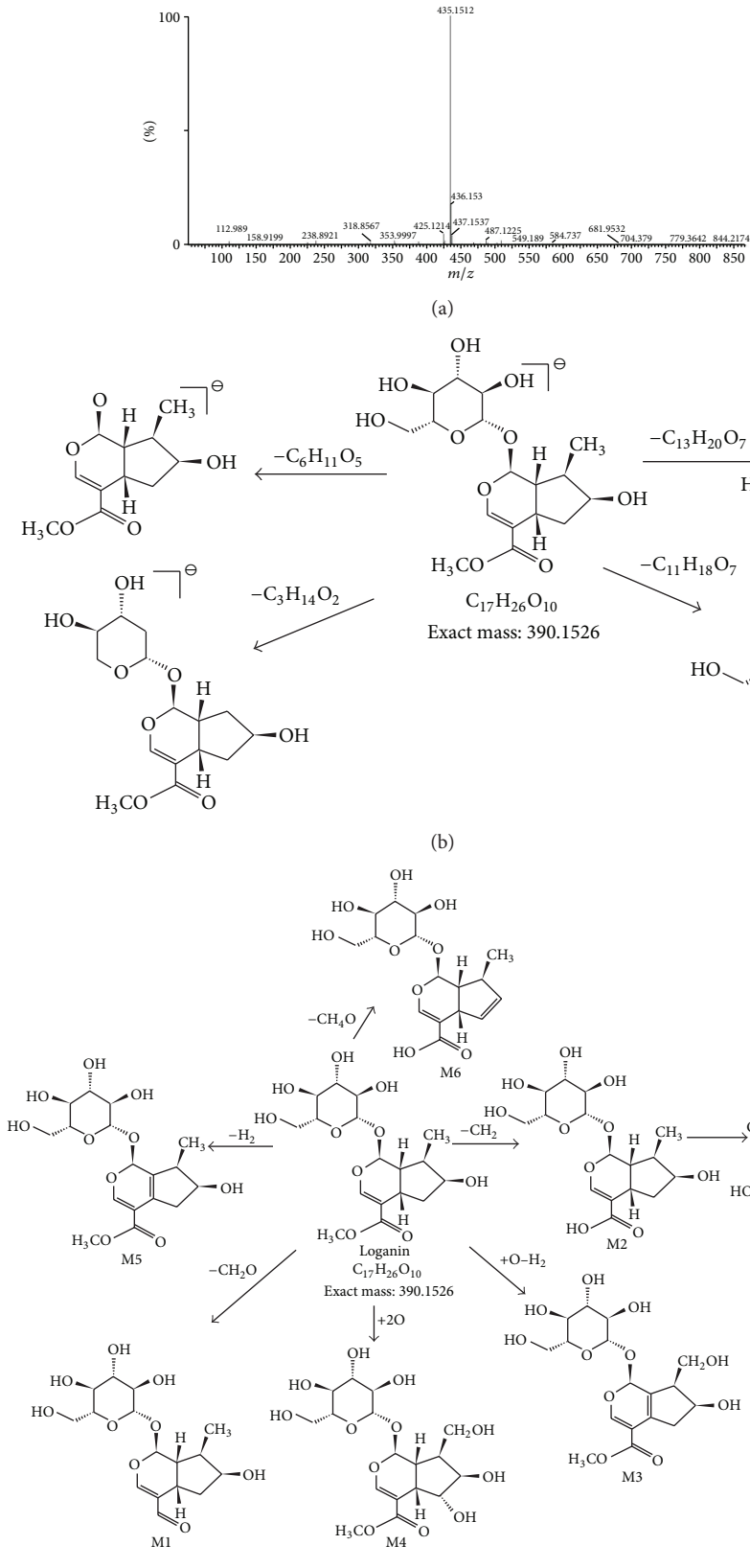

Figure 3: Proposed fragmentation pathways of loganin and its metabolites from analysis of the rat urine samples: (a) accurate MS spectra of loganin; (b) proposed fragmentation pathway of loganin; and (c) proposed metabolic pathway of loganin.

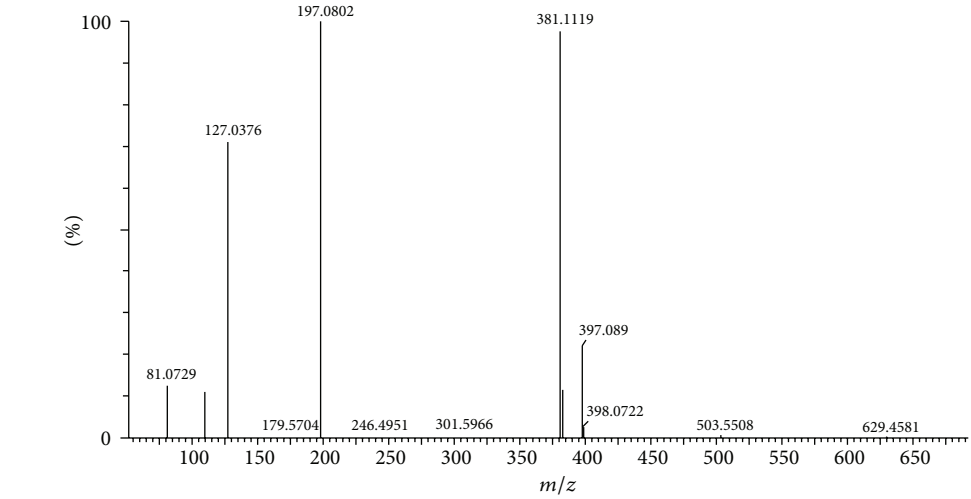

(a)

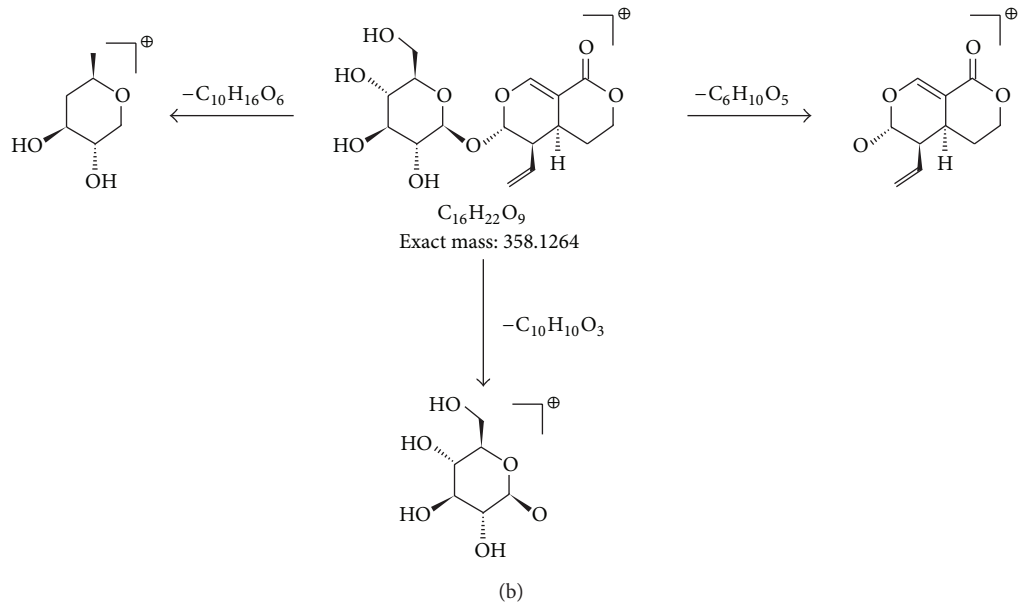

(b)

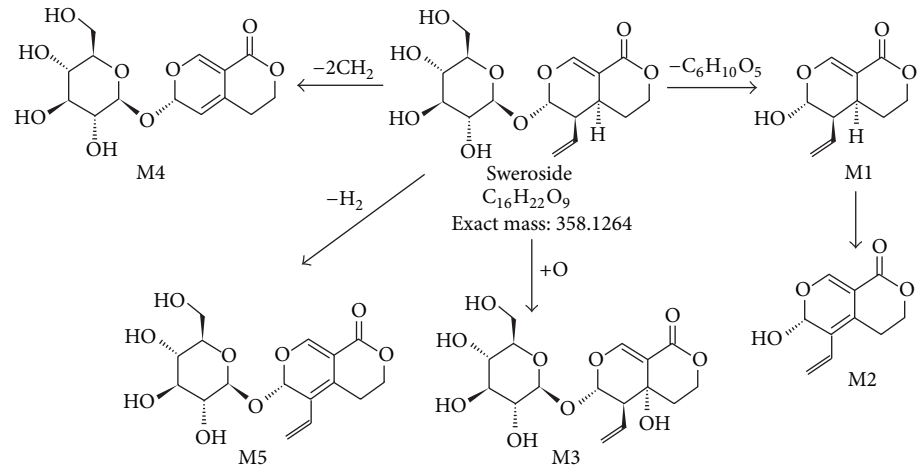

(c)

Figure 4: Proposed fragmentation pathways of sweroside and its metabolites from analysis of the rat urine samples: (a) accurate MS spectra of sweroside; (b) proposed fragmentation pathway of sweroside; and (c) proposed metabolic pathway of sweroside.

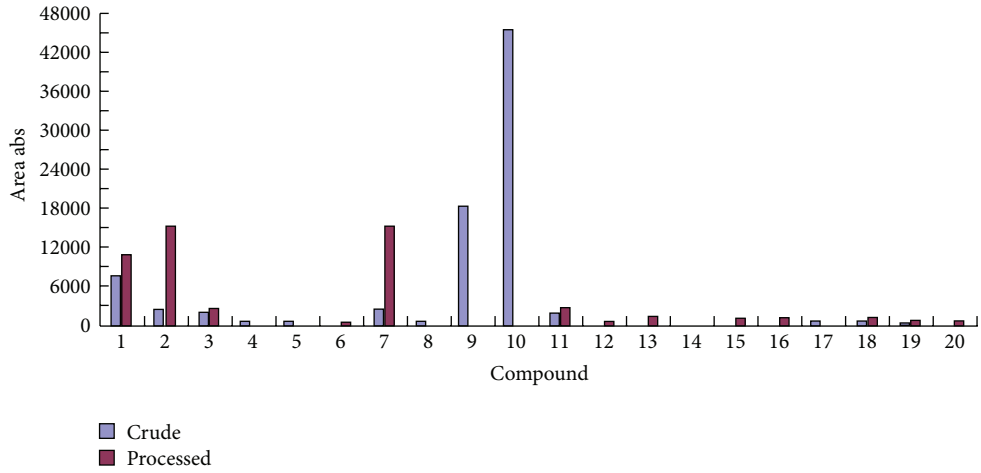

Figure 5: Parent compounds and metabolites detected in rat urines after oral administration of crude and processed *cornus officinalis*, respectively.

Table 1: The mass data of metabolites and parent components acquired using UPLC-QTOF/MS.

No.	Compound	T_R (min)	Molecular formula	Molecular weight	QTOF/MS	Mass accuracy (ppm)
1	Morroniside	8.08	$C_{17}H_{26}O_{11}$	406.1473	$[M+COOH]^-$	0
2	M1-1	10.73	$C_{17}H_{26}O_{10}$	390.1526	$[M-O]^-$	0.6
3	M1-2	8.08	$C_{17}H_{26}O_{12}$	422.1195	$[M+O]^-$	0.5
4	M1-3	8.72	$C_{10}H_{14}O_5$	214.1053	$[M-C_7H_{12}O_6]^-$	0.4
5	M1-4	5.53	$C_{11}H_{14}O_5$	225.061	$[M-C_6H_{12}O_6]^-$	0.3
6	M1-5	23.9	$C_{18}H_{28}O_{13}$	452.159	$[M+COOH_2]^-$	0.4
7	Loganin	10.60	$C_{17}H_{26}O_{10}$	390.1520	$[M+COOH]^-$	0
8	M2-1	7.5	$C_{16}H_{24}O_9$	360.1420	$[M-OCH_2]^-$	0.6
9	M2-2	6.28	$C_{16}H_{24}O_{10}$	376.1363	$[M-CH_2]^-$	0.2
10	M2-3	7.42	$C_{17}H_{24}O_{11}$	404.1313	$[M+O-H_2]^-$	0.3
11	M2-4	8.05	$C_{17}H_{26}O_{12}$	422.1233	$[M+O_2]^-$	0.5
12	M2-5	7.5	$C_{17}H_{24}O_{10}$	388.1369	$[M-H_2]^-$	0.3
13	M2-6	10.47	$C_{16}H_{22}O_9$	358.1264	$[M-CH_4O]^-$	0.1
14	M2-7	23.96	$C_{11}H_{14}O_7$	452.1590	$[M-CH_2-C_6H_{10}O_5]^-$	0.4
15	Sweroside	10.47	$C_{16}H_{22}O_9$	358.1256	$[M+Na]^+$	0
16	M3-1	10.48	$C_{10}H_{12}O_4$	196.0736	$[M-C_6H_{10}O_5]^+$	0.6
17	M3-2	8.08	$C_{10}H_{10}O_4$	194.0579	$[M-C_6H_{10}O_5-H_2]^+$	0.2
18	M3-3	7.33	$C_{16}H_{22}O_{10}$	374.0818	$[M+O]^+$	0.5
19	M3-4	2.65	$C_{14}H_{18}O_9$	330.0951	$[M-CH_2-CH_2]^+$	0.3
20	M3-5	6.35	$C_{16}H_{20}O_9$	356.1107	$[M-H_2]^+$	0.4

The corresponding fragment ions, including *m/z* 101.0273 $[M-C_{13}H_{20}O_8]^-$, *m/z* 123.0373 $[M-C_{10}H_{18}O_9]^-$, *m/z* 141.0547 $[M-C_{10}H_{16}O_8]^-$, *m/z* 155.0334 $[M-C_{10}H_{18}O_7]^-$, *m/z* 179 $[M-C_{11}H_{14}O_5]^-$, *m/z* 243.0825 $[M-C_6H_{10}O_5]^-$, and *m/z* 405.1390 $[M-H]^-$, were also identified in MS spectra of high-collision energy scan. Compound 1 was identified as morroniside through comparison with standard.

Five metabolites of morroniside were detected from the rat urine using MS^E approach and MetaboLynx, with most of the constituents $[M-H]^-$ being observed in the (−) ESI-MS spectra from MS^E data. Moreover, the characteristic fragment peaks of the parent compound related to the metabolite were observed. The high-collision energy scan fragment ions of M1-1 at *m/z* 390.1526 $[M-O]^-$, M1-2 at *m/z* 422.1195 $[M+O]^-$, M1-3 at *m/z* 214.1053 $[M-C_7H_{12}O_6]^-$, M1-4 at *m/z* 225.061 $[M-C_6H_{12}O_6]^-$ (loss of a glucose group), and M1-5 at *m/z* 425.159 $[M+COOH_2]^-$ were observed. After being processed with the mass defect filter, their possible metabolites were detected in combination the with related literature data or METLIN's metabolite mass spectral database, shown in Table 1. The pathways of morroniside and metabolites are shown in Figure 2.

3.2.2. Identification of Parent Compound 2 and Its Metabolites. Compound 2 showed an $[M+COOH]^-$ ion at *m/z* 435.1512 at 30 V. It also yielded product ions, including *m/z* 101.0143

$[M-C_{13}H_{20}O_7]^-$, *m/z* 127 $[M-C_{11}H_{18}O_7]^-$, and *m/z* 227.0905 $[M-C_6H_{10}O_5]^-$. Compound 2 was identified as loganin by comparison with standard.

Seven metabolites of morroniside were identified in the rat urine according to their retention time qualities, and MS/MS fragment ions. The high-collision energy scan fragment ions of M2-1 at *m/z* 360.1420 $[M-OCH_2]^-$, M2-2 at *m/z* 376.1363 $[M-CH_2]^-$, M2-3 at *m/z* 404.1313 $[M+O-H_2]^-$, M2-4 at *m/z* 422.1233 $[M+O_2]^-$, M2-5 at *m/z* 388.1369 $[M-H_2]^-$, M2-6 at *m/z* 358.1264 $[M-CH_4O]^-$, and M2-7 at *m/z* 452.1590 $[M-CH_2-C_6H_{10}O_5]^-$ were observed. The pathways of loganin and metabolites are shown in Figure 3.

3.2.3. Analysis of Parent Compound 3 and Its Metabolites. Compound 3 gave an $[M+Na]^+$ ion at *m/z* 381.1119 with a fragmentor voltage of 25 V. It also yielded product ions at *m/z* 127.0376 $[M-C_{10}H_{16}O_6]^+$ and *m/z* 197.0802 $[M-C_6H_{10}O_5]^+$. Compound 3 was identified as sweroside by comparison with standard.

Five metabolites of sweroside were detected from the rat urine using MetaboLynx software. The high-collision energy scan fragment ions of M3-1 at *m/z* 196.0736 $[M-C_6H_{10}O_5]^+$, M3-2 at *m/z* 194.0579 $[M-C_6H_{10}O_5-H_2]^+$, M3-3 at *m/z* 374.0818 $[M+O]^+$, M3-4 at *m/z* 330.0951 $[M-CH_2-CH_2]^+$, and M3-5 at *m/z* 356.1107 $[M-H_2]^+$ were observed. The pathways of sweroside and metabolites are shown in Figure 4.

3.3. The Influence of Rice Wine on the Contents of Main Compounds and Their Metabolites. Three parent compounds and seventeen metabolites were identified in the rat urine by UPLC-QTOF/MS after i.g. administration of aqueous extracts of crude *Cornus officinalis* and its processed extracts. In crude *Cornus officinalis* samples, thirteen metabolites were detected, but metabolites including M1-5, M2-5, M2-6, M2-7, M3-1, M3-5, and one parent compound (sweroside) were not found in the rat urine. It is possible that sweroside may have been transformed into its metabolites. For processed *Cornus officinalis* samples, six metabolites, including M1-3, M1-4, M2-1, M2-2, M2-3, and M3-2, were not detected in the rat urine. The peak intensities of parent compounds and metabolites in both crude and processed *Cornus officinalis* varied significantly. Moreover, the contents of compounds were dramatically decreased in *Cornus officinalis* after processing by rice wine. The results are shown in Figure 5.

4. Conclusion

In this work, UPLC-QTOF/MS was used to investigate the excretion of extracts of crude and processed *Cornus officinalis* in rat urine. Three parent compounds and seventeen metabolites were identified, demonstrating the analytical potential of this method for metabolism studies. Our study highlights the importance of UPLC-QTOF/MS as a potential tool for uncovering the effect of rice wine on metabolites of the main components of herbal medicine, *in vivo*, to predict and discover processing mechanisms of herbal medicine. It can therefore be used for studies of excipient treatment in processing of herbal medicine.

Authors' Contribution

G. Cao and H. Cai contribute equally to this work.

Acknowledgments

The authors are grateful for the financial support from the following: the National Natural Science Foundation of China (nos. 81274056, 81202918, 30873438, 30940093, and 81173546), the Medical Scientific Research Foundation of Zhejiang Province, China (no. 2013KYB183), the Natural Science Foundation of Jiangsu Province, China (no. BK2009495), the International Science and Technology Cooperation Project of Zhejiang Province, China (nos. 2012D60SA1C0065 and 2012D60SA1C0066), the International Science and Technology Cooperation Project of Jiangsu Province, China (no. BZ2011053) the Open Project of National First-Class Key Discipline for Science of Chinese Materia Medica, Nanjing University of Chinese Medicine (no. 2011ZYX2-006, no. 2011ZYX2-001), the Project of Science and Technology for Chinese Medicine of Zhejiang province, China (no. 2009CB008), the fund of Zhejiang Modernization of Traditional Chinese Medicine Item ([2008]436), the Chinese Medicine Research Program of Zhejiang Province, China (nos. 2008ZA002, 2011ZB101), and the Science Foundation of Zhejiang Chinese Medical University (no. 7211093).

References

[1] H. W. Yao and Y. Liu, "Study of the processing of chinese herbal medicine: status quo and development strategy," *China Pharmacy*, vol. 30, pp. 2394–2396, 2008.

[2] K. M. Qin, Y. Shi, X. H. Tan, T. L. Lu, H. Wu, and B. C. Cai, "Application of modern instrumental analytical techniques in the mechanism research of chinese medicine processing," *Scientia Sinica*, vol. 6, pp. 668–678, 2010.

[3] Z. Y. Li, H. P. Zhang, L. Jiang, and T. N. He, "Analysis of frace elements from supplementary materials in traditional Chinese medicine," *Journal of Yunnan Normal University*, vol. 1, pp. 25–27, 2002.

[4] M. F. Ma, W. Lv, and Y. Y. Gao, "Reseach on excipient of traditional Chinese medicine," *The Journal of Chinese Medicine & Traditional Chinese Medicine*, vol. 3, pp. 22–24, 2005.

[5] M. A. Presta, B. Bruyneel, R. Zanella, J. Kool, J. G. Krabbe, and H. Lingeman, "Determination of flavonoids and resveratrol in wine by turbulent-flow chromatography-LC-MS," *Chromatographia*, vol. 69, no. 2, pp. S167–S173, 2009.

[6] M. Boban and D. Modun, "Uric acid and antioxidant effects of wine," *Croatian medical journal*, vol. 51, no. 1, pp. 16–22, 2010.

[7] S. Das, D. D. Santani, and N. S. Dhalla, "Experimental evidence for the cardioprotective effects of red wine," *Experimental and Clinical Cardiology*, vol. 12, no. 1, pp. 5–10, 2007.

[8] Z. Q. Mao and X. R. Xuan, "Innovations in the production of yellow rice wine," *Food and Fermentation Technology*, vol. 1, pp. 10–12, 2009.

[9] J. Z. Yu, X. Wang, Z. Y. He, and J. Chen, "Comparative analysis of nutritional and functional components of yellow rice wine from different fields," *Journal of Anhui Agricultural Sciences*, vol. 32, pp. 15989–15991, 2009.

[10] G. Cao, C. Zhang, Y. Zhang et al., "Global detection and identification of components from crude and processed traditional

Chinese medicine by liquid chromatography connected with hybrid ion trap and time-of-flight-mass spectrometry," *Journal of Separation Science*, vol. 34, no. 15, pp. 1845–1852, 2011.

[11] L. L. Zhou, G. G. Wu, Z. Q. Liu, and S. Y. Liu, "Studies on the components of crude and processed fructus corni by ESI-MS^n," *Chemical Research in Chinese Universities*, vol. 24, no. 3, pp. 270–274, 2008.

[12] Z. Q. Fu, M. Y. Wang, and B. C. Cai, "Discussion of 5-hydroxymethylfurfural (5-HMF) in Chinese native medicine research present situation," *Chinese Archives of Traditional Chinese Medicine*, vol. 26, pp. 508–510, 2008.

[13] X. Ding, M. Y. Wang, Z. L. Yu, W. Hu, and B. C. Cai, "Studies on separation, appraisal and the biological activity of 5-HMF in *Cornus officinalis*," *China Journal of Chinese Materia Medica*, vol. 33, no. 4, pp. 392–484, 2008.

[14] G. Cao, H. Cai, Y. Zhang, X. Cong, C. Zhang, and B. Cai, "Identification of metabolites of crude and processed Fructus Corni in rats by microdialysis sampling coupled with electrospray ionization linear quadrupole ion trap mass spectrometry," *Journal of Pharmaceutical and Biomedical Analysis*, vol. 56, no. 1, pp. 118–125, 2011.

[15] G. Cao, Y. Zhang, X. D. Cong, H. Cai, and B. C. Cai, "Research progress on the chemical constituents and pharmacological activities of Fructus corni," *Journal of Chinese Pharmaceutical Sciences*, vol. 18, pp. 208–213, 2009.

[16] G. Cao, Y. Zhang, Q. Y. Shan et al., "Pharmacokinetic parameters of morroniside in iridoid glycosides of Fructus corni processing based on back-propagation neural network," *Pharmaceutical Biology*, vol. 49, pp. 989–993, 2011.

[17] L. Liu, A. Sun, S. Wu, and R. Liu, "Preparative purification of morroniside and loganin from fructus corni by combination of macroporous absorption resin and HSCCC," *Journal of Chromatographic Science*, vol. 47, no. 5, pp. 333–336, 2009.

[18] T. Yokozawa, C. H. Park, J. S. Noh, T. Tanaka, and E. J. Cho, "Novel action of 7-O-galloyl-D-sedoheptulose isolated from Corni Fructus as a hypertriglyceridaemic agent," *Journal of Pharmacy and Pharmacology*, vol. 61, no. 5, pp. 653–661, 2009.

[19] X. Li, Q. Wang, X. Zhang et al., "HPLC study of pharmacokinetics and tissue distribution of morroniside in rats," *Journal of Pharmaceutical and Biomedical Analysis*, vol. 45, no. 2, pp. 349–355, 2007.

[20] L. T. Zhang, L. M. Ren, and J. K. Wun, "Studies on pharmacokinetics of loganin and morroniside in *Cornus officinalis* injection in mice," *China Journal of Chinese Materia Medica*, vol. 28, no. 6, pp. 509–512, 2003.

[21] Y. D. Luo, J. Chen, J. Cao, X. D. Wen, and P. Li, "Determination of sweroside in rat plasma and bile for oral bioavailability and hepatobiliary excretion," *Chemical and Pharmaceutical Bulletin*, vol. 57, no. 1, pp. 79–83, 2009.

Hindawi Publishing Corporation
Evidence-Based Complementary and Alternative Medicine
Volume 2013, Article ID 496036, 8 pages
http://dx.doi.org/10.1155/2013/496036

Research Article

Effects of "Bu Shen Huo Xue Decoction" on the Endometrial Morphology and Expression of Leukaemia Inhibitory Factor in the Rat Uterus during the Oestrous Cycle

Xin Gong,[1] Yanyan Yu,[1] Qing Tong,[1] Ying Ren,[2] and Zhe Jin[1]

[1] *Reproductive Endocrinology Centre, Dongfang Hospital of Beijing University of Chinese Medicine, No. 6 Fangxingyuan 1 Qu, Fengtai District, Beijing 100078, China*
[2] *Dongzhimen Hospital of Beijing University of Chinese Medicine, No. 5 Haiyuncang, Beijing 100700, China*

Correspondence should be addressed to Zhe Jin; zjin0129@163.com

Received 15 February 2013; Revised 27 March 2013; Accepted 7 April 2013

Academic Editor: Chris J. Branford-White

The purpose of this study was to explore the positive effects of Bu Shen Huo Xue Decoction (BSHXF) on assisted reproduction. The study aimed to evaluate whether BSHXD could improve endometrial morphology and increase the expression of LIF in a gonadotrophin-releasing hormone agonists (GnRHa) long protocol-induced rat model during metestrus, diestrus, proestrus, and oestrus. The BSHXD group presented significantly increased endometrium thickness and decreased MVD compared with the GnRHa long protocol group. In addition, the expression of LIF was significantly higher in the BSHXD group. There were no significant differences between the control group and the BSHXD group in terms of MVD and LIF expression. These results suggested that BSHXD can improve the endometrium development, reduce the abnormal angiogenesis, and increase the expression of receptivity markers in a GnRHa long protocol-induced rat model during the oestrous cycle, which might result in an endometrial environment better suited for female reproduction.

1. Background

Infertility remains a prevalent disease worldwide, and its incidence is still increasing. Assisted reproductive technology (ART) is one current treatment. However, the fertility rate following ART is very low [1]. Impaired endometrial receptivity is a major limitation and reason for this low fertility.

It has been well documented that endometrial receptivity is a complex and multifactorial process [2] involving a good-quality embryo, a receptive endometrium, and the synchronisation between the developmental stages of the embryo itself [3]. Previous observations have demonstrated that when using a GnRHa long protocol, advanced endometrial maturation is present on the oocyte retrieval day of in vitro fertilisation (IVF), which may possibly result in a failure to correctly synchronise the timing between the embryo and a receptive endometrium [4]. Many studies have shown that the periovulatory uterine characteristics in ovarian stimulation treatment (OS) are considerably different compared with the natural cycle [4, 5]. It has been hypothesised that this change has already started by the follicular phase [5].

A large amount of evidence indicates that angiogenesis may play an important role during the implantation window [6–8], because the endometrial receptivity requires complex remodelling and angiogenesis to support foetal development [9–12]. Our previous small-sample study demonstrated that the GnRHa long protocol results in abnormal angiogenesis in the rat endometrium during the first oestrous cycle after OS. These results indicate that the side effects of the GnRHa long protocol treatment may trigger negative angiogenesis in the endometrium and impact later receptivity. The strong exposure of the endometrium to supraphysiological steroid hormone levels during the follicular phase might be responsible for this phenomenon [4].

In China, traditional Chinese medicine is widely used in assisted reproductive technology to enhance the success of IVF treatment. Bu Shen Huo Xue Decoction (BSHXD), a Chinese herbal formula, consists of *Placenta Hominis*, *Radix*

Rehmanniae Preparata, *Radix Salviae Miltiorrhizae*, *Radix Angelicae Sinensis*, *Radix Dipsacus asperoides*, *Eucommia ulmoides*, *Dioscorea opposita*, *Flos Rosae Rugosae*, *Rhizoma Ligustici Chuanxiong*, and *Semen Coicis*. This formula is used to tonify the kidney, regulate the uterine function, and promote blood circulation according to traditional Chinese medicinal prescriptions. Numerous studies have reported that many traditional Chinese medicinal herbs are rich sources of compounds that regulate angiogenesis [13]. Our recent clinical observations suggest that BSHXD has a positive effect on angiogenesis in the endometrium. Therefore, the potential benefits of regulating angiogenesis and enhancing the success of IVF need to be thoroughly studied.

Microvessel density (MVD) is one of the most common methods of indirectly assessing angiogenesis factors [14]. The maximal expression of leukaemia inhibitory factor (LIF) is observed in the midsecretory phase of the menstrual cycle, coinciding with the time of implantation in both the human and murine endometria [15, 16]. The strong expression of LIF is more likely to initiate a pregnancy than weak LIF during the luteal phase prior to IVF treatment in humans [17, 18]. LIF is one of very few cytokines to be a critical factor for implantation [19]. LIF null mutation female mice are infertile because of the failure of implantation [20] and LIF is significantly reduced in the endometria of infertile women [21].

The primary aim of this study was to explore whether BSHXD ameliorates the side effects of the GnRHa long protocol on endometrium histology, endometrium receptivity cytokines, and endometrial angiogenesis in a GnRHa long protocol-induced rat model. In addition, this study aimed to provide evidence of the usefulness of BSHXD in assisted reproduction.

2. Methods

2.1. Animals. SD (Sprague-Dawley) rats of 9-10 weeks of age were used for the experiments. All the procedures were performed according to the guidelines of the Beijing University of Chinese Medicine Animal Care and Use Committee. The rats were kept under standard 12 h light and 12 h dark conditions and under controlled temperature ($23 \pm 3^{\circ}$C) with 45%–65% humidity.

2.2. Treatment. Oestrus was identified by vaginal smear. Only the rats with regular cycles were used in the study. Suitable rats were randomly allocated into three groups: control, GnRHa long protocol, and BSHXD.

The animals in the GnRHa long protocol group were given 1 mL/100 g of distilled water for 12 days and then treated using the GnRHa long protocol. Briefly, a GnRH agonist (1.5 μg/100 g bw/day) (triptorelin, Diphereline, France) was i.p. injected from the 3th to 9th days of oestrous. The pregnant mare's serum gonadotropin (40 IU/100 g bw) (PMSG, China) was i.p. injected on the 9th day of oestrous, followed by the injection of hCG (40 IU/100 g) (Human Chorionic Gonadotropin, China) 28 h later.

BSHXD granules were provided by the Pharmacy Department of Dongfang Hospital of Beijing University of Chinese Medicine. The BSHXD granules contain equal weights of the ingredients of the BSHXD formula: *Placenta Hominis* 10 gram, *Radix Rehmanniae Preparata* 15 gram, *Radix Salviae Miltiorrhizae* 10 gram, *Radix Angelicae Sinensis* 12 gram, *Radix Dipsacus Asperoides* 15 gram, *Eucommia ulmoides* 12 gram, *Dioscorea opposita* 15 gram, *Flos Rosae Rugosae* 6 gram, *Rhizoma Ligustici Chuanxiong* 6 gram, and *Semen Coicis* 12 gram. The granules were dissolved in 200 mL of distilled water and kept at 2–8°C until use. The animals in the BSHXD group were given the drugs 1 mL/100 g daily for 12 days and then were subjected to the GnRHa long protocol treatment as the GnRHa long protocol group.

The rats in the control group were given distilled water for 12 days, followed by injections with saline at the same time and volume as those used in the GnRHa long protocol group.

2.3. Tissue Collection and Preparation. The whole uteri were collected from the GnRHa long protocol group and the BSHXD group on days 2, 3, 4, and 5 after hCG injection, and the uteri of the control group were collected on days 2, 3, 4, and 5 after ovulation. Day 2 was the day of metestrus. Day 3 was the day of diestrus. Day 4 was the day of proestrus. Day 5 was the day of oestrus. The tissue was divided into 2 parts after being rinsed with cold saline. One part was fixed in 4% paraformaldehyde and then embedded in paraffin for HE and immunohistochemical assays. The other part was stored at −80°C for later Western blot analysis.

2.4. Haematoxylin Eosin (HE) Staining. The paraffin-fixed tissues were divided into the 4 μm. After dewaxing, rehydration, and staining in Harris haematoxylin, the slides were counterstained in eosin-phloxine. The morphological changes were captured with a digital camera (Olympus, Inc., Tokyo, Japan).

2.5. Immunohistochemistry for CD34 and LIF. The paraffin-fixed tissues were divided into 4 μm sections. After dewaxing, rehydration, and blocking, the slides were incubated with the following primary antibodies: CD34 antibody (AF-4117, R&D Systems, USA) at a dilution of 1 : 39 and LIF antibody (sc-1336, Santa Cruz Biotechnology, USA) at a 1 : 200 dilution overnight at 4°C. After washing with PBS, the tissues were incubated with secondary antibodies for 25 minutes, followed by incubation with a DBA Kit (ZLI-9018, ZSGB-BIO, China). The negative controls were treated with the same procedure except with the PBS during the primary antibody incubation step.

The staining intensity of each slide was graded (0, absence; 1, weak; 2, moderate; 3, strong) by two examiners in a blinded fashion and assessed with the HSCORE. The HSCORE was calculated as follows:

$$\text{HSCORE} = P_i\,(\,i + 1)\,, \tag{1}$$

where i is the staining intensity and P_i is the percentage of stained glandular epithelium cells at each level of intensity.

Table 1: Comparison of the endometrial thickness during the oestrous cycle.

Endometrial thickness (μm)	Control group	GnRHa long protocol group	BSHXD group	*P* valve		
D2 (Metestrus)	541.97 ± 19.43	602.92 ± 6.39	485.98 ± 26.53	0.00[a]	0.00[b]	0.24[c]
D3 (Diestrus)	543.61 ± 37.37	431.48 ± 10.82	549.07 ± 27.09	0.00[a]	0.00[b]	0.82[c]
D4 (Proestrus)	563.86 ± 16.68	434.05 ± 5.77	750.08 ± 29.23	0.00[a]	0.00[b]	0.00[c]
D5 (Oestrus)	669.76 ± 24.10	494.25 ± 6.52	829.40 ± 22.65	0.00[a]	0.00[b]	0.00[c]

[a]Control group versus the GnRHa long protocol group.
[b]BSHXD group versus the GnRHa long protocol group.
[c]Control group versus the BSHXD group.

2.6. Density of Microvessels. Microvessels densities were viewed at 400x magnification (40x objective lens and 10x ocular lens; 0.24 mm^2/field). The images were captured with a digital camera (Olympus, Inc., Tokyo, Japan). For each section, at least 5 random fields were selected to determine the average vessel density within the uterus.

The number of CD34-positive vessels was quantified using Diagnostic Instruments Spot-II digital software (Diagnostic instruments, Inc., USA). The microvessel density was calculated as the number of CD34-positive vessels/(40 × 0.24 mm^2).

2.7. Western Blot for LIF. Rat endometrium tissue was homogenised and lysed in RIPA Lysis Buffer (C1053, Applygen, China) and proteinase inhibitor (P1265, Applygen, China). The protein concentration was quantified with bicinchoninic acid (BCA) (P1511, Applygen, China). The protein was used for Western blot with an LIF primary antibody (sc-1336, Santa Cruz Biotechnology, Europe) at a 1 : 500 dilution and incubated overnight at 4°C. After incubation, the membranes were washed three times with TBS-T and then incubated with the secondary antibody at a dilution of 1 : 2500 at room temperature for 1 h. The blots were visualised with Super ECL Plus Detection Reagent (P1010, Applygen, China). The ECL signals were detected with Quantity One software (Bio-Rad). GAPDH (ab8245, Abcam, UK) was used as an internal control to validate the amount of protein loaded onto the gels.

2.8. Statistical Analysis. The data are shown as the mean ± SEM. The Mann-Whitney *U* test was used to compare the two groups. Significance was set at *P* value < 0.05. Graphs of the data were produced using Excel software.

3. Results

3.1. Endometrial Thickness. The outcome of endometrial thickness was obtained by two independent observers blinded to treatment. The morphological change parameters and data are shown in Figure 1 and Table 1. The endometrial thickness of the GnRHa long protocol group was thicker than that of the control group and BSHXD group in metestrus (*P* values of 0.004), but the GnRHa long protocol group endometrial thickness was thinner than the control group mean (*P* values of 0.009, 0.002, and 0.002, resp.) and the BSHXD group mean (*P* values of 0.002, 0.002, and 0.002, resp.) in diestrus, proestrus, and oestrus periods. There was no significant difference between the BSHXD group and the control group in metestrus and diestrus (*P* values of 0.24 and 0.82, resp.). The thickness in the BSHXD group was significantly thicker than that in the control group in proestrus and oestrus (*P* values of 0.002 and 0.002, resp.).

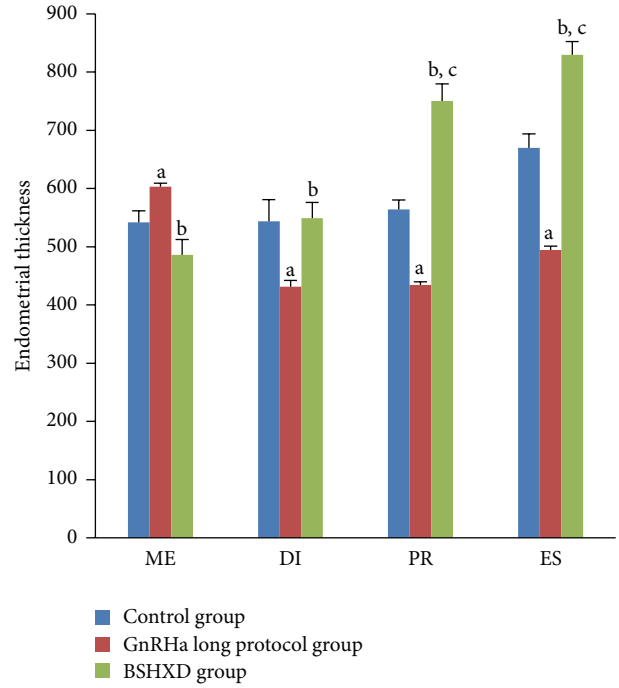

Figure 1: HE staining to evaluate the rat endometrial thickness. Comparison of thickness of rat uteri during metestrus (ME), diestrus (DI), proestrus (PR), and estrus (ES). (a) *P* values < 0.01 compared with the control group; (b) *P* values < 0.01 compared with the GnRHa long protocol group; (c) *P* values < 0.01 compared with the control group. The bar graphs represent daily data from 6 different animals.

3.2. Expression of Microvessel Density (MVD). Accompanying the GnRHa long protocol treatment-induced downregulation of LIF expression, there was a significant increase in endometrial MVD in rats (MVD: 3.77 ± 0.24 in metestrus,

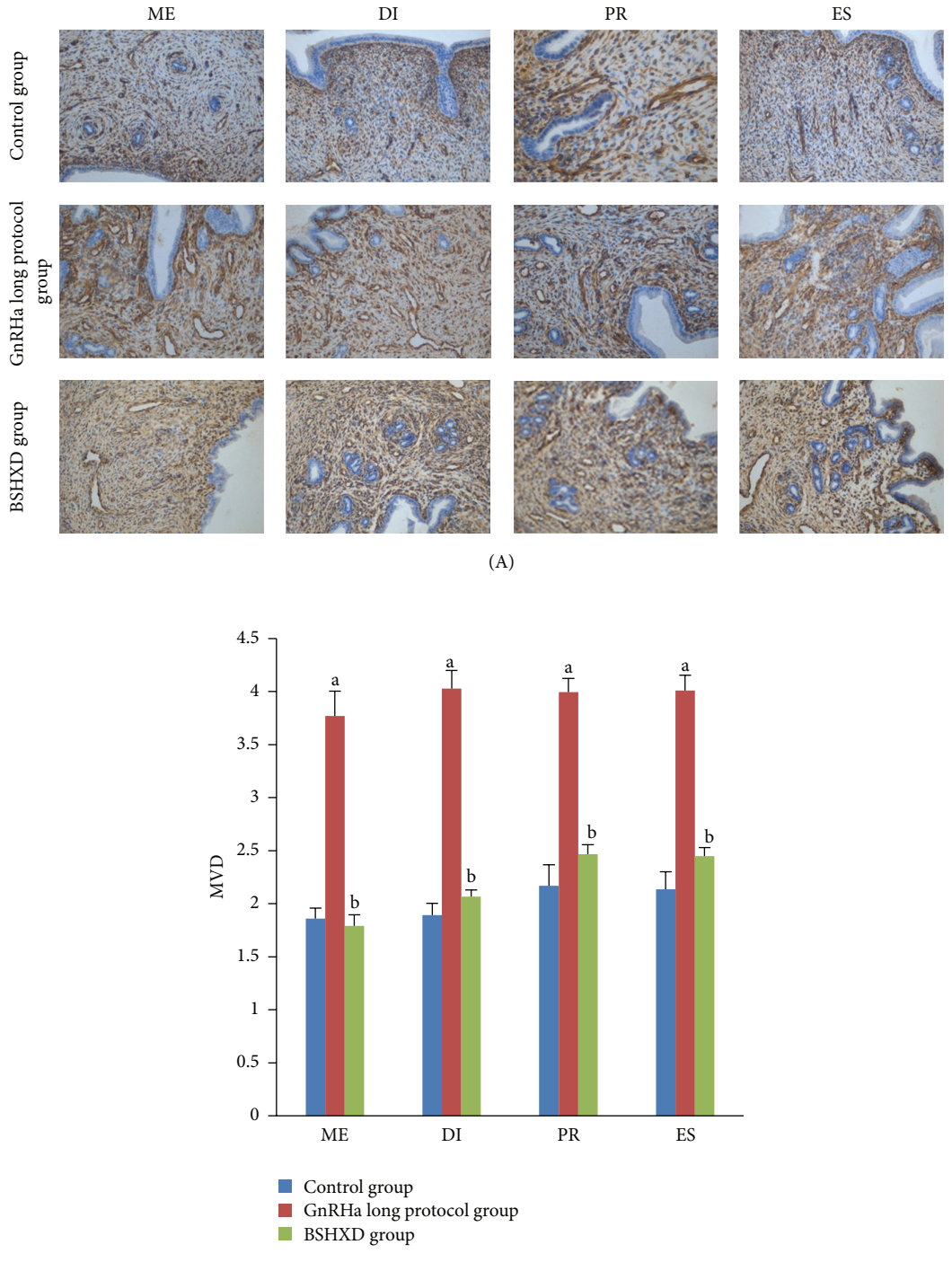

Figure 2: Expression of microvessel density (MVD) during metestrus (ME), diestrus (DI), proestrus (PR), and oestrus (ES). (A) Comparison of the MVD of rat uteri during metestrus (ME), diestrus (DI), proestrus (PR), and oestrus (ES). Magnification: 200x. (B) The number of CD34-positive vessels was quantified. The bar graphs represent daily data from 6 different animals. (a) P values < 0.01 compared with the control group; (b) P values < 0.01 compared with the GnRHa long protocol group.

4.03 ± 0.17 in diestrus, 3.99 ± 0.13 in proestrus, and 4.01 ± 0.14 in oestrus) (Figure 2). Related to the GnRHa long protocol group, no increase was observed in the control and the BSHXD groups in metestrus, diestrus, proestrus, and oestrus (P values of 0.002, 0.002, 0.002 and 0.002, resp.).

3.3. Expression of Endometrial LIF as Evaluated by Immunohistochemistry. LIF immunostaining was predominantly detected in glandular and luminal epithelial cells in rat endometrium. The LIF staining intensity in the GnRHa long protocol group was weaker than that in the control group

in metestrus, diestrus, proestrus, and oestrus (P values of 0.002, 0.002, 0.002, and 0.015, resp.) and weaker than that of the BSHXD group (P values of 0.002, 0.002, 0.015, and 0.002, resp.). During the oestrus cycle, there were no significant differences between the control group and BSHXD group in metestrus, diestrus, proestrus, and oestrus (P values of 0.093, 0.24, 0.065, and 0.31, resp.). The staining intensities are depicted in Figure 3.

3.4. Western Blot Expression of Endometrial LIF. Consistent with the results of the immunohistochemical staining, the LIF protein expression trends were confirmed by Western blot analysis (Figure 4). GAPDH was used as an internal loading control in each lane. Normalised with the GAPDH expression level, the expression of LIF protein in the GnRHa long protocol group was lower than that in the control group (P values of 0.026, 0.004, 0.015, and 0.009, resp.) and the BSHXD group (P values of 0.041, 0.015, 0.041, and 0.015, resp.) in metestrus, diestrus, proestrus, and oestrus. There were no significant differences between the control group and BSHXD group (P values of 0.485, 0.699, 0.065, and 0.065, resp.).

4. Discussion

The present study is a pilot, prospective, randomized, and controlled comparison study of the effects of BSHXD on the endometrial morphology and expression of LIF and MVD in a GnRHa long protocol-induced rat model during the oestrus cycle. The process of implantation only takes place during a limited "implantation window." This window is a restricted period of endometrial receptivity between days 4 and 6 of pregnancy in rats [22] and between days 20 and 24 of a regular menstrual cycle (day LH+7 to LH+11) in humans [23]. Implantation involves a complex sequence of signalling events that are crucial to the pregnancy. Most of these identified molecular mediators are under the influence of ovarian hormones [24, 25]. However, the GnRHa long protocol will result in the endometrium exposure to supraphysiological steroid hormone levels. The dosage in our experiment produced thin and impaired endometria in our rat models and abnormal expression of LIF and MVD, which may impact later endometrial implantation capacity. Predictably, the GnRHa long protocol impaired the endometrium and implantation at a very early stage even at the follicular phase. Our observations are in agreement with a previous study that confirmed the negative impact of GnRHa ovarian stimulation treatment [26–28], which may cause a relatively low rate of implantation despite advances in ATR [29]. Indeed, the average implantation rate in IVF is approximately 25% [30].

Endometrial thickness is an important bioassay. According to our present study results, the endometrial thickness in the GnRHa long protocol group was significantly lower than that of the control and BSHXD groups during diestrus, proestrus, and oestrus. These results suggest that the uterus is quite sensitive to hormonal change. Although some researchers have argued that histological endometrial data do not predict and influence the reproductive failure [31], increased endometrial thickness is associated with improved pregnancy rates [32]. Some studies have revealed that below a certain thickness cut-off limit, pregnancy will not be achieved [33–35]. We observed that BSHXD had positive effects on endometrial morphology in rats after they were subjected to a GnRHa long protocol treatment. There were no significant differences between the control group and BSHXD group in metestrus and diestrus. Compared with the control group, the BSHXD group presented enhanced endometrial thickness during the proestrus and oestrus stages. Thus, we suggest that BSHXD may have the capacity to stimulate the growth of the endometrium.

Because adequate blood flow to the embryo is critical for normal growth, it is not surprising that angiogenesis plays an important role during implantation. Dysregulated endometrial angiogenesis underlies infertility [36–38]. Therefore, appropriate angiogenesis is central to implantation and pregnancy. There was an approximately 2-fold increase in MVD in the GnRHa long protocol group compared with the control and BSHXD groups. However, there was no difference between the control group and BSHXD group. These results demonstrate that pretreatment with BSHXD can significantly ameliorate the negative effects of the GnRHa long protocol on MVD. We suggest that BSHXD may regulate angiogenesis during the oestrous cycle.

The present study demonstrated that BSHXD improved the expression of LIF protein in rat uteri during the oestrous cycle. LIF is a biomarker that is largely accepted as an indicator of endometrial receptivity both in humans, mice, and rats. LIF-deficient mice are mostly infertile [20], clearly indicating the important role. Our research confirmed the result of a previous study that indicated that LIF protein is maximally expressed in the murine endometrial glandular epithelium [39, 40]. Our results demonstrated that the GnRHa long protocol affected cytokine production at a very early stage, even before the "implantation window," because the staining intensity of LIF in the GnRHa long protocol group was weaker than the other two groups (P values < 0.05). However, there were no significant differences between the control and BSHXD groups (P values > 0.05). Our results indicate that BSHXD improves the LIF expression and brings its level closer to normal, which may help improve the later endometrial implantation capacity.

Most TCM remedies are formulated using individual herbs in combination because different herbs are thought to increase therapeutic efficacy and reduce adverse effects simultaneously through multiple targets and biological pathway [41]. The biological mechanisms underlying the effect of BSHXD on assisted reproduction remain unclear. However, our study demonstrated that the positive effects of BSHXD may be associated with the following: (a) increasing endometrial thickness, (b) regulation of angiogenesis to improve the endometrial environment, and (c) modulating cytokines that are associated with the pregnancy rates of IVF. According to the principles of TCM, BSHXD can nourish the uterus and adjust its function.

In conclusion, BSHXD improved the uterine environment by advancing endometrial development, reducing

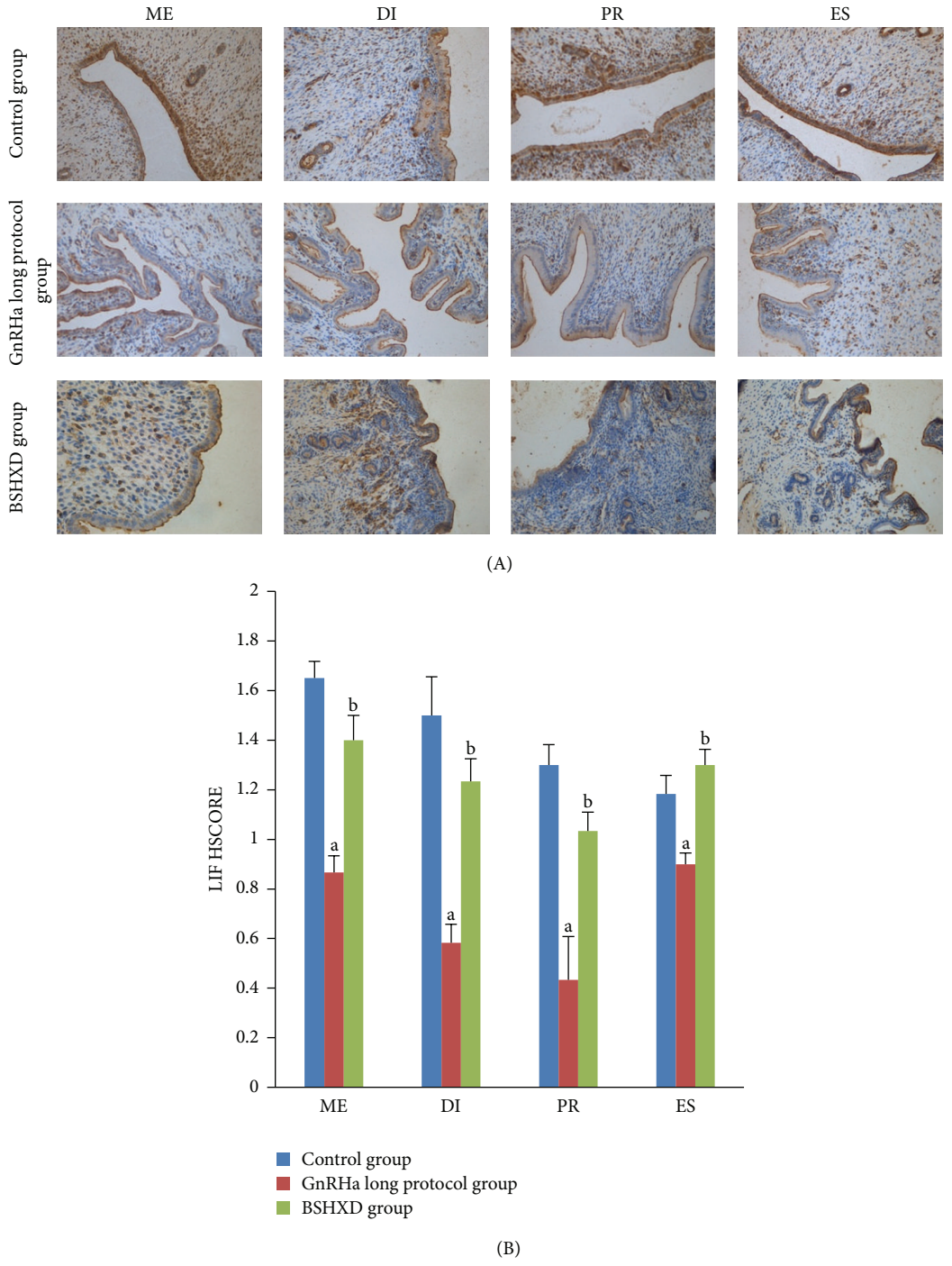

Figure 3: LIF immunohistochemical staining in the endometrium. (A) Immunohistochemical staining to evaluate the expression of endometrial LIF during metestrus (ME), diestrus (DI), proestrus (PR), and oestrus (ES). Magnification: 200x. (B) HSCORE for the immunohistochemical staining intensity of the endometrial LIF during metestrus (ME), diestrus (DI), proestrus (PR), and oestrus (ES). The bar graphs represent daily data from 6 different animals. (a) P values < 0.05 compared with the control group; (b) P values < 0.05 compared with the GnRHa long protocol group.

abnormal angiogenesis, and increasing expression of the protein receptivity marker LIF during the oestrous cycle. BSHXD may be useful aid for female reproduction. A further clinical evaluation needs to be conducted to confirm these results in human subjects.

Authors' Contribution

Gong Xin and Yu Yanyan conducted the experiment. Tong Qing provided the reagents and materials. Gong Xin performed all the immunohistochemical staining and Western

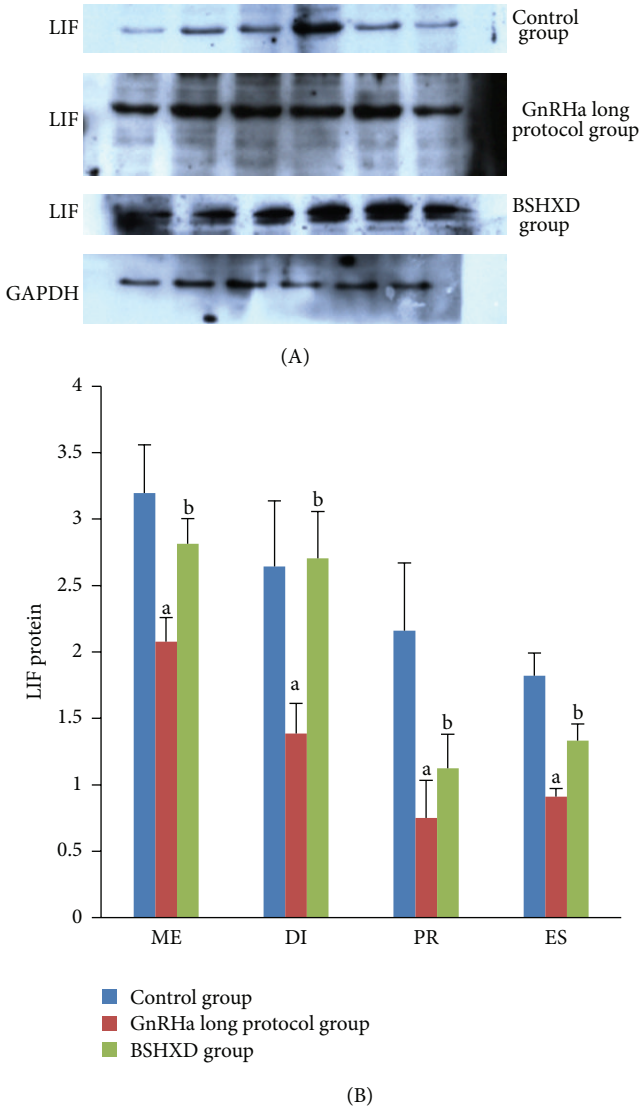

Figure 4: Expression of endometrial leukaemia-inhibitory factor (LIF) protein during metestrus (ME), diestrus (DI), proestrus (PR), and oestrus (ES). The bar graphs represent daily data from 6 different animals. (a) P values < 0.05 compared with the control group; (b) P values < 0.05 compared with the GnRHa long protocol group.

blot studies and drafted the paper. Jin Zhe performed the statistical analysis, drafting, and critical revision of the paper. All authors read and approved the paper.

Conflict of Interests

The authors declare that they have no conflict of interests.

Acknowledgments

The authors thank Dai Xin and Cheng Juan of the Dongzhimen Hospital of Beijing University of Chinese Medicine, for their helpful discussion and advice on the immunohistochemistry, and Fang Tingyu of the Beijing University of Chinese Medicine for his helpful advice on the English language. The authors are grateful to He Xinyi and Long Hongzhu for providing reagents. This project was supported by the Natural Science Foundation of China. The project no. is 81173292.

References

[1] A. P. Ferraretti, V. Goossens, J. de Mouzon et al., "Assisted reproductive technology in Europe, 2008: results generated from European registers by ESHRE," *Human Reproduction*, vol. 27, no. 9, pp. 2571–2584, 2012.

[2] F. W. Bazer, G. Wu, T. E. Spencer et al., "Novel pathways for implantation and establishment and maintenance of pregnancy in mammals," *Molecular Human Reproduction*, vol. 16, no. 3, pp. 135–152, 2010.

[3] H. Cakmak and H. S. Taylor, "Implantation failure: molecular mechanisms and clinical treatment," *Human Reproduction Update*, vol. 17, no. 2, Article ID dmq037, pp. 242–253, 2011.

[4] B. C. J. M. Fauser and P. Devroey, "Reproductive biology and IVF: ovarian stimulation and luteal phase consequences," *Trends in Endocrinology and Metabolism*, vol. 14, no. 5, pp. 236–242, 2003.

[5] E. G. Papanikolaou, C. Bourgain, E. Kolibianakis, H. Tournaye, and P. Devroey, "Steroid receptor expression in late follicular phase endometrium in GnRH antagonist IVF cycles is already altered, indicating initiation of early luteal phase transformation in the absence of secretory changes," *Human Reproduction*, vol. 20, no. 6, pp. 1541–1547, 2005.

[6] D. L. Carlone and V. Rider, "Embryonic modulation of basic fibroblast growth factor in the rat uterus," *Biology of Reproduction*, vol. 49, no. 4, pp. 653–665, 1993.

[7] V. Rider and A. Psychoyos, "Inhibition of progesterone receptor function results in loss of basic fibroblast growth factor expression and stromal cell proliferation during uterine remodelling in the pregnant rat," *Journal of Endocrinology*, vol. 140, no. 2, pp. 239–249, 1994.

[8] S. K. Das, K. C. Flanders, G. K. Andrews, and S. K. Dey, "Expression of transforming growth factor-β isoforms (β2 and β3) in the mouse uterus: analysis of the periimplantation period and effects of ovarian steroids," *Endocrinology*, vol. 130, no. 6, pp. 3459–3466, 1992.

[9] K. Red-Horse, P. M. Drake, and S. J. Fisher, "Human pregnancy: the role of chemokine networks at the fetal-maternal interface," *Expert Reviews in Molecular Medicine*, vol. 6, no. 11, pp. 1–4, 2004.

[10] D. S. Charnock-Jones, P. Kaufmann, and T. M. Mayhew, "Aspects of human fetoplacental vasculogenesis and angiogenesis. I. Molecular regulation," *Placenta*, vol. 25, no. 2-3, pp. 103–113, 2004.

[11] P. Kaufmann, T. M. Mayhew, and D. S. Charnock-Jones, "Aspects of human fetoplacental vasculogenesis and angiogenesis. II. Changes during normal pregnancy," *Placenta*, vol. 25, no. 2-3, pp. 114–126, 2004.

[12] T. M. Mayhew, D. S. Charnock-Jones, and P. Kaufmann, "Aspects of human fetoplacental vasculogenesis and angiogenesis. III. Changes in complicated pregnancies," *Placenta*, vol. 25, no. 2-3, pp. 127–139, 2004.

[13] X. Yu, Y. Tong, H. F. Kwok et al., "Anti-angiogenic activity of erxian decoction, a traditional Chinese herbal formula, in zebrafish," *Biological and Pharmaceutical Bulletin*, vol. 35, no. 12, pp. 2119–2127, 2012.

[14] P. A. W. Rogers, F. Martinez, J. E. Girling et al., "Influence of different hormonal regimens on endometrial microvascular density and VEGF expression in women suffering from breakthrough bleeding," *Human Reproduction*, vol. 20, no. 12, pp. 3341–3347, 2005.

[15] A. Arici, O. Engin, E. Attar, and D. L. Olive, "Modulation of leukemia inhibitory factor gene expression and protein biosynthesis in human endometrium," *Journal of Clinical Endocrinology and Metabolism*, vol. 80, no. 6, pp. 1908–1915, 1995.

[16] B. A. Lessey, A. J. Castelbaum, C. A. Buck, Y. Lei, C. W. Yowell, and J. Sun, "Further characterization of endometrial integrins during the menstrual cycle and in pregnancy," *Fertility and Sterility*, vol. 62, no. 3, pp. 497–506, 1994.

[17] H. D. Tsai, C. C. Chang, Y. Y. Hsieh, and H. Y. Lo, "Leukemia inhibitory factor expression in different endometrial locations between fertile and infertile women throughout different menstrual phases," *Journal of Assisted Reproduction and Genetics*, vol. 17, no. 8, pp. 415–418, 2000.

[18] S. M. Laird, E. M. Tuckerman, C. F. Dalton, B. C. Dunphy, T. C. Li, and X. Zhang, "The production of leukaemia inhibitory factor by human endometrium: presence in uterine flushings and production by cells in culture," *Human Reproduction*, vol. 12, no. 3, pp. 569–574, 1997.

[19] P. Paiva, E. Menkhorst, L. Salamonsen, and E. Dimitriadis, "Leukemia inhibitory factor and interleukin-11: critical regulators in the establishment of pregnancy," *Cytokine and Growth Factor Reviews*, vol. 20, no. 4, pp. 319–328, 2009.

[20] C. L. Stewart, P. Kaspar, L. J. Brunet et al., "Blastocyst implantation depends on maternal expression of leukaemia inhibitory factor," *Nature*, vol. 359, no. 6390, pp. 76–79, 1992.

[21] E. Seli, U. A. Kayisli, H. Cakmak et al., "Removal of hydrosalpinges increases endometrial leukaemia inhibitory factor (LIF) expression at the time of the implantation window," *Human Reproduction*, vol. 20, no. 11, pp. 3012–3017, 2005.

[22] W. Tassell, M. Slater, J. A. Barden, and C. R. Murphy, "Endometrial cell death during early pregnancy in the rat," *Histochemical Journal*, vol. 32, no. 6, pp. 373–379, 2000.

[23] H. Achache and A. Revel, "Endometrial receptivity markers, the journey to successful embryo implantation," *Human Reproduction Update*, vol. 12, no. 6, pp. 731–746, 2006.

[24] B. A. Lessey, L. Damjanovich, C. Coutifaris, A. Castelbaum, S. M. Albeida, and C. A. Buck, "Integrin adhesion molecules in the human endometrium. Correlation with the normal and abnormal menstrual cycle," *Journal of Clinical Investigation*, vol. 90, no. 1, pp. 188–195, 1992.

[25] C. Simon, J. C. Martin, and A. Pellicer, "Paracrine regulators of implantation," *Best Practice & Research Clinical Obstetrics & Gynaecology*, vol. 14, no. 5, pp. 815–826, 2000.

[26] J. A. Horcajadas, A. Riesewijk, J. Polman et al., "Effect of controlled ovarian hyperstimulation in IVF on endometrial gene expression profiles," *Molecular Human Reproduction*, vol. 11, no. 3, pp. 195–205, 2005.

[27] S. Mirkin, G. Nikas, J. G. Hsiu, J. Díaz, and S. Oehninger, "Gene expression profiles and structural/functional features of the peri-implantation endometrium in natural and gonadotropin-stimulated cycles," *Journal of Clinical Endocrinology and Metabolism*, vol. 89, no. 11, pp. 5742–5752, 2004.

[28] J. A. Martínez-Conejero, C. Simón, A. Pellicer, and J. A. Horcajadas, "Is ovarian stimulation detrimental to the endometrium?" *Reproductive Biomedicine Online*, vol. 15, no. 1, pp. 45–50, 2007.

[29] A. N. Andersen, L. Gianaroli, R. Felberbaum et al., "Assisted reproductive technology in Europe, 2001. Results generated from European registers by ESHRE," *Human Reproduction*, vol. 20, no. 5, pp. 1158–1176, 2005.

[30] M. J. de los Santos, A. Mercader, A. Galán, C. Albert, J. L. Romero, and A. Pellicer, "Implantation rates after two, three, or five days of embryo culture," *Placenta*, vol. 24, pp. S13–S19, 2003.

[31] M. J. Murray, W. R. Meyer, R. J. Zaino et al., "A critical analysis of the accuracy, reproducibility, and clinical utility of histologic endometrial dating in fertile women," *Fertility and Sterility*, vol. 81, no. 5, pp. 1333–1343, 2004.

[32] X. Zhang, C. H. Chen, E. Confino, R. Barnes, M. Milad, and R. R. Kazer, "Increased endometrial thickness is associated with improved treatment outcome for selected patients undergoing in vitro fertilization-embryo transfer," *Fertility and Sterility*, vol. 83, no. 2, pp. 336–340, 2005.

[33] N. Noyes, H. C. Liu, K. Sultan, G. Schattman, and Z. Rosenwaks, "Endometrial thickness appears to be a significant factor in embryo implantation in in-vitro fertilization," *Human Reproduction*, vol. 10, no. 4, pp. 919–922, 1995.

[34] P. Sundström, "Establishment of a successful pregnancy following in-vitro fertilization with an endometrial thickness of no more than 4 mm," *Human Reproduction*, vol. 13, no. 6, pp. 1550–1552, 1998.

[35] J. H. Check, C. Dietterich, M. L. Check, and Y. Katz, "Successful delivery despite conception with a maximal endometrial thickness of 4 mm," *Clinical and Experimental Obstetrics and Gynecology*, vol. 30, no. 2-3, pp. 93–94, 2003.

[36] C. Siristatidis, C. Nissotakis, C. Chrelias, H. Iacovidou, and E. Salamalekis, "Immunological factors and their role in the genesis and development of endometriosis," *Journal of Obstetrics and Gynaecology Research*, vol. 32, no. 2, pp. 162–170, 2006.

[37] D. J. Barker, "Developmental origins of adult health and disease," *Journal of Epidemiology and Community Health*, vol. 58, no. 2, pp. 114–115, 2004.

[38] E. R. Norwitz, "Defective implantation and placentation: laying the blueprint for pregnancy complications," *Reproductive Biomedicine Online*, vol. 14, no. 1, pp. 101–109, 2007.

[39] H. Bhatt, L. J. Brunet, and C. L. Stewart, "Uterine expression of leukemia inhibitory factor coincides with the onset of blastocyst implantation," *Proceedings of the National Academy of Sciences of the United States of America*, vol. 88, no. 24, pp. 11408–11412, 1991.

[40] Z. M. Yang, S. P. Le, D. B. Chen et al., "Leukemia inhibitory factor, LIF receptor, and gp130 in the mouse uterus during early pregnancy," *Molecular Reproduction and Development*, vol. 42, no. 4, pp. 407–414, 1995.

[41] L. Wang, G. B. Zhou, P. Liu et al., "Dissection of mechanisms of Chinese medicinal formula Realgar-*Indigo naturalis* as an effective treatment for promyelocytic leukemia," *Proceedings of the National Academy of Sciences of the United States of America*, vol. 105, no. 12, pp. 4826–4831, 2008.

Hindawi Publishing Corporation
Evidence-Based Complementary and Alternative Medicine
Volume 2013, Article ID 219472, 12 pages
http://dx.doi.org/10.1155/2013/219472

Research Article

Ganoderma tsugae Extract Inhibits Growth of HER2-Overexpressing Cancer Cells via Modulation of HER2/PI3K/Akt Signaling Pathway

Han-Peng Kuo,[1] Shih-Chung Hsu,[2] Chien-Chih Ou,[3] Jhy-Wei Li,[4] Hsiu-Hsueh Tseng,[5] Tzu-Chao Chuang,[6] Jah-Yao Liu,[7] Shih-Jung Chen,[8] Muh-Hwan Su,[9] Yung-Chi Cheng,[10] Wei-Yuan Chou,[11] and Ming-Ching Kao[1,11]

[1] *Department of Biological Science and Technology, College of Life Sciences, China Medical University, 91 Hsueh-Shih Road, Taichung 40402, Taiwan*
[2] *Kang-Ning Junior College of Medical Care and Management, Taipei 11486, Taiwan*
[3] *Oncology New Drug Division, SynCore Bio, Taipei 11070, Taiwan*
[4] *Department of Pathology, Da-Chien General Hospital, Miaoli 36052, Taiwan*
[5] *Graduate Institute of Life Sciences, National Defense Medical Center, Taipei 11490, Taiwan*
[6] *Department of Chemistry, Tamkang University, Tamsui, New Taipei 25137, Taiwan*
[7] *Department of Obstetrics & Gynecology, Tri-Service General Hospital, Taipei 11490, Taiwan*
[8] *Luo-Gui-Ying Fungi Agriculture Farm, Taoyuan 33043, Taiwan*
[9] *Sinphar Group Headquarter, Sinphar Group, Yilan 26944, Taiwan*
[10] *Department of Pharmacology, Yale University School of Medicine, New Haven, CT 06520-8066, USA*
[11] *Department of Biochemistry, National Defense Medical Center, Taipei 11490, Taiwan*

Correspondence should be addressed to Ming-Ching Kao; mckao@mail.cmu.edu.tw

Received 11 December 2012; Accepted 25 February 2013

Academic Editor: Chris J. Branford-White

Ganoderma, also known as Lingzhi or Reishi, has been used for medicinal purposes in Asian countries for centuries. It is a medicinal fungus with a variety of biological properties including immunomodulatory and antitumor activities. In this study, we investigated the molecular mechanisms by which *Ganoderma tsugae* (GT), one of the most common species of *Ganoderma*, inhibits the proliferation of HER2-overexpressing cancer cells. Here, we show that a quality assured extract of GT (GTE) inhibited the growth of HER2-overexpressing cancer cells *in vitro* and *in vivo* and enhanced the growth-inhibitory effect of antitumor drugs (e.g., taxol and cisplatin) in these cells. We also demonstrate that GTE induced cell cycle arrest by interfering with the HER2/PI3K/Akt signaling pathway. Furthermore, GTE curtailed the expression of the HER2 protein by modulating the transcriptional activity of the *HER2* gene and the stability/degradation of the HER2 protein. In conclusion, this study suggests that GTE may be a useful adjuvant therapeutic agent in the treatment of cancer cells that highly express HER2.

1. Introduction

Human epidermal growth factor receptor 2 (HER2) is a 185-kDa transmembrane receptor tyrosine kinase (RTK), belonging to the epidermal growth factor receptor (EGFR) family, which contains four homologous members: EGFR/HER1, HER2, HER3, and HER4. Ligand stimulation induces dimerization of the HER receptor (homo- or heterodimer), which leads to self-phosphorylation (except for HER3) on tyrosine residues localized to the C-terminal domain of HER receptors. Then, the phosphorylated HER receptors (activated form) activate a variety of downstream signaling pathways, such as the phosphatidylinositol-3-kinase (PI3K)/Akt and the Ras/mitogen-activated protein kinase (MAPK) pathways, which in turn promote cell proliferation, survival, and metastasis [1].

Aberrant upregulation of HER2 is found in approximately 25–30% of breast cancers [2] and in 6–50% of ovarian cancers [3]. Patients with HER2-positive cancer have a high risk for diminished effectiveness of cancer treatments, increased cancer metastasis, and poor clinical outcomes [4]. Therefore, inhibition of HER2 expression or its kinase activity may be an effective approach for the treatment of HER2-overexpressing cancers. In fact, a number of HER2-targeting agents, including monoclonal antibodies (e.g., trastuzumab) and small-molecule tyrosine kinase inhibitors (e.g., lapatinib), have been developed for the treatment of cancers with HER2-overexpression [1]. However, there is still a need for novel therapies to treat HER2-overexpressing cancers. For example, traditional Chinese medicine (TCM) and botanical products are currently considered to be safer and may be used as alternative therapeutic agents for treatment of cancers that overexpress HER2 [5, 6].

Ganoderma (also known as Lingzhi) has a long history of use in folk medicines in Asian countries. *Ganoderma lucidum* (GL) and *Ganoderma sinense* (GS), listed in *Chinese Pharmacopoeia* (2010 edition) [7, 8], are two of the most common species of *Ganoderma* and have been used for medicinal purposes in China for centuries. The biological activities of GL and GS, particularly their immunomodulatory and antitumor properties, have been well documented [9]. In addition, *Ganoderma tsugae* (GT), another well-cultivated species of *Ganoderma*, has been shown to have many biological and pharmacological properties, such as antiautoantibody formation [10], antifibrosis [11], antiinflammation [12], and antioxidation characteristics [13]. A number of reports show that GT has growth-inhibitory effects in a variety of human cancer cells, such as MDA-MB-231 and MCF-7 breast cancer cells [14], COLO 205 colorectal cancer cells [15], A431 epidermoid carcinoma cells [16], Hep3B hepatoma cells [17], and H23 and H23/0.3 lung adenocarcinoma cells [18]. Although GT has antitumor activity in many human cancer cells, the mechanisms that underlie its growth-inhibitory effect on HER2-overexpressing cancer cells remain unclear.

In this study, we produced a quality assured extract of GT (GTE) and characterized its antitumor effects and relevant molecular mechanisms in HER2-overexpressing cancer cells *in vitro* and *in vivo*. Our results show that GTE inhibits cancer cell growth and induces cell cycle arrest via modulation of the HER2/PI3K/Akt signaling pathway. We also show that combining GTE with taxol or cisplatin significantly slows the growth of HER2-overexpressing cancer cells, indicating a potential use of GTE in the treatment of cancers that overexpress HER2.

2. Materials and Methods

2.1. Cell Culture. Human ovarian carcinoma cell lines, SKOV-3 ($HER2^{high}$) and OVCAR-3 ($HER2^{low}$), and breast carcinoma cell lines, SKBR-3 ($HER2^{high}$) and BT-474 ($HER2^{high}$), were obtained from the American Type Culture Collection (ATCC, Manassas, VA, USA). The MCF-7/HER2 ($HER2^{high}$) human breast carcinoma cell line (MCF-7 of an HER2-transfected stable line) was kindly provided by Dr. M. C. Hung (Department of Molecular and Cellular Oncology, University of Texas, M. D. Anderson Cancer Center, Houston, TX, USA). The MDA-MB-435/HER2 ($HER2^{high}$) human melanoma cell line (MDA-MB-435 of an HER2-transfected stable line) was kindly provided by Dr. T. D. Way (Department of Biological Science and Technology, China Medical University, Taichung, Taiwan). All cells were cultured in DMEM/F12 medium (Gibco BRL, Grand Island, NY, USA) supplemented with 10% fetal bovine serum (FBS) in a humidified atmosphere of 5% CO_2 at 37°C.

2.2. Chemicals and Antibodies. The thiazolyl blue tetrazolium bromide (MTT), cycloheximide (CHX), and N-acetyl-L-leucinyl-L-leucinyl-norleucinal (LLnL) were obtained from Sigma-Aldrich (St. Louis, MO, USA). Antibodies against cyclins D1 and E, p21, p27, phospho-Akt (Ser308), Akt1, and ubiquitin (Ub) were purchased from Santa Cruz Biotechnology, Inc. (Santa Cruz, CA, USA). Antibodies against phospho-PI3K, PI3K, phospho-Erk 1/2, and Erk 1/2 were purchased from Cell Signaling Technology, Inc. (Beverly, MA, USA). Antibodies against phospho-HER2 (Ab-18), HER2 (Ab-3), β-actin, and Ki-67 (Clone MIB-1) were purchased from Neomarkers Inc. (Fremont, CA, USA), Calbiochem (San Diego, CA, USA), Chemicon International Inc. (Temecula, CA, USA), and Dakocytomation Inc. (Carpinteria, CA, USA), respectively. Taxol (paclitaxel) was purchased from Bristol-Myers Squibb (Wallingford, CT, USA), and cisplatin was purchased from Pharmacia & Upjohn S.p.A. (Via Robert Koch 1.2, Milan, Italy).

2.3. Preparation of Ganoderma tsugae Extracts. *Ganoderma tsugae* (GT) was kindly provided by the Luo-Gui-Ying Fungi Agriculture Farm (with a registered name of Tien-Shen Lingzhi), Taoyuan, Taiwan. The extract of GT (GTE) was prepared as described previously [15]. Briefly, the powder of the GT fruiting body (5 g) was soaked in 99.9% methanol (200 mL), mixed, and shaken for 24 h on a rotating shaker. After centrifugation, the supernatant was poured through filter paper (Whatman, cat. no. 1001-110), and the residues were extracted with methanol two additional times as mentioned above. The filtrates were collected together and subjected to concentration under reduced pressure (i.e., evaporated to dryness under reduced pressure) to produce a brown gel-like GT extract (GTE). The yield was approximately 30%. The GTE was then prepared as a stock solution with methanol solvent (100 mg/mL) and stored at −80°C until use. For animal experiments, the dry GTE was redissolved in ethanol and diluted with a suspension solution (74.5% corn oil, 16% PEG-400, 4% Tween-80, 4% Cremophor EL, and 1.5% Ethanol, v/v) to a concentration of 10 mg/mL.

2.4. Quality Control of GTEs via Bioresponse Fingerprinting. The quality of the GTEs was assessed as described previously [18, 19]. Briefly, the genomic bioresponse to the GTEs was determined in SKOV-3 cells treated with 0.5 mg/mL of GTE. The total RNA was extracted from the GTE-treated cells, cleaned with a commercial kit (Qiagene RNA extraction kit, cat. no. 75144), and then used to obtain transcription

profiles in GeneChip hybridization studies using Affymetrix technology. The changes in the individual gene expression levels obtained by the GeneChip experiments were measured by Affymetrix MAS 5.0 software. A statistical pattern comparison method from the PhytomicsQC platform, Phytomics Similarity Index (PSI), was applied to determine the batch-to-batch similarity of the botanical products. In general, clinically similar batches have a PSI more than 0.95.

2.5. Cell Proliferation Assay. Cell viability was determined using an MTT assay as previously described [6]. Briefly, cells were seeded at a density of 6,000 cells/well into 96-well plates and incubated overnight in a medium containing 10% FBS. After the cells adhered to the plate, various doses of GTE were added to the cells, and then the cultures were incubated at 37°C for 72 h. After incubation with MTT reagent (0.5 mg/mL) for 4 h, the relative viable cell numbers were directly proportional to the production of formazan crystals solubilized by DMSO. The final solution was measured using a spectrophotometer at a wavelength of 545 nm against a reference wavelength of 690 nm.

2.6. Soft Agar Colony Formation Assay. The effect of GTE on the potential for anchorage-independent growth was determined by soft agar colony formation assay as described previously [20] with slight modifications. The cells (2×10^4 cells/well) were seeded in 6-well plates containing 0.7% base agar, 0.35% top agar and exposed to different concentrations of GTE or an equal volume of DMEM/F12 twice/week, and incubated at 37°C for 3 weeks. Colonies were stained with MTT reagent (5 mg/mL) and then photographed using a phase contrast microscope (100X) equipped with a CCD camera.

2.7. Flow Cytometric Analysis. For the analysis of the cell cycle, the phase distribution was detected by flow cytometry as described previously [6]. In brief, cells were incubated with GTE or the vehicle for 24 h and then fixed with ice-cold 70% ethanol overnight at 4°C. Prior to analysis, the cells were washed twice with PBS buffer and then incubated with propidium iodide (PI) solution (50 μg/mL PI in PBS with 1% Tween-20 and 10 μg RNase) for approximately 30 min in the dark at room temperature. The DNA content was measured using flow cytometry (BD FACS Canto). The FCS Express v2.0 software was used to analyze the results from the flow cytometric experiment.

2.8. Reporter Gene Assay. Cells were cotransfected with pHER2-luc (a HER2 promoter-driven luciferase gene plasmid construct) and pCMV-β-gal plasmids for 6 h and then incubated with GTE or the vehicle for 24 h. The HER2 promoter and β-galactosidase (β-gal) gene activity assays were performed as previously described [21]. The relative light units of luciferase activity were normalized to β-gal activity.

2.9. Semiquantitative Reverse Transcriptase-Polymerase Chain Reaction (RT-PCR). Total RNA was isolated using TRIzol solution (Invitrogen, San Diego, CA, USA). Two micrograms of total RNA were used for first-strand cDNA synthesis. The appropriate primers (HER2 sense: 5′-CAATGGAGA-CCCGCTGAAC-3′; HER2 antisense: 5′-CAGTGCGCG-TCAGGCTCT-3′; glyceraldehyde-3-phosphate dehydrogenase (GAPDH) sense: 5′-ACCACAGTCCATGCCATCAC-3′; GAPDH antisense: 5′-TCCACCACCCTGTTGCTGTA-3′) were used to perform the polymerase chain reaction (for 1 cycle at 94°C for 5 min, 32 cycles of 94°C for 15 s, 56°C for 30 s, and 72°C for 1 min with a final extension at 72°C for 5 min). The PCR products were separated by electrophoresis on a 1.2% agarose gel and detected by ethidium bromide (EtBr) staining.

2.10. Immunoprecipitation and Western Blotting. Proteins were extracted from the cells by the addition of lysis buffer (20 mM Hepes buffer pH 7.0, 10 mM KCl, 2 mM $MgCl_2$, 0.5% NP-40, and protease inhibitors). Following cell lysis, the extracts were centrifuged at 16,000 ×g for 10 min at 4°C. The protein content of the supernatant was measured using the Bio-Rad protein assay kit. Immunoprecipitation was carried out as previously described [22] with a slight modification. Briefly, 300 μg of total protein was incubated with anti-HER2 antibody overnight at 4°C, followed by protein A/G PLUS-Agarose (Santa Cruz) for 3 h at 4°C. The precipitates were resolved using sodium dodecyl sulfate polyacrylamide gel electrophoresis (SDS-PAGE) and then transferred onto a polyvinylidene fluoride (PVDF) membrane. For Western blotting as described previously [22], total protein (40 μg) was loaded to the gel and blotted onto the PVDF membrane. The membranes were blocked using 5% nonfat milk in tris-buffered saline with Tween-20 (TBST) for 1 h at room temperature. After blocking, the PVDF membranes were incubated with primary antibodies for 1 h at room temperature, followed by an HRP-conjugated secondary antibody. The reactive signals were visualized using the Enhanced Chemiluminescence Kit (Amersham Biosciences, Arlington Heights, IL, USA). The bands were scanned and quantified using the ImageJ software.

2.11. Animal Experiments. The animal experiments were performed as described previously [15] with slight modifications. Briefly, 5×10^6 SKOV-3 cells were subcutaneously implanted into the flank region of female BALB/c nude mice (BALB/cAnN.Cg-*Foxn1*^{nu}/CrlNarl). In total, 19 mice were used for this experiment; the tumor-implanted mice were treated with GTE ($n = 12$) or with the vehicle ($n = 7$), respectively. The GTE-treated mice were fed with GTE daily at a dose of 200 mg/kg ($n = 5$) or 1,000 mg/kg ($n = 7$) body weight; this dosing schedule was initiated when the developing tumor was approximately 50–100 mm^3 in volume (approximately 2-3 weeks after the cancer cells were implanted). The tumor volume and body weight were monitored daily. The mice were sacrificed for pathology examinations when the tumor volume exceeded 1,000 mm^3. The tumors were then completely excised from the subcutaneous tissue and weighed. Biochemical and hematological parameters were used to evaluate potential drug toxicity.

2.12. Immunohistochemical (IHC) Staining. SKOV-3 xenografted tumors and the surrounding tissues were excised, fixed in formalin, embedded in paraffin, cut in 4-μm serial sections, and then placed onto glass slides. The tumor tissue-coated slides were then dewaxed with xylene and gradually hydrated with graded alcohols. After antigen retrieval was achieved by pressure-cooking in 10 mM citrate buffer (pH 6.0) for 6 min, immunostaining for Ki-67, HER2, and cyclin D1 (1 : 150 dilution) was then performed as described previously [23].

2.13. Statistical Analysis. All data are presented as the mean ± SD from three independent experiments. Statistical analysis was performed by one-way ANOVA. Differences between treatment groups were analyzed for significance by multiple comparisons using analysis of variance. $^{*}P < 0.05$ and $^{**}P < 0.01$ versus the vehicle-treated control group.

3. Results

3.1. Quality Control of GTE Using Bioresponse Fingerprint Analysis. The quality of TCMs are potentially influenced by many factors, such as the growth conditions and processing procedures [24]. To assess the quality of the GTE, the bioresponse fingerprints were analyzed by the pattern comparison method from the PhytomicsQC platform [19], which showed highly concordant biological profiles for GTEs (GTE1, GTE2, and GTE3), and extracted from three batches of GT, acting on SKOV-3 cells with a PSI value more than 0.95 (See Supplementary Figure S1A available online at http://dx.doi.org/10.1155/2013/219472). Under this PSI value, 376 genes with specifically altered expression (149 upregulations and 227 downregulations) were observed as bioresponse fingerprints of GTEs (See Supplementary Figure S1B). These results suggest that the GT powder products used in this study were stable, consistent, and of high quality.

3.2. GTE Inhibits Proliferation of HER2-Overexpressing Cancer Cells. To determine whether GTE inhibits the growth of HER2-overexpressing cancer cells, we first evaluated the impact of GTE on cell proliferation using the MTT assay. As shown in Figure 1(a), the treatment of SKOV-3 cells ($HER2^{high}$) with various concentrations of GTE (0.1–1 mg/mL) for 24–72 h resulted in significant dose- and time-dependent suppressive effects on the proliferation of SKOV-3 cells, accounting for a 0–56% reduction at 24 h, a 13–95% reduction at 48 h, and a 24–98% reduction at 72 h. Moreover, the trypan blue exclusion assay also clearly demonstrated that the GTE exhibited growth suppression effect at doses of 0.1–0.5 mg/mL while a less cytotoxic effect at 1.0 mg/mL on SKOV-3 cells (Figure 1(b)). Similar antiproliferative effects of GTE were also observed in other HER2-overexpressing cancer cells, for example, BT-474 and SKBR-3 (Supplementary Figures S2A and S2B). In addition, we assessed the influence of GTE on the potential for anchorage-independent growth, a hallmark of malignant cancer cells, using the soft agar colony formation assay. We found that GTE dramatically reduced anchorage-independent growth of SKOV-3 cells in a dose-dependent manner (Figure 1(c)). These results suggest that GTE is capable of inhibiting the proliferation of HER2-overexpressing cancer cells.

Resistance to chemotherapeutic agents (such as taxol and cisplatin) is a major problem in the treatment of cancers that overexpress HER2 [25, 26]. We therefore examined whether GTE could enhance the growth-inhibitory effects of anticancer drugs on SKOV-3 cells, by incubating the cells with both anticancer agents and GTE. As shown in Figure 1(d), GTE significantly enhanced the growth-inhibitory effects of taxol and cisplatin on SKOV-3 cells. We found that the proliferation of SKOV-3 cells was reduced by 30%, 45%, and 37% in cells exposed to GTE (0.25 mg/mL), taxol (10 ng/mL), and cisplatin (10 μg/mL) alone, respectively. However, the proliferation of SKOV-3 cells was reduced by 73% and 77% in cells exposed to GTE combined with taxol and cisplatin, respectively. Similarly, we also found that GTE could increase the chemotherapeutic efficacy of anticancer drugs against other HER2-overexpressing cancer cell lines, for example, MDA-MB-453/HER2 (Supplementary Figures S3A and S3B). These findings suggest that GTE can chemosensitize HER2-overexpressing cancer cells to anticancer drugs (e.g., taxol and cisplatin).

3.3. GTE Induces G1 Phase Arrest by Modulating the Expression of Cell Cycle Regulatory Proteins. As mentioned above, we observed a growth-inhibitory influence of GTE on SKOV-3 cells (Figures 1(a)–1(c)). To determine if the antiproliferative property of GTE was due to the disruption of cell cycle, flow cytometry was used to analyze the cell cycle change in SKOV-3 cells. As illustrated in Figure 2(a), treatment of SKOV-3 cells with GTE resulted in a distinct increase (approximately 24%) in the number of G1 phase cells at a concentration of 0.5 mg/mL GTE. This increase in the number of cells in the G1 phase was accompanied by a concordant decrease in the number of cells in the S and G2/M phases. Similar GTE-mediated cell cycle distribution patterns were observed in BT-474 ($HER2^{high}$) cells (Supplementary Figure S4A). These findings suggest that GTE inhibits the growth of HER2-overexpressing cancer cells by modulating the progression of the cell cycle.

Different cell cycle regulators, such as cyclins, cyclin-dependent kinases (CDKs), and CDK inhibitors (CKIs), are involved in multiple cellular pathways that tightly regulate the progression of the cell cycle [27]. To elucidate the molecular mechanisms of GTE-induced cell cycle arrest, we assessed the impact of GTE on the expression of cell cycle regulators. We demonstrated that, after GTE treatment, the protein levels of cyclins D1 and E were downregulated, while the protein levels of p21 and p27 were upregulated in SKOV-3 cells (Figures 2(b) and 2(c)). Similarly, GTE also dramatically affected the expression of cell cycle regulators (e.g., cyclins D1 and E) in two more HER2-overexpressing cancer cell lines, that is, BT-474 (Supplementary Figure S4B) and SKBR-3 cells (data not shown). These results suggest that GTE inhibits cell growth by regulating the expression of cell cycle regulators in HER2-overexpressing cancer cells.

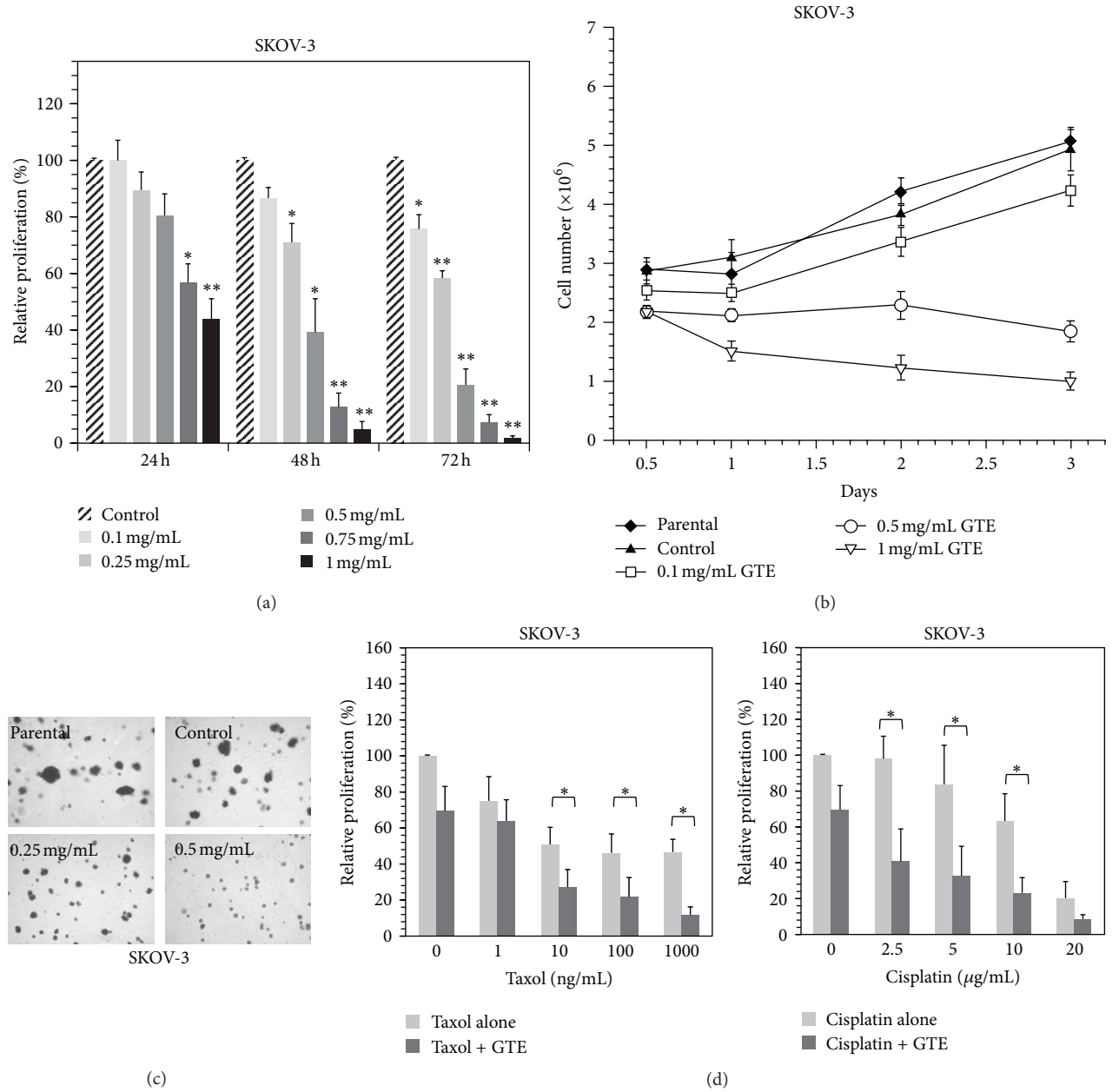

Figure 1: Effect of GTE on cell proliferation in HER2-overexpressing cancer cells. (a) SKOV-3 cells were treated with 0.5% methanol (vehicle control) or various concentrations of GTE (0.1, 0.25, 0.5, 0.75, and 1 mg/mL) for 72 h. Cell proliferation was measured using the MTT assay as described in Section 2. (b) SKOV-3 cells were treated with either vehicle control or GTE (0.1, 0.5, or 1.0 mg/mL) for 0.5, 1, 2, and 3 days. Cell numbers were determined using trypan blue staining. The parental SKOV-3 cells were not treated with vehicle (0.5% methanol) or GTE. (c) SKOV-3 cells were treated with different doses of GTE (0.25 and 0.5 mg/mL) twice a week for 3 weeks in the soft agar colony formation assay as described in Section 2. (d) SKOV-3 cells were treated with various concentrations of taxol (1, 10, 100, and 1000 ng/mL) or cisplatin (2.5, 5, 10, and 20 μg/mL) with or without GTE (0.25 mg/mL) for 72 h. Cell proliferation was determined by MTT assay. The results are expressed as the mean ± SD of three independent experiments. $^{*}P < 0.05$; $^{**}P < 0.01$.

3.4. GTE Inhibits HER2/PI3K/Akt Signaling Cascades. Based on the results mentioned above, there was a significant growth-inhibitory effect of GTE on HER2-overexpressing cancer cells (Figure 1). We next explored whether the inhibition of proliferation was caused by regulating the expression of HER2 protein. As shown in Figures 3(a) and 3(b), treatment of SKOV-3 cells with GTE resulted in a marked dose- and time-dependent decrease in HER2 protein levels. Similarly, GTE also decreased the protein expression of HER2 in other $HER2^{high}$ cell lines, such as SKBR-3, BT-474, and MCF-7/HER2 (Figure 3(d), Supplementary Figure S5A) and an $HER2^{low}$ cell line, OVCAR-3 (Supplementary Figure S5B).

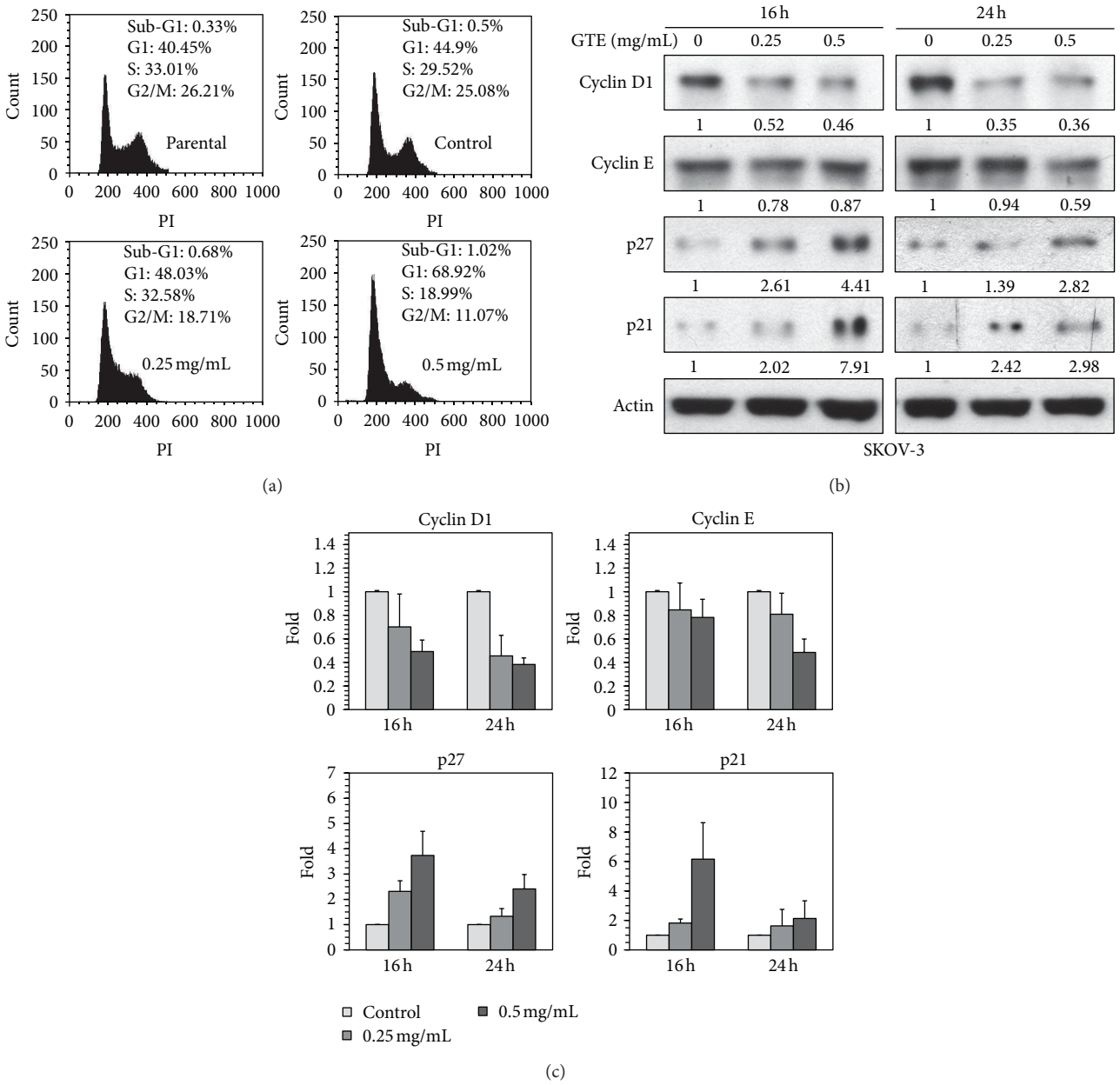

Figure 2: Effect of GTE on cell cycle distribution in HER2-overexpressing cancer cells. (a) SKOV-3 cells were treated with vehicle control (0.5% methanol) or various concentrations of GTE (0, 0.25, and 0.5 mg/mL) for 24 h. Cell cycle distribution was analyzed by flow cytometry as described in Section 2. The parental SKOV-3 cells were not treated with vehicle (0.5% methanol) or GTE. (b) SKOV-3 cells were treated with various concentrations of GTE (0, 0.25, and 0.5 mg/mL) for 16 h and 24 h. The expression of G1 phase regulators was determined by Western blotting as described in Section 2. (c) A histogram showing the relative protein levels from (b). Data are presented as the mean ± SD of three independent experiments. $^{*}P < 0.05$ and $^{**}P < 0.01$ versus the vehicle-treated control group.

The HER2 signaling pathway is known to be associated with cell proliferation; therefore, we tested the impact of GTE on two main downstream pathways of HER2: the PI3K/Akt and Ras/MAPK signaling cascades [1]. As shown in Figure 3(c), GTE exhibited inhibitory effects on phospho-HER2, phospho-PI3K, and phospho-Akt without a noticeable reduction in phospho-Erk 1/2 in SKOV-3 cells. Moreover, GTE showed similar effects on phospho-HER2 and phospho-Akt in other HER2-overexpressing cell lines, for example, SKBR-3 and BT-474 (Figure 3d)). These data clearly indicate that GTE exerts inhibitory effects on the HER2/PI3K/Akt signaling cascades in cancer cells with HER2-overexpression.

3.5. GTE Downregulates HER2 Protein Expression by Modulating the Gene Expression and Protein Stability of HER2. As mentioned above, our results showed a dramatic inhibitory influence of GTE on the expression of HER2 protein in

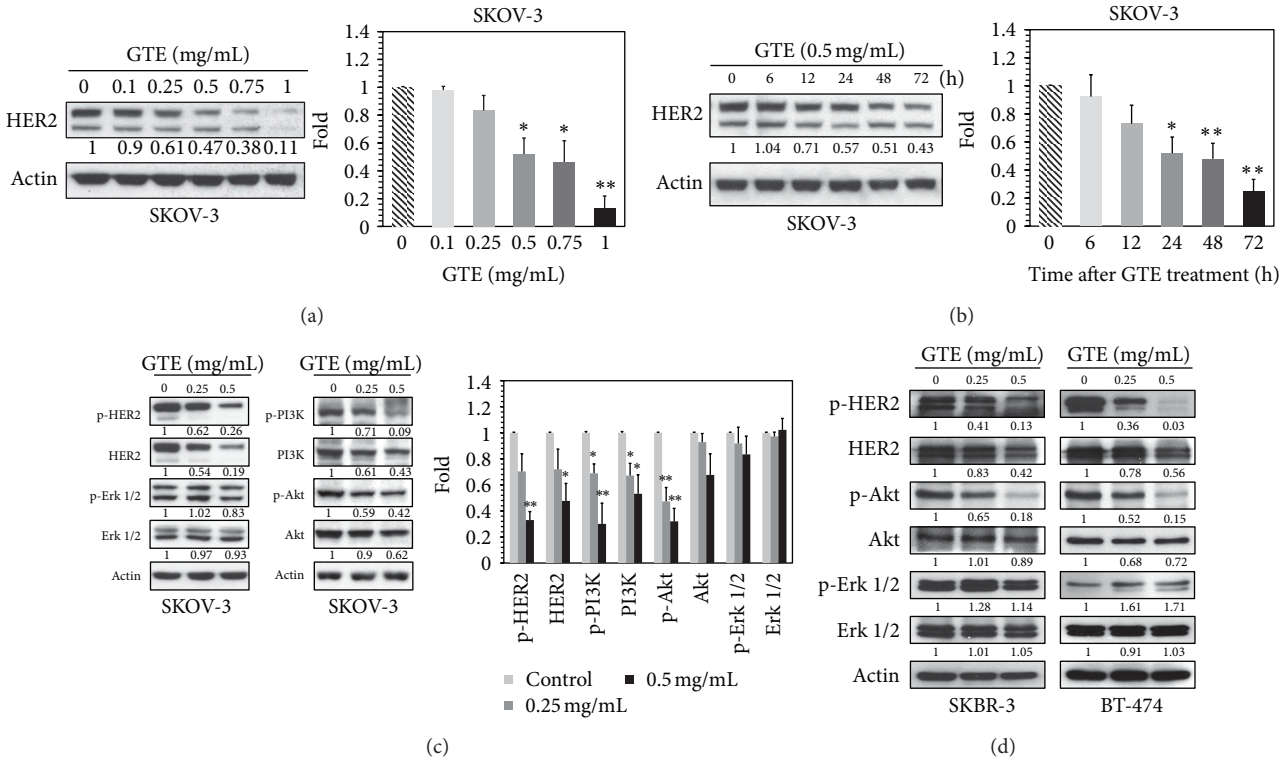

Figure 3: Effect of GTE on HER2/PI3K/Akt and Ras/MAPK signaling cascades in HER2-overexpressing cancer cells. (a) SKOV-3 cells were treated with various concentrations of GTE (0, 0.1, 0.25, 0.5, 0.75, and 1 mg/mL) for 24 h. The expression of HER2 protein was measured by Western blotting. (b) SKOV-3 cells were treated with 0.5 mg/mL GTE for 6, 12, 24, 48, and 72 h. The protein level of HER2 was determined by Western blotting. (c) Treatment of SKOV-3 cells with GTE (0, 0.25, or 0.5 mg/mL) for 24 h inhibited HER2/PI3K/Akt but not HER2/Erk signaling. (d) Treatment of SKBR-3 and BT-474 cells with GTE (0, 0.25, 0.5 mg/mL) for 24 h led to inhibition of the HER2/Akt but not the HER2/Erk signaling pathway. The results are expressed as the mean ± SD of three independent experiments. $^{*}P < 0.05$; $^{**}P < 0.01$.

HER2-overexpressing cancer cells (Figure 3). To determine the underlying molecular mechanisms of the GTE-mediated downregulation of HER2, we tested the effect of GTE on the transcriptional activity of *HER2* gene. The expression of HER2 mRNA was distinctly decreased in SKOV-3 (Figure 4(a)) and BT-474 (Supplementary Figure S6A) cells exposed to 0.25 and 0.5 mg/mL of GTE for 24 h, as determined by RT-PCR. Furthermore, the reporter gene assay indicated that GTE decreased the HER2 promoter activity in a dose-dependent manner in SKOV-3 cells (Figure 4(b)). Consistent with the decreased expression of HER2 protein, both the mRNA level and the promoter activity of HER2 were downregulated by GTE. Taken together, we conclude that GTE depletes the protein levels of HER2 via modulation of the *HER2* gene activity.

Because an overall decrease in protein stability could also be responsible for the reduced HER2 protein levels, we examined the effect of GTE on HER2 protein stability and found that the half-life of HER2 was clearly shortened by GTE treatment in SKOV-3 (Figure 4(c)) and BT-474 (Supplementary Figure S6B) cells. In general, proteins such as HER2 are tagged with polyubiquitin and then degraded by the ubiquitin-proteasome system (UPS). We tested whether the GTE-mediated HER2 protein stability was due to the activation of the UPS. As shown in Figure 4(d), the amount of polyubiquitinated HER2 (HER2-$Ub_{(n)}$) protein was significantly increased in SKOV-3 cells exposed to 0.5 mg/mL GTE for 24 or 48 h. In addition, the treatment of SKOV-3 cells with LLnL, a proteasome inhibitor, effectively prevented the GTE-mediated degradation of HER2 protein (Figure 4(e)). These observations suggest that the curtailment of HER2 by GTE may also occur through the induction of HER2 protein instability/degradation.

3.6. GTE Inhibits the Growth of SKOV-3 Xenografted Tumors by Modulating HER2 Protein. To determine the potential for anticancer effects of GTE *in vivo*, we used xenografted tumor-bearing nude mice. After the volume of the SKOV-3 xenografted tumors reached approximately 50–100 mm^3, the mice were orally (p.o.) administered either GTE (200 and 1,000 mg/kg/day) or vehicle for 31 days. As illustrated in Figure 5(a), the nude mice treated with 200 or 1,000 mg/kg/day of GTE exhibited a marked inhibition in the growth of SKOV-3-implanted tumors relative to that of the control group. There was no significant alteration in the body weights of the nude mice with or without GTE treatment, indicating GTE had no apparent toxicity (Figure 5(b)). In addition, in comparison to the vehicle

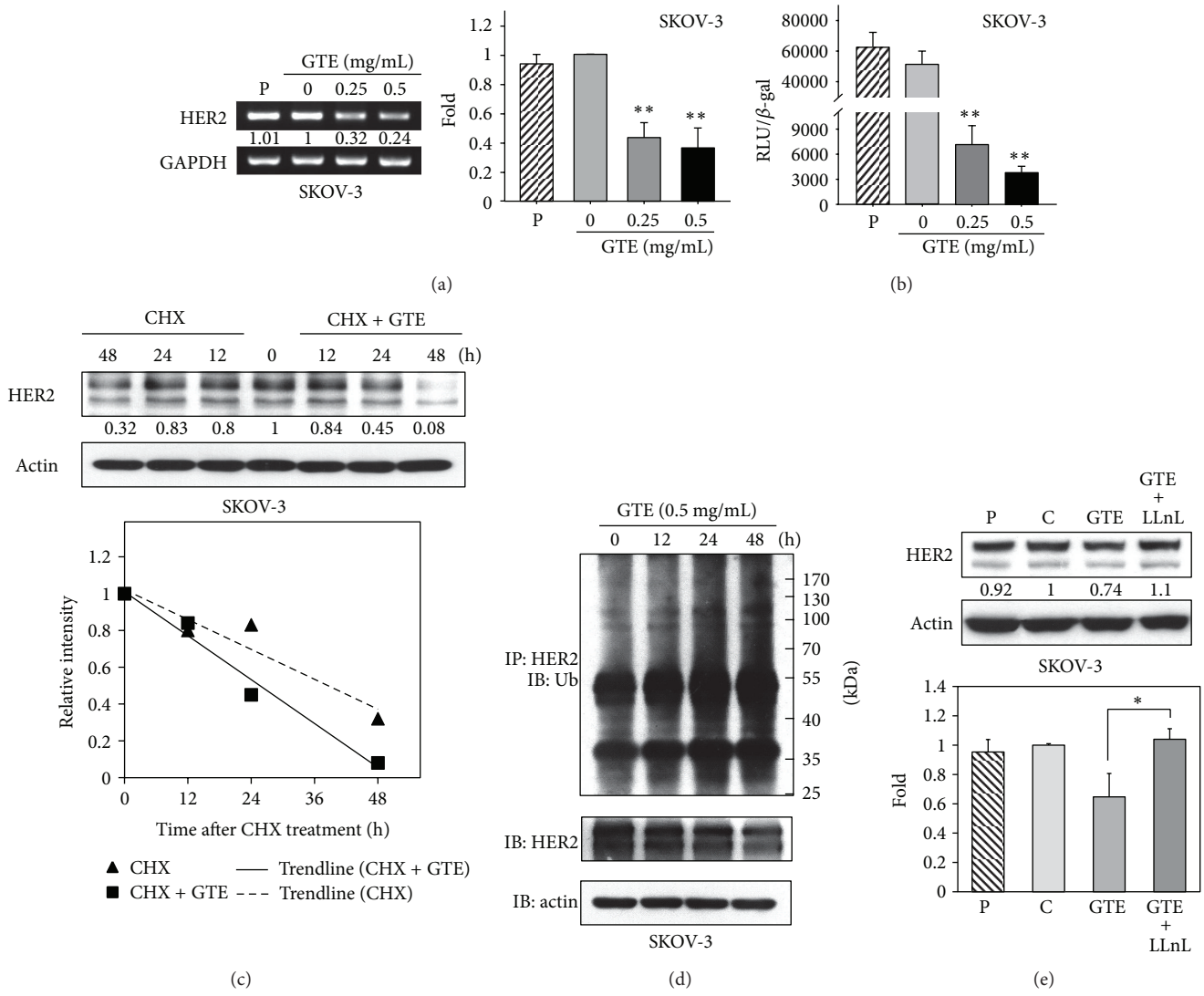

Figure 4: Effect of GTE on the gene expression and protein stability of HER2. (a) SKOV-3 cells were treated with GTE (0.25 or 0.5 mg/mL) or the vehicle for 24 h. The mRNA level of HER2 was measured by semiquantitative RT-PCR as described in Section 2. (b) SKOV-3 cells were transfected with a luciferase gene plasmid construct driven by HER2 promoter (pHER2-luc) for 6 h and then treated with various concentrations of GTE (0, 0.25, and 0.5 mg/mL) for 24 h. The activity of HER2 promoter was measured by a reporter gene assay, as described in Section 2. The relative light units (RLU) of luciferase activity were normalized against β-gal activity. (c) SKOV-3 cells were pretreated with 20 μg/mL of cycloheximide (CHX) for 30 min and then treated with GTE (0.5 mg/mL) or the vehicle for 12, 24, and 48 h. Stability of HER2 was determined by measuring the protein's half-life. (d) SKOV-3 cells were treated with GTE (0.5 mg/mL) for 12, 24, and 48 h. To detect polyubiquitinated HER2 (HER2-$Ub_{(n)}$), HER2 was immunoprecipitated and subjected to Western blot analysis using an antibody to ubiquitin. The total protein levels of HER2 and actin in the whole-cell extracts were also detected by Western blotting. (e) SKOV-3 cells were pretreated with proteasome inhibitor (LLnL) or the vehicle for 30 min and then treated with GTE (0.5 mg/mL) for 24 h. The protein level of HER2 was measured by Western blotting. P, parental SKOV-3 cells; C, vehicle control. Data are presented as the mean ± SD of three independent experiments. $^{*}P < 0.05$ and $^{**}P < 0.01$ versus the vehicle-treated control group.

controls, the expression of Ki-67 protein, a proliferation marker, was significantly decreased in GTE-treated tumors (Figure 5(c)), indicating that GTE inhibited cell proliferation of SKOV-3 xenografted tumors *in vivo*.

In our *in vitro* studies, we showed that GTE inhibited cell proliferation and induced G1 cell cycle arrest in HER2-overexpressing cancer cells through the modulation of HER2 expression. To determine the underlying molecular mechanisms of the GTE-mediated anticancer effect observed in the SKOV-3 xenografted tumors, tumor sections were immunostained for HER2 protein and cyclin D1, the first cyclin that is activated during G1/S phase progression. In comparison to the control group, the staining intensities of HER2 and cyclin D1 were dramatically downregulated in GTE-treated tumor cells (200 mg/kg/day) (Figure 5(c)). Together, these data suggest that GTE inhibited tumor cell proliferation by inducing cell cycle arrest and modulating the HER2 pathway *in vitro* and *in vivo*.

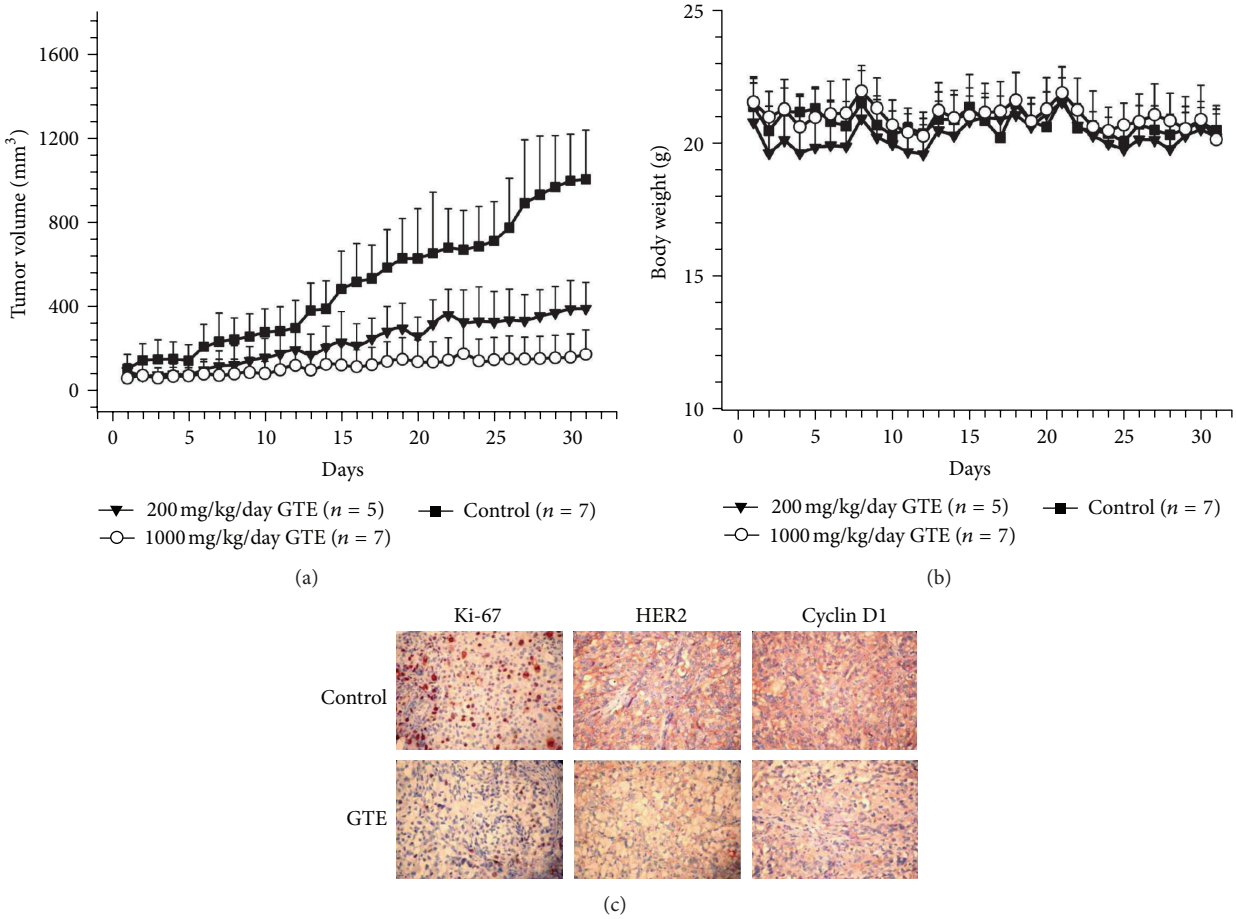

Figure 5: Effect of GTE on the growth of SKOV-3 xenografted tumors *in vivo*. (a) Tumor growth rate was significantly slower in the GTE-treated group (200 mg/kg/day, $n = 5$; or 1,000 mg/kg/day, $n = 7$) versus the control group ($n = 7$). The tumor volumes were estimated from the caliper measurements of three dimensions of the tumor. The estimated tumor volumes were calculated as $L \times W^2 \times 0.5$, where L is the major axis and W is tumor width. The results are represented as the mean ± SD. (b) The body weight of nude mice was not significantly different between the control and GTE-treated groups. (c) Downregulation of Ki-67, HER2, and cyclin D1 expression by GTE in SKOV-3 xenografted tumors on nude mice. The IHC analysis was performed on SKOV-3-induced xenografted tumors. The two representative specimens appear to show that GTE-treated mice (200 mg/kg/day) have lower protein expression than vehicle controls, for Ki-67, HER2, and cyclin D1 (400X magnification).

4. Discussion

HER2-overexpression is associated with a high risk for cancer metastasis and a poor response to antitumor therapies [4]. Treatment with therapeutic agents that specifically target cancer cells with HER2-overexpression, such as lapatinib and trastuzumab, has improved clinical outcomes. In addition to the anticancer agents, a number of TCMs and botanical products have been shown to be effective and useful adjuvant agents for the treatment of HER2-overexpressing cancer [5, 6, 26]. *Ganoderma tsugae* (GT), one of the most common species of *Ganoderma* cultivated in Taiwan, has been shown to have antiproliferative effects on human cancer cells [15, 16, 18]. In this study, we report for the first time that the extract of GT (GTE) has a distinct growth-inhibitory effect on HER2-overexpressing cancer cells *in vitro* (Figures 1(a)–1(c)) and *in vivo* (Figure 5(a)).

Perturbation of cell cycle progression in cancer cells is a useful strategy to arrest cancer growth [28]. Furthermore, cell cycle arrest also provides an occasion for cells to undergo either repair or programmed cell death. A number of TCMs (e.g., GT) exhibit marked growth-inhibitory effects on cancer cells via disruption of cell cycle progression. Previous reports show that GT inhibits cell proliferation by inducing cell cycle arrest in the G2/M phase in Hep3B hepatoma and COLO205 colorectal cancer cells [15, 17] and in the S phase in H23/0.3 lung adenocarcinoma cells [18]. In this study, our *in vitro* results indicate that GTE treatment induces G1 phase arrest via modulation of cell cycle regulators (e.g., cyclins D1 and E, p21, and p27) in HER2-overexpressing SKOV-3 ovarian cancer and BT-474 breast cancer cells (Figure 2 and Supplementary Figure S4). The varying effects of GTE on the cell cycle may be due to cell-type specificity and/or result from modulation of different signal transductions and cell cycle regulatory molecules.

Two major therapeutic approaches to the treatment of HER2-overexpressing cancers involve agents that curtail the expression and activation/phosphorylation of the HER2

receptor [29]. In this study, we demonstrate that GTE downregulates both the level of HER2 and its phosphorylated form in SKOV-3, BT-474, and SKBR-3 cells (Figure 3). We surmised that the inhibitory effect of GTE on the levels of phospho-HER2 may be due to its inhibition of the expression of HER2. In agreement with this hypothesis, we observed a significant decrease in the expression of HER2 mRNA (Figure 4(a)) and the activity of its promoter (Figure 4(b)) following treatment with GTE. Moreover, we have established a number of HER2 promoter deletion constructs (F1: −1067~−103, F2: −871~−103, F3: −495~−103, and F4: −207~−103) and found that GTE interacts with the HER2 promoter in the −871~−495 region (unpublished data). Based on Genomatix software predictions, there are several putative transcription factor binding sites located in this area, such as T-cell factor (TCF), forkhead-box K2 (FOXK2), and GATA-binding protein 2 (GATA2). Therefore, further studies are needed to clarify the molecular basis by which the transcription of the *HER2* gene is regulated to ultimately aid in the development of better strategies for the treatment of cancers with HER2-overexpression.

We also investigated the regulation of HER2 protein stability/degradation as another possible explanation as to how GTE controls HER2 protein expression. We found that the half-life of the HER2 protein is noticeably reduced by GTE in SKOV-3 (Figure 4(c)) and BT-474 cells (Supplementary Figure S6B). This observation led us to hypothesize that the decreased stability of the HER2 protein may be due to the induction of polyubiquitination of HER2 by GTE (Figure 4(d)), leading to its degradation by the proteasome complex. We used LLnL, a proteasome inhibitor, to confirm that the effect of GTE on the degradation of HER2 protein involves the activation of the ubiquitin-proteasome system (Figure 4(e)). Furthermore, several molecules, such as heat shock protein 90 (Hsp90), casitas B-lineage lymphoma (c-Cbl), and peptidyl-prolyl cis/trans isomerase 1 (Pin1), are reported to be required for the maintenance of the stability and activation of HER2 [30–32]. It would be worthwhile to determine if these molecules are involved in the GTE-induced degradation/instability of the HER2 protein.

Generally, cancer cells overexpressing HER2 respond poorly to chemotherapeutic agents. Suppression of the HER2 pathway by HER2-targeting therapeutics potentiates the anticancer activity of chemotherapeutic agents in the treatment of HER2-overexpressing cancers [25, 33]. A number of reports show that the combined usage of some extracts from TCMs (e.g., coptis rhizome and glycyrrhizae radix) with antitumor agents results in synergistic growth inhibition in cancer cells [34, 35]. It has also been reported that combining anticancer agents with GTE slows the growth rate of cancer cells [15, 18]. Herein, we demonstrate for the first time that the combined usage of GTE with taxol (Figure 1(d)), cisplatin (Supplementary Figure S3), or doxorubicin (data not shown) results in synergistic growth inhibition of HER2-overexpressing cancer cells. These results indicate that GTE may be a promising adjuvant therapeutic agent in the treatment of cancers with HER2-overexpression.

In conclusion, we provide a schematic presentation of possible molecular mechanisms *in vitro* and *in vivo* for the inhibitory effects of GTE on the proliferation of HER2-overexpressing cancer cells (Figure 6). Our results indicate that GTE induces G1 cell cycle arrest via regulation of the HER2/PI3K/Akt signaling pathway, thereby leading to a reduction in the growth of cancer cells overexpressing HER2. Our data also demonstrate that the depletion of HER2 protein by GTE involves an inhibition in the transcriptional activity of the *HER2* gene and an increase in the proteasome-dependent degradation of the HER2 protein. In addition, we have also shown that a combination of GTE with anticancer drugs (e.g., taxol, cisplatin, and doxorubicin) exerts synergistic growth-inhibitory effect on HER2-overexpressing cancer cells. Taken together, our findings suggest that GTE may be a useful and effective adjuvant therapeutic agent for the treatment of cancers that highly express HER2.

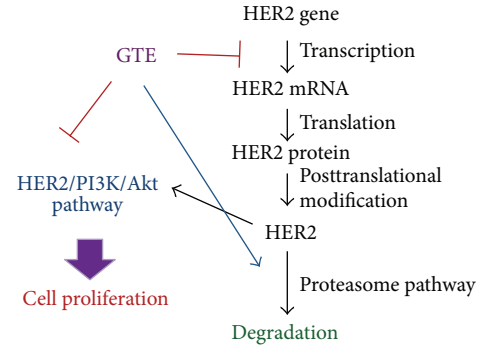

Figure 6: A schematic model of the GTE-mediated antiproliferative effect on HER2-overexpressing cancer cells. Ligand stimulation induces the activation of the HER2 receptor, which in turn activates the PI3K/Akt signaling pathway and then promotes cell growth and survival. After GTE treatment, the proliferation is inhibited because of an induction of cell cycle arrest. The GTE-mediated growth repression coincides with a reduction in the transcriptional activity of *HER2* gene and an induction in the degradation of HER2 protein, leading to a downregulation of the HER2/PI3K/Akt pathway.

Authors' Contribution

C.-C. Ou and J.-W. Li contributed equally to this study.

Acknowledgments

This work was supported by Grants from the National Science Council (NSC100-2313-B-039-005-MY3) and partly from the China Medical University (CMU) (CMU95-296), Taiwan. The authors also wish to thank members of the Medical Research Core Facilities Center (Office of Research & Development, CMU, Taichung, Taiwan) for their excellent technical support.

References

[1] J. Baselga and S. M. Swain, "Novel anticancer targets: revisiting ERBB2 and discovering ERBB3," *Nature Reviews Cancer*, vol. 9, no. 7, pp. 463–475, 2009.

[2] A. C. Wolff, M. E. H. Hammond, J. N. Schwartz et al., "American Society of Clinical Oncology/College of American Pathologists guideline recommendations for human epidermal growth factor receptor 2 testing in breast cancer," *Archives of Pathology and Laboratory Medicine*, vol. 131, no. 1, pp. 18–43, 2007.

[3] E. Verri, P. Guglielmini, M. Puntoni et al., "HER2/neu oncoprotein overexpression in epithelial ovarian cancer: evaluation of its prevalence and prognostic significance: clinical study," *Oncology*, vol. 68, no. 2-3, pp. 154–161, 2005.

[4] D. Yu and M. C. Hung, "Overexpression of ErbB2 in cancer and ErbB2-targeting strategies," *Oncogene*, vol. 19, no. 53, pp. 6115–6121, 2000.

[5] J. H. Ju, M. J. Jeon, W. Yang, K. M. Lee, H. S. Seo, and I. Shin, "Induction of apoptotic cell death by *Pharbitis nil* extract in HER2-overexpressing MCF-7 cells," *Journal of Ethnopharmacology*, vol. 133, no. 1, pp. 126–131, 2011.

[6] H. P. Kuo, T. C. Chuang, M. H. Yeh et al., "Growth suppression of HER2-overexpressing breast cancer cells by berberine via modulation of the HER2/PI3K/Akt signaling pathway," *Journal of Agricultural and Food Chemistry*, vol. 59, no. 15, pp. 8216–8224, 2011.

[7] National Commission of Chinese Pharmacopoeia, *Pharmacopoeia of Peoples Republic of China*, China Medical Science and Technology Press, Beijing, China, 2010.

[8] J. Da, W. Y. Wu, J. J. Hou et al., "Comparison of two officinal Chinese Pharmacopoeia species of *Ganoderma* based on chemical research with multiple technologies and chemometrics analysis," *Journal of Chromatography A*, vol. 1222, pp. 59–70, 2012.

[9] X. Zhou, J. Lin, Y. Yin et al., "Ganodermataceae: natural products and their related pharmacological functions," *The American Journal of Chinese Medicine*, vol. 35, no. 4, pp. 559–574, 2007.

[10] N. S. Lai, R. H. Lin, R. S. Lai, U. C. Kun, and S. C. Leu, "Prevention of autoantibody formation and prolonged survival in New Zealand Black/New Zealand White F1 mice with an ancient Chinese herb, *Ganoderma tsugae*," *Lupus*, vol. 10, no. 7, pp. 461–465, 2001.

[11] Y. W. Wu, K. D. Chen, and W. C. Lin, "Effect of *Ganoderma tsugae* on chronically carbon tetrachloride-intoxicated rats," *The American Journal of Chinese Medicine*, vol. 32, no. 6, pp. 841–850, 2004.

[12] H. H. Ko, C. F. Hung, J. P. Wang, and C. N. Lin, "Antiinflammatory triterpenoids and steroids from *Ganoderma lucidum* and *G. tsugae*," *Phytochemistry*, vol. 69, no. 1, pp. 234–239, 2008.

[13] J. L. Mau, H. C. Lin, and C. C. Chen, "Antioxidant properties of several medicinal mushrooms," *Journal of Agricultural and Food Chemistry*, vol. 50, no. 21, pp. 6072–6077, 2002.

[14] G. G. L. Yue, K. P. Fung, G. M. K. Tse, P. C. Leung, and C. B. S. Lau, "Comparative studies of various *Ganoderma* species and their different parts with regard to their antitumor and immunomodulating activities in vitro," *Journal of Alternative and Complementary Medicine*, vol. 12, no. 8, pp. 777–789, 2006.

[15] S. C. Hsu, C. C. Ou, J. W. Li et al., "*Ganoderma tsugae* extracts inhibit colorectal cancer cell growth via G_2/M cell cycle arrest," *Journal of Ethnopharmacology*, vol. 120, no. 3, pp. 394–401, 2008.

[16] S. C. Hsu, C. C. Ou, T. C. Chuang et al., "*Ganoderma tsugae* extract inhibits expression of epidermal growth factor receptor and angiogenesis in human epidermoid carcinoma cells: in vitro and in vivo," *Cancer Letters*, vol. 281, no. 1, pp. 108–116, 2009.

[17] K. H. Gan, Y. F. Fann, S. H. Hsu, K. W. Kuo, and C. N. Lin, "Mediation of the cytotoxicity of lanostanoids and steroids of *Ganoderma tsugae* through apoptosis and cell cycle," *Journal of Natural Products*, vol. 61, no. 4, pp. 485–487, 1998.

[18] Y. H. Yu, H. P. Kuo, H. H. Hsieh et al., "Ganoderma tsugae induces S phase arrest and apoptosis in doxorubicin-resistant lung adenocarcinoma H23/0. 3 cells via modulation of the PI3K/Akt signaling pathway," *Evidence-Based Complementary and Alternative Medicine*, vol. 2012, Article ID 371286, 13 pages, 2012.

[19] R. Tilton, A. A. Paiva, J. Q. Guan et al., "A comprehensive platform for quality control of botanical drugs (PhytomicsQC): a case study of Huangqin Tang (HQT) and PHY906," *Chinese Medicine*, vol. 5, article 30, 2010.

[20] B. Hu, H. M. An, K. P. Shen et al., "*Polygonum cuspidatum* extract induces anoikis in hepatocarcinoma cells associated with generation of reactive oxygen species and downregulation of focal adhesion kinase," *Evidence-Based Complementary and Alternative Medicine*, vol. 2012, Article ID 607675, 9 pages, 2012.

[21] T. C. Chuang, S. C. Hsu, Y. T. Cheng et al., "Magnolol downregulates HER2 gene expression, leading to inhibition of HER2-mediated metastatic potential in ovarian cancer cells," *Cancer Letters*, vol. 311, no. 1, pp. 11–19, 2011.

[22] H. P. Kuo, T. C. Chuang, S. C. Tsai et al., "Berberine, an isoquinoline alkaloid, inhibits the metastatic potential of breast cancer cells via Akt pathway modulation," *Journal of Agricultural and Food Chemistry*, vol. 60, no. 38, pp. 9649–9658, 2012.

[23] J. W. Li, T. C. Chuang, A. H. Yang, C. K. Hsu, and M. C. Kao, "Clinicopathological relevance of HER2/neu and a related gene-protein cubic regression correlation in colorectal adenocarcinomas in Taiwan," *International Journal of Oncology*, vol. 26, no. 4, pp. 933–943, 2005.

[24] B. Boh, M. Berovic, J. Zhang, and L. Zhi-Bin, "*Ganoderma lucidum* and its pharmaceutically active compounds," *Biotechnology Annual Review*, vol. 13, pp. 265–301, 2007.

[25] D. Yu, B. Liu, M. Tan, J. Li, S. S. Wang, and M. C. Hung, "Overexpression of c-erbB-2/neu in breast cancer cells confers increased resistance to Taxol via mdr-1-independent mechanisms," *Oncogene*, vol. 13, no. 6, pp. 1359–1365, 1996.

[26] L. Y. Shiu, C. H. Liang, Y. S. Huang, H. M. Sheu, and K. W. Kuo, "Downregulation of HER2/neu receptor by solamargine enhances anticancer drug-mediated cytotoxicity in breast cancer cells with high-expressing HER2/neu," *Cell Biology and Toxicology*, vol. 24, no. 1, pp. 1–10, 2008.

[27] X. Grana and E. P. Reddy, "Cell cycle control in mammalian cells: role of cyclins, cyclin dependent kinases (CDKs), growth suppressor genes and cyclin-dependent kinase inhibitors (CKIs)," *Oncogene*, vol. 11, no. 2, pp. 211–219, 1995.

[28] K. Collins, T. Jacks, and N. P. Pavletich, "The cell cycle and cancer," *Proceedings of the National Academy of Sciences United States of America*, vol. 94, no. 7, pp. 2776–2778, 1997.

[29] K. Imai and A. Takaoka, "Comparing antibody and small-molecule therapies for cancer," *Nature Reviews Cancer*, vol. 6, no. 9, pp. 714–727, 2006.

[30] S. Chandarlapaty, A. Sawai, Q. Ye et al., "SNX2112, a synthetic heat shock protein 90 inhibitor, has potent antitumor activity against HER kinase—dependent cancers," *Clinical Cancer Research*, vol. 14, no. 1, pp. 240–248, 2008.

[31] L. N. Klapper, H. Waterman, M. Sela, and Y. Yarden, "Tumor-inhibitory antibodies to HER-2/ErbB-2 may act by recruiting c-Cbl and enhancing ubiquitination of HER-2," *Cancer Research*, vol. 60, no. 13, pp. 3384–3388, 2000.

[32] P. B. Lam, L. N. Burga, B. P. Wu, E. W. Hofstatter, K. P. Lu, and G. M. Wulf, "Prolyl isomerase Pin1 is highly expressed in Her2-positive breast cancer and regulates erbB2 protein stability," *Molecular Cancer*, vol. 7, article 91, 2008.

[33] D. W. Miles, W. H. Harris, C. E. Gillett et al., "Effect of c-erbB2 and estrogen receptor status on survival of women with primary breast cancer treated with adjuvant cyclophosphamide/methotrexate/fluorouracil," *International Journal of Cancer*, vol. 84, no. 4, pp. 354–359, 1999.

[34] J. Liu, C. He, K. Zhou et al., "Coptis extracts enhance the anticancer effect of estrogen receptor antagonists on human breast cancer cells," *Biochemical and Biophysical Research Communications*, vol. 378, no. 2, pp. 174–178, 2009.

[35] K. Takara, S. Horibe, Y. Obata, E. Yoshikawa, N. Ohnishi, and T. Yokoyama, "Effects of 19 herbal extracts on the sensitivity to paclitaxel or 5-fluorouracil in HeLa cells," *Biological and Pharmaceutical Bulletin*, vol. 28, no. 1, pp. 138–142, 2005.